MITNE-186,c.3

THE REACTOR ENGINEERING OF THE MITR-II CONSTRUCTION AND STARTUP

G. C. Allen, Jr., L. Clark, Jr.,
J. W. Gosnell, D. D. Lanning

MASSACHUSETTS INSTITUTE OF TECHNOLOGY

Department of Nuclear Engineering

Cambridge, Massachusetts

THE REACTOR ENGINEERING OF THE MITR-II

CONSTRUCTION AND STARTUP

by

G. C. Allen, Jr., L. Clark, Jr.,

J. W. Gosnell, D. D. Lanning

June, 1976

MITNE-186

THE REACTOR ENGINEERING OF THE MITR-II
CONSTRUCTION AND STARTUP

Abstract

The heavy water moderated and cooled research reactor, MITR-I, has been replaced with a light water cooled, heavy water reflected reactor called the MITR-II. The MITR-II is designed to operate at 5 thermal megawatts. The MITR-I was shutdown in May, 1974, dismantling, construction, and preoperational testing continued until the MITR-II went critical on August 14, 1975. Cadmium absorbers were fixed in the upper core of the first fuel loadings to shorten the active core height and provide reactivity control. Solid non-fueled elements were also loaded for additional reactivity control.

Swelling of the original cadmium fixed absorbers necessitated a second core configuration. The second core contained additional solid non-fueled elements and no fixed absorbers.

The compact core of the MITR-II causes thermal neutron flux and power peaking to occur at the core outer boundaries and incore locations with excess moderator. The active core power density is in the range of 100 to 150 watts/cm^3 with peaks up to 300 watts/cm^3. The power, flow, and temperature distributions of the initial core loadings were determined analytically and experimentally in order to evaluate the safety limit factor and limiting operating conditions. Neutron flux, core temperature, coolant flow, and power distributions were measured by various experimental techniques.

The thermal-hydraulic parameters of the initial fuel loadings are evaluated and shown to satisfy the acceptance criteria for operation of the MITR-II.

TABLE OF CONTENTS

LIST OF FIGURES

Figure

Figure

Figure

Figure

Figure

Figure

LIST OF TABLES

Table

Table

ACKNOWLEDGEMENTS

CHAPTER 1

INTRODUCTION

1.1 General

The Massachusetts Institute of Technology Research Reactor has been serving the academic, industrial and medical research needs of MIT and the surrounding community since the initial facility went critical on July 21, 1958. The original design of the Massachusetts Institute of Technology, hereafter called MITR-I, operated successfully from 1958 until May, 1974 when it was shutdown for modification. During the design of the MITR-I, it had been estimated that the life of the facility based on technical obsolescence would be approximately ten years and thus, features were incorporated into the original design that would permit eventual modification. When the competitiveness of the MITR-I relative to other research facilities decreased in the late sixties, the decision was made to begin the process of designing a new reactor, hereafter called the MITR-II.

The design objectives of the MITR-II were established by the late Dr. Theos J. Thompson and carried to their successful realization in the completed MITR-II by Dr. David D. Lanning. Numerous Department of Nuclear

Engineering students performed research necessary to the re-
design effort and safety evaluation of the new facility.
One of the areas of concern was an analysis of the power
distribution and thermal-hydraulic limiting conditions for
the MITR-II. The purpose of this work is to evaluate the
power distribution limits of the initial MITR-II cores and
to recommend procedures to be used for future core loadings.

This chapter provides a brief description of the MITR-I
in order to understand the advantages of the modification.
In addition, basic features of the MITR-II are described in
order to give a familiarity with the new system which will
be useful in understanding conditions which affect the power
distribution.

1.2 MITR-I

The MITR-I was operated to steady-state powers up to
5 thermal megawatts. The reactor was moderated and forced
connection cooled by heavy water and utilized MTR type fuel
elements of highly enriched uranium-235. The fuel elements
consisted of curved plate-type uranium and aluminum alloy
fuel which was clad with aluminum. Figure 1.2-1 shows a
vertical cross section of the MITR-I. The reactor core was
contained in an aluminum tank four feet in diameter and
seven feet high which was surrounded by a graphite reflector
region. The entire core tank region was shielded by thick
high density concrete penetrated by experimental facilities.

FIG. 1.2-1

EMERGENCY D₂O COOLING TANK

ROTARY LID

LOWER SHIELD PLUG

UTILITY SHELF

BORAL SHUTTER

LEAD SHUTTER

THERMAL SHIELD

TYPICAL BEAM PORT

THERMAL COLUMN

H₂O SHUTTER TANK

PIPE PASSAGE TO BASEMENT

BORAL AND LEAD SHUTTERS

MEDICAL THERAPY ROOM
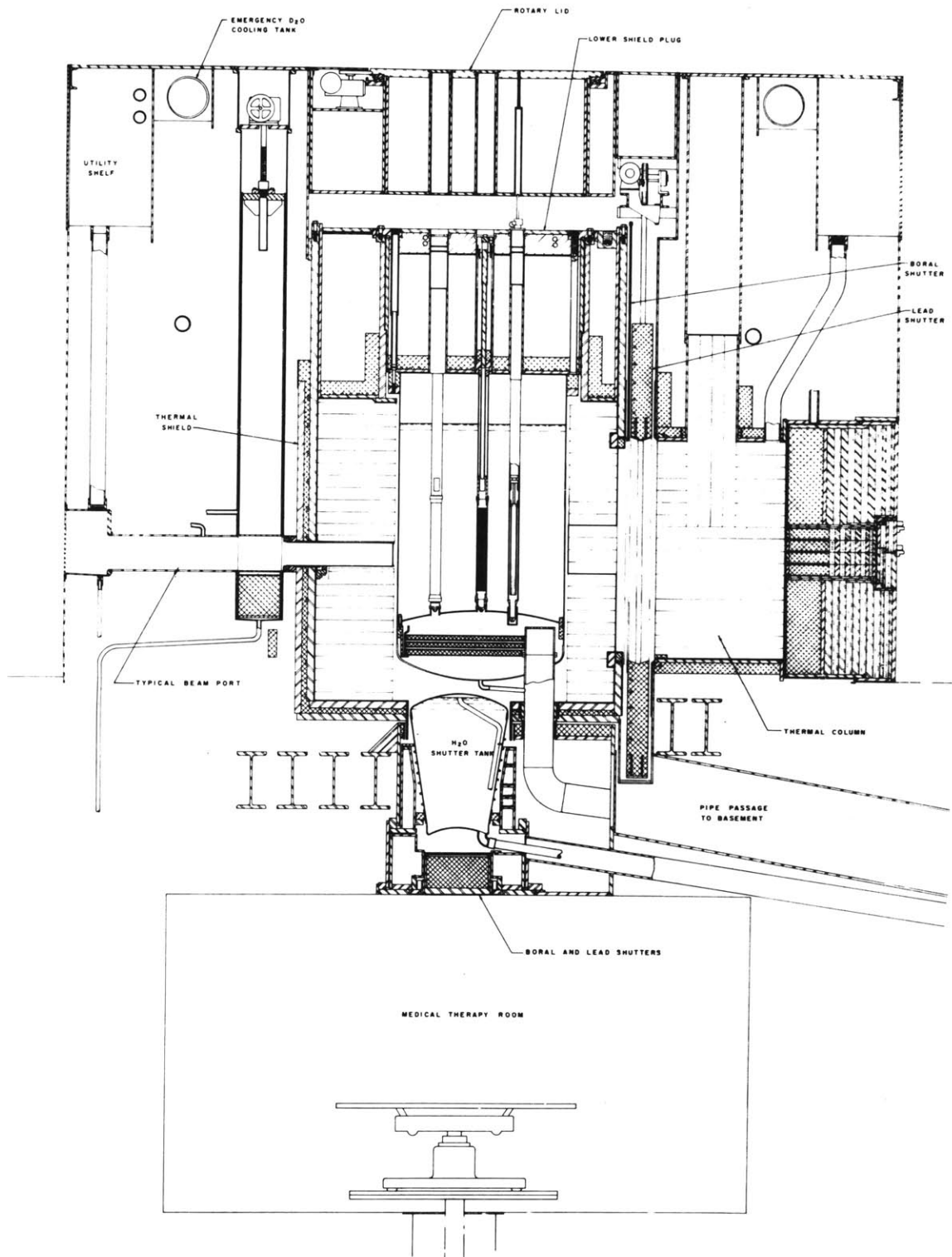
VERTICAL SECTION OF THE MITR-I

Access to the reactor core was only possible through the plug above the core. The centerline of the beam ports was located on a horizontal plane about two inches below the centerline of the fuel.

1.2.1 Core Arrangement and Operation

The fuel elements were arranged in a widely spaced manner in concentric rings with fuel elements being located approximately six inches apart. The central fuel element was located in the radial center of the tank. Figure 1.2-2 shows a horizontal cross section through the reactor and the thirty numbered fuel element positions. In the place of several fuel elements in the outer ring, sample assemblies were located. The sample assemblies were used to tailor the flux to specific beam ports, reduce core reactivity, provide experimental facilities, and in some cases act as check valves to allow natural circulation cooling during absence of flow. In addition to the above, the core also contained six shim safety rods and one regulating control rod.

The operating limit of the MITR-I was the prevention of boiling in the reactor core. The refueling cycle was basically an out-in loading. Fresh fuel would be loaded in the outer rings and moved closer to the core center as the uranium was burned up. Table 1.2-1 shows the limits on element loading per ring for elements containing 169 grams of U^{235} when fresh.

FIG. 1.2-2
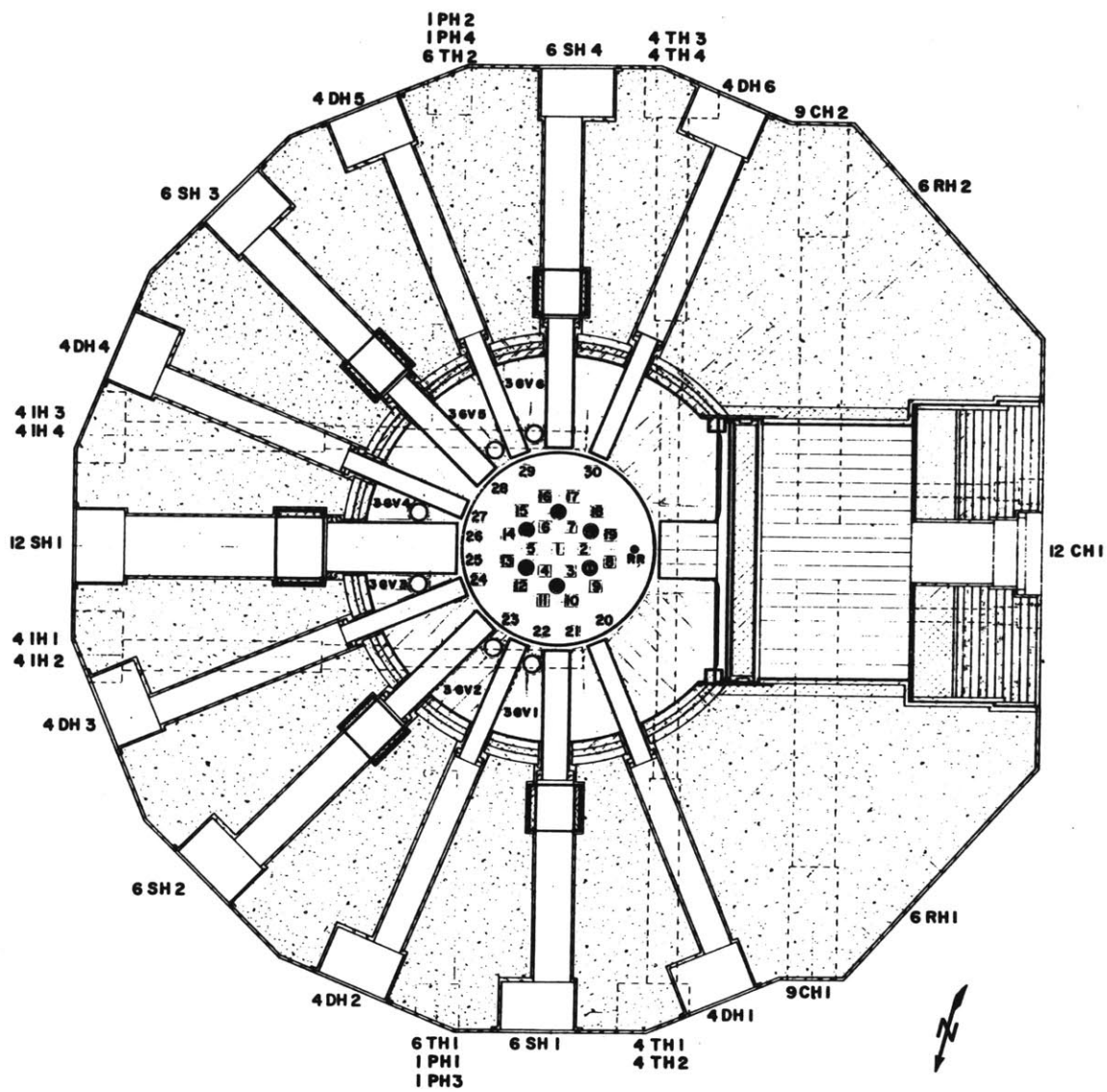
HORIZONTAL SECTION OF THE MITR-I

TABLE 1.2-1

MITR-I FUEL LOADING CRITERIA

<u>Limit</u>

Position 1	Grams of U^{235} in Element x Number of Fueled Elements Incore < 3270
Positions 2-7	Grams of U^{235} in Element x Number of Fueled Elements Incore < 3700
Remaining Positions	No Limit

By meeting the criteria in Table 1.2-1, the power produced in a given element would be less than the power required to cause boiling in the core. An additional limit on each fuel cycle step was that the element burnup could not exceed 43 atom percent. The reactor was operated in a steady state mode for approximately 100 hours per week. The total power generated by the MITR-I during its operation slightly exceeded one quarter of a million megawatt-hours.

1.2.2 <u>Facility Limitations</u>

The MITR-I had operated successfully and safely for sixteen years but in technical terms it had become an old facility. Many major components were only available for limited surveillance inspection and the facility was less competitive than newer research reactors. Because of the desire for continued safe and competitive operation, it was decided that the time had come to either perform extensive

renovation or modify the reactor. The MITR-I was con-
structed at a time when reactor licensing requirements
were less stringent than present and it may have been that
the decision to renovate would not have been acceptable
upon an up-to-date safety review. Coolant pipes entering
and leaving the bottom of the core tank, an adverse coupling
between reflector dump and fuel cooling, and lack of any
seismic analysis are examples of licensing problems which
might have arisen if the renovation of the MITR-I had been
the chosen alternative.

The MITR-I was also limited in reactor fuel handling
and core access. Refueling and core access was only avail-
able through a double plug arrangement above the core and
thus, refueling was performed in the blind. Incore irradi-
ation facilities were limited in size as to what could fit
through a fuel element hole in the lower shield plug. The
complexity of incore refueling and maintenance increased
personnel radiation exposure and required a high inventory
of radioactive hardware.

The neutron flux density and the neutron energy spec-
trum for the MITR-I were less desirable than competing
facilities. The flux distribution for the MITR-I is de-
scribed in the following section.

1.2.3 Thermal Neutron Flux Distribution

The thermal flux distribution across the MITR-I core
is shown in Fig. 1.2-3. The peak thermal flux was approx-
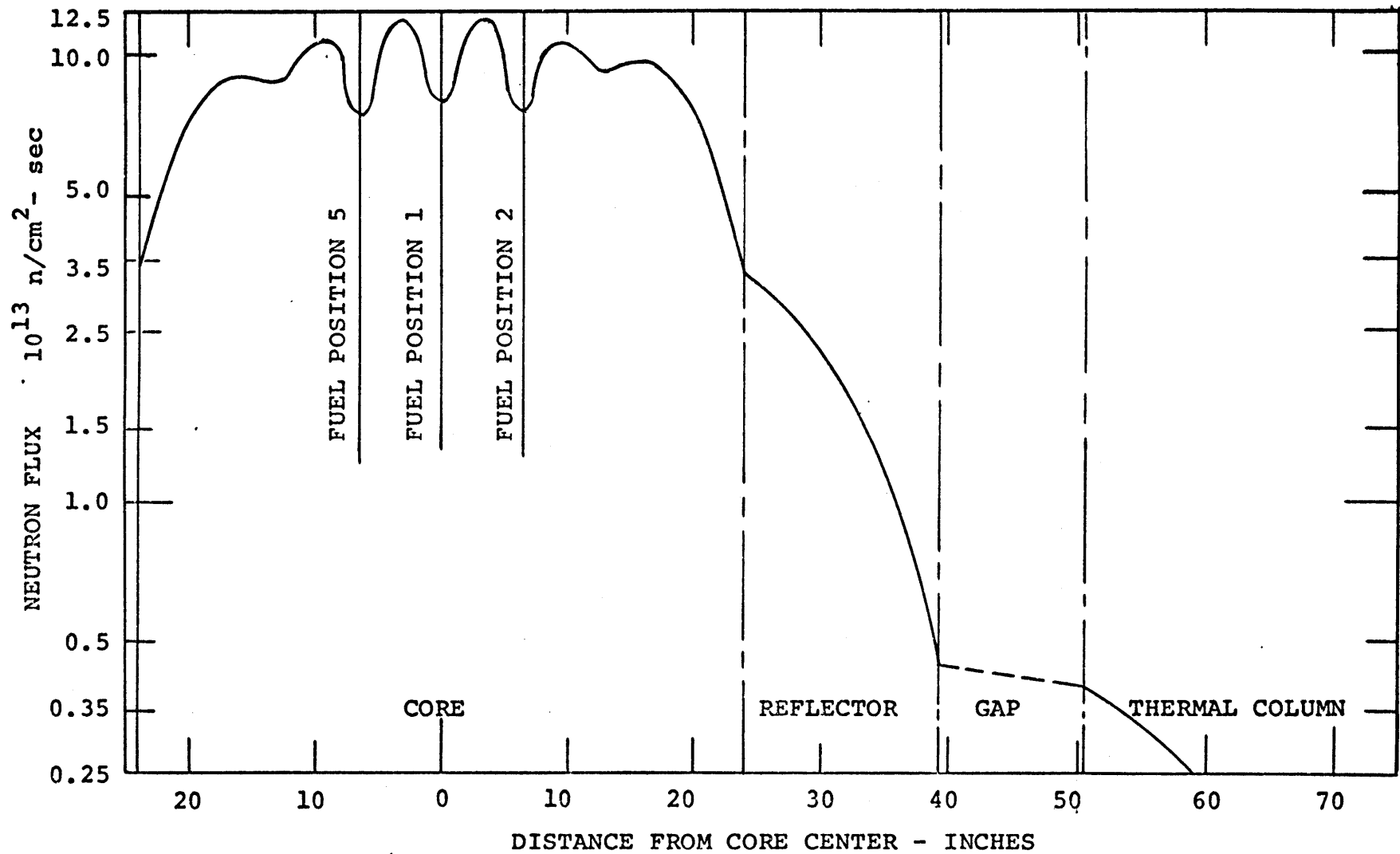
FIG. 1.2-3 MITR-I NEUTRON FLUX AT CORE AXIAL CENTERLINE THROUGH
THE CORE AND THERMAL COLUMN AT 5.0 MW

imately 1.2×10^{14} n/cm^2-SEC which occurred at the center

of the core. The peak thermal flux that was usable by beam

port experimenters at the core tank wall was approximately

2×10^{13}. Because the beam ports looked directly at the

reactor fuel elements, the beam port neutron flux had a

high first flight to thermal flux ratio which was not a

satisfactory condition for some experimenters. Since the

MITR-I was primarily used as a source of neutrons, its use-

fulness as a research tool was greatly dependent on the

magnitude and quality of the neutron fluxes at its experimen-

tal facilities.

1.3 MITR-II

The MITR-II is located in the same shielding and con-

tainment structure as the MITR-I. Many of the supporting

and process facilities are identical for the MITR-II when

compared to the MITR-I. The MITR-II is a heavy-water

reflected and light water cooled and moderated nuclear

reactor which utilizes flat plate-type, finned aluminum clad

fuel elements highly enriched in U-235. Like the MITR-I,

the MITR-II was designed to operate in a steady state mode

to powers of 5 thermal megawatts. Figure 1.3-1 shows a

cross sectional layout of the MITR-II. A new tank and

pool system was installed to replace the old tank and the

top plugs.

The core is located inside of two concentric tanks and

a core housing. The outermost tank is a 4 ft. diameter

FIG. 1.3-1

FLOW SHROUD

COOLANT
INLET

SPENT FUEL
STORAGE

H_2O
CORE TANK

CRYOGENIC
BEAM SOURCE

D_2O REFLECTOR TANK

D_2O
SHUTTER

CADMIUM SHUTTER

H_2O
SHUTTER TANK

MEDICAL ROOM CEILING
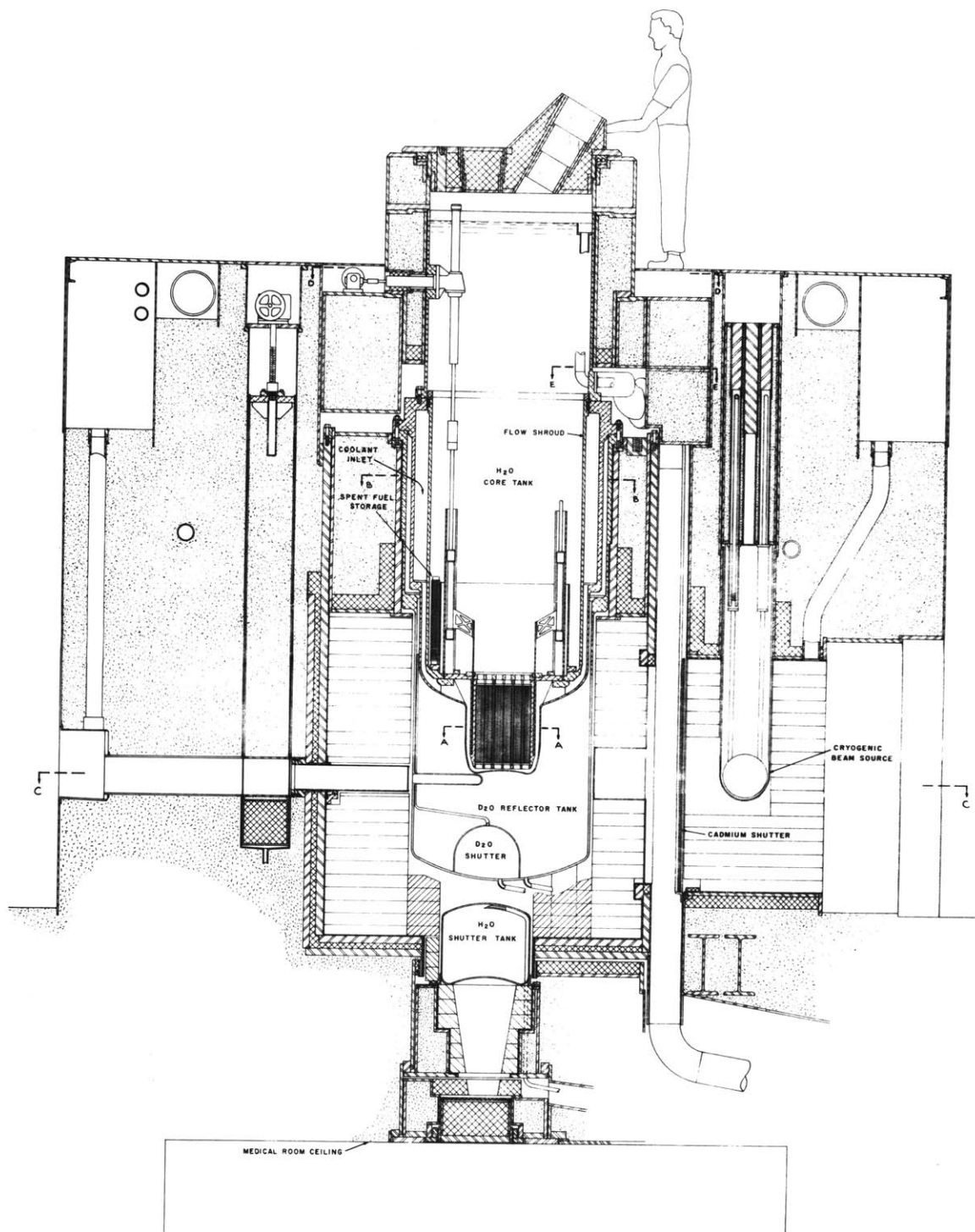
VERTICAL SECTION OF THE MITR-II

D_2O reflector tank and is used to maintain a D_2O level
for neutron reflection. The D_2O system includes the
capability of rapidly lowering the D_2O level in the reflector
tank for a rapid reduction of reactivity as an alternate
shutdown means. Re-entrant thimbles are included in the
reflector tank which act as extensions of the existing
beam ports into the high flux region directly beneath the
reactor core.

The core tank holds the primary system light water and
the core housing assembly. The water surface level at the
top of the core tank pool is maintained close to atmospheric
pressure and thus, the entire system is operated at low
pressures. Heat generated in the core is removed by forced
convection. H_2O coolant enters the reactor through the
inlet plenum into the annular region between the core tank
and the flow shroud. It then flows downward in this annulus
until it reaches the bottom of the core housing where it is
directed upward through the fuel elements into the water
pool above the core. At a water level near the inlet pipe
level, the water discharges out the exit plenum. Siphon
breakers and natural convection valves which are maintained
in the closed position by primary pump pressure, open auto-
matically upon loss of flow to prevent siphoning of water
out of the core tank in the unlikely event of a pipe break
and to allow natural circulation cooling of the core.

The fuel is arranged in a compact core configuration in the core housing assembly which is at a higher elevation than the MITR-I core. The fuel elements are held in place by a rotating upper grid. The control blades come down around the outside of the core and are effective by cutting off thermal neutron transport between the reflector and the core. In the initial design of the MITR-II, the control blades were made with cadmium in an aluminum sandwich. There are six control blades and one regulating rod in the MITR-II.

The graphite reflector and radiation shielding for the MITR-II are very similar to the MITR-I configuration. The exceptions are a little additional graphite beneath the reflector tank and the modified upper shielding around the top of the core tank pool.

1.3.1 Core Arrangement and Operation

Fuel elements are arranged in a compact core arrangement as shown in Fig. 1.3-2. The core is a hexagonal cylinder about 15 inches across the flats formed by 27 rhombic fuel element positions. Fuel elements may be loaded into any of three concentric rings; A, B, and C. The positions are numbered around the ring in a clockwise fashion with the number one position in each ring being the first position which is clockwise of a line drawn between the core center and regulating rod. Figure 1.3-2 shows the number

FIG. 1.3-2

core tank

core housing assembly

spider hole #3

spider hole #1

#5

#4

#6

C-10 C-11

C-9   C-12

C-8   B-6   B-7   C-13

B-5   B-8

C-7   A-3   C-14

B-4   A-2   A-1   B-9   C-15

C-6   B-3   B-1

#3   C-5   B-2   C-1

C-4   C-2

C-3

#2

REGULATING ROD

shim blade (6)

corner hole

hexagonal fixed absorber location

radial fixed absorber location
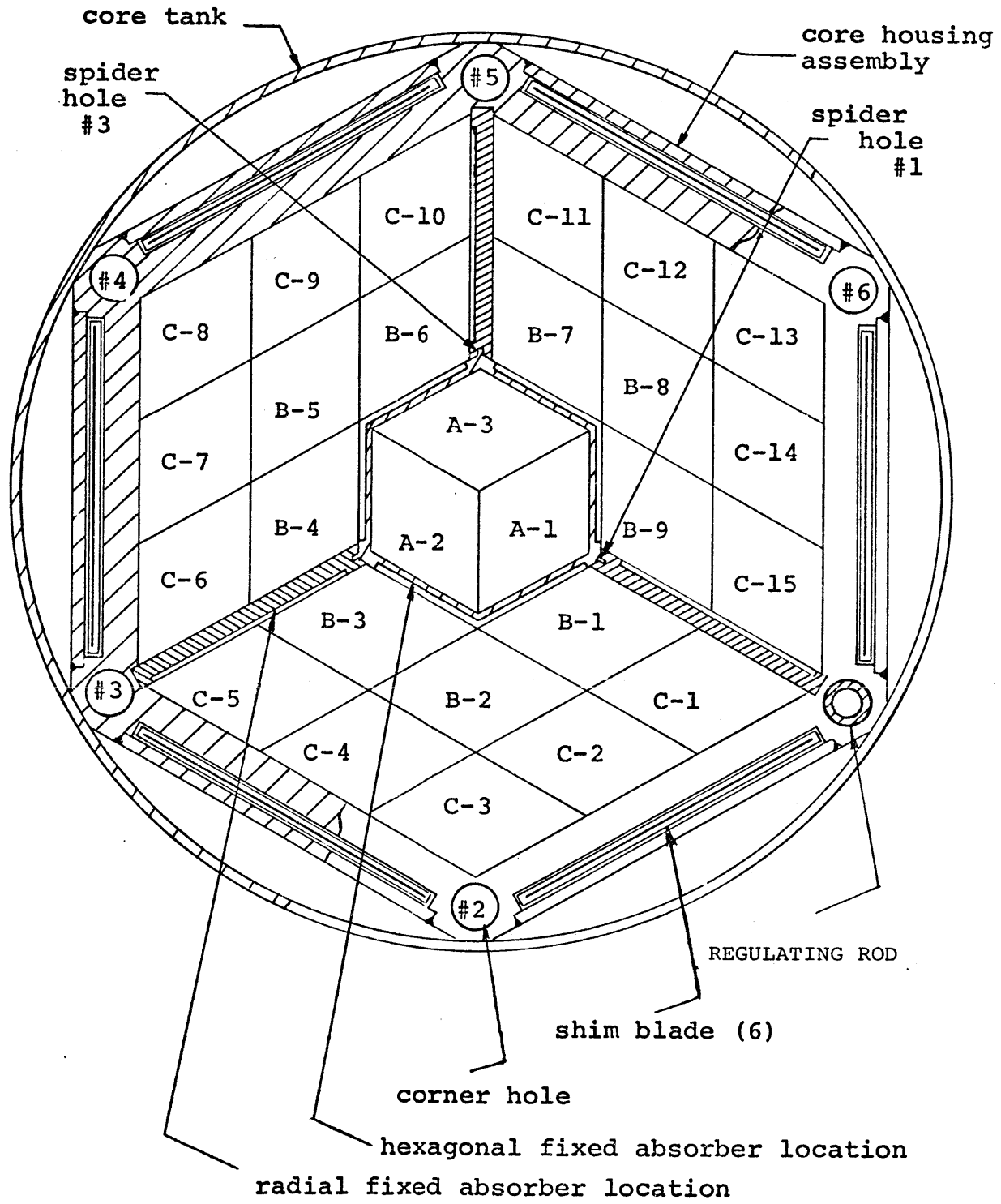
CORE SECTION M.I.T.R. - II

designation for each fuel position. The inner ring
(ring A) contains 3 element positions, the middle ring
(ring B) contains 9 element positions and the outer ring
(ring C) contains 15 element positions.

The upper portion of the core is poisoned by fixed
absorbers which are attached to the absorber spider which
is part of the core housing assembly. A vertical cross
section through the core showing the fixed absorbers is
shown in Fig. 1.3-3. The absorber spider separates the core
into four regions as shown in Fig. 1.3-2. The fixed ab-
sorbers in the spider depress the power in the upper half
of the core and make the active core to be about 12 inches
or about one half the fueled length of an element. The
fact that the compact core is undermoderated combined with
the poisoned upper core results in peak thermal fluxes
occurring at the lower edges of the core.

A fueled element is shown in Fig. 1.3-4. The element
is rhombic in shape and composed of fifteen flat fuel plates.
Each plate contains a core of highly enriched uranium in the
form of U-Al$_x$ cermet which is clad with aluminum. The
fuel plate surfaces are finned in order to increase the effective
heat transfer area. The increase was needed because
the compact core generates the same total power as the
MITR-I, but has a smaller fuel plate surface area in the
active core and greater power spiking than the MITR-I. Each
element has a uniform loading of approximately 445 grams of

FIG. 1.3-3

H_2O

shim
blade

D_2O

absorber
spider

D_2O

core
tank

lower

spider

beam port

D_2O
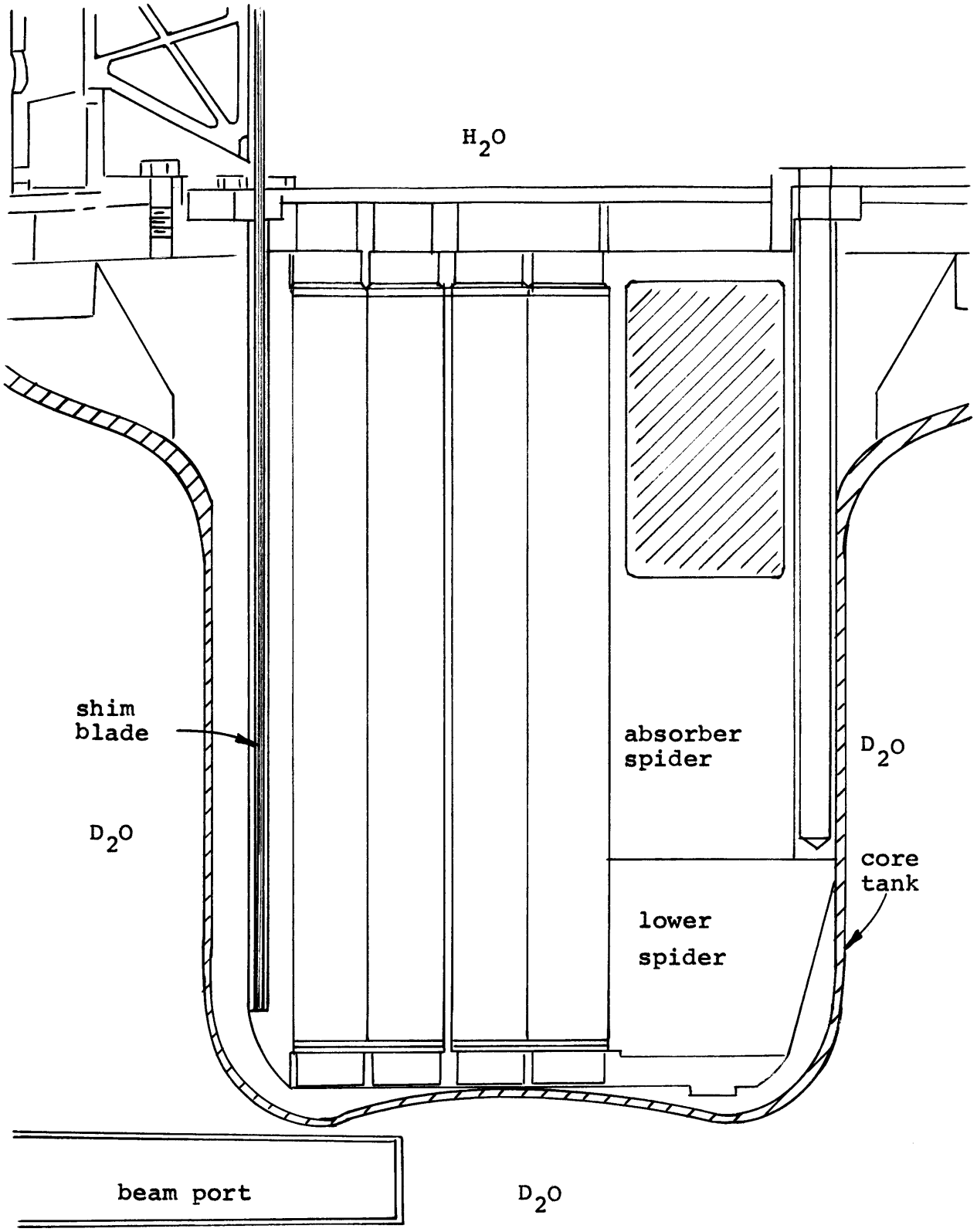
VERTICAL SECTION OF THE MITR-II CORE
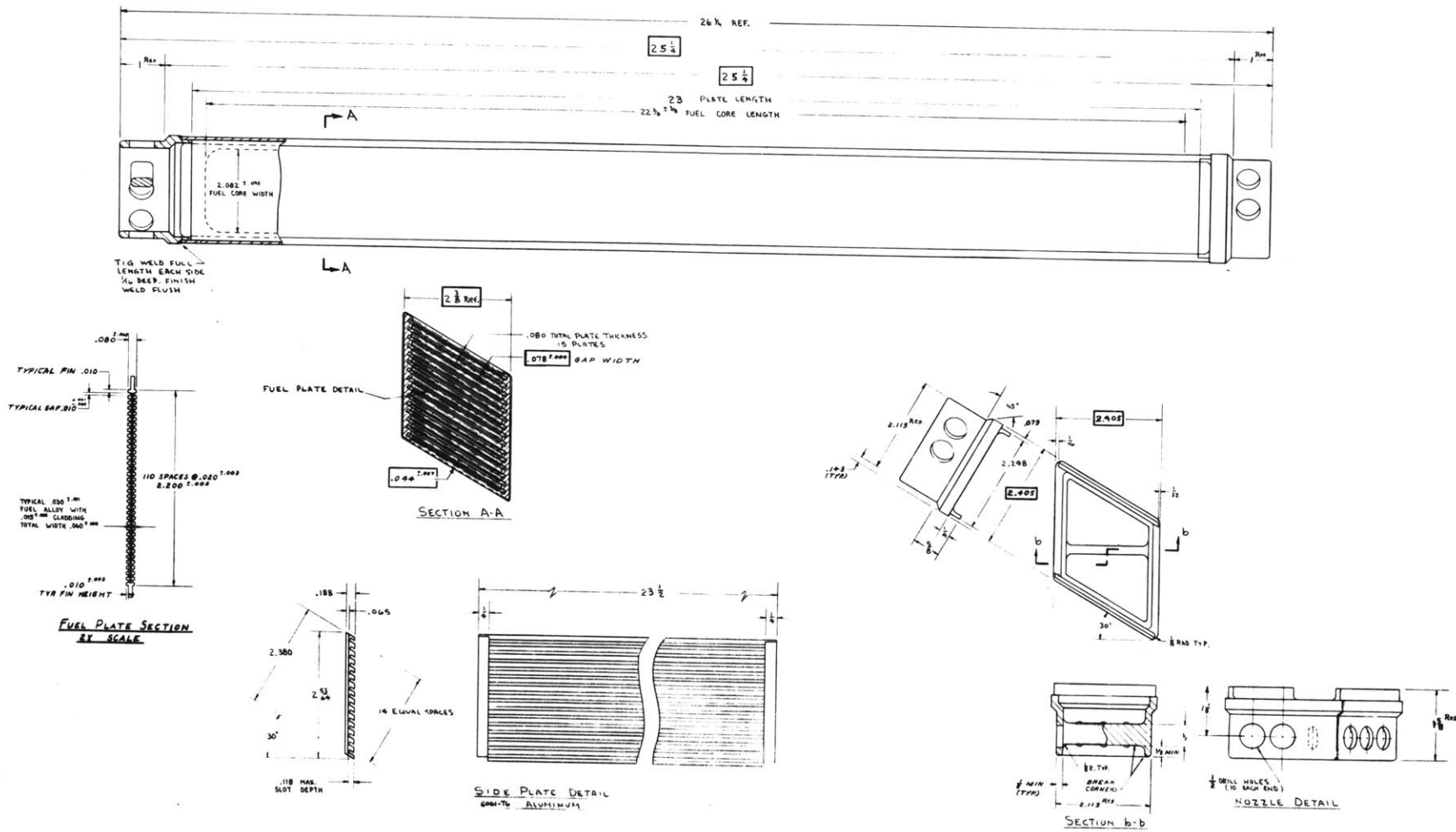
FIG. 1.3-4   MITR-II FUEL ELEMENT

U-235. All elements have a nozzle at each end and the elements are completely reversible in the core allowing either end to be down.

Irradiation facilities may be positioned incore by filling one or more fuel positions with the experimental facility. The incore facility must be designed to prevent unacceptable reactivity or power peaking conditions. An Incore Sample Assembly (ICSA) shown in Fig. 1.3-5 was designed to fill a central element position in the original core. This particular design proved to cause unacceptable power peaking.

The core was designed to burn the lower half of the elements. The upper half of the elements were intended to be protected from burnup by the fixed absorber and the control blades outside of the elements. When the lower half has been used to an appropriate life, the element may be inverted, or flipped, and placed in the same or different ring. The already depleted uranium in the top half of the flipped element will also help to hold the flux into the lower portion of the core. Fuel elements may be flipped or exchanged in such a manner as desired to give the proper burnup, reactivity, and power peaking arrangement.

1.3.2 Advantages of the MITR-II

The MITR-II was constructed because of improvements in research capability, safety, and operations over the previous reactor. The MITR-II provides a higher source

FIG. 1.3-5   INCORE   SAMPLE ASSEMBLY

Left end view note: NOZZLE IS NOT SHOWN FOR CLARITY.

Right end view note: NOZZLE IS NOT SHOWN FOR CLARITY.

T.I.G. WELD FULL LENGTH EACH SIDE 1/16 DEEP. FINISH WELD FLUSH.

FUEL NOZZLE

A SLIP FIT ON NOZZLE

1.880 DIA HOLE

2.248

A SLIP FIT ON NOZZLE

2.100 DIA C'BORE

intensity for neutron beam experiments and an increased ratio of thermal flux to first flight fast neutrons. This is possible because of reentrant thimbles which extend into the high flux region beneath the core and because the core was raised so that the beam ports no longer look directly at the fuel. The new reactor has a higher fast flux in the core for fast flux irradiations and an improved and more flexible neutron beam in the medical therapy room. The pool type design gives more flexibility in designing incore irradiation facilities.

The MITR-II is a safer facility because of the complete replacement of the core tank and core structures with new, corrosion free, unirradiated materials built to meet current code and quality assurance requirements. The shutdown and emergency cooling system is better for the MITR-II and the back up reactivity shutdown by dumping the D_2O is separated from the core cooling system. The review and modification process has helped upgrade the entire facility.

Refueling and maintenance are simpler on the MITR-II than they were on the MITR-I because of the pool design. Direct view of core components make surveillance inspections easier. Lower radiation exposure of maintenance personnel is expected with the MITR-II.

1.3.3 New Core Limitations and Problems

Constructing a   unique   facility means that one is

starting at the beginning of the learning curve. The unique design has led to various shakedown difficulties and added expenses. Startup problems have proved to be both frustrating and educational.

The light water moderated MITR-II is more susceptible to power peaking difficulties than the MITR-I. Because the core is undermoderated, power peaks occur at the core-reflector interface or anywhere an abundance of moderator is near the fuel, such as corner holes in the core housing assembly or the coolant channel in the original design of the ICSA. Power peaking must be carefully considered in the following:

1) High control blade positions

2) Refueling proposals

3) Irradiation facilities.

CHAPTER 2

OBJECTIVES

The primary objectives of this work are as follows:

1) To determine experimentally and analytically neutron flux, core power, temperature and coolant distributions of the MITR-II,

2) To relate the predicted distributions to the measured distributions,

3) To evaluate the limiting operating conditions for initial cores of the MITR-II,

4) To recommend the procedures to be used for the establishment of the limiting operating conditions after future refueling operations.

These objectives were accomplished as a part of the completion of the final design, construction, and startup of the MITR-II.

2.1 Core Distributions

As described in Chapter 1, the MITR-II is a unique reactor. The power and flux distributions are far from typical "classical" distributions found in many reactors. Because of this uniqueness, it is especially important to accurately evaluate the core temperature, power and flow distributions. By determining core wide distributions, it is possible to be certain that the most conservative case is being analyzed in evaluating the operating and safety limits.

A best estimate of a distribution was determined by analytical calculations or by scale model testing. Then the following means were employed to empirically measure core-wide distributions in the completed MITR-II for comparison with the original best estimate:

1. Neutron flux and core power mapping
   A. Gamma scanning of removable fuel plates
   B. Flux wires
   C. Self-powered incore detectors

2. Flow mapping
   A. Establishment of relative fuel element flow rates by differential measurements using an above core flow meter assembly
   B. Channel flow measurements of an individual element

3. Temperature mapping
   A. Thermocouple instrumented fuel plates
   B. Thermocouples on assembly outlets

The experimental and analytical results were compared to determine both the accuracy of the prediction method and areas where the prediction method could be improved. Chapters 4, 5, 6, 7, and 8 describe the calculated and measured core-wide distributions for the initial MITR-II cores. Chapter 10 is a summary of the distributions and gives a discussion of the agreement between predictions and measurements.

2.2 Safety Limits and Operating Conditions

The design of the MITR-II core has been made with emphasis on safe and useful operability. As part of the startup program for the MITR-II, the safety limits and limiting conditions for operation must be evaluated in

order to prove the validity of the design analysis. The
values of several core factors with an estimate of their un-
certainty must be determined in order to evaluate the safety
limits and limiting condition for operation. The factors
to be evaluated are defined as follows:

F_f is the fraction of primary flow cooling the fuel,

d_f is the flow disparity, the ratio of the minimum
expected flow in the hot channel to the average
channel flow,

F_r is the ratio of channel power to the average
channel power,

F_a is the peak power per unit volume in the plate
relative to the average power per unit volume
in that plate,

Z is the ratio of the power released into the
channel between the inlet and the hot spot to
the total power released into that channel.

Chapter 7 contains the safety limit evaluation of the
initial cores of the MITR-II.

2.3 Future Procedures for Determining Operating Conditions

It would be an unacceptable burden to perform a large
scale experimental program with each reactor refueling.
Consequently, a procedure for evaluating the safety limits
of future MITR-II cores must be developed. Section 7.5 lists
a proposed procedure for future evaluations and Chapter 10
also gives a summary of the results.

CHAPTER 3

CONVERSION FROM MITR-I to MITR-II

3.1 Conversion Schedule

When the idea to replace the MITR-I with the MITR-II
was first conceived it was estimated that it would take
six weeks to complete the project. The first actual con-
struction schedule indicated that the conversion would take
three and one half months. In the end, it took fourteen
months to obtain a critical reactor after shutting down the
MITR-I. A chronological listing of highlights during
the conversion is shown in Table 3.1-1. The variance
between original estimates and actual required time was
caused by an underestimation of the conversion difficulty
and by several conversion problems.

3.2 Major Conversion Problems

An overiding concern in all projects is lack of
money and difficulty in completing the project within the
originally scheduled time. The conversion to the MITR-II was
no exception to this rule. The actual problems seemed
magnified at the time because of financial limitations and
not necessarily because of difficulty of the technical
solutions. In all cases, a conservative solution was
applied to the problem, once the problem was recognized.

TABLE 3.1-1

MITR-II CONVERSION SCHEDULE

February, 1973	Final decision to proceed with MITR-II
April, 1973	Construction permit issued
May, 1973	Contracts signed for tanks and core housing
July, 1973	Contracts signed for shielding
September, 1973	Contracts signed for control mechanisms
November, 1973	Completed initial lattice modification
December, 1973	Modified medical H_2O shutter system
January, 1974	Problems found in first core housing casting and delay in core tank delivery
April, 1974	Shielding and control rods shipped to M.I.T.
May, 1974	Core tank shipped to M.I.T.
	Shutdown MITR-I
June, 1974	Reflector tank shipped to M.I.T.
	Dismantled MITR-I
July, 1974	Completed dismantling MITR-I
September, 1974	Documentation review of MITR-II tanks
November, 1974	Contracts signed to build weldment core housing
December, 1974	Reflector Tank installed
	Assembled core tank components except for core housing
January, 1975	Installed core tank
	Completed primary piping
March, 1975	Perform system hydro tests
April, 1975	Installed shielding
June, 1975	Core housing and control blades installed
July, 1975	Pre-operational tests completed
August, 1975	Initial criticality achieved

However, conservative solutions are not necessarily the fastest or least expensive, which added to the financial burden.

Delays and problems during construction do not reflect upon the safety of the MITR-II. The MITR-II conforms to the requirements of its Technical Specifications and Safety Analysis Report. The reason for listing conversion problems here is to provide a reference for some of the occurrences during construction.

3.2.1 Lack of Quality Assurance Group

The MITR-II was constructed by the same group of people that had operated the MITR-I successfully for many years. This group was familiar with the facility as it had previously existed and with the necessary radiation procedures. Lack of skills and experience in construction was expected to be secondary to the necessity to be familiar with the reactor physical plant. Time would have been required to train construction workers and still in the end both construction workers and operating personnel would be on the payroll. The exception to the above is the case of an independent quality assurance group. The purpose of quality assurance is to provide adequate documentation that a system, structure or com-ponent will perform satisfactorily in service and in conformance with Safety Analysis Report and Technical Specifications requirements.

The Nuclear Regulatory Commission is responsible for enforcing Title 10, Chapter 1, Code of Federal Regulations. Part 50, Appendix B of the above regulations explains the quality assurance criteria for nuclear power plants and fuel reprocessing plants. Construction of the MITR-II was required to meet the intent of this section. During final operation of the MITR-I, a quality assurance program was developed which was expected to carry over to the construction phase of the MITR-II. The group was too small to assign separate individuals who would be solely devoted to quality assurance requirements. Given the limited resources of the operating group and the numerous demands on time, quality assurance documentation was not given high priority. The problem was compounded by the initial infrequency of Nuclear Regulatory Commission (NRC) inspections with respect to the construction schedule, which allowed much to occur without an explanation of what was truly desired by the NRC.

Much concern and action had gone into assuring the safety of the MITR-II, but some documentation was poorly organized or incomplete when compared to power plant standards. As a result, the MITR-II staff was criticized on the implementation of their quality assurance plan. To improve this situation, the Stone and Webster Engineering Corporation (S&W) was retained as an outside consultant. Stone and Webster is a large engineering firm with con-

siderable experience in constructing nuclear power plants and satisfying NRC requirements. S&W provided the necessary experience in quality assurance matters and provided an independent quality assurance consultant for the completion of the construction phase of the MITR-II.

At no time was the MITR-II staff intending not to live up to its quality assurance commitments, but an initial desire to save resources by not having an independent full-time quality assurance group resulted in construction schedule slippage and considerable expense in the end. Given present NRC regulations, future conversion projects should consider an independent, full-time experienced quality assurance group as necessary as any items of hardware.

3.2.2 Lack of Knowledge Concerning MITR-I Field Dimensions

The MITR-I was constructed in the 1950's and at that time there were few formal requirements for quality assurance and record keeping. Timely installation of several MITR-II components was dependent upon field dimensions agreeing with recorded print dimensions. Tight assembly tolerances allowed little room for error.

In several cases, the field dimension differed enough from the expected dimension to create installation problems, i.e., the components would not fit without being reworked. Operation of the MITR-I had precluded verifying these field dimensions prior to component fabrication.

Installation of the D_2O reflector tank and the primary system aluminum transition pipes was delayed several months by difficulties caused by inaccurate field dimensions. These components had to be trial fitted several times prior to final installation. Several other components would not fit the first time, but they resulted in much shorter delays.

The source of the problem was in expecting the field dimensions to be correct in the first place. A program of trial fitting was planned but this was more to verify the expected dimensions rather than determine the actual dimensions. Initial construction should have been planned to work around critical dimensions until they were determined. It is questionable whether such a program would have saved much time but it would have saved some expense. Future conversions of existing facilities should in so far as possible avoid reliance on existing field dimensions until they can be verified.

3.2.3 Difficulty with Aluminum Fabrication

Fabricating numerous components out of aluminum proved to be more difficult than expected. Problems were encountered in aluminum casting, corrosion prevention, weld radiography, welder certification, and dimensional stability. The MITR-II primary and D_2O systems are expected to be high integrity systems and as such, defects were not accepted during construction. Tight dimensional tolerances were required to allow the compact reactor core to operate as designed.

Aluminum fabrication to tight tolerances and low defects proved to be time consuming.

The MITR-II core housing assembly was first made from a 356-T6 aluminum casting. This alloy was first chosen because of its corrosion resistance and low neutron absorption. Problems arose because the casting process entrains a certain amount of impurities and porosity into the cast metal. Machining the casting to final dimensions revealed these deficiencies. The first casting obtained was rejected because of excessive porosity. Several other castings were made by a different manufacturer until one was obtained, which according to radiographs, was acceptable. Upon machining, this casting also revealed defects which required repair. During a weld repair of one of these defects, the casting cracked at a point where considerable weld material had been machined away. As a result of difficulty with obtaining a large acceptable casing the final core housing was fabricated using 6061-T6 aluminum plate.

Considerable effort was required to prevent unacceptable levels of corrosion in the aluminum components. Protection against contamination by halogens and various heavy metals was necessary. Water in the system required constant cleanup and Ph control to prevent corrosion. This requirement complicated the need to have various systems partially filled with water for radiation shielding.

Butt welds which could not be inspected inservice or during system hydrostatic tests were required to successfully pass weld radiography. In the Boston area there was little experience with preparing and testing radiograph acceptable aluminum joints. As a result, weld radiographs were compared with the requirements of other common metals that are used to fabricate pressure vessels. Considerable time and expense was required to learn how to make aluminum joints that could pass a stringent radiograph criteria.

In the same manner that it was difficult to obtain the expertise to make radiograph acceptable weld joints, it was difficult to have welders obtain certification on aluminum joints. Since welding was performed in the field and not on a production line, the welders had to be certified for all positions, a range of material thicknesses, and several aluminum alloys. Several procedure steps, which would be standard in production welding and would make certification easier, had to be omitted because of restrictions in field welding.

Welding on aluminum components results in some initial distortion during welding and additional distortion with time as the welding stresses relieve. Considerable attention to this problem was required during fabrication to assure that the final product would meet tight dimensional tolerances. Machining after welding was often required to make up for distortion during welding. Credit for

structural strength anywhere in a component could only be taken for aluminum in the welded condition because of large decreases in strength of aluminum from welding and the large heat affected weld zone in the component.

Considerable time was spent learning to deal with aluminum because of its desirable properties in a neutron efficient research reactor. Other metals would have been more forgiving could they have been employed.

3.2.4 One of a Kind Fabrication

The MITR-II is an original fabrication which was built to replace another original fabrication, the MITR-I. Progress was hindered by being at the beginning of the learning curve. The cost and time for mistakes, procedure generation, and experience gathering could not be amortized over several units. Many of the major problems which occurred were merely the first trial in an attempt to build a satisfactory end product. Choices of fabrication techniques, material, and assembly procedures would certainly be much easier on a second conversion project.

Several construction problems could have been avoided if the manufacturer were made more familiar with the design intent and assembly requirements of the components being fabricated. In future conversion projects, more emphasis should be placed on familiarizing the fabricator with the total project. As a minimum requirement, the fabricator should draft his own shop drawings.

3.2.5 Preventing Loss of Neutron Economy

Being a research reactor, optimal neutron economy
is extremely important to the MITR-II. Thought was
given to the choice of materials used in the reactor to
limit neutron parasitic capture, as well as, to the de-
sign and assembly of reactor components. Boron or cadmium
contamination was prevented by assuring minimum concentra-
tions in source materials and thorough cleaning prior to
installation. Attention to neutron economy led to the
use of a casting material for the first core housing and
it was only with reluctance that a higher absorption
material was finally used. Field dimension errors led to
some misalignment between the re-entrant thimbles to the
reflector tank and the reactor beam ports which took time
to determine and to achieve the optimal alignment.

Neutron economy was important to the eventual util-
ization of the facility and time spent on its optimization
was time well spent. The problem was that some compro-
mises required to obtain a safe functioning reactor seemed
to have an adverse effect on neutron economy.

3.3 Fuel Loading

Fuel loading into the core of the MITR-II reactor
began on July 30, 1975. A plutonium-beryllium neutron
source was positioned in the center of the core and fuel
elements were loaded one at a time, symmetrically around

the source. All nuclear instrumentation was around the core in the graphite reflector region. Neutron count rates were measured with all control blades inserted and all blades withdrawn prior to loading each fuel element. The neutron count rates were used to determine the amount of subcritical multiplication and thus, predict when the reactor would become critical.

Subcritical multiplication is defined as the ratio of the total neutron flux, due to both the source and fission neutrons, to the flux due to the source only (Ref. 3.3-1). The steady state multiplication of neutrons in the core can be represented by:

$$\frac{\text{Measured Count Rate}}{\text{Source Count Rate}} \sim \frac{1}{1 - K_{eff}} \quad , \qquad (3.3-1)$$

where Source Count Rate is the count rate obtained from the source alone and the Measured Count Rate is the measurement of the count rate with fuel in the core. The count rates were measured by four channels of nuclear instrumentation surrounding the core. For Eq. 3.3-1 to be true, K_{eff} must be less than one, i.e., the reactor is subcritical. As additional fuel is loaded and the reactor approaches critical, K_{eff} tends to unity, and the multiplication becomes infinite. In order to determine the actual critical loading, the reciprocal of the count rate is plotted against the number of fuel elements loaded (all fuel elements have approximately the same uranium loading). The plot is extrapolated

to the zero value of the reciprocal multiplication, i.e.,
infinite multiplication, to give the critical loading of
the core. Count rates were obtained with control blades
fully inserted and with blades fully withdrawn in order to
determine the critical loading with blades full in and
blades full out.

Fuel loading was carried out with the reactor coolant
systems shutdown and bypassed. Prior to each day of fuel
loading, coolant was circulated to sweep out any bubble
buildup in the core from oxidation of newly inserted aluminum
clad fuel elements. Each position contained a water filled
dummy element which would be replaced by an enriched uranium
loaded element. One central element position was occupied
by the neutron source.

3.3.1 Core I Initial Criticality

On August 14, 1975, the MITR-II reactor went critical
for the first time. The plot of reciprocal multiplication
versus fuel loading for the first critical loading is shown
in Fig. 3.3-1. The reactor went critical with twenty
fuel elements loaded which was considerably less than the
twenty-seven positions available for fuel. The shim bank
worth was smaller than expected and was only worth approx-
imately 8.5% $\Delta K/K$. The reactor had gone critical with less
fuel than expected and consequently had six water filled
fuel positions and one position containing the source
upon initial criticality. Figure 3.3-2 shows the core

FIG. 3.3-1

INVERSE MULTIPLICATION PLOT FOR FIRST CRITICAL LOADING OF CORE I

blades inserted

blades withdrawn

number of fuel elements loaded in core
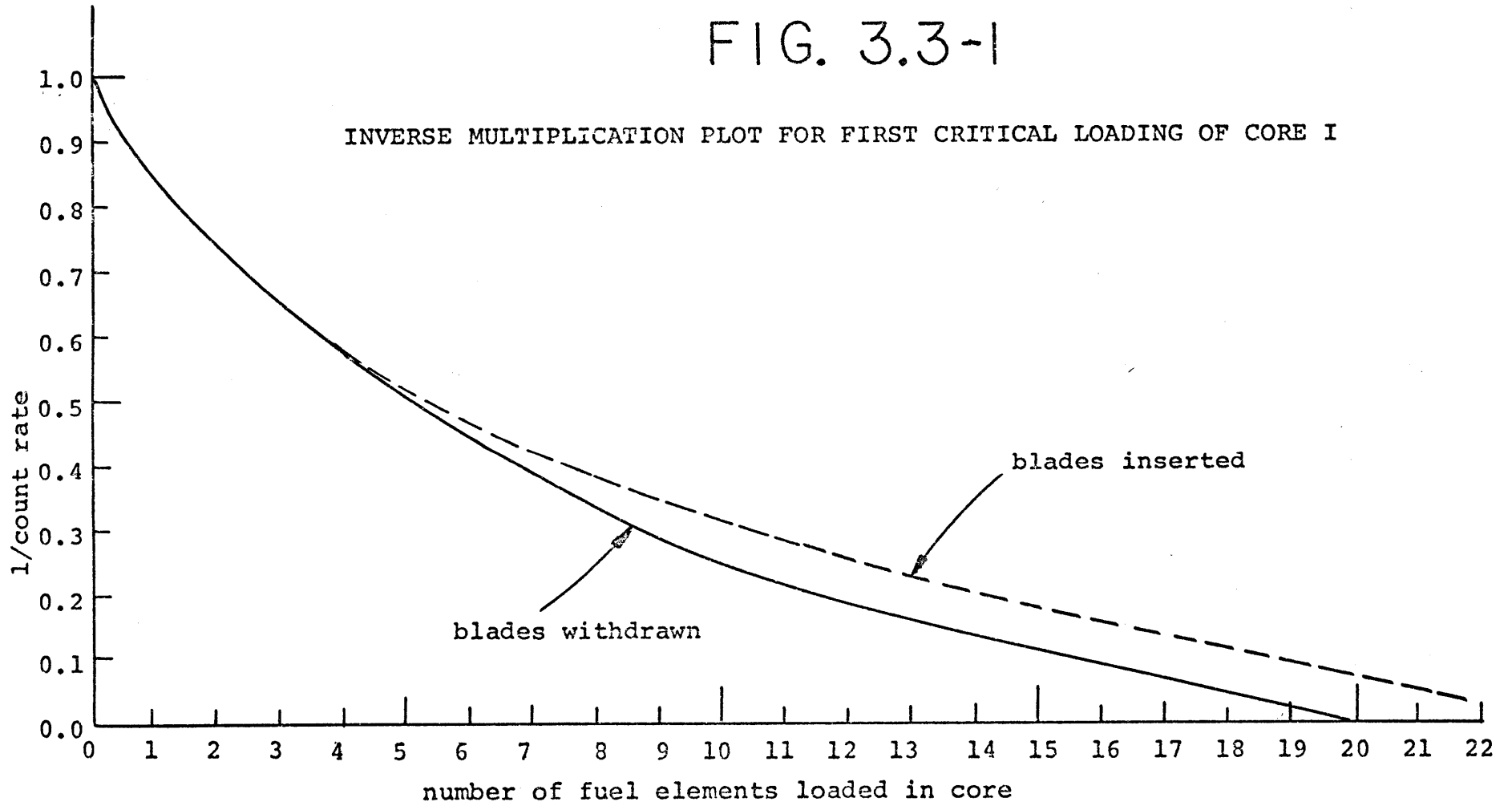
configuration for initial criticality.

Because of the small control bank worth, only one additional element could be added to the core without exceeding the shutdown margin required by the Technical Specifications (the reactor must be subcritical by at least 1% ΔK/K with the most reactive shim blade and the regulating rod fully withdrawn). A twenty-one element core (with 445 grams of U^{235} loading per element) would be unacceptable for long-term operation, because the reactor would not have sufficient excess reactivity for overcoming xenon and fission product poisoning, the empty fuel positions would allow too much bypass flow, and the power peaking would be unacceptable. The problem was caused by the large amount of water in the core in the empty fuel positions. The control blades are effective because they block thermal neutrons in the reflector from re-entering the core. The core should operate somewhat undermoderated and thus, depends on the reflector as a source of thermalized neutrons. Having excess light water in the core results in sources of thermalized neutrons in the core that decrease the worth of reflector neutrons. For the condition of the near fully loaded core, water in the core is worth more for its moderating value than its negative absorber effect.

In order to load more fuel into the reactor core two measures were considered. First, the height of the fixed cadmium absorber in the central spider could be lowered and

FIG. 3.3-2

CORE CONFIGURATION FOR INITIAL CRITICALITY OF CORE I

REGULATING ROD
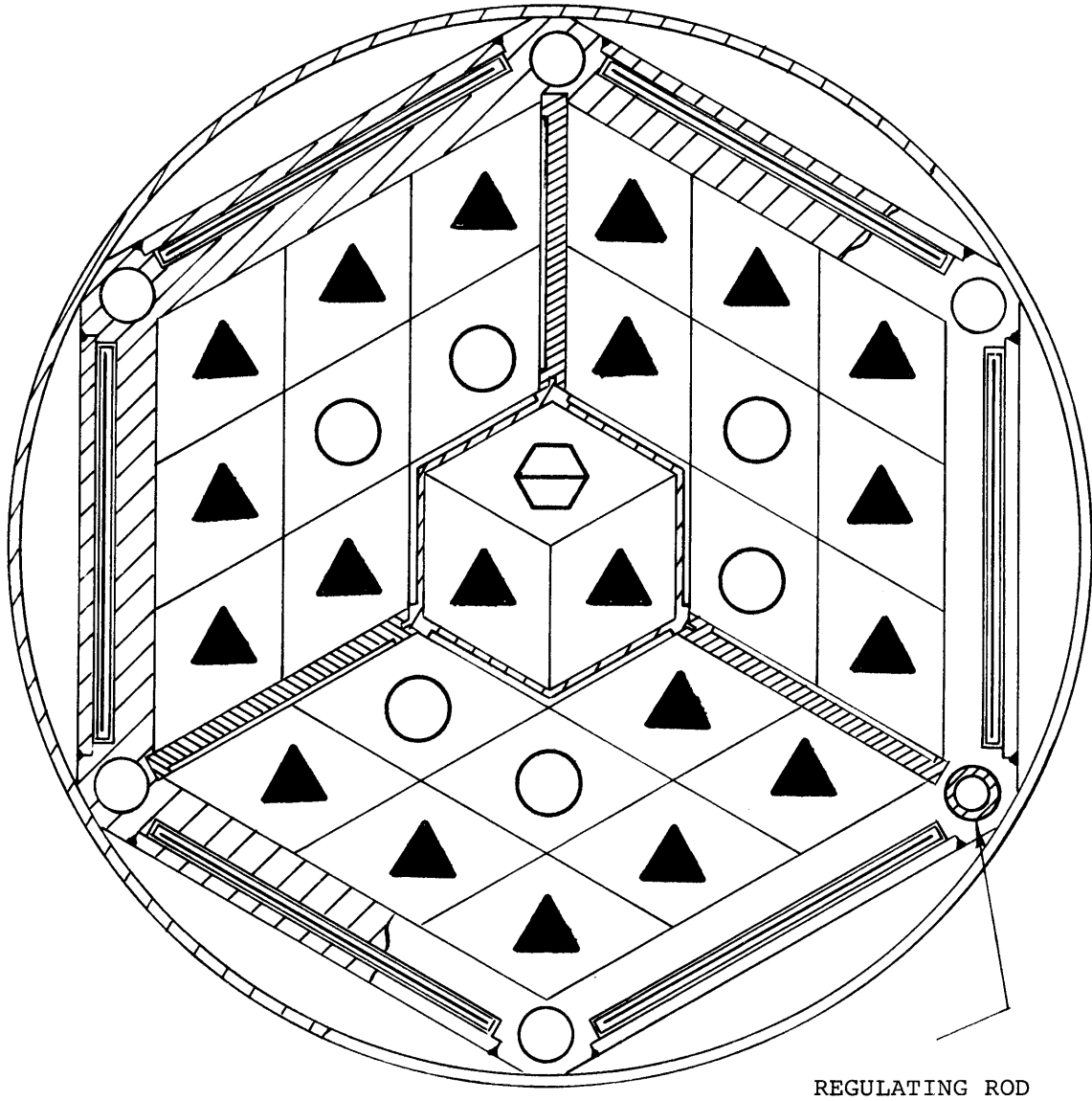
▲ – 445 gram U^{235} fuel element

◯ – water filled dummy element

⬡ – incore sample assembly

second, several fuel element positions could be filled with solid aluminum dummies to displace water in the core. Several computer calculations were made using a CITATION code three-dimensional model (CITATION model and results are discussed in Section 5.2.3). These calculations showed that power peaking was less adversely affected by lowering the fixed absorber than it was by increasing the number of solid dummies. As a result, the fixed absorber was lowered four inches and three solid dummies (see Fig. 3.3-3A for detail of solid dummy loaded in Core I and Fig. 3.3-3B for detail of additional solid dummies loaded into Core II) were loaded into the core for a seond criticality loading.

3.3.2 Core I Second Criticality

The plot of reciprocal multiplication versus fuel loading for the second loading is shown in Fig. 3.3-4. The reactor went critical with a loading of twenty-two active fuel elements, three solid dummy elements, and one sample assembly containing a neutron source.

The shim bank worth increased to approximately 14% $\Delta K/K$. Figure 3.3-5 shows the core configuration for the second criticality.

Two additional active elements were loaded and one solid dummy was unloaded. The core loading at the beginning of power distribution measuring consisted of twenty-four active elements, two solid dummies, and one incore sample assembly. The neutron source was moved from an in-core position to a position in the graphite reflector. Chapter
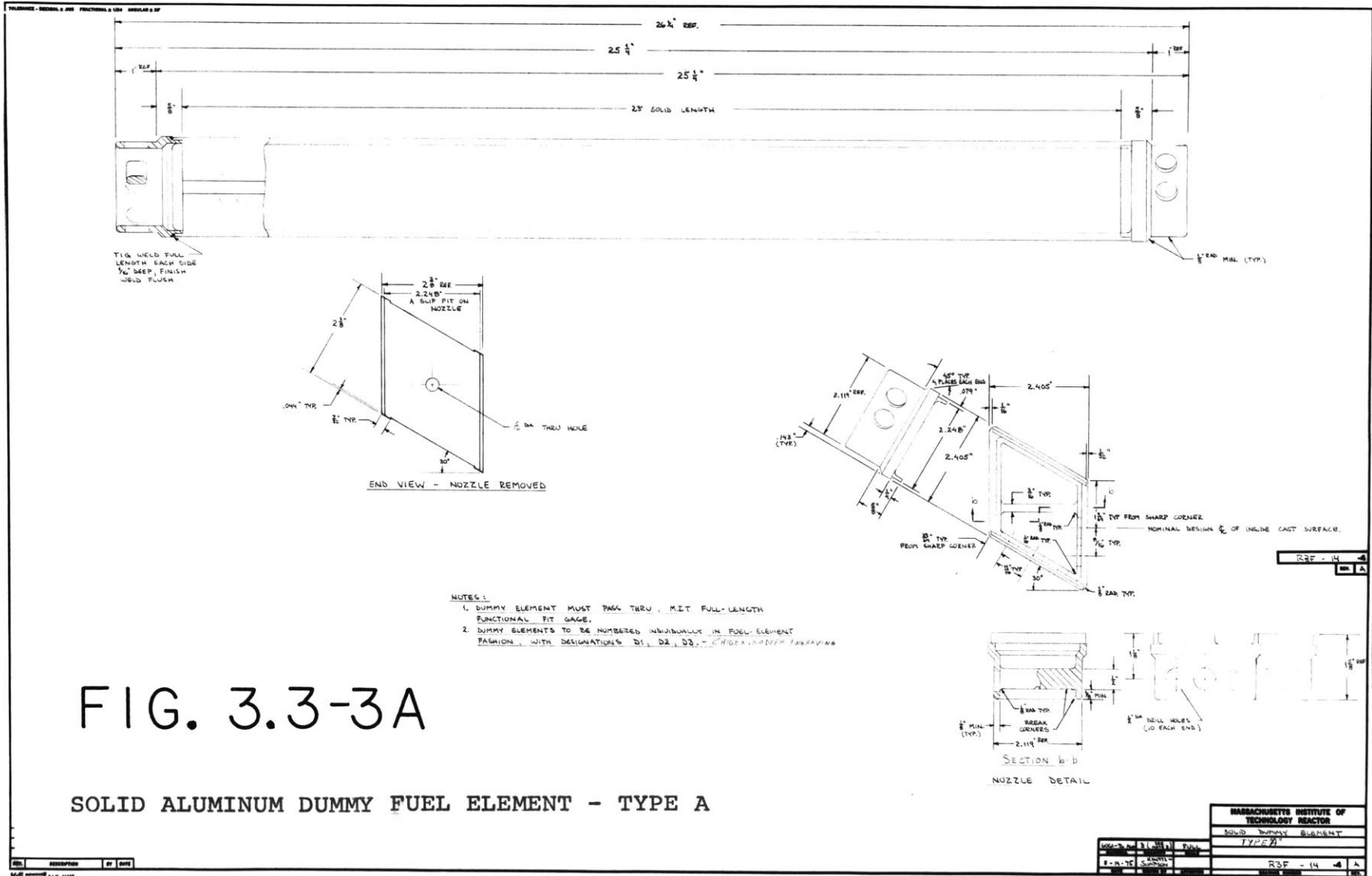
FIG. 3.3-3A

SOLID ALUMINUM DUMMY FUEL ELEMENT — TYPE A

NOTES :
1. DUMMY ELEMENT MUST PASS THRU. M.I.T FULL-LENGTH FUNCTIONAL FIT GAGE.
2. DUMMY ELEMENTS TO BE NUMBERED INDIVIDUALLY IN FUEL ELEMENT FASHION, WITH DESIGNATIONS D1, D2, D3, - 1" HIGH, 1/16" DEEP ENGRAVING

END VIEW - NOZZLE REMOVED

SECTION b-b

NOZZLE DETAIL

TIG WELD FULL LENGTH EACH SIDE 3/16" DEEP, FINISH WELD FLUSH

NOTES:
1. DUMMY ELEMENT MUST PASS THRU, M.I.T. FULL-LENGTH FUNCTIONAL FIT GAGE.
2. DUMMY ELEMENTS TO BE NUMBERED INDIVIDUALLY IN FUEL-ELEMENT FASHION, WITH INSIGNATIONS D1, D2, D3,-2"HIGH×.010 DEEP ENGRAVING
3. THERE IS A LEFT HAND AND RIGHT HAND END ON EACH DUMMY

FIG. 3.3-3B

SOLID ALUMINUM DUMMY FUEL ELEMENT - TYPE B

END VIEW - NOZZLE REMOVED

SECTION b-b
NOZZLE DETAIL

FIG. 3.3-4

INVERSE MULTIPLICATION PLOT FOR SECOND CRITICAL LOADING OF CORE I

blades inserted

blades withdrawn

number of fuel elements loaded in core
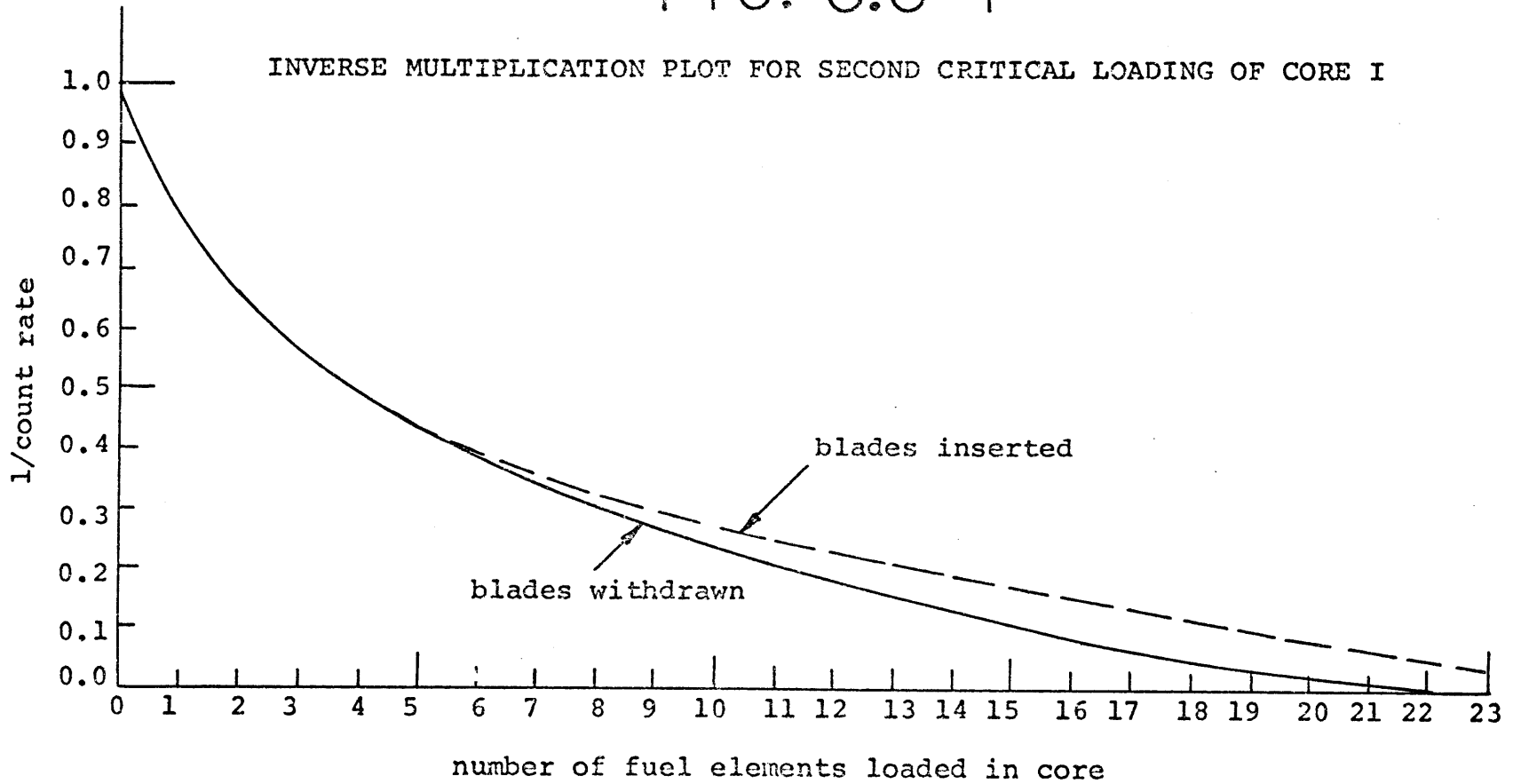
FIG. 3.3-5

CORE CONFIGURATION FOR SECOND CRITICALITY OF CORE I
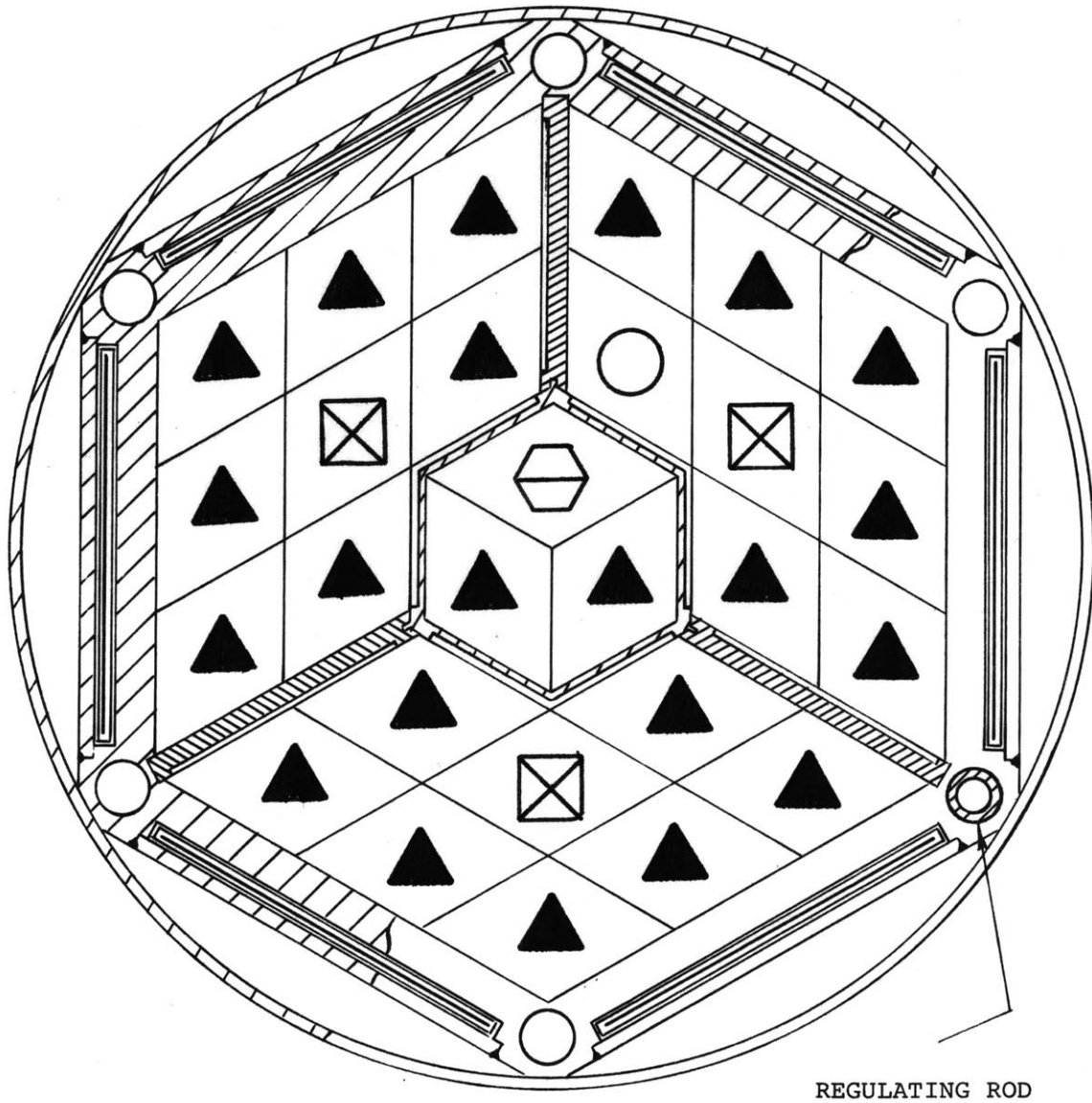
REGULATING ROD

▲ – 445 gram U^{235} fuel element

◯ – water filled dummy element

⬡ – incore sample assembly

⊠ – solid dummy element, type A

5 contains the power distribution measurements for Core I.

3.4 Fuel Loading for Core II

On February 9, 1976, during an attempt to remove a fuel element from the reactor core it was discovered that numerous fuel elements were not movable. Approximately two-thirds of the reactor fuel elements were stuck in the core because the cadmium fixed absorber sandwiches were swollen beyond acceptable tolerances for the compact core arrangement. The absorber sandwich expansion was not unexpected because of a control blade sandwich swelling which occurred several weeks earlier. The mechanism that has been hypothesized to have caused the swelling was based on leakage of the cadmium sandwiches. The fixed absorber sandwiches were composed of a cadmium sheet (0.040 inches) sandwiched between two aluminum plates that are seal welded around the outside edge in order to seal the cadmium inside. Figure 3.4-1 shows an idealized version of the cadmium swelling mechanism. Water leaked into the sandwich through small cracks in the seal weld. The water corroded the cadmium which yielded a supply of corrosion products inside the sandwich. Hydrogen from the corrosion process, and/or radiolytically decomposed water built up a slight gas pressure inside the sandwich. As the gas attempted to escape from the sandwich via the weld leaks, corrosion products were carried into the cracks and plugged the original water leaks. As the gas pressures

FIG. 3.4-1

SUSPECTED CADMIUM SANDWICH
SWELLING MECHANISM

seal
weld

1/16 inch
aluminum
plate

0.040 inch-thick
cadmium sheet

water leaks in pin
hole crack which
develops

Radiolytic decomposition
of water creates
gas in sandwich

sandwich
expands as
gas pressure
builds up

gas escapes through original
crack but corrosion products
eventually seal crack
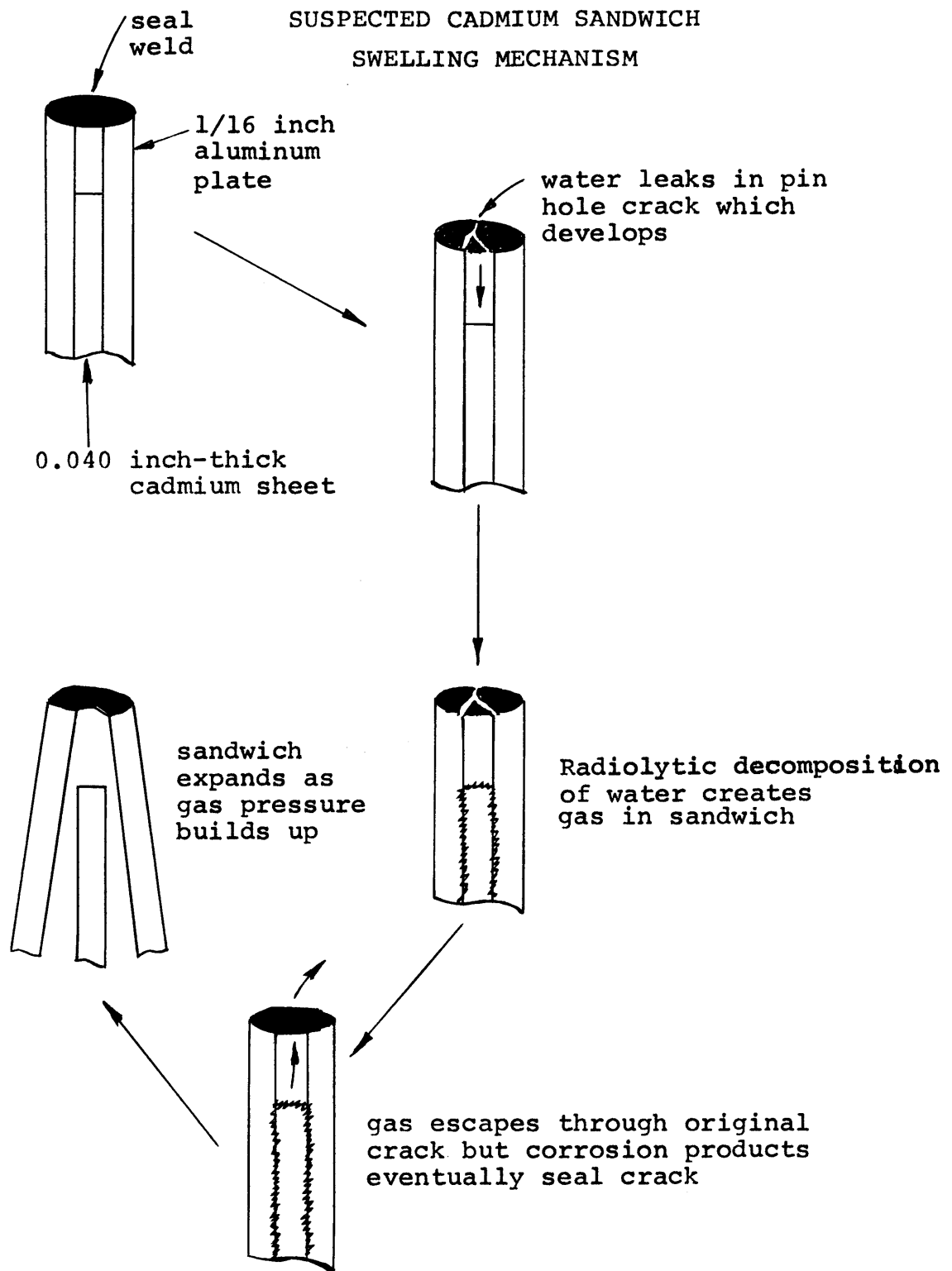
continued to build up, the cadmium sandwich swelled. The flat plate structure of the sandwiches meant that only low pressures (~1 to 3 psig) were necessary to cause unacceptable amounts of swelling in the fixed absorbers.

As a result of the fixed absorber swelling, it was necessary to remove the fixed absorbers in order to prevent damage to the fuel elements. The reactor fuel was successfully unloaded and then the swollen fixed absorbers were removed. In order to continue service to the experimenters during the time it took to develop an alternative fixed absorber, calculations were performed to evaluate operating the reactor without any fixed absorber.

3.4.1 Core Loading Arrangement

In order to counter balance the positive reactivity effect of removal of the fixed cadmium absorbers, Core II was designed to contain fewer fuel elements and more solid dummies. The initial core arrangement was expected to contain 6 solid dummy elements and 21 fully loaded elements. CITATION calculations were made to determine the desired core reactivity level and perform preliminary power peaking analysis. Figure 3.4-2 shows the core loading arrangement that was initially predicted to be the eventual Core II loading. The MITR Safeguard Committee reviewed the planned operation without fixed absorbers and permitted initial fuel loading.

FIG. 3.4-2

PROSPOSED SIX DUMMY CORE WITHOUT FIXED ABSORBERS

REGULATING ROD
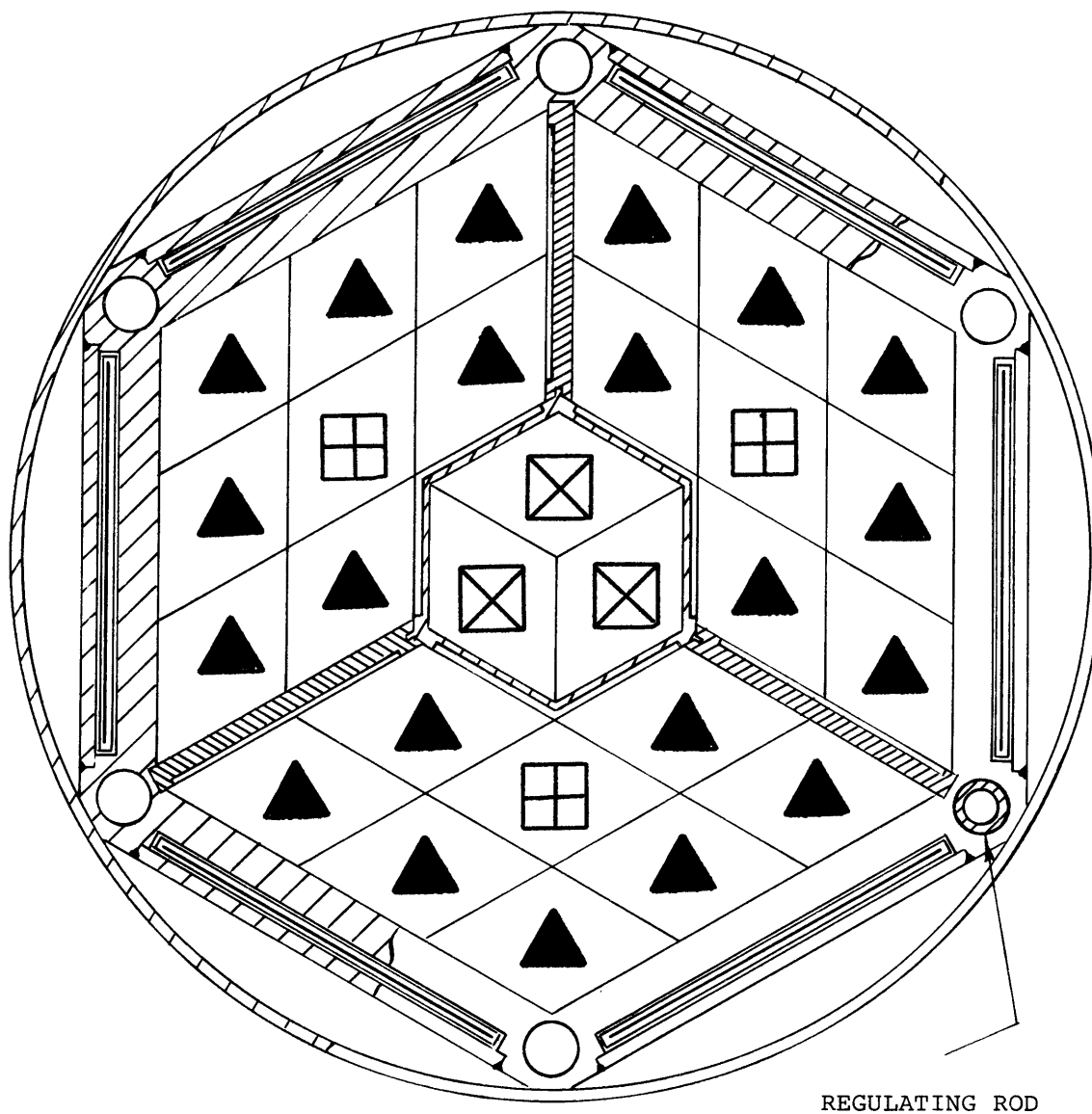
▲ – 445 gram U^{235} fuel element

⊠ – solid dummy element – type A

⊞ – solid dummy element – type B

3.4.2 Criticality

On March 9, 1976, the reactor went critical with 20 fuel elements loaded. Figure 3.4-3 shows the initial critical loading with no fixed absorbers in the core. Figure 3.4-4 shows the 1/M plot for the approach to critical for Core II.

The reactivity worth of removal of solid dummies from B-ring positions B-2, B-5, and B-8 was estimated to be close to 1.8% $\Delta K/K$. In order to decrease the worth of solid dummies in the B-ring and in order to minimize the power peaking effect of the water gap caused by removal of the fixed absorbers, the B-ring solid dummies were loaded into positions B-3, B-6, and B-9. By placing solid dummies in these B-ring positions and because of the "notch-up" plate arrangement, no single plate would be directly against the water gap caused by removal of the fixed absorbers. Figure 3.4-5 shows the plate and dummy arrangement for one section.

In order to lower the shim bank height to prevent unacceptable peaking effects in the upper portion of the core, a fuel element was loaded in position A-1 replacing a solid aluminum dummy. The final Core II loading arrangement is shown in Fig. 6.1-1. Chapter 6 contains the power distribution measurements for Core II.

FIG. 3.4-3

CORE CONFIGURATION FOR INITIAL CRITICALITY OF CORE II
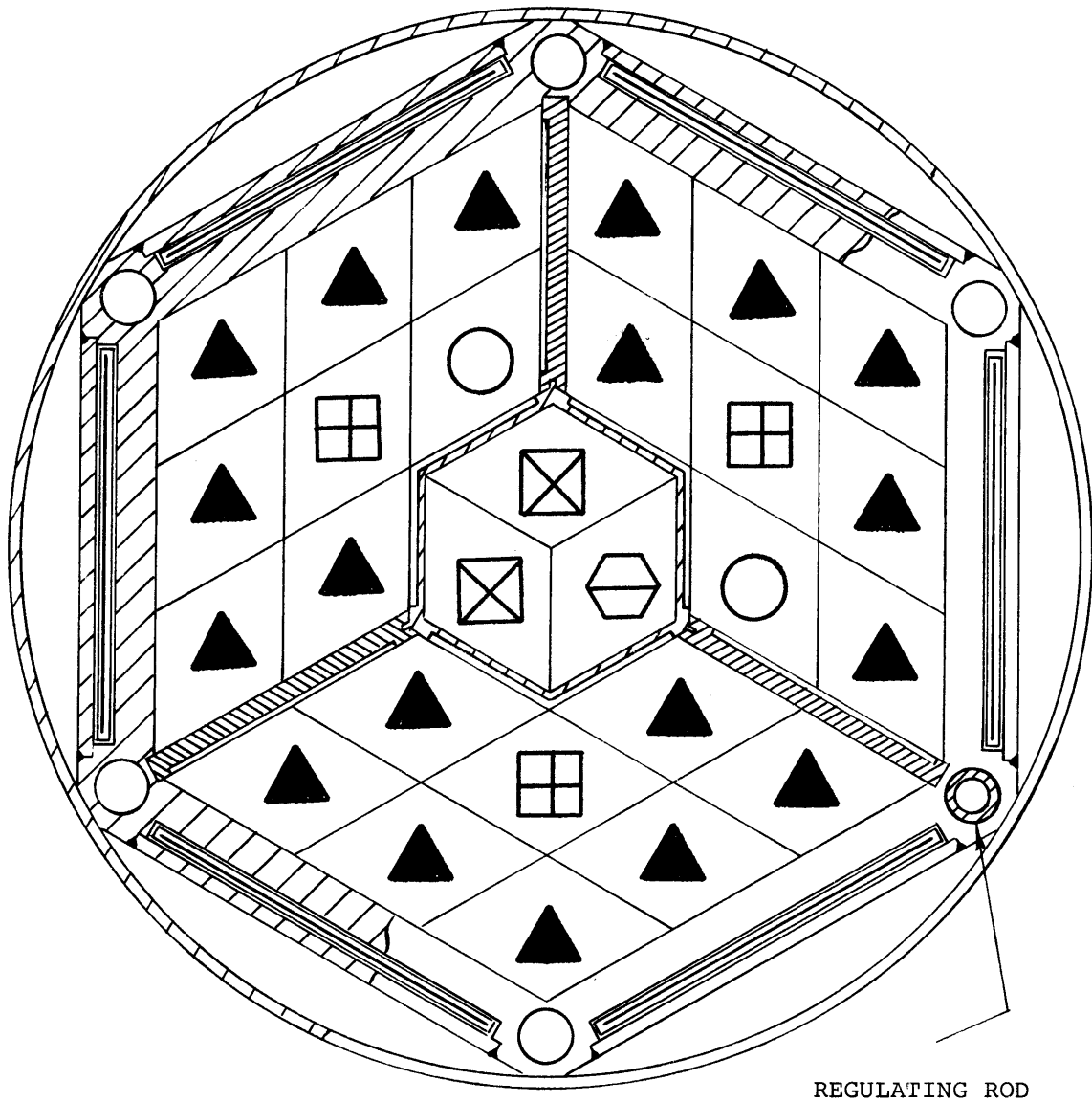
REGULATING ROD

▲ – 445 gram U^{235} fuel element

◯ – water filled dummy element

⬡ – incore sample assembly

⊠ – solid dummy element – type A

⊞ – solid dummy element – type B

FIG. 3.4-4

INVERSE MULTIPLICATION PLOT
FOR CRTICAL LOADING OF CORE II
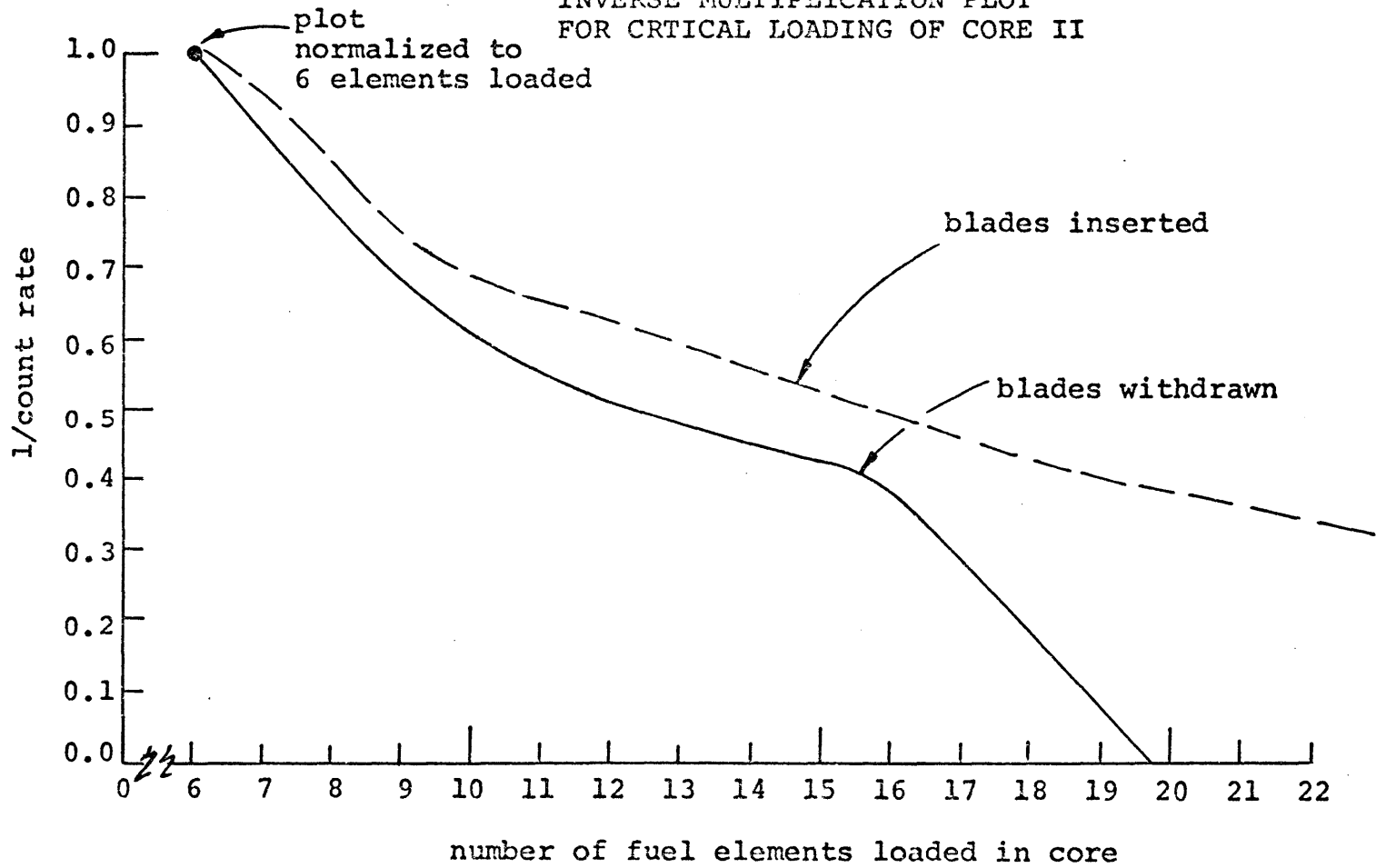
FIG. 3.4-5

NOTCH-UP FUEL PLATE ORIENTATION IN OUTER GROUP OF CORE II

REGULATING ROD

water gap caused by
removal of radial
fixed absorber

water gap caused by
removal of hexagonal
fixed absorber

solid dummy element
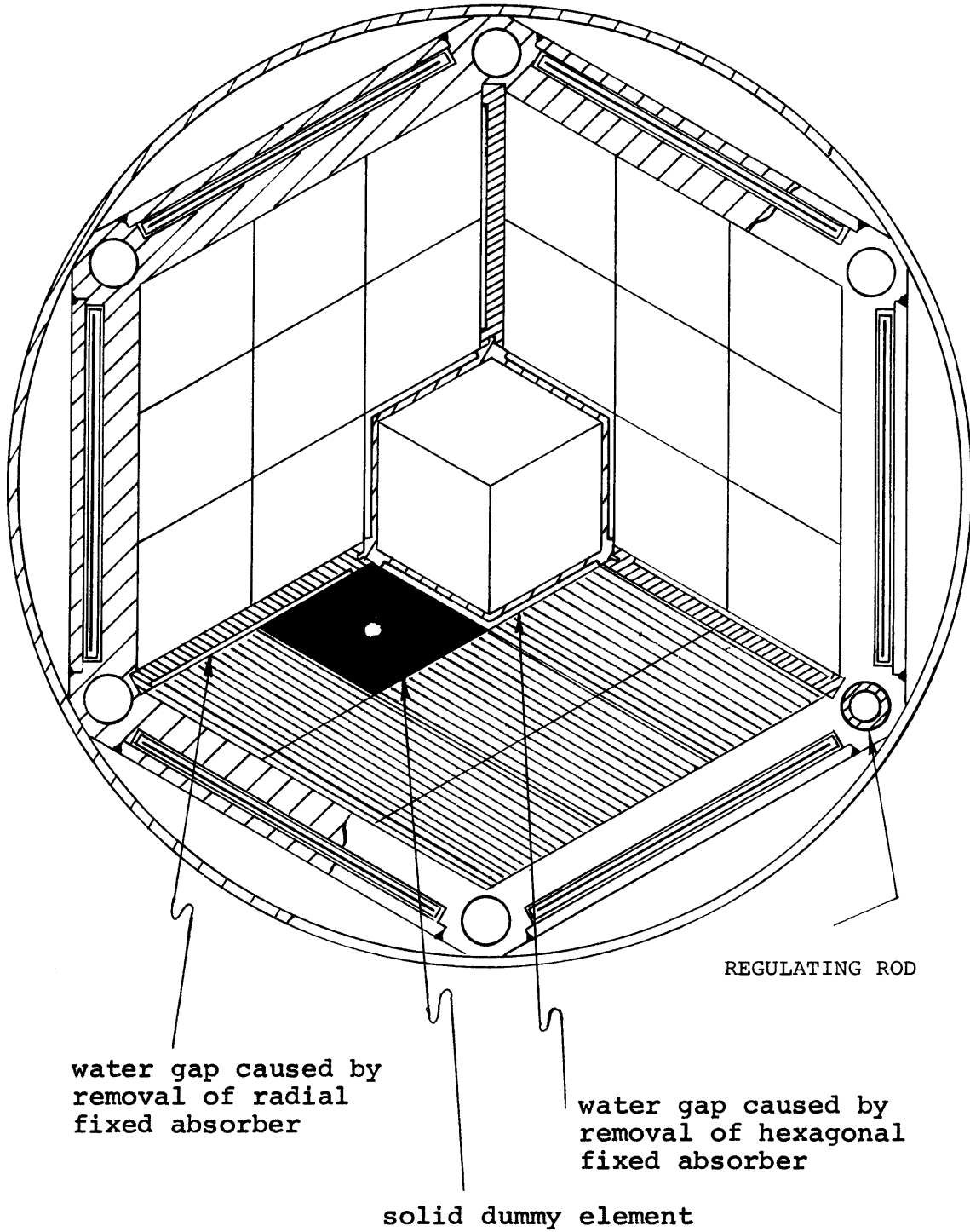
CHAPTER 4

PRIMARY COOLANT FLOW DISTRIBUTIONS

Coolant flow distributions in the MITR-II are discussed in this chapter. Section 4.1 describes the flow tests that were performed to evaluate the design of the MITR-II core tank. Section 4.2 describes flow tests on MITR-II fuel elements. The fuel position relative flow measurements for Core I are described in Section 4.3 and the bypass flow measurements for Core I are described in Section 4.4. Flow distribution results for Core I are summarized in Section 4.5. Section 4.6 describes the flow distribution measurements and results for Core II.

4.1 Design Flow Tests

Flow tests were performed as an aid in determining and evaluating the flow characteristics of the initial and final designs of the MITR-II. The flow tests used to determine the core tank bottom shape are described in this section.

4.1.1 History

In the fall of 1969 an experimental test stand was operated at the M.I.T. Reactor site to study hydraulic and vibration characteristics of the core and tank assembly

of the proposed reactor modification. The test stand
design was based on the initial core design and was a
full scale model capable of operating under full coolant
flow conditions. Initially, the program was intended to
determine flow resistances and distributions throughout
the inlet plenum and fuel matrix. In later tests, a
fully operating control blade assembly was added to
measure vibrations and drop times under full coolant
flow perturbations.

The test stand was operated from the reactor second-
ary coolant pumps, so that runs had to be scheduled during
reactor shut-down periods. Because of this limitation, a
quarter size model was simultaneously tested in the labor-
atory and these results were then used to prepare and to
supplement full scale tests. A sketch of the full size
test stand is shown in Fig. 4.1-1.

During February, 1970, a full scale assembly of the
initially proposed finned plate fuel element was tested
under simulated operating conditions. The total pressure
drop across the assembly and the individual fuel channel
pressure drops were measured at various flow rates up to
120% of 5 MW operating flow. The results of these tests
are summarized in Section 4.2.1 and a sketch of the test
system is shown in Fig. 4.1-2.

In the summer of 1970, it was discovered that for
criticality reasons the proposed core diameter had to be

FIG. 4.1-1

CORE DESIGN FLOW TEST LOOP

manometer bank

pressure gage

pressure gage

pump - HM-2A

pump - HM-2

test section

cooling tower basin

flowmeter

pump - HM-1A

pump - HM-1
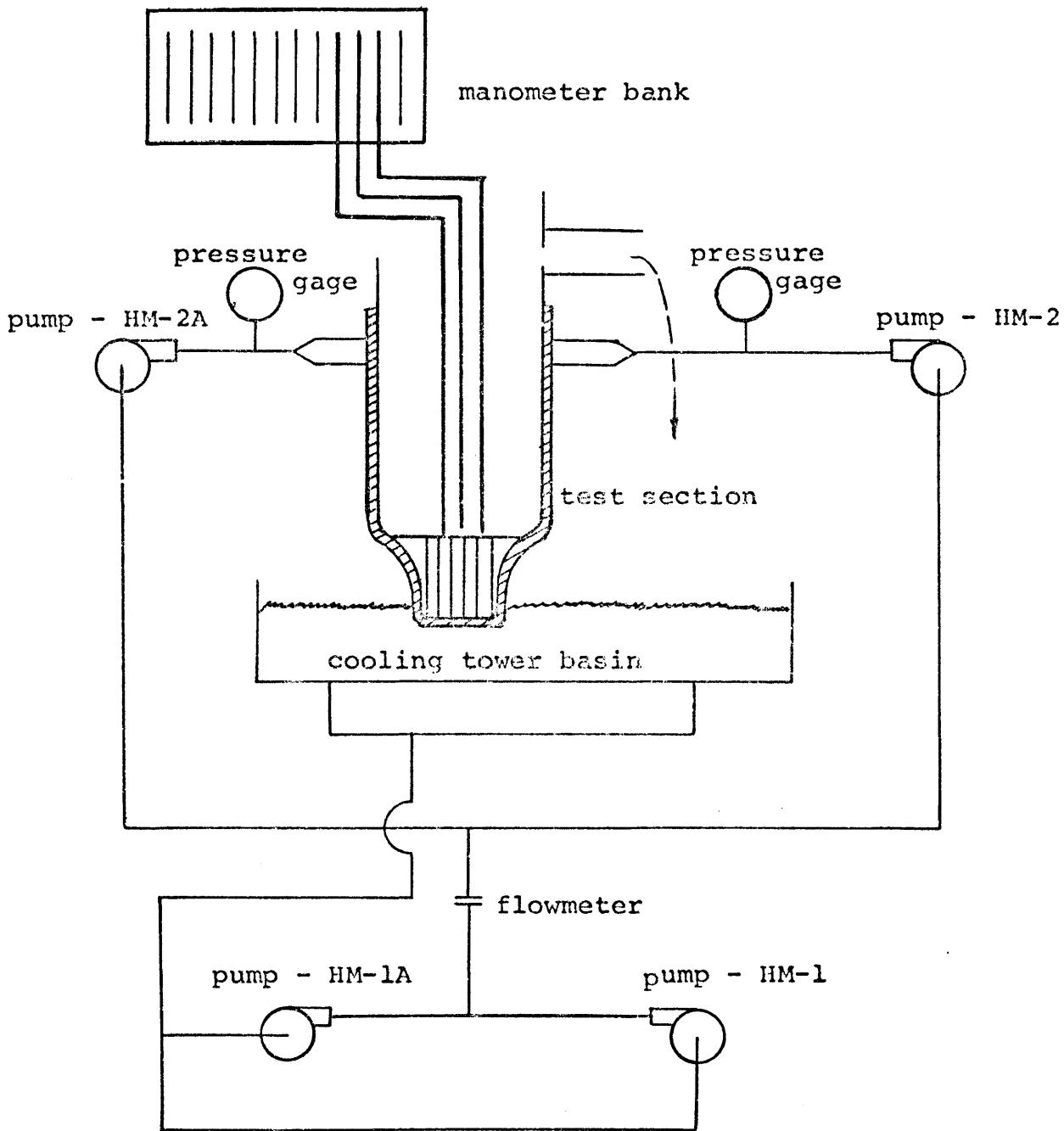
FIG. 4.1-2

FUEL ELEMENT DESIGN FLOW TEST LOOP

flow timing tank

manometer bank

flow orifice

flow manometer

test section

flow control valve

pump
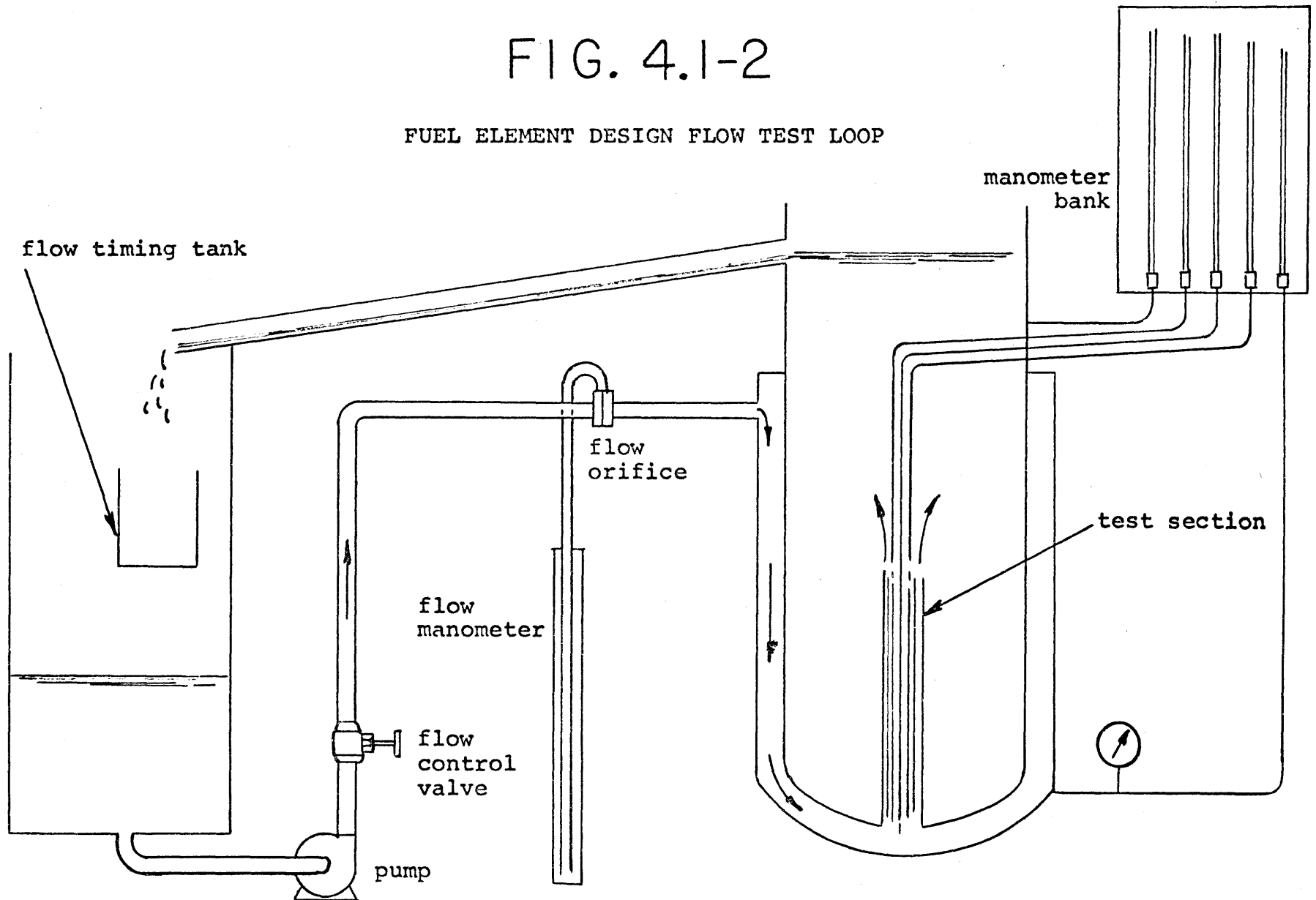
increased. At the same time design studies were made to reduce the inlet plenum volume to a minimum. These design changes negated all data collected prior to that point. It was decided to modify the existing test stand to reflect the design changes at a reduced scale rather than completely rebuild the facility to the new full size. The resulting model was about 80% of the expected final size. The size difference was considered trivial when scaling factors were used. This assumption was confirmed by good correlation between the quarter size test stand results and the larger unit results. The final design of the inlet plenum was based on this second series of tests.

4.1.2 Test Program and Limitations

The mock-up test program led to the gradual development of the lower core tank shape, arrangement of the flow deflectors, and lower plenum gap (distance between core tank and bottom of lower grid), which resulted in the optimal fuel element flow distribution. Initial testing was performed on the quarter size model, in order to minimize the number of variations on the 80% full size test stand.

The larger hydraulic test loop consisted of two reactor secondary system pumps in series with two secondary system booster pumps, the test stand, and the cooling tower basin. The system is shown in Fig. 4.1-1. The hydraulic measurements were made by calibrated bourdon gages at the test stand inlet and matched impact pitot

tubes in selected fuel element positions. Total flow was measured by a calibrated orifice in the main secondary coolant pipe. Fuel elements were simulated by using orificed tubes in the test stand.

The major differences between the test stand mock-up and the actual core are:

A) Test stand was 80% of full size which results in dependence on accurate scaling factors,

B) Fuel elements are simulated by orificed tubes,

C) The static head of water over the core was four feet instead of the actual eleven feet,

D) The inlet flow to the shroud in test stand was at two locations 180 degrees apart rather than at one location.

4.1.3 Test Summary

The flow distribution for the test which most closely resembles the actual core is shown in Fig. 4.1-3. The flow deflectors and plenum shape are the same for the test case and actual case. The plenum gap for the test case was 9/64 of an inch and for the actual core the plenum gap is 10/64 of an inch.

The minimum flow to an element position is 7% less than the average element position flow. Consequently, in the MITR-II Safety Analysis Report, the factors for increases in the enthalpy and film temperature differences were taken to be 1.08 and 1.06, respectively.

FIG. 4.1-3

PLENUM FLOW DISPARITY IN DESIGN FLOW TEST LOOP
(9/64" plenum gap)

REGULATING ROD
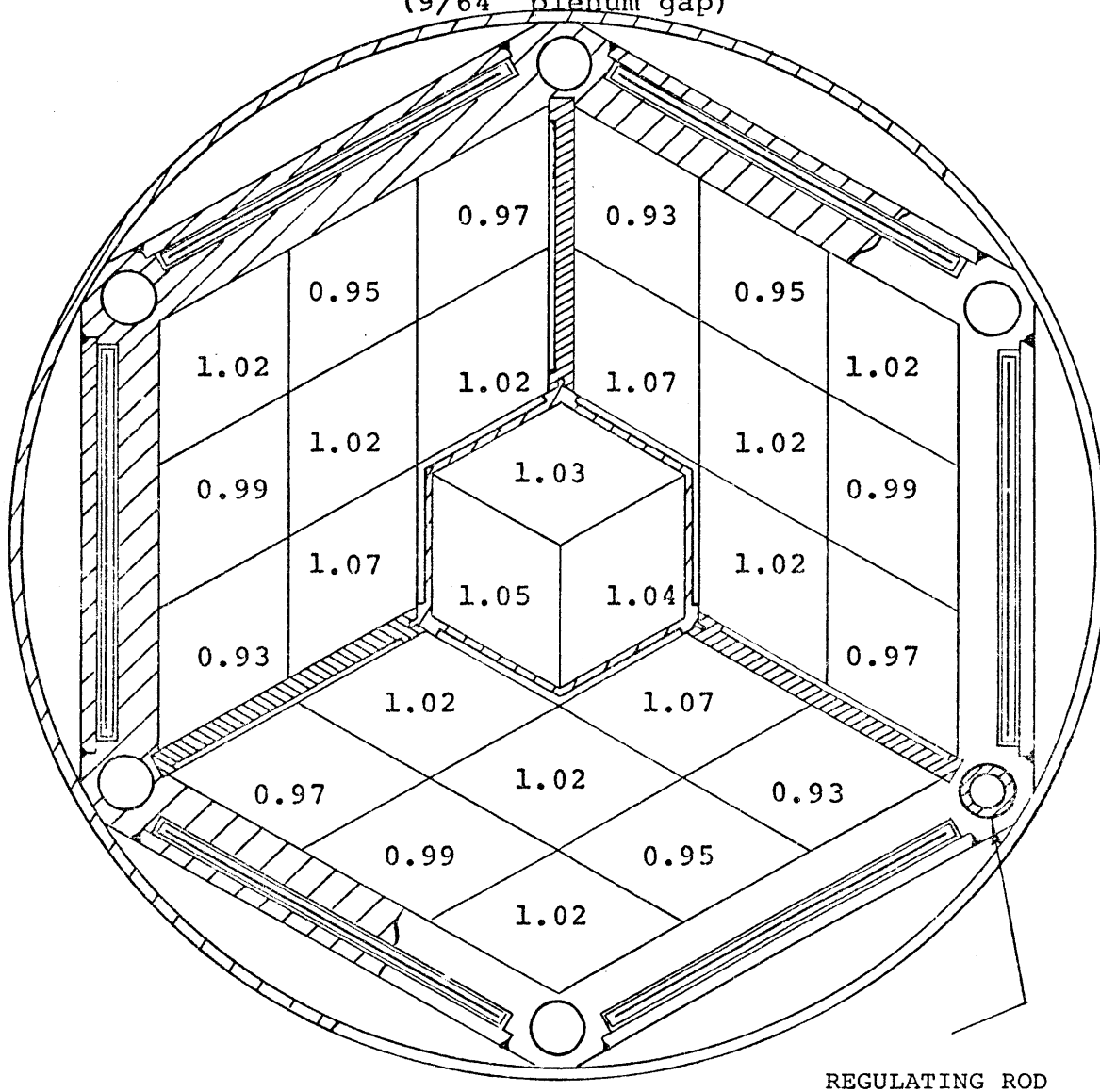
$$\text{plenum flow disparity} = d_{f_p} = \frac{\text{fuel position flowrate}}{\text{average fuel position flowrate}}$$

4.2 Fuel Element Flow Tests

Fuel element flow tests were performed to evaluate the mechanical stability and coolant channel flow disparity of MITR-II fuel elements.

4.2.1 Summary of Design Fuel Element Flow Tests

In 1970, a full scale assembly of the initial design of the finned plate fuel element was tested under simulated operating conditions. The test loop setup is shown in Fig. 4.1-2. The final design of the fuel element was different from the design tested so the specific results of the test are not applicable. The following general results were found:

A)   The pressure drop across the new fuel element design can be calculated accurately using the standard Darcy formula,

B)   The individual channel flows for all interior channels were within 3.5 percent of each other,

C)   The simulated outer channel between two fuel elements had a much higher flow rate than interior channels,

D)   The simulated outer channel between a fuel element and core housing wall had a 30% lower flow than an average interior channel, but this channel is required to remove heat from one side of a fuel plate where all the other channels cool two sides.

4.2.2 Dummy Element Flow Test

In 1974, a non-fueled element, constructed in an identical manner and by the same vendor as all of the fuel elements for the first core of the MITR-II, was flow tested.

The primary concern of this test was to check the dimensional stability of the fuel element under varying flow conditions. In addition, the test was used to determine variations in flow velocities between channels of the element and to measure the pressure drop across the element.

The fuel element test loop is shown in Fig. 4.2-1. The element tested was "Non-Fueled 001" which was constructed by Gulf United Nuclear Fuels (GUNF) in New Haven, Connecticut. Bourdon tube pressure gages were used to measure the pressure drop across the fuel element. Three pitot tubes were used to scan the discharge of the element across the left, center, and right of the end discharge as shown in Fig. 4.2-2. Impact pressures on the pitot tubes were measured using a water manometer. Flows rate variations were obtained by throttling the discharge of a 100 gpm capacity centrifugal pump. Flow was measured by a rotameter on the pump discharge. A bypass of the test section was throttled to provide back pressure equivalent to the static head at the discharge of the actual core.

The test section was constructed to provide the same space for the fuel element as would be provided by surrounding fuel elements in the core housing. The flow direction in the inlet plenum is the same as the actual case. The lower grid and top grid plate openings were also identical to the final housing. Upon discharging from the upper grid opening, the water in the test loop

FIG. 4.2-1

FLOW TEST APPARATUS FOR DUMMY FUEL ELEMENT

2200 gallon
water storage
tank

flowmeter

flowmeter

bypass

manometer

fuel element
test section

pump
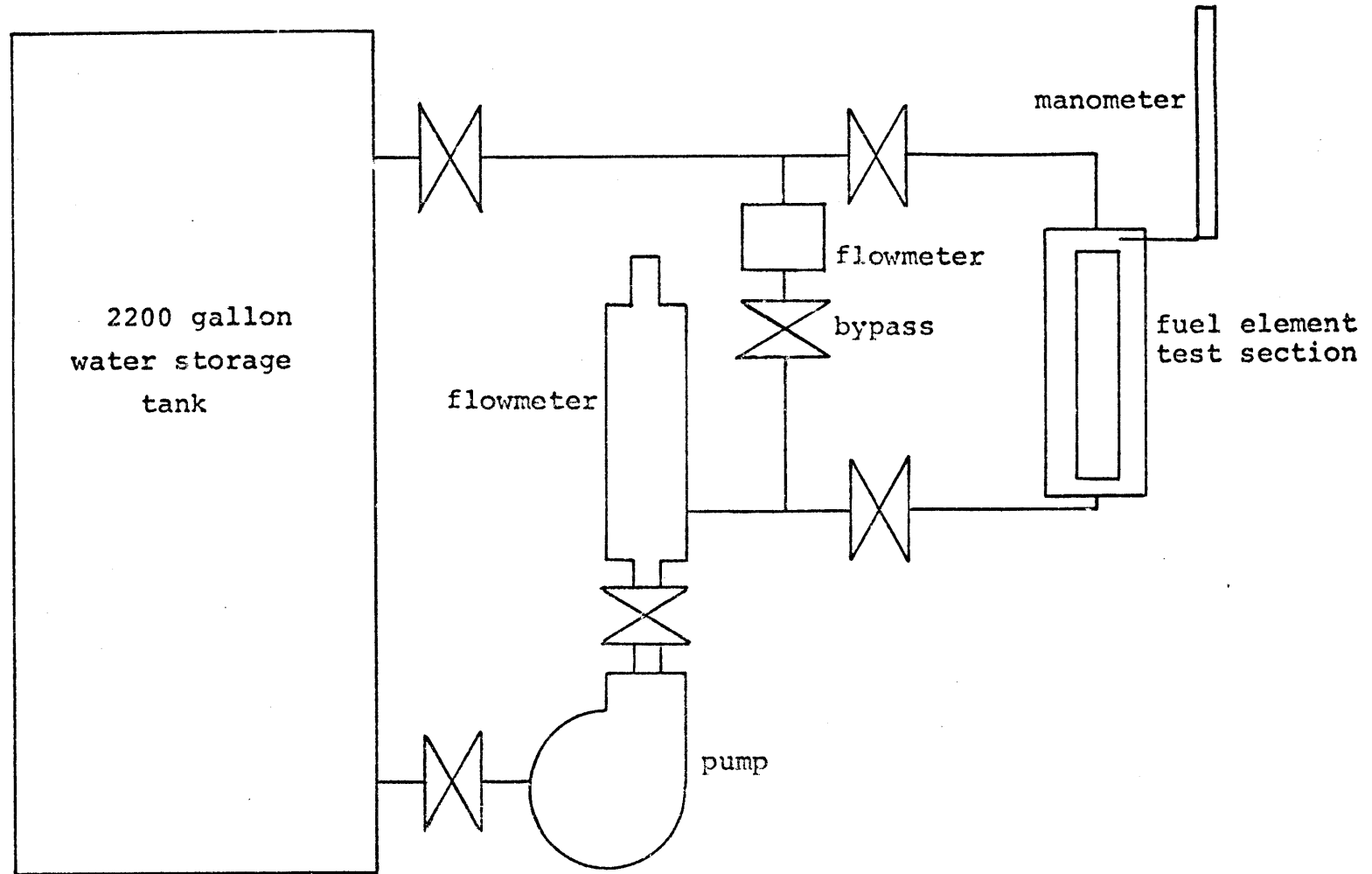
FIG. 4.2-2

POSITION OF SCANNING PITOT TUBES
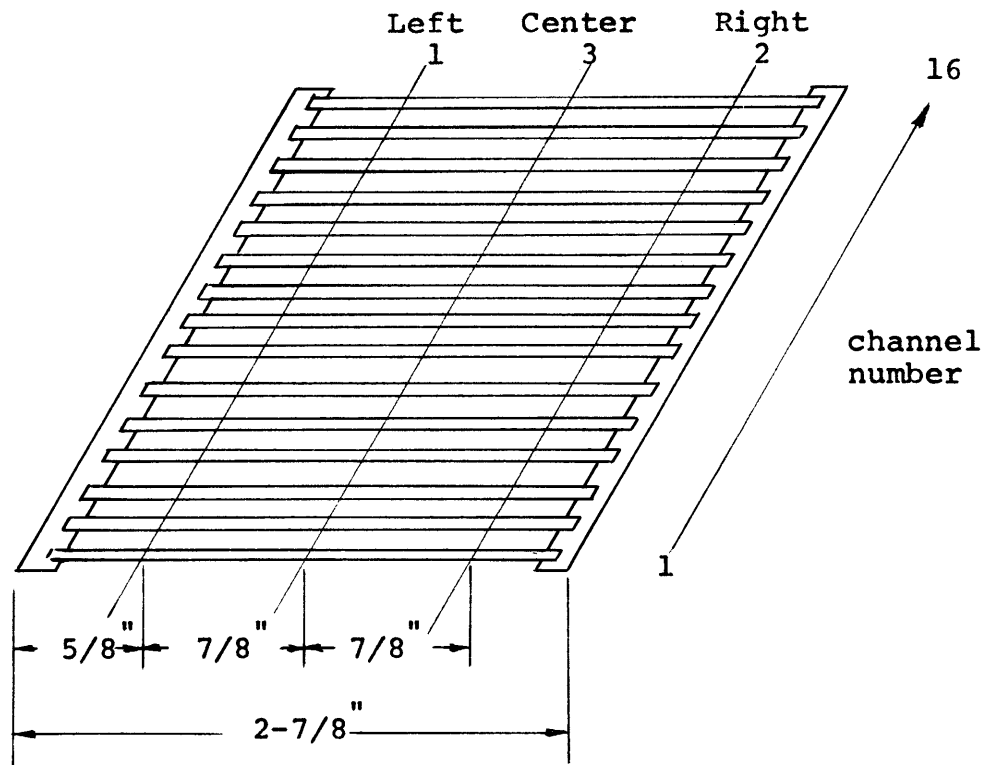
Note: Channels 1 and 16 are outside half channels.

also underwent a sudden expansion.

Two limitations on the accuracy of the test mock-up
are the absence of element to element flow via gaps in the
fuel element end nozzles and inaccuracy in modeling the lower
inlet plenum.

4.2.3 Mechanical Stability of Fuel Element

The mechanical stability of a dummy fuel element was
tested in the fuel element test loop. The element,
"Non-Fueled 001", was dimensionally checked at GUNF and
channel width measurements were made for each fuel element
coolant channel prior to flow testing. During this initial
measuring, GUNF found some local channel positions that
were close to exceeding the channel width tolerance. GUNF
reworked those channels by bending to bring them well with-
in the channel tolerance. The dimensions of the element
were checked at M.I.T. using a functional fit gauge.

The element was inserted into the test section and
subjected to the following flows:

A) Three hours at 120% operating flow (91 gpm),

B) Twelve cycles from 30 gpm to 90 gpm ,

C) Three hours at 100% operating flow (76 gpm).

After the test, the element still fit in the functional
fit gauge and was returned to GUNF to have the coolant
channel measurements repeated. Exterior measurements of the
element appeared to be unchanged after the flow test. Most
of the coolant channels underwent a uniform expansion of

0.0005 to 0.002 inches; i.e., the plates expanded outward
from the center of the element. Coolant channels which had
been reworked because they were too large (and thus were
bent smaller) appeared to have returned to the pre-worked
conditions very quickly. The same trend was not true for
reworked channels that had been too small. No channel was
significantly smaller after the test.

Thus, there appears to be a small uniform expansion
of coolant channels during flow at the expense of the
channels between elements. The tests indicate the element
is mechanically acceptable with the added information that
channels reworked because they are too large will probably
return to the pre-worked size after coolant flow is
initiated.

4.2.4 Channel Flow Measurements

Relative channel flow measurements were taken using
impact pitot tubes shown in Fig. 4.2-3. After flow was
established, the pitot tube would be bled to remove any
air bubbles. While scans were being made with one pitot
tube, the remaining two tubes would be withdrawn into the
side wall. The pitot tube measured the impact pressure
directly at the discharge of each individual channel by
traveling in the gap between the fuel element plates and
the end nozzle and moving at a 90° angle to the plates.
Static pressure was measured at the same elevation as the
pitot tubes. The pitot tube was moved to the postion that

FIG. 4.2-3

DETAIL OF SCANNING PITOT TUBE

to manometer

to manometer

static pressure tap

fuel plates in dummy element

coolant flow direction
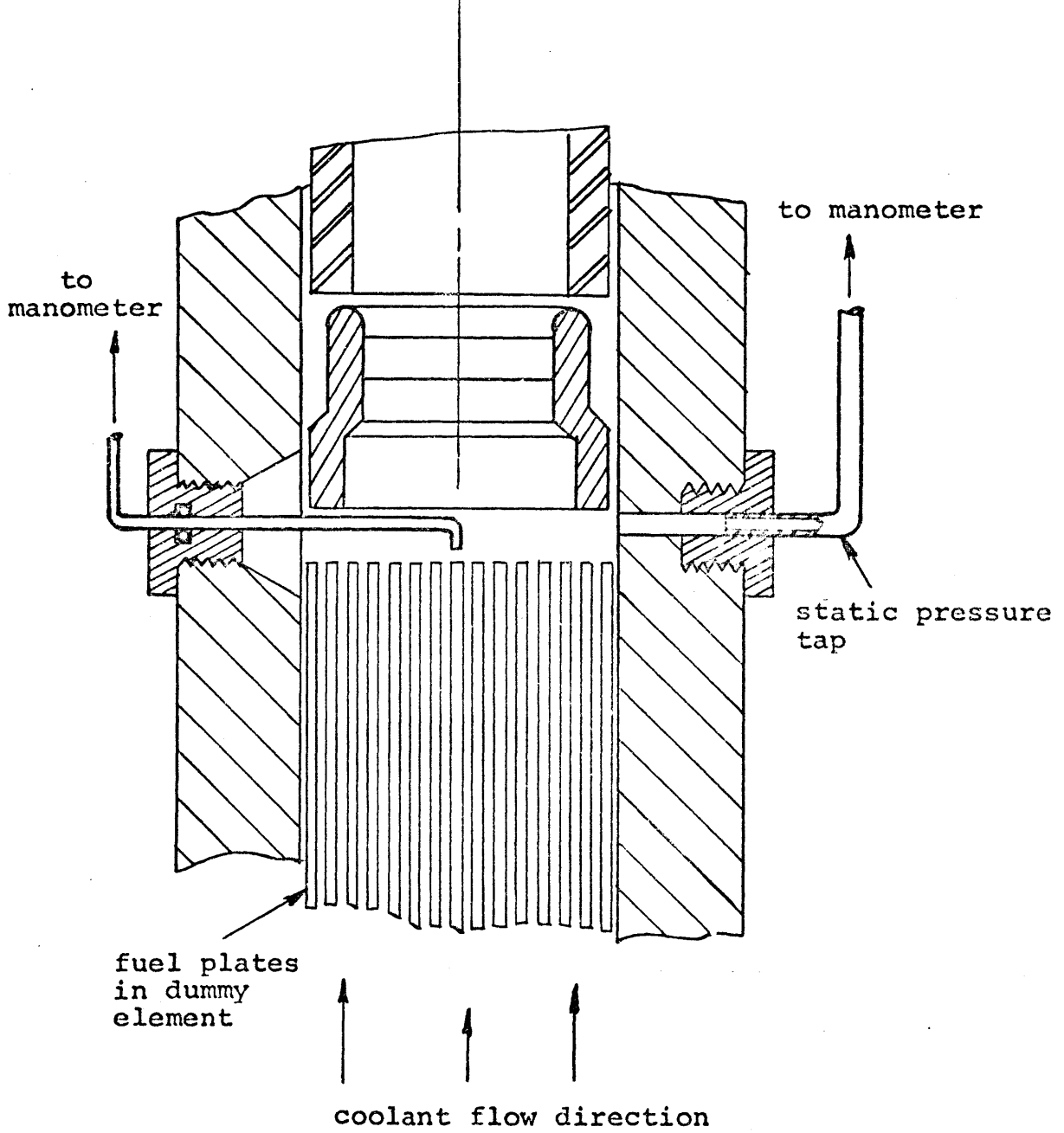
gave the peak impact pressure on the water manometer for each channel discharge. Each pitot tube would measure the impact pressure at one discharge location on each of the coolant channels. By using three pitot tubes, three locations for each channel were measured as shown in Fig. 4.2-2.

Several initial tests were required to become familiar with operating the test loop and to determine that an on-line filter was necessary to prevent collection of foreign material in the dummy element (the storage tank in the test loop had not been used for a number of years prior to this test). Complete tests were then made at flows of 74 gpm and 85 gpm and results are shown on Table 4.2-1. The values of Δh are the difference between the impact pressure and the static pressure. The subscripts on the values, i.e., Δh_1, Δh_2, and Δh_3, represent the values for the left, right, and central pitot tubes, respectively. For incompressible fluids, the following equation is valid:

$$\Delta h \propto V^2, \qquad\qquad (4.2-1)$$

where,

V is fluid velocity.

Thus, the values of $\sqrt{\Delta h}$ shown in Table 4.2-1 are proportional to the coolant channel discharge velocity.

Looking at Table 4.2-1, several conclusions can be made. First, the central pitot tube yields a flow velocity

TABLE 4.2-1

CHANNEL FLOW MEASUREMENTS DATA FOR LEFT, CENTRAL, AND
RIGHT MEASUREMENTS IN ELEMENT TEST LOOP

$A = \sqrt{\Delta h_1}$ for pitot tube on left side of element outlet.

$B = \sqrt{\Delta h_2}$ for pitot tube on right side of element outlet.

$C = \sqrt{\Delta h_3}$ for pitot tube in center of element outlet.

$D = \sum_{i=1}^{3} \dfrac{\sqrt{\Delta h_i}}{3}$, $\dfrac{C-D}{D} \times 100$ = % error between central
                                                                                    measurement and average.

Δh = inches of water on manometer.

Channels 1, 16 are outside half channels.

Channels 2 through 15 are interior channels.

TABLE 4.2-1 (Continued)

Element Total Flow = 74.0 GPM

Channel #	A	B	C	D	$\frac{C-D}{D} \times 100$
1	4.53	4.37	4.47	4.46	+0.22
16	5.0	4.18	4.47	4.55	-1.8
2	4.85	4.86	4.69	4.80	-2.3
3	5.05	5.08	5.20	5.11	+1.8
4	4.9	5.11	5.0	5.0	0.0
5	5.05	4.80	5.15	5.0	+3.0
6	4.80	5.01	5.10	4.97	+2.6
7	4.90	4.86	4.95	4.90	+1.0
8	4.85	5.11	4.80	4.92	-2.4
9	4.80	4.79	4.90	4.83	+1.4
10	4.24	4.29	4.24	4.26	-0.47
11	4.36	4.57	4.47	4.47	0.0
12	4.24	4.35	4.36	4.32	+0.93
13	4.47	4.32	4.58	4.36	+5.0
14	4.74	4.80	4.80	4.78	+0.42
15	5.0	4.18	4.47	4.55	-1.8

Average Error = 1.6%

TABLE 4.2-1 (Continued)

Element Total Flow = 85.0 GPM

Channel #	A	B	C	D	$\frac{C-D}{D} \times 100$
1	5.15	5.0	5.15	5.10	+0.98
16	5.52	4.88	5.24	5.22	+0.38
2	5.66	5.68	5.57	5.64	+1.2
3	5.92	5.83	5.87	5.87	0.0
4	5.74	6.0	5.87	5.87	0.0
5	5.79	5.78	6.0	5.86	+2.4
6	5.61	5.96	5.96	5.84	+2.1
7	5.74	5.81	5.66	5.74	-1.4
8	5.66	5.80	5.61	5.69	-1.4
9	5.57	5.78	5.79	5.71	+1.4
10	4.95	5.07	4.9	4.97	-1.4
11	5.1	5.18	5.15	5.14	+0.19
12	5.0	5.01	5.15	5.08	+1.4
13	5.15	5.19	5.43	5.26	+3.2
14	5.43	5.75	5.66	5.61	+0.89
15	6.2	6.2	6.24	6.22	+0.32

Average Error = 1.2%

which is within a few percent of average of the three pitot
tubes and thus gives a good representation of the coolant
channel flow velocity. Second, the exterior channels,
channels 1 and 16 have a flow velocity which is about
10% less than the interior channels. Channels 1 and 16
simulate channels that would exist between a fuel element
and core housing wall. The significance of this lower flow
velocity is discussed in Section 4.2.5. Third, there
appears to be a large difference between the flows of the
individual interior channels.

Because of this large disparity between the interior
channel flows, an attempt was made to minimize (or average
out) effects caused by the test loop setup and flow
measuring apparatus. This was achieved by removing the
element and flipping it 180° and repeating the flow scan
with the central pitot tube. The data for the 0° and 180°
cases at 74 and 85 gpm are shown in Table 4.2-2. Note
that channel 4, for instance, is the same physical channel
in both 0° and 180° tests but that its position in the
test loop would be different. Table 4.2-2 shows that the
average of the 0° and 180° cases yields a much more uniform
interior channel flow velocity. The minimum channel flow
velocity is about 7% less than the average flow. Mean
values and standard deviations for the results are shown
on Table 4.2-2.

TABLE 4.2-2

CHANNEL FLOW MEASUREMENT DATA FOR 0° AND 180°
ELEMENT MEASUREMENTS IN ELEMENT TEST LOOP

$A = \sqrt{\Delta h_{c-0°}}$ for measurements across center of element outlet with notch end up.

$B = \sqrt{\Delta h_{c-180°}}$ for measurements across center of element outlet with notch end down.

$C = \dfrac{\sqrt{\Delta h_{c-0°}} + \sqrt{\Delta h_{c-180°}}}{2}$ = average of notch up and notch down measurements.

Δh = inches of water on manometer

Channels 1, 16 are outside half channels.

Channels 2 through 15 are interior channels.

TABLE 4.2-2 (Continued)

Element Total Flow = 74.0 GPM

Channel #	A	B	C
1	4.47	4.75	4.61
16	4.47	4.63	4.55
2	4.69	5.18	4.94
3	5.20	4.93	5.07
4	5.0	4.76	4.88
5	5.15	4.72	4.94
6	5.10	5.13	5.12
7	4.95	5.15	5.05
8	4.80	5.43	5.12
9	4.90	5.50	5.20
10	4.24	5.08	4.66
11	4.47	5.26	4.87
12	4.36	5.43	4.90
13	4.58	5.54	5.06
14	4.80	5.35	5.08
15	5.05	5.57	5.31

	Mean	Standard Deviation
Outside Channel	4.58	0.042
Interior Channel	5.01	0.163

TABLE 4.2-2 (Continued)

Element Total Flow = 85.0 GPM

Channel #	A	B	C
1	5.15	5.39	5.27
16	5.24	5.24	5.24
2	5.57	5.91	5.74
3	5.87	5.74	5.81
4	5.87	5.31	5.59
5	6.0	5.41	5.71
6	5.96	5.51	5.74
7	5.66	5.47	5.57
8	5.61	5.88	5.75
9	5.79	6.31	6.05
10	4.90	5.91	5.41
11	5.15	6.08	5.62
12	5.15	6.25	5.70
13	5.43	6.32	5.88
14	5.66	6.15	5.91
15	6.24	6.40	6.32

	Mean	Standard Deviation
Outside Channel	5.255	0.021
Interior Channel	5.77	0.224

4.2.5 Channel Flow Disparity

In Section 3.3.4.3.3 of the MITR-II Safety Analysis Report, hot channel factors for channel dimensional tolerances were derived. Differences in the channel diameter give rise to small inequities in the flow distribution among the channels. These flow inequities led to variations in the channel enthalpy rise and in the film temperature difference. All uncertainties in the film temperature difference are included in the heat transfer coefficient and effectiveness uncertainty factor (1.20) which is included in F_o in the MITR-II Technical Specifications equation for evaluating the limiting conditions for operation.

The uncertainty factor for the channel enthalpy rise is included separately, both in the Safety Limit and limiting conditions for operation, and is dependent on the channel to channel flow disparity. Using channel dimensional tolerances, the channel flow disparity can be calculated (Ref. 4.2-2). The channel flow disparity is defined as follows:

$$\frac{W_{min}}{W_{nom}} = \frac{(AV)_{min}}{(AV)_{nom}} = \text{Channel Flow Disparity, (4.2-2)}$$

where,

W = channel mass flow rate,

A = channel area,

V = flow velocity.

By assuming that entrance and exit losses are proportional to friction losses within the channel, the channel pressure drop can be calculated using the standard Darcy equation:

$$\Delta P = \rho \frac{fLV^2}{D_e 2g} \qquad (4.2\text{-}3)$$

For narrow rectangular channels D_e can be approximated as 2d where d is the channel width, thus by equating pressure between channels:

$$(\frac{fV^2}{d})_{\substack{\text{nominal} \\ \text{channel}}} = (\frac{fV^2}{d})_{\substack{\text{minimum} \\ \text{channel}}} , \qquad (4.2\text{-}4)$$

where,

f is the channel friction factor.

For typical turbulent flows, the following relationship for the friction factor holds:

$$f \propto (D_e V)^{-0.2} \propto (dV)^{-0.2} . \qquad (4.2\text{-}5)$$

Combining Eqs. 4.2-4 and 4.2-5, the velocity ratio between the minimum and nominal channels becomes:

$$\frac{V_{min}}{V_{nom}} = (\frac{d_{min}}{d_{nom}})^{2/3} . \qquad (4.2\text{-}6)$$

Since $A \propto d$, the channel flow disparity becomes:

$$d_{f_c} = \frac{W_{min}}{W_{nom}} = (\frac{d_{min}}{d_{nom}})^{2/3} \frac{A_{min}}{A_{nom}} = (\frac{d_{min}}{d_{nom}})^{2/3} (\frac{d_{min}}{d_{nom}}) = (\frac{d_{min}}{d_{nom}})^{5/3} .$$

$$(4.2\text{-}7)$$

Based on the fuel fabrication specifications for the MITR-II, the ratio d_{min}/d_{nom} is equal to 0.955. Substituting this value into Eq. 4.2-7 yields the following value of the flow disparity based on fuel channel tolerances:

$$d_{f_c} = 0.926 \quad . \tag{4.2-8}$$

Using the results of the interior channel flow measurements in Section 4.2.4, an experimentally determined velocity ratio can be determined. Taking the average flow velocity, subtracting two standard deviations, and dividing by the average flow velocity gives a minimum to average velocity ratio. The average of the ratios for the 74 and 85 gpm cases yields a velocity ratio of 0.929. Thus, the channel flow velocity ratio based on a minimum channel velocity that is two standard deviations less than the average is:

$$\frac{V_{min}}{V_{nom}} = 0.929 \quad . \tag{4.2-9}$$

Combining the experimentally based value of the velocity ratio with the area ratio based on fuel channel tolerances yields the following value of the flow disparity:

$$d_{f_c} = \frac{V_{min}}{V_{nom}} \frac{A_{min}}{A_{nom}} = (0.929)(0.955) = 0.887 \tag{4.2-10}$$

The experimentally based flow disparity yields a larger disparity than the calculated disparity. Channel widths

vary within the allowable tolerance along the channel length. Because of these variations, it has not been possible to correlate the experimental flow velocities with actual measured channel widths. For the purpose of evaluating the core performance, the experimentally based value of channel flow disparity will be used, even though it may only be the uncertainty in the flow measurement methods that make it larger than the expected calculated value. No measured flow velocity was more than two standard deviations less than the average. The flow disparity was greater than the 1970 test because the original test element was manufactured using tight tolerances and the present test used a production line element.

The simulated exterior channels between the outer fuel plate and core housing wall had a flow velocity which was approximately 90 percent of the average interior channel (see Table 4.2-2). The ratio of flow in an exterior channel to an interior channel is:

$$\frac{W_{exterior}}{W_{interior}} = \frac{V_{exterior}}{V_{interior}} \frac{A_{exterior}}{A_{interior}} = 0.9 \frac{0.044}{0.078} = 0.51$$

$$(4.2\text{-}11)$$

Thus, the exterior channel has approximately 50% of the coolant flow of an interior channel, but this channel is required to remove heat from only one side of a fuel plate whereas, the interior channels are required to cool two sides. The 1970 test gave a higher exterior channel flow, but it did not have proper nozzle openings for flow.

4.3   Fuel Position Flow Measurements for Core I

Relative flow measurements of the reactor core fuel positions were necessary to determine the plenum chamber flow disparity. The plenum flow disparity is defined as the ratio of the coolant flow in the fuel element position of interest to the flow in the average fuel element position in the core. These measurements were obtained by positioning flow velocity measuring devices at the discharge of each fuel element position. The tests were performed using the fully loaded reactor core with both one and two main pump operation. The flow measuring methods and the results for Core I are described in this section.

4.3.1   Incore Flow Meters

Two flow meters were used to measure relative flow distribution. The first was a simple pitot tube and is shown in Fig. 4.3-1. This flow measuring device was used for scanning the core outlet area and making a qualitative check on the second flowmeter which was used as the primary flow measuring device.

The second flowmeter was a flow averaging pitot bar. This type of flowmeter was chosen because of the limitations that: materials used in the core tank must be made from either stainless steel or aluminum; be able to function under a 10 foot head of water; and be possible to fabricate within a reasonable cost. The flowmeter is shown in Fig. 4.3-2. Basically, the meter consists of a

FIG. 4.3-1

SIMPLE FLOW MEASURING PITOT TUBE

to water manometer

9- 1/2"

14- 1/2"

3/4"
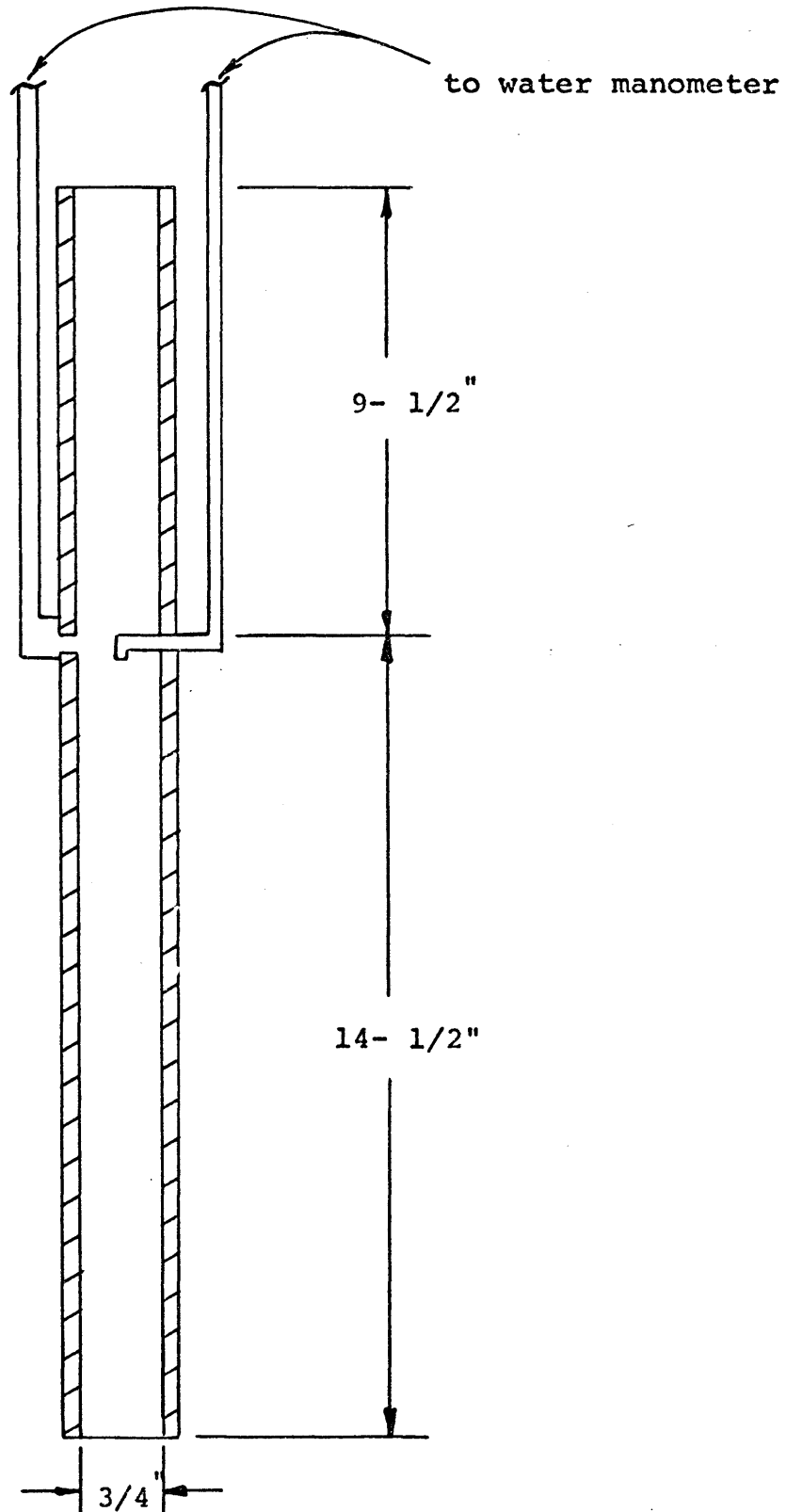
FIG. 4.3-2

INCORE PRIMARY FLOWMETER

upper support extension

11"

37"

2" I.D.

detail of pitot bar

holder to fit into holddown grid plate
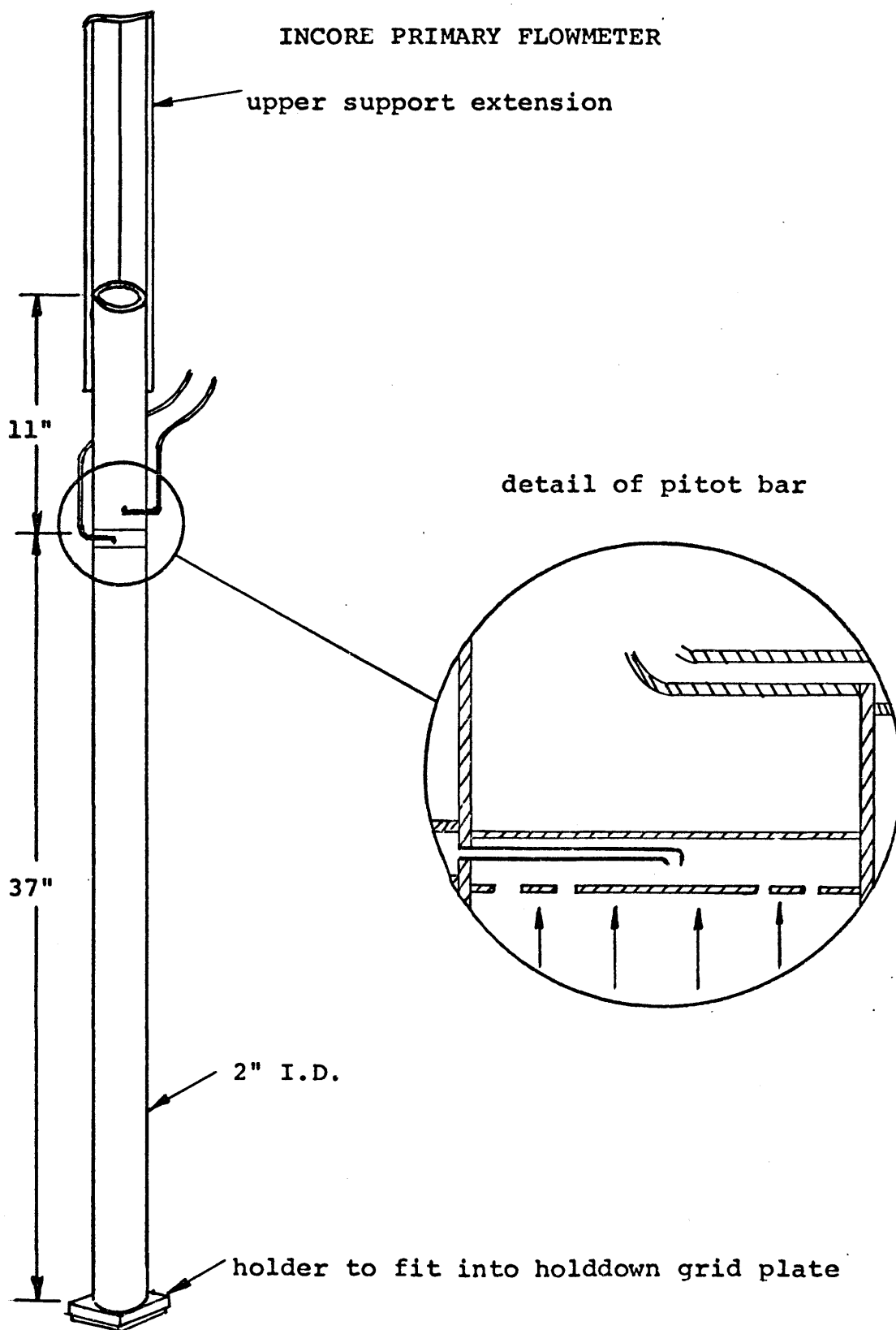
four feet long, two inch I.D. tube with a pitot bar and pressure tap, located approximately three feet from the entrance of the   e. An adapter (which fits snuggly in the discharge   zzle of a MITR-II fuel element) is welded to the en ance of the tube. Water flowing into the flowmeter from the fuel element travels up the tube and discharges from the tube into the core tank pool.

The pitot bar itself is constructed from two concentric tubes (see Fig. 4.3-2). The outer tube has an inner diameter of 0.25 inches and 0.02-inch-thick walls. There are four holes in the tube which face upstream to measure an average impact pressure over the velocity profile in the main two-inch tube. A small inside tube with an inner diameter of 3/32 of an inch and 0.01-inch-thick walls measures the average impact pressure at cenline between the four holes. The pressure on this small inside tube is measured on one leg of a water manometer with the downstream suction pressure being measured on the second leg. Flowmeters of this design and hole spacing are commercially available (Ref. 4.3-1).

4.3.1.1 Flow Meter Characteristics

The pitot tube and pitot bar in both incore flow meters measure the flow velocity in a tube with a known flow area. Thus, the output from these flowmeters is proportional to a flow rate. For the main incore flowmeter (utilizing the averaging pitot bar) most of the water

discharging from a fuel position is assumed to exit through the flowmeter with the effect of flow resistance from the flowmeter on the element being measured proportional to the normal flow out of the element. Thus, the flowmeter will measure the relative flow between elements only.

For incompressible fluids, the square root of the measured impact pressure minus the measured static pressure is proportional to the velocity. For the primary flowmeter, the impact pressure and downstream pressure were measured (downstream pressure was measured by a pressure tap 180° from the pitot bar openings). The downstream pressure is thus the static pressure minus flow suction effects. The use of these pressures gives a larger differential pressure on the water manometer and for this reason yields increased measuring accuracy, but it causes the output to deviate slightly from the true square root relation. In order to determine the true relationship between differential pressure and flow rate, a calibration described in Section 4.3.1.2 was performed.

The pitot bar was located 18 diameters upstream from the entrance and 5 diameters downstream from the exit of the tube. Thus, the flow in the tube should be fully developed at the location of the pitot bar.

4.3.1.2 <u>Testing and Calibration</u>

The primary flowmeter with the flow averaging pitot bar as described in Section 4.3.1.1 was tested and cali-

brated in a test section shown in Fig. 4.3-3. The flow
was measured by using a calibrated rotameter in the test
loop and the differential pressure in the flowmeter was
measured with a water manometer. The test was performed
by varying the flow through the test loop and recording
the manometer and rotameter readings. The results of
the test are shown in Fig. 4.3-4. A least squares fit
was performed and the slope was found to be 0.477. Thus,
for the primary flowmeter:

$$W \propto (\Delta h)^{0.477} \quad , \qquad (4.3-1)$$

where,

W   is flow in flowmeter,

Δh the difference between impact pressure
     and downstream pressure as measured by
     manometer.

The relative flows per element are obtained by com-
paring the $(\Delta h)^{0.477}$ for each fuel element position.

4.3.2 Incore Flow Measurements

Incore flow measurements were taken as part of MITR-II
Startup Procedure 5.9.2. Initial flow measurements
were made with fuel loadings typical of operating con-
ditions including the effect of solid dummies and an
incore sample assembly in various reactor fuel positions.
The reactor fuel positions can be divided into four groups
which are separated by the lower and absorber spiders.
Changes which affect a fuel position (such as loading a

FIG. 4.3-3

INCORE PRIMARY FLOWMETER CALIBRATION TEST LOOP

rotameter

water manometer

2200 gal. water storage tank

pump

test section where primary flowmeter was located

FIG. 4.3-4

CALIBRATION CURVE

FOR INCORE PRIMARY FLOWMETER

differential pressure (cm. of H_2O)

flowrate

(gallons per minute)
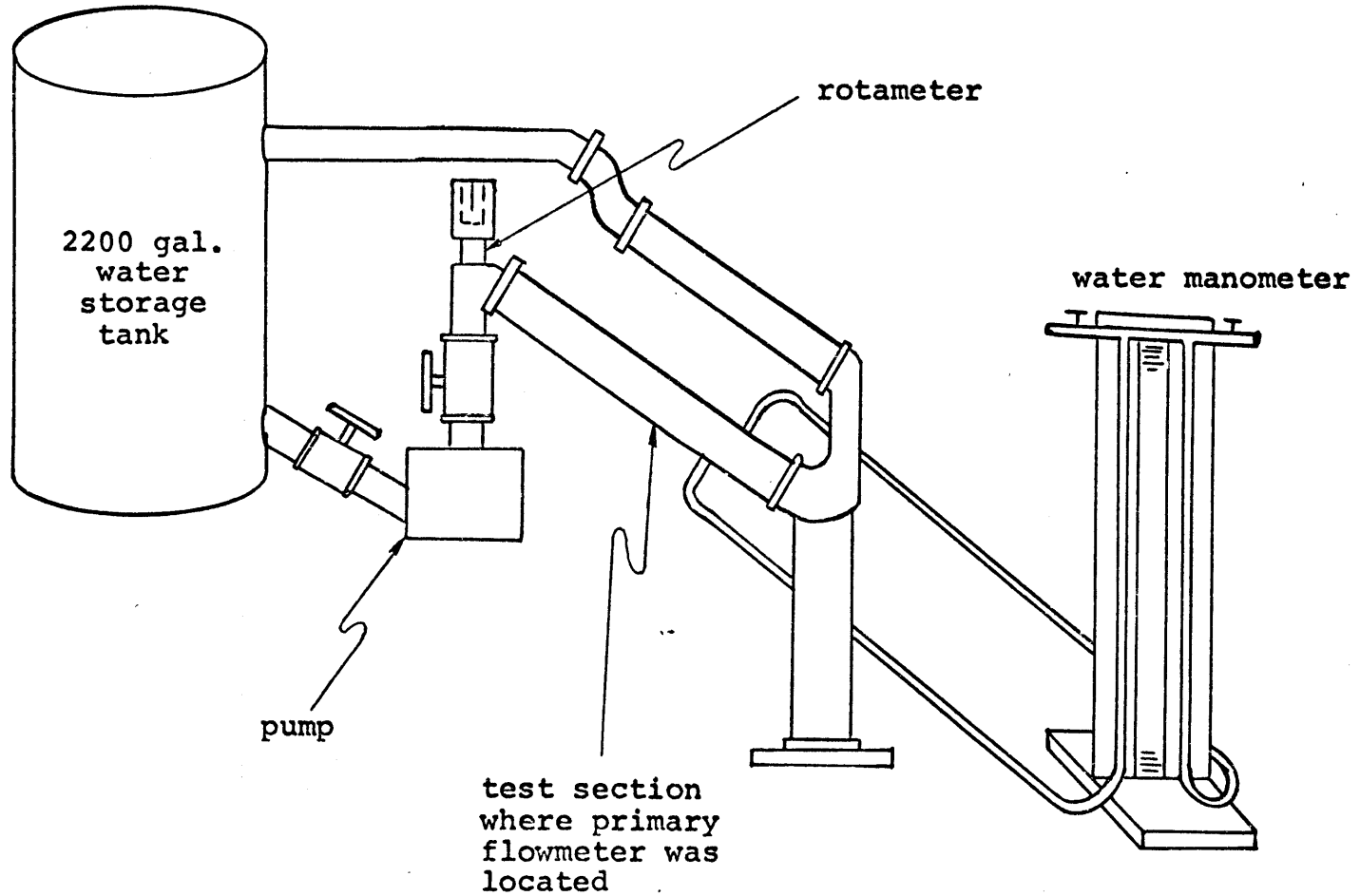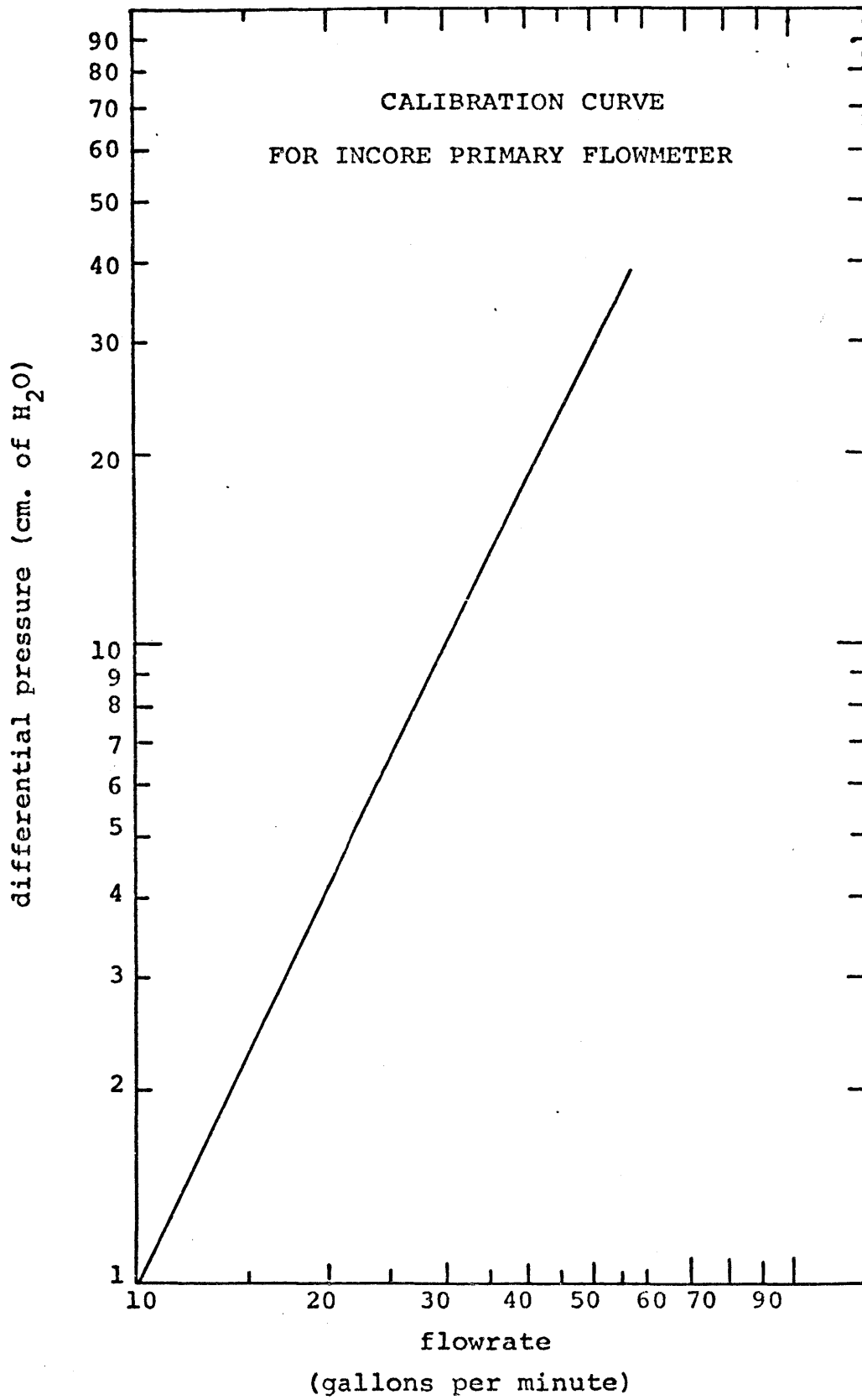
solid dummy where an element had been previously) appeared
to have most of its effect on the other positions within
its group and have little effect on individual positions
in other groups. The four groups of elements are as
listed below (see Fig. 1.3-2 for core arrangement).

Group 1	Group 2		Group 3		Group 4	
A-1	B-1	C-2	B-4	C-7	B-7	C-12
A-2	B-2	C-3	B-5	C-8	B-8	C-13
A-3	B-3	C-4	B-6	C-9	B-9	C-14
	C-1	C-5	C-6	C-10	C-11	C-15

Relative flow ratios for the different fuel element
positions are shown in Table 4.3-1 for the initial measure-
ments of several core loading arrangements. Measurements
were made with both one and two pumps operating.

After the arrangement for Core I of the MITR-II was
decided upon, a second set of flow measurements were taken
with the Core I fuel element configuration. Measurements
for each fuel element position were repeated three times
in order to reduce experimental uncertainty. Two fuel
positions could not be measured with the primary flow
measuring device because of interference with the hold
down grid latch. These positions were C-5 and C-6. The
pitot tube flowmeter was used to scan all fuel positions
to verify that neither of these positions had the lowest
coolant flow. The pitot tube was not as accurate as the
primary flowmeter since it did not fit snuggly into the
fuel element nozzle, but the pitot tube did show the same
trends as the flowmeter. Results of final relative flow

TABLE 4.3-1

RATIO OF ELEMENT POSITION FLOW TO CORE AVERAGE ELEMENT FLOW WITH VARIOUS SOLID DUMMY AND ICSA CONFIGURATIONS IN GROUPS FOR ONE AND TWO PUMP OPERATION

Position in Reactor	Dummy Element in Group		Dummy Element not in Group		ICSA in Group	
	1 Pump	2 Pump	1 Pump	2 Pump	1 Pump	2 Pump
Group 1						
A-1	*	*	0.854	0.844	//	//
A-2	--	1.017	0.940	0.913	0.894	0.965
A-3	--	0.9857	0.894	0.911	1.007	0.983
Group 2						
B-1	1.066	1.082	1.076	1.068	--	--
B-2	*	*	1.056	1.055	--	--
B-3	0.980	1.009	1.026	1.025	--	--
C-1	1.013	1.001	0.980	1.013	--	--
C-2	0.970	0.975	0.950	0.966	--	--
C-3	1.003	1.008	1.003	0.994	--	--
C-4	0.960	0.990	0.931	0.937	--	--
C-5	--	--	--	--	--	--
Group 3						
B-4	--	1.037	1.036	1.080	--	--
B-5	*	*	1.076	1.049	--	--
B-6	--	1.083	1.086	1.091	--	--
C-6	--	--	--	--	--	--
C-7	0.964	0.967	0.954	0.903	--	--
C-8	--	1.026	1.020	0.971	--	--
C-9	--	0.991	0.960	0.977	--	--
C-10	--	0.996	0.993	1.006	--	--

TABLE 4.3-1 (Continued)

Position in Reactor	Dummy Element in Group		Dummy Element not in Group		ICSA in Group	
	1 Pump	2 Pump	1 Pump	2 Pump	1 Pump	2 Pump
Group 4						
B-7	1.086	1.070	1.079	1.031	--	--
B-8	//	//	1.083	1.041	--	--
B-9	1.056	1.074	1.083	1.052	--	--
C-11	1.013	1.006	1.003	0.959	--	--
C-12	0.980	0.983	0.954	0.935	--	--
C-13	1.030	1.017	1.036	0.944	--	--
C-14	1.026	0.979	0.980	0.943	--	--
C-15	1.036	1.034	1.040	1.024	--	--

* Solid dummy in fuel position

// ICSA in fuel position

-- Data not taken

Note: All measurements made using incore flowmeter (Fig. 4.3-2)

measurements with two primary pumps operating are shown in Table 4.3-2.

4.3.2.1 One Primary Pump Versus Two Primary Pumps

Relative element flow ratios appear to be the same for both one pump and two pump operation. Data for one and two pump operation is shown on Table 4.3-1. Thus, the flow disparity will be independent of the number of pumps operating.

4.3.2.2 Solid Dummy Element Effects

A dummy element only seems to affect flow ratios in element positions that are in the same group (see Section 4.3.2 for groupings) as the dummy element itself. The outer three groups (composed of B and C-ring elements) appear to be affected in an identical manner by a dummy element. Inserting a solid dummy in the center B-position in a group caused the flow in the other elements of the group to increase. Element positions in the C-ring with full sides adjacent to the dummy element seem to experience the greatest increase in flow. Without a dummy element in the group, the minimum ratio of element flow to core average element flow for any of the three outer groups was approximately 0.94. With a dummy in the group, the minimum flow ratio is raised to approximately 0.97. The similar results for each of the outer groups indicate that the core is flow symmetric and that no one side of the

TABLE 4.3-2

COMPARISON OF RATIOS OF ELEMENT POSITION FLOW TO CORE
AVERAGE ELEMENT FLOW OBTAINED USING SCANNING
PITOT TUBE AND INCORE FLOWMETER

Position in Reactor	Scanning Pitot Tube (Figure 4.3-1)	Incore Flowmeter (Figure 4.3-2)
A-1	*	*
A-2	1.065	1.017
A-3	0.997	0.986
B-1	1.060	1.049
B-2	*	*
B-3	1.039	0.997
C-1	0.993	0.942
C-2	0.974	0.960
C-3	0.964	0.981
C-4	0.968	0.977
C-5	0.917	--
B-4	1.011	1.007
B-5	1.121	1.057
B-6	1.100	1.073
C-6	0.980	--
C-7	0.907	0.945
C-8	1.004	1.011
C-9	0.867	0.9377
C-10	0.949	0.9811
B-7	1.073	1.082
B-8	*	*
B-9	1.098	1.092
C-11	0.974	0.985
C-12	0.983	0.946
C-13	1.010	0.997
C-14	0.932	1.025
C-15	1.010	1.001

* solid dummy in fuel position
-- data not taken because of interference with grid latch

core receives a disproportionate share of the flow. The average flow ratio per element for each group is shown in Table 4.3-3.

TABLE 4.3-3

AVERAGE ELEMENT FLOW IN GROUP WITH AND
WITHOUT SOLID DUMMY IN GROUP

1 Dummy in Group		Dummy not in Group
Group 1	1.001	0.889
Group 2	1.01	1.008
Group 3	1.016	1.011
Group 4	1.02	0.991

(Data taken from averaging data in Table 4.3-1)

Note in the above table, that with the exception of Group 1, there is little difference in average flow ratio per element in a group between the one dummy and no dummy cases. However, for these outer three groups, adding a solid dummy improves the flow distribution within that group by increasing flow to the lower than average flow C-ring element positions by diverting the flow from a normally above average flow B-ring element positions.

The flow distribution in the A-ring elements of Group 1 is greatly improved by adding a solid dummy element to the group. There appears to be insufficient flow to the group for three elements without having a large flow disparity. This problem is not serious since during reactor operation, at least one A-ring position is expected to be filled by a

solid dummy or In-core Sample Assembly (both have much
lower flow than a fuel element).

Because of limitations on reactor shutdown margin and
because of an insufficient number of non-fueled elements,
it was not possible to perform flow tests without some solid
dummies somewhere in the core. The data indicates that
dummies exert only a local influence on flow disparity and
that this limitation is not important.

4.3.2.3 ICSA Effects

Coolant flow through the Incore Sample Assembly (ICSA)
tested (see Fig. 1.3-5) was a fraction of a normal element
flow. Consequently, the effect of the ICSA was between a
fuel element and solid dummy element. Table 4.3-1 veri-
fies this effect. Design of an ICSA for A-ring positions
must insure that there is a sufficient flow restriction
in the ICSA to provide adequate cooling for the remaining
A-ring elements.

4.3.3 Plenum Flow Disparity for Core I

As a result of the second set of measurements with
the primary flowmeter, plenum flow disparity factors for
each fuel element position for Core I of the MITR-II were
determined. Factors for each position are shown in
Fig. 4.3-5. In general, the values for Groups 2 and 4
represent flow disparity factors for outer groups which
have a solid dummy in the center B-position. The values
for Group 3 represent a typical outer group with no solid

FIG. 4.3-5

PLENUM FLOW DISPARITIES FOR CORE I

REGULATING ROD
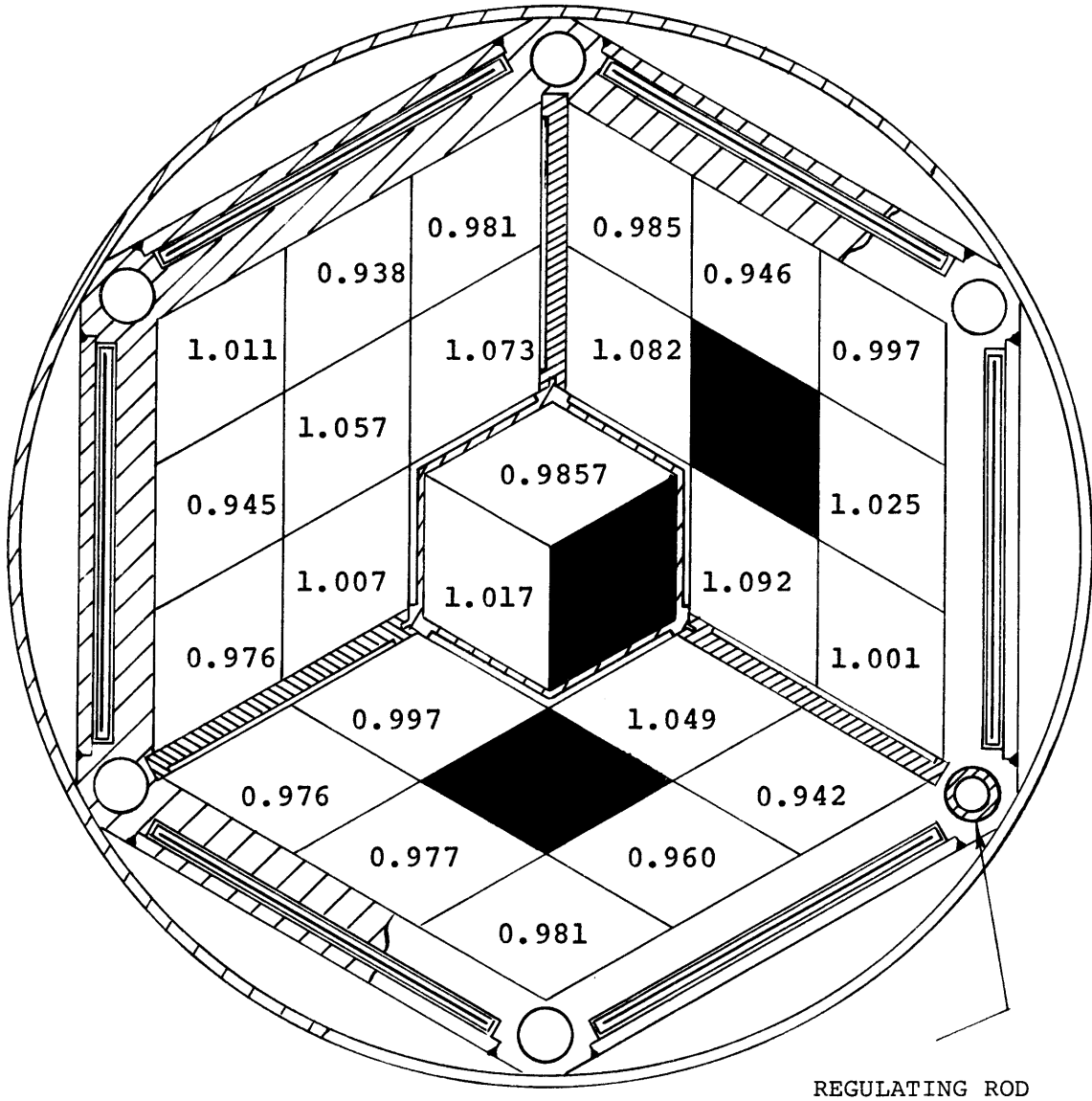
▰ - solid dummy element

dummy elements present.

4.4 Core Bypass Flows

There are several sources which allow coolant to by-pass the active fuel elements in the core. Some of these sources are controllable by design (ICSA, solid dummy elements, etc.) and others are small leakage flows. It is important to obtain an estimate of these bypass flows in order to determine the fraction of coolant that cools the active core (F_f). Because many of these flows are small, they are difficult to accurately measure in core in the presence of the turbulence effects from the large primary coolant flow.

The bypass flows were estimated by three manners:

A) Calculated, knowing leakage area and pressure drop,

B) Out core test loops,

C) Using pitot tube scans incore and comparing flows seen to fuel element position flows.

The results of these estimates are shown on Table 4.4-1.

4.4.1 Check Valve Flow Tests

Because of a valve sticking problem encountered during the preoperational testing of the natural circulation and anti-syphon valves (Ref. 4.4-1), a flow test was made to verify the new design of the natural circulation valves. The test loop setup is shown in Fig. 4.4-1. After being tested for 1000 cycles, a

FIG. 4.4-1

NATURAL CIRCULATION VALVE TEST LOOP

valve being tested

pressure gage

discharge valve for
adjusting back-
pressure

quick
closing
valve

flowmeter

pump

test section

water tank
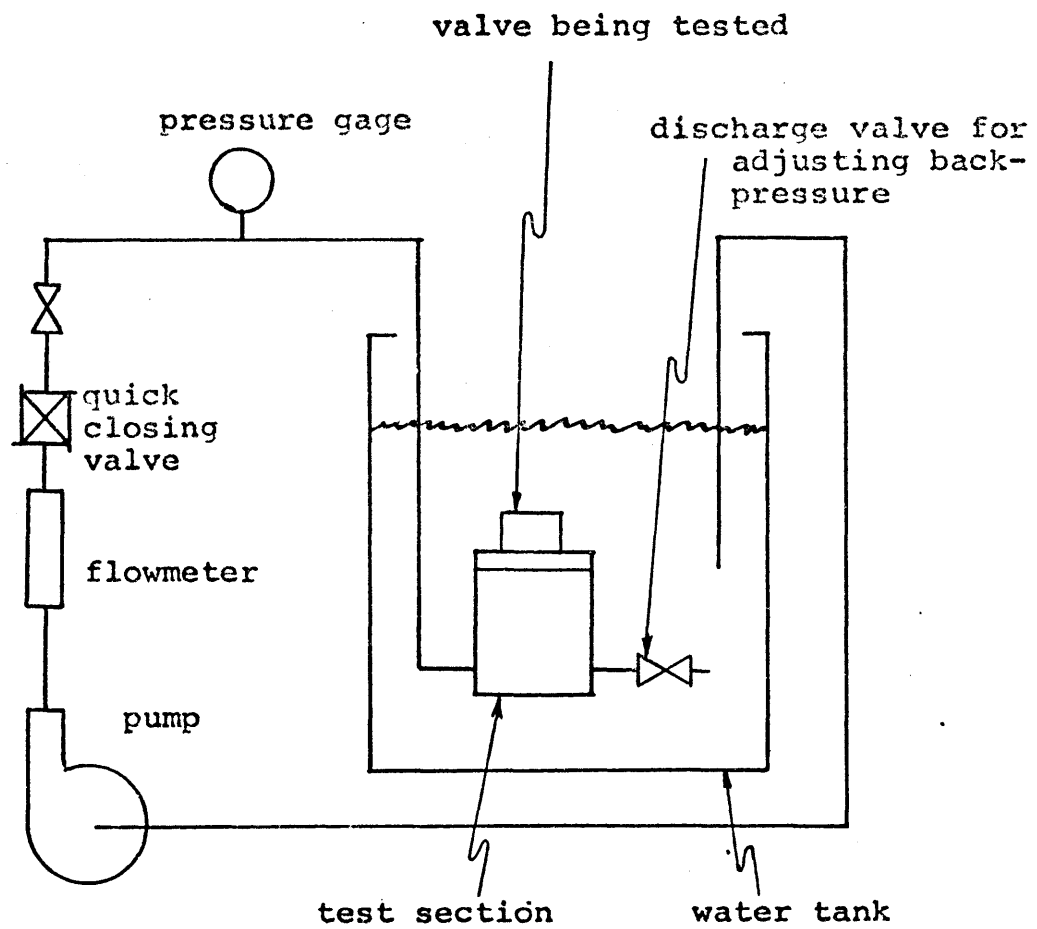
prototype valve still yielded low leakage flows. Four valves for use incore were constructed and each was tested in the test loop prior to installation. Leakage flow was measured on the test loop rotameter.

The volume of check valve leakage varied directly with the pressure on the check valve. This indicates that once the valve closes, there is no additional deformation of the seating surface to reduce flow as pressure increases. Thus the higher the pressure, the higher the leakage flow and vice-versa. At pressures that correspond to reactor values, the average leakage of the natural circulation valves was 1.5 gpm/valve. No valve had a greater leakage than 2 gpm at these pressures.

4.4.2 Bypass Flow Evaluation for Core I

Table 4.4-1 shows the sources of bypass flow for Core I and estimates for their quantities. The means for obtaining those estimates is also listed. The leakages listed in the table are not adjustable except for the bypass flow for the dummy elements. The bypass flow for the dummy elements could be reduced by replacing the dummy elements with active elements or by reducing the flow cooling the dummies if operating experience shows that this is possible.

For Core I of the MITR-II, the bypass flow totaled approximately 105 gpm. This yields a F_f of 0.9487 from

TABLE 4.4-1

SUMMARY OF BYPASS FLOWS FOR CORE I

Source	Estimated Bypass Flow	Source of Estimate
Control blade cooling holes	13.4 gpm	Calculated by knowing pressure drop and hole sizes
Core housing corner holes	3.9 gpm	
Natural Circulation check valves (4)	6.0 gpm	Test loop data
Anti-syphon valves (2)	3.0 gpm	Comparison with natural circulation valves
Solid dummy elements (3)	68.3 gpm	Measured with primary flowmeter
Annular partition gasket	5.0 gpm	No flow measured, source of estimate is minimum flow detectable using pitot tube
Annular partition and core housing joint	5.0 gpm	

the following equation:

$$F_f = \frac{\text{Total coolant flow - bypass flow}}{\text{Total coolant flow}} \quad , \quad (4.4\text{-}1)$$

Flow through an Incore Sample Assembly (ICSA) would have to be added to the bypass flow and thus would make F_f a smaller number if an ICSA was loaed in the core. The uncertainty on bypass flow for Core I is less than 20gpm which would yield an uncertainty of F_f approximately one percent (20 gpm represents a 15% uncertainty in the bypass flow which is estimated to be greater than the actual uncertainty).

4.5 Summary of Flow Distributions for Core I

The channel and plenum flow disparities have been experimentally determined for Core I of the MITR-II. The channel flow disparity is:

$$\text{Channel flow disparity} = d_{f_c} = 0.887. \quad (4.5\text{-}1)$$

Plenum flow disparities are shown in Fig. 4.3-5. The fuel position which contained the lowest element flow in Core I was position C-9. The plenum flow disparity for C-9 with a Core I loading is:

$$\text{C-9 plenum flow disparity} = d_{f_p} = 0.9377. \quad (4.5\text{-}2)$$

For the C-9 fuel position in Core I, this yields a total maximum flow disparity:

$$d_f = 0.887 \times 0.9377 = 0.832 \quad . \qquad (4.5\text{-}3)$$

Similar maximum flow disparities can be obtained for each fuel element position by multiplying the channel disparity d_{f_c} by the d_{f_p} for the position in Fig. 4.3-5. Repeat measurements indicate that the relative flow measurements have a two standard deviation uncertainty of one percent.

For Core I of the MITR-II, the fraction of coolant cooling the core was:

$$F_f = 0.9487 \quad . \qquad (4.5\text{-}4)$$

F_f also has an uncertainty of approximately one percent.

4.6   Flow Distribution for Core II

Flow measurements were made on Core II of the MITR-II. Flow considerations for Core II differed from Core I in the following manner:

A)   Removal of fixed absorbers resulted in additional solid dummies being loaded into the reactor,

B)   Solid dummies were loaded into side B-ring positions (B-3, B-6, B-9) rather than central B-ring positions (B-2, B-5, B-8).

As a result of these differences, flow measurements were made for Core II using the incore flowmeter described in Section 4.3.

4.6.1 Plenum Flow Disparity

Table 4.6-1 shows the measured plenum flow disparity between element positions for the Core II loading configuration. Note that the highest flows still occur in the B-ring and that the range of flow disparities is similar to the Core I loading. The range of plenum flow disparities for Core I is 1.092 to 0.937 and the range for Core II is 1.084 to 0.93.

Figure 4.6-1 shows the plenum flow disparities, d_{f_p}, that were used in evaluating the safety limit and limiting conditions for operation of Core II.

4.6.2 Bypass Flows

The fraction of the flow that cools the active fuel elements, F_f, is smaller for Core II because of additional bypass flow through the added solid dummies. Table 4.6-2 gives a summary of bypass flows for Core II. The total bypass flow is approximately 159 gpm. This yields a F_f of 0.9205 using Eq. 4.4-1.

4.6.3 Summary of Flow Distribution for Core II

The channel flow disparity is the same as for Core I and is equal to 0.887. Plenum flow disparities, d_{f_p}, are shown in Fig. 4.6-1 and the total flow disparity, d_f, is the product of the channel and plenum disparities.

TABLE 4.6-1

RATIO OF ELEMENT POSITION FLOW TO CORE AVERAGE ELEMENT FLOW OBTAINED USING INCORE FLOWMETER ON CORE II

Position in Reactor	Ratio
A-1	1.009
A-2	*
A-3	*
B-1	1.074
B-2	1.049
B-3	*
C-1	0.989
C-2	0.930
C-3	0.951
C-4	0.949
C-5	--
B-4	1.032
B-5	1.058
B-6	*
C-6	--
C-7	0.954
C-8	0.993
C-9	0.953
C-10	1.019
B-7	1.084
B-8	1.032
B-9	*
C-11	1.009
C-12	0.944
C-13	0.944
C-14	0.972
C-15	1.036

* Solid Dummy in fuel position

-- Data not taken because of interference with grid latch

FIG. 4.6-1

PLENUM FLOW DISPARITIES FOR CORE II

REGULATING ROD
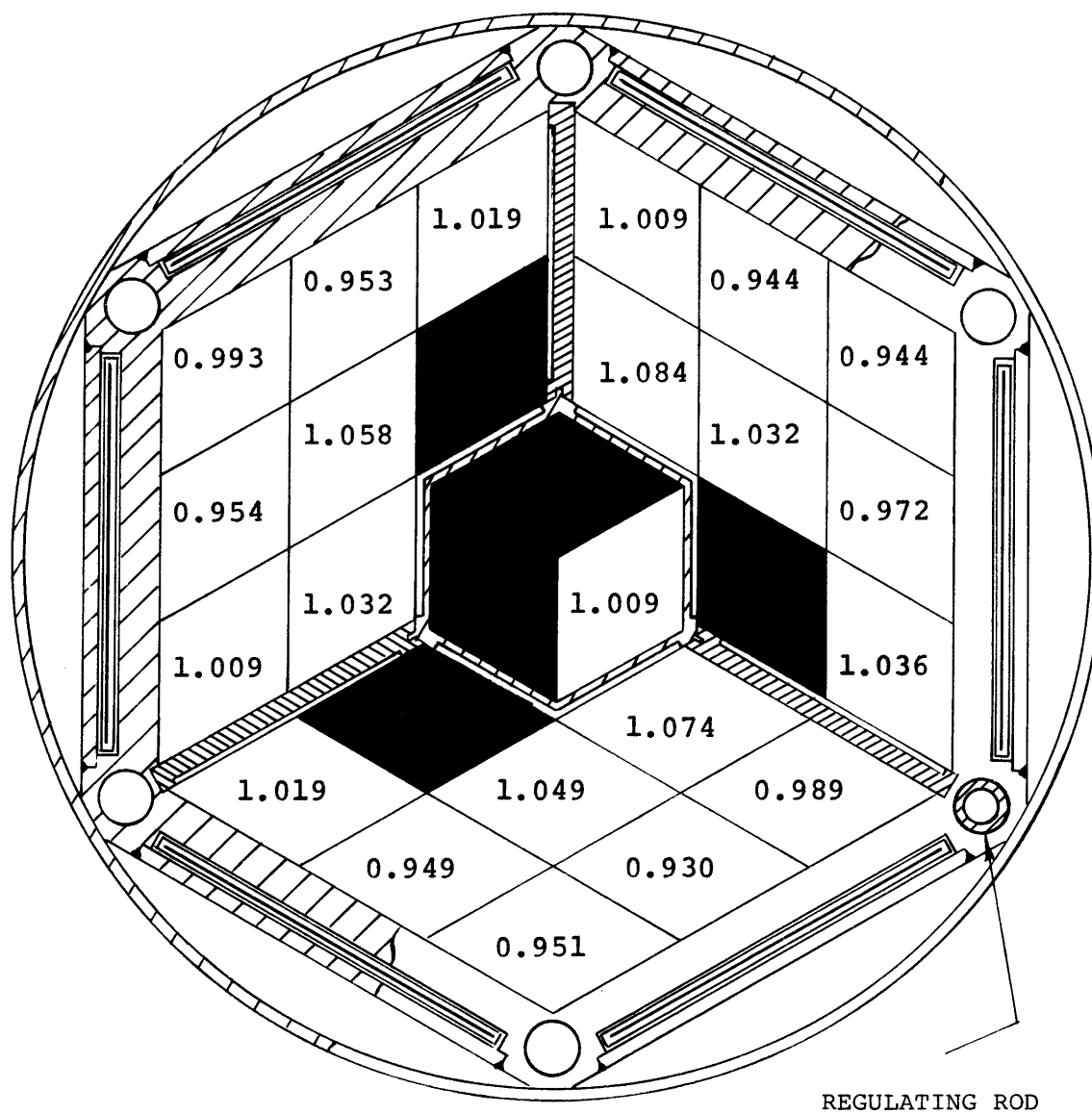
▰ - solid dummy element

TABLE 4.6-2

SUMMARY OF BYPASS FLOWS FOR CORE II

Source	Estimated Bypass Flow	Source of Estimate
Control blade cooling holes	13.4 gpm	Calculated by knowing
Core housing corner holes	3.9 gpm	pressure drop and hole size
Natural Circulation check valves (4)	6.0 gpm	Test loop data
Anti-syphon valves (2)	3.0 gpm	Comparison with natural circulation valves
Solid dummy elements (3)	122.8 gpm	Measured with primary flowmeter
Annular position gasket	5.0 gpm	No flow measured, source
Annular partition and core housing joint	5.0 gpm	of estimate is minium flow detectable using pitot tube

For Core II of the MITR-II, the fraction of coolant cooling the core, F_f, was equal to 0.9205.

The uncertainty on F_f and d_f remains at one percent for each.

CHAPTER 5

POWER DISTRIBUTIONS IN CORE I

Power distributions in Core I of the MITR-II are discussed in this chapter. Section 5.1 summarizes the predictions used to evaluate the initial design of the MITR-II. Section 5.2 describes the design check predictions used to evaluate the final design of the MITR-II and used to compare with the experimental power distribution measurements. The experimental measurement of power distribution by gamma scanning of removable fuel plates in an MITR-II fuel element is discussed in Section 5.3. Section 5.4 describes neutron flux measurements in Core I by copper wire activation. The results of power and neutron flux measurements and calculations of Core I are summarized in Section 5.5.

5.1 Design Predictions

Initial design studies of the MITR-II were performed by numerous members of the MITR staff and Nuclear Engineering Department students. The goal of the initial work was to determine a final design of the MITR-II and to prepare a Safety Analysis Report (Ref. 5.1-1) for the project. The completed Safety Analysis Report (SAR) is a summary of the design predictions and conclusions. Design predictions

regarding power distribution are further summarized in this section.

The base core for most original design studies consisted of a fully loaded core with one sample assembly in a center ring position. In most cases the sample assembly was mocked up by using a "lead fuel element".

5.1.1 Power Density Distribution

Reactor physics methods used to evaluate the MITR-II were developed by Addae (Ref. 5.1-2). A finite difference diffusion code, Exterminator-II, provided the basic power distributions used in evaluating core power densities. Homogeneous average power densities were obtained from Exterminator-II (Ref. 5.1-3) and these were converted into heterogeneous values using a method described in Section 3.3.4.3.3 of the MITR-II Safety Analysis Report. A similar method was used to evaluate the design check results from CITATION and is described in Section 5.2.3.1 of this work. The major difference between the two methods is the additional normalization factor required for Exterminator-II since its output is in fissions/cm^3 and CITATION prints out power densities in watts/cm^3.

Figure 5.1-1 shows the predicted axial heat flux distribution along the hottest fuel plate at an edge of the core and at a central core position as predicted by Exterminator-II. Values of the axial and radial power peaking were determined using Exterminator-II calculations.

FIG. 5.1-1

AXIAL HEAT FLUX DISTRIBUTION ALONG THE HOTTEST FUEL PLATE
(reactor power 6 Mw + primary coolant flow rate: 1800 GPM)

Heat flux at the edge of the
core next to the D_2O reflector

Curve 1: blades at 8 inches
Curve 2: blades at 10 inches
Curve 3: blades at 14 inches

Heat flux on a central plate

Curve 4: blades at 8 inches

(y-axis) heat flux on one surface of a fuel plate $(Btu/hr-ft^2)$

(x-axis) distance from bottom of fuel (inches)

The axial peaking factor, F_a, is the ratio of the maximum power density in a fuel plate to the average power density in that fuel plate. The radial peaking factor, F_r, is the ratio of the total power generated in a fuel plate to that generated in the average fuel plate in the core. Table 5.1-1 gives a summary of F_a and F_r as evaluated using Exterminator-II at several shim bank heights (Ref. 5.1-1).

The product $F_r \times F_a$ is a measure of the power density at a point compared to the average power density in the core. For Table 5.1-1 which was used as an example in the SAR analysis, all maximum $F_a \times F_r$ values are at the bottom edge of the fuel. As seen from Table 5.1-1, the effect of lowering the shim bank is important. Lowering the shim bank raises the peak by shortening the core.

Figure 5.1-2 shows the predicted power density distribution for a vertical section of the core. Figures 5.1-3 and 5.1-4 show power density distributions for a horizontal cross section at core mid-height for a hexagonal model and a R-Z model, respectively. These three figures were made by Addae (Ref. 5.1-2) for a smaller diameter core than the final design and the latter two were normalized such that the average power density equals 1.0. Note that the R-Z model misses the power peak that occurs because of the water hole at the corner of the core housing.

TABLE 5.1-1

SUMMARY OF AXIAL AND RADIAL POWER PEAKING FACTORS

Shim Blade Height above Fuel Bottom	F_a		F_r		$F_r \times F_a$	
	Center Plate	Edge Plate	Center Plate	Edge Plate	Center Plate	Edge Plate
14 inches	2.19	2.01	1.20	1.45	2.63	2.91
10 inches	2.29	2.66	1.30	1.22	2.98	3.24
8 inches	2.44	3.17	1.36	1.07	3.32	3.39

FIG. 5.1-2

0.5

1.0

2.0

3.0

4.0

5.0×10^{12}

core

5.0×10^{12}

6.0

7.0

core tank

D_2O tank

beam port
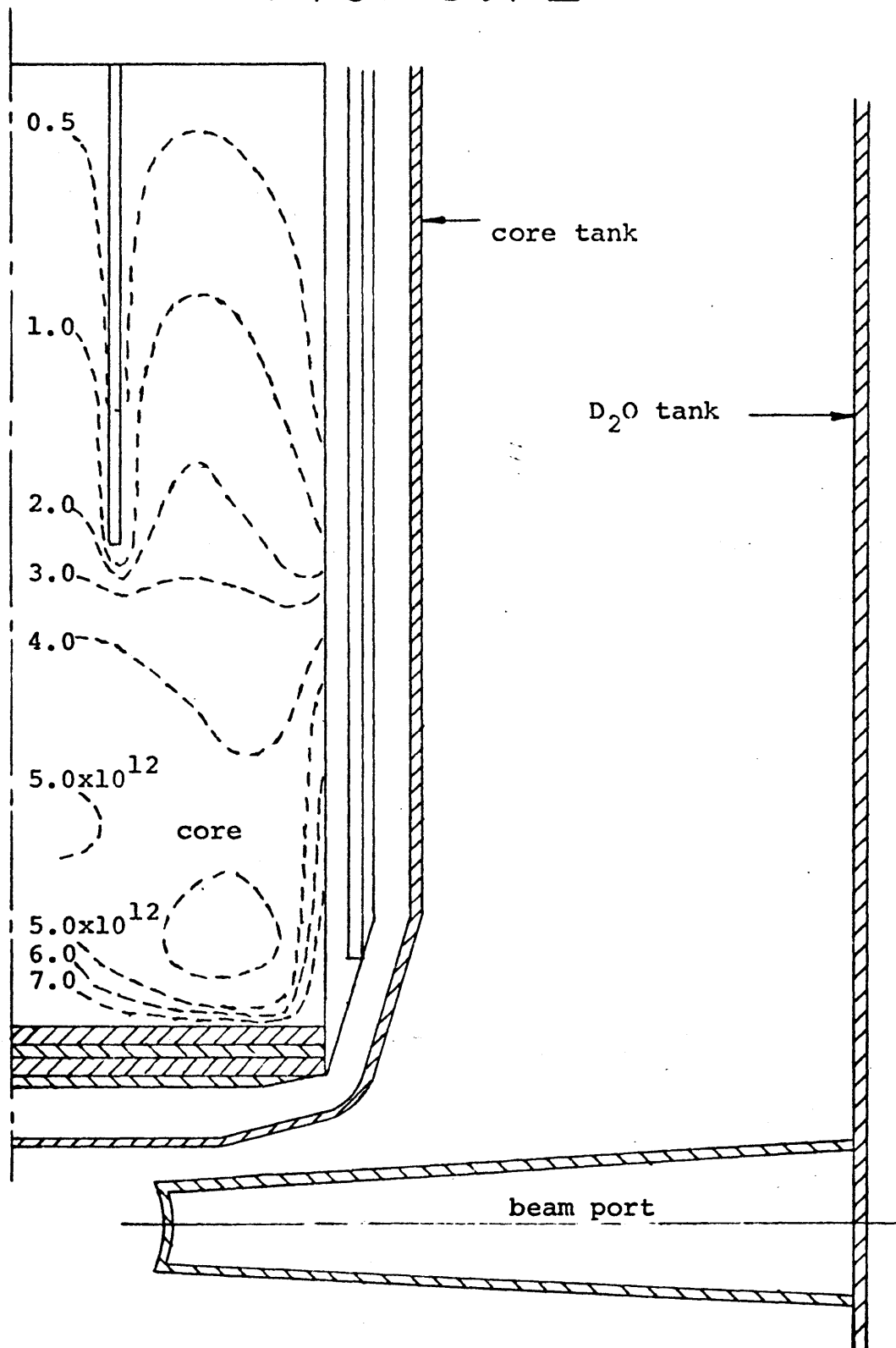
POWER DENSITY DISTRIBUTION FOR VERTICAL SECTION
(10^{12} fissions/cm³-sec)

FIG. 5.1-3
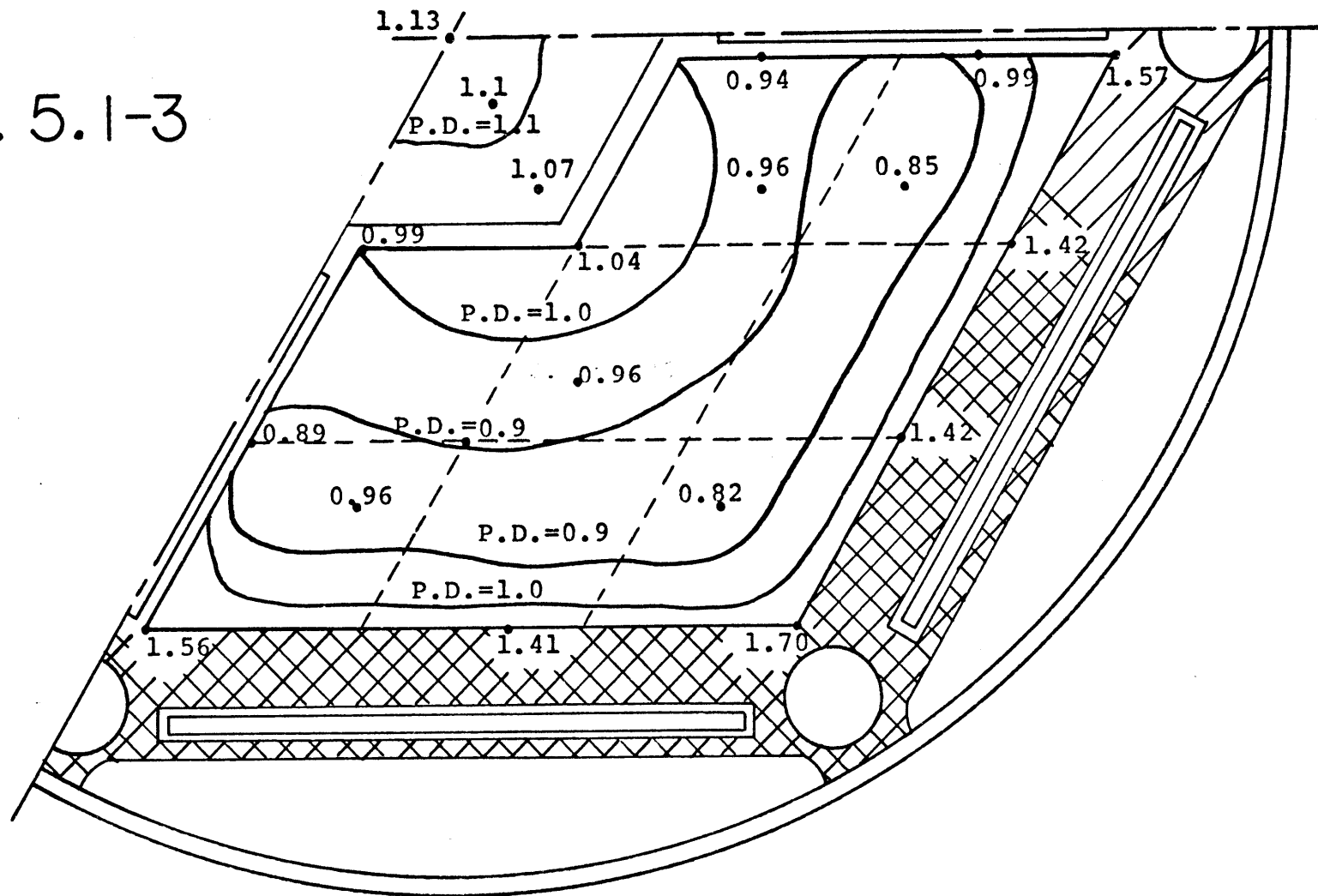
RADIAL NORMALIZED POWER DENSITY DISTRIBUTION IN THE ACTUAL HEXAGONAL CORE AT
MID-HEIGHT

FIG. 5.1-4

light water tank

light water coolant

1.224

1.217
1.95
1.129
1.070
1.00
0.956
0.890
1.379

___ normalized power density
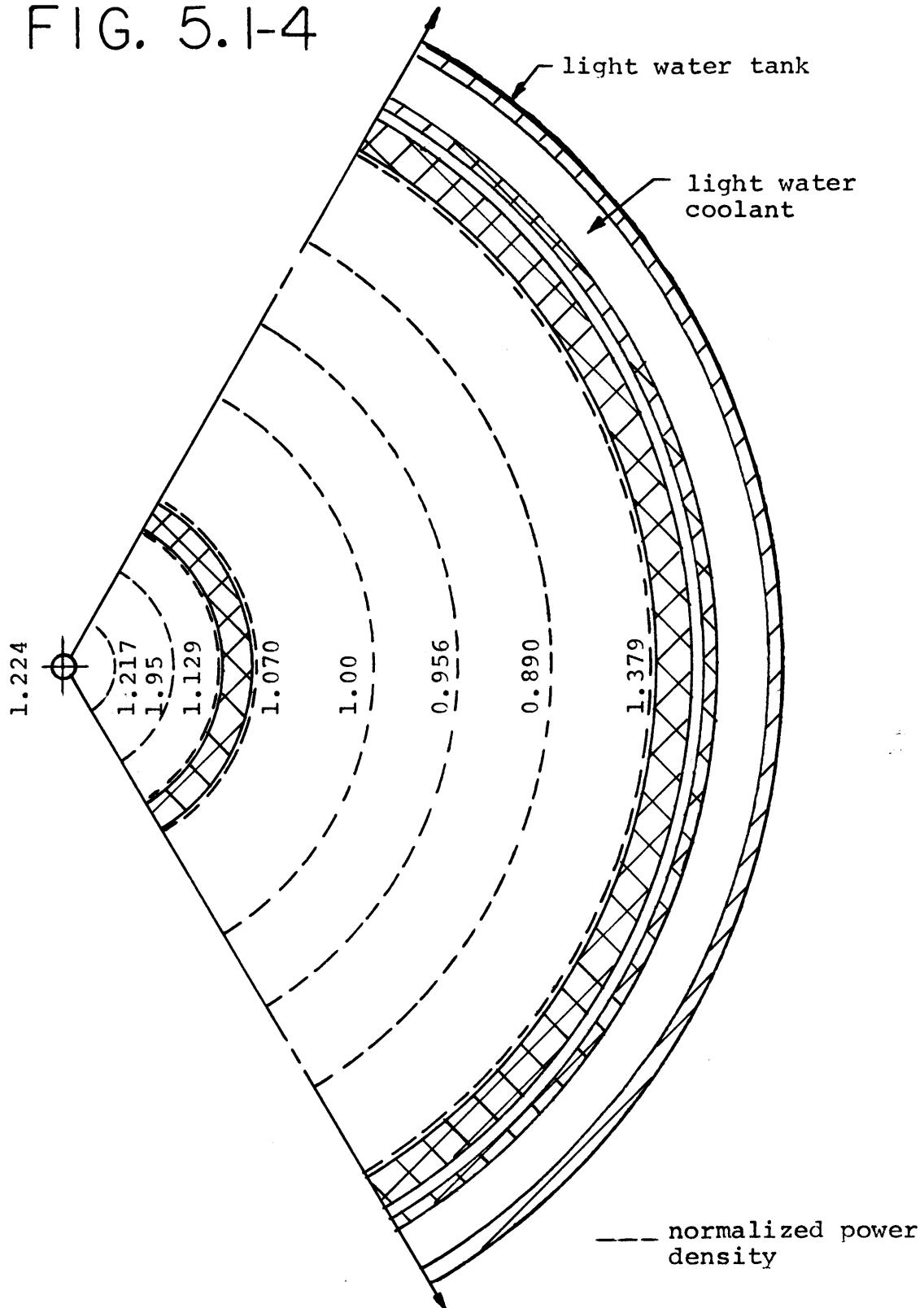
RADIAL NORMALIZED POWER DENSITY DISTRIBUTION IN THE
CYLINDRICAL CORE MODEL AT MID-HEIGHT

5.1.2 Neutron Flux Distribution

One goal of the reactor modification was to increase the neutron source intensity for neutron beam experiments. Figure 5.1-5 shows the thermal neutron flux surrounding the reactor core as calculated by Kadak (Ref. 5.1-4). The predicted thermal neutron flux at the outside edge of the heavy water tank for the MITR-II core is predicted to be about the same as that flux at the same region for the MITR-I core. The advantage of the redesign is derived from the greater flux that the re-entrant thimbles extending into the heavy water tank view.

Figure 5.1-5 shows that the thermal flux at the beam port tip is approximately 8.5×10^{13} neutrons/cm^3. This is an optimistic prediction because it neglects such factors as beam port perturbation, but even including several factors that will lower the beam port flux, the flux enhancement to neutron beam experiments is expected to be approximately a factor of three increase in thermal neutron flux over levels in the MITR-I.

5.2 Design Check Predictions

Computer calculations were made as a design check and to predict power and flux distributions in various core configurations of the MITR-II. The main tool used in design check predictions was the computer code CITATION (Ref. 5.2-1).

FIG. 5.1-5

core tank

fixed
absorber

D_2O tank

core

11.0

10.

8.8

8.5

8.0×10^{13} 6.0×10^{13} 4.0×10^{13} 2.5×10^{13}
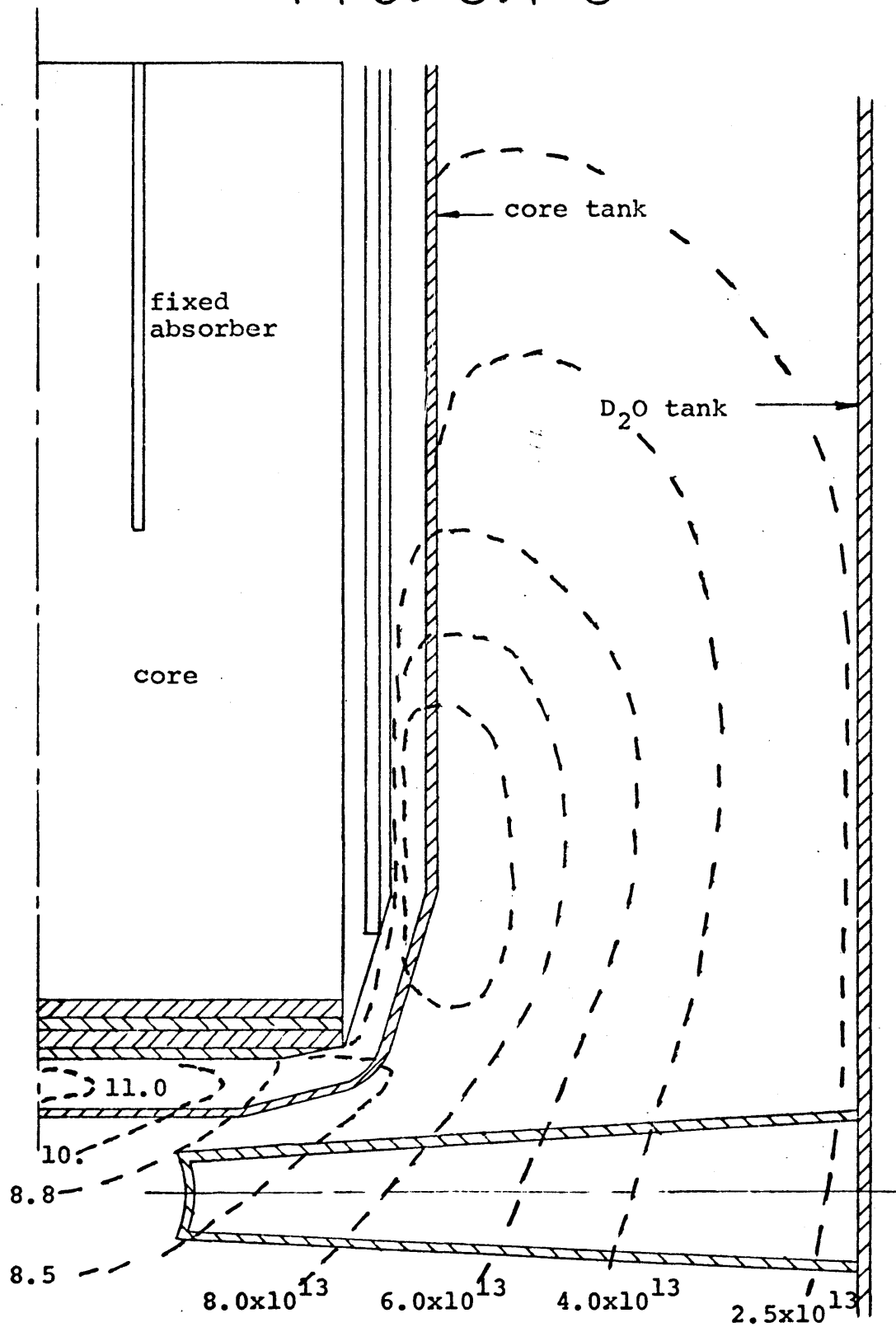
DESIGN 5 MW THERMAL NEUTRON FLUX

5.2.1 CITATION Code and Neutron Cross Section Set

CITATION is designed to solve problems involving the finite difference representation of diffusion theory, treating up to three space dimensions with arbitrary group-to-group scattering. X-Y-Z, θ-R-Z, hexagonal-Z and triangonal-Z geometrics may be treated. Depletion problems may be solved and fuel mangaged for multi-cycle analysis. The code is designed to effectively use computers in the IBM-360 series.

The cross sections used in CITATION were developed by Kadak (Ref. 5.1-4) following the procedures set forth by Addae (Ref. 5.1-1). The cross sections were updated by Emrich (Ref. 5.2-2). The basic cross section data used is that of Hansen and Roach (Ref. 5.2-3).

For the energy range above 1 ev. the diffusion length of neutrons was considered long enough so that the flux distribution would not be sensitive to the fine structure of the material distribution in the core. The first 13 higher energy group cross sections from Hansen and Roach were used for energies above 1 ev. .

In the energy range below 1 ev., the diffusion length of neutrons is of the same order at the thickness of the fuel plates and hence, self-shielding would be important. To obtain good cross sections for the fuel below 1 ev., it was necessary to account for heterogeneous effects of an individual fuel cell. The procedure that was developed

was to find equivalent homogeneous cross sections in two steps. The first step involved the homogenization of an individual fuel plate, while the second step used the data obtained from the first step to complete the homogenization of the rest of the fuel element. The integral transport theory code THERMOS (Ref. 5.2-4) was used to perform these calculations and to perform whole core radial and axial calculations to obtain core wide thermal cross sections for the fuel. The results of the whole core calculations yielded two sets of thermal cross sections whose energy structure corresponded to the two lowest energy groups contained in a modified 15 group cross section set (2 thermal groups plus 13 epithermal and fast groups). The 15 group space dependent cross sections were then collapsed to three using the EXTERMINATOR-II diffusion theory code (Ref. 5.1-3). Cross sections for the three energy groups shown in Table 5.2-1 were used in the present work.

The beam port and sample assembly void cross sections were calculated by Lukic (Ref. 5.2-5) for the two dimensional model and Emrich for the three-dimensional model. The void effective cross sections were obtained from a diffusion theory model derived by Kennedy (Ref. 5.2-6). Kennedy's model replaces the voids across which neutrons stream without making any collisions by a fictitious pure scattering material.

For control blades, cross sections were obtained by representing the cadmium absorbers by fictitious diffusion

regions having the same net absorption effect as the actual cadmium absorbers. The control blade cross sections in the present work were calculated by Emrich (Ref. 5.2-2).

Up to 80 nuclides were used to represent homogenized elements in various locations. The nuclides were combined to form various compositions at each location. Table 5.2-2 lists the composition numbers, nuclide numbers, and nuclide names used in the three-dimensional computer model.

TABLE 5.2-1

MITR-II Three Group Energy Structure

Fast	3 kev. - ∞ kev.
Epithermal	.4 ev. - 3 kev.
Thermal	0.00025 ev. - .4 ev.

5.2.2 Two-Dimensional Calculation

A two-dimensional R-Z mock-up of the reactor core was used for initial flux calculations and reactivity measurements in the present work. Areas investigated using the two-dimensional model were beam port length optimization, D_2O blister tank flux and reactivity effects, and the effect of changing core housing aluminum alloys. Figure 5.2-1 shows the R-Z core model analyzed by CITATION. Figure 5.2-2 shows the group 3, thermal flux, predicted by CITATION for the base case fully loaded core.

The beam port length optimization resulted in the beam ports extending within 4 inches of the centerline of the reactor. The calculations indicated that the closer to the

TABLE 5.2-2

MATERIAL COMPOSITIONS OF THE VARIOUS REGIONS IN THE
REACTOR USED IN CITATION CALCULATIONS

Composition	Nuclide Number	Nuclide Number	Volume Percent
1	1	U-235	.91%
	2	U-238	.07%
	4	Al	52.82%
	3	H_2O	46.20%
2	32	Al	50.00%
	33	H_2O	50.00%
3	5	U-235	.91%
	6	U-238	.07%
	8	Al	52.82%
	7	H_2O	46.20%
4	9	U-235	.91%
	10	U-238	.07%
	11	Al	52.82%
	12	H_2O	46.20%
5	15	U-235	.91%
	16	U-238	.07%
	13	Al	52.82%
	14	H_2O	46.20%
6	17	U-235	.91%
	18	U-238	.07%
	20	Al	52.82%
	19	H_2O	46.20%
7	21	D_2O	98.60%
	22	Al	.30%
	47	H_2O	.50%
8	34	Pb	100.00%
9	35	Al	85.00%
	36	Cd	15.00%
10	37	Al	100.00%
11	54	Al	100.00%
12	55	D_2O	100.00%

TABLE 5.2-2 (Continued)

Composition	Nuclide Number	Nuclide Name	Volume Percent
13	24	U-235	.91%
	25	U-238	.07%
	26	Al	52.82%
	27	H_2O	46.20%
14	28	U-235	.91%
	29	U-238	.07%
	30	Al	52.82%
	31	H_2O	46.20%
15	39	H_2O	50.00%
	40	Al	50.00%
16	41	C	100.00%
17	42	D_2O	50.00%
	43	Al	50.00%
18	44	H_2O	100.00%
19	45	H_2O	94.5 %
	46	Al	5.5 %
20	47	H_2O	100.00%
21	48	H_2O	100.00%
22	28	U-235	.91%
	29	U-238	.07%
	30	Al	52.82%
	31	H_2O	9.24%
	--	Void	36.96%
23	15	U-235	.91%
	16	U-238	.07%
	13	Al	52.82%
	14	H_2O	9.24%
	--	Void	36.96%
24	51	H_2O	90.00%
	52	Al	10.00%
25	21	D_2O	40.00%
	22	Al	9.00%
	56	Void	51.00%

TABLE 5.2-2 (Continued)

Composition	Nuclide Number	Nuclide Name	Volume Percent
26	21	D_2O	63.00%
	22	Al	5.00%
	56	Void	32.00%
27	22	Al	14.80%
	56	Void	82.20%
28	21	D_2O	46.00%
	22	Al	8.00%
	56	Void	46.00%
29	21	D_2O	30.00%
	22	Al	10.00%
	56	Void	60.00%
30	21	D_2O	52.00%
	22	Al	7.00%
	56	Void	41.00%
31	21	D_2O	60.00%
	22	Al	6.00%
	56	Void	41.00%
32	21	D_2O	78.00%
	22	Al	3.00%
	56	Void	19.00%
33	5	U-235	.91%
	6	U-238	.07%
	8	Al	52.82%
	-	Void	46.20%
34	9	U-235	.91%
	10	U-238	.07%
	11	Al	52.82%
	--	Void	46.20%
35	15	U-235	.91%
	16	U-238	.07%
	13	Al	52.82%
	--	Void	46.20%

TABLE 5.2-2 (Continued)

Composition	Nuclide Number	Nuclide Name	Volume Percent
36	24	U-235	.91%
	25	U-238	.07%
	26	Al	52.82%
	---	Void	46.20%
37	28	U-235	.91%
	29	U-238	.07%
	30	Al	52.82%
	---	Void	46.20%
38	17	U-235	.91%
	18	U-238	.07%
	20	Al	52.82%
	---	Void	46.20%
39	1	U-235	.91%
	2	U-238	.07%
	4	Al	52.82%
	-	Void	46.20%
40	47	H_2O	42.00%
	54	Al	58.00%
41	57	Void	100.00%

FIG. 5.2-I
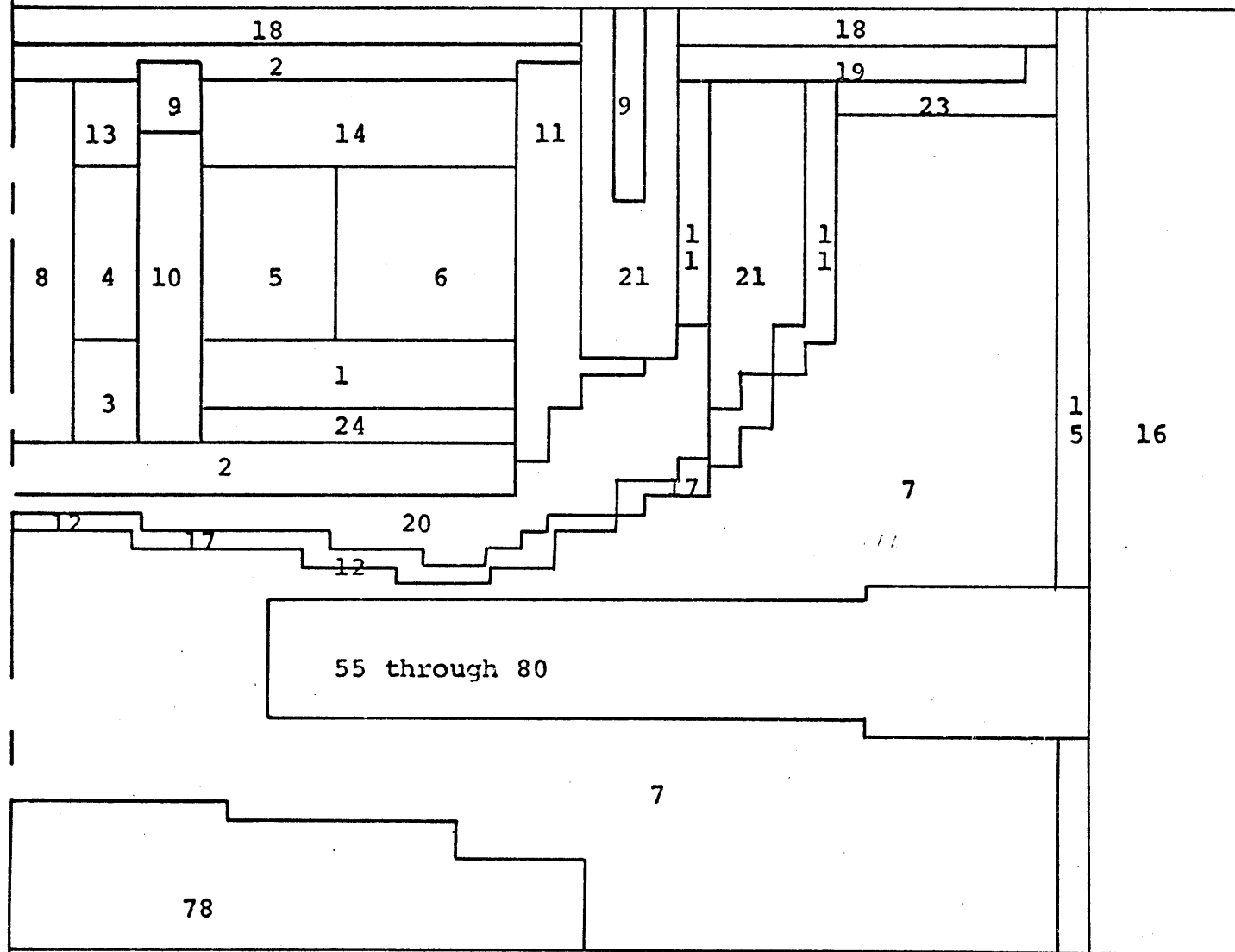
CITATION TWO DIMENSIONAL (R-Z) CORE MODEL   (not to scale)

FIG. 5.2-2

5 MW THERMAL NEUTRON FLUX FROM 2-D CITATION
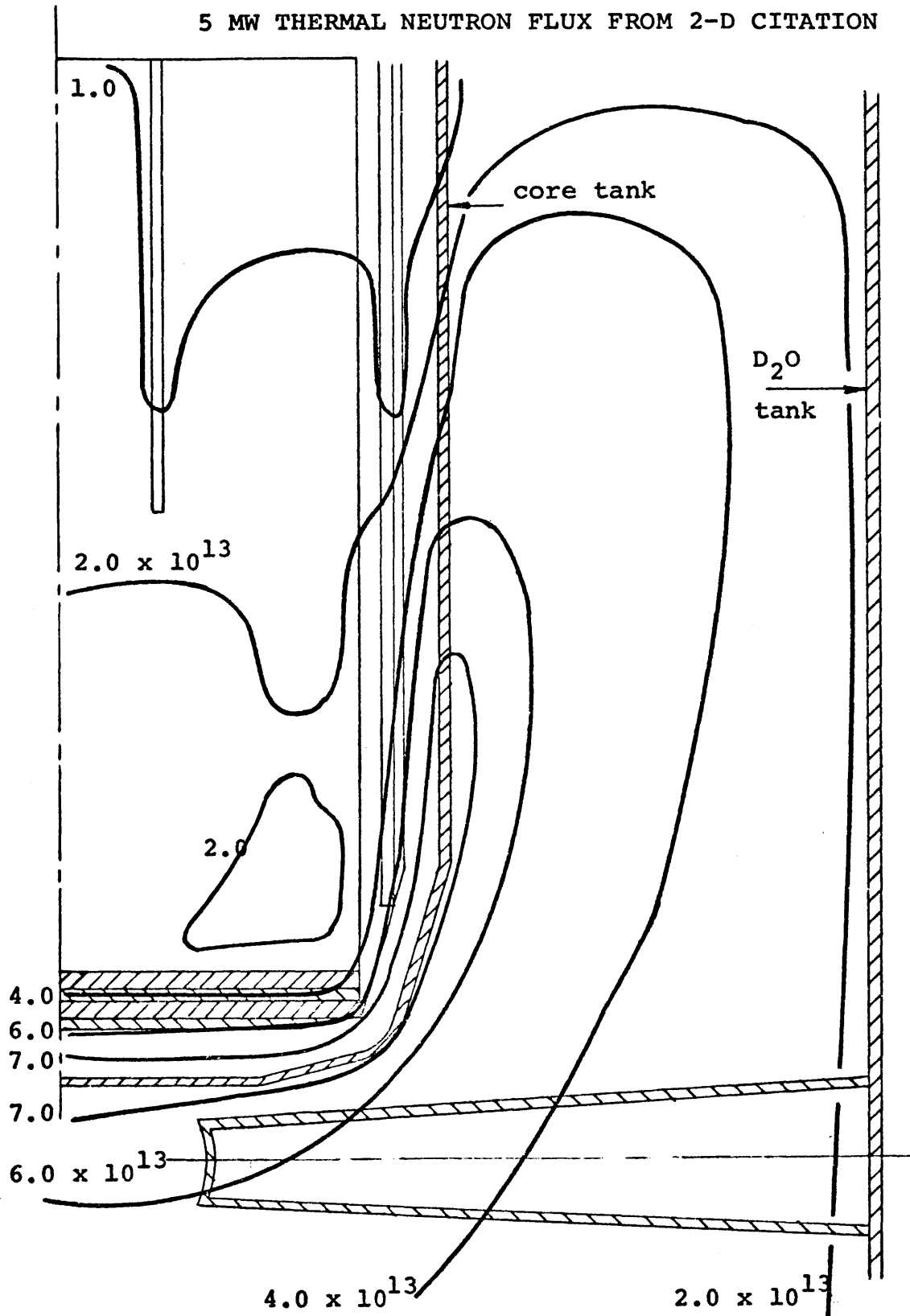
group 3 flux, 26 fuel elements, blades at 8 inches,
fixed cadmium absorber 14 inches from fuel bottom edge

centerline of the core that the beam ports extended
the higher the flux they viewed. If the beam ports extended
to the centerline of the core there would be no scattering
material at the end of the beam port to scatter neutrons
out the beam port. As a result, the beam port ends were
selected to be 4 inches from the centerline of the core,
where 4 inches represented several neutron scattering mean
free paths in D_2O.

D_2O blister tank studies resulted in raising the
height of the D_2O blister tank in order to increase the
neutron flux available to the medical therapy room.
CITATION predicted a reactivity change for opening the
raised shutter of -0.036% $\Delta K/K$ or -46mβ. The actual
measured reactivity worth of emptying the blister tank was
approximately -70 mβ. This is actually good agreement
considering the large mesh spacing at the blister tank
and statistical error induced by determining a small
number from the difference of two large numbers.

The change in the core housing alloy was necessitated
by core housing fabrication problems as described in
Section 3.2.3. The effect of the alloy change was ex-
pected to be a 15% increase in the aluminum absorbtion
cross section. The two-dimensional calculation predicted
that this change would result in a reactivity decrease
of 0.274% $\Delta K/K$ and would decrease the peak thermal flux
at the beam port ends by approximately 0.5%.

The two-dimensional model was useful for modeling

effects which were symmetric about the core centerline.

For a more detailed analysis, the three-dimensional model

was used.

5.2.3 Three-Dimensional CITATION Calculation

Initial cores of the MITR-II were mocked-up using

a three-dimensional (R, θ, Z) approximation to the hex-

agonal cylinder shaped core. Only half of the core was

mocked-up in these calculations since the MITR-II is

approximately symmetric along a line passing through

the center of the core and the center of the regulating

rod. Using half core symmetry allowed additional mesh

points in the R and Z direction up to the limit of the

M.I.T. computer core space. Figure 5.2-3 shows a

schematic representation of an R-θ plane used to mock-up

the reactor core in CITATION. Figure 5.2-4 shows an

example of the core model for R-Z slice through the core

at one of the θ's. The initial model used by this work

was based on the model by Yeung (Ref. 5.2-7).

The CITATION core model divides the active core into

8 sections in the R direction and 11 sections in the θ

direction. The mesh points were set up so that fuel

elements in the A and B rings could be changed easily.

In the axial direction, the active core is divided into

3 main sections: the upper section in which the fuel is

strongly affected by the fixed absorbers and control

FIG. 5.2-3

THREE DIMENSIONAL CITATION MODEL R-Θ REPRESENTATION OF CORE
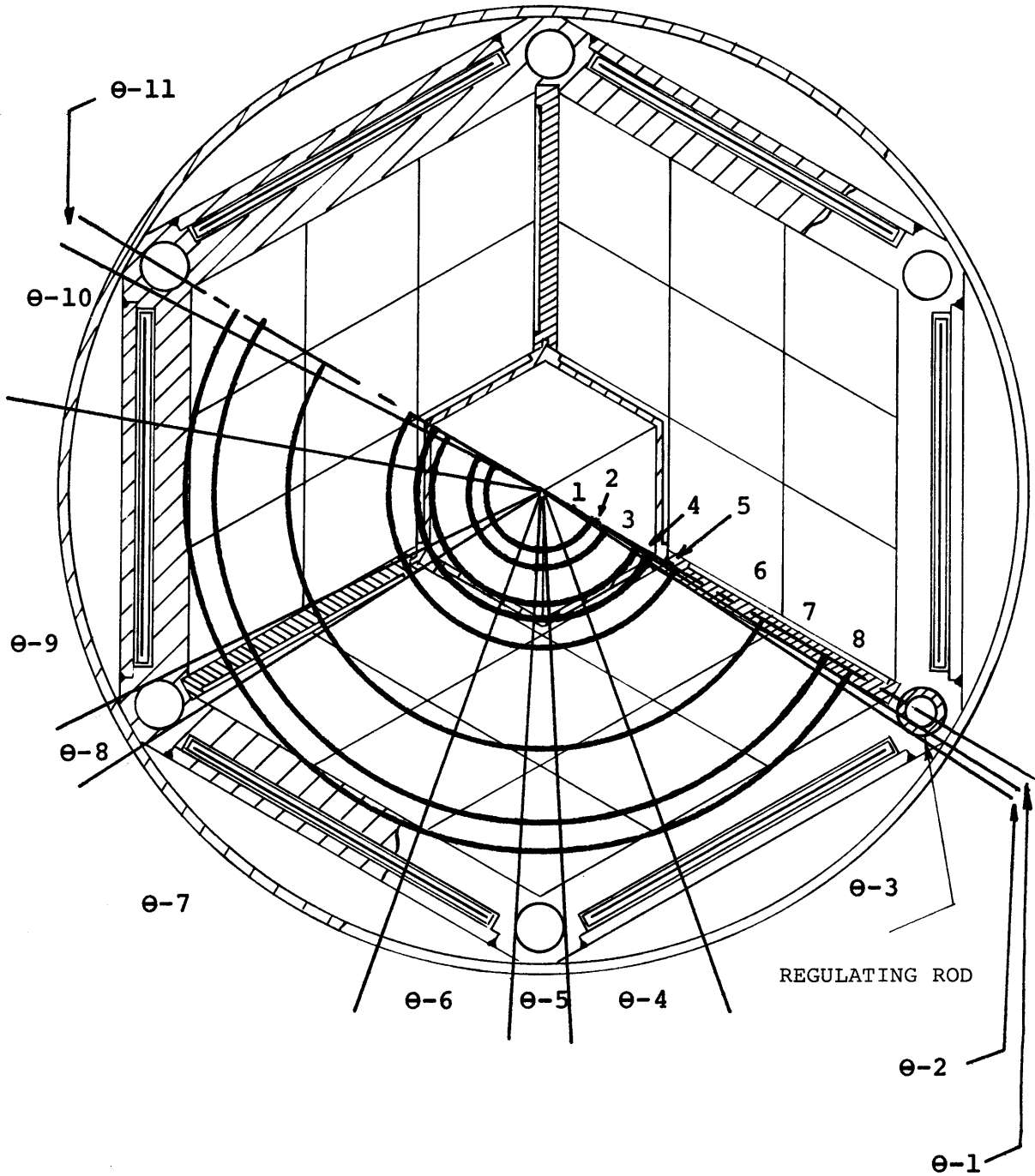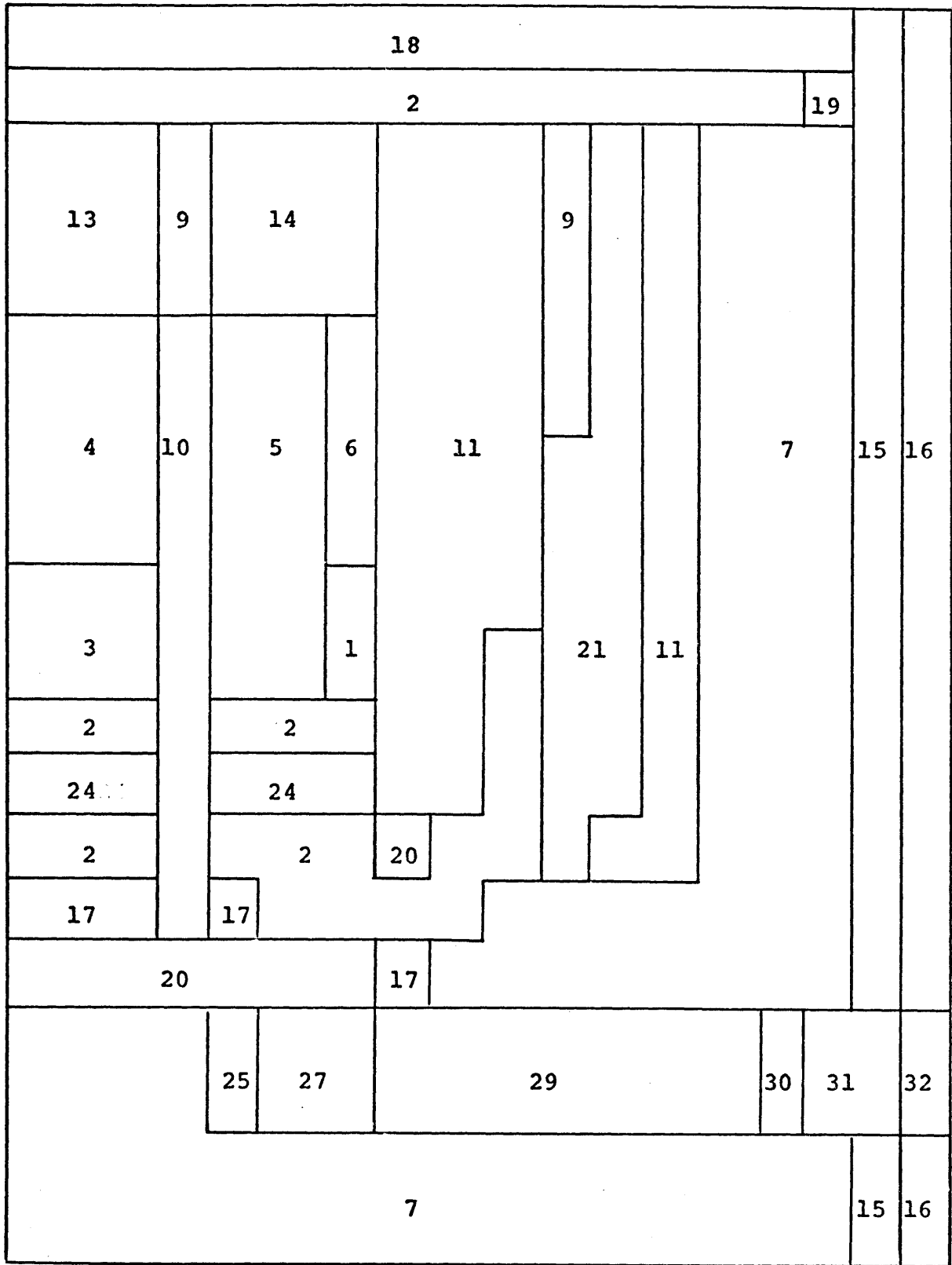
THREE DIMENSIONAL CITATION R-Z PLANE THROUGH θ-5
(not to scale)

FIG. 5.2-4

blades, the lower section in which the fuel is adjacent
to the heavy water reflector and subjected to thermal
flux peaking, and the middle section of the core which
is little affected by either the control blades or the
heavy water reflector.

While it will be shown in this work that CITATION
gives good predictions for neutron flux, power density,
and reactivity changes, CITATION predictions for absolute
K_{eff} missed the actual K_{eff} by 4 to 5% ΔK/K. Table 5.2-3
gives the CITATION prediction and measured K_{eff} for some
early core configurations. The error may have been
caused by error in the cross sections with large amounts
of H_2O present in the core and possibly by an error in
the effective core diameter used in R, Z, θ model.

5.2.3.1 Power Density

One feature of CITATION is that if a total core power
is specified, the code will print out average mesh point
specific volume power densities for each mesh point con-
taining fissile material. The values of these average
power densities, $P(R,Z,\theta)$, are normalized such that the
total integrated power over the core is equal to the
specified total power. Using the local power densities
from CITATION, fuel plate heat fluxes, channel powers, and
fuel plate wall temperatures can be calculated.

The fuel plate heat flux, $(Q/A)_i$, generated in the
i^{th} mesh point volume is calculated by multiplying the

TABLE 5.2-3

MEASURED AND PREDICTED K_{eff} FOR CORE I CONFIGURATIONS

Case	Citation 3-D	Measured	Difference
Original base case 26 elements, fixed at 14", blades at 10"	1.063		
First critical case 21 elements, fixed at 14", blades at 10", 4 waterfilled positions	0.918	0.998	0.08
23 elements, fixed at 12", 3 dummies, blades at 10"	0.969		
23 elements, fixed at 10", 3 dummies, blades at 10"	0.954	0.996	0.042
23 elements, fixed at 10", 3 dummies, blades full in	0.834	0.892	0.058
24 elements, fixed at 12", 2 dummies, blades at 10"	1.000		
24 elements, fixed at 10", 2 dummies, blades at 10"	0.981	1.023	0.042
24 elements, fixed at 10", 2 dummies, blades at 8"	0.959	1.005	0.046

average local power density, $P(R,Z,\theta)$, by the ratio of

unit volume of homogenized core heat transfer area in

a unit volume of core and by a correction factor that

converts the watts/cm^3 obtained from CITATION to BTU/hr-ft^3.

For fuel elements in the first core of MITR-II the

following holds:

$$(Q/A)_i \text{ BTU/hr-ft}^2 = 833 \ P(R,Z,\theta)_i \quad , \quad (5.2-1)$$

where,

$(Q/A)_i$ is the fuel plate heat flux (off one side of the fuel plate) for the ith mesh point,

$P(R,Z,\theta)_i$ is the average power density in the ith mesh point in watts/cm^3.

The ratio of the local power density to the core

average power density is equal to the product $F_r F_a$

where:

F_r is the radial peaking factor, the ratio of the power produced in a fuel plate to the power produced in the average fuel plate,

F_a is the axial peaking factor, the ratio of the power density at a local spot on a plate to the average power density in that plate.

The value of $F_r F_a$ for the ith mesh point is evaluated as

follows:

$$(F_r F_a)_i = \frac{P(R,Z,\theta)_i}{\displaystyle\sum_{j=1}^{m} \frac{P(R,Z,\theta)_j \ V_q(R,Z,\theta)_j}{V(R,Z,\theta)_j}} \quad , \quad (5.2-2)$$

where,

$V(R,Z,\theta)_j$ is the volume of the jth mesh point,

m is the total number of fueled mesh points.

The denominator of Eq. 5.2-2 which represents the core average power density may also be determined in the following manner:

$$P(R,Z,\theta)_{AVE} = \sum_{j=1}^{M} \frac{P(R,Z,\theta)_j \ V(R,Z,\theta)_j}{V(R,Z,\ )_j}$$

$$= \frac{Total\ Core\ Power}{Total\ Fueled\ Volume\ in\ CITATION\ Model} \cdot$$

$$(5.2-3)$$

Combining Eqs. 5.2-1 and 5.2-3 yields the core average fuel plate heat flux:

$$(Q/A)_{AVE} \ BTU/hr\text{-}ft^2 = 833 \ P(R,Z,\theta)_{AVE} \ , \qquad (5.2-4)$$

where,

$P(R,Z,\theta)$ is in units of watts/cm^3.

PC_k, the power deposited in a coolant channel between two fuel plates, can be calculated by assuming that all of the heat from the two fuel plate sides facing a channel is deposited in the channel. The following equation represents the heat deposited in a channel K:

$$PC_k = 2 \int_{0}^{L} W \ Q/A(z) \ dz \ , \qquad (5.2-5)$$

where,

W is the fueled width of the fuel plate,

Q/A(z) is the area heat flux from a fuel plate side as a function of Z,

L is the fueled height of the fuel plate.

Note that the factor 2 is required because there are 2 fuel plate sides per channel. For CITATION results the following equation replaces Eq. 5.2-5:

$$PC_k = 2W \sum_{i=1}^{n} (Q/A)_i \, z_i \quad , \qquad (5.2\text{-}6)$$

where,

$(Q/A)_i$ is the fuel plate area heat flux for constant R and θ corresponding to the channel of interest,

z_i is the height in the Z direction of the ith mesh point,

n is the number of fueled mesh point volumes in the Z direction for a constant R and θ.

The individual value of F_r for the Kth channel can be obtained by the following equations:

$$(F_r)_k = \frac{PC_k}{2W \, (Q/A)_{AVE} \sum_{i=1}^{n} z_i} \quad , \qquad (5.2\text{-}7)$$

$$\text{or} \quad (F_r)_k = \frac{\sum_{i=1}^{n} (Q/A)_i \, z_i}{(Q/A)_{AVE} \sum_{i=1}^{n} z_i} \quad . \qquad (5.2\text{-}8)$$

The value of F_a for the ith mesh point in the Kth channel is given by the following equation:

$$(F_a)_{ik} = \frac{(Q/A)_i}{\dfrac{\sum\limits_{i=1}^{n} (Q/A)_i z_i}{\sum\limits_{i=1}^{n} z_i}} \quad . \qquad (5.2-9)$$

The fuel plate wall temperature is calculated by using the following general equations:

$$Q/A(z) = \eta h \left(T_W(z) - T_f(z) \right) , \qquad (5.2-10)$$

$$2 \int_0^z W \, Q/A(z) \, dz = mC_p (T_f(z) - T_o) , \qquad (5.2-11)$$

where,

$Q/A(z)$ is the plate heat flux as a function of z,

η is the clad fin effectiveness,

$T_W(z)$ is the wall temperature as a function of z,

$T_f(z)$ is the fluid temperature as a function of z,

W is the constant fuel plate width,

m is the mass flow rate,

C_p is the fluid heat capacity,

T_o is the fluid inlet temperature.

Equations 5.2-10 and 5.2-11 can be combined to give:

$$T_W(z) - T_o = \frac{Q/A(z)}{\eta h} + \frac{2W}{mC_p} \int_0^z Q/A\,(z)dz. $$

$$(5.2-12)$$

Knowing the values of η, h, W, m, C_p, and T_o, the fuel plate wall temperature, $T_w(z)$, can be calculated at the mesh point interfaces using the CITATION results by the following equation:

$$T_w(Z_n) - T_o = \frac{(Q/A)_i}{\eta h} + \frac{2W}{mC_p} \sum_{i=1}^{n} (Q/A)_i Z_i \qquad (5.2-13)$$

where,

n is the number of mesh points from the bottom of the fueled region,

Z_n is the axial height that corresponds to n mesh points from the bottom of the fueled region.

By utilizing Eqs. 5.2-1, 5.2-6, and 5.2-13, the safety limits and limiting conditions for operation as explained and evaluated in Sections 7.2 and 7.3 are obtained using the three-dimensional results of CITATION.

Power density distributions for Core I of the MITR-II were obtained using a three-dimensional CITATION calculation. Core I had solid aluminum dummies in core positions A-1, B-2, and B-8. The bottom of the fixed absorber was 10 inches from the bottom of the fuel and the shim bank was at 8 inches for these calculations. Figure 5.2-5 shows the axial power distribution for an outside plate in element C-8. CITATION predicts that this will be the hottest fuel plate.

Figure 5.2-6 shows the axial power distribution for a plate next to a solid dummy in A-2. Note the large power spike at the bottom of the element and the power

depression at the top because of the fixed absorber.

Figure 5.2-7 shows the axial power distribution for an interior plate in B-5. B-5 has the highest total element power density of any element in the Core I configuration.

Figures 5.2-8, 5.2-9, and 5.2-10 show power density distributions on respective horizontal planes through the core at 0.53, 4.05, and 13 inches from the bottom of the fuel (Core I CITATION predictions for fuel element powers are shown in Fig. 6.4-1).

5.2.3.2 Flux Distributions

CITATION prints out the neutron flux for each of the three energy groups at each mesh point. Figure 5.2-11 shows the predicted thermal neutron flux for a vertical cross section through Core I of the MITR-II. A detail listing of the neutron flux at each mesh point for each energy group is listed in Appendix B.

Comparisons between CITATION flux predictions and copper wire data are found in Section 5.4.

5.2.3.3 Sensitivity to Shim Bank Height

The power distribution in the core changes with variations in the shim bank height. Figures 5.2-12 and 5.2-13 illustrate two potential effects of concern from changing the shim bank height. For a plate in the C-ring near the edge of the core, raising the shim bank increases the total power produced by the plate (F_r increases) but decreases the actual power peak itself (F_a decreases).

FIG. 5.2-5

CITATION RELATIVE POWER DISTRIBUTION
ON PLATE 1 OF ELEMENT IN C-8

(Core I, blades at 8 inches)
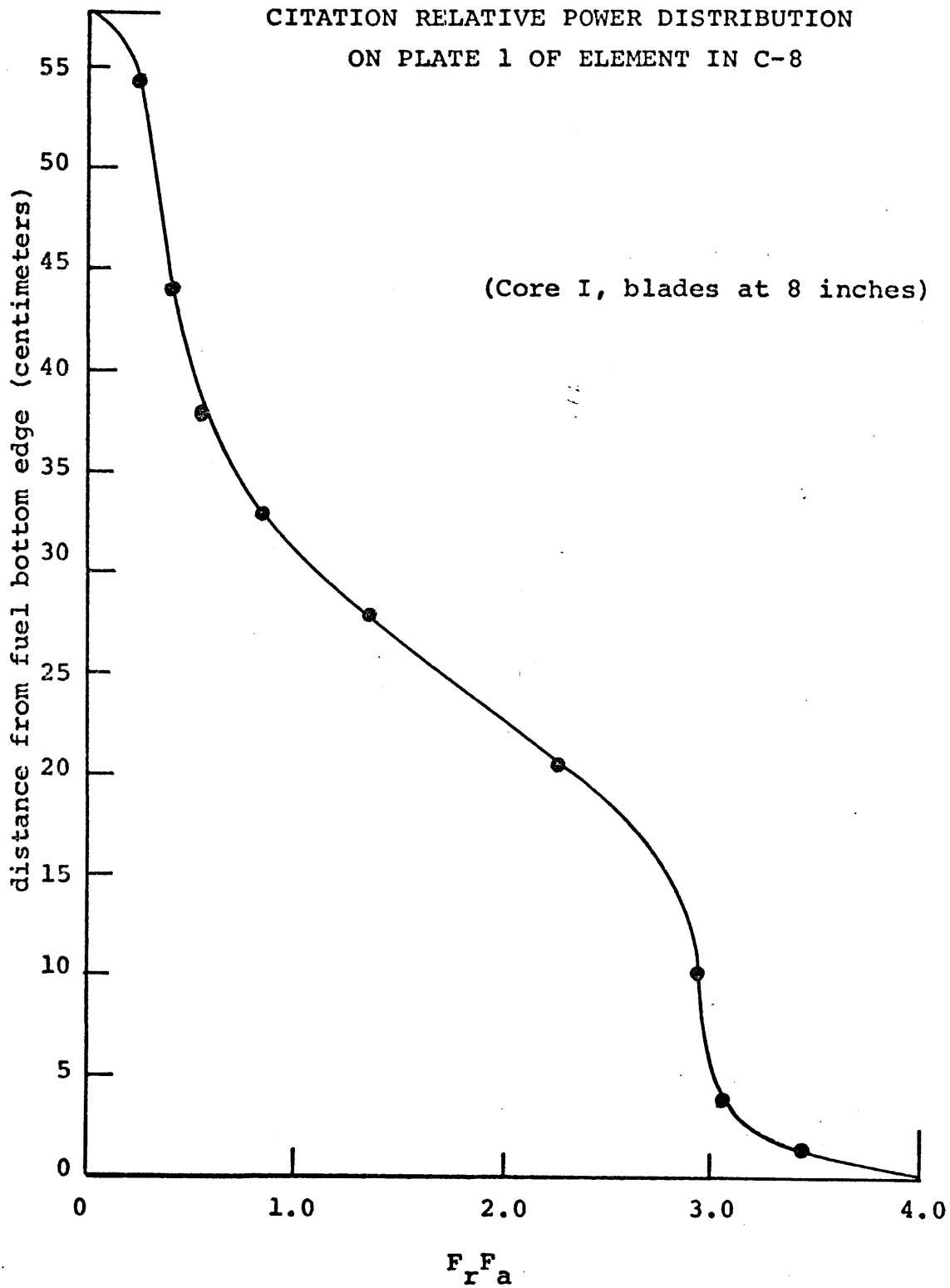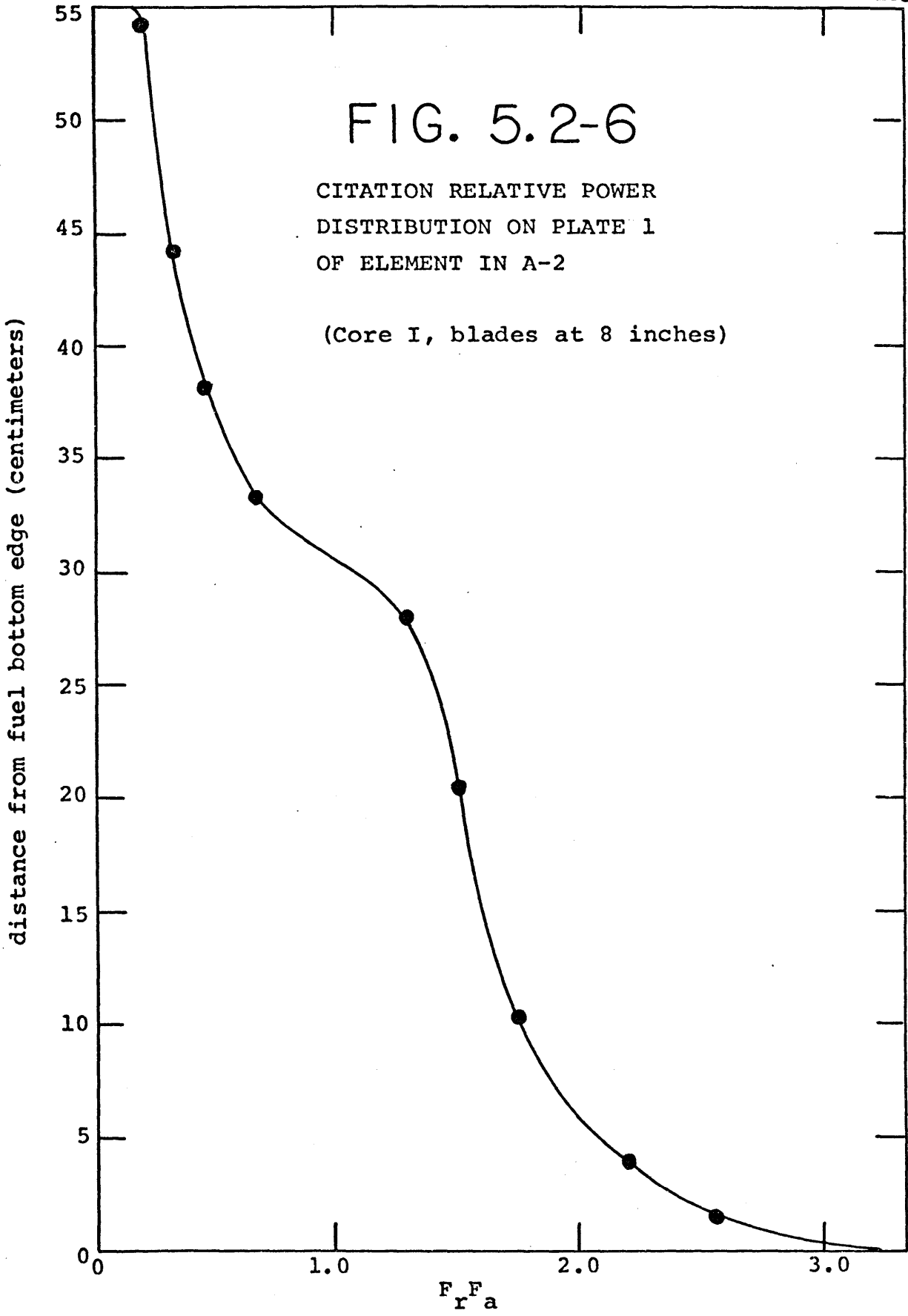
FIG. 5.2-6

CITATION RELATIVE POWER
DISTRIBUTION ON PLATE 1
OF ELEMENT IN A-2

(Core I, blades at 8 inches)

FIG. 5.2-7

CITATION RELATIVE POWER
DISTRIBUTION ON CENTRAL
PLATE IN ELEMENT B-5

(Core I, blades at 8 inches)
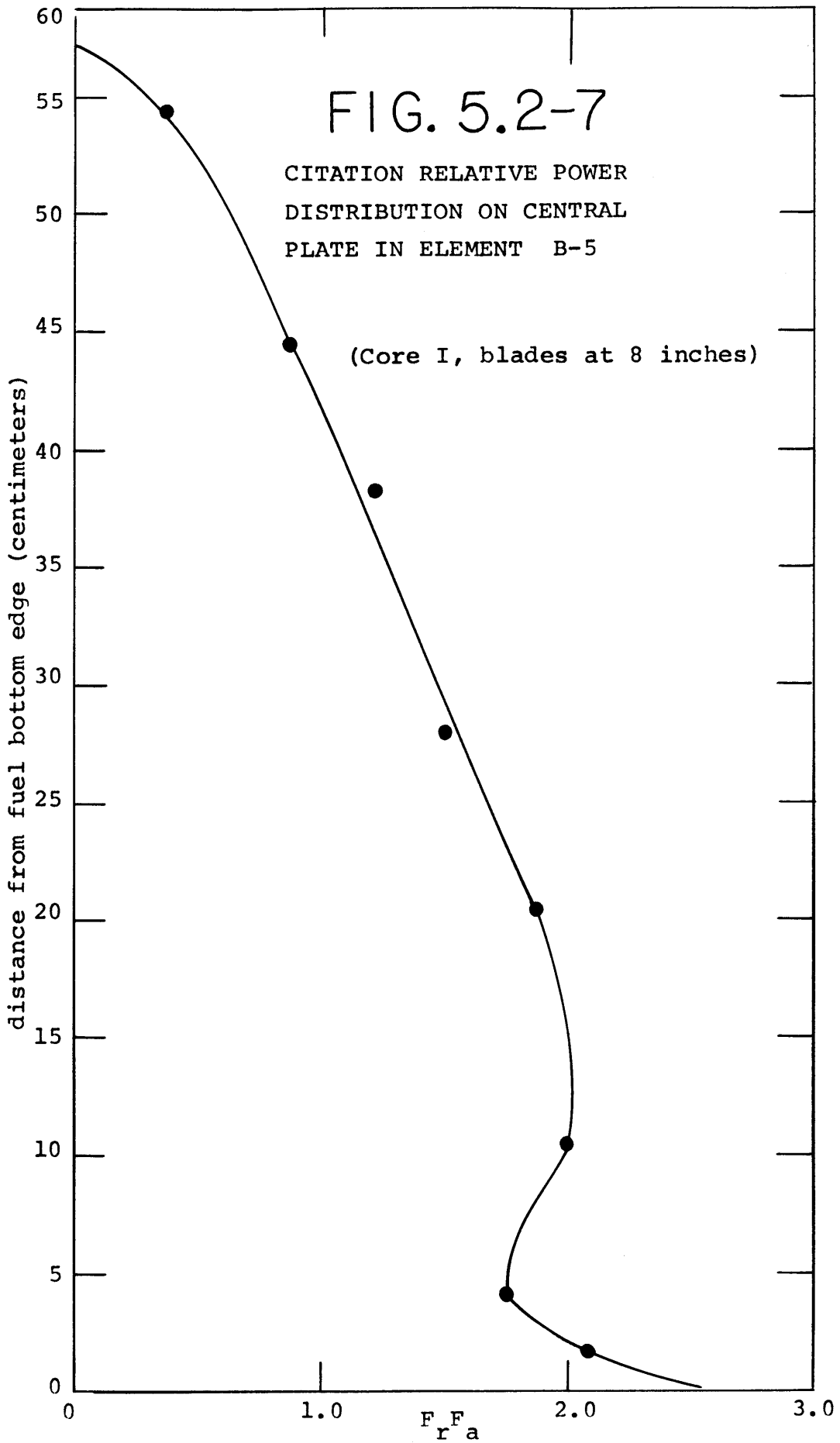
FIG. 5.2-8

CITATION RELATIVE POWER DISTRIBUTION FOR HORIZONTAL LAYER 11

(horizontal layer 11 is 0.53 inches from bottom of fuel)
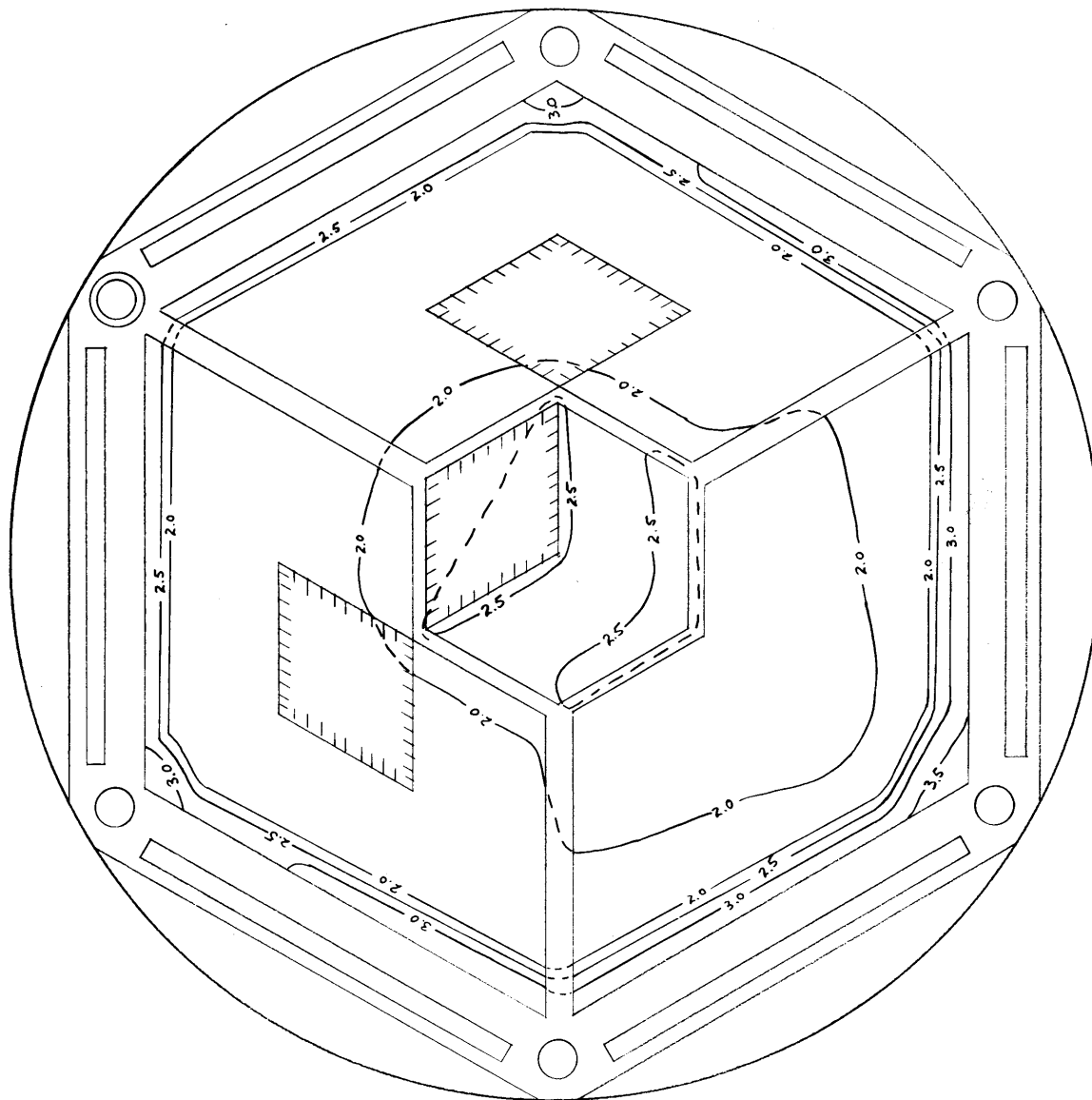
contour lines are constant values of $F_r F_a$

FIG. 5.2-9

CITATION RELATIVE POWER DISTRIBUTION FOR HORIZONTAL LAYER **9**

(horizontal layer 9 is 4.05 inches from bottom of fuel)
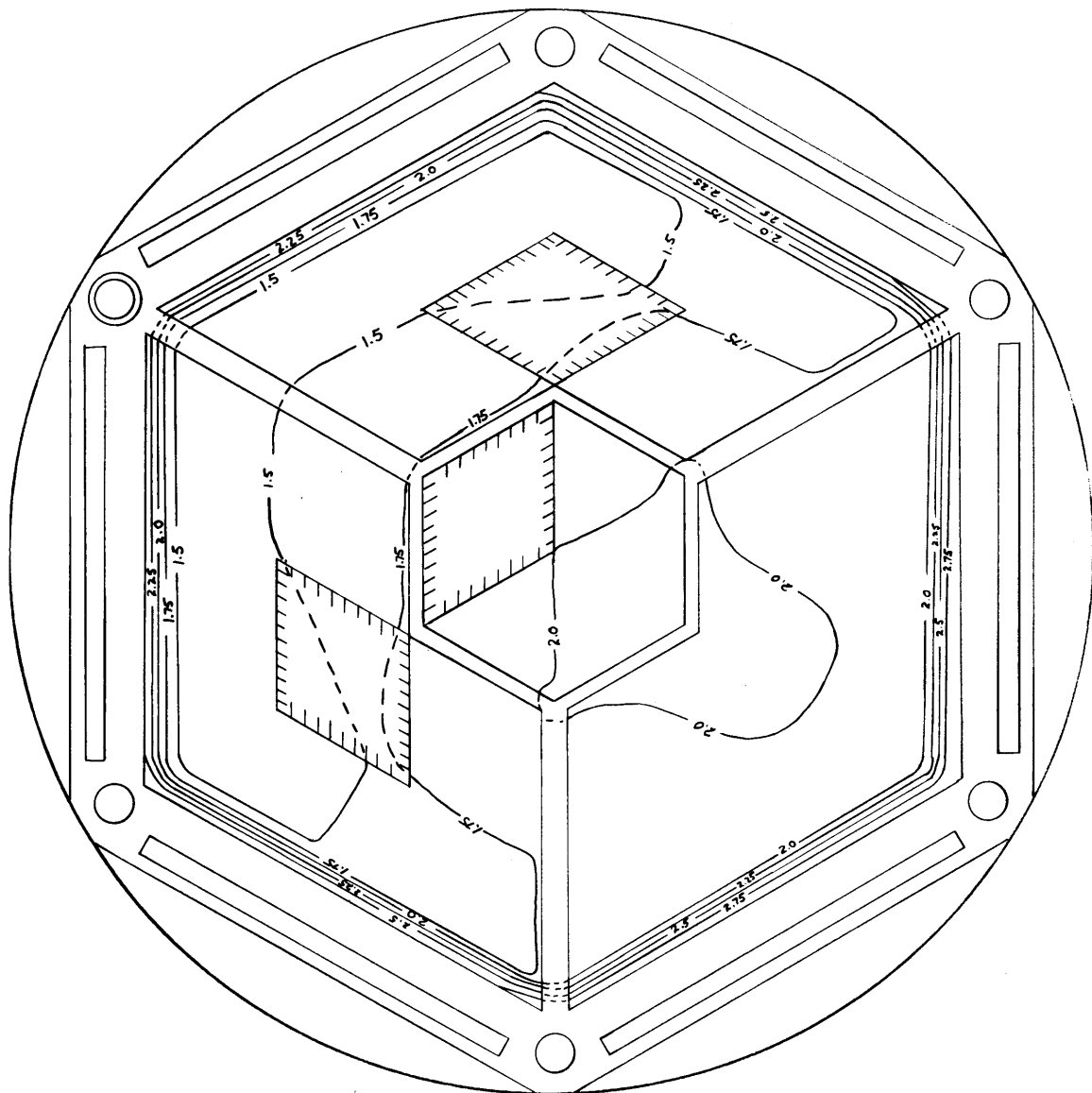
contour lines are constant values of $F_r F_a$

FIG. 5.2-10

CITATION RELATIVE POWER DISTRIBUTION FOR HORIZONTAL LAYER 6

(horizontal layer 6 is 13.0 inches from bottom of fuel)

contour lines are constant values of $F_r F_a$

FIG. 5.2-11

5 MW THERMAL FLUX FROM 3-D CITATION

core tank

D_2O tank

1.0

2.0 x 10^{13}

4.0 x 10^{13}

6.0
8.0
10.0

10.0 x 10^{13}

8.0 x 10^{13} 6.0   4.0   2.0 x 10^{13}
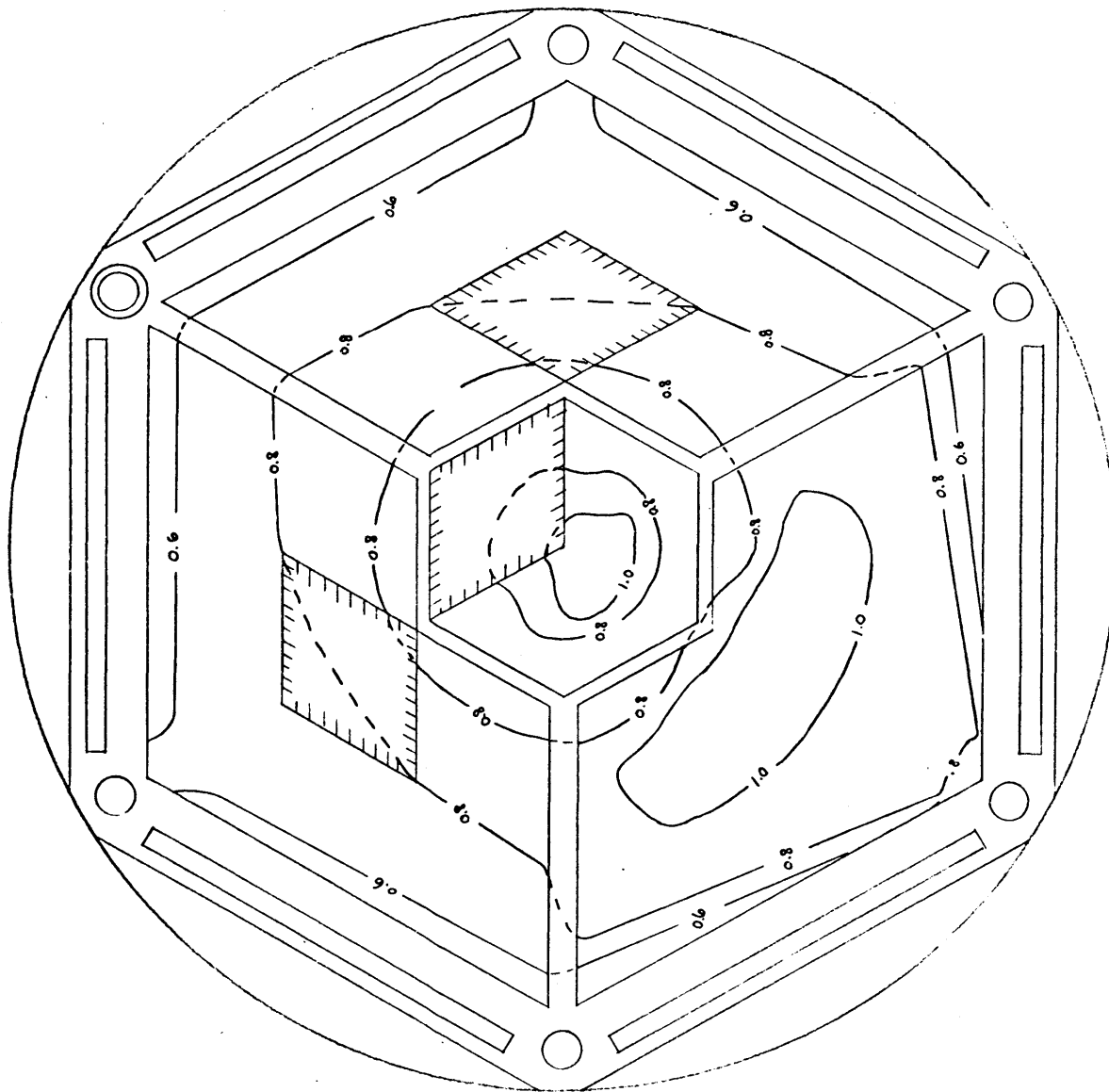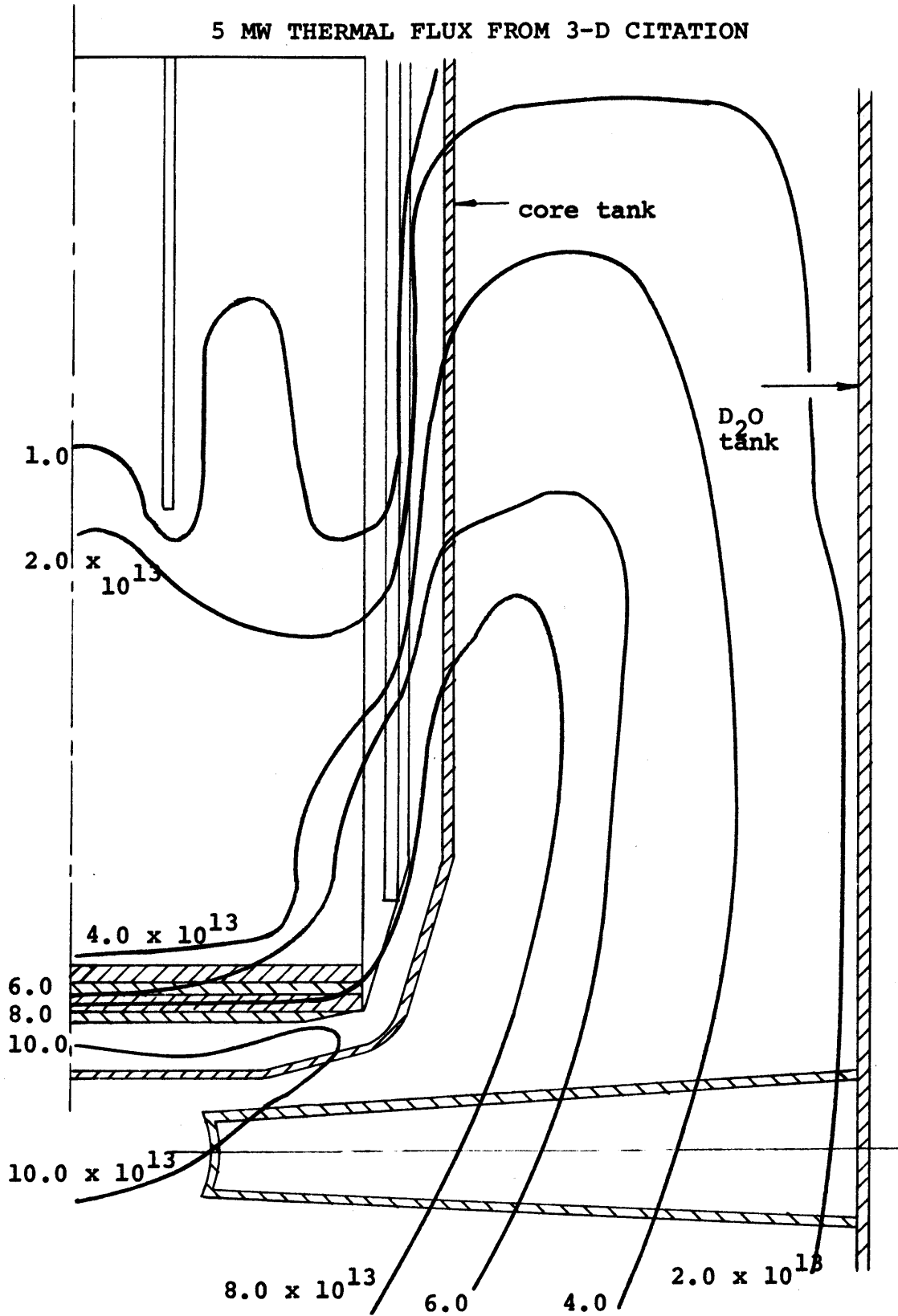
group 3 flux, Core I loading, blades at 8 inches,
fixed cadmium absorbers 10 inches from fuel bottom edge

This effect can be seen in Fig. 5.2-12. For a plate in the A-ring near the center of the core, raising the shim bank decreases the total power produced by the plate (F_r decreases) because more power is bein produced by C-ring elements. If, however, the element in the center of the core has a power peak at a z position above the bottom edge of the core, as is the case with the initially designed ICSA, then the axial peak will occur at a higher position on the plate as the shim bank is raised. This effect can be seen on Fig. 5.2-13.

Chapter 7 covers safety limits and operating limits for the MITR-II. It is shown in Chapter 7 that the safety limit is proportional to the total power produced on a plate. The greater the power produced on a plate, the closer the approach to the safety limit. If a factor, SLF, represents the safety limit, then the higher the value of the SLF is, the closer one is to the safety limit. It is also shown in Chapter 7 that the limiting condition for operation is proportional to the peak power generated and its axial location. If an equation, OLE, represents the limiting condition for operation, then the higher the value of the OLE is, the higher one is to the limiting condition for operation. The SLF and OLE are defined and evaluated in Chapter 7. Table 5.2-4 shows that for an element in the C-ring, raising the shim bank increases the value of the SLF and decreases the value of the OLE (compare case 3 and 5). The same table also shows that for an element in the A-ring with its peak above the bottom edge, raising

FIG. 5.2-12

CITATION POWER DENSITY PREDICTION ON
PLATE 1 IN ELEMENT IN POSITION C-8

(plate 1 is next to core housing)
(Core I, evaluated for two blade heights)
(power = 5.0 MW)
(power density is for homogenized core)

blades at 10
inches

blades at 8 inches

distance from fuel bottom edge (centimeters)

power density (watts/cm^3)
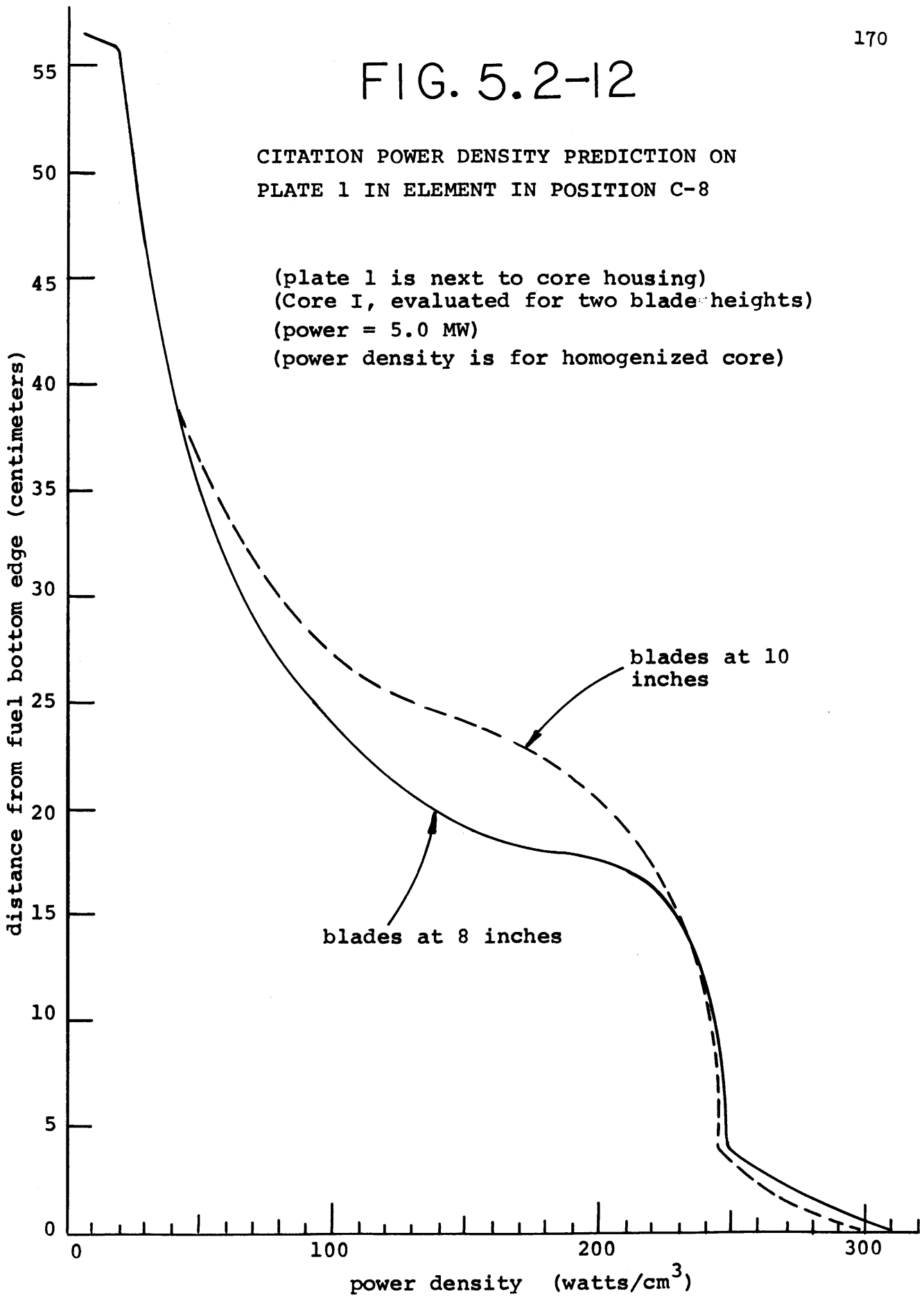
FIG. 5.2-13

CITATION POWER DENSITY PREDICTION FOR
PLATE 1 IN ELEMENT IN POSITION A-2
WHERE PLATE 1 IS NEXT TO THE ICSA IN A-1

(Core I, ICSA in position A-1 instead
of solid dummy element)

(power density is for homogenized core)
(power = 5.0 MW)

blades at 8
inches

blades at 10 inches

distance from fuel bottom edge (centimeters)

power density (watts/cm^3)
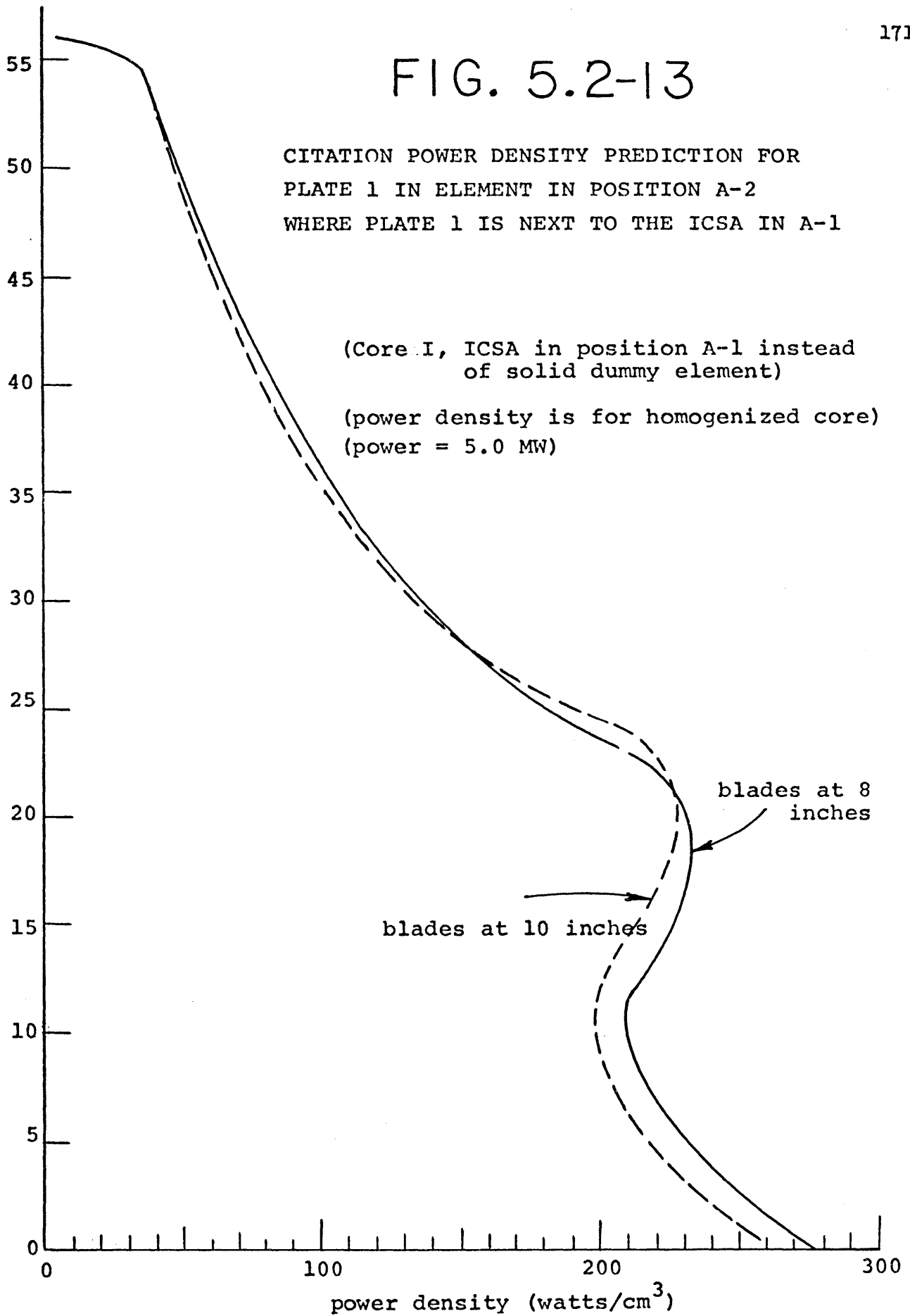
TABLE 5.2-4

EFFECT OF ICSA AND BLADE HEIGHT ON INITIAL
CORE FACTOR EVALUATION ESTIMATES

Case	Core Configuration	Channel Location	SLF*	OLE*
1	23 elements, 3 dummies, blades at 10", ICSA	A-2 next to ICSA	2.74	4.05
2	24 elements, 2 dummies, blades at 10", ICSA	A-2 next to ICSA	2.68	3.92
3	24 elements, 2 dummies, blades at 10", ICSA	C-8 next to outer edge	2.41	3.63
4	24 elements, 2 dummies, blades at 8", ICSA	A-2 next to ICSA	2.78	3.77
5	24 elements, 2 dummies, blades at 8", ICSA	C-8 next to outer edge	2.21	3.80

* These factors are derived and explained in Chapter 7.

the shim bank decreases the value of the SLF and increases

the value of the OLE (compare cases 2 and 4). For an

A-ring element which only has its peak at the bottom,

raising the shim bank would decrease the total power pro-

duced by the plate and decrease the power at the peak.

For this case, raising the shim bank decreases the value of

the SLF and can either increase or decrease the value of the

OLE depending upon the new axial distribution in the plate.

This shift with blade height will not be a problem

for Core I because there is adequate margin in the safety

limit for elements in the C-ring and adequate margin in

the A-ring for the limiting condition for operation with

the ICSA removed.

5.2.3.4 Sensitivity to the Number of Solid Dummies

For Core I, CITATION power density data can be used

to show that the fewer the number of solid dummies, the

more slightly favorable the core in terms of the safety

limit and limiting condition for operation. Comparing

cases 1 and 2 on Table 5.2-4 confirms this conclusion.

This trend occurs because the core power is being averaged

over more elements and there is more heat transfer area

available. There is a limit as to how many solid dummies

could be replaced by fuel elements (neglecting the addi-

tional problem of shutdown reactivity margin) before this

trend would reverse because lowering the shim bank to com-

pensate for the reactivity addition of the fuel element

would begin to cause excessive peaking in the lower core.

5.2.3.5 Sensitivity to the Incore Sample Assembly (ICSA)

Figure 5.2-13 shows the axial power distribution
in the fuel plate next to the ICSA as predicted by CITATION.
Insertion of the originally designed ICSA into the A-ring
causes excessive power peaking in surrounding elements.
As is discussed in Chapter 7, the unacceptable power peaking
caused by the ICSA as predicted by CITATION and confirmed
by the experimental measurements resulted in the originally
designed ICSA being removed for Core I of the MITR-II.

5.3 Experimental Measurement of Power Density

The power distribution in the MITR-II core was
experimentally measured by gamma scanning of removable
fuel plates in an MITR-II fuel element and is described
in this section. Before operation above 1 KW was per-
mitted, low power testing was required in order to
determine initial power peaking and to measure the rela-
tive core power distribution of the cold and unpoisoned
Core I of the MITR-II.

5.3.1 General Description of Gamma Scanning

The gamma scanner design was initially developed by
Donald Labbe, Gamma Scanner for MITR-II Fuel Plates
(Ref. 5.3-1). Some modification and initial construction
was performed by Steven Grill, Construction of the Gamma
Scanner for MITR-II Fuel Plates (Ref. 5.3-2).

The fission product density in a fuel element is directly proportional to the power density history of the fuel element. The purpose of the gamma scanner is to measure the fission product gamma rays emitted from a specific volume of a fuel plate while shielding out the gamma rays from the remainder of the fuel plate. Comparison of the count rates from different volumes of the fuel plate will show the relative power distribution. Appropriate corrections must be made for background, backscatter radiation, decay times, edge effects and previous irradiation history of the fuel plate. A fuel element was constructed with removable plates so that it could be irradiated in various locations throughout the core and then removed and scanned after each irradiation. From the scanning data, relative core power maps were developed for the first core loading.

5.3.2 Scanner Apparatus

The gamma scanner apparatus consists of a lathe table, collimator, lead shielding, electronics, removable plate element, and transfer cask.

5.3.2.1 Removable Plate Element

A special fuel element was constructed for use in the gamma scanning experiment. The element was constructed by Gulf United Nuclear Fuels and was labeled 4M41. The element is shown in Fig. 5.3-1 and is identical with a

FIG. 5.3-1

REMOVABLE PLATE FUEL ELEMENT

standard fuel element except that five fuel plates and one end nozzle are removable.

The removable plates were not swaged into the element as were the remaining ten plates. The five plates were free to slide out of the element when the removable end nozzle was unscrewed. The removable plate element was only loaded in core for low power testing with the main coolant pumps off because of the element's decreased structural integrity caused by the loose plates. The element was constructed to tight tolerances in order to simulate channel dimensions in a standard element. Alcohol was required to lubricate any plate to be removed in order to prevent galling of the aluminum.

Each of the removable plates was radiographed in order to determine the fuel density distribution in each fuel plate. Fuel densities are measured by making densitometer readings on the radiographs. Densitometer maps for each of the five removable plates are shown in Figs. 5.3-2 through 5.3-6. Lower densitometer readings indicate high fuel concentrations. Densitometer values for nominal fuel density vary because of radiograph development techniques and must be normalized against a standard for each radiograph.

3" 1/4 typ

typ

1/4"

2"

GP-64

139	133	131	130	121	117	112	107	107	105	103	107
140	139	121	126	117	117	111	103	101	100	96	102
141	136	127	125	122	121	111	101	104	101	99	104
137	142	129	126	120	119	110	105	103	98	101	99
142	139	134	127	121	125	110	107	101	101	99	96
144	137	132	129	118	118	112	105	100	101	94	95
142	141	137	130	121	119	110	105	99	96	99	97
142	133	130	124	119	115	109	107	105	106	101	105

1"

108	111	114	111
110	109	116	109
118	113	113	115
113	111	113	111
113	113	110	112
104	109	112	114
111	107	109	110
114	115	117	114

←CL plate

(nominal density
of fuel would
give reading ∼104,
density decreases
as reading
increases)

3"

111	110	114	112	115	112	115	119	123	131	132	140
108	112	113	111	115	112	115	120	119	124	132	127
107	107	109	115	112	114	116	118	115	124	124	131
107	111	112	118	116	119	114	118	122	126	125	126
107	110	110	117	119	114	116	115	123	129	125	128
106	104	112	110	118	118	118	118	122	119	128	125
110	109	112	110	118	116	119	123	121	125	127	134
111	113	112	116	120	118	120	122	121	125	126	135

(0,0)

FIG. 5.3-2   DENSITOMETER MAP OF PLATE 1 IN REMOVABLE
PLATE ELEMENT   (plate 1 in GAMSCAN)

3"

1/4 typ

typ

1/4"

3"

GR-05

136	129	124	121	116	107	106	104	101	100	105	107
137	126	126	122	114	109	104	101	97	98	100	102
133	128	124	117	109	105	101	98	97	100	98	99
127	120	128	115	112	105	102	97	97	97	94	100
130	118	122	110	109	102	99	96	95	96	95	97
124	120	118	113	108	101	101	97	94	96	96	99
123	123	115	110	109	102	102	100	99	99	101	99
120	120	116	114	109	103	105	104	99	101	102	105

1"

108	104	109	102
106	104	100	107
107	104	105	104
102	101	102	103
99	100	104	104
103	101	100	102
103	99	106	102
108	107	108	109

←CL plate

(nominal density of fuel would give reading~104, density decreases as reading increases)

3"

109	107	107	104	105	106	108	114	115	111	114	126
107	105	105	103	107	103	108	110	111	111	113	118
108	104	101	105	108	105	103	108	110	111	117	119
104	106	103	100	100	105	105	106	109	110	113	116
103	105	104	99	104	106	102	109	107	109	109	116
106	105	104	101	102	105	106	102	106	109	111	118
105	106	105	101	102	107	112	110	110	116	112	116
110	113	107	106	105	105	111	115	117	117	120	122

(0,0)

FIG. 5.3-3   DENSITOMETER MAP OF PLATE 4 IN REMOVABLE
PLATE ELEMENT   (plate 2 in GAMSCAN)

typ

GT-124

3"

1/4 typ

1/4"

2"

127	123	116	114	110	113	110	107	105	108	106	104
124	117	115	111	107	109	109	104	101	104	106	104
127	113	115	109	107	107	105	101	98	105	104	105
133	115	114	111	106	106	104	100	101	102	104	104
125	116	115	111	107	105	104	101	102	105	104	105
132	121	118	115	107	103	103	105	99	104	102	106
132	124	123	117	112	109	107	101	105	107	108	109
137	126	126	125	119	115	113	112	106	113	110	112

1"

110	109	109	108
107	106	105	109
104	102	104	104
103	104	104	103
102	103	103	103
101	104	106	104
106	107	105	107
111	113	112	111

CL plate

(nominal density
of fuel would
give reading ~104,
density decreases
as reading
increases)

3"

102	104	106	109	110	115	119	121	125	130	127	135
102	103	100	102	104	108	112	118	122	126	133	131
104	100	102	103	103	106	112	116	124	126	128	128
104	103	100	98	104	104	107	115	120	127	122	124
100	101	99	99	101	104	111	114	119	122	125	132
102	101	102	101	101	106	113	115	126	123	125	138
100	102	101	103	103	108	116	115	122	126	129	140
110	110	109	106	110	111	116	118	128	131	134	138

(0,0)

FIG. 5.3-4   DENSITOMETER MAP OF PLATE 8 IN REMOVABLE
PLATE ELEMENT   (plate 3 in GAMSCAN)

3" 1/4 typ

typ

1/4"

2"

GT-118

125	121	118	116	116	113	116	113	113	109	112	111
117	118	114	110	113	104	109	108	109	105	111	115
118	115	113	113	105	105	109	106	104	102	105	105
122	121	113	115	108	107	104	103	103	103	104	104
124	115	115	108	109	104	106	103	102	104	107	105
126	118	113	112	109	107	102	101	103	102	104	106
119	119	115	110	110	105	108	102	100	102	102	102
125	121	120	109	117	107	107	106	105	102	108	108

1"

110	109	110	110
107	107	108	106
103	105	104	104
102	102	101	103
101	103	103	102
104	107	104	101
103	105	102	100
106	106	103	103

← CL plate

(nominal density
of fuel would
give reading ~104,
density decreases
as reading
increases)

3"

111	108	105	109	107	113	115	117	126	124	133	131
105	103	104	102	102	105	107	115	119	127	136	127
104	98	100	98	98	102	104	110	117	126	131	122
100	102	99	93	101	101	100	109	117	125	124	130
104	99	100	98	102	101	104	110	115	125	124	135
106	100	104	99	104	103	107	112	120	128	130	137
108	102	103	101	101	103	107	112	122	128	128	134
109	105	103	103	108	108	113	116	124	126	133	138

(0,0)

FIG. 5.3-5   DENSITOMETER MAP OF PLATE 10 IN REMOVABLE
PLATE ELEMENT   (plate 4 in GAMSCAN)

GT-17 (3" wide, 1/4" typ, 2" tall)

126	127	122	120	115	114	107	106	107	103	106	107
124	125	119	115	110	107	102	100	101	99	99	100
125	123	121	115	111	103	98	101	98	99	96	100
127	125	122	115	111	106	104	103	98	96	97	97
128	127	123	117	113	107	105	102	98	100	98	102
124	123	124	120	114	111	109	106	102	103	102	103
126	127	123	122	113	116	110	107	104	103	103	102
	125	128	120	120	114	114	113	112	108	107	108

(1" wide)

107	105	105	109
107	105	105	109
105	103	106	105
105	104	106	103
104	102	104	104
104	103	106	102
107	108	106	108
109	107	107	108

← CL plate

(nominal density of fuel would give reading ∼104, density decreases as reading increases)

(3" wide)

107	107	105	108	109	111	115	118	123	130	142	152
106	100	102	105	107	106	112	114	121	126	132	146
103	103	102	103	107	109	112	113	117	123	125	144
107	107	104	105	106	108	110	116	120	122	123	139
104	108	103	105	108	110	113	116	118	119	126	137
107	106	104	106	111	110	115	119	119	120	128	140
108	106	108	107	112	112	116	112	118	122	125	142
111	111	111	113	118	116	118	116	122	125	129	135

(0,0)

FIG. 5.3-6 DENSITOMETER MAP OF PLATE 14 IN REMOVABLE PLATE ELEMENT   (plate 5 in GAMSCAN)

5.3.2.2 Collimator and Shielding

The collimator designed by Labbe (Ref. 5.3-1) and constructed by Grill (Ref. 5.3-2) is shown in Fig. 5.3-7. The collimator was designed to maximize the count rate from a one-sixteenth square inch area of fuel plate while minimizing the effect of collimator leakage, background, and backscatter radiation. Because of longitudinal variations in the fuel plate power density were expected to be much greater than transverse variations, a rectangular slot collimator was developed. Care was taken during assembly of the collimator section to avoid shielding weaknesses and gamma streaming.

The complete collimator and shielding arrangement is shown in Fig. 5.3-8. Lead shielding was positioned completely around the tunnel where the fuel plate would be located in order to limit backscattered radiation from reaching the detector and to shield the experimenters. The fuel plate was movable in the tunnel so that any point on the plate could be placed under the collimator. Parts of the shielding were machined to allow proper overlapping of shielding, to allow free motion of the fuel plate, and to allow shielding to fit in several tight positions.

A removable section of the collimator was constructed to allow repeatable positioning of a standard source used to check electronics drift. The location of the removable section is shown in Fig. 5.3-8.

FIG. 5.3-7
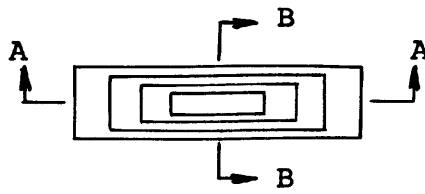
GAMMA SCANNER COLLIMATOR DIMENSIONS

dimensions
shown
are in
inches

A-A   B-B

FIG. 5.3-8

detector cavity

collimator source insert

transverse control

steel plate

collimator

longitudinal control
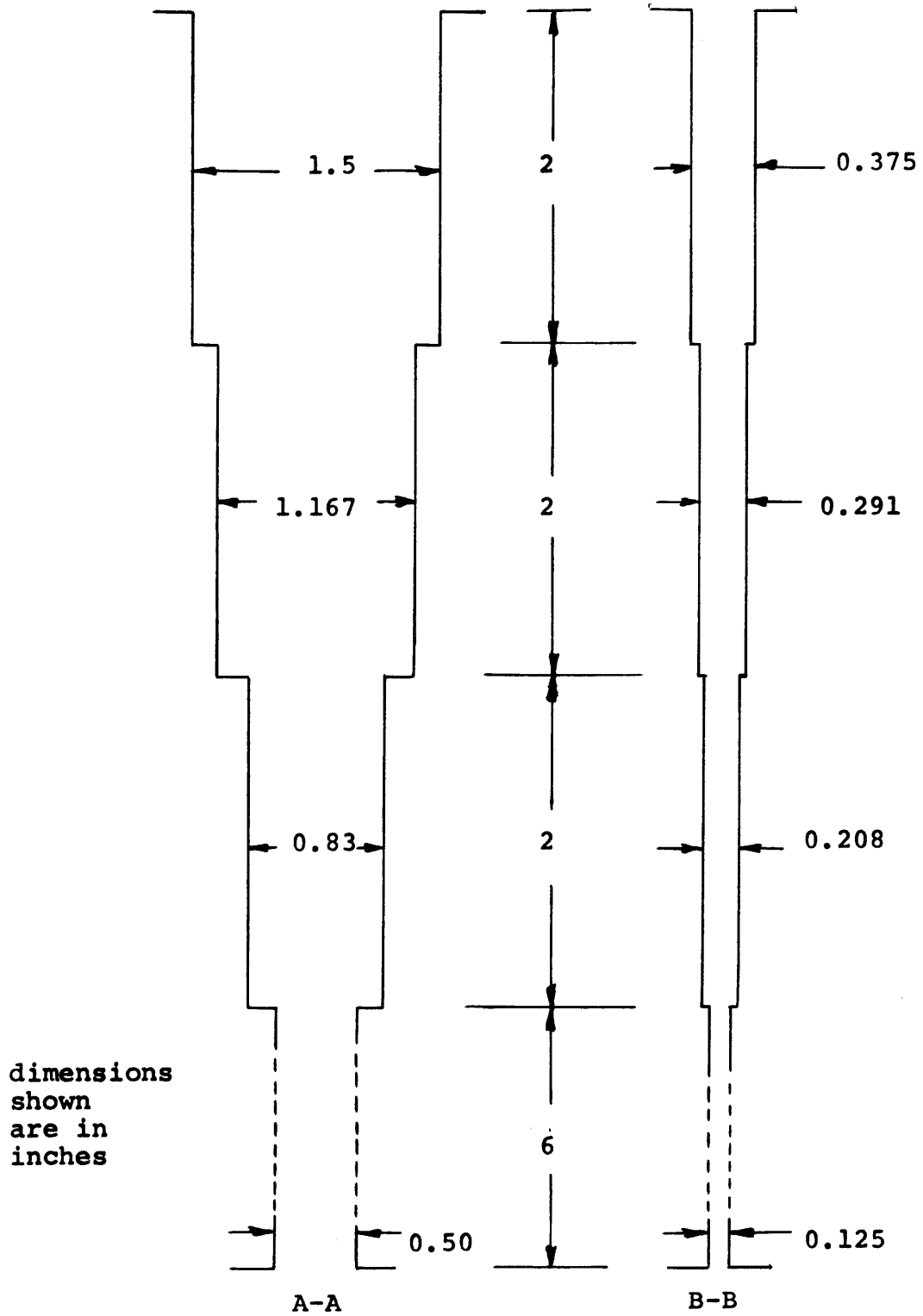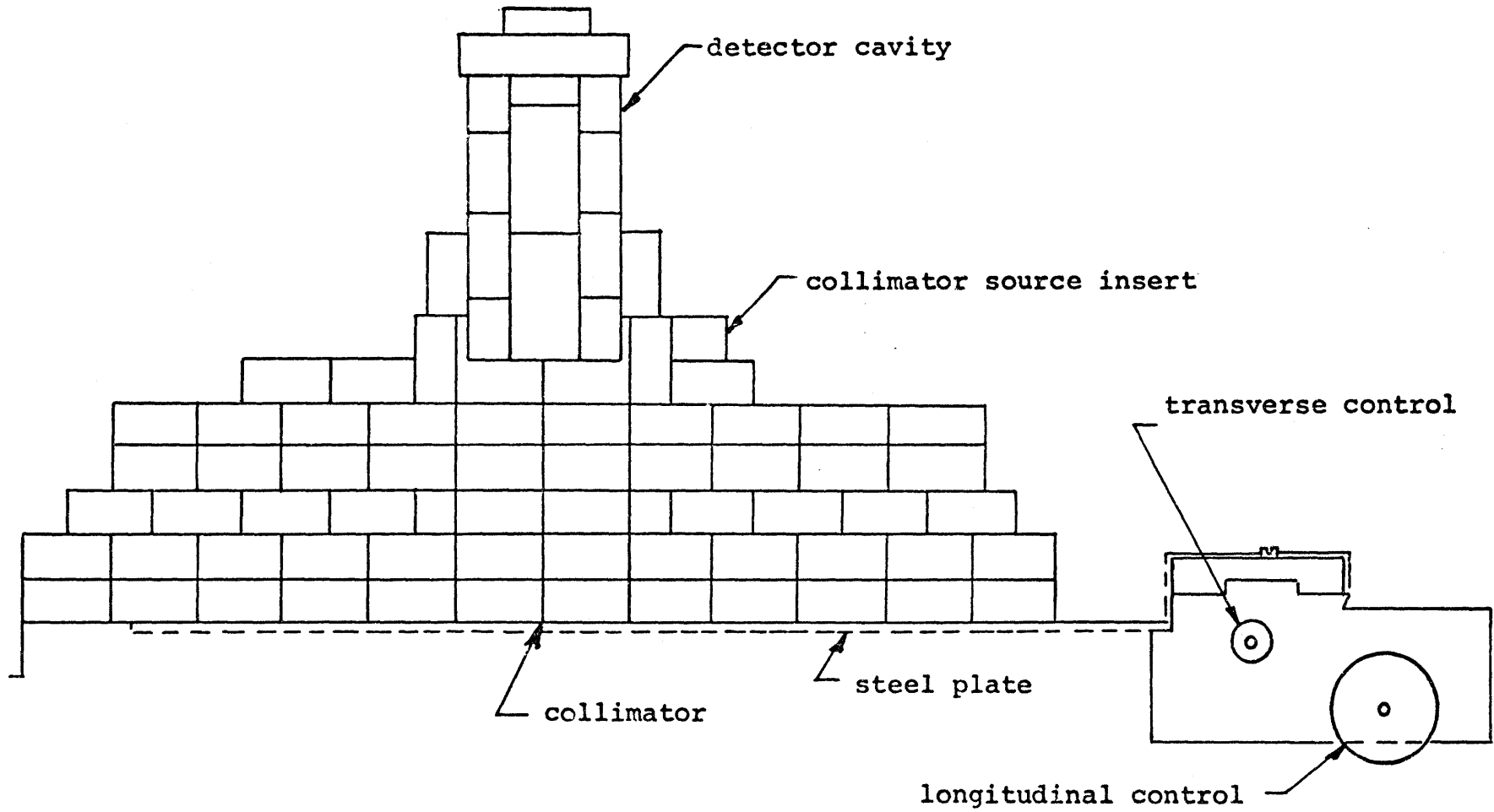
GAMMA SCANNER

A second collimator was installed in the gamma scanning apparatus for measuring activated copper wires. Details of this second collimator and copper wire counting are described in Section 5.4.

5.3.2.3 Electronics

A block diagram of the electronics used in gamma scanning fuel plates is shown in Fig. 5.3-9. The NaI (Th) crystal, phototube, and preamplifier were positioned above the collimator. After initial alignment and testing of the counting setup, the detector was wedged into a fixed position and remained in the same position for all scans.

5.3.2.4 Plate Movement

The movement of individual fuel plates under the collimator section must be accurately determined. Positions must be repeatably obtained within the desired experimental accuracy. A precision lathe table was used to accomplish these goals.

A long steel plate, 0.250 inch thick and 3.0 inches wide, was secured to the lathe table. A slot on the plate was machined for accurate and repeatable positioning of fuel plates. The steel plate with the fuel plate riding piggy-back could be moved transversely and longitudinally in the tunnel under the collimator shielding. Indicators attached to the lathe table gave the transverse (Y-axis) and longitudinal (X-axis) position of the steel plate.

The zero positions for the indicators were determined by sighting through the collimator to an end position on the machined slot on steel plate. The repeatability of steel plate positions was verified by using dial indicators. The transverse and longitudinal dimensions were repeatable in all cases to within 1/32 of an inch (±0.08 cm.).

5.3.3 Scanning Procedure

Fuel plate gamma scanning was performed as part of MITR-II Startup Procedure 5.9.1. A separate procedure was developed for handling of the removable plate element. Details of these two procedures are given in Appendix A. The development of scanning techniques is described in the following sections.

5.3.3.1 Initial Tests

No fuel plate scans were performed by Labbe (Ref. 5.3-1) or Grill (Ref. 5.3-2) to verify the initial design and construction of the scanner apparatus because of delays in the MITR-II construction schedule. Both Labbe and Grill tested the detection system with a variety of standard gamma sources in order to determine the detector resolution and the electronics drift. The NaI crystal resolution was found to be acceptable and electronics drift which would result in changing the low energy gamma ray cutoff was found to be acceptable provided that the detection system was allowed to warm up for several days.

Labbe scanned some irradiated foils in order to
verify the repeatability of the plate positioning apparatus.

5.3.3.2 Preparations for Scanning

Preparations for scanning included final testing and
modification of the gamma scanner apparatus and develop-
ment and testing of scanning procedures. The basic components
of the scanner had been assembled well in advance of the
actual experiment.

After the electronics were warmed up for several days,
a final check was performed on the detector resolution and
the discriminator settings were determined. The baseline
discriminator setting was chosen so that fission product
gamma rays with energies greater than approximately 0.35
Mev would be detected. A standard I^{131} source provided
a means to set the low energy cutoff and check for any
electronics drift. Differential counts for a 0.2 volt
window and I^{131} source versus discriminator voltage for
the scanner detector system are shown in Fig. 5.3-10.
For the scanning experiment, the discriminator was set at
0.5 volts, this setting corresponded to a position on the
lower energy side of the 0.3645 Mev iodine peak. A point
was chosen on the slope of the peak, rather than the peak
itself, so that the direction of the electronics drift
could be determined. Normal scanning took place with
counting in the integral mode, i.e., all detected gammas
above the cutoff energy would be counted. Placing an I^{131}

source in a repeatable position and no fuel plate in the
scanner, differential counts were taken using the same
baseline cutoff and a small voltage window. Thus by
looking at a small energy band on the slope of the iodine
peak, the drift of the energy cutoff up or down could be
indicated by respective increases or decreases in the
standard source counts.

A uranium foil counter was set up near the gamma
scanner apparatus. A block diagram of the foil counter
detection system is shown in Fig. 5.3-9. This setup was
needed to count uranium foils which would be irradiated
in a reactor pneumatic irradiation facility at the same
time the removable plate element was irradiated. The
foils would be counted simultaneously with the fuel plates,
resulting in data which indicated the fission product
decay rate. The uranium foil counter was checked with
standard sources and the baseline discriminator setting
was also determined using an I^{131} standard source.
Differential counts for a 0.2 volt window and I^{131} source
versus discriminator voltage for the foil detector system
are shown in Fig. 5.3-10.

Some modification of the scanner apparatus was nec-
essary to allow free movement of the lathe table and
attached steel plate. Labbe (Ref. 5.3-1) had suggested a
series of points to be scanned on the fuel plates, but
limitations in the transverse movement of the fuel plate

FIG. 5.3-9

PLATE SCANNING ELECTRONICS BLOCK DIAGRAM

(A) gamma scanning electronics
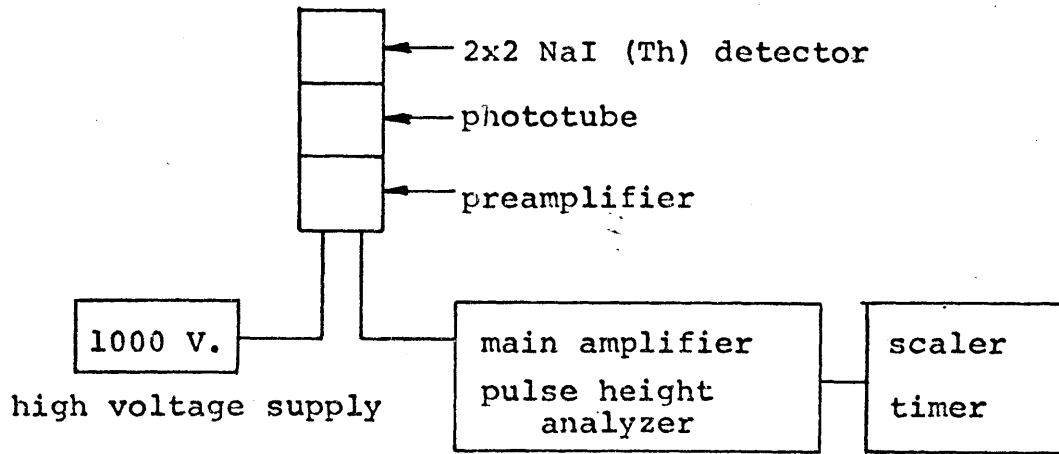
(B) uranium foil counting electronics
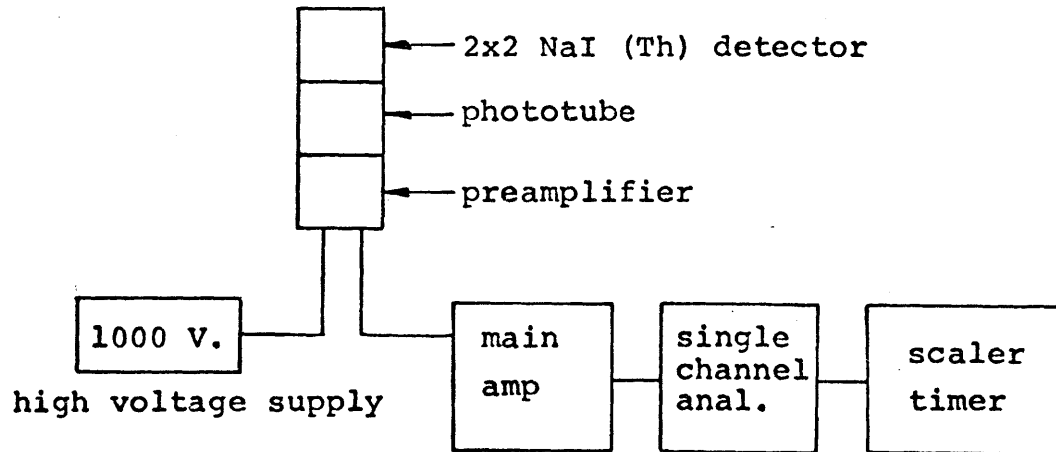
FIG. 5.3-10

CALIBRATION CURVES OF
DETECTOR SYSTEMS

I^{131} source
differential counting
mode with 0.2 volt
window

——————— gamma scanner
detector

– – – – – – uranium foil
detector

counts per minute

discriminator baseline setting (volts)
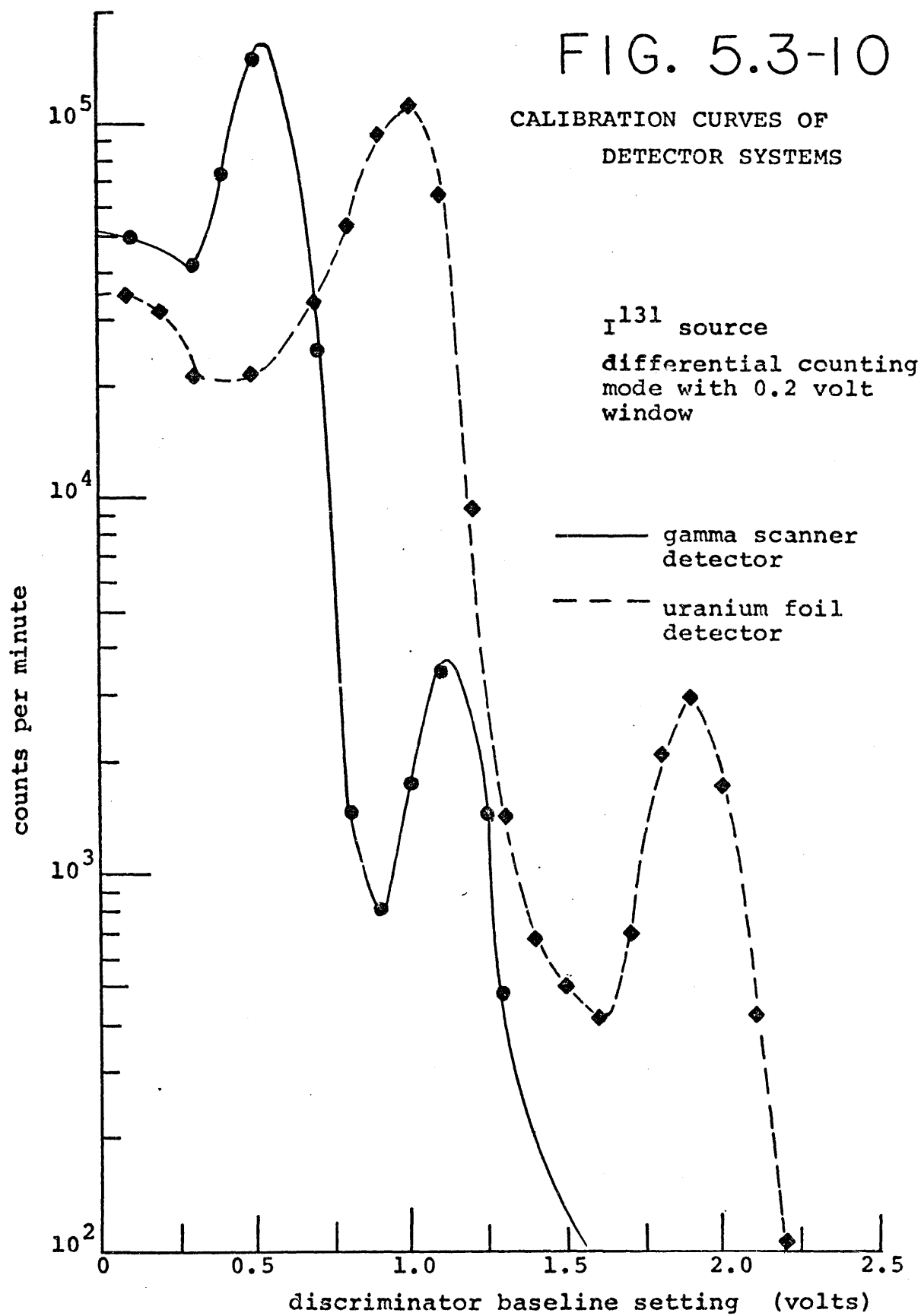
in the shielding tunnel made it impossible to scan some of his suggested points for backscattering corrections. The shielding tunnel had to be shortened to obtain additional longitudinal freedom to fully scan the fuel plates. Indicators were also added to the lathe table to allow accurate measurement of fuel plate positions.

A transfer and handling procedure for the removable plate element was developed. The procedure is given in Appendix A. A steel cask was used to transfer the irradiated fuel element from the reactor floor to the counting location. Once at the counting location, the element was transferred from the steel cask to a lead cave. The cave was open on both ends to allow easy disassembly of the element and removal of fuel plates. The cave was oriented in the counting location to minimize backscattered radiation from reaching the scanner detector. All scans were done with all parts of the removable plate element in the cave except the single plate in the process of being scanned. A sketch of the transfer cask and lead cave is shown in Fig. 5.3-11.

A dry run was carried out using the unirradiated removable plate element. This was done to insure that the actual scanning with hot fuel plates, would be accomplished smoothly and with a minimum of personnel exposure. The fuel plates were scanned to determine background measurements but no counts above normal background (no

FIG. 5.3-11

steel gun barrel
with stainless
steel liner

TRANSFER CASK

AND

LEAD CAVE

42 inches

transporter

transfer cask

shadow shielding
on open end

side toward gamma
scanner and personnel

bricks staggered
to prevent streaming

stainless steel
tray holding element

side view

end view
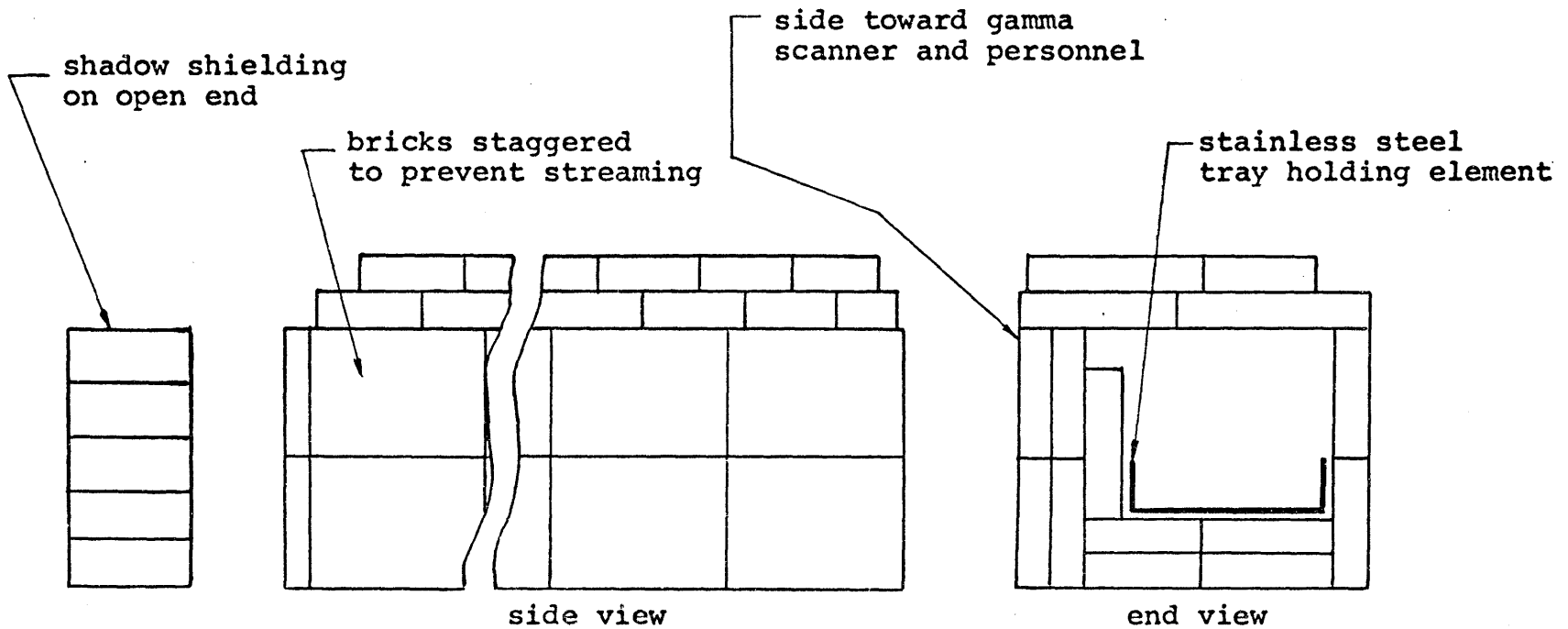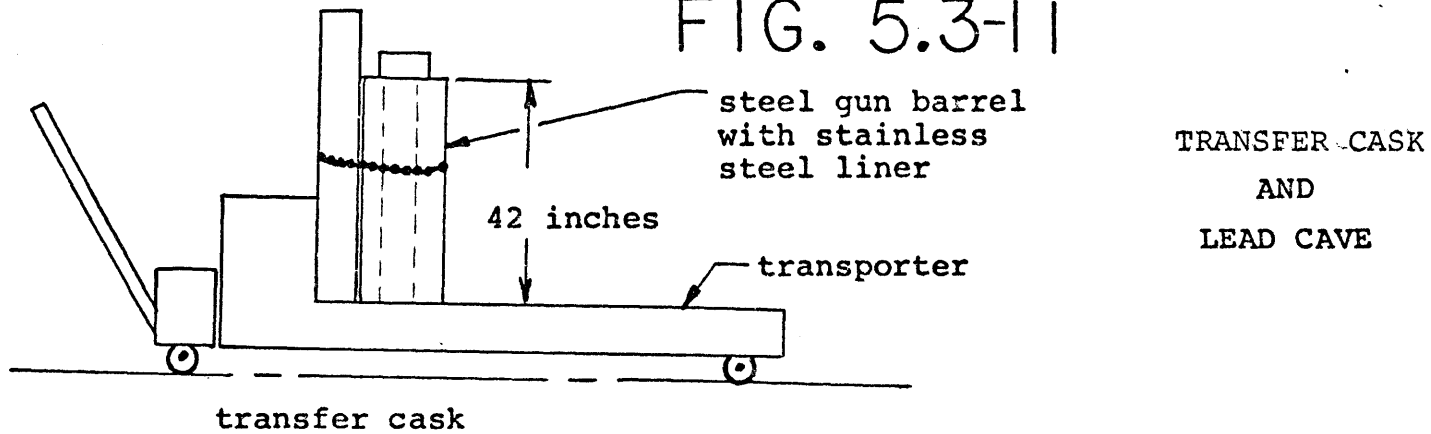
lead cave exterior dimensions approximately 12x12x40 inches

plates in the scanner) were found. The geometric efficiency of the scanner was too low to see the natural activity of the uranium in the fuel plates. A standard source (Na^{22}) was then scanned to verify that all components were working.

The procedure used for gamma scanning was Startup Procedure 5.9.1 (a copy is included in Appendix A). Because of uncertainty in the reactor power level and projected fuel plate activation levels, an initial fuel plate activation was required to determine the power level and irradiation and decay times required to give good statistics for scanning measurements. A thirty minute irradiation was performed at a power of approximately 100 watts nominal (best estimate based on later calibrations is that this corresponded to approximately 10 to 20 watts). This irradiation yielded peak count rates around 4000 counts per minute. Because of the desire to have peak count rates greater than 10,00 counts per minute in order to have greater than 1% accuracy, the irradiation time was increased to one hour, the power level was increased by a factor of two, and the decay time (approximately 2 hours) was held constant for the remaining fuel plate irradiations. This resulted in an increase in the activation level and count rate by a factor of four.

The position of the fuel meat inside the fuel plate was determined using fuel plate radiographs supplied by

Gulf United Nuclear Fuels. The distance from the fuel plate end to the fuel plate meat could be directly measured since the radiographs were full size. The relationship between the fuel plate end and collimator position was previously determined by sighting through the collimator and was related using the lathe table indicators. Thus a correlation between the collimator position and the fuel position was determined for each of the five removable plate.

The fuel plates were scanned in the trial irradiation using the points suggested by Labbe (Ref. 5.3-3). This scanning program (114 points scanned per plate) took an excessive length of time and would result in low activities in the last plates scanned. The major problem was the numerous transverse scan points across the fuel element. The power distribution changes of greatest interest were in the longitudinal direction and thus the scanning points were changed to increase the longitudinal point scans and decrease the transverse scans. Sufficient transverse scan points were retained to indicate transverse trends and unexpected power peaking. Once a scanning program was outlined, all scans had to conform to that program because of limitations on decay corrections and inter-plate comparisons in the computer analysis. Sixty-six scanning points were chosen and are shown in Fig. 5.3-12. Data sheets developed for recording scanning data are shown in Appendix F.

FIG. 5.3-12

SCANNING POINT LOCATIONS FOR CORE I

effective area of
enclosed point
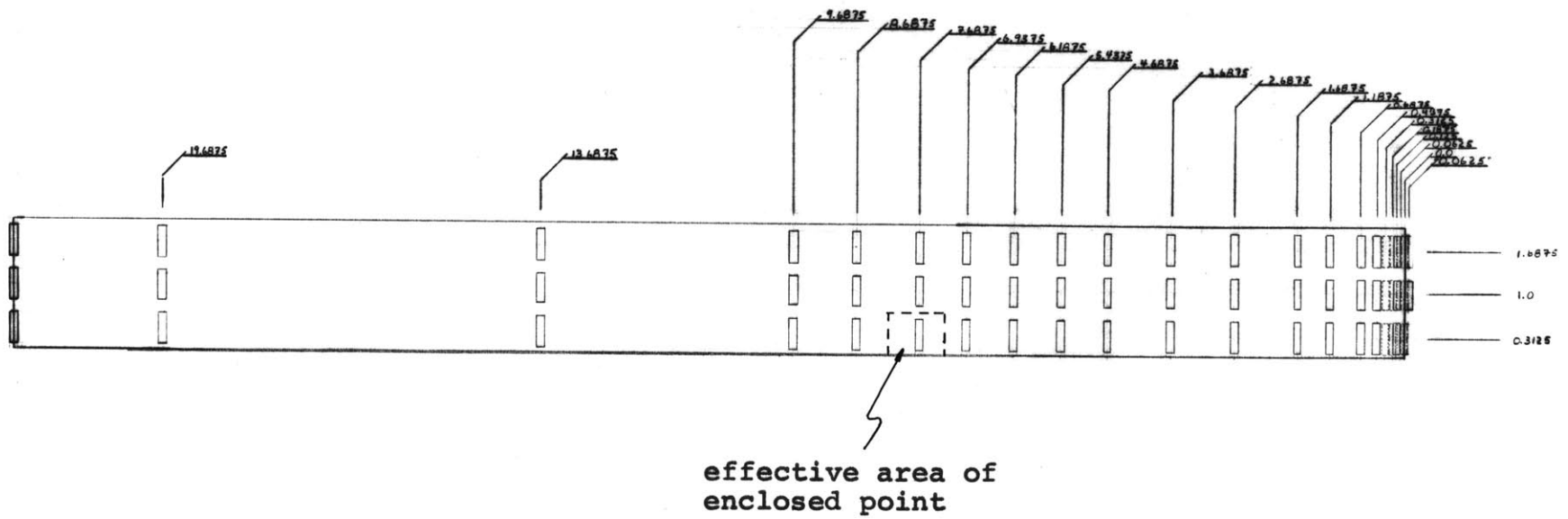
5.3.3.3 Irradiation and Counting

The removable plate element was irradiated fourteen times in various core positions. The element would be irradiated for one hour at 200 nominal watts (later best estimates indicate that this was approximately 20 to 50 watts), then the reactor would be shut down. During the irradiation, two foils, a uranium foil and a cobalt foil, would be irradiated in a repeatable position in a reactor pneumatic irradiation facility (1PH2). After cooling incore for approximately one and one half hours, the removable plate element would be removed to the lead cave in the counting location (see procedure in Appendix A). Plates would be removed from the element one at a time and scanned. The uranium foil from the pneumatic facility would be counted simultaneously on the foil counter (1 minute counts) and the cobalt foil was removed to storage for later counting. Plate scanning would usually commence two hours after the irradiation was completed.

Background counts and standard source checks would be made prior to commencing each element scan (Note: no detector drift was detected). With a fuel plate inserted in the scanner, one minute counts would be taken at each of sixty-six locations. The sixty-six positions were aligned in a rectangular array with three points across the plate in the transverse direction for each of twenty-two longitudinal postions. The sixty-six positions are shown in

Fig. 5.3-12. Gamma scans were always performed on the same five plates and usually in the same order. Upon completion of scanning the five plates for an irradiation, the plates would be stored in the transfer cask and transferred inside the reactor containment. The element would be allowed to cool until shortly before the next irradiation when it would be cleaned, reassembled, and refueled back into the next reactor core position.

Table 5.3-1 lists the core positions and removable plate element orientations for each of the fourteen irradiations. Figure 5.3-13 shows the incore location for each of the irradiation positions. Irradiations were performed with a few variables in the configuration. These variables were dummy element location, incore sample assembly location, and shim bank height. Table 5.3-1 lists the status of these variables when they affect an irradiation. Sufficient core positions were measured to be able to predict the power distribution in every core position by utilizing core symmetry. Raw data for the element scan is filed with Startup Procedure 5.9.1 in the MITR Headquarters file. Samples of the raw data are found in Appendix F.

5.3.3.4 Cobalt Irradiations

A 0.250 inch diameter by 0.003 inch thick cobalt foil was irradiated in pneumatic facility 1PH2 during each removable plate element irradiation. The cobalt

TABLE 5.3-1

POSITION OF REMOVABLE PLATE ELEMENT DURING CORE I IRRADIATIONS

Irradiation #	Core Position	Element Orientation
1	C-9	Plate 1 next to core housing
2	A-2*	Plate 1 next to ICSA in A-1
3	C-5	Plate 1 next to core housing
4	B-4	Plate 1 next to radial spider
5	A-2$^+$	Plate 1 next to solid dummy in A-1
6	C-8	Plate 1 next to core housing
7	B-5	Plate 1 toward outer boundary of core
8	C-10	Plate 1 next to core housing
9	C-8**	Plate 1 next to core housing
10	B-9	Plate 1 next to hexagonal spider and solid dummy in A-1
11	C-14	Plate 1 next to core housing
12	C-13	Plate 1 next to core housing
13	B-3	Plate 1 next to hexagonal spider
14	C-8***	Reference removable plate (plate 1 in removable plate element) is the 15th plate in element away from core housing

*   Incore Sample Assemble next to A-2
+   Solid dummy next to A-2
**   Irradiation performed with fuel element in C-13 removed and replaced with a solid dummy so that blade height was at 8.90 inches (blade height at 7.65 for other irradiations)
*** Element rotated 180° from position in irradiation #6

FIG. 5.3-13

REMOVABLE PLATE ELEMENT IRRADIATION POSITIONS

Irr.8

Irr.1

Irr.6
Irr.9
Irr.14

Irr.7

Irr.12

Irr.11

Irr.4

Irr.2
Irr.5

Irr.10

Irr.13

Irr.3

REGULATING ROD
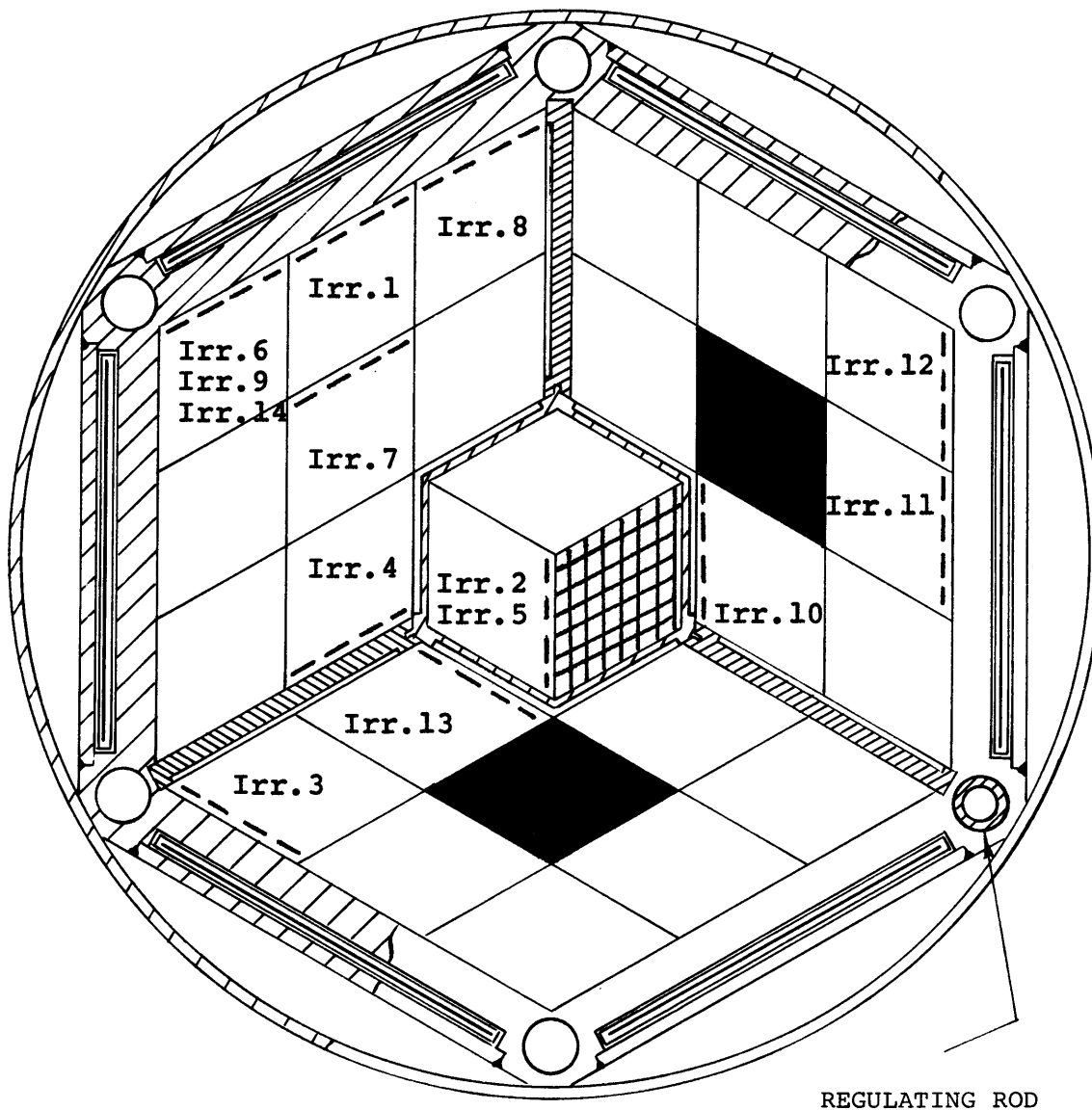
— — — plate 1 position

solid dummy element

solid dummy element except for Irr.2
when an ICSA was in this position

Blade height was 7.65 inches except for Irr.9
when blade height was 8.9 inches.

foils were always positioned in the same manner in the
polyethylene sample holder to achieve a repeatable geometry.
The polyethylene sample holder, which is usually referred
to as a rabit, has interior cylindrical dimensions of
1 inch in diameter by 2 3/8 inches in lenth. A hollow
polyethylene cyliner (3/4 inch outside diameter by 2 inches
long) was inserted into the rabit with a cobalt foil taped
(with mylar tape) on one end and a uranium foil taped on
the other end. Both foils were heat sealed into small
polyethylene bags and the rabit was always inserted into
1PH2 so that the cobalt foil was closer to the send-receive
station than the uranium foil. The cobalt foils were used
to standardize power level to one irradiation. Variations
between irradiations occurred because of differences in rates
of achieving desired power level and small fluctuations at
the desired power level because of nuclear instrument
inaccuracy at low power levels.

The cobalt foils were thoroughly cleaned to eliminate
contamination from affecting the count rates. The foils
were counted for one hour in a counting setup for which
a block diagram is shown in Fig. 5.3-14. Discriminator
settings were adjusted so that gamma rays with energies
of the two Co^{60} peaks would be counted. Raw counts were
corrected for background, foil mass, and cobalt decay to
counting time. Table 5.3-2 gives counting data for cobalt
foils used during removable plate element irradiations.

FIG. 5.3-14

COBALT FOIL COUNTING ELECTRONICS BLOCK DIAGRAM
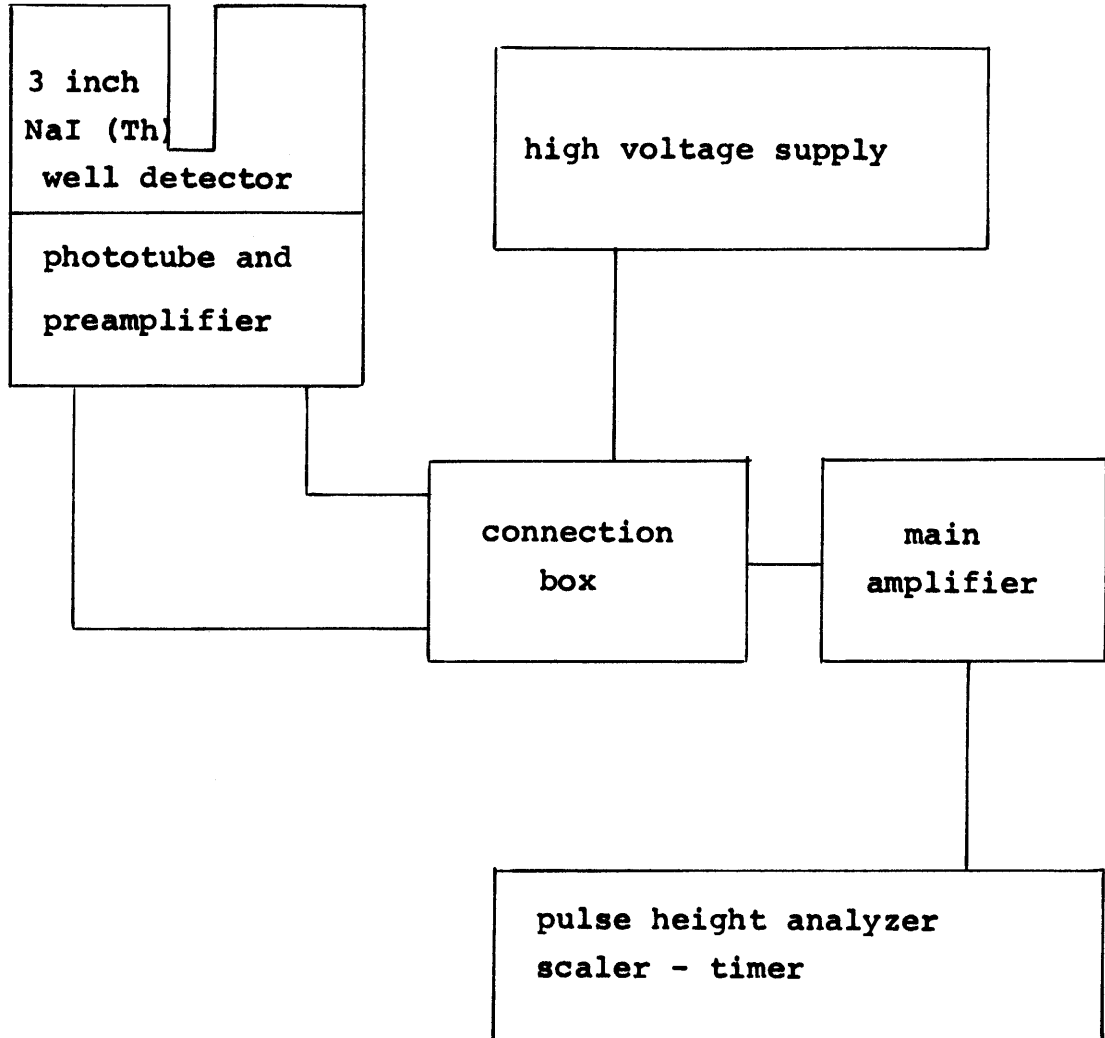
TABLE 5.3-2

CORE I REMOVABLE PLATE IRRADIATION COBALT FOIL DATA

Irradiation #	Raw Counts	Corrected for Background	Corrected for Mass and Background	Total Counts Corrected for Decay, Mass, and Background
1	27617	13696	12854	12924
2	27199	13278	13278	13327
3	27191	13270	13037	13089
4	27125	13204	12588	12635
5	28723	14802	13409	13454
6	27206	13285	13081	13043
7	26904	12983	12392	12412
8	27513	13592	12998	13016
9	26545	12624	12338	12352
10	28008	14087	12792	12803
11	27742	13821	12812	12822
12	27710	13789	12949	12954
13	27121	13200	13156	13157
14	28086	14165	13196	13196

Total corrected counts for the Kth irradiation = COB(K)

5.3.4 Data Analysis

Gamma scanning the removable plate element yielded raw counts for various longitudinal and transverse positions on fuel plates. The decay time from each irradiation was also recorded for each individual count. Sample data sheets used to compile and transcribe approximately 500 pages of raw data are shonw in Appendix F. From this large amount of data, power distributions were predicted.

5.3.4.1 Computer Code GAMSCAN

Computer code GAMSCAN is used to calculate the corrections to the raw fuel plate counting data for fission product decay, effects of previous irradiations, and background activity. This yields corrected counts for input to computer code COREFAC. Appendix C contains a listing of GAMSCAN.

5.3.4.1.1 General Description

The initial version of GAMSCAN was written by Labbe and is described in Gamma Scanner for MITR-II Fuel Plates (Ref. 5.3-1). Gamma scanning irradiated fuel plates yields raw counts of fission product decay in the given plate. The fission product decay rate depends upon the duration and power level of the irradiation period and upon the history of previous irradiations. By correcting the raw data to determine a fission product decay rate for each point two hours after an irradiation as a result

of only that irradiation, the correct fission product decay rates can be correlated to the power distribution. Because of the difficulty of performing decay corrections by hand, GAMSCAN was written to perform the calculations.

The initial version of GAMSCAN was divided into two parts. The first part performed the appropriate decay and background corrections and the second part corrected for edge and area averaging effects. The front (and main) part of the code was improved and debugged and used for correcting the raw data. The second part has been discarded because it did not properly correct for edge and area averaging effects. These latter effects were corrected by a hand calculation for fuel plates of interest.

GAMSCAN was written in Fortran IV computer language and was run on the IBM System 360 at the MIT Computation Center. The code was expanded in size from its original version in order to evaluate all of the data input.

5.3.4.1.2 Decay Corrections and Input Requirements

GAMSCAN utilizes an experimentally determined fission product decay curve derived from U^{235} foil irradiations in the MITR-I. Fission product activity versus time for a ten minute irradiation at approximately 100 watts is shown in Fig. 5.3-15. Activity two hours after the ten minute irradiation is set equal to one and all other activities are measured relative to the two hour activity. The fraction of the activity at a given time relative to a two hour

FIG. 5.3-15

TEN MINUTE IRRADIATION DECAY CURVE
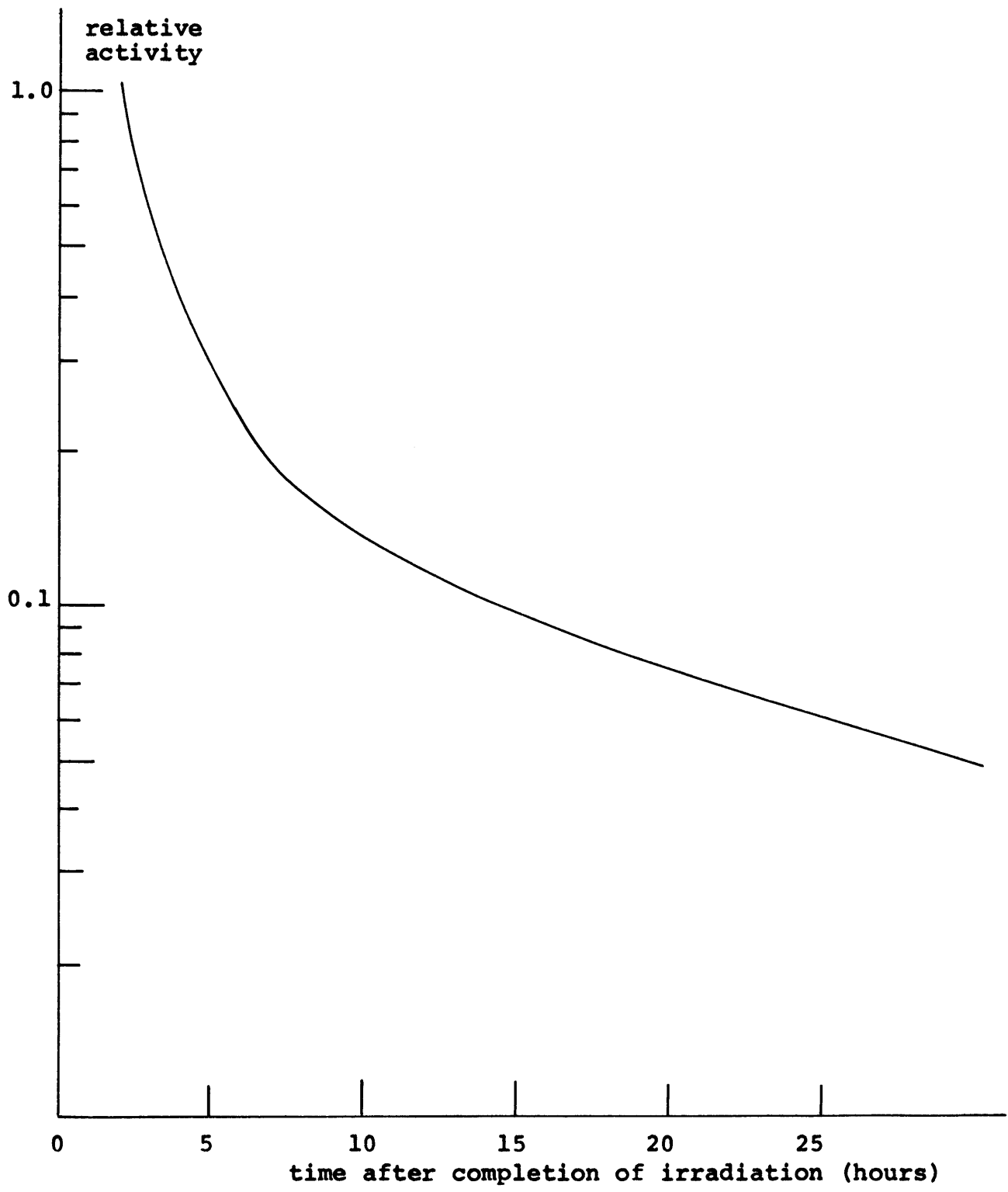
decay can be read off Fig. 5.3-15. By dividing the
curve shown in Fig. 5.3-15 into linear approximations
for small time segments, a fission product decay equa-
tion is used by GAMSCAN.

The decay curves of fission products gamma rays
for irradiations greater than ten minutes were determined
by relating a longer irradiation to a series of ten
minute irradiations. For example, the count rate at
two hours from the completion of a sixty minute irradiation
is the sum of the ten minute irradiation count rates at
the following six decay times:

    1)   2.833 hours,
    2)   2.667 hours,
    3)   2.500 hours,
    4)   2.333 hours,
    5)   2.167 hours,
    6)   2.000 hours.

Because of low powers, depletion and poisoning effects
are small, the method of using ten minute intervals to
determine decay curves for longer intervals is valid.
The advantage of using ten minute intervals is two-fold.
First, irradiations of different lengths can be handled
by the code. Second, fluctuations in power only have to
be averaged over ten minute intervals rather than obtaining
an average power for the complete irradiation. Note that
for an irradiation time of greater than ten minutes the
actual reference time will be somewhat greater than two
hours from the first ten minute interval. However, the
reference time is identical for each irradiation of the

same time length and for future discussion, this reference
time is referred to as the two hour reference time.

Raw counts are normalized to the two hour reference
time by dividing the raw count by the fraction of activity
relative to the two hour reference activity at the time the
raw count was taken. The power level of the irradiation
for each of the ten minute segments is normalized to a
reference power for all irradiations. For a given irradia-
tion period divided into N ten minute intervals, the decay
corrected counts would be:

$$CC_R = (C_R - B - C_{R-1}) \sum_{i=1}^{N} \frac{P_i}{Af_i} \quad , \qquad (5.3-1)$$

where,

CC_R is the count corrected for decay for the Rth irradiation,

C_R is the raw count for the Rth irradiation,

B_R is the background count for the Rth irradiation,

C_{R-1} is the count from all irradiations previous to irradiation R,

P_i is the power level of the ith ten minute interval,

A is the reference power level,

f_i is the fraction of activity present at time t_i,

t_i is the decay time from the ith irradiation interval to the middle of the counting period,

N is the number of ten minute irradiation intervals.

The method of obtaining corrections for background and
backscatter counts is found in Section 5.3.4.4. The activity

of previous irradiations must be subtracted from the raw
counts before the decay correction can be made. The decay
time of previous irradiations is the sum of the time between
irradiations and the decay time from the last irradiation.
The activity due to previous irradiations can be calculated
as follows:

$$C_{R-1} = \sum_{K=1}^{R-1} (\text{Counts}_K - B_K) \sum_{i=1}^{N_K} \frac{P_{ki}}{A} f_{R-K,i} \quad , \quad (5.3-2)$$

where,

C_{R-1} is the activity due to all irradiations previous to irradiation R,

Counts_K is the counts of the Kth irradiation,

B_K is the background for the Kth irradiation,

P_{Ki} is the power level of the ith interval of the Kth irradiation,

A is the reference power level,

$f_{R-K,i}$ is fraction of activity present from the ith interval of the Kth irradiation at the time of count after the Rth irradiation,

R is the number of the last irradiation,

N_K is the number of ten minute irradiation intervals in the Kth irradiation.

Required input to GAMSCAN is listed as follows:

NO   is the number of times the fuel plates are irradiated,

NZG   is the number of fuel plates irradiated,

MZS   is the number of points counted per plate,

A   is the reference power level,

MP(K)   is the number of points to be counted per plate for the Kth irradiation,

LI(K)   is the number of ten minute irradiation
        intervals for the Kth irradiation,

DT(K)   is the time between irradiations in minutes,
        e.g., PT(3) is the time between the starts
        of irradiation 2 and 3,

P(K,I) is the power level of the Ith ten minute
        interval of the Kth irradiation,

XX(I)   are the x and y coordinates of the Ith
YY(I)   point on the plate,

B(K)   is the input background count for a plate
        in the Kth irradiation,

T(K,J) is the time in minutes between the start
        of the Kth irradiation and the middle of
        the counting of the Jth point,

C(K,J) is the counts/minute recorded at point J for
        the Kth irradiation.

For the present GAMSCAN code, the following restrictions

exist:

1) The number of irradiations (NO) cannot exceed 14,

2) The number of points scanned (MZS, MP(K)) cannot
    exceed 67 and must be the same points for all
    irradiations and inputed in the same order,

3) The number of plates counted (NZG) cannot exceed 5,

4) The number of ten minute irradiation intervals can-
    not exceed 7,

5) XX(I) is the distance in the longitudinal direction
    from the lower left corner of the fuel plate meat
    to the center of the point being scanned,

6) YY(I) is the distance in the transverse direction
    from the left edge of the fuel meat.

GAMSCAN yields corrected counts for input to COREFAC.

These corrected counts correspond to the expected count rate

at a point on a fresh fuel plate that would exist two hours

after an irradiation at a reference power. Sample input and

output data can be found in Appendix F.

5.3.4.1.3 Code Limitations

The initial version of GAMSCAN was streamlined to
eliminate area averaging and edge correction routines which
were not successful. The final code merely corrected the
raw counting data for fission product decay, background,
and backscatter. The number of irradiations and points
scanned is limited by the allowable computer core space.
The accuracy of the output is limited by counting statistics
and background corrections.

Raw counts on the fuel plates were on the order of
10,000 counts per minute which would give a statistical
accuracy of approximately 1%. Because some counts were
taken a considerable time after the irradiation, the raw
counts would be multiplied by a factor as much as 8 in
order to yield normalized two hour counts. Because of this
potential for multiplication of error, there is considerable
importance in making sure that the decay and background
corrections are accurate and minimizing statistical in-
accuracy by maximizing the count rate.

The limiting factor on count rate was the allowable
personnel radiation exposure during removable plate element
handling. Table 5.3-3 gives radiation dose levels for a
typical irradiation of the removable plate element. Because
the removable plate element had to be disassembled and re-
assembled manually a total of at least fourteen times for

TABLE 5.3-3

RADIATION SURVEY RESULTS OF TRANSFER OF REMOVABLE PLATE
ELEMENT FOLLOWING A 1 HOUR IRRADIATION AT 200
NOMINAL WATTS AND A 70 MINUTE DECAY

Survey Results

A. Transfer from Core (unshielded) to Gun Barrel - Reactor
Floor

1. 300 mR/hr at 1 meter
2. 15 mR/hr at 4 meters
3. 300 mR/hr - Surface - Gun Barrel
4. 500 mR/hr - Top Gun Barrel (unshielded)

B. Transfer from Gun Barrel to Pb Cave (in hotshop)

1. Outside Pb Cave   10-15 mR/hr
2. 1 Fuel Plate Removed
    a. 50 Rad/hr - contact,   hot end
    b. 20 mR/hr at 3 feet - partially shielded
3. Radiation Dose Rates of Worker Disassembling Fuel Plate
   (partially shielded - cold end exposed)
    a. Hands   100 mR/hr γ , 700 mRad/hr Beta and Gamma
    b. Body   50 mR/hr

C. Estimated Beta and Gamma Exposure to Hands for each
Assembly and Disassembly (approximately one each day)
and based on a Total Exposure Time of 10 Minutes:

1. Gamma dose rate = 100 mR/hr = 20 mR
2. Beta and Gamma dose rate = 700 mRad/hr = 100 mRad

Core I, the activity from a one hour irradiation at 200 nominal watts was taken to be the upper limit.

As stated in Section 5.3.4.1.2, the decay curve for fission products was derived by combining an experimentally determined tem minute irradiation decay curve into a series of ten minute irradiations to determine the decay curve for a long irradiation. All irradiations used to determine the power distribution were sixty minutes long. Figure 5.3-16 shows the decay curve which GAMSCAN predicts would occur from a sixty minute irradiation of a plate with no previous irradiation history. A uranium foil (10% U^{235} by weight in aluminum) was irradiated in a pneumatic facility and subjected to the same irradiation history as the removable plate element. As can be seen by Fig. 5.3-16, the measured decay rate of the foil agrees well with the GAMSCAN decay rate. Foil data for irradiation 2 is plotted on Fig. 5.3-16 because there was a four day decay between irradiation 2 and irradiation 1, thus approximating a foil with no previous irradiations. Also, in case of irradiation 1, sufficient shielding had not been placed around the foil counter to shield against background radiation in the room which changed with time because of decay of the removable plate element.

In order to verify the accuracy of the corrections for background and previous irradiations, several fuel plates were rescanned a second time after the completion of initial scans. Figure 5.3-17 shows the difference between predicted

FIG. 5.3-16

ONE HOUR IRRADIATION DECAY CURVE
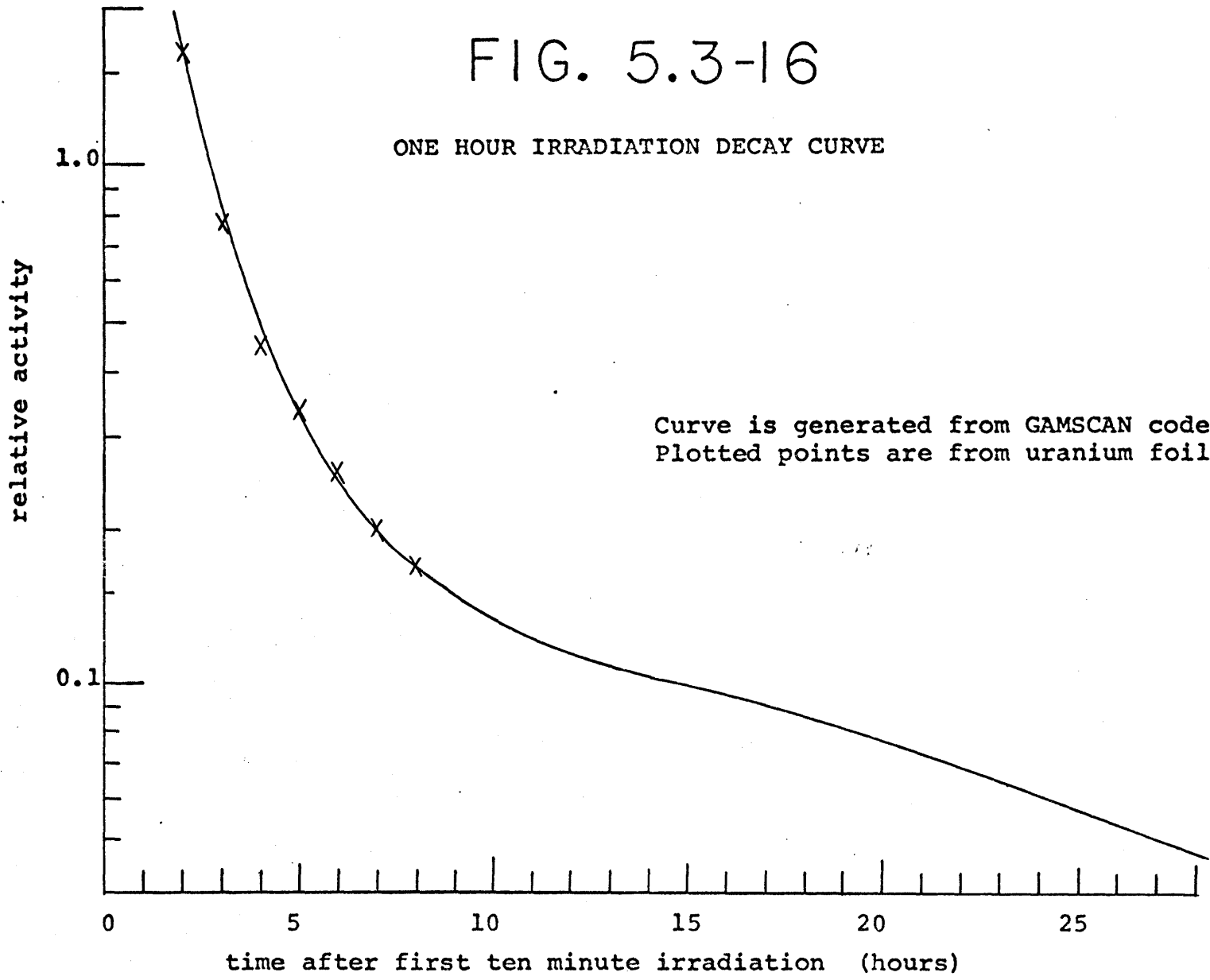
Curve is generated from GAMSCAN code.
Plotted points are from uranium foil data.

relative activity

time after first ten minute irradiation (hours)

FIG. 5.3-17

COMPARISON BETWEEN ACTUAL DECAY AND GAMSCAN PREDICTED DECAY FOR

PLATE HAVING COOLED 24 HOURS

(raw counts   1500 c.p.m.)

distance from bottom of fuel   (inches)
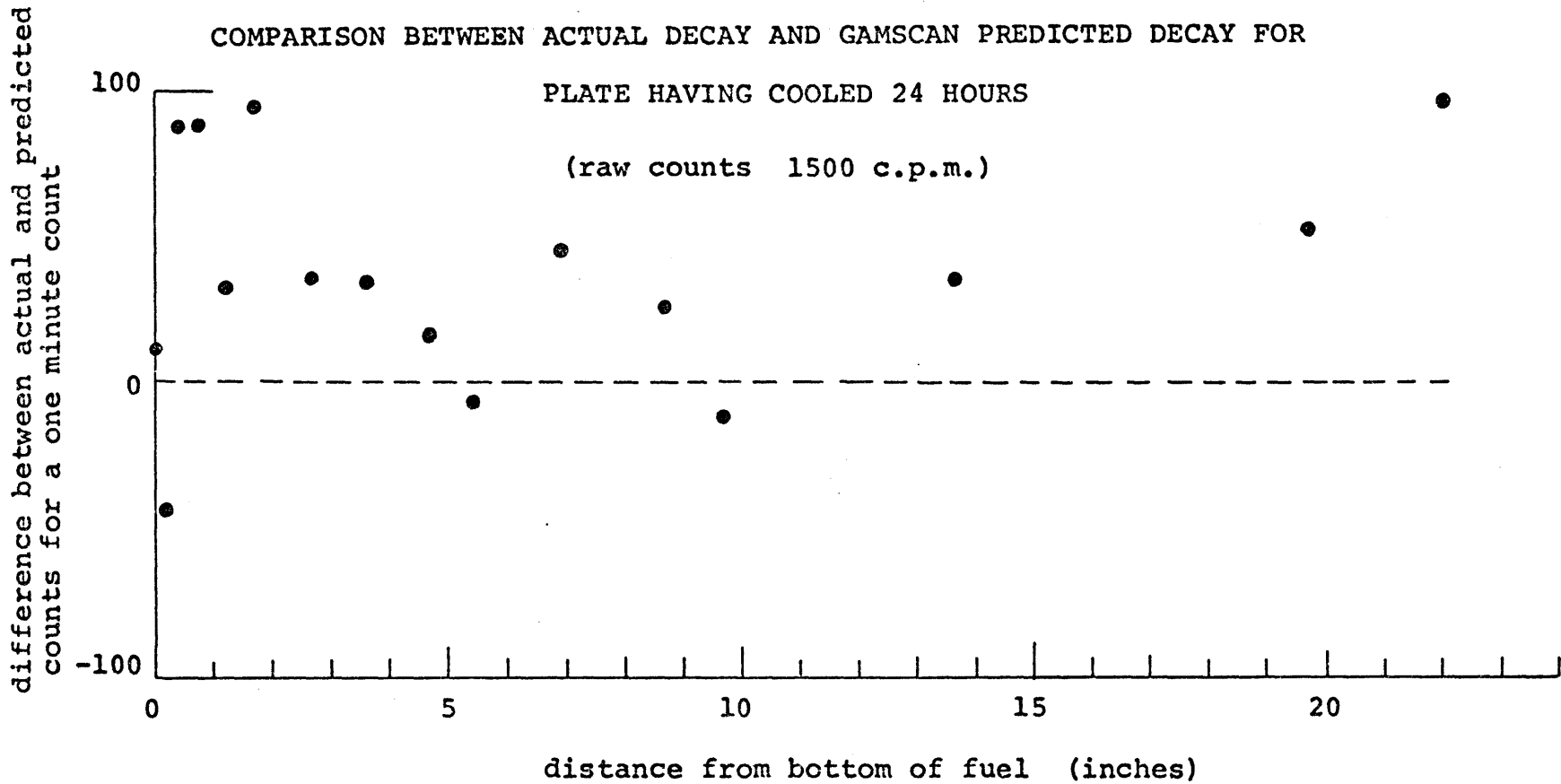
and actual decay evaluations for a plate that had cooled twenty-four hours. The difference is less than 100 counts which is less than a seven percent error in the background and previous irradiation correction. Since the background and previous irradiation correction is about five to ten percent of the raw counts taken immediately after an irradiation, the error in correcting the raw counts is less than one percent which compares favorably with counting uncertainty.

The greatest accuracy in the decay correction occurs when the counts are made two to seven hours after the irradiation when the log of decay versus time is somewhat linear. For a second count which was taken approximately seven hours after the first count to test the previous irradiation and background correction, the error in the correction resulted in an error in the corrected counts of approximately 2-3%. For this case, the log of the decay versus time was non-linear. For all of the irradiations performed in measuring the power distribution, the second irradiation occurred more than eighteen hours after the first so that the correction error should be small.

5.3.4.2 Computer Code COREFAC

Computer code COREFAC is used to calculate both plate and core wide distribution factors from data from GAMSCAN. Appendix D contains a listing of COREFAC.

5.3.4.2.1 General Description

COREFAC was developed to handle the large amount of data output from GAMSCAN in order to determine F_r, the radial peaking factor, and F_a, the axial peaking factor. Corrected counts for each of the 66 points for each of the five plates for each of the fourteen irradiations are punched on cards by GAMSCAN for input to COREFAC. Cobalt foil data is used by COREFAC to normalize the corrected counts from the fourteen irradiations in Core I to one irradiation power and time length. For each plate the average counts per unit area of plate was determined and thus a point to average ratio was determined for each of the sixty-six points on the plate. This point to average value is equivalent to the F_a at each of the points. For points on the lower edge of the plate, additional correction was required to obtain a true value of F_a because of area averaging effects. Section 5.3.4.5 explains the edge peaking correction.

Knowing the average counts per plate and applying symmetry to the core, a core average counts per plate by the average counts per plate for the core, plate to core average ratios were obtained. These ratios correspond to F_r, the radial peaking factor.

COREFAC was written in Fortran IV computer language and was run on the IBM System 360 at the MIT Computation Center. Required input values for COREFAC are the following:

NO is the number of irradiations evaluated,

NZG is the number of plates/element counted,

MZS is the number of points/plate counted,

COB(K) is the cobalt foil count for the Kth irradiation,

X(I), Y(I) are the x,y coordinates for the Ith point on the plate counted,

NWT(K,J) is the core average weighting factor for the Jth plate in the Kth irradiation (NWT(K,J)=CORWT(K) x PLTWT(K,J), see Section 5.3.4.2.4),

ARWT(I) is the area weighting factor for the Ith point,

CORRAT(J,I) is the corrected count from GAMSCAN of the Ith point of the Jth plate for each representative irradiation.

5.3.4.2.2 Cobalt Corrections

Cobalt foils were irradiated in a repeatable position in an experimental facility 1PH2 for each irradiation. The computer code GAMSCAN has the capability of correcting for power variations during an irradiation because GAMSCAN treats all irradiation as a series of ten minute irradiations. For all fourteen irradiations the power level was constant during the irradiation and thus the same reference power was used in GAMSCAN for all ten minute intervals of all fourteen irradiations. However, GAMSCAN did not have the capability to adjust for varying rates of achieving desired power and because nuclear instrumentation was not sensitive to small fluctuations in power and was susceptible to drift between irradiations, the cobalt foil data was

used to standardize power between irradiations in COREFAC.

Corrected cobalt foil data is shown on Table 5.3-2. A cobalt foil count for each irradiation was inputed to COREFAC. The minimum count was determined and each count inputed from GAMSCAN was corrected as follows:

$$CORRAT(K,J) = \frac{CORRAT(K,J) \times SMCOB}{COB(K)} , \qquad (5.3-3)$$

where,

CORRAT(K,J)   is the corrected count for the Jth position of the given plate for the Kth irradiation,

SMCOB   is the smallest cobalt foil count,

COB(K)   is the cobalt foil for the Kth irradiation.

All cobalt counts were greater than 10,000 so that the counting statistical error in cobalt correction should be less than 1%.

5.3.4.2.3 Plate Area Weighting Factors

Sixty-six points were scanned on each removable fuel plate. Each point was representative of a local section of the fuel plate. Figure 5.3-12 shows the scanning point locations. Most scanning points were taken in areas of highest power density or maximum power gradient in order to determine as accurately as possible the power distribution.

Counts per unit area were obtained for each point scanned by dividing the number of counts at that point by

the collimator area (0.0625 square inches). These counts per unit area were then multiplied by the amount of area for which each of the points was representative. The respective areas for each point are listed in Table 5.3-4. The area for each point was defined as being a rectangle whose sides were located at the median position between the point of interest and the surrounding points. For points near the border of the fuel meat, the fuel meat boundary was the respective side of the effective rectangle. Figure 5.3-12 shows some examples of point effective areas.

By summing up the counts for all areas on the plate and dividing by the fuel meat area, the average counts per unit area for the plate is determined. Dividing the average counts per unit area of the total plate into the counts per unit area of each point yields the ratio of point power to average plate power. The ratio for a point X is represented by the following equation:

$$\frac{\text{Unit Power at Local Point}}{\text{Average Unit Power on Plate}} = \frac{(\text{Counts/unit area})_x}{\dfrac{\sum\limits_{x=1}^{66} (\text{Counts/unit area})_x \times \text{Representative Area}_x}{\text{Total Area of Fuel Meat}}} .$$

$$(5.3-4)$$

The above ratio actually represents the F_a at each point on the plate. The spike at the bottom edge must be

TABLE 5.3-4

FUEL PLATE EFFECTIVE AREAS FOR GAMSCAN POINTS IN CORE I

J	Area (in.^{2})	J	Area (in.^{2})	J	Area (in.^{2})
1	0.0	23	0.2578	45	0.4922
2	0.0	24	0.2461	46	0.5391
3	0.0	25	0.3593	47	0.5156
4	0.0225	26	0.3437	48	0.4922
5	0.0215	27	0.3281	49	0.6289
6	0.0205	28	0.5391	50	0.6016
7	0.0449	29	0.5156	51	0.5742
8	0.0430	30	0.4922	52	0.7188
9	0.0410	31	0.7188	53	0.6875
10	0.0674	32	0.6875	54	0.6563
11	0.0645	33	0.6562	55	1.797
12	0.0615	34	0.7188	56	1.719
13	0.0898	35	0.6875	57	1.641
14	0.0860	36	0.6562	58	3.594
15	0.0820	37	0.6289	59	3.438
16	0.0898	38	0.6016	60	3.281
17	0.0860	39	0.5742	61	3.009
18	0.0820	40	0.5391	62	2.879
19	0.1348	41	0.5156	63	2.748
20	0.1289	42	0.4922	64	0.8086
21	0.1231	43	0.5391	65	0.7734
22	0.2695	44	0.5156	66	0.7383

corrected for by hand, but because it adds only a very small amount to the actual power produced by the plate, the error in determining the average plate power by neglecting it is small.

5.3.4.2.4 Core Average Weighting Factors

In the previous section, plate average counts were determined for each fuel plate irradiated. The plate averages must be properly weighted in order to determine a core wide average counts per plate.

The first task is to weight the plates within the element since in all cases only five plates out of fifteen could be scanned in each irradiation. This weighting was accomplished by plotting the power distribution through the element at several elevations. By dividing the distribution curve up into a series of blocks in which the integral of the area under the blocks approximately equals the integral of the area under the distribution curve, the number of plates that each plate counted represents can be determined. Figure 5.3-18 shows an example for the case of the removable plate element irradiated in position B-5.

Similar curves were made for all irradiations in order to determine plate weighting factors for the plates in each irradiation. Table 5.3-5 shows how plates were weighted in each element for all the irradiations.

Core symmetry was used to relate element positions for which irradiations were performed to element positions for

FIG. 5.3-18

EXAMPLE OF PLATE WEIGHTING IN ELEMENT IN
POSITION B-5 BY BLOCK REPRESENTATION OF
GAMSCAN CORRECTED COUNTS CURVE
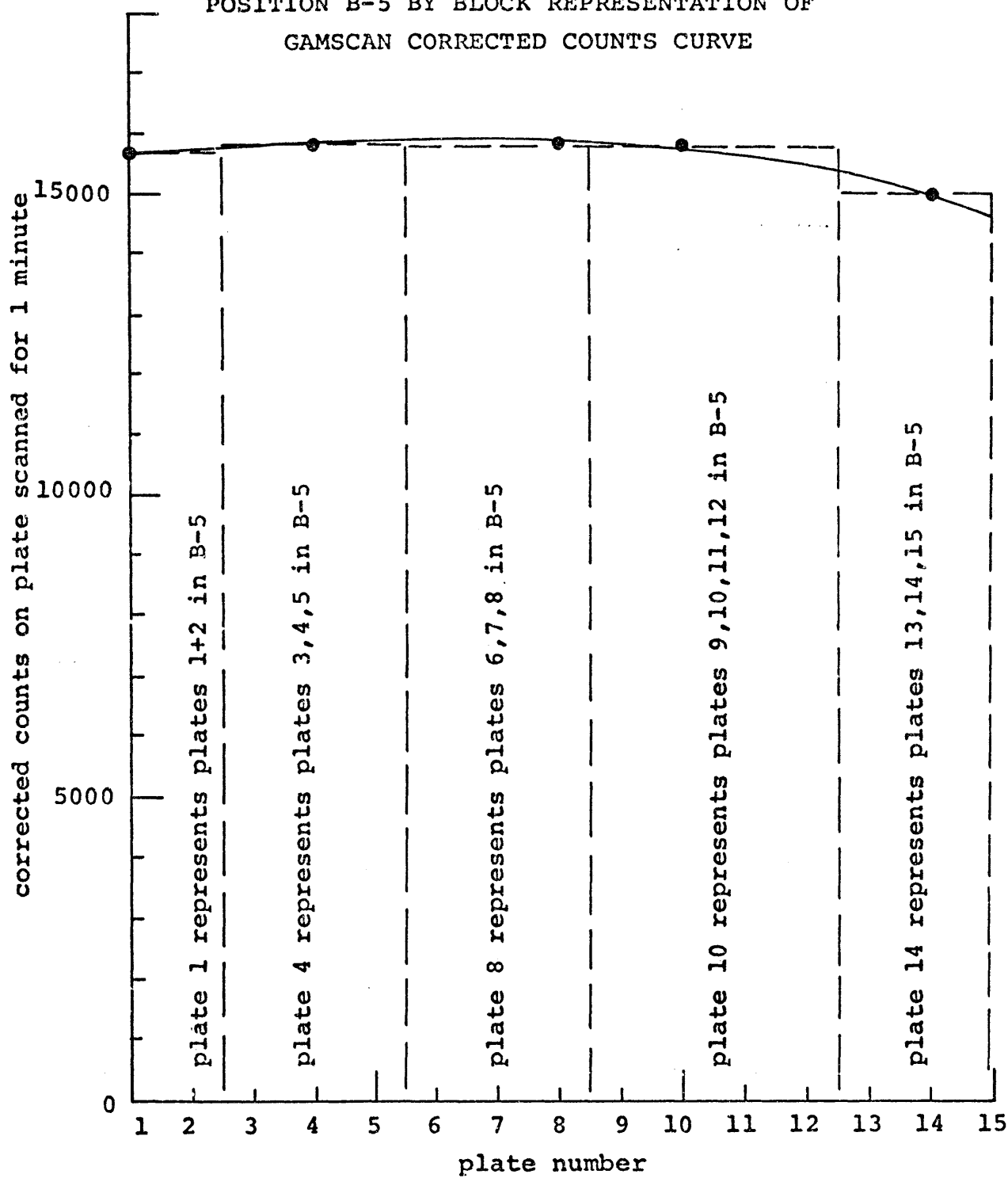
which irradiations were not performed. Figure 5.3-19

shows which element positions were considered to be

equivalent. The plate weighting factors for each element

were then increased by a factor equal to the number of

elements similar to the element irradiated in order to

derive a core wide weighting factor for each plate counted.

Derivation of a core average power per plate is summarized

by the following equation:

$$CORAVG = \frac{\sum_{k=1}^{14} CORWT(K) \sum_{J=1}^{5} PLATEAVE(K,J) \times PLTWT(K,J)}{Total\ Plates} ,$$

(5.3-5)

where,

CORAVG is the core average counts per unit plate area,

CORWT(K) is the number of elements in the final core that can be represented by the Kth irradiation,

PLATEAVE(K,J) is the average counts per unit area on the Jth plate for the Kth irradiation,

PLTWT(K,J) is the number of plates in the element irradiated in K^{th} irradiation that can be represented by the Jth plate.

Values of CORWT(K) x PLTWT(K,J) used for evaluation of

Core I can be found on Table 5.3-5. For some cases CORWT(K)

is zero and thus the product is equal to zero because some

irradiations are not representative of elements in Core I,

for example, the case of A-2 position next to the ICSA

was not present in the final core.

FIG. 5.3-19

REMOVABLE PLATE ELEMENT IRRADIATIONS WHICH REPRESENT THE CORE I FUEL POSITIONS

Irr.8   Irr.3

Irr.1   Irr.11

Irr.6
Irr.14   Irr.4   Irr.13   Irr.12

Irr.7   Irr.5   Irr.11

Irr.1   Irr.10

Irr.4   Irr.5   Irr.3

Irr.8

Irr.13   Irr.10

Irr.3   Irr.3

Irr.11   Irr.11

Irr.12

REGULATING ROD
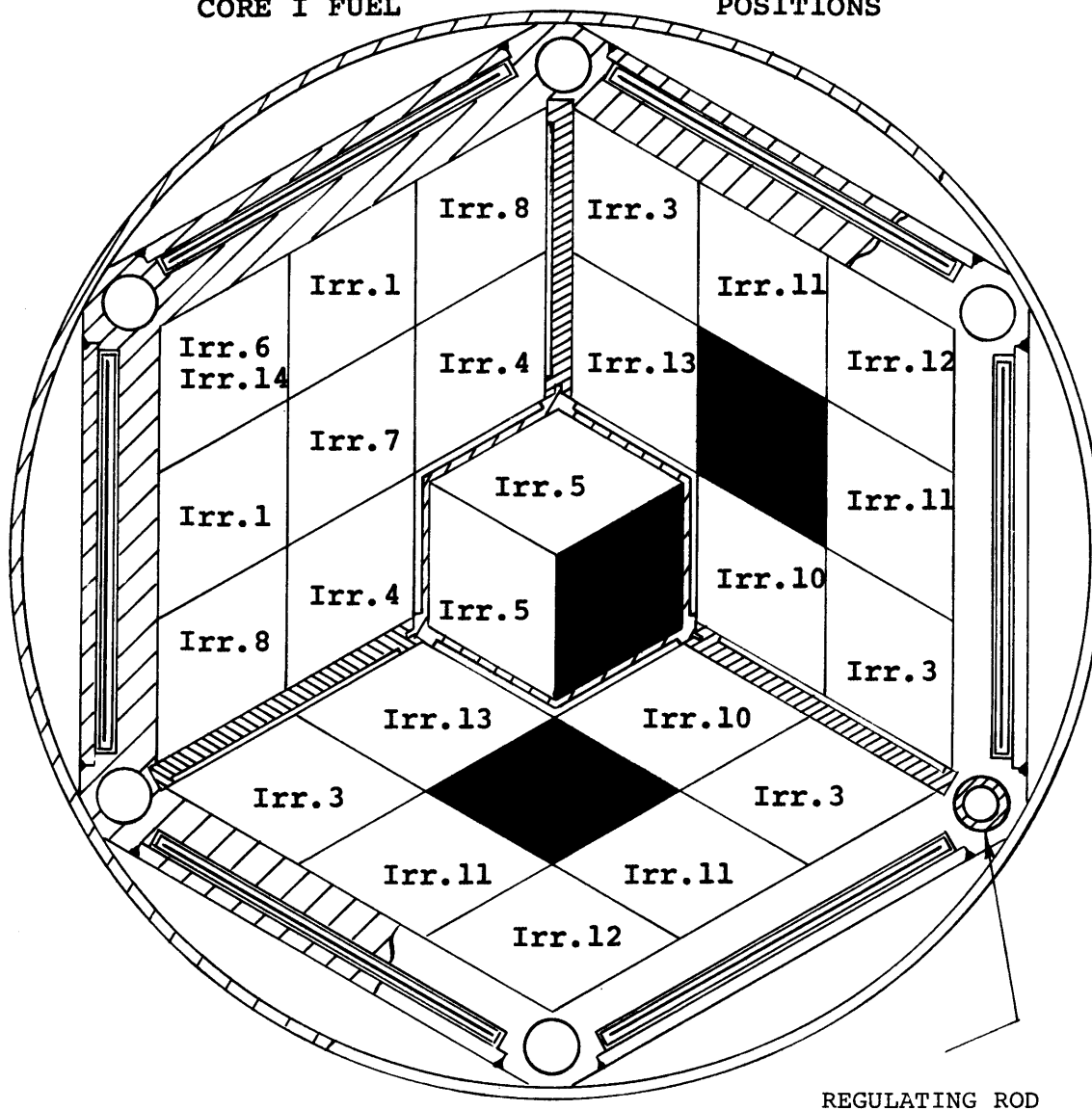
◪ solid dummy element

TABLE 5.3-5

PLATE WEIGHTING FACTORS FOR USE IN COREFAC
TO MODEL CORE I FINAL CONFIGURATION

Core Element Position (Irradiation #)	GAMSCAN Plate #	Number of Plates in Element Represented by Plate	Number of Plates in Core Represented by Plate
C-9 (Irradiation #1)	1	1 1/2	3
	2	3 1/2	7
	3	3	6
	4	3	6
	5	4	8
A-2 (Irradiation #2) (ICSA in A-1)	1	0	0
	2	0	0
	3	0	0
	4	0	0
	5	0	0
C-5 (Irradiation #3)	1	2	8
	2	3	12
	3	3	12
	4	4	16
	5	3	12
B-4 (Irradiation #4)	1	2	4
	2	3	6
	3	3	6
	4	3	6
	5	4	8
A-2 (Irradiation #5) (Solid dummy in A-1)	1	2	4
	2	3	6
	3	4	8
	4	3	6
	5	3	6

TABLE 5.3-5 (Continued)

Core Element Position (Irradiation #)	GAMSCAN Plate #	Number of Plates in Element Represented by Plate	Number of Plates in Core Represented by Plate
C-8 (Irradiation #6)	1	1	1
	2	2	2
	3	2	2
	4	1	1
	5	2	2
B-5 (Irradiation #7)	1	2	2
	2	3	3
	3	3	3
	4	4	4
	5	3	3
C-10 (Irradiation #8)	1	1 1/2	3
	2	3 1/2	7
	3	3	6
	4	3	6
	5	4	8
C-8 (Irradiation #9) (Blades at 8.9", C-13 removed)	1	0	0
	2	0	0
	3	0	0
	4	0	0
	5	0	0
B-9 (Irradiation #10)	1	2	4
	2	3	6
	3	3	6
	4	3	6
	5	4	8
C-14 (Irradiation #11)	1	1 1/2	6
	2	3 1/2	14
	3	3	12
	4	3	12
	5	4	16

TABLE 5.3-5 (Continued)

Core Element Position (Irradiation #)	GAMSCAN Plate #	Number of Plates in Element Represented by Plate	Number of Plates in Core Represented by Plate
C-13 (Irradiation #12)	1	1 1/2	3
	2	3 1/2	7
	3	3	6
	4	3	6
	5	4	8
B-3 (Irradiation #13)	1	2	4
	2	3	6
	3	3	6
	4	3	6
	5	4	8
C-8 (Irradiation #14)	1	1	1
	2	2	2
	3	1	1
	4	2	2
	5	1	1

Total Plates in Core = 360

Once the core average counts per unit area are determined, the plate average counts to core average counts ratio can be determined for each plate by dividing plate average counts by the core average counts. This ratio corresponds to F_r, the ratio of the power produced in a plate to the average power produced per plate in the core.

5.3.4.2.5 Code Limitations

COREFAC performs straight-forward numerical manipulations. The main limitations of the code are the approximations on input accuracy for plate weighting factors and element weighting factors. Also, the code does not calculate the lower edge peak which must be corrected by hand. At present, the code is limited to being able to handle fourteen irradiations because of DIMENSION limitations. Counts for all irradiations for a given plate must be inputed before counts are inputed for the next plate.

5.3.4.3 Collimator Effective Width

In order to properly determine the actual edge peaking from experimental data, it is necessary to determine the effective collimator width. The effective collimator width will be somewhat greater than the actual physical collimator width because of leakage through the collimator shield. The effective collimator width used in edge peaking

correction was experimentally determined.

Figure 5.3-20 shows how the counts at the edge of a uniform plate source would vary as the edge of the plate source moves through a perfect collimator opening. A "perfect" collimator opening has no shield leakage and thus even the smallest amount of shield completely attenuates the source. As can be seen on Fig. 5.3-20, the distance between the breaks in count rate curve is equal to the collimator width. In reality, some shield leakage exists and thus radiation from points beneath the collimator shield leak through the shield and are counted by the detector. By scanning a distinct edge of a uniform plate source, the effective collimator width can be experimentally determined. The effective width corresponds to the distance between the two breaks in the experimentally determined count rate versus edge position curve.

It was not possible to accurately determine the effective width from fuel plate data because of uranium density variation at the edge of the fuel meat. Therefore, a large indium foil was irradiated in a uniform flux and scanned to determine the effective collimator width. Figure 5.3-21 shows the indium foil which was used for the following reasons:

A)   Indium has a large capture cross section and thus is easily activated to dose rates that approximate a fuel plate and,

B)   Activated indium has numerous short-lived gamma rays with a wide spectrum of energies which helps simulate fission product gamma rays.

FIG. 5.3-20

EXAMPLE OF A PERFECT COLLIMATOR SCANNING A UNIFORM
EDGE SOURCE DISTRIBUTION

edge source

source intensity

distance in x-direction from reference point

count rate versus position

width of perfect collimator

detector counts

distance in x-direction of centerline of
collimator from reference point
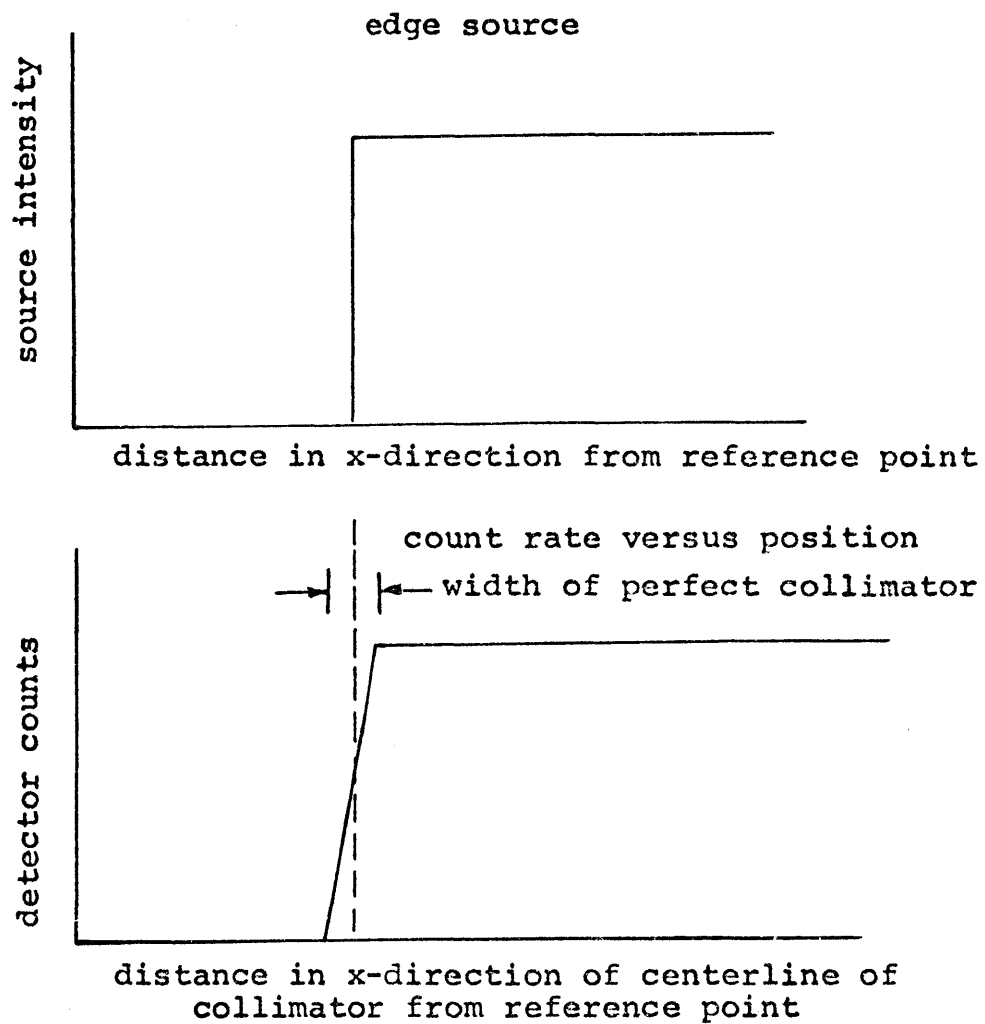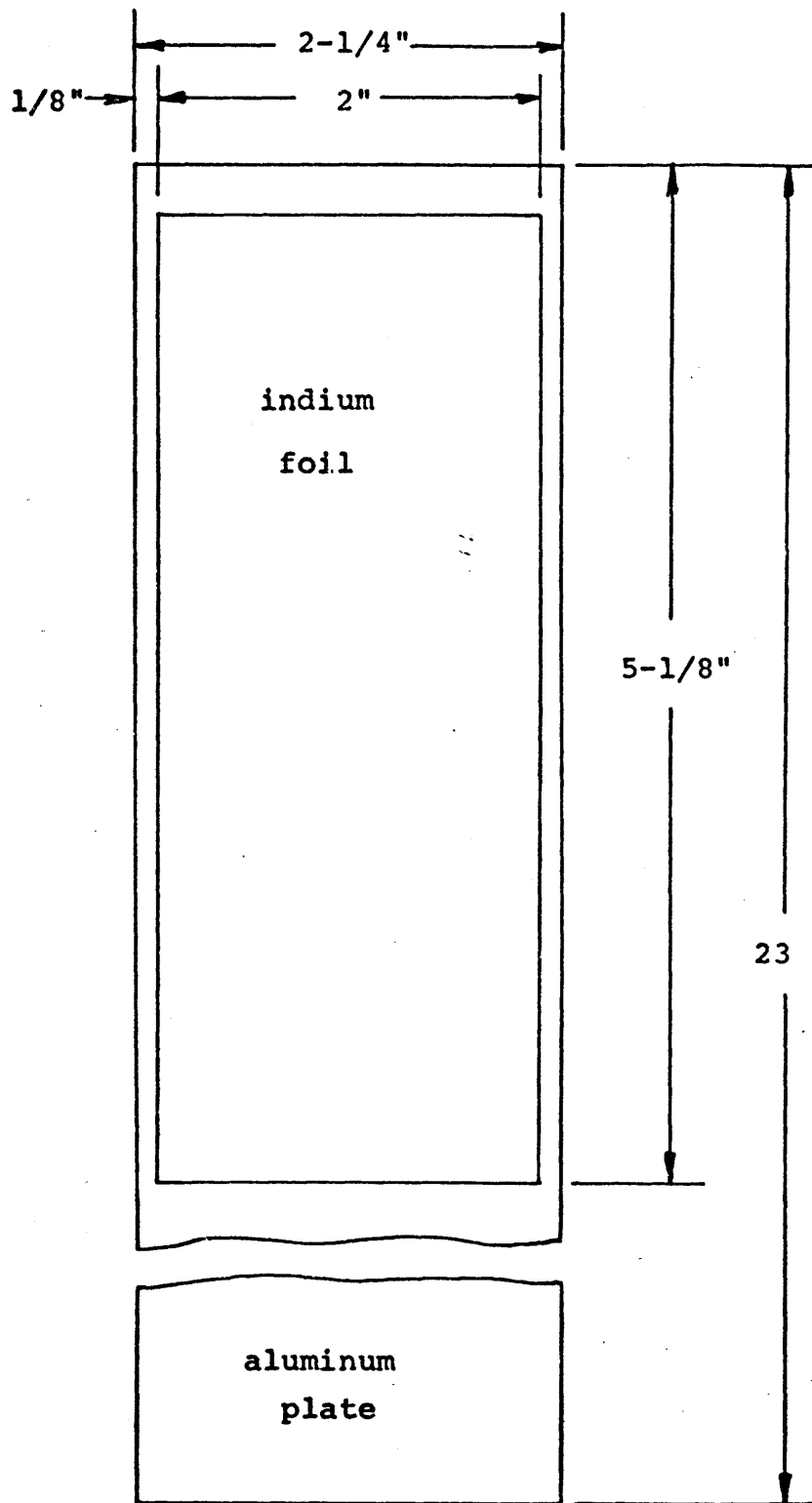
FIG. 5.3-21   INDIUM FOIL DIMENSIONS

The indium foil was positioned on a blank aluminum plate to approximate the fuel meat in a fuel plate. The lower edge of the foil was a distinct edge whose position in the gamma scanning apparatus could be accurately determined relative to the collimator opening. The foil and blank plate were irradiated at a nominal power of 200 watts in 3GV6 for twenty minutes (3GV6 is an irradiation facility located in graphite reflector region surrounding the reator). The neutron flux shape is nearly flat in the facility and thus the foil was uniformly activated. The foil was oriented in the facility to avoid self shielding which would give nonuniform activation.

The "indium fuel plate" was removed from 3GV6 and scanned in the gamma scanning apparatus. A scan of the longitudinal centerline of the "indium fuel plate" is shown in Fig. 5.3-22. The distance between the breaks in the curve correspond to 0.2 inches (actual collimator width is 0.125 inches). Thus the effective collimator width is taken as 0.2 inches.

5.3.4.4 Background and Backscatter Correction

The amount of background and backscatter correction at a point scan on a fuel plate is dependent upon the position of the fuel plate in the scanner apparatus and the total activity of the fuel plate being scanned. The correction, B(K), varies with fuel plate total activity because shield leakage is proportional to the total plate

FIG. 5.3-22

EFFECTIVE COLLIMATOR WIDTH DETERMINATION

distance from center of collimator to edge of indium foil
(inches)
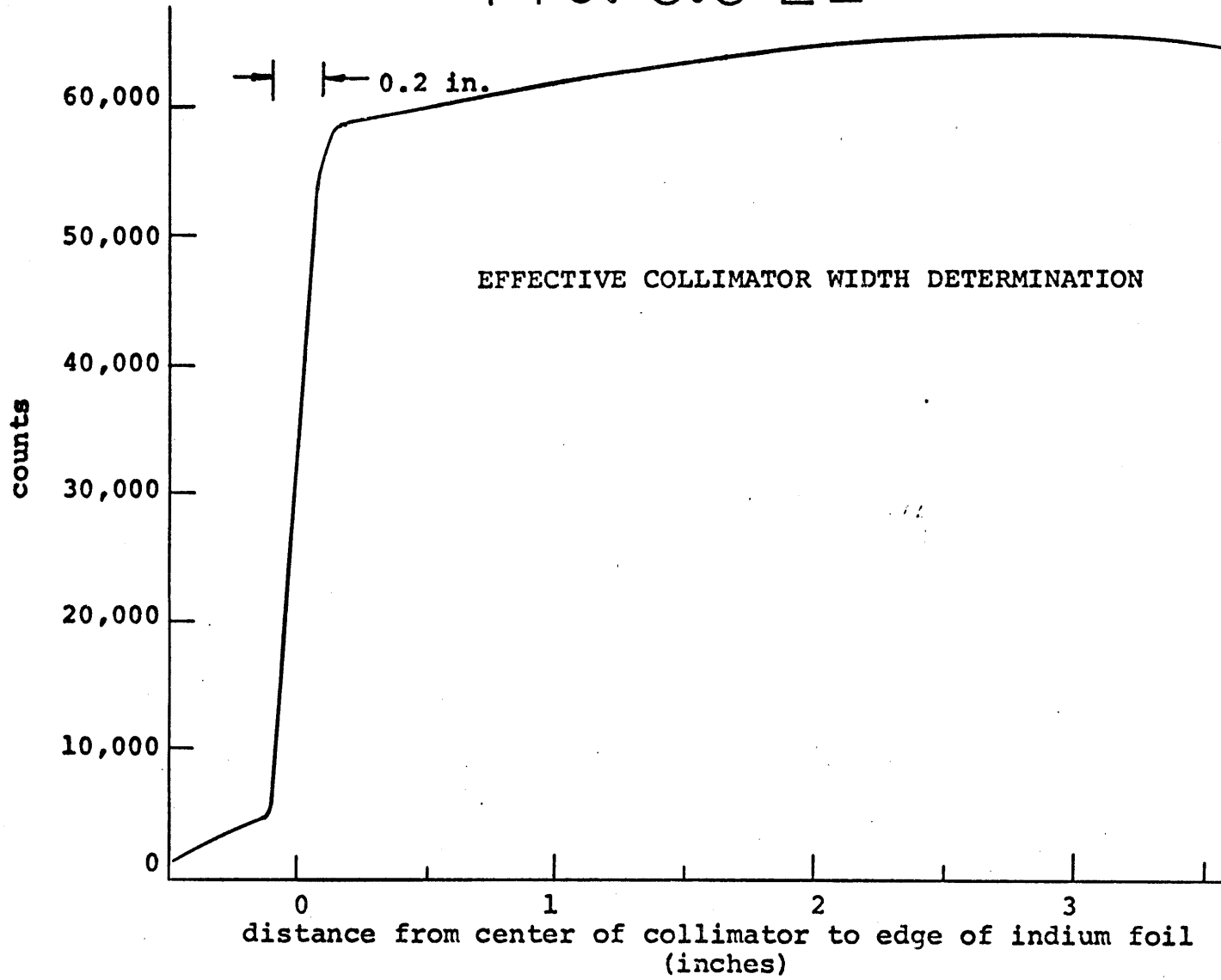
activity. Also, shield leakage seen by the detector is dependent upon the physical location of the fuel plate in the scanner.

The original correction method proposed by Labbe (Ref. 5.3-1) was to take background counts off the transverse edge of the fuel plate (i.e., no fuel meat directly under collimator) at various longitudinal positions. In this manner, a specific correction curve would be generated for each fuel plate. This curve would include effects from both the activity of the plate being counted and the longitudinal positioning of the fuel plate (the variation of B(K) with the lateral positioning of the fuel plate is small because of the narrowness of the fuel meat). This correction method was not possible because of limitation in the lateral motion of the scanner apparatus which prevented taking counts off the edge of the fuel meat at various longitudinal positions.

A generalized correction curve was developed in order to determine how the shape of the background and backscatter correction B(K) varied with longitudinal position of the fuel plate. When each plate was inserted into the gamma scanner apparatus, a position off the lower end of the fuel meat was counted as a reference background point. This reference count was proportional to the activity of the fuel plate. Figure 5.3-23 shows the generalized curve of the ratio of B(K) to reference point count versus long-

itudinal fuel plate position. An equation for this generalized curve is included in GAMSCAN. Using the inputed reference count and the longitudinal position of a given point, GAMSCAN calculates a background and backscatter correction, $B(K)$, for that given point using the generalized equation. In a similar manner, values of $B(K)$ are determined for all points scanned on a plate.

The generalized curve was experimentally determined and tuned to give accurate decay and background correction when compared with repeat scans of fuel plates. Figure 5.3-23 also shows experimental data for the ratio of counts off the edge of the fuel meat to counts at the reference point at various points along the length of the fuel plate for one plate in an irradiation. It was possible to obtain these counts by placing the fuel plate next to the machined slot used to hold the fuel plate and locating the edge of the fuel meat slightly offset from the colli-mator. The sample data points slightly disagree with the generalized curve at positions near the top of the fuel but this is because these experimental points were counted in a short time period during which little additional decay of the fuel plate would have occurred. During the actual complete scanning of a fuel plate the top of the plate would have decayed for an hour longer than the bottom of the fuel plate because of the time required to perform the scan. As a result the total activity of the plate

FIG. 5.3-23

GAMSCAN BACKGROUND AND BACKSCATTER CORRECTION CURVE

Curve is included in GAMSCAN computer code.
Plotted points are experimental data points.

distance from lower edge of fuel meat (inches)

ratio of B(K) to reference point counts
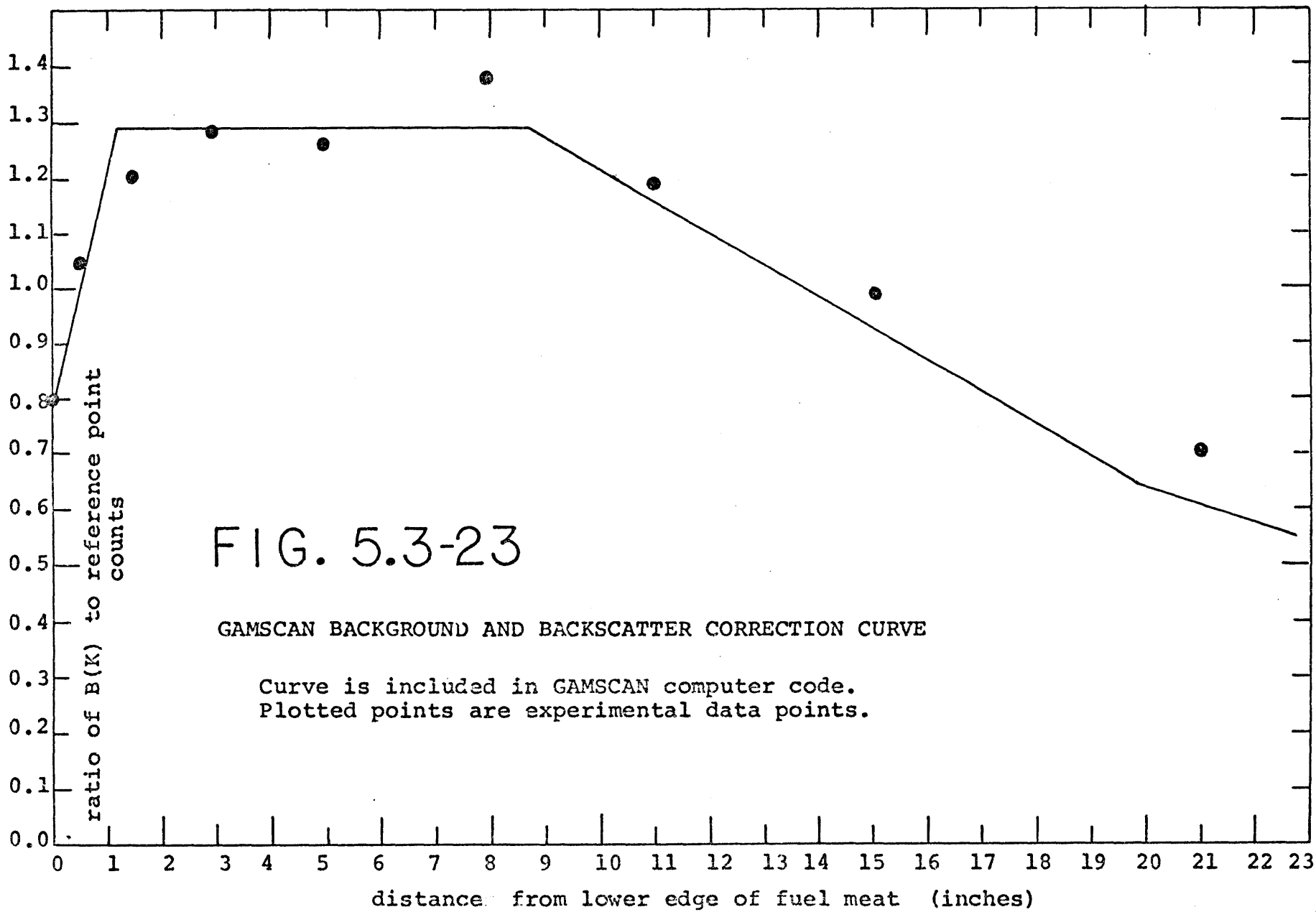
will be lower during the final point scanning and thus
B(K) will be lower than what would be the case if all
points were counted in a short time period.

5.3.4.5 Edge Peaking Correction

In order to determine the expected edge peaking
properly an extremely narrow collimator width would have
to be used to prevent the peak from being averaged out
over the coolimator width. An extremely narrow collimator
opening would give low count rates which would result in
statistical inaccuracies and cause high background and
backscatter count rates relative to the actual count.
The collimator opening used (0.5 inches x 0.125 inches)
is a compromise between maximum resolution and maximum
count rate. The collimator width of 0.125 is not small
relative to the distance over which the edge peak occurs,
therefore additional correction is required. Because the
collimator length in the direction parallel to the edge
peak is smaller than the length of the edge peak, the
following one-dimensional model is valid.

The fission product activity, which is directly
proportional to the power at the edge during operation,
is found to be represented by the distribution as shown
in Fig. 5.3-24 and can be approximated by the following
function:

$$P(x) = 0 \qquad \text{for } x < x_o , \qquad (5.3\text{-}6)$$

$$P(x) = Ae^{-a(x - x_o)} + B \qquad \text{for } x > x_o , \quad (5.3\text{-}7)$$

FIG. 5.3-24

ASSUMED POWER PEAK SHAPE AT BOTTOM EDGE OF FUEL
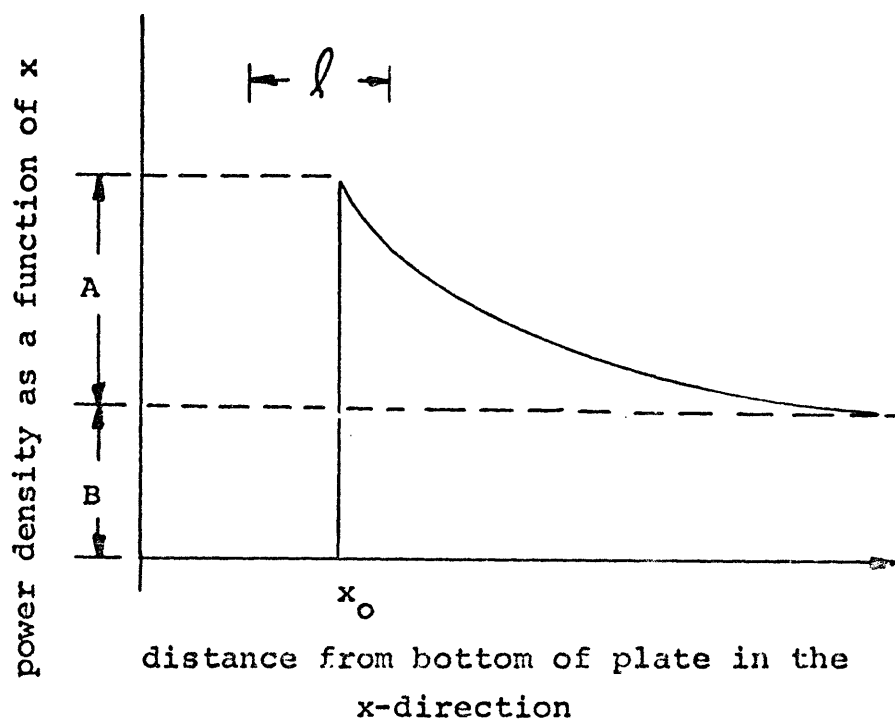
ℓ is the collimator width

where,

P(x)   is the fission product activity at point
       as a function of x,

A   is the amplitude of the exponential,

B   is the constant base level of activity
    beneath the actual peak,

x_o is the location of the end of the fuel,

a   is the reciprocal of the relaxation length
    for x the peaking at the end.

If the detector integrates over length ℓ, where ℓ is the effective width of a collimator whose center is at x, the counts obtained assuming detector efficiency constant and equal to one will be:

$$C(x) = \int_{x - \ell/2}^{x + \ell/2} P(x)\,dx \ . \qquad (5.3-8)$$

The above equation can be divided into the following for various values of x:

$$C(x) = 0 \qquad \text{for } x \leq x_o - \ell/2 \ , \qquad (5.3-9)$$

$$C(x) = \int_{x_o}^{x + \ell/2} P(x)\,dx \qquad \text{for } x_o - \ell/2 < x \leq x_o + \ell/2 \ . \qquad (5.3-10)$$

$$C(x) = \int_{x - \ell/2}^{x + \ell/2} P(x)\,dx \qquad \text{for } x > x_o + \ell/2 \ . \qquad (5.3-11)$$

Substituting Eq. 5.3-7 for P(x) and integrating for general limits yields:

$$C(x) = \int_{x_1}^{x_2} P(x)\,dx = A \int_{x_1}^{x_2} e^{-a(x - x_o)}\,dx + \int_{x_1}^{x_2} B\,dx,$$

(5.3-12)

giving,

$$C(x) = \frac{A e^{-a(x - x_o)}}{a} \Bigg/ \begin{array}{c} x_1 \\[2ex] x_2 \end{array} + B(x_2 - x_1) \quad . \quad (5.3\text{-}13)$$

The integral limits from Eqs. 5.3-10 and 5.3-11 are put into the general Eq. 5.3-13. For Eq. 5.3-10 where,

$$x_o - \ell/2 < x \leq x_o + \ell/2 \ ,$$

$$x_1 = x_o$$

$$x_2 = x + \ell/2 \ ,$$

Eq. 5.3-13 becomes:

$$C(x) = \frac{A}{a} [e^{-a(x_o - x_o)} - e^{-a(x + \ell/2 - x_o)}] +$$

$$B[x + \ell/2 - x_o] \ , \quad (5.3\text{-}14)$$

which simplifies to:

$$C(x) = \frac{A}{a} [1 - e^{-a(x + \ell/2 - x_o)}] + B[x + \ell/2 - x_o].$$

(5.3-15)

For Eq. 5.3-11 where,

$$x_o + \ell/2 < x ,$$

$$x_1 = x - \ell/2 ,$$

$$x_2 = x + \ell/2 ,$$

Eq. 5.3-13 becomes:

$$C(x) = \frac{A}{a}[e^{-a(x - \ell/2 - x_o)} - e^{-a(x + \ell/2 - x_o)}] + B\ell , \tag{5.3-16}$$

which simplifies to:

$$C(x) = \frac{A}{a}[e^{-a(x + \ell/2 - x_o)} [e^{a\ell} - 1]] + B\ell . \tag{5.3-17}$$

The value of $C(x)$ for all values of x is given by three expressions:

$$C(x) = 0 \qquad \text{for } x < x_o - \ell/2, \tag{5.3-18}$$

$$C(x) = \frac{A}{a} [1 - e^{-a(x - x_o + \ell/2)}] + B[x - x_o + \ell/2] \tag{5.3-19}$$
$$\text{for } x_o - \ell/2 < x \leq x_o + \ell/2,$$

$$C(x) = \frac{A}{a} [e^{-a(x - x_o + \ell/2)} [e^{a\ell} - 1]] + B\ell \tag{5.3-20}$$
$$\text{for } x > x_o + \ell/2.$$

Now the peak measured number of counts will occur when $x = x_o + \ell/2$ because the detector will be viewing the maximum amount of activity. If the detector viewed the peak activity over the whole collimator effective width ℓ,

C_{peak} would be:

$$C_{peak} = (A + B)\ell. \tag{5.3-21}$$

Thus the ratio of the actual peak to the measured peak using Eq. 5.3-19 and substituting $x_o + \ell/2$ for x becomes:

$$\frac{C_{peak}}{C(x_o + \ell/2)} = \frac{(A + B)\ell}{[\frac{A}{a}[1 - e^{-a\ell}] + B\ell]} . \tag{5.3-22}$$

Note that if the detector efficiency was not equal to one, but still a constant, it would have divided away at this point.

Because the constant base level measurement is not subject to collimator area averaging and can be easily measured, the rise factor above the base level is the value of interest. If the base level counts is equal to $B\ell$, the rise factor is:

$$D^* = \frac{\text{Actual peak-base level}}{\text{Measured peak-base level}} = \frac{(A + B)\ell - B\ell}{\frac{A}{a}(1 - e^{-a\ell}) + B\ell - B\ell}, \tag{5.3-23}$$

which simplifies to:

$$D^* = \frac{a\ell}{1 - e^{-a\ell}} , \tag{5.3-24}$$

or

$$\text{Actual peak above base level} = (\frac{a\ell}{1 - e^{a\ell}}) \times \text{measured peak above base level}. \tag{5.3-25}$$

In order to determine the actual peak from the measured peak, B, ℓ, P_M, and a must be determined where:

B   is the base level activity,

ℓ is the effective collimator width,

P_M is the measured peak above the base level,

a   is the reciprocal of the relaxation length for the peaking at the end.

The effective collimator width, ℓ, was determined experimentally as described in Section 5.3.4.3. The remaining parameters B, P_M, and a were determined for each plate of interest by graphically interpreting the power distribution data obtained from gamma scanning. Figure 5.3-25 is an example of plots used to determine B, P_M, and a. Because the actual uranium density tapers off at the fuel plate ends, this extrapolation gives a conservative value of the bottom edge peak for the plates as constructed.

Table 5.3-6 shows the measured peak and the calculated actual peak at the lower end of several plates of interest. Note that the sharpness of the peak (compare F_a to B) increases as the distance from the outer cylindrical edge of the core increases. However, the actual power produced at the lower edge peak increases only slightly from the outer cylindrical edge to the center as witnessed by the slight increase in the product $F_a F_r$. The importance of this lower edge peak is discussed in Section 7.3.2.

FIG. 5.3-25

BOTTOM EDGE PEAK PLOT USED TO DETERMINE B, P_M, AND a

A-2 plate 1

C-9 plate 1

C-8 plate 8

F_a

expected distance from bottom edge of fuel meat
(inches)
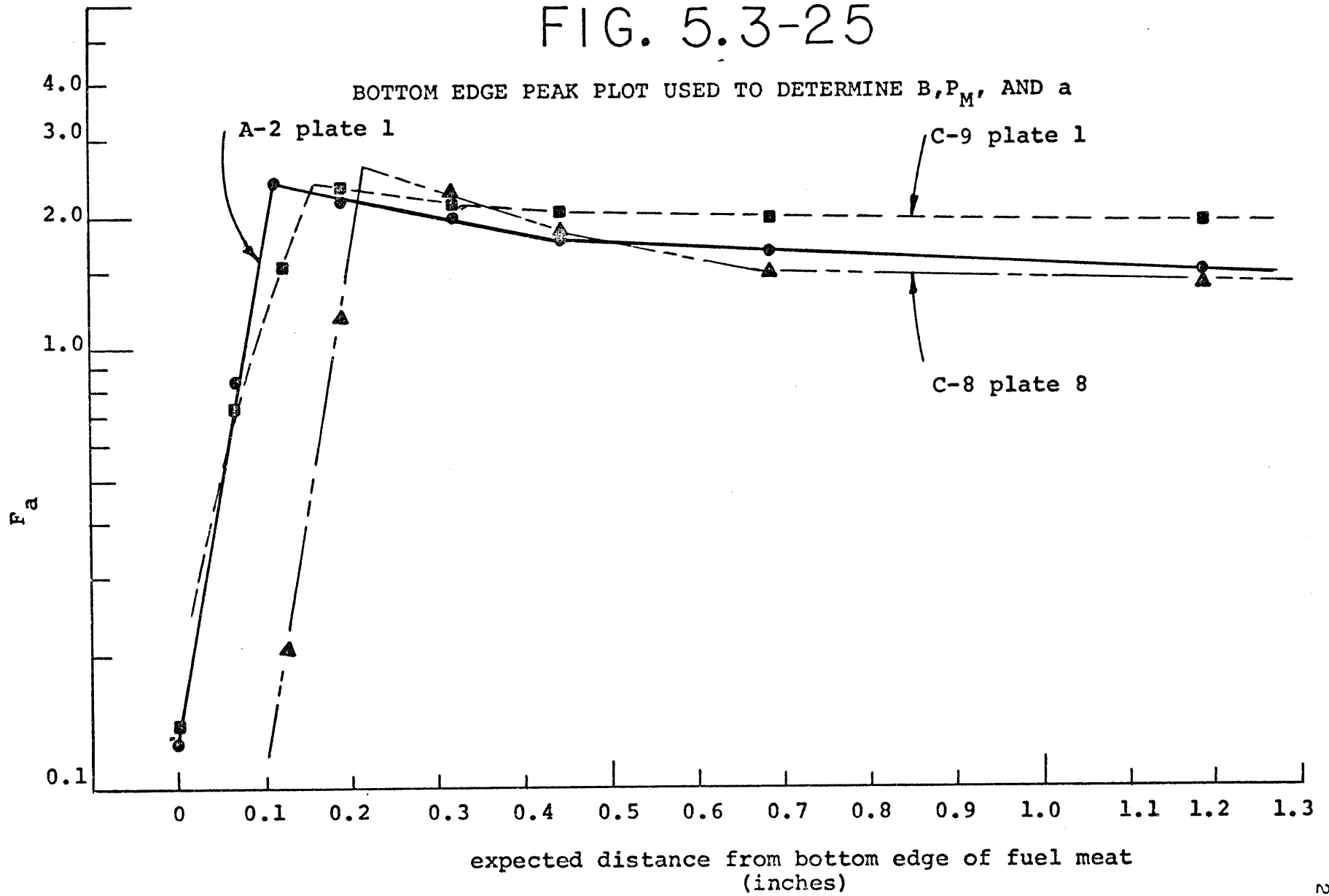
TABLE 5.3-6

COMPARISON BETWEEN EXTRAPOLATED VALUES OF F_a AT FUEL
PLATE BOTTOM EDGE AND PEAK MEASURED VALUE

Plate Position*	Extrapolated F_a	Peak Measured F_a	B
C-8, Plate 1	2.22	1.95	1.64
C-8, Plate 2	1.92	1.83	1.58
C-8, Plate 8	3.31	2.25	1.40
C-9, Plate 1	2.49	2.32	1.90
B-9, Plate 1	2.79	2.41	1.60
A-2, Plate 1	2.57	2.26	1.48

* Element orientations listed in Table 5.3-1.

5.3.5 Power Distribution from Gamma Scanning

By using the results of COREFAC, power distributions
at various positions of interest in the core can be plotted.
In order to simplify comparison between various plots, the
value of the product F_r x F_a is plotted versus position.
The quantity $F_r F_a$, which is the product of the radial
peaking factor and axial peaking factor at the point
being plotted, is a measure of the power generated at the
point relative to the average core power.

The power distribution across the fuel element in
position B-5 is shown in Fig. 5.3-18. Note that the
power distribution is fairly flat across B-5 indicating
a uniform power production at the given height in the
element. Figure 5.3-26 shows the power distribution
across a fuel element in position C-9 as several different
heights. For C-9 the power distribution is spiked either
up or down on the plate next to the control blade de-
pending upon whether the height in the element is above
or below the height of the control blade. The power dis-
tribution across a fuel element in position C-8 is shown
in Fig. 5.3-27. The power shape is similar to that found
in C-9 with the exception that the control blades do not
depress the power distribution as much as in C-9 for
heights above the height of the control blade.

Figure 5.3-28 shows power distributions across fuel
elements in B-3 and A-2. The element in A-2 has one side

FIG. 5.3-26

POWER DISTRIBUTION ACROSS ELEMENT C-9 AT SEVERAL ELEVATIONS

Irradiation 1 shown here.
Plate 1 is next to control blade slot.
Z is distance in inches from bottom
    of fuel meat.

$Z = 0.438$

$Z = 5.438$

$Z = 13.688$

$F_r F_a$

plate number

• $Z = 0.438$
♦ $Z = 5.438$
▲ $Z = 13.688$
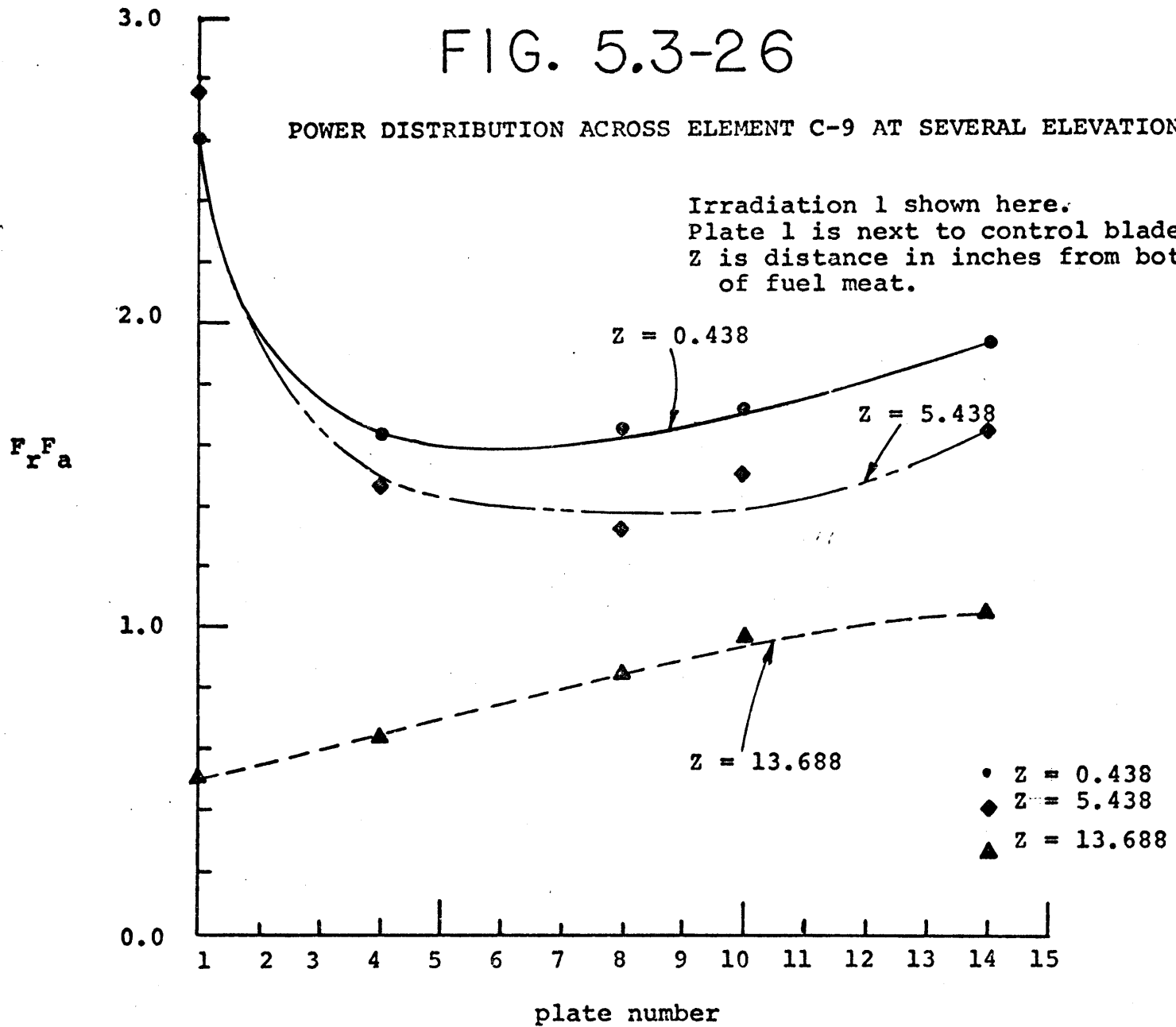
FIG. 5.3-27

POWER DISTRIBUTION ACROSS ELEMENT C-8 AT SEVERAL ELEVATIONS

Irradiations 6 and 14 shown here.
Plate 1 is next to core housing.
Z is distance in inches from bottom
of fuel meat.

Z = 0.438

Z = 5.438

Z = 13.688

$F_r F_a$

• Z = 0.438
◈ Z = 5.438
▲ Z = 13.688

plate number

FIG. 5.3-28

- A-2 @ Z=0.438 ⎫ Irradiation 5, plate 1 is next to solid
- A-2 @ Z=13.688 ⎭ dummy

- B-3 @ Z=0.438 ⎫ Irradiation 13, plate 1 is next to
- B-3 @ Z=13.688 ⎭ hexagonal spider

Z is distance in inches from bottom of fuel meat.

$F_r F_a$

Z = 0.438 (B-3)

Z = 0.438 (A-2)

Z = 13.688 (A-2)

Z = 13.688 (B-3)

plate number
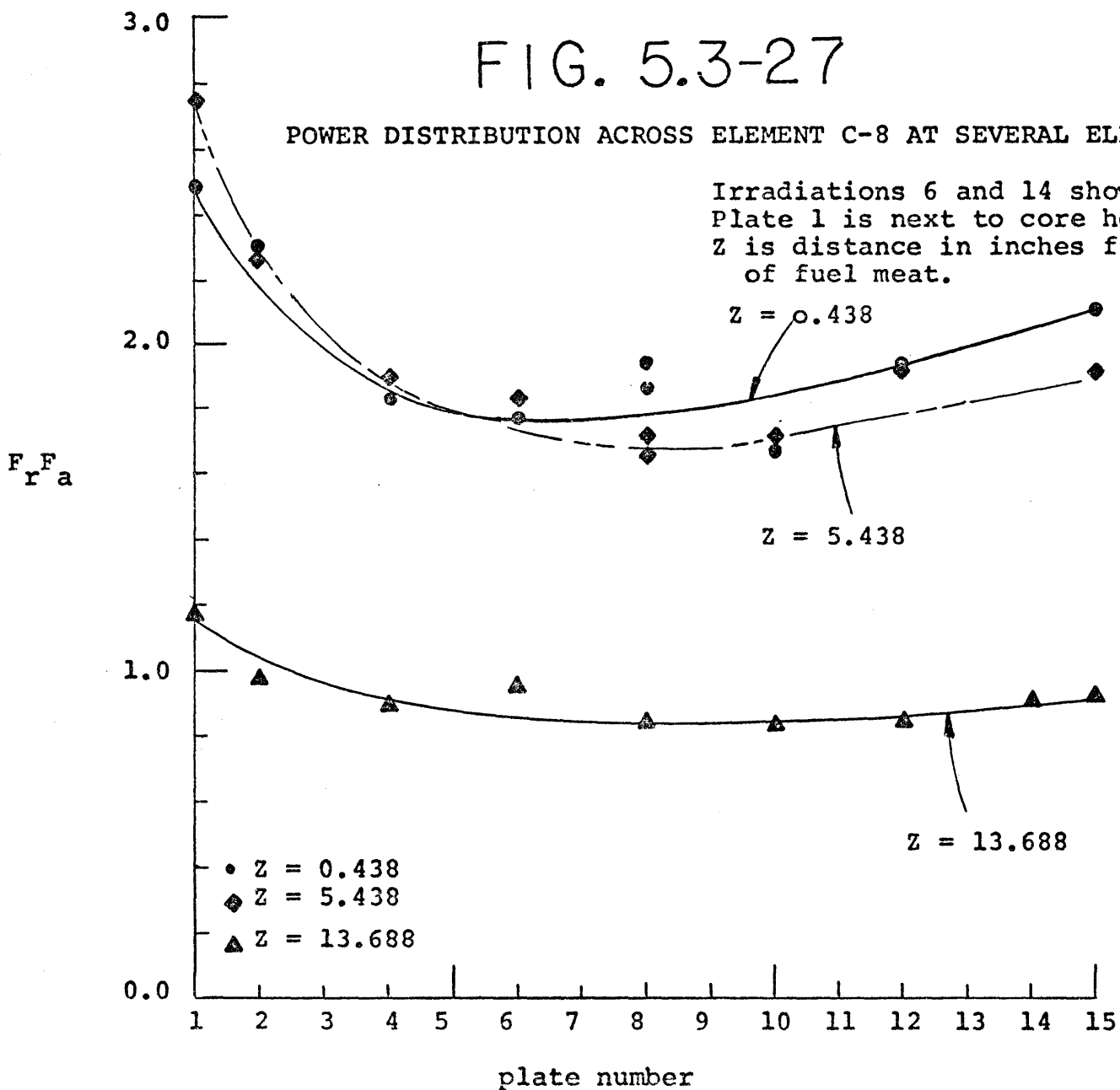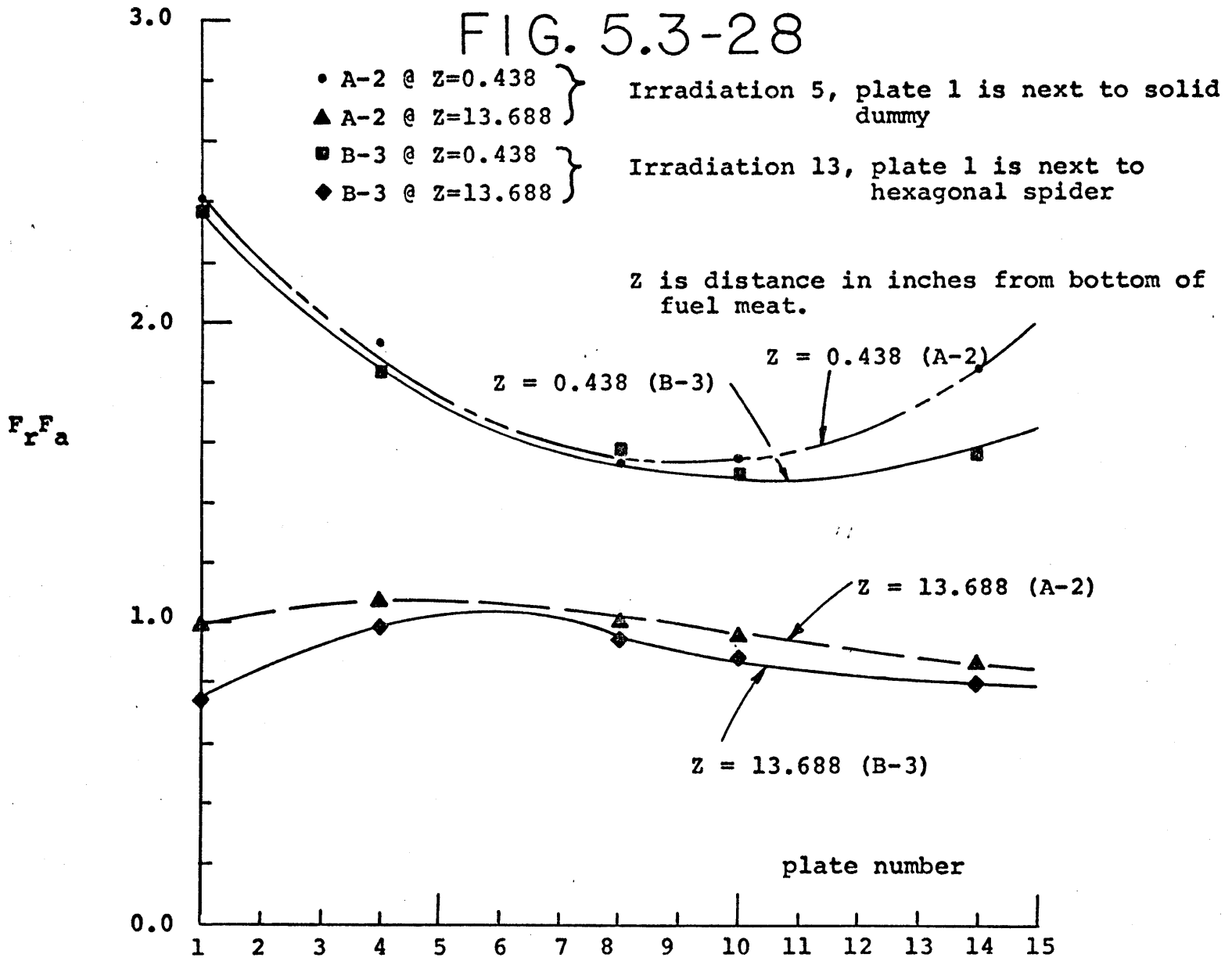
POWER DISTRIBUTIONS ACROSS ELEMENTS B-3 AND A-2 AT SEVERAL ELEVATIONS

next to a solid dummy and the other side next to the absorber spider. The element in B-3 has two sides next to the absorber spider and one side next to a solid dummy. The distributions are shown at two different heights in the element, in order to show the difference caused by the absorber spider: whether the height of the distribution is above or below the cadmium absorber in the spider.

Figure 5.3-29 shows the axial power distribution in C-8 next to the corner water hole for two different shim bank heights. For Core I of the MITR-II this channel gave the highest total power. Note that raising the shim bank lowered the peak even though the actual power generated increased slightly.

Figure 5.3-30 shows the axial power distribution for C-9 which is on the outer edge of the core, next to a shim blade. For plate 1 which is next to the shim blade, a large power peak occurs because of water replacing the shim blade in the shim blade slot. Note that this peak is quickly suppressed above the height of the shim blade. Also note that this large peak does not exist several plates into the element.

Figure 5.3-31 shows the power distribution in B-9 for plate 1 which is next to both a solid dummy and the hexagonal spider. The largest bottom edge spikes occurred for this element and the element in A-2. The calculated

value of F_rF_a using the edge correction method agrees
very well with the extrapolated graphical value. Note
that the power drops off rapidly at heights in the
element above the height of the fixed absorber.

Figure 5.3-32 shows the axial power distribution
in B-5. Element B-5 is nearly completely surrounded by
other fuel elements and has the highest total element
power of any element in Core I.

Figure 5.3-33 shows the axial power distribution
for plate 1 in A-2 for the plate next to a solid dummy
or next to the original In-core Sample Assembly (ICSA).
The large peak caused by the ICSA was the determining
factor used in eliminating the ICSA from Core I.

Table 5.3-7 shows the core power distribution for
Core I elements where the removable plate element was
irradiated averaged over plates and elements. Figure
5.3-34 shows the element average powers in their relative
core positions.

Figures 5.3-35 through 5.3-37 show values of F_rF_a
at various horizontal slices through the core. These
slices are at 0.438, 5.438, and 13.688 inches from the
bottom of the fuel, respectively.

5.4 Neutron Flux Measurements by Copper Wire Activation

Flux distribution measurements as indicated by activa-
tion of foils and wires were made at several locations incore
and in experimental facilities in order to be able to compare

FIG. 5.3-29

CORE I AXIAL POWER DISTRIBUTION IN ELEMENT POSITION C-8
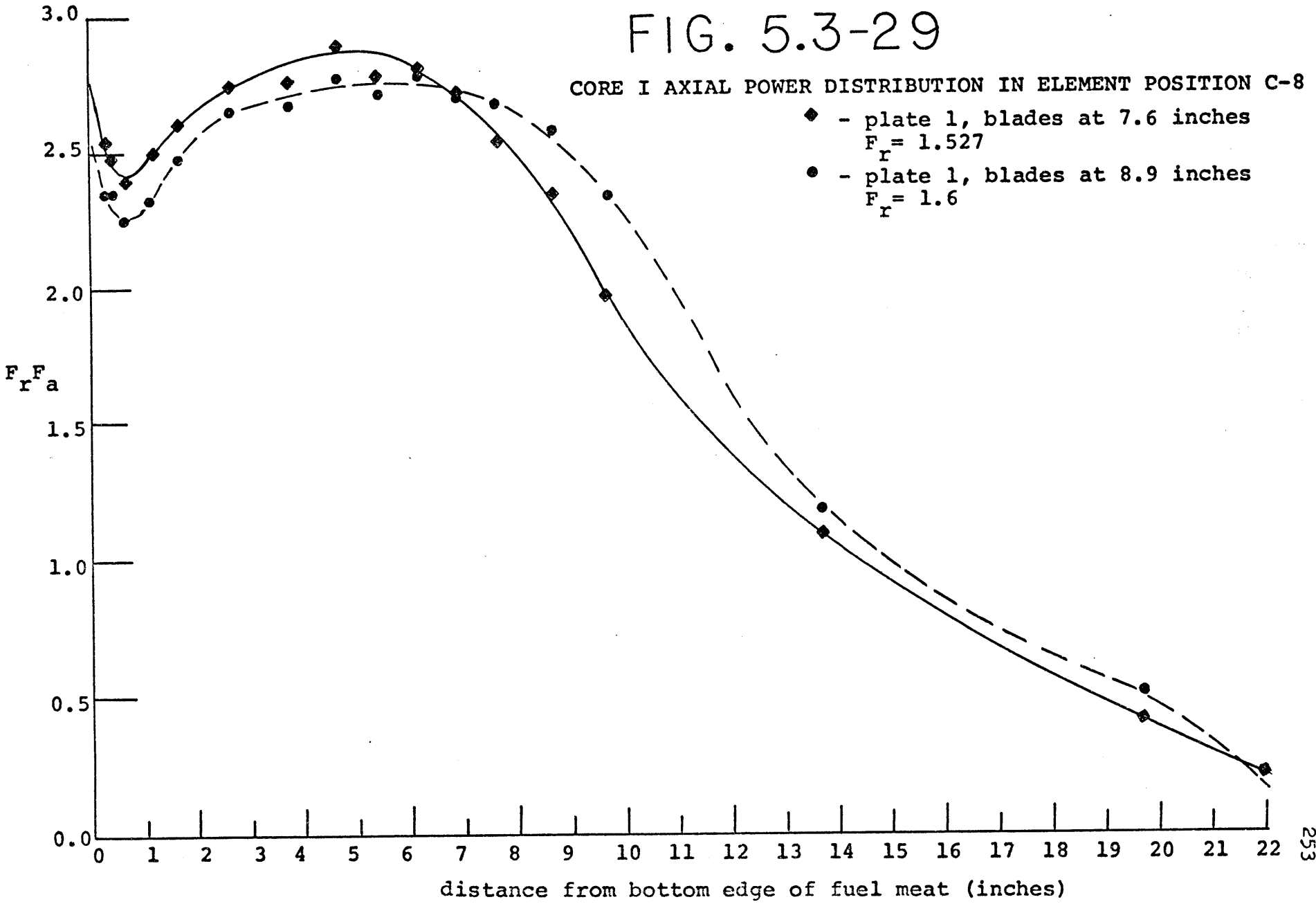
♦ - plate 1, blades at 7.6 inches
  F_r = 1.527

● - plate 1, blades at 8.9 inches
  F_r = 1.6

$F_r F_a$

distance from bottom edge of fuel meat (inches)

FIG. 5.3-30

CORE I AXIAL POWER DISTRIBUTION IN ELEMENT POSITION C-9

♦ — plate 1, blades at 7.6 inches
F_r = 1.266

● — plate 4, blades at 7.6 inches
F_r = 0.93

F_rF_a

distance from bottom edge of fuel meat (inches)

FIG. 5.3-31

CORE I AXIAL POWER DISTRIBUTION IN ELEMENT POSITION B-9

Using edge correction method
the calculated value of the
bottom edge spike is: $F_r F_a = 3.43$.

$\bullet$ - plate 1, blades at 7.6 inches
$F_r = 1.23$

$F_r F_a$

distance from bottom edge of fuel meat (inches)
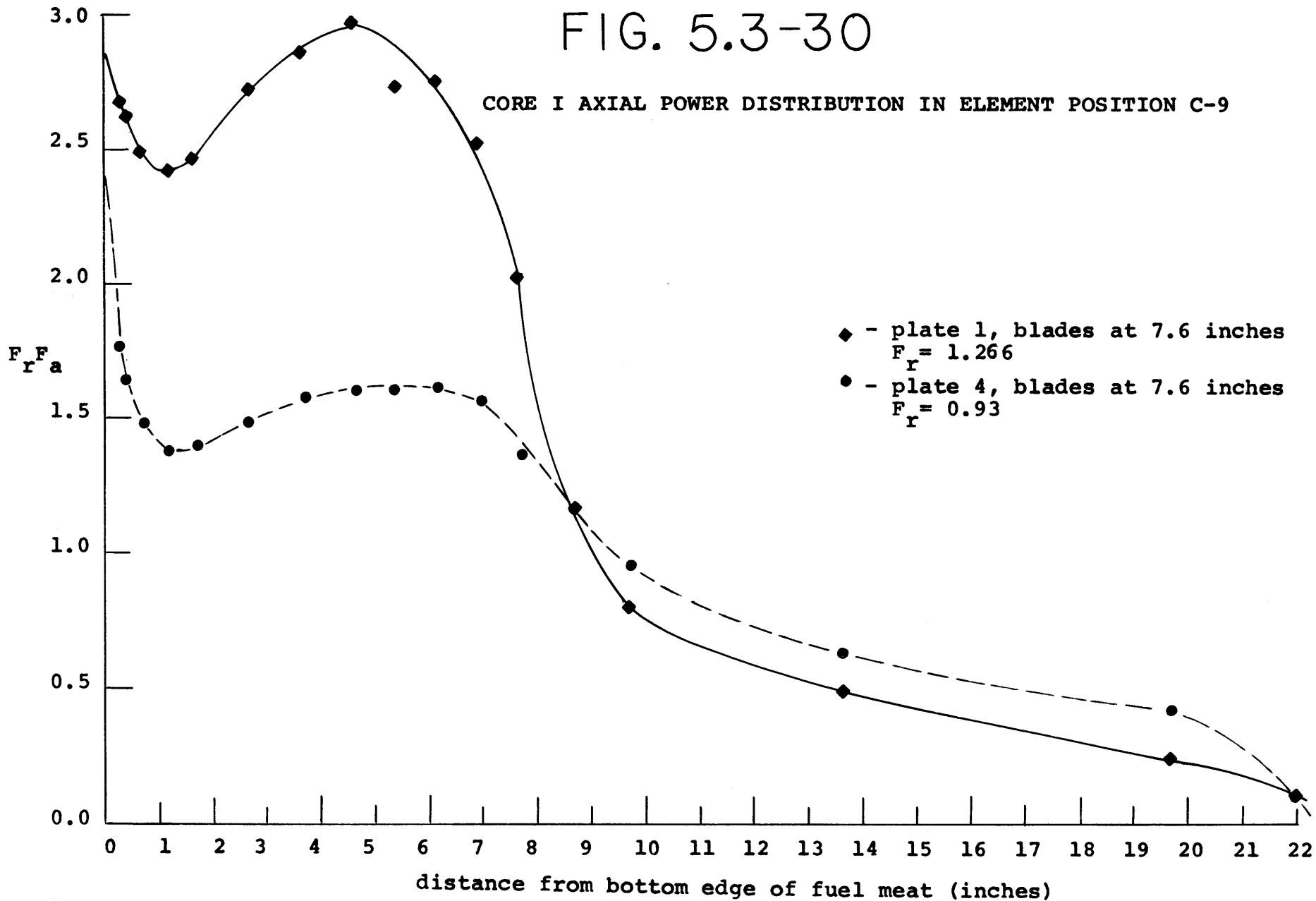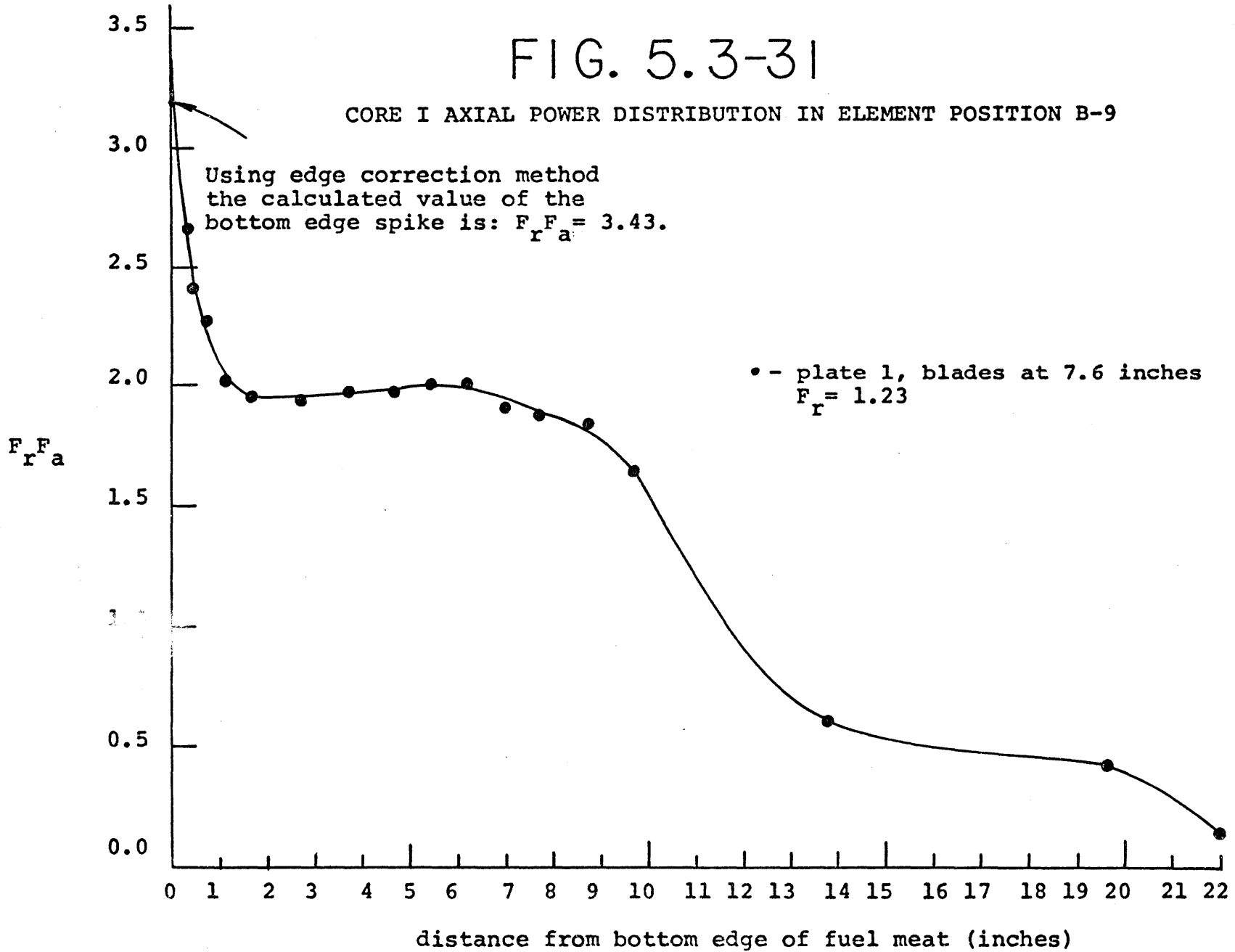
FIG. 5.3-32

CORE I AXIAL POWER DISTRIBUTION IN ELEMENT POSITION B-5

- plate 1, blades at 7.6 inches
$F_r = 1.275$

$F_r Fa$ (y-axis)

distance from bottom edge of fuel meat (inches) (x-axis)

FIG. 5.3-33

CORE I AXIAL POWER DISTRIBUTION IN ELEMENT POSITION A-2

▲ - plate 1, blades at 7.4 inches
ICSA in A-1, F_r = 2.13

● - plate 1, blades at 7.6 inches
solid dummy in A-1, F_r = 1.333

$F_r F_a$

distance from bottom of fuel meat (inches)
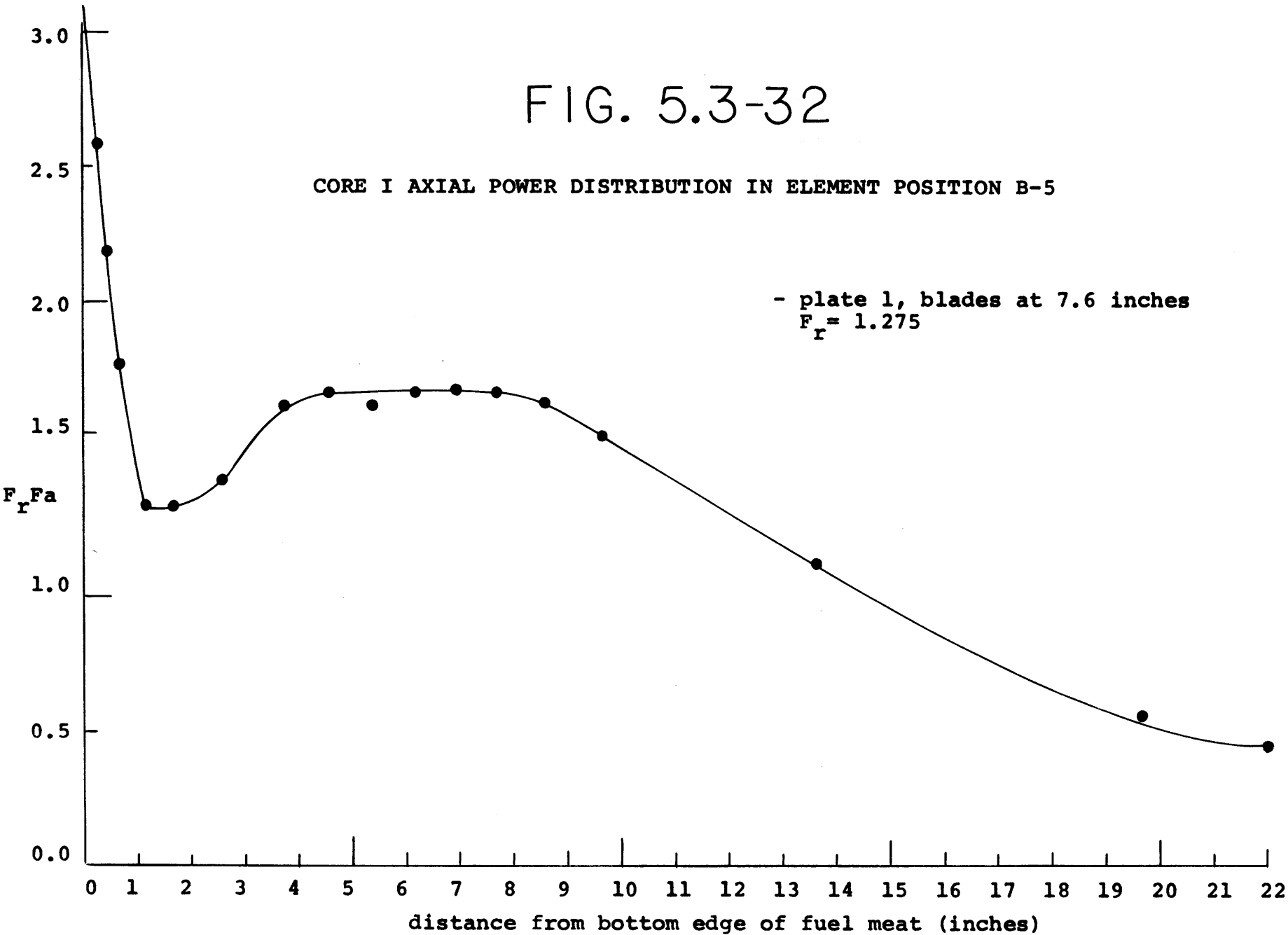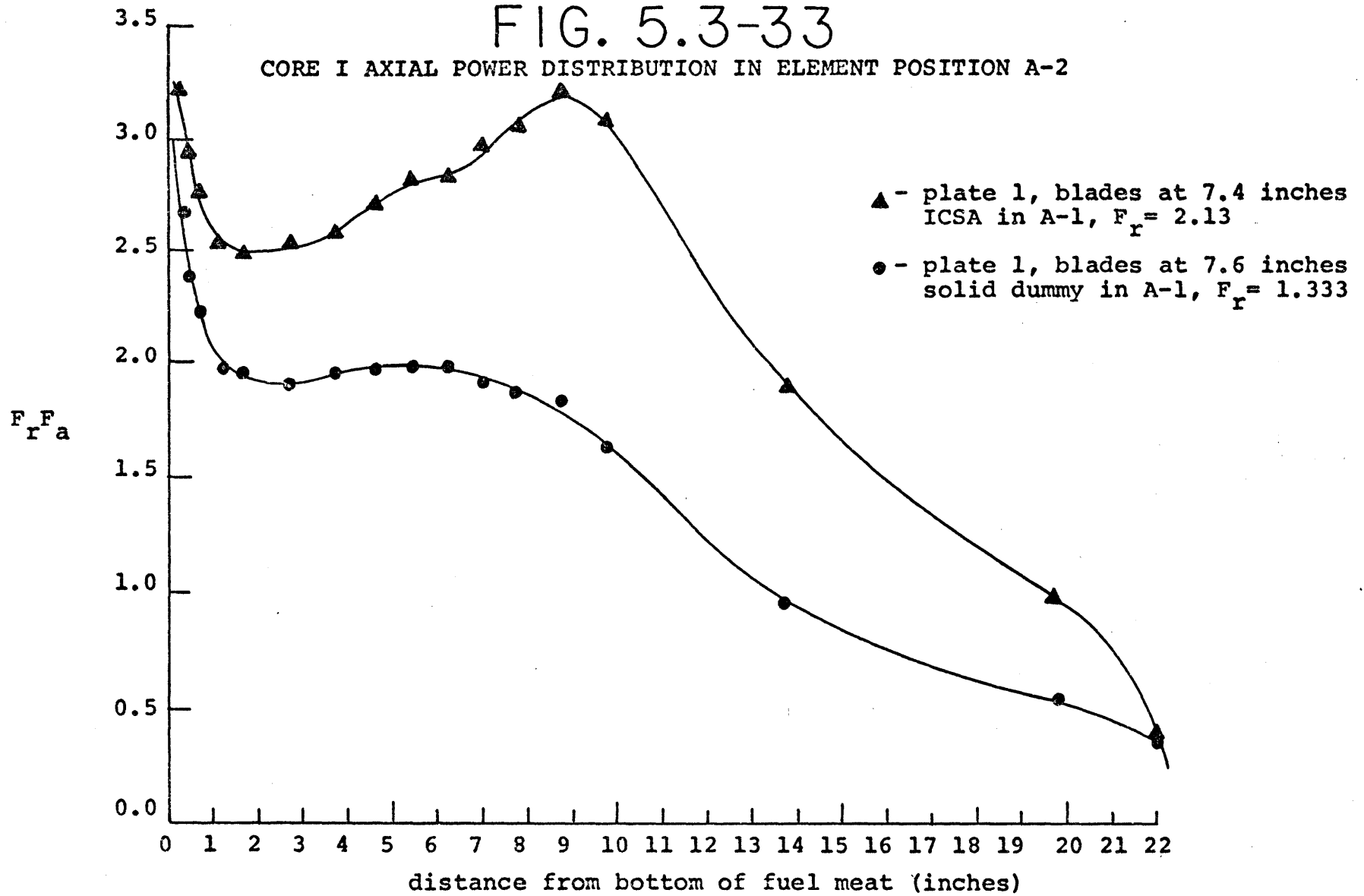
FIG. 5.3-34

RELATIVE POWERS OF ELEMENTS IN CORE I WHERE THE REMOVABLE PLATE ELEMENT WAS IRRADIATED

REGULATING ROD
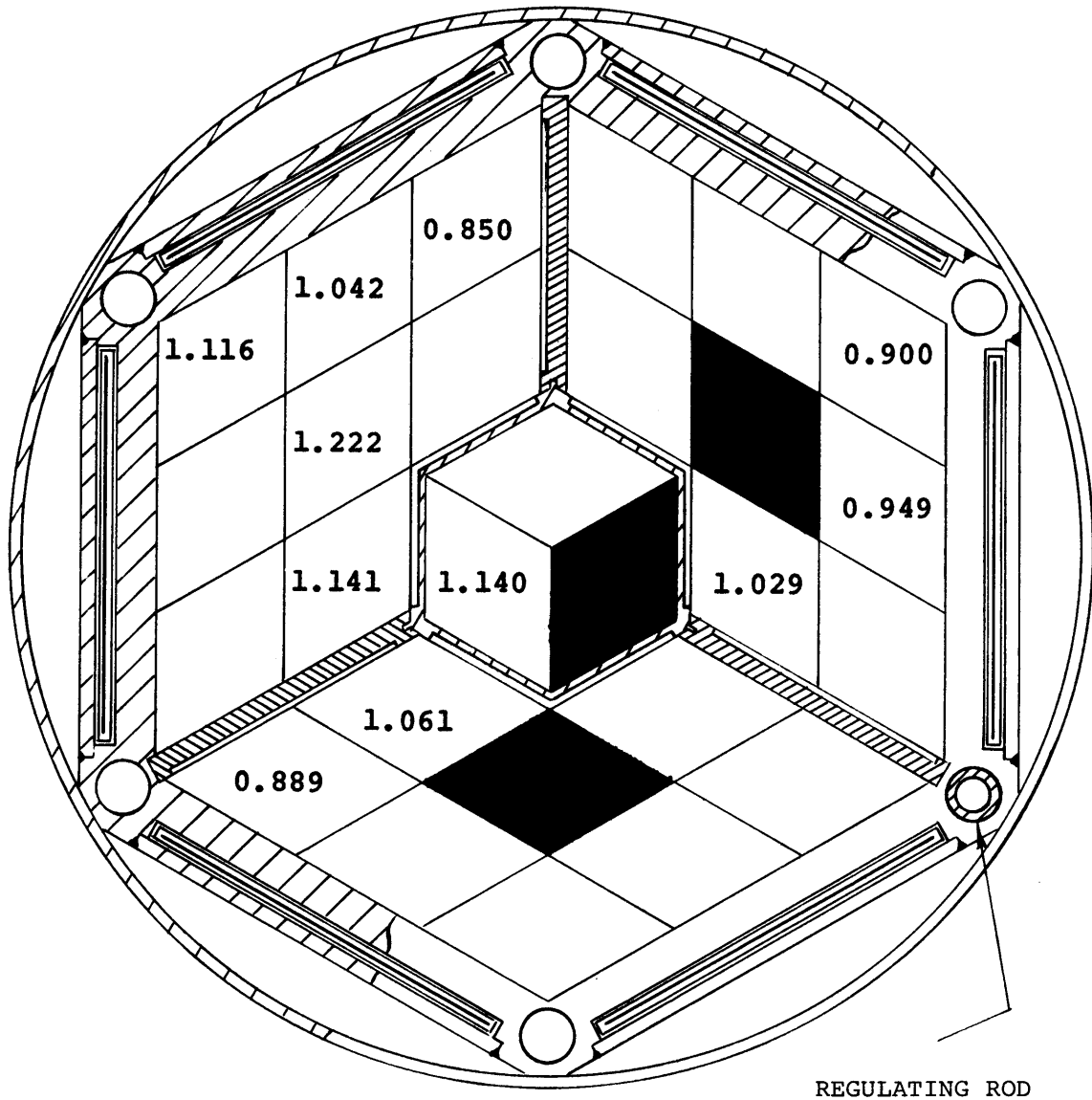
Above numbers are the ratios of the COREFAC predicted element power for that position to the average element power in the core.

▰ - solid dummy element

TABLE 5.3-7

RELATIVE POWER DISTRIBUTION IN PLATES AND ELEMENTS OF
CORE I WHERE THE REMOVABLE PLATE ELEMENT WAS
IRRADIATED – BLADES AT 7.6 INCHES

Core Element Position (Irradiation #)	Plate* Number	Ratio of Plate to Power of Average Plate in Core	Ratio of Element to Power of Average Element in Core
C-9 (Irradiation #1)	1	1.2661	
	4	.9299	
	8	.9504	1.042
	10	1.0687	
	14	1.1064	
C-5 (Irradiation #3)	1	1.3556	
	4	.8833	
	8	.8224	0.889
	10	.7614	
	14	.8209	
B-4 (Irradiation #4)	1	1.2018	
	4	1.1703	
	8	1.1662	1.141
	10	1.0884	
	14	1.1083	
A-2 (Irradiation #5)	1	1.3333	
	4	1.1671	
	8	1.1205	
	10	1.0612	1.140
	14	1.0908	
C-8 (Irradiation #6)	1	1.5274	
	4	1.0960	
	8	1.0047	1.116
	10	1.0003	
	14	.9227	

TABLE 5.3-7 (Continued)

Core Element Position (Irradiation #)	Plate* Number	Ratio of Plate to Power of Average Plate in Core	Ratio of Element to Power of Average Element in Core
B-5) (Irradiation #7)	1	1.2758	
	4	1.2663	
	8	1.2301	1.222
	10	1.1994	
	14	1.1639	
C-10 (Irradiation #8)	1	1.2844	
	4	.8567	
	8	.8188	0.85
	10	.8427	
	14	.7050	
B-9 (Irradiation #10)	1	1.2296	
	4	1.1435	
	8	1.0324	1.029
	10	.9399	
	14	.9062	
C-14 (Irradiation #11)	1	1.2255	
	4	.9165	
	8	.8969	0.9494
	10	.8964	
	14	.9539	
C-13 (Irradiation #12)	1	1.3969	
	4	.9585	
	8	.8299	0.90
	10	.7742	
	14	.8074	
B-3 (Irradiation #13)	1	1.1935	
	4	1.1823	
	8	1.0741	1.061
	10	1.0349	
	14	.9139	

TABLE 5.3-7 (Continued)

Core Element Position (Irradiation #)	Plate* Number	Ratio of Plate to Power of Average Plate in Core	Ratio of Element to Power of Average Element in Core
C-8 (Irradiation #14)	15**	1.1828	
	12	1.1236	
	8	1.0327	1.116
	6	1.0797	
	2	1.3152	

*   Position of plate 1 in core position is listed in Table 5.3-1. In comparing GAMSCAN results to actual plate position the following is true except for Irradiation #14:

GAMSCAN Plate #	Actual Plate #
1	1
2	4
3	8
4	10
5	14

**For Irradiation #14, the following relationship between GAMSCAN Plate # and Actual Plate # is true:
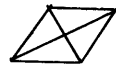
GAMSCAN Plate #	Actual Plate #
1	15
2	12
3	8
4	6
5	2

"Plate 1" in C-8 position is next to core housing.

FIG. 5.3-35

CORE I EXPERIMENTAL POWER DISTRIBUTION FOR A HORIZONTAL
CROSS-SECTION 0.438 INCHES FROM BOTTOM EDGE OF FUEL MEAT

regulating rod
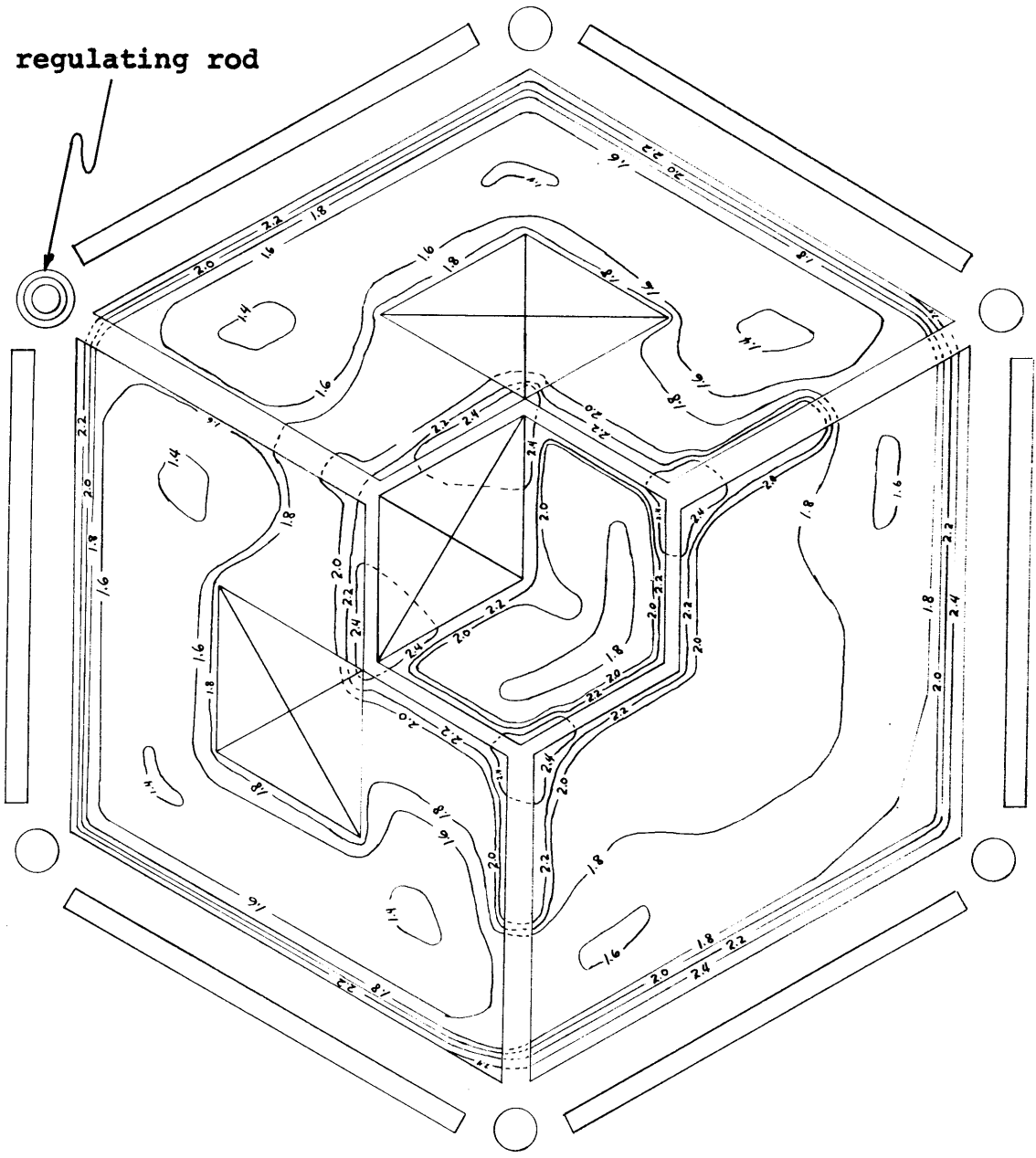
⬦ - solid dummy element

Contour lines are equal values of $F_r F_a$.

FIG. 5.3-36

CORE I EXPERIMENTAL POWER DISTRIBUTION FOR A HORIZONTAL
CROSS-SECTION 5.438 INCHES FROM BOTTOM EDGE OF FUEL MEAT

regulating rod
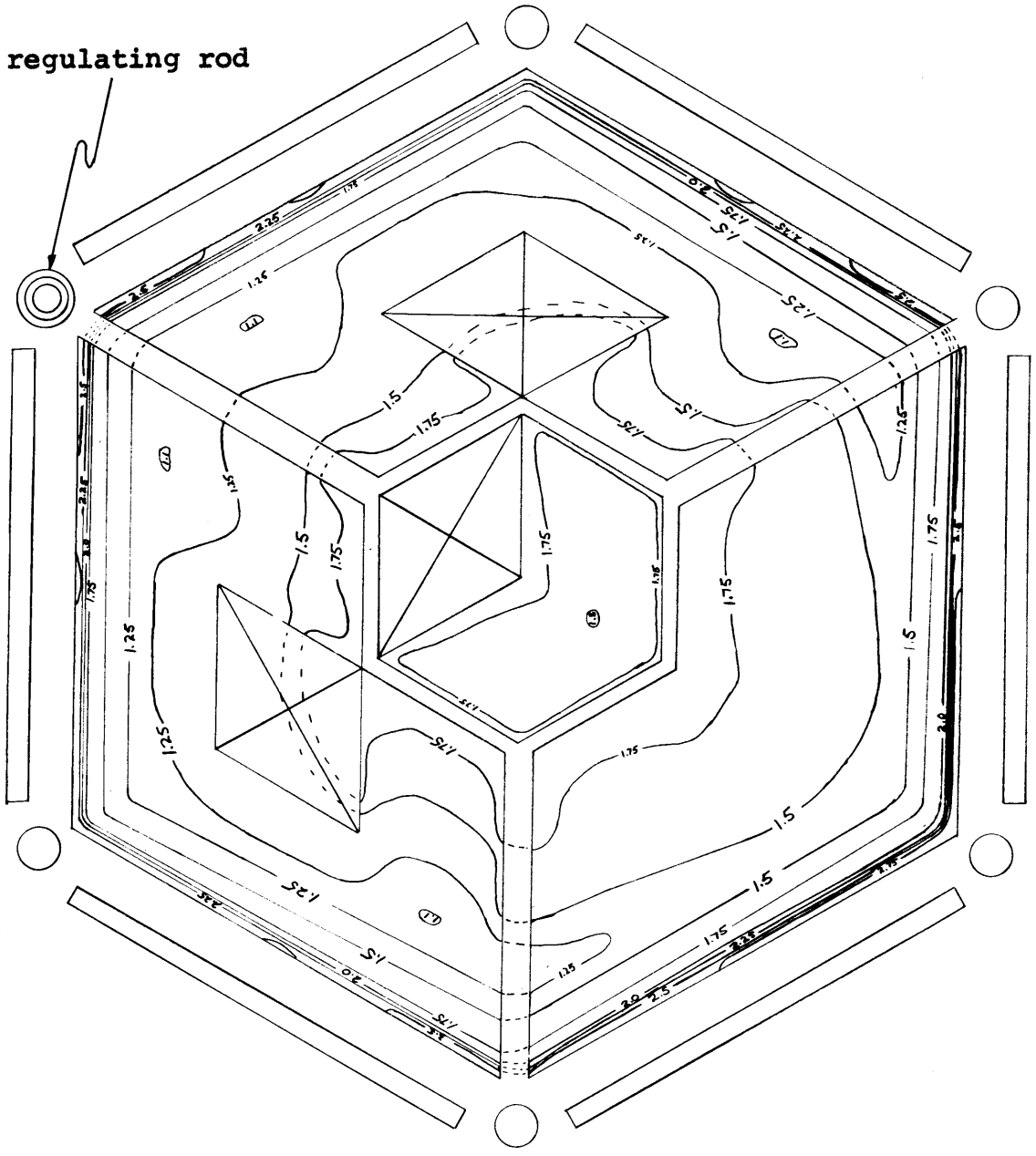
- solid dummy element

Contour lines are equal values of $F_r F_a$.

FIG. 5.3-37

CORE I EXPERIMENTAL POWER DISTRIBUTION FOR A HORIZONTAL
CROSS-SECTION 13.688 INCHES FROM BOTTOM EDGE OF FUEL MEAT

regulating rod
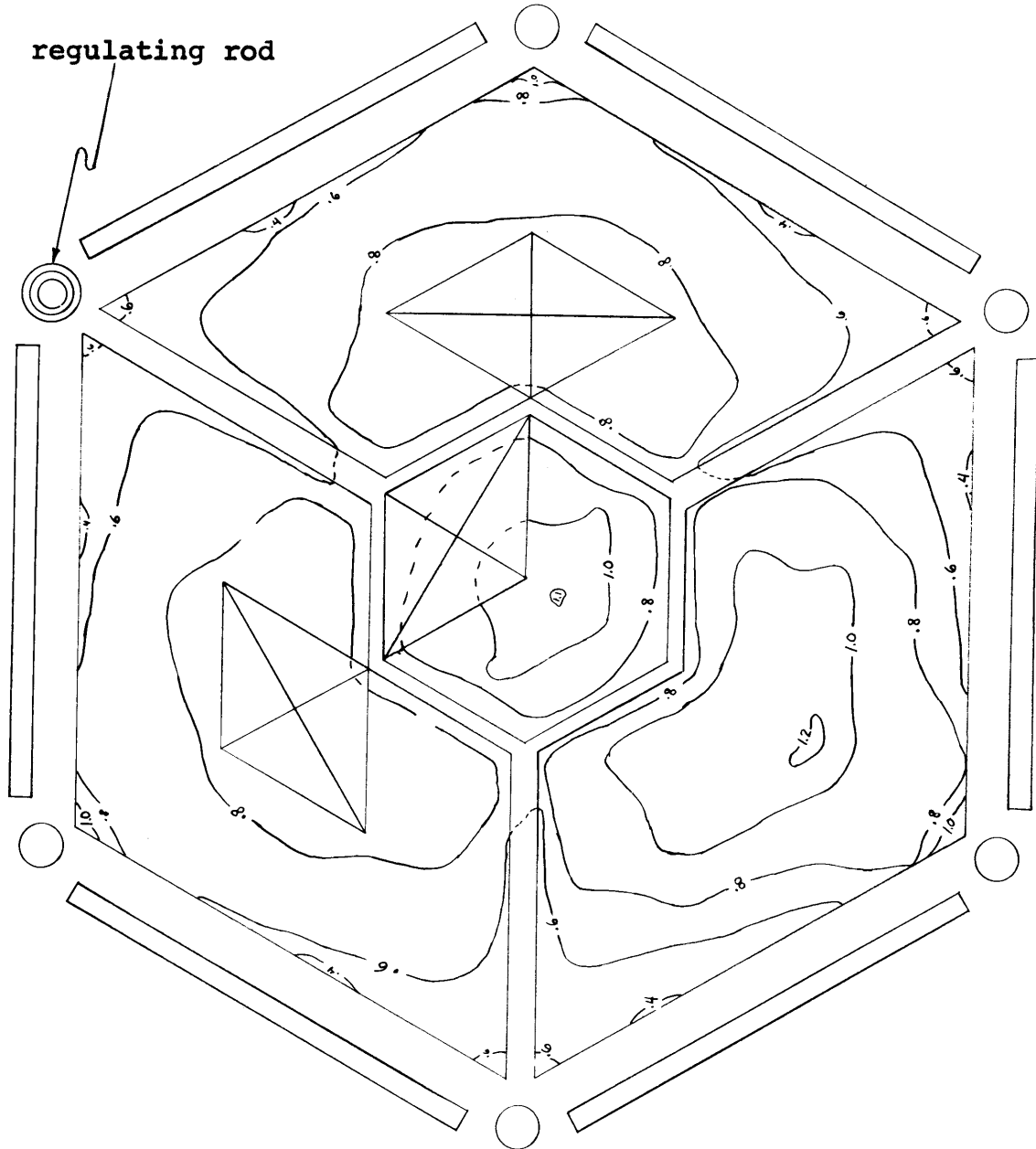
◿◺ – solid dummy element

Contour lines are equal values of $F_r F_a$.

between several methods of experimental and analytic flux evaluation. Copper wire irradiation was one method used for experimental measurements.

5.4.1 General Description

Copper is commonly used as a thermal neutron flux monitor because its cross section is fairly well known, it produces by irradiation a radionuclide that emits gamma rays with a convenient half-life, it exhibits small neutron self-shielding, and it is conveniently available in wire form. Copper wires were prepared and irradiated in the following positions:

1) Coolant channels between fuel plates,

2) Spider holes,

3) Core housing corner holes,

4) 3GV facilities and,

5) 6RH2 facility.

The copper wires were removed after the irradiation and allowed to decay for 1 1/2 hours before scanning in order to allow the Cu^{66} activity to decay away. The wires were scanned using a second collimator located in the gamma scanner (see Section 5.3.2) and activities at various axial positions on the wire were recorded. The activities were corrected for decay and different irradiations were correlated to one power by using results from cobalt foils which were irradiated in the pneumatic facility 1PH2.

The purpose of the copper wire flux measurement is to compare the thermal flux in the positions measured with the thermal flux as predicted by the computer code CITATION.

5.4.2 Experimental Procedure

Copper wire flux mapping was included in MITR-II Startup Procedure 5.9.1. A copy of this procedure is included in Appendix A.

5.4.2.1 Wire Preparation

High purity copper wire (0.99999) which had a 0.64 millimeter diameter was purchased for the flux wires. The wires were cut to length and thoroughly cleaned with acetone. Because it was not desirable to have copper in direct contact with the primary coolant water in order to avoid contamination of the primary water, the copper wires were completely covered as described below.

The copper wires were placed inside clear polyolefin (unsaturated polyethylene) shrinkable tubing. The tubing was heated with a hot air gun in order to shrink the tubing against the wire. This resulted in a 0.01 inch coating of polyolefin over the copper. The ends of the wire were sealed with BIPAX (TRA-BOND, BB-2101) epoxy which had been approved for short term use in the reactor. Because the coating over the copper wire was a thin coating of a hydrocarbon it was assumed that the perturbation caused

by the coating would be small (there appeared to be no
heavy metal contamination in the coating because the
resulting gamma scans of copper with coating showed only
the copper gamma spectrum). An engraved aluminum marker
was epoxied onto the upper end of each wire in order to
make identification of the wires easier. Several wires
were attached to long stainless steel extensions in order
to be able to locate the wires remotely in experimental
positions.

5.4.2.2 Electronics and Counting Setup

The activity of the copper wires was much less than
the activity of fuel plates and therefore, a different
sized collimator had to be installed. Because detector
discriminator settings could be adjusted so that only the
0.51 Mev gamma peak of Cu^{64} would be counted, collimator
leakage for other energy gamma rays was of no concern.
The dimensions of the installed collimator are shown
in Fig. 5.4-1. The NaI (Th) scintillation detector that
was used to count the uranium foils was positioned above
the collimator and shielded with lead bricks. The arrange-
ment of the detector and collimator for copper wire scanning
is shown in Fig. 5.4-2. A block diagram of the electronic
counting equipment is shown in Fig. 5.4-3.

A copper wire to be scanned was taped into a shallow
slot in an aluminum plate the same size as a fuel plate.
The aluminum plate was then placed in the same slot that

FIG. 5.4-1

width   depth

1.0   2.0

2.0

0.625

2.0   1.375
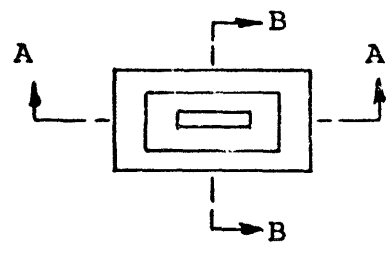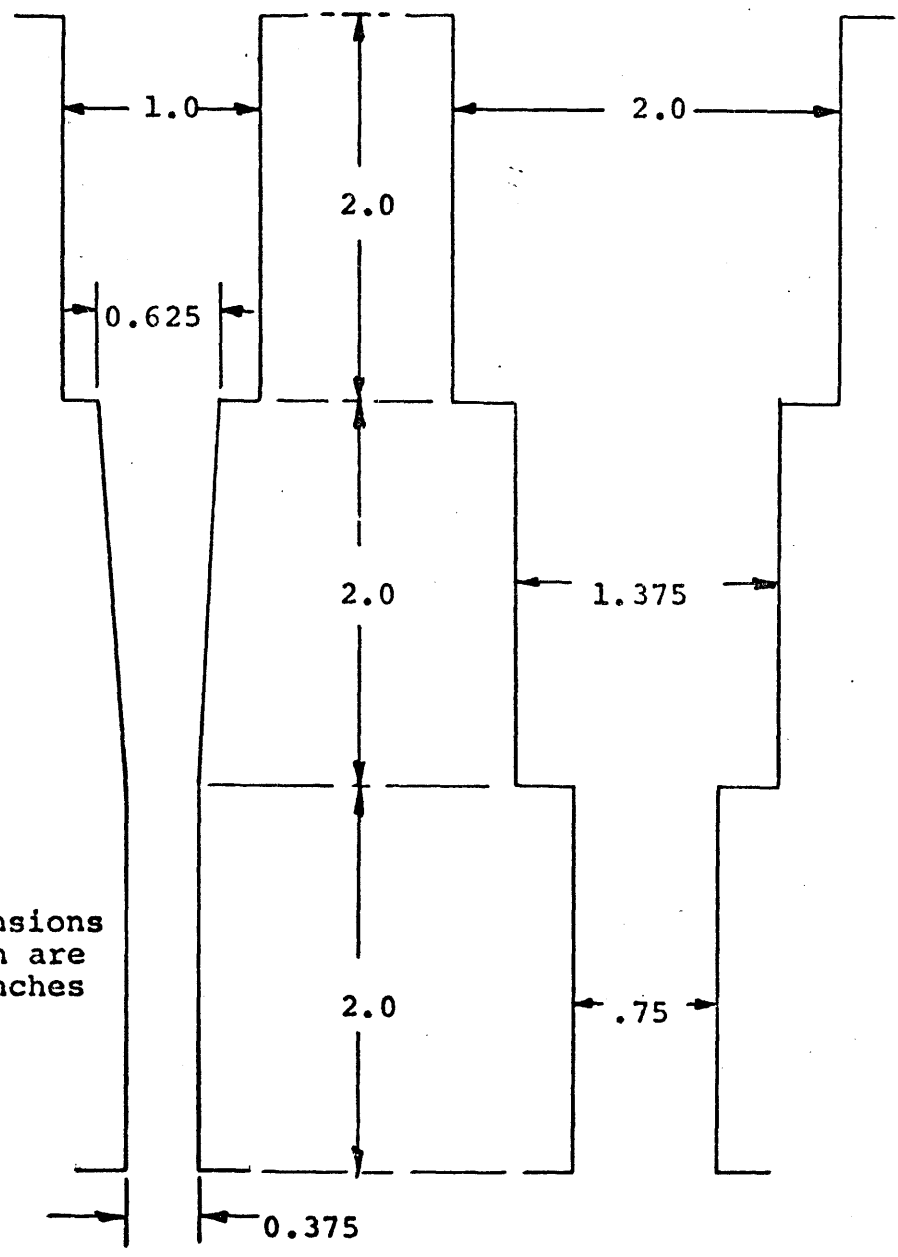
all
dimensions
shown are
in inches

2.0   .75

0.375

B-B   A-A

COPPER WIRE COLLIMATOR

FIG. 5.4-2

COPPER WIRE SCANNER

detector cavity

transverse
control

steel plate

collimator

longitudinal control
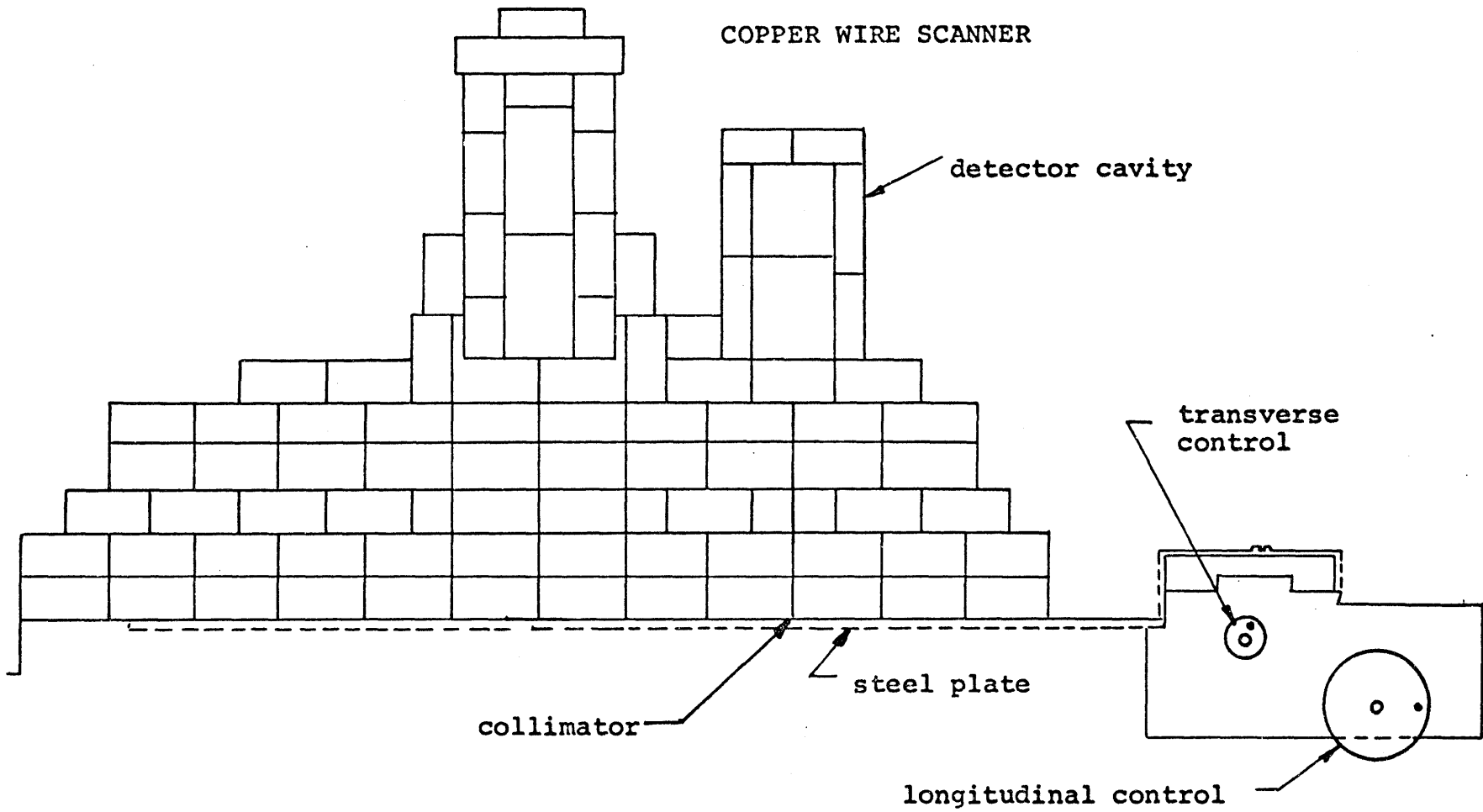
FIG. 5.4-3

BLOCK DIAGRAM OF COPPER WIRE COUNTING ELECTRONICS
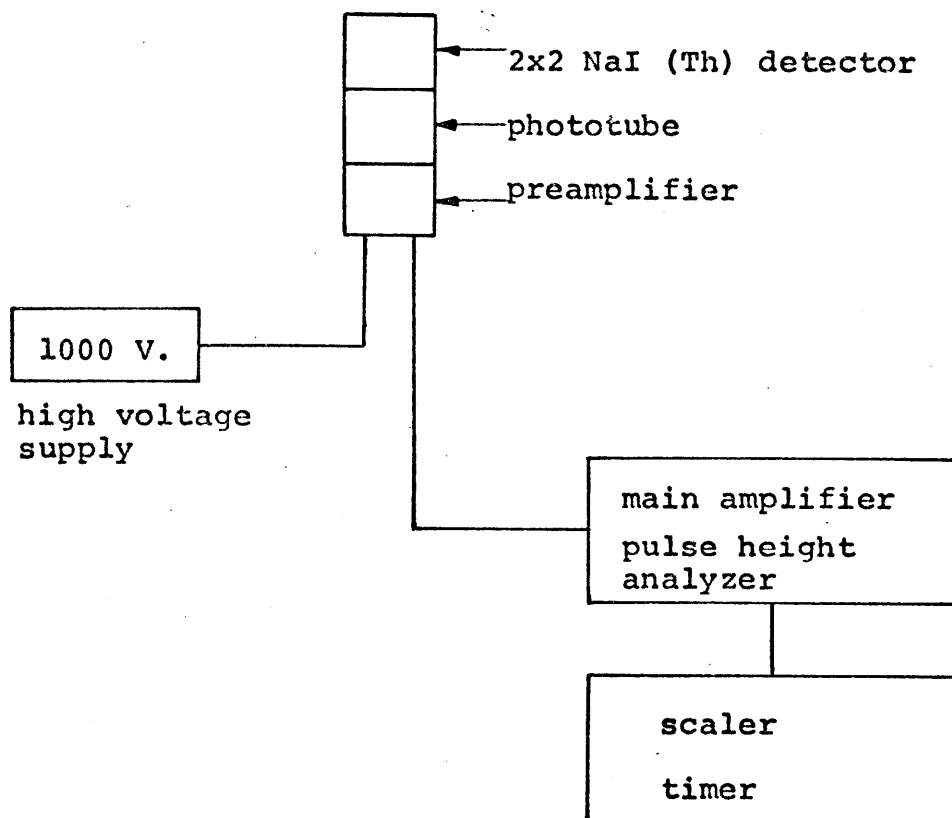
held a fuel plate during fuel plate scanning. The copper wire could be moved under the collimator by adjusting the lathe table controls in a similar manner as fuel plate scanning. The initial relationship between the lathe table positions and the position of the aluminum plate holding the copper wire was obtained by sighting through the collimator and viewing the bottom edge of the aluminum plate to obtain a reference point.

5.4.2.3 Irradiation and Counting

Copper wires were positioned and irradiated in the reactor in groups of up to five wires per irradiation. Table 5.4-1 lists the positions for each of the copper wires irradiated. Figure 5.4-4 shows the location of the wires for positions in the reactor core. The wires were irradiated at 200 nominal watts for one hour which corresponded to the same power and irradiation time as was used for the removable plate element during gamma scanning. Prior to beginning the irradiation, a cobalt foil was inserted into the same repeatable position in 1PH2 that was used for cobalt foils during the fuel plate scanning procedure.

After completion of the irradiation, the wires were allowed to decay at least one hour and then they were removed for scanning. The cobalt foil was also removed for later counting. At the counting location, the wires were thoroughly cleaned but the polyolefin coating was left on the wires. A wire would be taped with thin mylar

TABLE 5.4-1

COPPER FLUX WIRE IRRADIATION LOCATIONS

Case	Irradiation #	Wire Identification Letter	Location
1	15	J	Corner hole #4
2	16	A	10th channel from edge in C-8
3	16	B	2nd channel from edge in C-8
4	16	C	6RH2
5	16	L	Corner hole #2
6	16	K	Spider hole #3
7	17	E	11th channel from solid dummy in A-2
8	17	D	2nd channel from solid dummy in A-2
9	17	F	3GV5
10	17	M	Corner hole #4
11	17	N	Spider hole #1
12	18	G	3GV6
13	18	Q	Spider hole #3
14	18	P	Corner hole #5

FIG. 5.4-4

COPPER FLUX WIRE IRRADIATION LOCATIONS
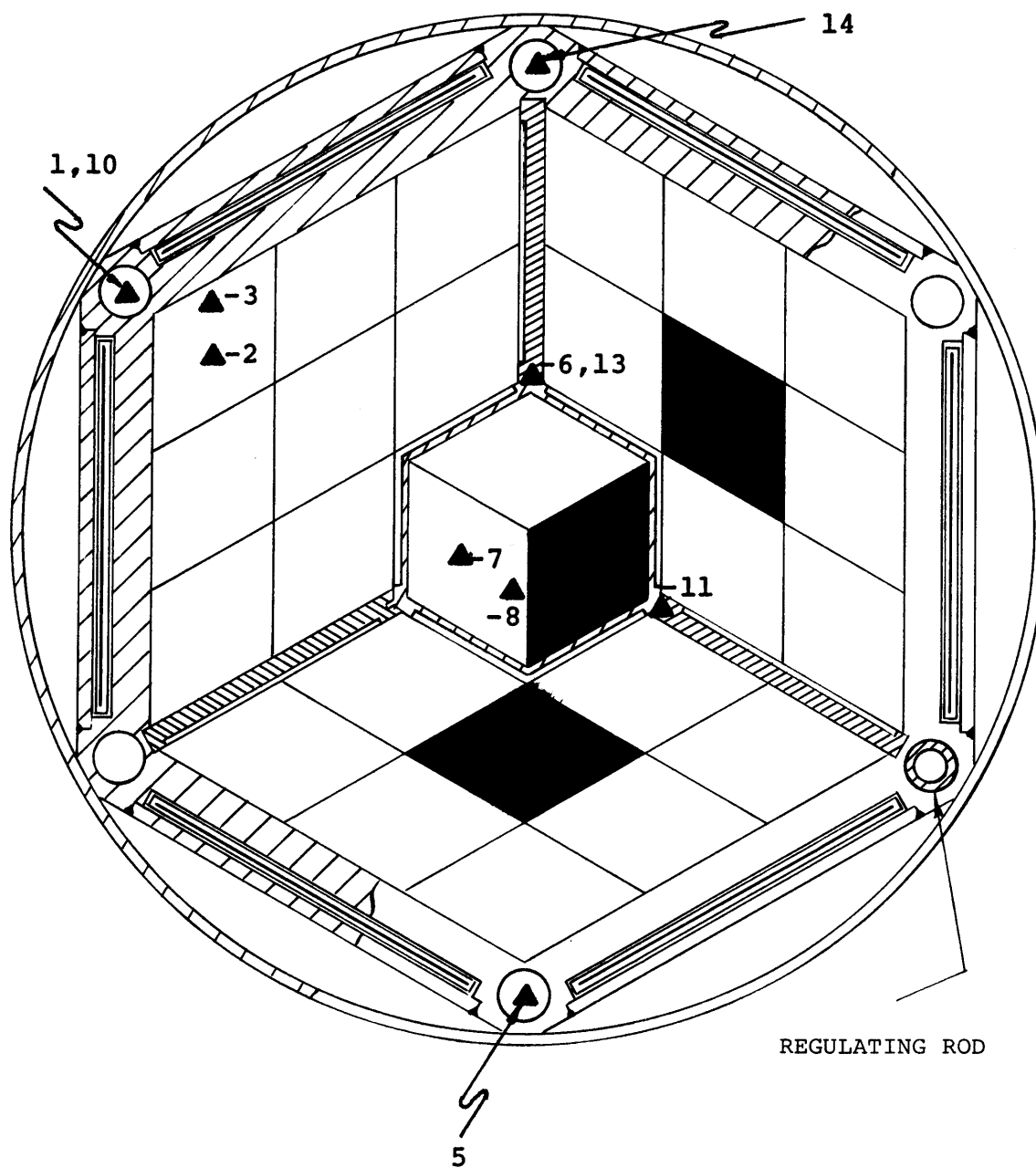
▲-4 6RH2

▲-9 3GV5

▲-12 3GV6

Numbers shown are case numbers for each wire.

tape onto the blank aluminum plate and positioned in the gamma scanner. The wire was counted for four minutes at various axial locations with the wire always located in the center of the collimator in the transverse direction. The raw count, time of the count, and axial position on each wire were recorded for each four minute count. A sample data sheet used for wire counting can be found in Appendix F. Each wire would be scanned in turn until all wires for a given irradiation were counted.

The cobalt foils were counted using the same method and electronics as described in Section 5.3.3.4.

5.4.3 Data Analysis

The raw counts obtained were corrected for the decay between irradiation completion and counting, background counts, power variations between irradiations and resonance activation in order to give corrected counts that would correspond to the activation by thermal neutrons alone. The raw data for the copper wire scanning is filed in the M.I.T. Reactor Headquarters office with the data for Startup Procedure 5.9.1. Samples of corrected counting data is included in Appendix F. Case #1 data was not corrected because this was only an initial irradiation to test activity levels and procedures; a repeat irradiation of that position is Case #10.

5.4.3.1 Decay, Power, and Background Corrections

For each point counted, the decay time after counting was recorded. The following equation relates the initial activity at the completion of the irradiation with the activity and the time the wire position was counted:

$$A_o = \frac{A_t}{e^{-\lambda t}} \quad , \qquad (5.4-1)$$

where,

A_o is the initial activity,

A_t is the activity at time t after the irradiation,

t is the time from the end of the irradiation to the beginning of the count,

λ is the decay constant for Cu^{64}.

Because Cu^{64} was the isotope being counted (0.51 Mev gamma peak) the decay constant used was 9×10^{-4} min.$^{-1}$ ($T_{1/2}$ = 12.82 hrs.). The activity, A_t, at the time of the count is proportional to the raw count rate, C_t, minus the background count rate, B, which makes Eq. 5.4-1 into:

$$A_o \propto \frac{(C_t - B)}{e^{-\lambda t}} \quad . \qquad (5.4-2)$$

The wire irradiations were all correlated to the same power level as the plate gamma scans for Core I of the MITR-II. Table 5.4-2 gives the cobalt count for each of the wire irradiations and lists the cobalt count for the reference cobalt count from the plate gamma scanning.

TABLE 5.4-2

CORE I COPPER WIRE IRRADIATION COBALT FOIL DATA

Irradiation #	Raw Counts	Corrected for Background	Corrected for Mass and Background	Total Counts Corrected for Decay, Mass and Background
15	29162	15241	13724	13792
16	26902	12981	12981	13042
17	26816	12895	12371	12425
18	26750	12829	12778	12816

Total corrected counts for the Kth irradiation = COB(K)

SMCOB = 12,352

The initial count rate at the completion of the irradiation corrected for decay, background, and power level is determined by the following equation:

$$C_o = (\frac{C_t - B}{e^{-\lambda t}}) (\frac{SMCOB}{COB(K)}) , \qquad (5.4-3)$$

where,

SMCOB is the reference cobalt count from plate scanning,

COB(K) is the cobalt foil for the Kth irradiation,

C_o is the normalized initial count rate,

C_t, B, λ, and t are as described above.

5.4.3.2 Resonance Corrections

The count rates obtained in Section 5.4.3.1 were caused by induced activity in the copper wire from both thermal and resonance neutrons. CITATION neutron flux results for the copper wire positions are used to determine resonance corrections to the counting data. The total activity induced in a stable flux monitor by CITATION thermal and resonance neutron fluxes can be represented by the following equation:

$$A_{TOT} = (N\phi_3\sigma_3 S) + (N\phi_2 I_o S) , \qquad (5.4-4)$$

where,

N   is the number of atoms of the stable flux monitor,

σ_3 is the thermal neutron activation cross section which has been averaged over the energy range of CITATION Group 3,

$\emptyset_3$ is the thermal neutron flux for CITATION Group 3,

S   is the saturation factor,

$\emptyset_2$ is the resonance neutron flux for CITATION Group 2,

I_o is the effective resonance integral for CITATION Group 2 flux,

A_{TOT} is the total activity.

The activity from thermal neutrons alone, A_{th}, would be:

$$A_{th} = N\emptyset_3\sigma_3 S \quad . \qquad (5.4-5)$$

Combining Eqs. 5.4-4 and 5.4-5 yields the ratio of thermal activity to total activity:

$$\frac{A_{th}}{A_{TOT}} = \frac{N\emptyset_3\sigma_3 S}{N\emptyset_3\sigma_3 S + N\emptyset_2 I_o S} , \qquad (5.4-6)$$

which reduces to,

$$\frac{A_{th}}{A_{TOT}} = \frac{1}{1 + \dfrac{\emptyset_2}{\emptyset_3}\dfrac{I_o}{\sigma_3}} \quad . \qquad (5.4-7)$$

Values for $\emptyset_2$, $\emptyset_3$, I_o, and σ_3 must be known to determine the ratio of the thermal activation to the total activation. The neutron flux ratio $\emptyset_2/\emptyset_3$ is obtained by taking the ratio of the Group 2 flux (.4ev - 3 kev) to

the Group 3 flux (0.00025ev - 0.4ev) at each wire position from the three-dimensional CITATION computer calculation. Values of σ_3 and I_o are derived from the work done by Mathews on wire and foil irradiations done on the MITR-I (Ref. 5.4-1). The copper cross section and effective resonance integral used by Mathews must be modified to the appropriate CITATION energy averaged value.

The thermal activation cross section for neutrons with a speed of 2200 meters per second for Cu^{63} which is the parent nuclide of Cu^{64} is 4.50 barns. The effective resonance integral, I_o, is made up of a 1/V component and a resonance component. The 1/V component of the resonance integral is:

$$I_{1/v} = \sigma_{act}^o \int_{E_c}^{E_f} (\frac{E_o}{E})^{1/2} \frac{dE}{E} , \qquad (5.4-8)$$

where,

$I_{1/v}$ is the 1/V component of the resonance integral,

E_o is the neutron energy corresponding to the most probable neutron velocity,

σ_{act}^o is the activation cross section for neutrons with energy E_o,

E_c is the lower energy limit of the CITATION resonance energy group,

E_f is the lower energy limit of the CITATION fast energy group,

Integrating Eq. 5.4-8 yields:

$$I_{1/v} = 2\sigma_{act}^o (\frac{E_o}{E})^{1/2} \Big/_{E_f}^{E_c} , \qquad (5.4-9)$$

which reduces to the following:

$$I_{1/V} = 2\sigma^{O}_{act} \left[(\frac{E_o}{E})^{1/2}_c - (\frac{E_o}{E_f})^{1/2} \right] . \quad (5.4\text{-}10)$$

The lower energy limits of the resonance and fast energy groups used in the three-dimensional CITATION calculation were $E_c = 0.4ev$ and $E_f = 3 \times 10^3 ev$. Taking $E_o = 0.0253ev$ and $\sigma^{O}_{act} = 4.50$ barns, Eq. 5.4-10 is evaluated to give:

$$I_{1/V} = 2.24 \text{ barns} . \quad (5.4\text{-}11)$$

The resonance component of I_o must include self-shielding effects of the wire thickness. Mathews (Ref. 5.4-1) determined the non-1/V component of the resonance integral for copper foils of various thicknesses. Figure 5.4-5 shows a curve of foil thickness versus effective resonance integral. In order to compare the values for a cylindrical wire to the values of a foil, the equivalency between foils and wires must be determined.

The fraction of incoming neutrons which are absorbed in a pure absorbing body is proportional to geometry in the following way (Ref. 5.4-1):

$$F_{abs} \propto \frac{4v}{S} , \quad (5.4\text{-}12)$$

where,

F_{abs} is the fraction of neutrons absorbed,

v is the volume of the body,

S is the surface area of the body.

FIG. 5.4-5

EFFECTIVE RESONANCE INTEGRAL FOR Cu^{63}

Copper resonance integral does not include
1/v component and is based on 2200 meter/sec.
cross-section of $\sigma_{act}(Cu^{63})$ = 4.50 barns.
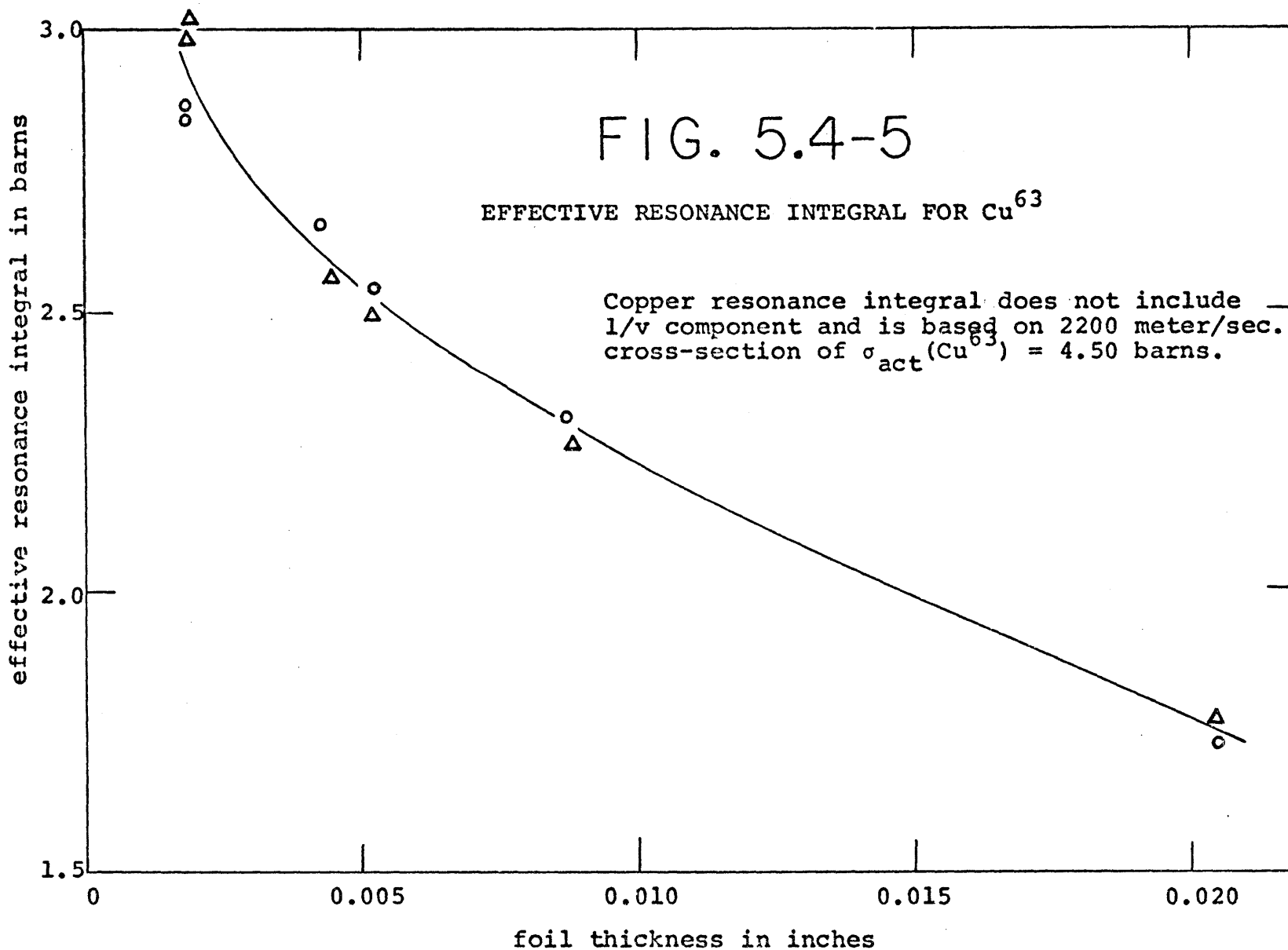
The ratio between fractions of neutrons absorbed in a foil and in a wire would be:

$$\frac{F_{abs}^{foil}}{F_{abs}^{wire}} = \frac{(\frac{4v}{S})_{foil}}{(\frac{4v}{S})_{wire}} \quad . \tag{5.4-13}$$

For an infinite foil of thickness t, the relationship between volume and surface area is:

$$S = \frac{2v}{t} \quad . \tag{5.4-14}$$

For an infinite wire of diameter D, the relationship between volume and surface area is:

$$S = \frac{4v}{D} \tag{5.4-15}$$

Substituting Eq. 5.4-14 and 5.4-15 into Eq. 5.4-13 yields:

$$\frac{F_a^{foil}}{F_a^{wire}} = \frac{2t}{D} \quad . \tag{5.4-16}$$

for the case where the same fraction of neutrons are absorbed in both the wire and the foil, $F_a^{foil}/F_a^{wire} = 1$, and Eq. 5.4-16 becomes:

$$D = 2t \quad . \tag{5.4-17}$$

From this equation it is seen that a wire of diameter "x" is approximately equivalent to a foil of thickness "x/2". Mathews (Ref. 5.4-1) determined the non-1/V effective resonance integral for a 0.020 inch in diameter copper wire

and found that $I_{non-1/v}$ = 2.195. Using Fig. 5.4-5, this corresponds to a foil of thickness 0.010 thus confirming Eq. 5.4-17.

The copper wires in the present irradiations had a diameter of 0.0252 inches and thus, from Fig. 5.4-5, $I_{non-1/v}$ = 2.13 barns. The total effective resonance integral is:

$$I_o = I_{1/v} + I_{non-1/v} \quad , \quad (5.4-18)$$

substituting values for 0.0252 inch copper wire Eq. 5.4-18 yields:

$$I_o = 4.37 \text{ barns} \quad . \quad (5.4-19)$$

CITATION uses thermal cross sections that is averaged over the thermal energy group. The relationship between an averaged cross section for a Maxwellian energy distribution and the cross section for neutrons with a speed of 2200 meters per second is as follows (Ref. 5.4-2):

$$\sigma_a(\bar{v}) = \frac{\pi^{1/2}}{2} \sigma_{act}^o \quad , \quad (5.4-20)$$

where,

$\sigma_a(\bar{v})$ is the energy averaged cross section,

σ_{act}^o is the 2200 meter per second cross section.

Since σ_{act}^o equals 4.50 barns for Cu^{63}, the energy averaged cross section which corresponds to the CITATION Group 3 cross section, σ_3, is 3.99 barns.

The derivation of I_o included averaging over the

resonance energy group and thus, the following ratio corresponds with the energy averaged CITATION flux ratio:

$$\frac{I_o}{\sigma_3} = \frac{4.37 \text{ barns}}{3.99 \text{ barns}} = 1.095 \quad . \qquad (5.4-21)$$

Substituting the value of Eq. 5.4-21 into Eq. 5.4-7 yields:

$$\frac{A_{th}}{A_{TOT}} = \frac{1}{1 + 1.095 \frac{\phi_2}{\phi_3}} \quad , \qquad (5.4-22)$$

where,

ϕ_2/ϕ_3 is the flux ratio taken from CITATION.

5.4.4 Summary of Copper Wire Flux Maps

The main purpose of copper wire flux mapping is to determine the thermal neutron flux shape in positions of interest and to compare this shape with the flux shape as predicted by CITATION. All of the copper wire data was corrected for power differences between irradiations and for resonance capture effects (using CITATION flux ratios). Sample corrected data is listed in Appendix F and the raw data is filed in the MITR Headquarters Office with Procedure 5.9.1.

The corrected counts were plotted versus wire position. CITATION Group 3 (thermal) fluxes from the three-dimensional model which corresponded to each respective wire

count position were also plotted on the same graphs. A
5 MW CITATION thermal flux of 1.0 x 10^{13} was chosen to
equal 186.5 counts because this yielded good agreement
between the copper wire and CITATION results at incore
locations where confidence in CITATION results is high.

Figures 5.4-6 and 5.4-7 show that CITATION and the
copper wires are in agreement with the exception of the
flux spike at each end of the element. This expected
difference is further discussed later in this section.
At the element ends, the CITATION spike is 60% of the
copper wire spike. Note that there is no large difference
between the flux shapes for the position that was next
to the solid dummy and the position that was next to
the fueled element.

Figure 5.4-8 shows the flux distributions in
channel 2 of element C-8. There is generally good
agreement between CITATION and copper wire results
with the exception of the spike at the bottom. Figure 5.4-9
shows the flux distribution for an interior channel in
C-8. Note that the shapes are in agreement, but that
CITATION predicted a higher thermal flux.

Figures 5.4-10 and 5.4-11 show flux distributions in
channels of an element in A-2. The copper wire in
channel 11 (Fig. 5.4-11) extended 1 3/4 inches below the
bottom of the fuel meat and thus shows the very large
thermal flux spike that occurs at the bottom of the fuel.

FIG. 5.4-6

THERMAL NEUTRON FLUX DISTRIBUTION IN ABSORBER SPIDER HOLE #1

distance from bottom tip of copper wire (inches)
to collimator centerline

FIG. 5.4-7

THERMAL NEUTRON FLUX DISTRIBUTION IN ABSORBER SPIDER HOLE #3

- - ● - CITATION results (group 3)

──△── copper wire scans, case 6 and 13

186.5 counts $\approx$ 1.0 x 10^{13} neut./cm^2-sec @ 5 MW

top of lower spider

distance from bottom tips of copper wires (inches)
to collimator centerline
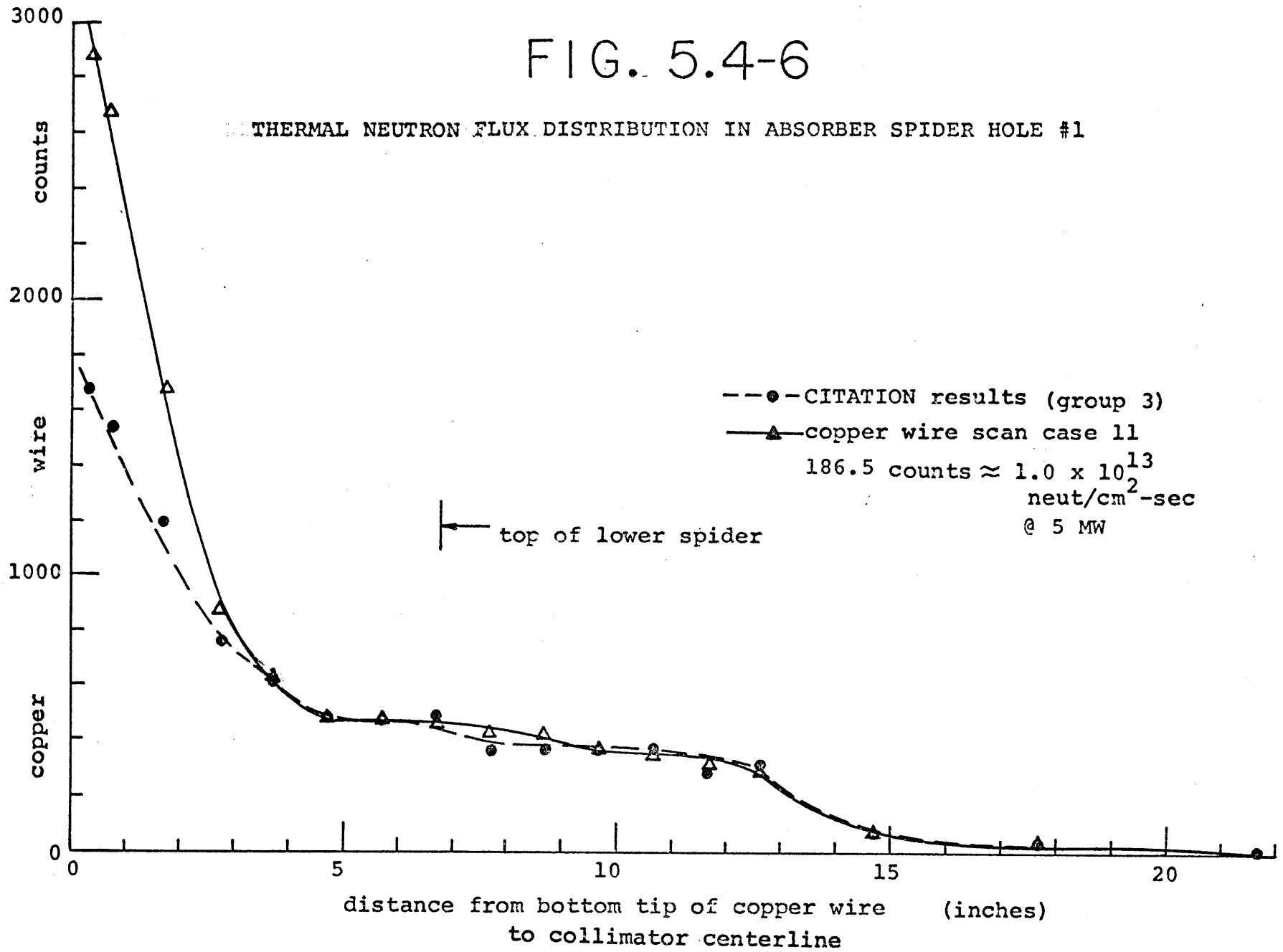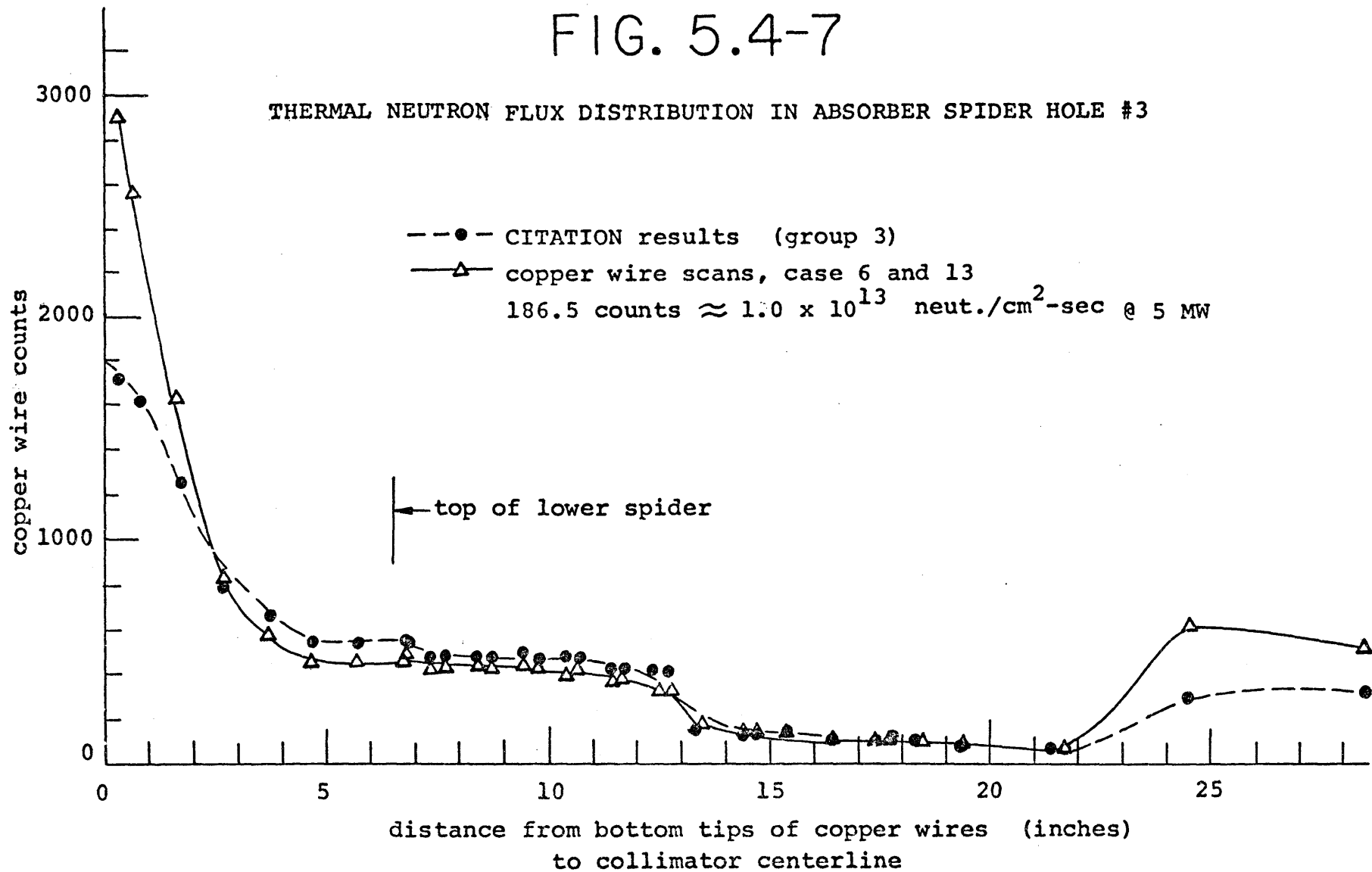
FIG. 5.4-8

THERMAL NEUTRON FLUX DISTRIBUTION IN CHANNEL #2 OF ELEMENT IN C-8

$--o--$ CITATION results (energy group 3)

$\underline{\quad\triangle\quad}$ copper wire scan, case 3

186.5 counts $\approx$ 1.0 x 10^{13} n/cm^{2}sec

Channel 2 is second channel from core housing in C-8.

Neutron flux normalized to 5 MW.
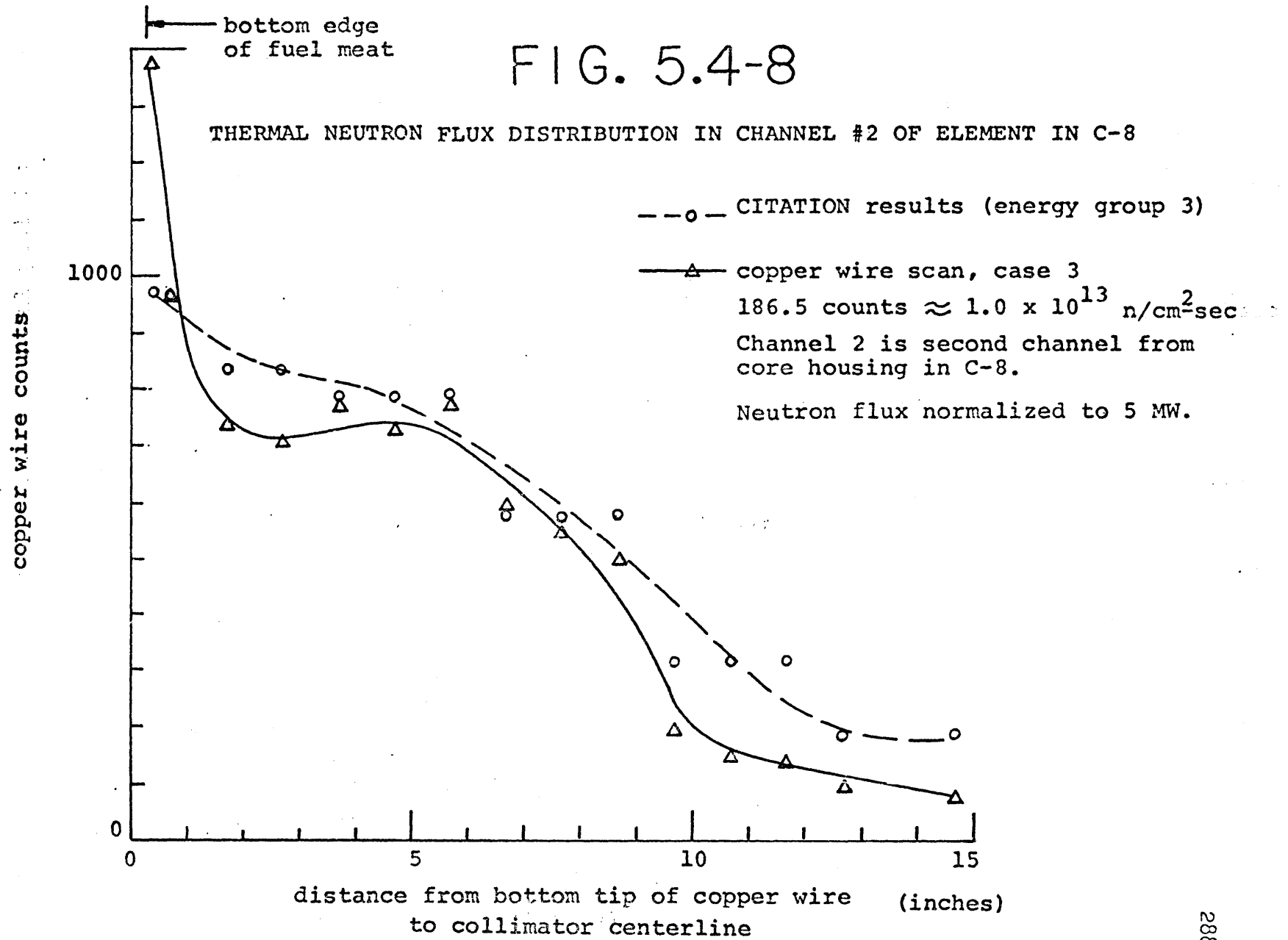
FIG. 5.4-9

THERMAL NEUTRON FLUX DISTRIBUTION IN CHANNEL #10 OF ELEMENT
IN POSITION C-8

bottom edge
of fuel meat

- -o- CITATION results (group 3)

-△- copper wire scan, case 2
186.5 counts ≈ 1.0 x 10^{13} @5MW

Channel 10 is the tenth
channel from core housing
in C-8.

distance from bottom tip of copper wire (inches)
to collimator centerline

FIG. 5.4-10

THERMAL NEUTRON FLUX DISTRIBUTION IN CHANNEL #2 OF ELEMENT IN A-2

bottom edge
of fuel meat

copper wire counts

1000

0

0   5   10   15

distance from bottom tip of copper wire   (inches)
to collimator centerline

- - ● - CITATION results (group 3 neutron flux)

—▲— copper wire scan, case 8

186.5 counts $\approx$ 1.0 x 10^{13} neut./cm^2-sec

Channel 2 is second channel in A-2
from solid dummy in A-1.

Neutron flux normalized to 5 MW.

FIG. 5.4-11

THERMAL NEUTRON FLUX DISTRIBUTION IN CHANNEL #11 OF ELEMENT IN A-2

- - ● - CITATION results (group 3)

────▲──── copper wire scan, case 7

18.5 counts $\approx$ 1.0 x 10^{13} neut/cm^{2}sec

Channel 11 is the eleventh channel in A-2 from solid dummy in A-1.

Neutron flux normalized to 5MW.

bottom edge of fuel meat

copper wire counts

distance from bottom tip of copper wire to collimator centerline

(inches)
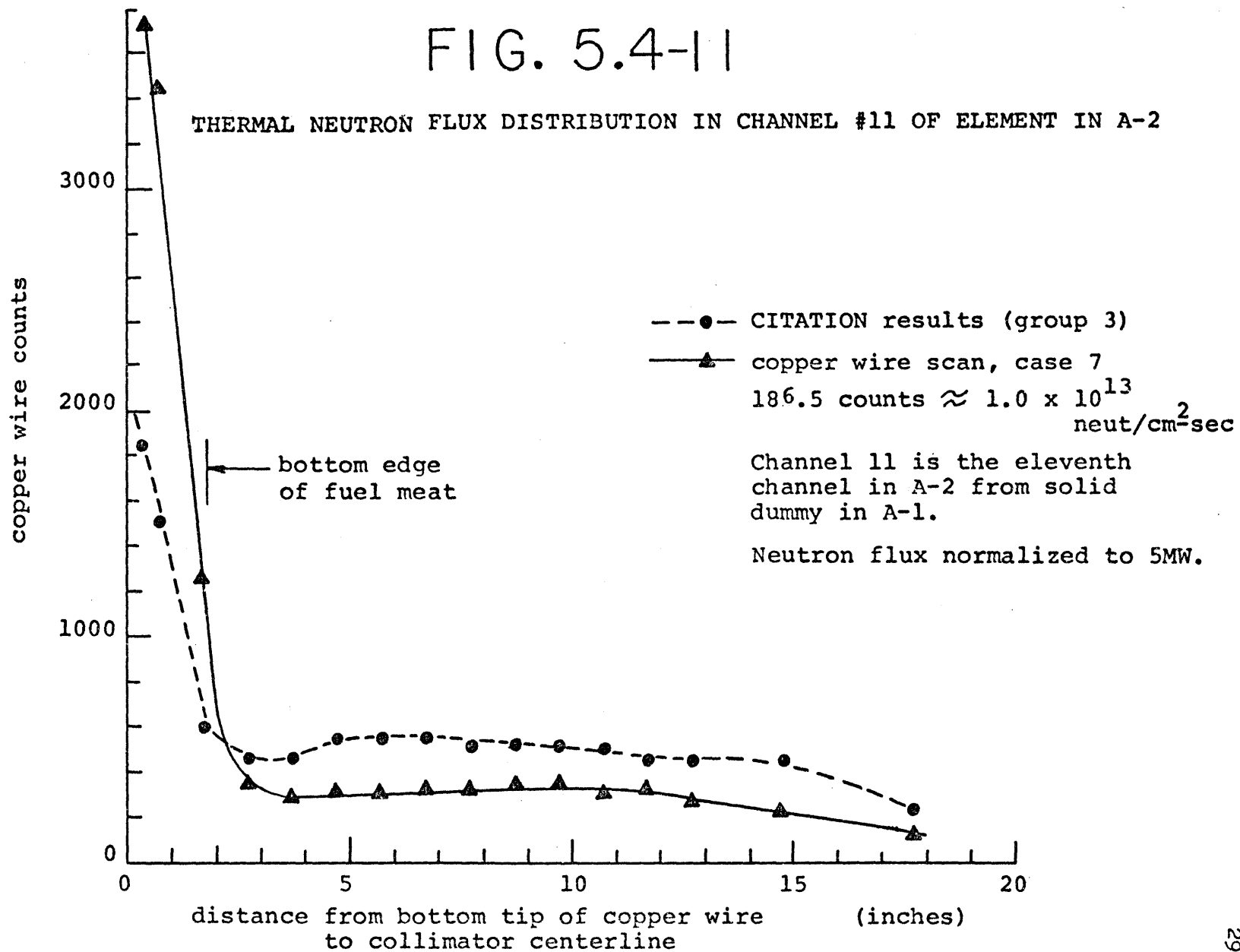
Figures 5.4-12, 5.4-13, and 5.4-14 show the thermal flux distributions in core housing corner holes #2, 4, and 5, respectively, (see Fig. 5.4-4 for locations). CITATION does not do well predicting the flux shape in the corner holes because of large mesh point spacing and because of homogenized materials cross sections. The copper wire flux shapes in each of the three different corners are very similar with only the magnitude of counts differing. The counts for corner hole #4 which is next to the C-8 element position are about 12% greater than the counts in the other two corner holes measured. There appears to be no variations in the corner holde distribution shape depending upon whether the corner hole is next to a radial spider arm or next to a fuel element.

Figures 5.4-15, 5.4-16, and 5.4-17 show the flux distributions for 6RH2, 3GV5, and 3GV6, respectively. CITATION cannot give good representations of the experimental locations because of the limited mesh points at the experimental locations. Note that the peak flux in the 3GV facilities does not occur at the bottom of the facility.

The copper wires showed a much greater thermal flux spike at the bottom of the fuel than was predicted by CITATION. Hove (Ref. 5.4-3) had shown that CITATION calculations using homogenized lower plenum cross sections under predicted the flux peak that occurred at the bottom of the fuel. The implications of this under prediction

FIG. 5.4-12
THERMAL NEUTRON FLUX DISTRIBUTION IN CORNER HOLE #2

— — ● — CITATION results (group 3 flux)

—△— copper wire scan, case 5
186.5 counts $\approx$ 1.0 x 10^{13} n/cm^2-sec
@5 MW

bottom of
corner hole #2
(by C-3)
Bottom of corner hole
is defined as lower end of
3/4 in. diameter corner hole.

distance from bottom tip of copper wire to collimator centerline
(inches)

FIG. 5.4-13

THERMAL NEUTRON FLUX DISTRIBUTION IN CORNER HOLE #4

bottom of corner hole #4 (near C-8)

— o — CITATION results (gr.3)

—△— copper wire scan, case 10

186.5 counts ≈

$1.0 \times 10^{13} n/cm^2 sec$

@ 5 MW

distance from bottom tip of copper wire to collimator centerline
(inches)
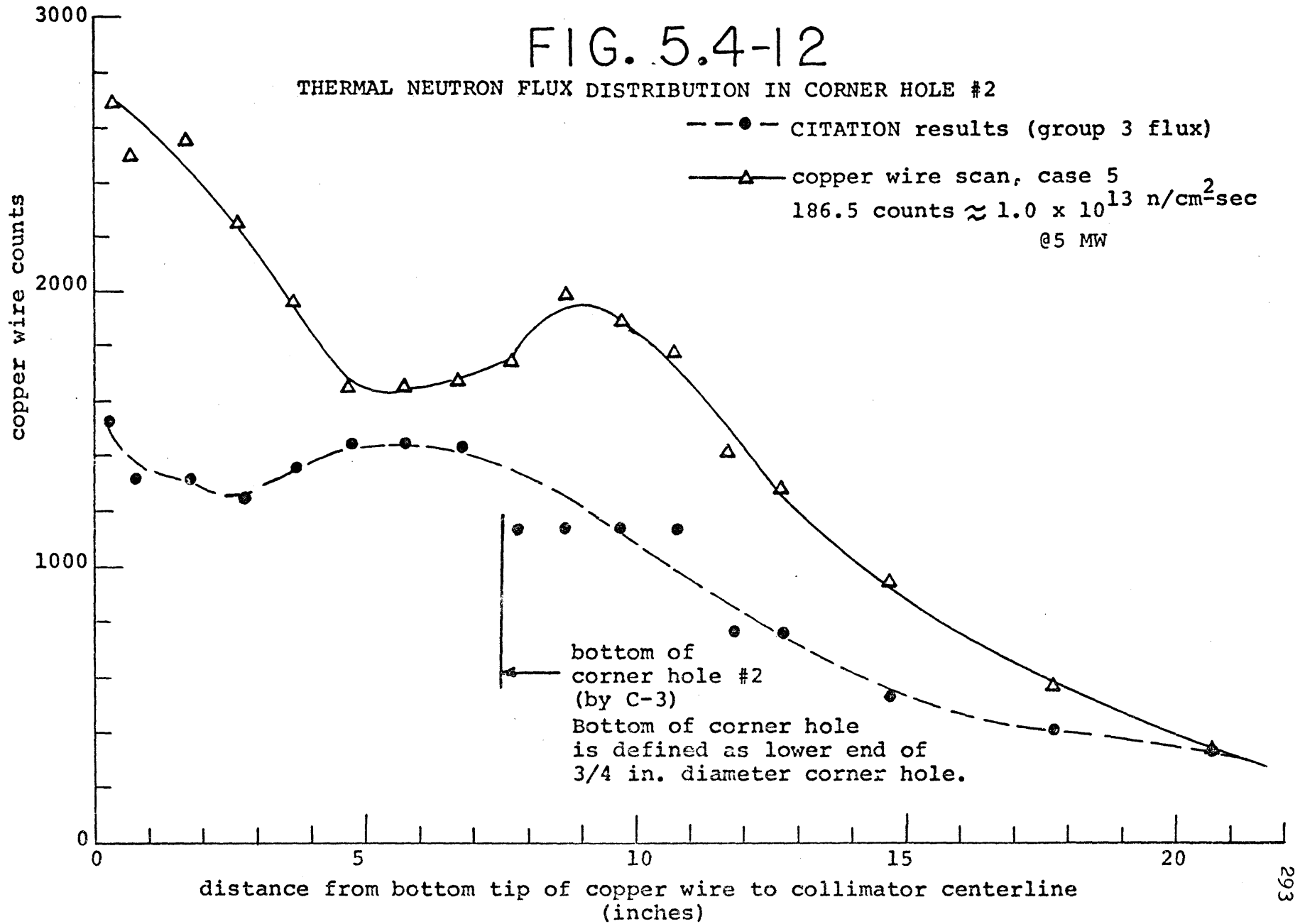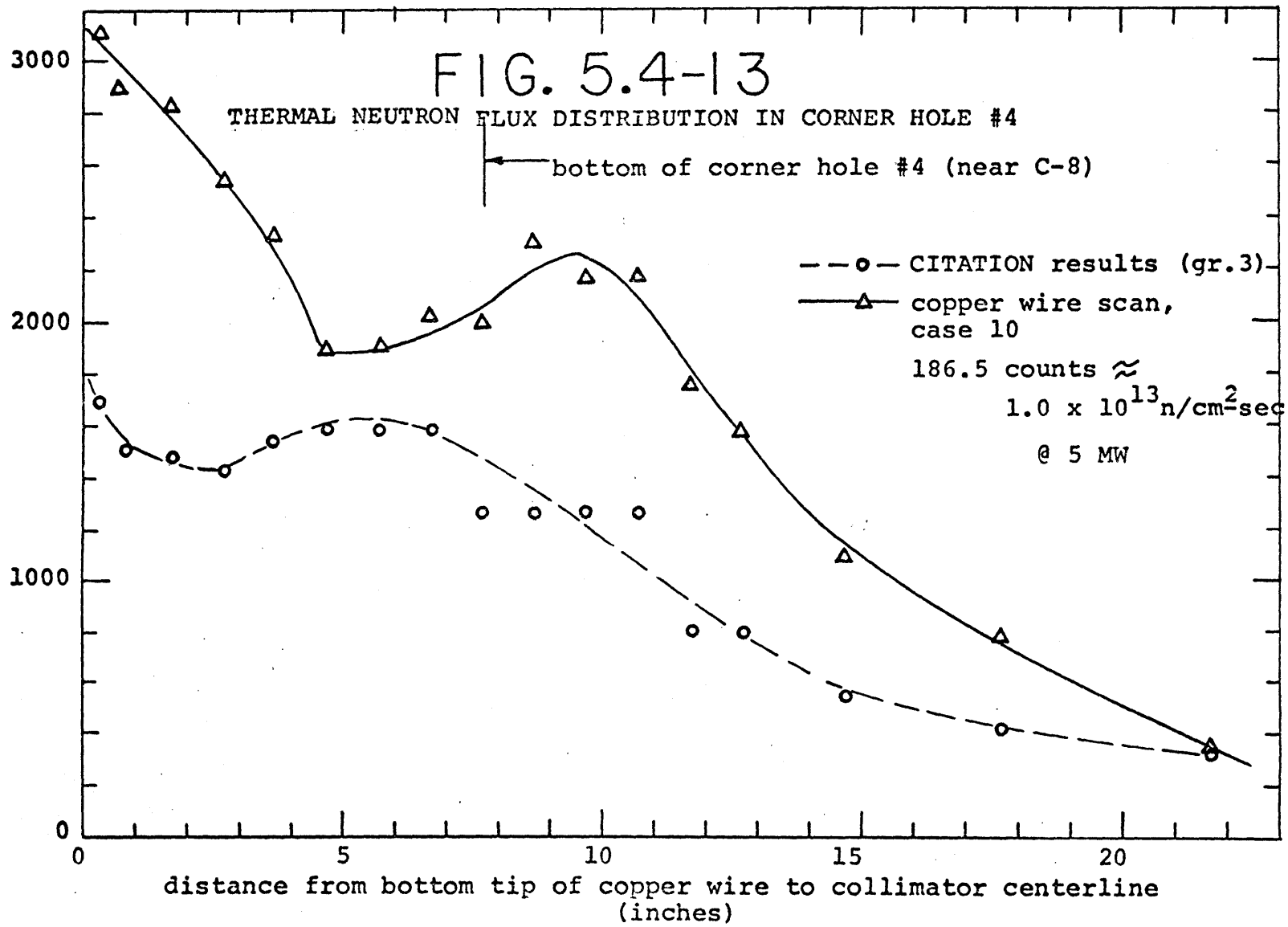
FIG. 5.4-14

THERMAL NEUTRON FLUX DISTRIBUTION IN CORNER HOLE #5

FIG. 5.4-15

THERMAL NEUTRON FLUX DISTRIBUTION IN 6RH2

FIG. 5.4-16

THERMAL NEUTRON FLUX DISTRIBUTION IN 3GV5

FIG. 5.4-17

THERMAL NEUTRON FLUX DISTRIBUTION IN 3GV6

bottom of 3GV6 thimble

— ● —CITATION results (group 3)

copper wire scan, case 12
186.5 counts $\approx$ 1.0 x 10^{13}
neut/cm^{2}sec
@ 5 MW

copper wire counts

distance from bottom tip of copper wire to collimator centerline (inches)
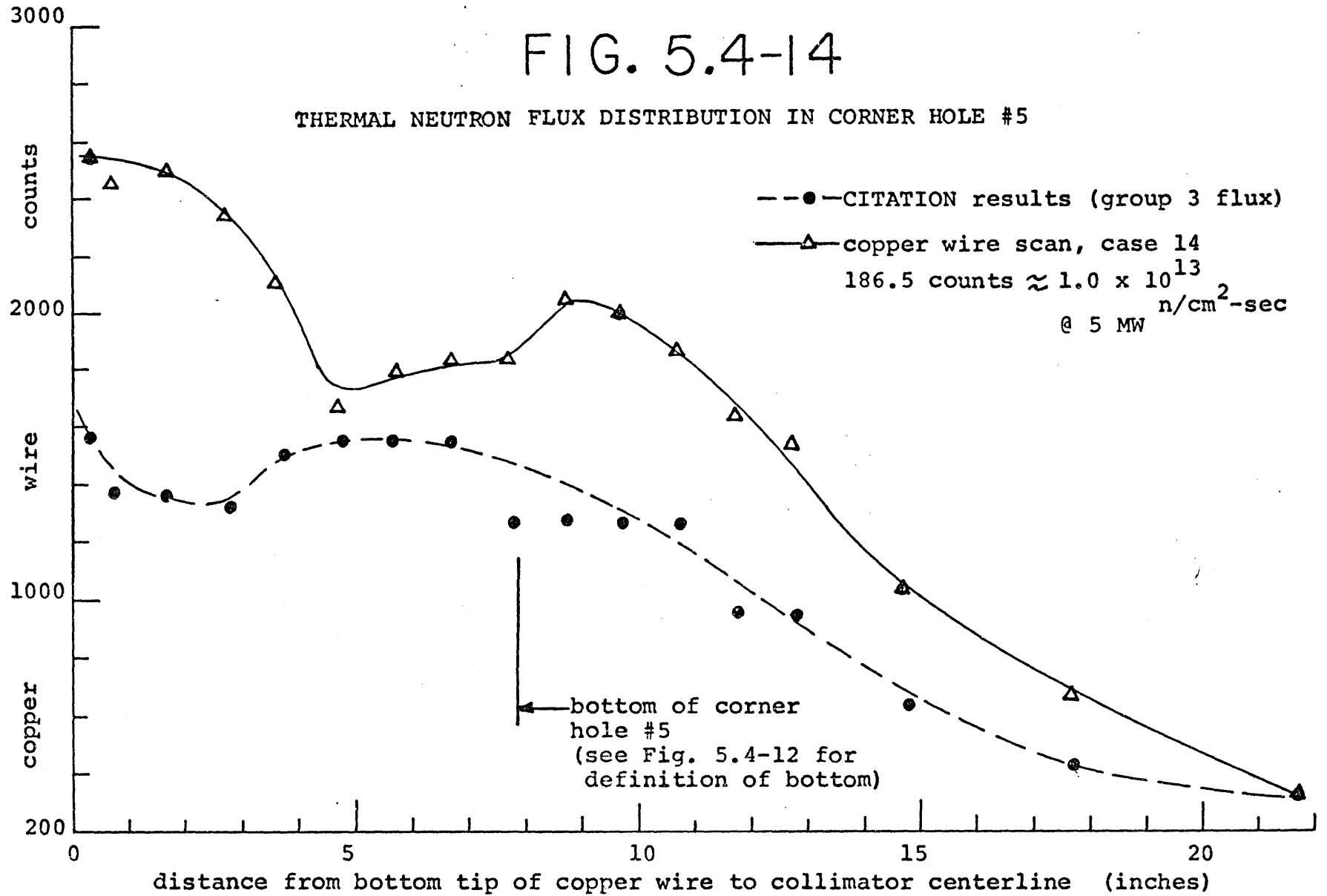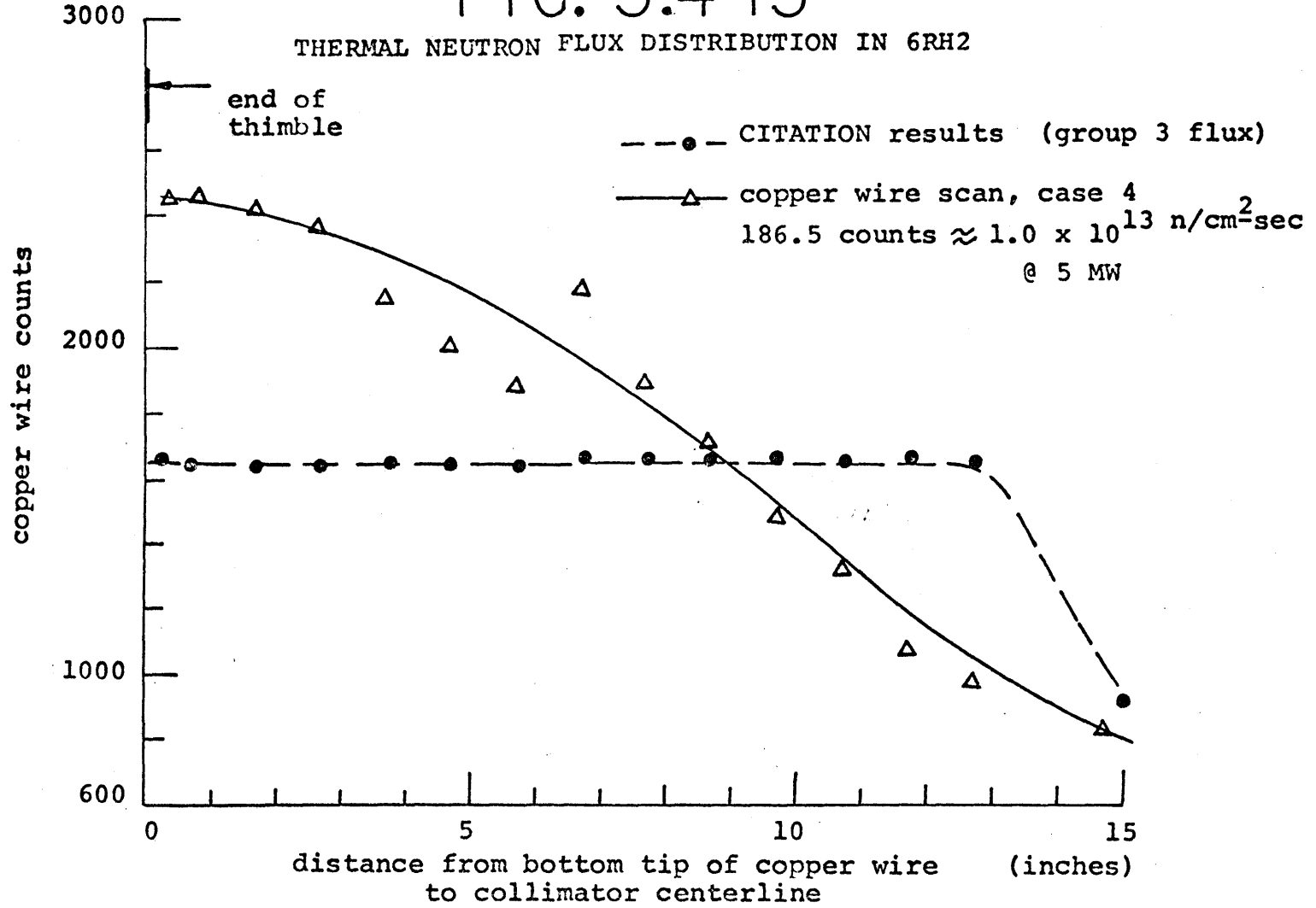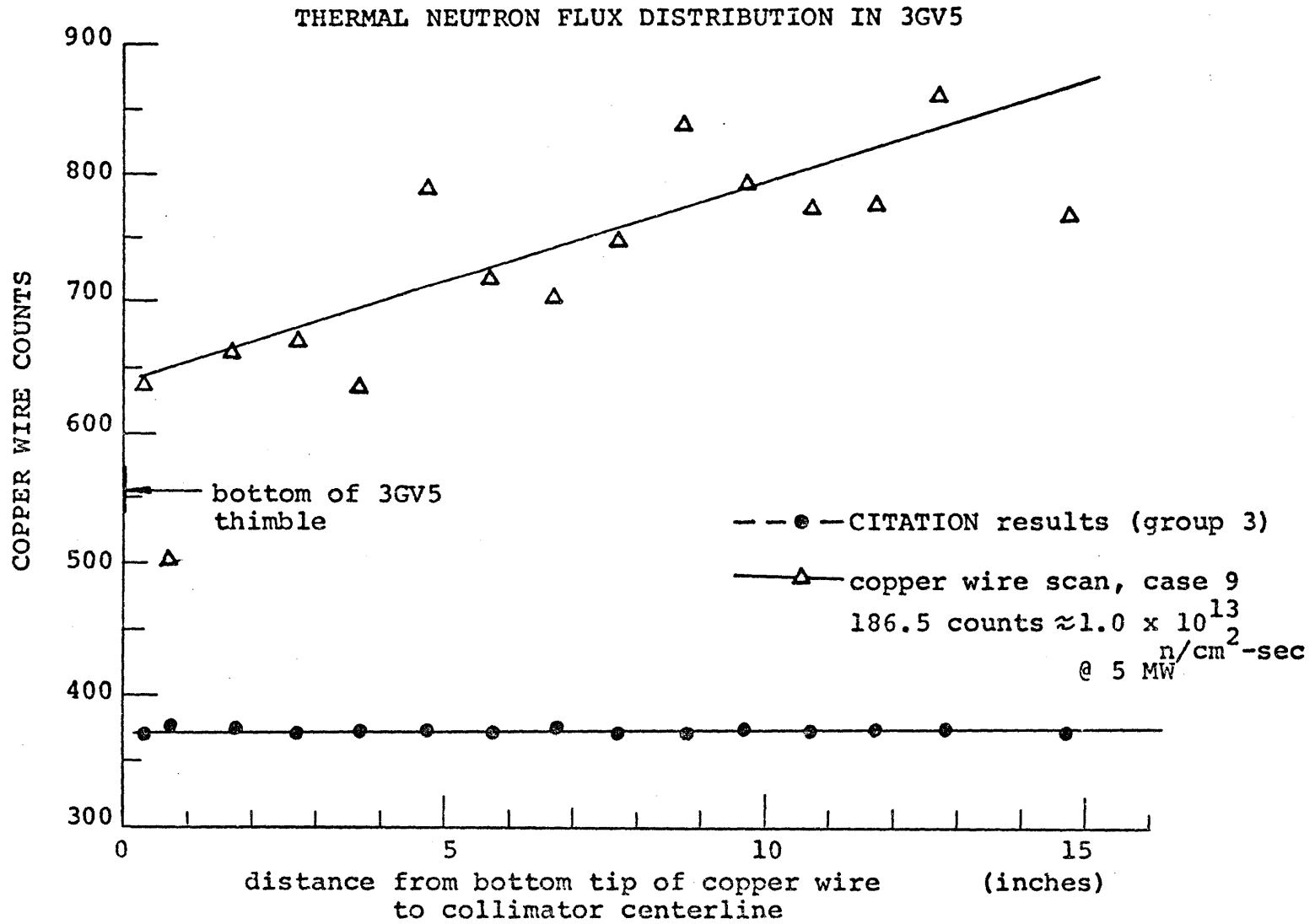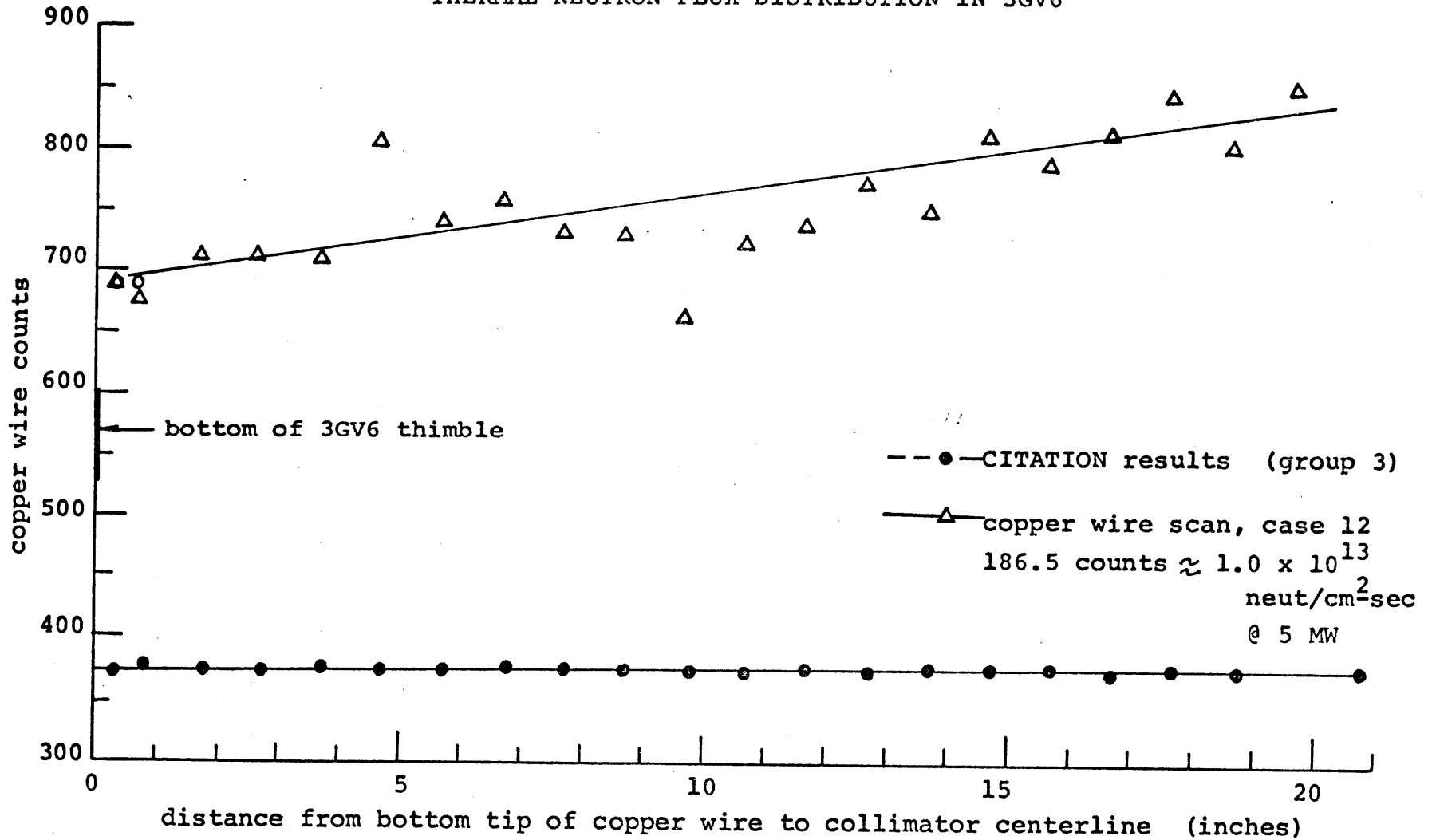
shall be further discussed in Sections 7.3 and 10.1.1.

5.5 Summary of Power and Flux Distributions for Core I

Three methods of determining the power and flux distributions were used in this chapter. The methods were:

1) CITATION computer code,

2) Gamma Scanning, and

3) Copper Wire Irradiations.

Tables 5.5-1, 5.5-2, and 5.5-3 summarize the figures which show the results for these respective methods. The importance and conclusion of these results are further discussed in Chapter 10.

TABLE 5.5-1

SUMMARY TABLE OF CORE I CITATION DISTRIBUTIONS

Figure Number	Title of Figure
5.2-2	5 MW Thermal Neutron Flux from 2-D CITATION
5.2-5	CITATION Relative Power Distribution of Plate 1 of Element in C-8
5.2-6	CITATION Relative Power Distribution of Plate 1 of Element in A-2
5.2-7	CITATION Relative Power Distribution on Central Plate in Element B-5
5.2-8	CITATION Relative Power Distribution for Horizontal Layer 11
5.2-9	CITATION Relative Power Distribution for Horizontal Layer 9
5.2-10	CITATION Relative Power Distribution for Horizontal Layer 6
5.2-11	5 MW Thermal Flux from 3-D CITATION
6.4-1	Comparison between CITATION and COREFAC Results for Core I

TABLE 5.5-2

SUMMARY TABLE OF POWER DISTRIBUTIONS FOR CORE I BASED ON PLATE SCANNING DATA

Figure Number	Title	Comments
5.3-26, 5.3-27, 5.3-28	Power Distributions across Elements C-9, C-8, and (A-2, B-3)	Shows variation in power across element for several positions.
5.3-29	Core I Axial Power Distribution in Element Position C-8	Shows power variation in hot channel in C-8 with control blade height and shows power peaking at corner hole.
5.3-30	Core I Axial Power Distribution in Element Position C-9	Shows power peaking at water filled control blade slot and how peak drops off a few plates into the element.
5.3-31	Core I Axial Power Distribution in Element Position B-9	Shows highest bottom edge peak which was measured. Element was next to a solid dummy and hexagonal spider. Power is depressed in upper part because of proximity to fixed absorber.
5.3-32	Core I Axial Power Distribution in Element Position B-5	Shows axial power distribution on a plate in the element with the highest average power distribution.

TABLE 5.5-2 (Continued)

Figure Number	Title	Comments
5.3-33	Core I Axial Power Distribution in Element Position A-2	Shows Power Distribution in A-2 both next to a solid dummy and next to the original ICSA (flooded)
5.3-34	Relative Powers of Elements in Core I where the Removable Plate Element was Irradiated	
5.3-35	Core I Experimental Power Distribution for a Horizontal Cross Section 0.438 inches from Bottom Edge of Fuel Meat	
5.3-36	Core I Experimental Power Distribution for a Horizontal Cross Section 5.438 inches from Bottom Edge of Fuel Meat	
5.3-37	Core I Experimental Power Distribution for a Horizontal Cross Section 13.688 inches from Bottom Edge of Fuel Meat	

Table Number		
5.3-7	Relative Power Distribution in Plates and Elements of Core I where the Removable Plate Element was Irradiated - Blades at 7.6 inches.	

TABLE 5.5-3

SUMMARY TABLE OF COPPER WIRE FLUX DISTRIBUTIONS

Figure Number	Description
5.4-6, 5.4-7	Thermal Neutron Flux Distributions in Absorber Spider Holes #1 and #3
5.4-8, 5.4-9	Thermal Neutron Flux Distribution in Channels #2 and #10 of Element in C-8
5.4-10, 5.4-11	Thermal Neutron Flux Distributions in Channels #2 and #11 of Channel in A-2
5.4-12, 5.4-13, 5.4-14	Thermal Neutron Flux Distributions in Corner Holes #2, #4, and #5
5.4-15	Thermal Neutron Flux Distribution in 6RH2
5.4-16	Thermal Neutron Flux Distribution in 3GV5
5.4-17	Thermal Neutron Flux Distribution in 3GV6

CHAPTER 6

POWER DISTRIBUTIONS IN CORE II

Power distributions in Core II of the MITR-II are
discussed in this chapter. Section 6.1 summarizes the
analysis methods and fuel loading arrangement for Core II.
The calculational model and design check predictions for
Core II are described in Section 6.2. The experimental
measurements of power distributions for several specifiec
element positions are described in Section 6.3. The power
distributions for Core II are summarized in Section 6.4.

6.1 Analysis Methods and Loading

Core II was intended as a short term core to be
operated during the period of time it would take to
obtain satisfactory substitutes for the original cad-
mium sandwich fixed absorbers. Core II was designed
to allow operation of the MITR-II without fixed absorb-
ers in the upper half of the core. This resulted in
a higher active core height and some loss of neutron
intensity at the beam ports beneath the reactor core.
The fuel loading for Core II is shown in Fig. 6.1-1.

The power and neutron flux distributions of Core II
were calculated by using the CITATION computer code.
Selected power distributions were experimentally verified

FIG. 6.1-1

CORE II FUEL LOADING
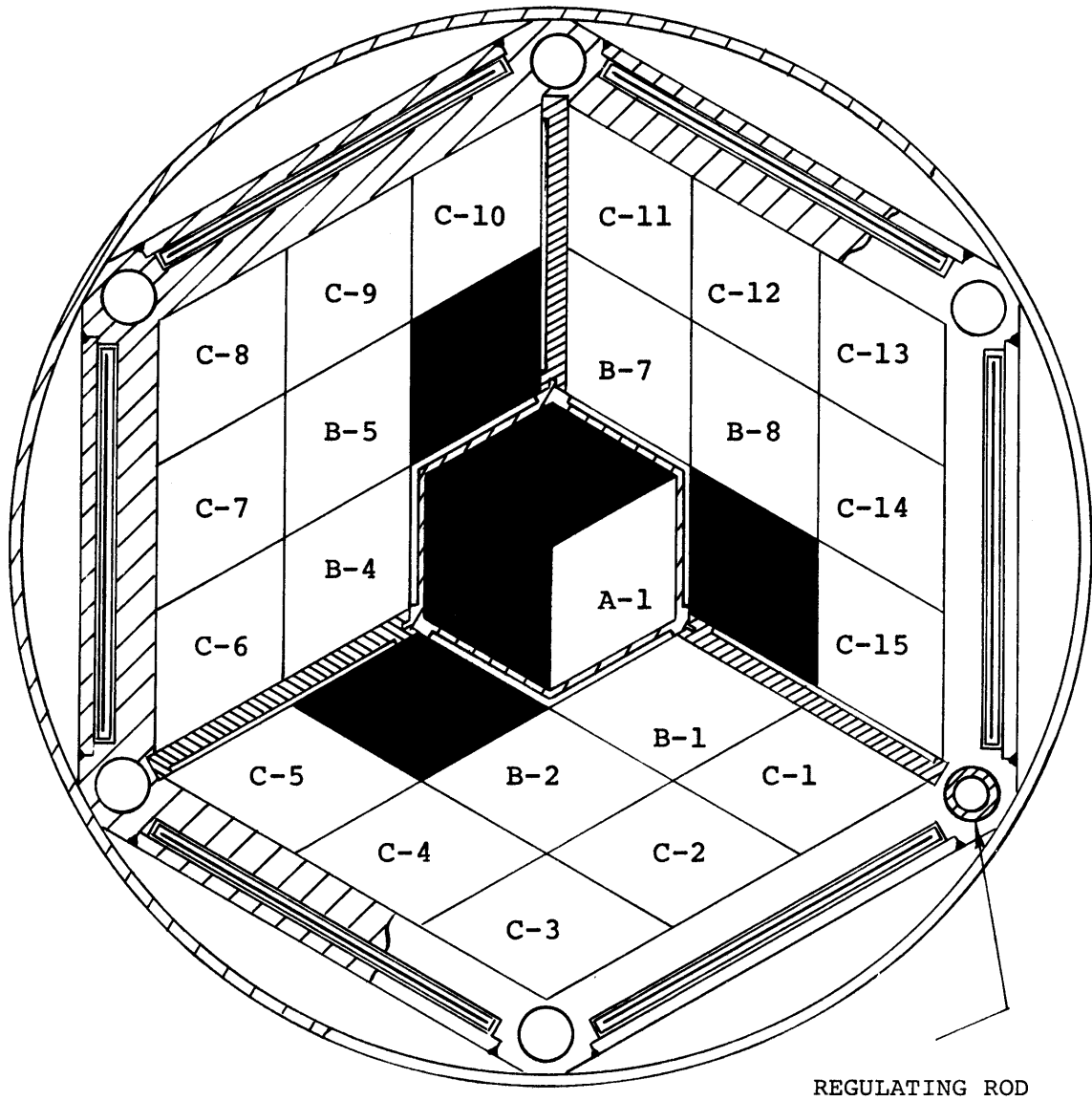
◣ - solid dummy element

by gamma scanning a removable plate fuel element after
irradiation in the specified positions. The use of
CITATION and gamma scanning techniques to determine
the power density is extensively described in Chapter 5
and will not be repeated here. Only the differences between
evaluating Core I and Core II are discussed in this chap-
ter. The differences arise in the means for evaluating
the radial peaking factor, F_r, since for Core II fewer
removable plate irradiations were performed.

6.2 Design Check Predictions

A three-dimensional model was developed to mock-up
the Core II fuel loading for use in the CITATION code
calculation. The CITATION code and cross sections set
are described in Section 5.2.1. A description of the
Core II calculational model is given in Section 6.2.1.

6.2.1 Mesh Spacing Arrangement

As can be seen in Fig. 6.1-1, Core II of the MITR-II
is not symmetric about a plane passing through the center
of the core and the center of the regulating rod. In
order to model Core II as symmetric about the center
plane, the solid dummies in the B-ring had to be smeared
as shown in Fig. 6.2-1. The total volume of fuel for
22 fuel elements was set equal to the amount of fuel in
the mock-up shown in Fig. 6.2-1. The axial direction
(Z direction) and radial (R direction) mesh boundaries

FIG. 6.2-1

CITATION R-θ MOCKUP OF CORE II

θ-11
θ-10
θ-9
θ-8
θ-7
θ-6
θ-5
θ-4
θ-3
θ-2
θ-1

REGULATING ROD

- solid dummy elements
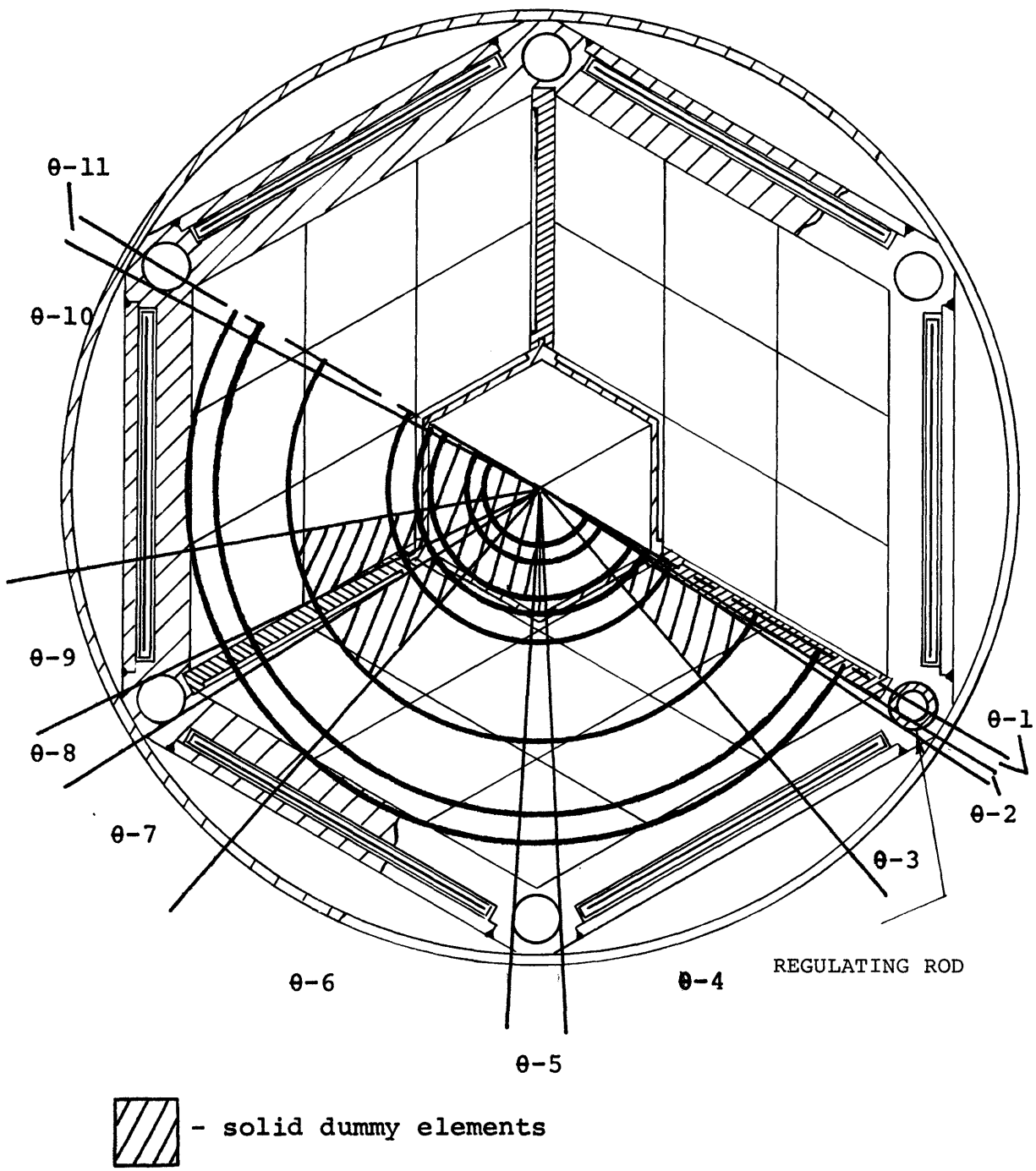
were maintained the same as for Core I. The θ direction

boundaries were altered to obtain the positions shown

in Fig. 6.2-1.

Table 6.2-1 shows the comparison between the CITATION

predictions for K_{eff} and power densities for the models

of Core I and Core II. The average power density multiplied

by the number of elements in the core comes to approximately

the same number for each loading which indicates that the

fuel volume ratio between the two cases is correct. The

fact that the error in K_{eff} (compared to the measured

$K_{eff} = 1.00$) is about the same for both cases indicates

that the symmetric model of the non-symmetric Core II is

probably not a bad assumption and the results will be

consistent with other CITATION calculations of the MITR-II.

6.2.2 Power Density

If a total core power is specified, CITATION prints

out the average mesh point power density for each mesh

point containing fissile material. For all CITATION com-

puter calculations in this work, the total core power was

specified as 5 thermal megawatts. Section 5.2.3.1 shows

how CITATION calculated power densities can be used to

obtain local fuel plate heat fluxes; heat deposited in

local coolant channels; values of F_r, F_a, and $F_r \times F_a$;

and fuel plate wall temperatures.

By employing the method to determine channel powers

described in Section 5.2.3.1, the average channel power

TABLE 6.2-1

COMPARISON OF CITATION K_{eff} AND POWER DENSITY
PREDICTIONS FOR CORE I AND CORE II

Comparison Between K_{eff} for CITATION Models

	Core I	Core II
Measured K_{eff}	1.0	1.0
CITATION Prediction for K_{eff} of Critical Core	0.947	0.954

Comparison Between Power Densities for
CITATION Models of Core I and II

	Core I	Core II
Number of Loaded Elements	24	22
Average Power Density in Fueled Volume	84 watts/cm^3	91.3 watts/cm^3
$\dfrac{\text{Average Power Density times Number of Elements}}{1000}$	2.016	2.008

for each element can be obtained. The power deposited

in the Kth channel, PC_K, is determined by the following

equation:

$$PC_K = 2W \sum_{i=1}^{n} (Q/A)_i \, Zi, \quad \text{watts} \qquad (5.2-6)$$

where,

$(Q/A)_i$ is the fuel plate area heat flux in watts/cm^2
for constant R and θ corresponding to the
channel of interest,

Z_i is the height in centimeters in the Z direction
of the ith mesh point,

W   is the fueled width of the fuel plate in
centimeters,

n   is the number of mesh point volumes in the
Z direction for constant R and θ.

The average channel power in an element is determined

by the following:

$$PC^M = \sum_{j=1}^{Q} PC_j f_j \quad , \qquad \text{watts} \qquad (6.2-1)$$

where,

PC^M is the average channel power in the Mth element,

PC_j is the channel power of the jth channel in the
M^{th} element,

f_j is the fraction of the Mth element power that is
represented by the jth channel,

Q   is number of channels in the Mth element for
which CITATION representations are available.

Note that the following must be made true for each evaluation:

$$\sum_{j=1}^{Q} f_j = 1.0. \tag{6.2-2}$$

The f_j's are evaluated by determining the volume fraction of the element that can be reprsented by a given channel in CITATION (a series of axial mesh points with a constant R and θ).

The ratio of element power to core average element power is defined to be F_r' and can be determined by the following equation:

$$(F_r')^M = \frac{\dfrac{PC^M}{P}}{\dfrac{\displaystyle\sum_{i=1}^{P} PC^i}{P}} \tag{6.2-3}$$

where,

$(F_r')^M$ is the ratio of power produced in the Mth element to the power produced in the average element,

P is the number of fueled elements in the reactor.

By using results and Eqs. 5.2-3, 6.2-1, and 6.2-3, the value of F_r' was calculated for each element in Core II. Figure 6.2-2 shows the value of F_r' for each element position.

The hottest channels in Core II are predicted to be in elements A-1 and C-13. Axial power distributions for the hottest channels in those elements are shown in Figs. 6.2-3 and 6.2-4. An axial power distribution for a

FIG. 6.2-2

CITATION RELATIVE FUEL ELEMENT POWER FOR CORE II

REGULATING ROD
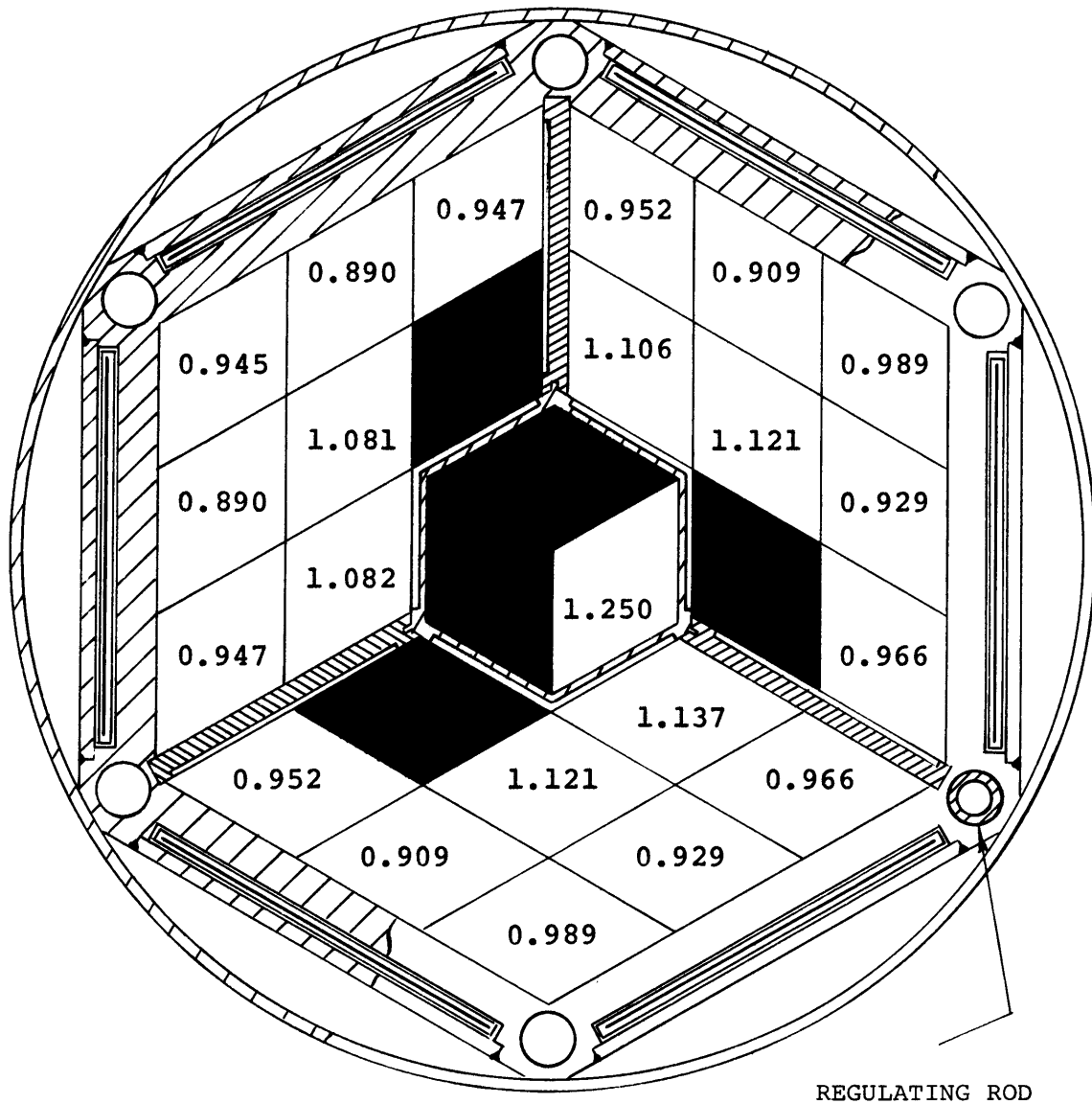
◢ - solid dummy elements

Above numbers are the ratio of the CITATION
predicted power in each element position
to the power in the average element in the
core for the blades at 8 inches.

FIG. 6.2-3

CITATION RELATIVE POWER
DISTRIBUTION OF PLATE 1
OF ELEMENT IN A-1 FOR
CORE II

(plate 1 is next to the
hexagonal spider)

blades at 8 inches

blades at 14
inches

FIG. 6.2-4

CITATION RELATIVE POWER
DISTRIBUTION OF PLATE 1 OF
ELEMENT IN C-13 FOR CORE II

(plate 1 is next to core
housing)

blades at 14 inches

blades at 8 inches

FIG. 6.2-5

CITATION RELATIVE POWER
DISTRIBUTION OF CENTRAL
PLATE OF ELEMENT IN B-7
FOR CORE II

central channel in a B-ring element is shown in Fig. 6.2-5. As would be expected, a higher fraction of element power is generated in the upper half of the element upon removal of the fixed absorbers.

Figures 6.2-3, 6.2-4, and 6.2-5 show the effects of raising the blade height on the axial power distribution. For interior element ring positions, the shape of the plate axial power distribution is nearly unchanged and the total power generated drops slightly. For fuel plates near the outside of the core, the shape of the power distribution changes considerably with blade height and the total power generated increases significantly. When peak values of the safety limit and limiting condition for operation occur in outside edge fuel channels, the values will increase toward the allowable limit as the shim bank is raised.

6.3 Experimental Measurement of Power Density

The power distribution in several fuel element positions was experimentally measured by gamma scanning of removable fuel plates. A description of gamma scanning techniques is found in Section 5.3. The removable plate element was only irradiated in four fuel element positions in the Core II loading for the following reasons:

A. A full irradiation program of all positions
    would have required an extended length of
    time,

B. Comparisons between CITATION and gamma scan-
    ning for Core I had given a good verification
    of accuracy of CITATION,

C. Future core evaluations will not involve
    gamma scanning techniques and thus it
    would be helpful to begin to formulate
    those evaluation techniques as early as
    possible with some limited additional
    experimental verification as a check.

The four element positions where fuel plate irradiations were performed were chosen by picking the positions which CITATION predicted to have the greatest power peaking and where characteristics of Core II differed sufficiently from Core I such that unexpected power peaking might occur; i.e., water gaps created by removal of the fixed absorbers. Figure 6.3-1 shows the four positions where the removable plate element was irradiated.

6.3.1   Variances Between Core I and Core II Gamma
                    Scanning Technique

The gamma scanning experimental technique and data evaluation was the same for Core II as for Core I with the exception of the following:

1) The counting electronics were different (see
    Fig. 6.3-2 for block diagram of new electronic
    equipment),

2) Uranium foil irradiations were not performed
    since they had been found to be unnecessary,

3) Scanning position points were changed and new
    effective areas inputed to COREFAC,

4) COREFAC was not utilized to obtain core-average
    weighting factors because sufficient irradiations
    were not performed to yield accurate core-wide
    plate weighting factors.

FIG. 6.3-1

CORE II REMOVABLE PLATE ELEMENT IRRADIATION POSITIONS

Irr.24

Irr.22

Irr.21

Irr.23

REGULATING ROD
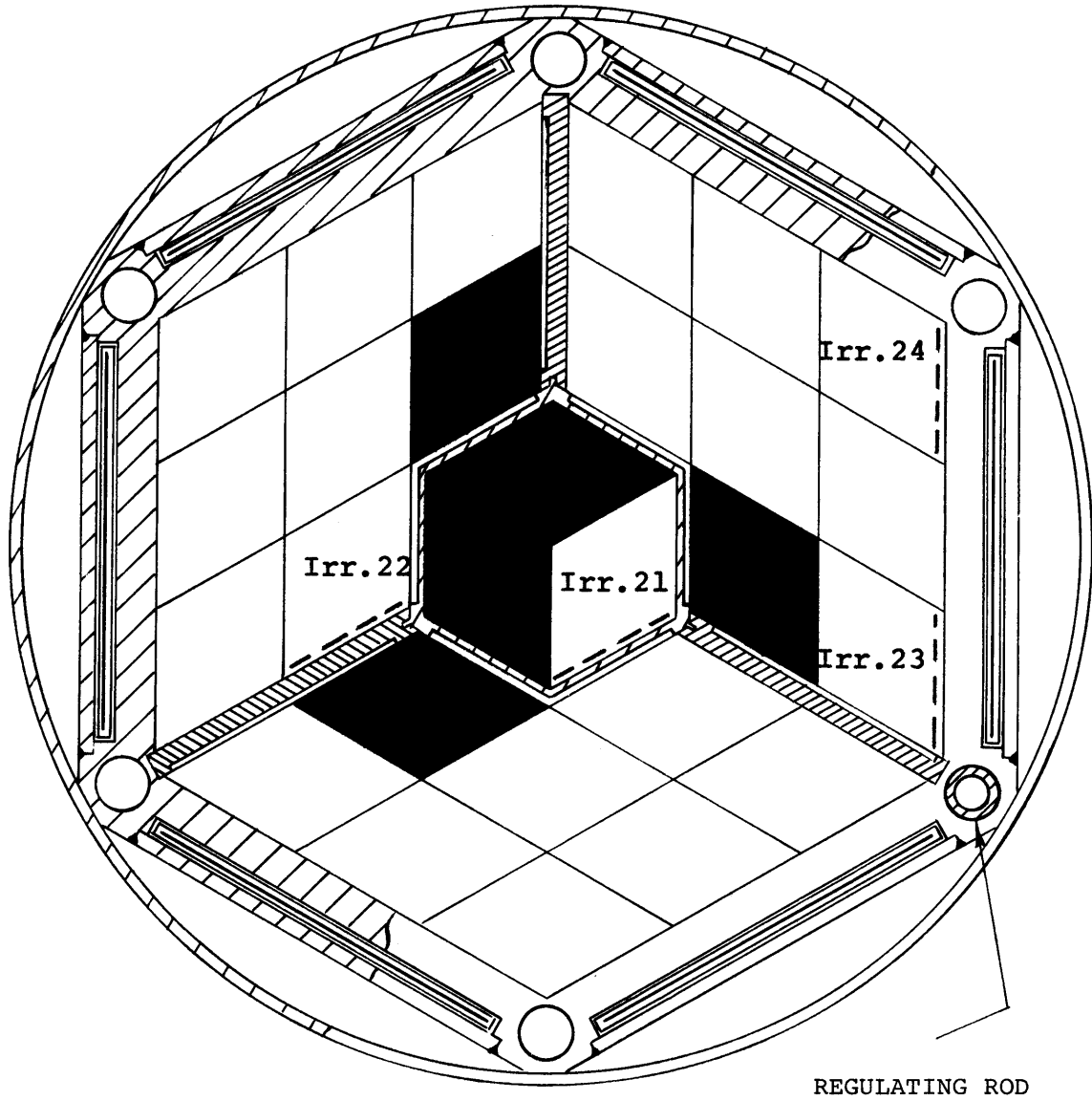
◢ - solid dummy element

┊ - orientation of plate 1 in element position

FIG. 6.3-2

BLOCK DIAGRAM OF CORE II GAMMA SCANNING ELECTRONICS

2x2 NaI (Th)

phototube

preamplifier

Mechtronics   #512

amplifier and single
channel analyzer

coarse gain = 64
fine gain = 1
baseline = 0.45 V.

high voltage
supply

1000 V.

Mechtronics   #714

scaler - timer
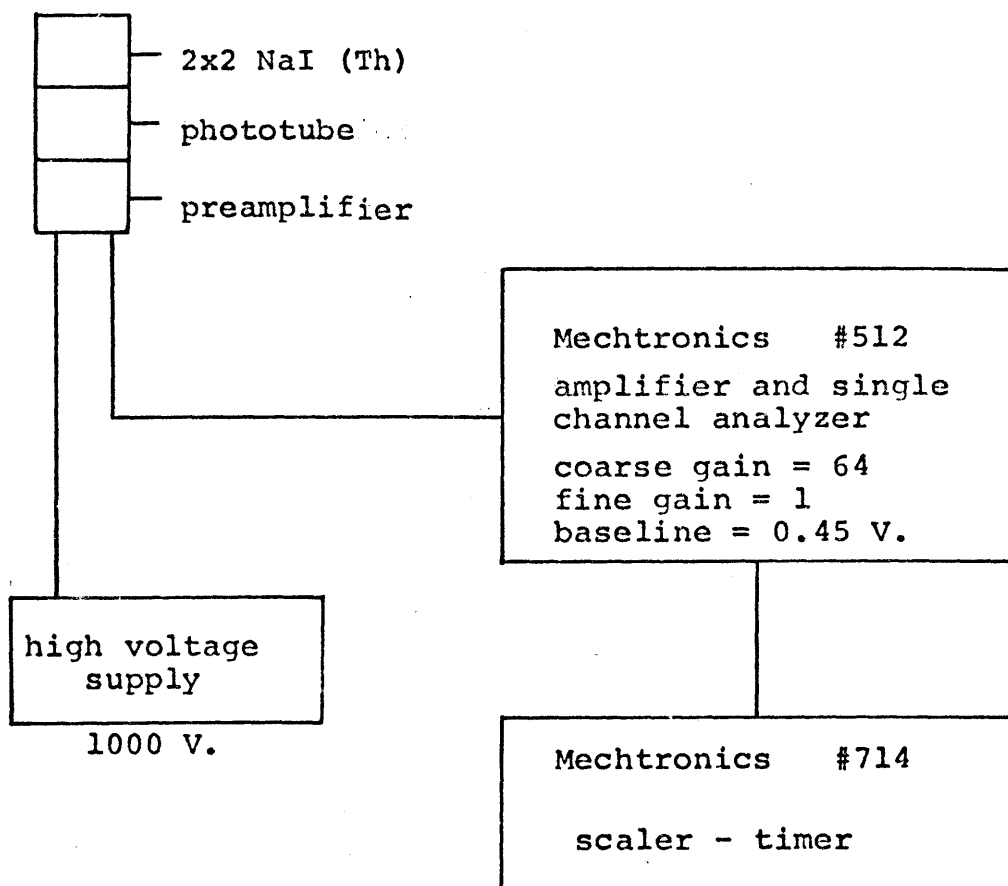
The electronics change had no effect on the results since the same I^{131} source used as Core I standard was used to calibrate and adjust the Core II setup to the same count rates and energy cutoff as Core I. Deleting the uranium foil counts was possible because the uranium foil data was not used in evaluating the scanning data.

The scanning positions were changed because more information was desired about the power distribution in the upper section of the core. Because the number of points scanned is limited to 66, some of the positions in the lower portion of the plate were deleted. A series of points were chosen at the top edge of the fuel plate in order to assure that no unacceptable peaking was occurring near the outlet of the elements with the fixed absorber removed. Table 6.3-1 gives the coordinates of the positions scanned with (0,0) corresponding to a lower left corner of the fuel meat when looking at the fuel plate with the number side up and the scan point effective areas.

COREFAC was only used to obtain the axial peaking factor F_a, and to provide data for evaluating F_r'', the ratio of the power produced in a plate to the power produced in the average plate in that element. Insufficient removable plate irradiations were performed to obtain data representative of every fuel plate in Core II. As a result, core wide weighting could not be obtained

TABLE 6.3-1

REMOVABLE PLATE SCAN POINT COORDIANTES FOR CORE II

Point	x*	y*	Effective Area
1	0.0	1.688	0.0225
2	0.0	1.000	0.0215
3	0.00	0.313	0.0205
4	0.063	1.688	0.0674
5	0.063	1.000	0.0644
6	0.063	0.313	0.0615
7	0.188	1.688	0.0898
8.	0.188	1.000	0.0859
9	0.188	0.313	0.0820
10	0.313	1.688	0.0898
11	0.313	1.000	0.0859
12	0.313	0.313	0.0820
13	0.438	1.688	0.1347
14	0.438	1.000	0.1289
15	0.438	0.313	0.1230
16	0.688	1.688	0.2695
17	0.688	1.000	0.2579
18	0.688	0.313	0.2461
19	1.188	1.688	0.3594
20	1.188	1.000	0.3438
21	1.188	0.313	0.3281
22	1.688	1.688	0.5391
23	1.688	1.00	0.5156
24	1.688	0.313	0.4922
25	2.688	1.688	0.7188
26	2.688	1.000	0.6875
27	2.688	0.313	0.6562
28	3.688	1.688	0.7188
29	3.688	1.000	0.6875

TABLE 6.3-1 (Continued)

REMOVABLE PLATE SCAN POINT COORDINATES FOR CORE II

Point	x*	y*	Effective Area
30	3.688	0.313	0.6562
31	4.688	1.688	0.7188
32	4.688	1.000	0.6875
33	4.688	0.313	0.6562
34	5.688	1.688	0.7188
35	5.688	1.000	0.6875
36	5.688	0.313	0.6562
37	6.688	1.688	0.7188
38	6.688	1.000	0.6875
39	6.688	0.313	0.6562
40	7.688	1.688	1.0781
41	7.688	1.000	1.0312
42	7.688	0.313	0.9844
43	9.688	1.688	1.4375
44	9.688	1.000	1.3750
45	9.688	0.313	1.3125
46	11.688	1.688	1.4375
47	11.688	1.000	1.3750
48	11.688	0.313	1.3125
49	13.688	1.688	1.7970
50	13.688	1.000	1.7190
51	13.688	0.313	1.6405
52	16.688	1.688	2.1562
53	16.688	1.000	2.0625
54	16.688	0.313	1.9687
55	19.688	1.688	1.6172
56	19.688	1.000	1.5469
57	19.688	0.313	1.4766

TABLE 6.3-1 (Continued)

REMOVABLE PLATE SCAN POINT COORDINATES FOR CORE II

Point	x*	y*	Effective Area
58	21.188	1.688	0.8086
59	21.188	1.000	0.7734
60	21.188	0.313	0.7383
61	21.938	1.688	0.3492
62	21.938	1.000	0.3297
63	21.938	0.313	0.3102
64	22.438	1.688	0.0140
65	22.438	1.000	0.0144
66	22.438	0.313	0.0140

*(0,0) corresponds to the lower left corner of the fuel meat when looking at the fuel plate with the number side up.

with sufficient accuracy to utilize the capability in
COREFAC to evaluate F_r, the ratio of power produced in
a plate to the power produced in the average plate in
the core.

6.3.2 Data Analysis

Computer code GAMSCAN was utilized to evaluate
counting data and correct for decay, background, and
backscatter. The output of GAMSCAN was used as input
to COREFAC along with cobalt foil counts and scan
point effective areas. Table 6.3-2 gives the element
orientation and the corrected cobalt count for each
irradiation. COREFAC output yielded the value of F_a
for each point scanned and an average counts per unit
area of plate for each plate scanned.

Figure 6.3-3 shows the axial distribution of F_a
for the hottest plate in A-2. Note that the power
distribution is fairly uniform in the plate. Power
peaks occur at the top and bottom of the plate where
water is plentiful in the inlet and outlet plenums.
Similarly, a power peak occurs above 10 inches as a
result of the water gap caused by removal of the fixed
absorbers.

Figure 6.3-4 shows the axial variation of F_a for
a plate in B-4 next to a radial wing of the absorber
spider. There is no unacceptable peaking caused by the
water gap created by removal of the fixed absorber sandwich.

TABLE 6.3-2

CORE II REMOVABLE PLATE ELEMENT ORIENTATION POSITIONS AND COBALT FOIL COUNTS

Irradiation Number	Fuel Element Position	Element Orientation in Position	Total Cobalt Foil Counts Corrected for Decay, Mass, and Background
21	A-1	Plate 1 next to hexagonal spider	15,066
22	B-4	Plate 1 next to absorber spider	28,742
23	C-15	Plate 1 next to core housing	28,459
24	C-13	Plate 1 next to core housing	28,439

*Blade height for irradiations was 8.6 inches.

FIG. 6.3-3

AXIAL PEAKING FACTOR FROM PLATE
SCANNING DATA ON PLATE 1 OF
ELEMENT IN A-1 FOR CORE II

(blades at 8.6 inches)

(plate 1 is next to the
hexagonal spider)

FIG. 6.3-4

AXIAL PEAKING FACTOR FROM PLATE
SCANNING DATA ON PLATE 1 OF
ELEMENT IN B-4 FOR CORE II

(blades at 8.6 inches)
(plate 1 is next to the
radial spider wing)   =

FIG. 6.3-5

AXIAL PEAKING FACTOR FROM PLATE
SCANNING DATA ON PLATE 1 OF
ELEMENT IN C-13 FOR CORE II

(blades at 8.6 inches)
(plate 1 is next to core
housing)

Figure 6.3-5 shows the axial variation of F_a for the outside fuel plate in C-13. The power distributions in this outside plate resembles distributions found in Core I where power was depressed in the upper core by fixed absorbers. The control blades have a major influence on the power distribution in the outside edge plates causing the power to decrease above the axial height of the shim bank. Because element positions C-3, C-8, and C-13 are relatively far from the fixed absorber locations, the power density distribution shape depends mainly on the shim bank height and is only slightly affected by whether fixed absorbers are or are not present. The effect of fixed absorbers would only be significant for high shim bank heights. (Compare Figs. 5.3-29 and 6.3-5 for similarity of distributions). The outside plate of C-13 becomes the hottest plate in the core as the shim bank height is raised.

For each irradiation position of the removable plate element, the average counts per plate of each plate scanned was plotted versus plate number in the element. These plots showed the power distributed through the fuel element. Since only five plates out of fifteen were scanned in each irraidation, each plate had to be weighted to determine how many plates that each plate counted actually represented. This weighting was accomplished by dividing the distribution curve up into a

series of blocks in which the integral of the area under the blocks approximately equals the integral of the area under the distribution curve. Figure 6.3-6 shows an example for the case of the removable plate element irradiated in position C-13.

The ratio of the power produced in a plate to the power produced in the average plate in that element is defined as F_r'' and is evaluated for each plate scanned by the following:

$$(F_r'')_{jk} = \frac{PLTAVG(K,J)}{\dfrac{\sum\limits_{i=1}^{5} W_{jk} P_{LTAVG(K,J)}}{15}} \tag{6.3-1}$$

where,

$(F_r'')_{jk}$ is the value of F_r'' for the jth plate scanned in the Kth element,

PLTAVG(K,J)   is the average counts per plate for the jth plate in the Kth element,

W_{jk} is the weighting factor that corresponds to the number of plates in the Kth element that the jth plate represents with the criteria that $\sum\limits_{j=1}^{5} W_{jk} = 15.$

The values of F_r'' for each plate scanned in Core II are listed in Table 6.3-3.

FIG. 6.3-6

PLATE POWER DISTRIBUTION THROUGH ELEMENT C-13

F_r vs plate number in element
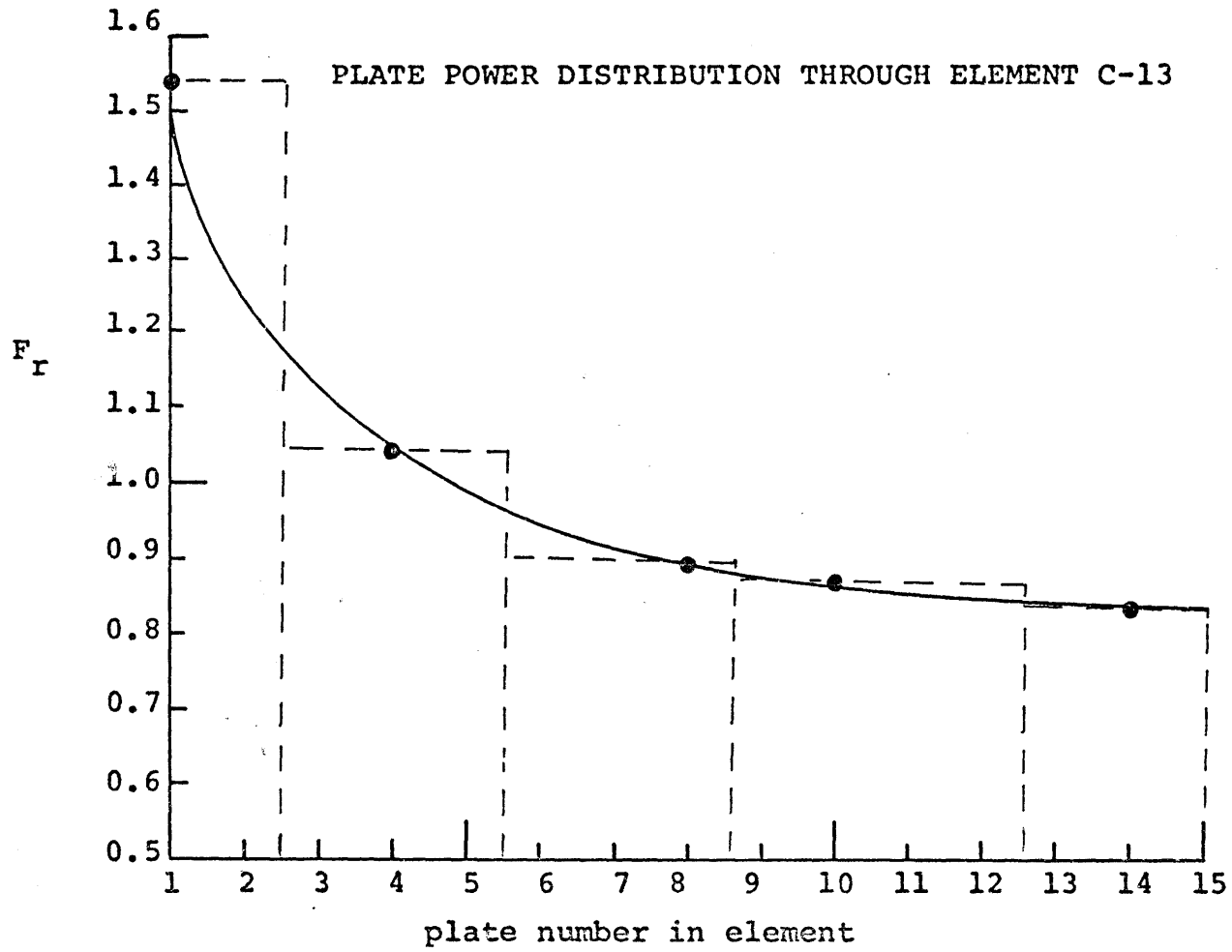
TABLE 6.3-3

VALUES OF F''_r FOR CORE II DETERMINED BY
REMOVABLE PLATE ELEMENT IRRADIATIONS

Element Position	Plate Number in Scanning Data	Plate Number in Element	Number of Plates in Element Represented by Plate which was Scanned W_{jk}	F''_r
A-1	1	1	2	1.27
	2	4	4	1.08
	3	8	2	.97
	4	10	3	.90
	5	14	4	.88
B-4	1	1	2	1.38
	2	4	3	.99
	3	8	3	.96
	4	10	4	.95
	5	14	3	.86
C-15	1	1	2	1.42
	2	4	3	.99
	3	8	3	.87
	4	10	4	.87
	5	14	3	1.03
C-13	1	1	2	1.55
	2	4	3	1.05
	3	8	3	.90
	4	10	4	.88
	5	14	3	.84

6.4 Summary of Power Distributions in Core II

Table 6.4-1 gives a summary listing of information in this chapter on the power distribution in Core II. The value of the radial peaking factor, F_r, which is of interest in determining the core safety limit and limiting conditions for operation is evaluated in the following manner:

$$F_r = F_r' \times F_r'' \quad , \qquad (6.3\text{-}2)$$

where,

F_r' is taken from Fig. 6.2-2 based on CITATION data,

F_r'' is taken from Table 6.3-3 based on plate scanning
data for the hot channel of interest.

The value of F_r is thus based on the product of CITATION data and an experimentally determined factor. CITATION results yield a value of F_r' that is sufficiently within uncertainty limits used in determining the safety limit and limiting condition for operations. Figure 6.4-1 shows a comparison between CITATION predicted values of F_r' for Core I and the COREFAC predicted values of F_r' for Core I. For higher power elements the agreement between the two methods is very good and for all element positions the average difference is 5%, which is less than the 10% uncertainty on power density used in evaluating the safety limit and limiting condition for operation.

FIG. 6.4-1

COMPARISON BETWEEN CITATION AND COREFAC RESULTS FOR CORE I

REGULATING ROD
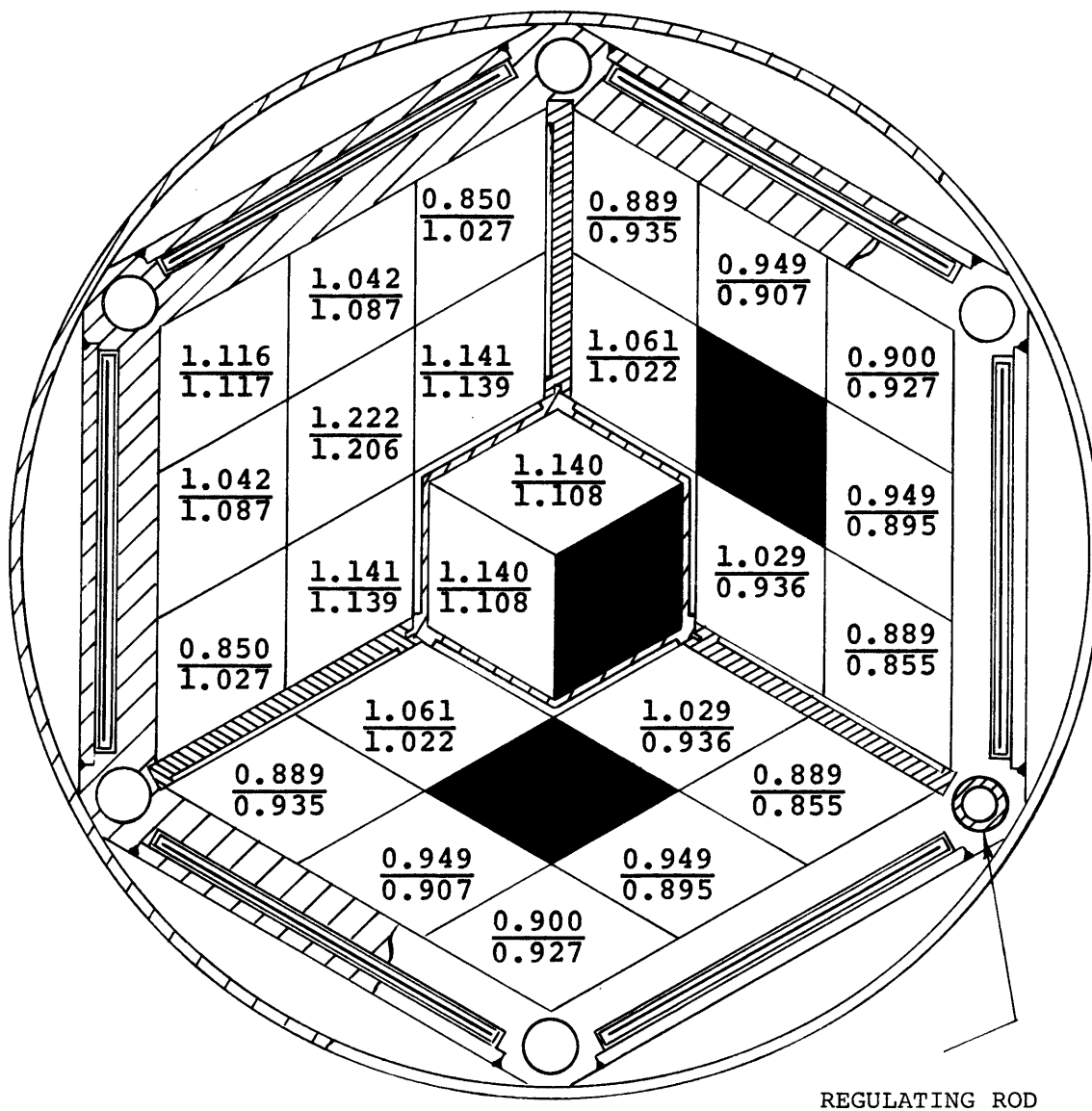
■ - solid dummy element

$$\frac{xxxxx}{yyyyy} = \frac{\text{ratio of COREFAC power per element to core average element power}}{\text{ratio of CITATION power per element to core average element power}}$$

TABLE 6.4-1

SUMMARY TABLE OF CORE II POWER DISTRIBUTIONS

Figure Number	Title	Description
Fig. 6.2-2	CITATION Relative Fuel Element Power for Core II	Shows value of F_r' for each Core II element position.
Fig. 6.2-3	CITATION Relative Power Distribution of Plate 1 of Element in A-1 for Core II	Shows value of $F_r F_a$ from CITATION calculations versus axial position for plate in A-1 next to hexagonal spider.
Fig. 6.2-4	CITATION Relative Power Distribution of Plate 1 of Element in C-13 for Core II	Shows value of $F_r F_a$ from CITATION calculations for plate next to core housing in C-13.
Fig. 6.2-5	CITATION Relative Power Distribution of Central Plate of Element in B-7 for Core II	Shows value of $F_r F_a$ from CITATION calculation for an interior B-ring plate.
Fig. 6.3-3	Axial Peaking Factor from Plate Scanning Data on Plate 1 of Element in A-1 for Core II	Shows value of F_a from COREFAC for plate next to hexagonal spider in A-1.
Fig. 6.3-4	Axial Peaking Factor from Plate Scanning Data on Plate 1 of Element in B-4 for Core II	Shows value of F_a from COREFAC for plate in B-4 next to the radial spider with the absorber removed.

TABLE 6.4-1 (Continued)

Figure Number	Title	Description
Fig. 6.3-5	Axial Peaking Factors from Plate Scanning Data on Plate 1 of Element in C-13 for Core II	Shows value of F_a from COREFAC for plate in C-13 that is next to the core housing.
Fig. 6.3-6	Plate Power Distribution Through Element C-13	Shows values of F through element in C-13.

CHAPTER 7

SAFETY LIMITS AND LIMITING OPERATING CONDITIONS

The thermal-hydraulic safety limit and limiting
conditions for operation of the MITR-II are described
in this chapter. The derivation of the thermal-hydrau-
lic safety limit of the MITR-II is found in Section 3.3.4
of the MITR-II Safety Analysis Report. Much of the work
shown in that SAR section is repeated in Sections 7.2.1
and 7.3.1 of this work because the best way to completely
understand the basis of the safety limit and limiting
conditions for operation is to review the complete deriva-
tion. New data from experiments completed since the SAR
was written are incorporated in this work to update the
SAR derivation when applicable.

The evaluations of the safety limit and limiting
condition for operation as defined by Technical Specifi-
cation Sections 2.1 and 3.1 are included in Sections 7.2
and 7.3 for the first two core loadings of the MITR-II.
Expected problems for future core loadings are discussed
in Section 7.4. Suggested methods for evaluation of future
core loadings are included in Section 7.5

338

7.1 General Descriptions

Conservative thermal-hydraulic limits are used for the MITR-II. A safety limit is set to prevent boiling induced flow instabilities which could lead to boiling burnout and limiting safety system settings are set to prevent incipient boiling from occurring anywhere in the core. The limiting condition for operation above 1.0 kw is that the power distribution in the operating core has been evaluated to assure that incipient boiling will not occur for the limiting safety system settings. These limits are established by utilizing the normally measured quantities of total reactor power, total primary coolant flow, and bulk coolant temperature of the reactor outlet and by utilizing the experimentally and analytically determined core factors together with an estimate of their uncertainty. The use of conservative assumptions and conservative values of uncertainties assure a wide margin between the true safety limit of prevention of boiling burnout and actual operating condition provided that the technical specification safety limit and limiting conditions for operation are met.

7.2 Safety Limit

The purpose of safety limit is to assure that the structural integrity of the fuel elements is maintained.

This assures that the fission products are contained, and that the fuel is maintained in a coolable geometry. The safety limit as defined in the Technical Specification Section 2.1 is:

> The point determined by the combination of the true values of P_T, W_T, and T_{out} shall not be above the line given in Fig. 2.1-1 (Fig. 7.2-1 in this work) corresponding to the true value of the water height, L;

where,

P_T is the total reactor thermal power(MW),
W_T is the reactor coolant flow rate (gpm),
T_{out} is the reactor coolant outlet temperature (°C),
L is the height above the outlet end of the heated section of the hottest fuel channel (feet).

The plot shown in Fig. 7.2-1 is valid if $F_{HC}F_p/d_f F_f$ is less than or equal to 2.9 where:

F_{HC} is the hot channel factor, the ratio of the power released into the hottest channel over the average (radial) channel power,

F_p is the fraction of the total power generated by the fuel,

d_f is the flow disparity, the ratio of the minimum expected flow in the hot channel to the average channel flow,

F_f is the fraction of primary flow cooling the fuel.

The ratio $F_{HC}F_p/d_f F_f$ has been evaluated for the initial core loadings of the MITR-II to insure the validity of Fig. 7.2-1.

FIG. 7.2-I

MITR - II SAFETY LIMITS

for $\dfrac{F_{HC} F_p}{d_f F_f} = 2.9$

WATER HEIGHT, L

12 feet
10 feet
8 feet
6 feet

POWER TO FLOW RATIO, P/W , $\times 10^4$ MW/gpm

REACTOR OUTLET TEMPERATURE, T_{out} (°C)
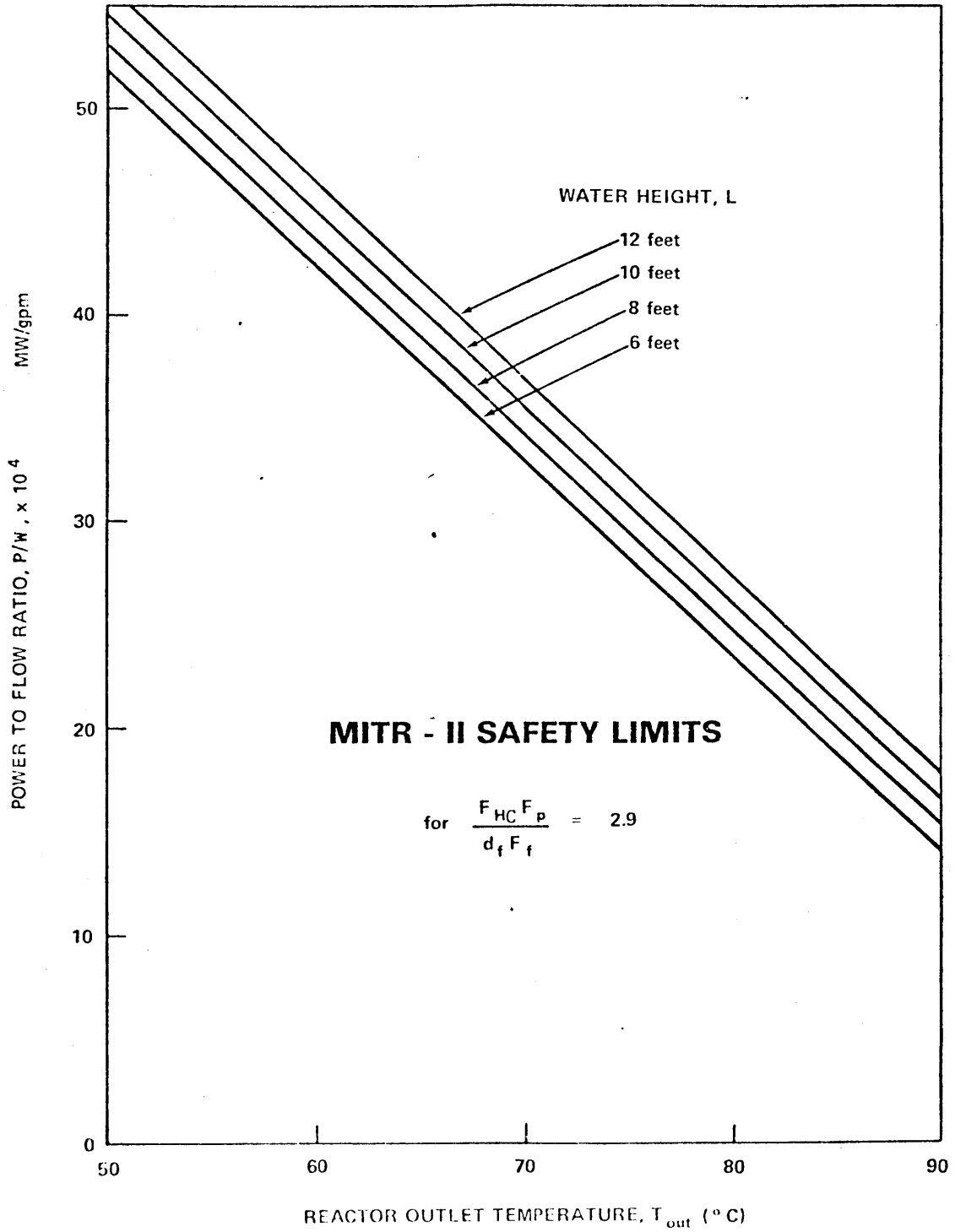
7.2.1 Basis of Safety Limit

The safety limit provides an upper bound for which operation below the safety limit assures the structural integrity of the fuel elements. Although aluminum melts at approximately 660°C it begins to soften significantly at about 450°C and this temperature of 450°C is thus taken as the upper limit on clad temperature.

Since the MITR-II operates at atmospheric pressure at the pool surface and since the fuel elements use thin aluminum cladding, the difference of about 350°C between 450°C and low pressure boiling temperatures could not be reached if boiling burnout is prevented. Because of the low pressure and multichannel design of the MITR-II, it is difficult to predict when boiling burnout would occur because of the problem of two-phase flow instabilities. The occurrence of an instability can result in the worst case in flow starvation and a premature "burnout" at heat fluxes well below the burnout heat flux predicted without an instability. Despite basic research in the area of stability in two-phase flows for at least the last twenty years, a good understanding of the total stability picture has been hampered by the existence of a great number of different mechanisms (Ref. 7.2-1). The exact amount of the effect of an instability on lowering the burnout heat flux is very difficult to predict at the present time. In view of this difficulty, it is

assumed here that the onset of flow instability causes a lower flow rate in one channel for the same pressure drop and thus causes burnout at a lower heat flux than would be computed from the average flow conditions of the channels. The MITR-II safety limit is set such that the reactor operates below conditions for onset of flow instability. This basis combined with the conservative assumptions used in predicting the onset of flow instability, produces a safety limit of the maximum steady state power that is considerably below values based on applicable burnout correlations. Thus, there appears to be a comfortable margin beyond this safety limit before reaching the point where a real threat to fuel element integrity exists.

The mechanism which can be used to explain the class of instability which would be expected to occur in the MITR-II core is the pressure drop-flow rate instability. This mechanism can arise whenever the pressure drop versus flow rate curve of a system element has a flat or negative sloping region. The following single spaced sections in quotations, except where noted otherwise, are excerpts from Section 3.3-4 of the MITR-II Safety Analysis Report. The equation, figure, table, and reference numbers in the excerpted section have been renumbered to be consistent with the numbering system in this work and to provide

easy reference for discussion in this work. These excerpts

combined with additional comments show the basis of the

MITR-II Safety Limit.

"The method of investigating the onset of flow
instability consists of calculating the pressure
drop as a function of flow rate for a given heat
flux. The minimum stable flow rate is that
which coincides with the minimum of the curve.
This is consistent with the stability criterion
below:
For instability:

$$\frac{\partial}{\partial W}(\Delta p \text{ external sys.}) - \frac{\partial}{\partial W}(\Delta p \text{ coolant channel}) \geq 0,$$

$$(7.2-1)$$

where,

p is the pressure drop,
W is the coolant flow.

Since, for a large number of channels,

$$\Delta p \text{ external sys.} = \text{constant}, \qquad (7.2-2)$$

the criterion reduces to:

$$- \frac{\partial}{\partial W}(\Delta p \text{ coolant channel}) \geq 0. \qquad (7.2-3)$$

This theoretical model has been proposed in
several references, Refs. 7.2-2, 7.2-3, and
7.2-4, and has been found to give excellent
agreement with experiment (Ref. 7.2-4 and 5).
    In case of the MITR fuel element some in-
terpretation is necessary in order to define the
coolant channel. The entire fuel element
could be considered a coolant channel, since
there are 24* to 27 elements in the core and
the assumption of a constant pressure drop
across the fuel elements is not significantly
affected by flow changes in any one element.
The alternative is to treat the individual
channels between fuel plates. This distinc-
tion has considerable bearing on the results
and as will be seen below the latter case is
the more conservative and has, therefore,
been used in this analysis.
    The pressure drop across the coolant
channel can be divided into four parts:

*There are only 22 fueled elements in Core II
of the MITR-II.

1) the entrance effect,
2) the friction factor drop along
   the length of the channel,
3) the exit effect,
4) the gravity drop - since the flow
   is vertical and upward.

In the absence of boiling, these pressure drops
are normally computed by standard methods and,
except for the last one which is independent
of flow rate, are an increasing function of
flow rate, i.e., the slope of the pressure
drop vs. flow curve is positive and there is
no flow instability. The presence of boiling
in the channel affects all except possibly the
first factor. In general, the entrance effect
and the exit effect are increasing functions
of flow rate, but their magnitudes may be de-
creased by the transition to two-phase flow.
The friction drop may have either a positive
or negative slope and may be considered the
determining factor.

Having defined the coolant channels as
the individual channels between fuel plates,
the entrance effect becomes both small and
difficult to calculate due to the geometry
of the MITR fuel element lower adapter. For
these reasons, this pressure drop has been
neglected, introducing a conservative factor.*
Since this term would be realtively large
and have a positive slope with respect to
flow rate for the case of an entire element
considered as a coolant channel, the selection
of the individual fuel plate channels as
the coolant channels is quite conservative.

The exit effect pressure drop is also
neglible for the individual channels, but
would be significant for the whole element.
It has, therefore, also been neglected and,
for reasons similar to those given above,
this represents another conservative factor.

Similarly, the gravity drop becomes an
increasing function of flow rate for two-
phase flow, but requires knowledge of the

*A relatively simple fuel element modification
incorporating orificing for the coolant channels
could probably produce a substantial improvement
in stability by adding an entrance effect
pressure drop.

void fraction which is extremely difficult
to predict. Neglecting this term then adds
still another conservative factor.

The remaining term is the friction
term, which for the no-boiling case is nor-
mally computed by:

$$\Delta P_{ADB} = 4f \frac{L}{D} \frac{v^2}{2g} \ , \qquad\qquad (7.2\text{-}4)$$

where,

f = dimensionless "Fanning" friction
factor,

L/D = dimensionless length to diameter
ratio and

D = equivalent diameter of the channel =
$4A/S$, where A is the flow area (ft^2)
and S is the channel perimeter (ft),

v = velocity, ft/sec,

g = conversion factor, 32.3 ft-lb force/lb.
mass-sec^2,

ΔP_{ADB} = pressure drop, ft. of coolant.

The friction factor f can be taken to be a
constant for the flow rates considered here, as
evidenced by the heat transfer correlation
measurements (Ref. 7.2-6). This pressure drop
is more complicated for the boiling case,
however, and must be modified accordingly.
Dormer (Ref. 7.2-7) has experimentally measured
this effect for small round tubes for subcooled
boiling over a wide range of parameters. The
use of Dormer's results gives a good insight
into the application of the experimental
results. Other experiments have also been made
with narrow coolant channels similar to the
MITR-II elements (Ref. 7.2-5). The instability
limit derived by using both Refs. 7.2-5 and 7.2-7
are presented below. The two methods give the
same result for the values of the Safety Limits.

Dormer found that the experimental results
could best be correlated by plotting:

$$\Delta p/\Delta P_{ADB} \ \text{vs.} \ q/q_{sat} \ , \qquad\qquad (7.2\text{-}5)$$

where,

$\Delta p, \Delta P_{ADB}$ = pressure drops with and without
boiling respectively,

$\dfrac{\Delta p}{\Delta P_{ADB}}$ = correction factor to be applied
to the results of Eq. 7.2-4,

$$q = \text{heat on surface of coolant channel,}$$
$$q_{sat} = \text{heat that would produce saturated boiling at the exit of the channel.}$$

Dormer's results are plotted for various L/D ratios in Fig. 7.2-2. Dormer's data involve parameters that are reasonably consistent with the case of interest.

If all other parameters are unchanged, a <u>reduction</u> in flow will <u>decrease</u> q_{sat} and thereby <u>increase</u> q/q_{sat}, hereafter referred to as R. Referring to Fig. 7.2-2, if R is sufficiently large (for the presecribed L/D curve), $\Delta p/\Delta p_{ADB}$ is an increasing function of R. This behavior may be interpreted as a pressure drop vs. flow relationship with a negative slope as opposed to the positive slope of Eq. 7.2-4. The flow rate at which the product Δp_{ADB} and $\Delta p/\Delta p_{ADB}$ is a minimum then corresponds to the minimum stable flow rate for the prescribed conditions.

The actual calculation of R used to enter Fig. 7.2-2 involves other system parameters, specifically: reactor power, and the power produced in the hottest plate in the core. The power produced in the hottest plate of any element in the core is obviously a function of the total reactor power and has to be taken as a function of fuel loading, control rod position and experimental sample assembly in-core design. Consequently, a radial hot channel factor "$F_{H.C.}$" is also included in the safety limit specifications. This factor is the ratio of the power produced in the hottest channel "P_{cMax}" divided by the average power per coolant channel "P_{cAVG}":

$$F_{H.C.} = \frac{P_{cMax}}{P_{cAvg}} = P_{cMax}\left(\frac{N}{P_T}\right) , \qquad (7.2\text{-}6)$$

(Note: $F_{H.C.}$ is the <u>radial</u> hot channel factor only)

where:

N is the number of coolant channels in the core, i.e., the number of fuel elements times the number of channels per element,

P_T is the total reactor power."
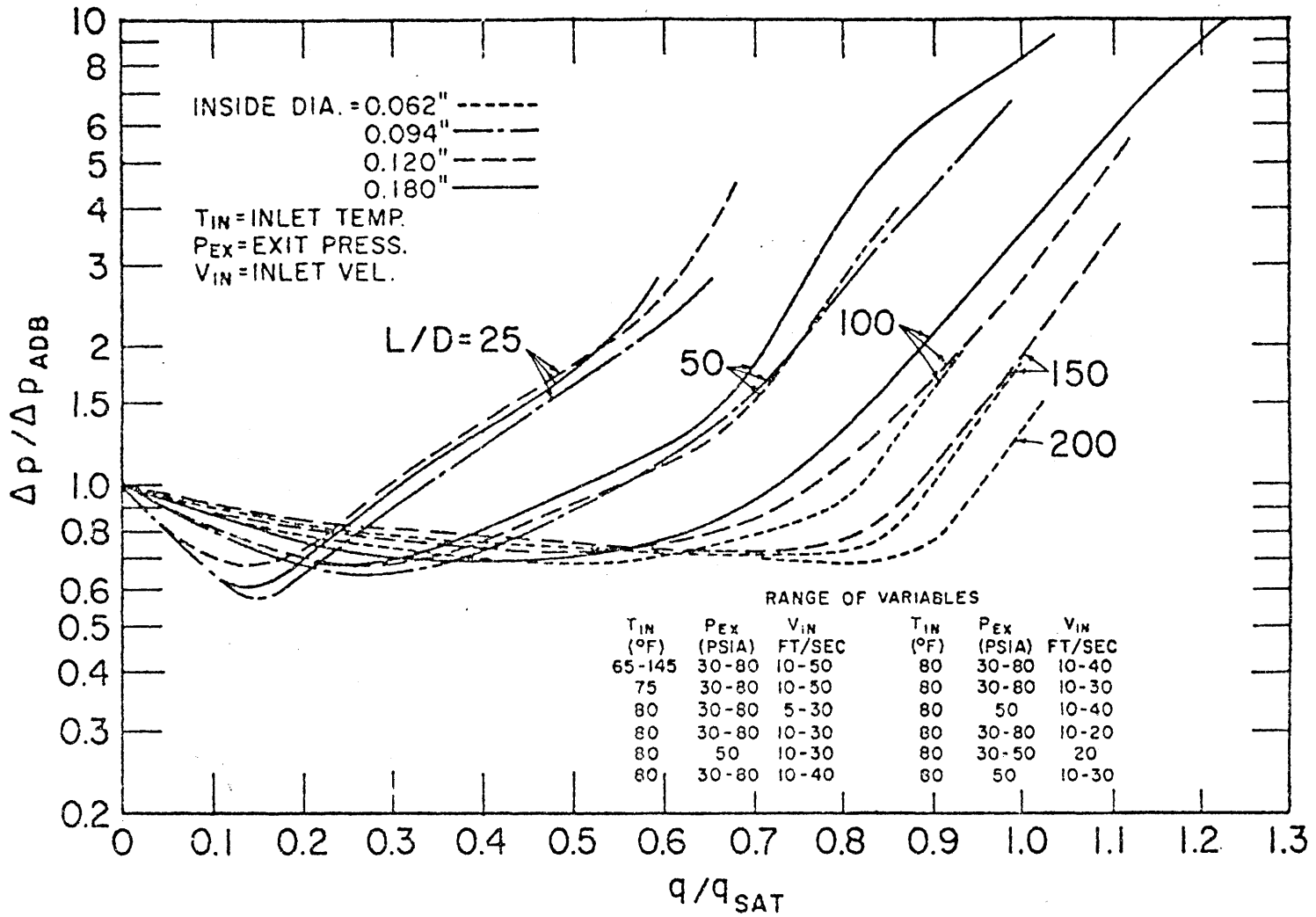
FIG. 7.2-2   CORRELATED PRESSURE DROP - ALL GEOMETRIES

348

The maximum operating value of $F_{H.C.}$ in this work is determined using plate gamma scanning data. The experimental data is compared with calculated CITATION results in order to derive a procedure for determining $F_{H.C.}$ for future core loadings.

"Since the reactor power is a variable parameter for the purpose of this calculation, there remains only the relationship with the main coolant inlet temperature. At a given time, the actual value of the inlet temperature will be determined by a number of factors, such as the outside wet bulb temperature, the cooling tower effectiveness, the secondary system flow rate, the overall heat exchanger heat transfer coefficient, and the H_2O flow rate. For a given power and flow, however, there is a simple relationship between the inlet and outlet temperature, and since Eq. 7.2-6 gives the hottest plate power as a function of reactor power, the ratio R can be determined independent of the secondary system provided a limiting bulk core coolant outlet temperature is established. This leads to the following derivation for R:

$$P_T = W_T C_p (T_{out} - T_{in}) \tag{7.2-7}$$
$$= (2.64 \times 10^{-4}) W_T (T_{out} - T_{in}) \,,$$

where,

P_T = reactor thermal power, Mw,
W_T = total H_2O flow rate, GPM; and
T_{out}, T_{in} = H_2O temperature, °C.

The value of R is given by:

$$R = q/q_{sat} = \frac{P_{cMax}}{P_{csat}} \tag{7.2-8}$$

where,
P_{csat} is the power required to raise the bulk coolant temperature in the hottest channel to saturation.

In terms of the hot channel factor $F_{H.C.}$ from Eq. 7.2-6, R becomes:

$$R = \frac{P_T F_{H.C.}}{N P_{csat}} \quad .$$ (7.2-9)

The quantity P_{csat} is related to the flow and temperature by the expression:

$$P_{csat} = \frac{d_F W_T C_p}{N} (T_{sat} - T_{in}) ,$$ (7.2-10)

where,

d_F is the hot channel flow disparity that is, the ratio of the flow through the hot channel to the average coolant channel flow,

T_{sat} is the saturated water temperature at the outlet end of the hot channel."

The value of d_F has been determined by flow measurements incore and by flow tests through a dummy fuel element. Chapter 4 shows the methods by which flow disparities were measured. Uncertainties in measuring d_F are included in the value of the hot channel factor, $F_{H.C.}$.

"The three expressions, Eqs. 7.2-7, 7.2-9, and 7.2-10 can be combined to eliminate P_{csat} and T_{in} as follows:

$$\frac{P_T}{W_T C_p} = T_{out} - T_{in} ,$$ (7.2-7')

$$\frac{P_T F_{H.C.}}{d_F R W_T C_p} = T_{sat} - T_{in} ,$$ (7.2-11)

thus,

$$\frac{P_T}{W_T C_p} \left(\frac{F_{H.C.}}{d_F R} - 1 \right) = T_{sat} - T_{out} .$$ (7.2-12)

It remains now to determine, "R_m" the value
of R corresponding to the minimum stable flow
condition. For constant power and outlet temp-
erature, it follows from Eq. 7.2-12 that W_m is
proportional to $\dfrac{F_{H.C.}}{(\dfrac{F_{H.C.}}{d_F R} - 1)}$ and since by Eq. 7.2-4

Δp_{ADB} is proportional to v^2 which in turn is pro-
portional to $W_T{}^2$, the value of Δp_{ADB} becomes

$$\Delta p_{ADB} = k [\frac{F_{H.C.}}{d_F R} - 1]^2 \quad , \qquad (7.2-13)$$

where,

k is the proportionality constant for
constant reactor power and outlet
temperature.

The minimum stable flow is determined by the
minimum in the value of p as a function of R.
Values of $\Delta p/\Delta p_{ADB}$ are given in Fig. 7.2-2
in this work. By plotting the quantity
$(\dfrac{\Delta p}{\Delta p_{ADB}}) (\dfrac{F_{H.C.}}{d_F R} - 1)^2$ as a function of R,
it is possible to determine the value of
R_m at which Δp will be a minimum. Examples of
this procedure are shown in Fig. 7.2-3, where
the value of $F_{H.C.}/d_F$ is taken to be 3.0 and
three values of the heated length to the
effective diameter are considered. Also two
plots are shown with $F_{H.C.}/d_F = 2.0$. The
equivalent diameter of a coolant channel
(with fins) is about 0.10 inches. The full
length of the coolant channel is 21 inches;
however, only the lower half of the core is
active and at startup with the rods below the
midpoint, the active length of the hottest
channel may be slightly less than 12 inches,
although some heat will certainly be added to
the channel up to 17" and above. A very con-
servative value of R_m is given by taking
L/D = 100 (L = 10") and by using the curve
for $F_{H.C.}/d_F = 3.0$. Thus, the value of $R_m = 0.78$
is derived and will be used for all values of
$F_{H.C.}/d_F$ less than 3.0. To be conservative,
the value of T_{sat} will be taken at the pressure
for 10 feet below the surface of the pool, which
is 21 inches above the core bottom.

The instability limit, derived from Dormer's
experiments, can be checked by using the results
presented by R. Forgan and R. H. Whittle in
Ref. 7.2-5. Their experiments are more directly

FIG. 7.2-3   DETERMINATION OF Rm
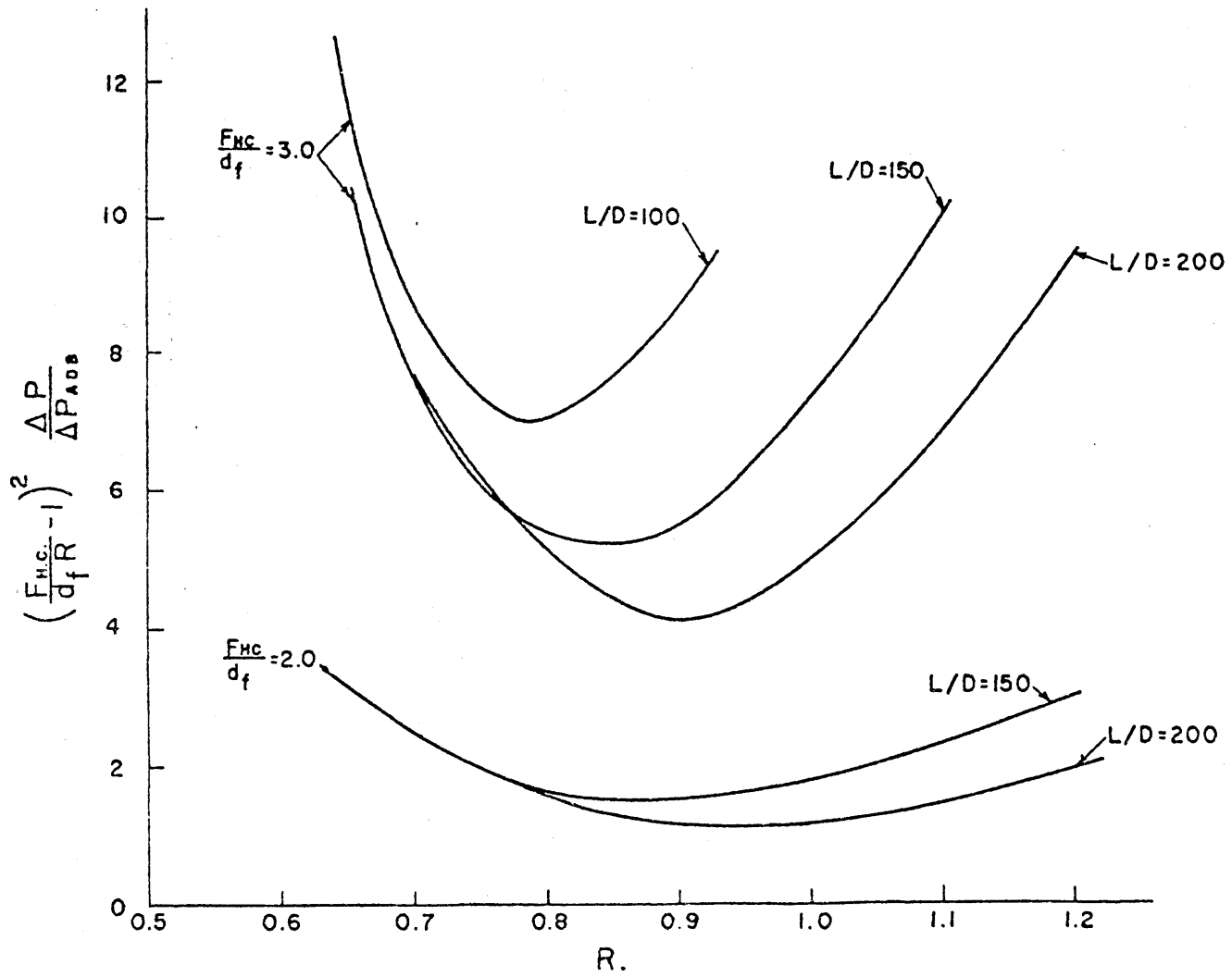
applicable to the MITR-II fuel design since
they involved the use of narrow rectangular
channels. The following quotations are taken
from Ref. 7.2-5.

'74. The results presented in Tables 4
to 8 show that, for a given test section, the
ratio of the bulk-water temperature rise to
that to produce saturated conditions at exit
from the test section ($\Delta T_c/\Delta T_{sat}$) is approx-
imately constant for the point of minimum
pressure drop on the demand curves. It would
be expected that, for a given test section,
this ratio would depend on system pressure,
heat flux, water velocity, axial and lateral
power distribution, direction of flow, inlet
temperature, condition of the heated surfaces,
and possibly a number of other factors not
identified.

'75. The results of the present tests,
together with those in Part I show that the
ratio is either independent of or insensitive
to some of these parameters over the limited
range of parameters investigated. The earlier
tests showed the ratio ($\Delta T_c/\Delta T_{sat}$) to be in-
dependent of water velocity, heat flux and
inlet temperature, and to be the same for a
uniform axial heat-flux distribution as for
a distribution wherein the heat flux is de-
creasing in the direction of the coolant
flow. The present tests indicate that flow
direction, gas content of the water, and
surface condition have little effect on the
ratio, which is unchanged by increase of system
pressure from approximately one atmosphere
to 1.7 atmospheres. This represents a
small change in system pressure but there are
indications discussed below, that the system
pressure in an insensitive parameter,.....'

'84. For rectangular flow channels having
a gap in the approximate range 0.050 in. to
0.130 in. and heated length in the range 16 to
24 in. and with either uniform axial distri-
bution of heat flux or a distribution which
falls toward the channel exit, the critical
value of $\Delta T/\Delta T$ (at the minimum in the ΔP/flow
curves) is given by Eq. 1.

85. There is evidence to suggest that
$\Delta T_c/\Delta_{sat}$ is insensitive to system pressure up
to 400 psi.

The expression for $\Delta T_c / \Delta T_{sat}$ at the minimum ΔP/flow given as Eq. 1 in Ref. 7.2-5 is: (for values of L_h / D_h in the range $100 < L_h / D_h < 200$)

$$\frac{\Delta T_c}{\Delta T_{sat}} = 0.732 + 6.45(10)^{-4} \frac{L_h}{D_h} , \qquad (7.2\text{-}14)$$

where L_h is defined as the heated length of the test section and D_h is erroneously labeled as the heated perimeter. An investigation of the reported data shows the D_h in Eq. 7.2-14 is actually the equivalent diameter (4A/S as described under Eq. 7.2-4. The ratio $(\Delta T_c / \Delta T_{sat})$ in this expression is the same as q/q_{sat} and thus Eq. 7.2-14 is a direct relationship for R_m as a function of L/D. When L/D is taken to be 100, the value of R_m given by Eq. 7.2-14 becomes:

$$R_m = 0.796.$$

This value is in excellent agreement with the value (0.78) for R_m derived from Dormer's experiments. For the MITR-II Safety Limits, the slightly more conservative value of $R_m = 0.78$ has been used as discussed in SAR Section 3.3.2.2.

The next step is to insert the values of the normal operating limits for the primary coolant flow rate, outlet temperature and hot channel factor, into the safety limit expression (Eq. 7.2-12) and solve for the reactor power flow instability safety limit. However, before this value can be established as the reactor safety limit, a calculation must be made to check that the flow instability does, in fact, occur prior to burnout.

Gambill (Ref. 7.2-8) gives the following correlation for the burnout heat flux:

$$\phi_{BO} = KL_v \rho_v \left(\frac{\sigma g_c a \Delta \rho}{\rho_v^2}\right)^{1/4} [1 + (\frac{\rho_\ell}{\rho_v})^{0.923}$$

$$(\frac{C_p \Delta T_{sub}}{25 L_v})] + K'(\frac{k}{D}) N_{Re}^m N_{Pr}^n (t_w - t_b)_{BO},$$

$$(7.2\text{-}15)$$

where,

K, K' = adjustable constants of boiling and conservative terms,

L_v = latent heat of vaporization,

ρ_v = density of vapor,

σ = surface tension,

g_c = conversion contant, $L \cdot M/F \cdot \theta^2$,

g = local acceleration,

$\Delta \rho$ = density difference $(\rho_\ell - \rho_v)$,

C_p = constant pressure specific heat of liquid,

ρ_ℓ = density of liquid

ΔT_{sub} = degree of subcooling $(t_{sat} - t_b)$,

K = thermal conductivity of liquid,

D = equivalent diameter of flow passage,

N_{Re} = Reynold's number,

N_{Pr} = Prandtl number,

m, n = exponents,

t_w = wall temperature at burnout,

t_b = bulk coolant temperature.

This correlation is based on a physical model and the first term corresponds to the boiling heat transfer at burnout while the second term corresponds to non-boiling or convective heat transfer at burnout. The use of the second term requires knowledge of t_w, the wall temperature at burnout, and the method proposed for predicting t_w, (Ref. 7.2-9) does not cover the temperatures of interest for low pressure cases. This apparently is a result of the fact that the convective term is significantly only for the higher pressures. In any event, this term has been neglected in the present case, and any error so introduced will be conservative.

Table 7.2-1 below gives the extreme ranges of some of the physical parameters covered by the data correlated.

TABLE 7.2-1

RANGE OF DATA (FOR RECTANGULAR CHANNELS) FOR REF. 7.2-8

Parameter	Range
Pressure (psia)	14-2,000
ΔT_{sub} (°F)	0-282
v (ft/sec)	4.8-85.4
ϕ_{BO} (Btu/hr ft^2 x 10^{-6})	0.42-11.41

Table 7.2-2 below gives the values of
the parameters used in Eq. 7.2-15.

TABLE 7.2-2

PARAMETERS FOR EQ. 7.2-15

(Physical properties evaluated at a static head
of 10 feet of H_2O)

$$K = 0.14$$

$$\sigma = 58.85 \text{ dynes/cm} = 4.032 \times 10^{-3} \text{ lb/ft}$$

$$a = g_c = 32.2 \text{ ft/sec}^2 = 4.17 \times 10^8 \text{ ft/hr}^2$$

$$L_v = 962 \text{ Btu/lb}$$

$$\rho_\ell = 59.5 \text{ lb/ft}^3$$

$$\Delta\rho = 59.45 \text{ lb/ft}^3$$

$$\rho_v = 4.74 \times 10^{-2} \text{ lb/ft}^3$$

$$C_p = 1.0 \text{ Btu/lb}°F$$

$$T_{sub} = 84.5°F \text{ (conservative at hot spot of hottest channel)}$$

The results of Eq. 7.2-15 give a burnout heat
flux of 1.5×10^6 Btu/hr·ft^2.

As shown in SAR Section 3.3.4.2, the hot
spot heat flux is less than $3.5(10)^5$ Btu/hr·ft^2
for 6 Mw operation. Thus, the burnout heat
flux is not reached until the reactor power
approaches 26 Mw. This value of power is well
above the limiting power level set by Eq. 7.2-12
for flow instability. Therefore, Eq. 7.2-12
is used for the evaluation of the safety limits."

As stated in the last paragraph of the section

excerpted from the SAR, the following equation is used

for the evaluation of the safety limits based on the

onset of multichannel flow instability:

$$\frac{P_t}{W_T C_p} \cdot \left(\frac{F_{H.C.}}{d_F R_m} - 1 \right) = T_{sat} - T_{out} \quad , \qquad (7.2\text{-}12)$$

where,

P_T is the total reactor thermal power,

W_T is the reactor coolant flow rate,

T_{out} is the reactor coolant outlet temperature,

T_{sat} is the saturation temperature at the outlet end of the heated section of channel,

C_p is the specific heat of the coolant,

$F_{H.C.}$ is the ratio of the power produced in the hottest channel divided by the average power per coolant channel,

d_f is the ratio of the flow through the hot channel to the average coolant channel flow,

R is the ratio (q/q_{sat}) given by the onset of the predicted flow instability.

By the time that the Technical Specifications were approved, Eq. 7.2-12 was slightly modified to yield the following:

$$\frac{P_T}{2.64(10)^{-4}W_T} \left(\frac{F_{H.C.}F_p}{d_f R_m F_f} - 1\right) = T_{sat} - T_{out} \qquad (7.2\text{-}16)$$

where,

$2.64(10)^{-4}$ is the value of C_p for water and includes the appropriate conversion factors for the units of the other factors,

F_p is the fraction of the total power generated by the fuel,

F_f is the fraction of primary flow cooling the fuel.

The factors F_p and F_f were included to correct de-
ficiencies in Eq. 7.2-12. The safety limit is related to
the absolute amount of power that is generated in the
hottest channel. Assuming that all of the total power
is generated by the fuel is very conservative because the
fraction of power from neutron and gamma heating that is
not generated in the fuel will be distributed more evenly
over the core than the fission product power distribution.
In addition, power generated in experimental facilities
which would be included in the measured P_T would not be
distributed through the core like the fission product
power distribution. By multiplying the previously
defined $F_{H.C.}$ by F_p, the product now stands for the
ratio of the power produced in the hottest channel by the
power produced in the fuel to the average power per
coolant channel by power produced in the fuel. This
product gives a more correct value of the ratio of the
power produced in the hottest channel to the power pro-
duced in the average channel. Thus Eq. 7.2-9 has been
modified to be:

$$R = \frac{P_T F_{H.C.} F_p}{N P_{csat}} \qquad (7.2-9')$$

The factor F_f is included because not all of the
primary coolant flow cools the fuel. Bypass flow is
caused by dummy elements, incore experiments, control

blade cooling and check valve leakage. Thus F_f is included as an additional flow disparity. Equation 7.2-10 would become:

$$P_{csat} = \frac{d_f F_f W_T C_p}{N} (T_{sat} - T_{in}).$$ (7.2-17)

The measured parameters W_T and T_{out} are not affected by F_f so Eq. 7.2-7' would remain:

$$\frac{P_T}{W_T C_p} = T_{out} - T_{in} .$$ (7.2-7')

Thus combining Eqs. 7.2-7', 7.2-9', and 7.2-17 yields:

$$\frac{P_T}{W_T C_p} (\frac{F_{H.C.} F_p}{d_f R_M F_f} - 1) = T_{sat} - T_{out} .$$ (7.2-16)

The value of T_{sat} depends on the coolant pressure at the outlet of the heated section. This pressure is directly proportional to the head of water above that point. By conservatively taking R_M to be 0.78 and setting $F_{H.C.} F_p / d_f F_f$ equal to 2.9, Eq. 7.2-16 is evaluated to determine the safety limits. The results are plotted in Fig. 7.2-1. The safety limits would be considered exceeded if the point defined by the true value of P_T, W_T, and T_{out} fell above the appropriate limiting line as determined by the water height L. The plot in Fig. 7.2-1 is valid if $F_{H.C.} F_p / d_f F_f$, now defined as the Safety Limit Factor (SLF), is shown to be less than 2.9. The SLF was evaluated for Core I and Core II

and shown to be less than 2.9 before operation above 1 KW
was permitted.

7.2.2 Safety Limit Evaluation

To assure the validity of Fig. 7.2-1 representing
the safety limit, the Safety Limit Factor, (SLF =
$F_{H.C.}F_p/d_f F_f$) must be shown to be less than 2.9 for each
core loading. The factors composing the SLF are deter-
mined in the following manner for the initial core loadings.

The hot channel factor, $F_{H.C.}$, is determined by multi-
plying the maximum value of the radial peaking factor, F_r,
by an enthalpy factor, F_H, that represents the uncertainty
of several parameters that affect the enthalpy rise in a
coolant channel. Peak values of F_r are obtained for
various fuel plates of interest from the gamma scanning
experimental data and from CITATION calculations. For most
coolant channels, heat is deposited into the channel from
the two plates bounding the channel. By assuming that the
heat deposited into the hottest channel is equal to the
amount of heat from two sides of the hottest plate, a
conservative value of the heat deposited into the channel
is obtained. This assumption remains valid for the out-
side channels where the coolant channel is bounded by a
fuel plate on one side and core housing structure on the
other side. For this case, only one side of a fuel plate
deposits heat into a channel which has one half of a normal

channel flow. The hot channel enthalpy factor, F_H, is obtained as the product of the following hot channel factors taken from Table 3.3.4.3.3-2 of the MITR-II SAR:

Reactor power measurement uncertainty   1.05
Power density measurement uncertainty   1.10
Fuel density tolerances
    (29.7 ± 0.8 grams U^{235}/plate   1.027
Eccentricity   1.001
Flow measurement uncertainty   1.02

$$F_H = \overline{1.2111}$$

The hot channel factors in SAR Table 3.3.4.3.3-2 for plenum chamber flow and channel tolerances are represented in d_f in the present work and thus do not have to be included in F_H. F_H is a conservative uncertainty factor in that it is the product of the worst cases rather than a statistical compilation. The uncertainty in measuring d_f and F_f is included in F_H. Thus $F_{H.C.}$ can be obtained by knowing the maximum radial peaking factors, F_r, using the following:

$$F_{H.C.} = (F_r)_{max} F_H \qquad (7.2-18)$$

$$= 1.211 \ (F_r)_{max}$$

F_p could be experimentally determined by performing an accurate heat balance on the reactor system and determining power generated in incore experimental facilities. For the present work, F_p has been assumed to be equal to 1.0 which is the most conservative assumption.

The flow disparity, d_f, is the product of the channel flow disparity, d_{fc}, and the plenum flow disparity, d_{fp}. The channel flow disparity was determined from fuel element flow tests described in Section 4.2 and is equal to 0.887. The plenum flow disparity is dependent upon the fuel element position and the core loading arrangement. Thus the flow disparity, d_f, is determined by the following equation:

$$d_f = 0.887 \, d_{fp} \quad , \qquad (7.2\text{-}19)$$

where d_{fp} depends upon the fuel element location and core loading arrangement for the channel of interest.

F_f is experimentally determined for each core loading arrangement. The uncertainties on F_f and d_f are included in F_H.

The values of $(F_r)_{max}$, $F_{H.C.}$, d_f, and F_f for core loadings I and II are shown on Tables 7.2-3 and 7.2-4, respectively. Values of the SLF are also shown in each table. The methods for determining the core factors varies for each core evaluation because of differences in the experimental program. Fewer gamma scans were performed for Core II than for Core I. Note that for all cases on Tables 7.2-3 and 7.2-4, the value of the SLF is less than 2.9. Note also that the "hottest channel" is not always the channel with the greatest F_r and that the flow disparity d_f, must also be considered. The next

TABLE 7.2-3

SAFETY LIMIT FACTORS FOR CORE I

Channel Location in Core	$(F_r)_{max}$		$F_{H.C.}$		d_{f_p} ++	d_f	F_f	SLF	
	P.S.D.*	CIT**	P.S.D.*	CIT**				P.S.D.*	CIT**
Blades at 7.6 inches									
C-8+, channel next to core housing	1.5274	1.354	1.85	1.64	1.011	0.897	0.9487	2.17	1.93
C-9+, channel next to core housing	1.266	1.26	1.53	1.53	0.9377	0.832	0.9487	1.94	1.94
A-2+, channel next to solid dummy	1.333	1.164	1.61	1.41	0.9857	0.8743	0.9487	1.94	1.7
Blades at 14 inches									
C-8, channel next to core housing	--	1.642	--	1.989	1.011	0.897	0.9487	--	2.34
C-9, channel next to core housing	--	1.60	--	1.938	0.9377	0.832	0.9487	--	2.46

+ Blades at 7.6 inches for plate scanning data and at 8 inches for CITATION calculations
* Based on plate scanning data
** Based on CITATION calculations
++ Lowest d_f for symmetric position chosen

TABLE 7.2-4

SAFETY LIMIT FACTORS FOR CORE II

Channel Location in Core	$(F_r)_{max}$		$F_{H.C.}$		d_{f_p}	d_f	F_f	SLF	
	P.S.D.* + CIT	CIT**	P.S.D.* + CIT	CIT**				P.S.D.* + CIT	CIT**
Blades at 8 inches+									
A-1, Channel next to hexagonal spider	1.59	1.245	1.926	1.51	1.009	0.895	0.9205	2.34	1.83
C-13, channel next to core housing	1.54	1.20	1.865	1.453	0.944	0.8373	0.9205	2.42	1.89
Blades at 14 inches									
A-1, channel next to hexagonal spider	--	1.137	--	1.377	1.009	0.895	0.9205	--	1.671
C-13, channel next to core housing	--	1.42	--	1.72	0.944	0.8373	0.9205	--	2.23

+ Blades were at 8.6 inches for removable plate irradiations.
* Based on plate scanning data and CITATION
** Based on CITATION calculation only

three sections respectively describe the derivation of the SLF for Core I, Core II, and the effect of the shim bank height on the SLF.

7.2.2.1 Core I

The core factor $(F_r)_{max}$ was determined by two independent means for Core I. Fuel plate gamma scanning data (GAMSCAN) from fourteen irradiations was compiled to yield a value of F_r for each plate (Section 5.3.5). Similarly, a value of F_r was calculated for the corresponding channels of interest using CITATION power density data and techniques shown in Section 5.2.3.1. For all cases the CITATION calculations yielded values of F_r that were less then the Gamscan values. The CITATION values were low because of large mesh spacings which averaged power over several plates and prevented accurate representation of physical conditions that caused local power peaking. The mesh spacing is limited by the allowable computer memory space.

For positions where local conditions had an effect on a single plate, CITATION underestimated the Gamscan values of F_r by 12 - 14%. For internal fuel element positions, not subject to local effects, CITATION and Gamscan were in good agreement on F_r. The values of F_r in Table 7.2-3 are for the shim blades at 8 inches. The effect of raising the blades is discussed in Section 7.2.2.3.

Initially it was planned to include an incore sample assembly (ICSA) into the first core loading. CITATION calculations had shown that the large amount of water in the ICSA might cause unacceptable power peaking in plates next to the ICSA. This prediction was true as shown by Table 7.2-5 which gives the value of the SLF for a fuel channel in the A-ring next to the ICSA. Core factors for this hot channel may give an acceptable safety limit, but the limiting condition for operation cannot be met as is shown in Section 7.3.2.

7.2.2.2 Core II

The core factor $(F_r)_{max}$ was determined using CITATION data alone in the same manner as was done for Core I, and $(F_r)_{max}$ was also determined using a combination of experimental and CITATION data. Only four gamma scanning irradiations were performed for Core II and this was an insufficient number to determine values of F_r from experimental data alone. Section 6.3 shows how values of F_r were determined using a combination of CITATION results and plate scanning data. In summary, F_r for a given channel is determined by the following product:

$$F_r = F'_r F''_r \quad , \qquad\qquad (7.2-20)$$

TABLE 7.2-5

SAFETY LIMIT FACTOR FOR CHANNEL NEXT TO
ORIGINAL DESIGN OF ICSA

Channel Location in Core	SLF	
	Based Plate Scanning Data	Based on CITATION Calculation
A-2*, channel next to ICSA	2.88	2.78

*Core Loading - 2 solid dummies
1 ICSA
Fixed absorbers at 10 inches
Blades at 8 inches

where,

F_r is the radial peaking factor; the ratio of power produced in a fuel plate to the power produced in the average plate in the core,

F_r' is the ratio of power produced in a fuel element to the power produced in the average fuel element in the core,

F_r'' is the ratio of power produced in a fuel plate in an element to the power produced in the average fuel plate in that same element.

The value of F_r' was obtained using CITATION results and the value of F_r'' was obtained using plate scanning results. Table 7.2-4 shows the values of the SLF for the hot channels in Core II. Note that for Core II the "CITATION only" results are about 25% less than the combination results.

7.2.2.3 Effects of Shim Bank Height

As predicted in Section 5.2.3.3, the SLF (ratio $F_{H.C.} F_p / d_f F_f$) approaches the limiting value of 2.9 for hot channels on the outside edge of the core as the height of the shim bank increases. Because no gamma scans could be made with a fully loaded core and the blades at near out positions, the effects of raising the shim bank had to be estimated using CITATION calculations. Table 7.2-6 shows the CITATION predictions for the hottest outside edge channels for Core I and Core II. Note that the core factor ratio increases by a factor of approximately 1.5 for both loadings as the blades are raised from 8 inches

TABLE 7.2-6

EFFECT OF SHIM BANK HEIGHT ON SAFETY LIMIT FACTOR

Case		SLF	Change in SLF for 1 inch Change in Shim Bank Height	$H = \dfrac{SLF_{bld\ @21"}}{SLF_{bld\ @8"}}$	SLF_E^+	$SLF_E \times H$
Core Loading	**Blade Height**					
C-8, channel next to core housing	8 inches	1.93	0.0683	1.46	2.17*	3.17[++]
	14 inches	2.34				
C-9, channel next to core housing	8 inches	1.94	0.0867	1.58	1.94*	3.06[++]
	14 inches	2.46				
Core II Loading						
C-13, channel next to core housing	8 inches	1.89	0.0566	1.39	2.42**	3.36[++]
	14 inches	2.23				

+ Experimental value of SLF from plate scanning data for blades at 8-inches
* Blades at 7.6 inches
** Blades at 8.6 inches
++ Shim bank height at which SLF exceeds 2.9: Core I - 18.4 inches, Core II - 14.6 inches.

to 21 inches. When the gamma scanning obtained values
of the SLF are increased by this factor now defined as H,
the value of the core factor ratio exceeds 2.9. By
assuming that the increase in the core factor is linear
with blade height, the shim bank height at which the
core factor ratio will exceed 2.9 can be determined for
each loading. The blades may not exceed these heights
with the clean-unburned core or the safety limit defined
by Fig. 7.2-1 will be invalid. This problem will be dis-
cussed in Section 7.5.

7.3 Limiting Condition for Operation

The safety limit was based on the prevention of a
flow instability which might lead to boiling burnout
with potential resultant damage to the aluminum cladding
and structure. The flow instability could only occur
with a certain amount of subcooled boiling in the chan-
nel. Thus, the limiting condition for operation was
conservatively set so that incipient boiling would be
prevented at all points in the core. This also prevents
nuclear noise from bubble growth and collapse.

In the Technical Specifications of the MITR-II, the
core is predicted to operate below incipient boiling at
every point in the core by the use of the following
equation:

$$[(\frac{W_T}{W_{T_o}})^{0.2}G + \frac{F_p F_r Z}{d_f F_f} - 1] - 2.77[\frac{P_T F_r F_a}{\eta A}]^{0.466} \le 3.72$$

$$(7.3-1)$$

where,

P_T is the limiting safety system setting of the reactor power in megawatts,

W_T is the total coolant flow rate in gallons/minute,

W_{T_o} is the normalizing flow of 1800 gpm used to calculate the heat transfer coefficient h_o.

G is the core design constant defined as

$$\frac{F_r F_a F_p}{\eta (F_f d_f)^{0.8}} \quad \frac{W_{T_o} C_p}{h_o A} F_o \quad ,$$

F_r is the radial peaking factor, the ratio of the power produced in a fuel plate with the hot spot to power produced in the average fuel plate,

F_a is the axial peaking factor, the ratio of the power density in the plate at the given axial position to the average in the given plate,

A is the total heat transfer area of all the fuel meat, i.e., two sides of the flat fuel plate,

d_f is the flow disparity in the channel with the highest fuel clad temperature,

η is the clad fin effectiveness, i.e., effective area over smooth channel area,

F_p is the fraction of the total power generated by the fuel,

F_f is the fraction of primary flow cooling the fuel,

F_o is the total uncertainty factor to account for the uncertainty in the heat transfer coefficient, power peaking factors, and flow,

Z is the axial location factor, the ratio of the power released into the channel containing the hot spot between the inlet and the hot spot relative to the total power released into that channel,

c_p is the coolant heat capacity,

T_{out} is the limiting safety system setting of the bulk outlet temperature in °C,

L is the height of water above the outlet end of the heated section of the hot channel in feet.

The measured values of the limiting safety system settings on P_T, W_T, L, and T_{out} shall be as follows:

	2 Primary Pumps	1 Primary Pump	0 Primary Pump
W_T	1800 gpm (MIN)	900 gpm (MIN)	0 (MIN)
P_T	6.0 MW (MAX)	3.0 MW (MAX)	100 KW (MAX)
L	Top surface water level being at most 4 inches below overflow condition which is a fixed system parameter		
T_{out}	60°C (MAX)	60°C (MAX)	60°C (MAX)

If the measured values of P_T, W_T, L, and T_{out} remain within the limits of the limiting safety system settings, incipient boiling will be prevented from occurring if Eq. 7.3-1 has been shown to be valid.

7.3.1 Limiting Condition for Operation Basis

Prior to operation above 1.0 KW, it must be shown that the maximum wall temperature at every point in the operating core is below the wall temperature that will lead to incipient boiling when the measured system parameters (P_T, T_{out}, W_T, and L) are at the limiting safety system settings. The following single spaced sections in quotations, except where noted otherwise, are direct excerpts from the MITR-II Safety Analysis Report. The equation, figure, table, and reference numbers have been changed to be consistent with the present work. Most of the parameter definitions are found in Section 7.3 and new parameters are defined as they are introduced.

The wall temperature at a point is determined by the following expression:

$$Q/A = \eta h [T_{WALL} - T_c(z)], \qquad (7.3-2)$$

where,

Q/A is the local heat transfer rate,

T_{WALL} is the wall temperature at the local point,

h is the heat transfer coefficient at the local point,

$T_c(z)$ is the bulk fluid temperature at the same axial, z, point as the wall point of interest.

The relationship between the maximum value of the local heat flux involves the radial and axial power peaking factors and the fraction of the power generated in the fuel, F_p, i.e.:

$$(Q/A)_{MAX} = F_p F_r F_a P_T/A \ . \tag{7.3-3}$$

The local heat transfer coefficient, h, is calculated from the following equation:

$$h = h_o \frac{R_e^{0.8}}{R_{e_o}^{0.8}} = \frac{h_o (F_f d_f W_T)^{0.8}}{(W_{T_o})^{0.8}} \tag{7.3-4}$$

where,

h_o is the value of the heat transfer coefficient calculated using the Boelter correlation for the average coolant channel flow of W_{T_o}/N with N the total number of coolant channels in all fuel assemblies and W_{T_o} is the normalizing total flow rate of 1800 gpm. (The Boelter correlation is: $Nu = 0.023 \, Re^{0.8} P_r^{0.3}$ where Nu, Re, and P_r are the Nusselt, Reynolds, and Prandtl numbers, respectively). The normalized h_o is modified to the local h by using the Boelter relation between heat transfer coefficient and coolant flow.

The bulk coolant channel fluid temperature, $T_c(z)$ for a given channel can be related to the reactor inlet temperature in the following manner:

$$T_c(z) = T_{in} + \frac{F_p F_r P_T Z}{d_f F_f W_T C_p} , \qquad (7.3-5)$$

(Note that if the peak occurs at the bottom, $Z=0$ and $T_c(z) = T_{in}$).

The measured bulk outlet temperature, T_{out}, can be related to the bulk inlet temperature with the following expression:

$$P_T = W_T C_p (T_{out} - T_{in}) . \qquad (7.3-6)$$

Equations 7.3-2, 7.3-3, 7.3-4, 7.3-5, and 7.3-6 can be combined to form the following equation for the maximum wall temperature:

$$T_{out} = (T_{WALL})_{MAX} - \left[\frac{\frac{F_p F_r F_a (W_{T_o})^{0.8}}{(d_f F_f)^{0.8} \eta}}{\frac{h_o A}{C_p (W_T)^{0.2}}} + \right.$$

$$\left. \frac{F_p F_r Z}{d_f F_f} - 1 \right] \frac{P_T}{W_T C_p} \qquad (7.3-7)$$

To simplify the operating limit considerations, G' is defined as:

$$G' \equiv \frac{F_p F_r F_a W_{T_o} C_p}{(d_f F_f)^{0.8} \eta A h_o} , \qquad (7.3-8)$$

and therefore, Eq. 7.3-7 becomes,

$$T_{out} = (T_{WALL})_{MAX} - \left[G' \left(\frac{W_T}{W_{T_o}} \right)^{0.2} + \frac{F_p F_r Z}{d_f F_f} - 1 \right] \frac{P_T}{W_T C_p} .$$

$$(7.3-9)$$

"The value of (T_{WALL}) is established conservatively as the onset of incipient boiling at the static pressure 12 inches above the fuel bottom (i.e., the top of the active core). The coolant head is 132 inches when the level is at the reactor scram point of four inches below the normal overflow level. Based upon a semi-theoretical approach, Bergles and Rohsenow obtained a correlation (Ref. 7.3-1) for predicting incipient boiling that is dependent only on pressure and wall temperature. For water over a pressure range from 15 to 2000 psia, the heat flux at incipient boiling is given by:

$$q''_{IB} = 15.6 p^{1.156}(T_{WIB} - T_{sat})^{2.30/p^{0.0234}} \qquad (7.3\text{-}10)$$

where,

q''_{IB} = incipient boiling heat flux, BTU/hr-ft^2;

p = pressure, psia

T_{WIB} = local wall temperature at incipient boiling, °F

T_{sat} = fluid saturation temperature, °F

When the absolute pressure is taken to be 4.75 + 14.7 = 19.45 psia, Eq. 7.3-10 becomes:

$$T_{WIB} = 107 + \frac{5}{9}(\frac{q''_{IB}}{482})^{0.466} \qquad (7.3\text{-}11)$$

for T_{WIB} in °C.

At the limiting power P_T,

$$q''_{IB} = \frac{3.413 P_T}{\eta A} F_r F_a (10)^6 \qquad (7.3\text{-}12)$$

for P_T in megawatts and A in ft^2."

Combining Eqs. 7.3-9, 7.3-11, and 7.3-12 yields:

$$T_{out} = 107 + 35(\frac{P_T F_r F_a}{\eta A})^{0.466} - \left[(\frac{W_T}{W_{T_o}})^{0.2} G' + \frac{F_r F_p Z}{d_f F_f} - 1\right]\frac{P_T}{2.64(10^{-4})W_T} \qquad (7.3\text{-}13)$$

where,

T_{out} is in °C,

P_T is in Megawatts,

W_T is in gallons/minute,

$2.64(10^{-4})$ is a constant for C_p and an units conversion factor.

The limiting safety system setting of T_{out} is 60°C for all cases, and for both one pump and two pump operation $P_T/W_T = 3.33 \times 10^{-3}$ MW/gpm. Inserting these values of T_{out} and P_T/W_T into equation 7.3-13 and multiplying G' by an uncertainty factor, F_o, yields the condition for the hot spot being less than the onset of incipient boiling which is found in the technical specifications:

$$[(\frac{W_T}{W_{T_o}})^{0.2}G + \frac{F_p F_r Z}{d_f F_f} - 1] - 2.77[\frac{P_T F_r F_a}{\eta A}]^{0.466} \leq 3.72,$$

$$(7.3-1)$$

where,

$G = G'F_o$.

In order to evaluate equation 7.3-1, the following parameters must be determined: F_p, F_r, F_a, Z, d_f, F_f, W_T, W_{T_o}, P_T, η, A, and G. The parameters are defined or determined in the following manner for Core I and Core II of the MITR-II.

W_T is set equal to the limiting safety system setting in gallons/minute for total coolant flow,

W_{T_o} is equal to 1800 gallons/minute,

F_p is conservatively set to equal to 1.0,

F_r is evaluated using plate scanning data and CITATION results as described in Section 7.2,

d_f is evaluated in the manner as described in Chapter 4,

F_f is evaluated in the manner as described in Chapter 4,

P_T is set equal to the limiting safety system setting of total reactor power in megawatts,

A is equal to the total heat transfer area of all the fuel for the given core loading and is evaluated using the following equation:

$$A \text{ in } ft^2 = 9.704N \qquad (7.3\text{-}14)$$

where N is the number of fueled elements loaded in the core,

η is set equal to 1.9. The finned fuel surface was found to have a heat transfer coefficient of 1.9 times greater than the coefficient predicted by the Boelter correlation for smooth surfaces. A theoretical study of the surface effectiveness was performed by Taborda (Ref. 7.3-2) and an experimental evaluation of the surface effectiveness was performed by Szymcsak(Ref. 7.3-3),

F_a is evaluated using plate scanning data and CITATION results. The computer code COREFAC gives values of F_a for each point counted on every plate scanned. Values of F_a are obtained from CITATION for each mesh point by the following equation:

$$F_{a_i} = \frac{(Q/A)_i}{\dfrac{\sum\limits_{i=1}^{n} (Q/A)_i Z_i}{\sum\limits_{i=1}^{n} Z_i}}, \qquad (7.3\text{-}15)$$

where,

$(Q/A)_i$ is the volumetric heat flux for constant R and θ for the channel of interest,

Z_i is the height in the Z direction of the ith mesh point,

n is the number of fueled mesh point volumes in the Z direction for a constant R and θ,

Z is evaluated using plate scanning data and CITATION results. Z is determined in the following manner from CITATION:

$$Z = \frac{\sum\limits_{i=1}^{\gamma} (Q/A)_i Z_i}{\sum\limits_{i=1}^{n} (Q/A)_i Z_i} \quad , \qquad (7.3\text{-}16)$$

where,

$(Q/A)_i$, Z_i, and n are as defined for determination of F_a and,

γ is the number of fueled mesh points from the bottom of the channel of interested up to and including the mesh point for which the Z is being determined,

The value of Z is determined using COREFAC output in the following manner:

$$Z = \frac{\sum\limits_{i=1}^{\gamma'} CTAR_i + \sum\limits_{i=\gamma'+1}^{\gamma'+3} \frac{CTAR_i}{2}}{\sum\limits_{i=1}^{66} CTAR_i} \quad , \qquad (7.3\text{-}17)$$

where,

      CTAR   is the number of counts in the effective area
               for the ith point scanned,

      γ' is the number of the last point scanned below
               the level of the point where Z is being deter-
               mined (there are 3 points to an axial position
               with points being numbered starting at the
               bottom and 66 points total).

G has been defined as:

$$\frac{F_r F_a F_p}{\eta (F_f d_f)^{0.8}} \quad \frac{W_{T_o} C_p}{h_o A} F_o \quad , \tag{7.3-18}$$

where the evaluation of all of the factors has been deter-

mined except the uncertainty factor, F_o. The value of F_o

is made up of the product of the following uncertainty

factors:

Source of Uncertainty	Uncertainty Factors
Reactor power measurement uncertainty	1.05
Power density estimate uncertainty	1.10
Fuel density tolerances*	1.10
Flow measurement uncertainty	1.02
Heat transfer coefficient and effectiveness uncertainty	<u>1.20</u>
Estimated Value of F_o	1.55

*The power density estimate uncertainty is different
for the case where a point location is being analyzed in
comparison with the safety limit where only the uncertainty
for the total plate was of interest.

Core I and Core II were evaluated with an additional uncertainty factor not found in Eq. 7.3-1. A factor, F_o', was included into Eq. 7.3-1 as shown below and this new equation was defined as the Operating Limit Equation (OLE),

$$OLE \equiv [(\frac{W_T}{W_{T_o}})^{0.2}G + \frac{F_p F_r Z F_o'}{d_f F_f} - 1] - 2.77[\frac{P_T F_r F_a}{nA}]^{0.466} \leq 3.72.$$
$$(7.3-19)$$

No uncertainty factor was included into the final term $2.77[\frac{P_T F_r F_a}{A}]^{0.466}$ since this term is negative and it is more conservative not to include an uncertainty factor which would increase it by a factor proportional to F_o.

The value of F_o' is made up of the product of the following uncertainty factors:

Uncertainty in determining $F_r Z$
(same as uncertainty $F_r F_a$)   1.10

Flow measurement uncertainty   <u>1.02</u>
                                            1.122.

7.3.2 Incipient Boiling Evaluation

The OLE (Eq. 7.3-19) was evaluated for both Core I and II before power levels were raised above 1.0KW. The parameters are for Core I and II that did not vary with position are shown in Table 7.3-1. The parameters that varied with position are F_r, F_a, Z, and d_{f_p}. The means for evaluating each of these factors were discussed in the preceding chapters but they are summarized in Table 7.3-2.

TABLE 7.3-1

CONSTANT CORE FACTORS FOR EACH CORE LOADING

Core Factor	Value for Core I	Value for Core II
F_p	1.0	1.0
F_f	0.9487	0.9205
W_T	1800 gpm (2 pumps) 900 gpm (1 pump)	1800 gpm (2 pumps) 900 gpm (1 pump)
P_T	6.0 MW (2 pumps) 3.0 MW (1 pump)	6.0 MW (2 pumps) 3.0 MW (1 pump)
η	1.9	1.9
A	232.9 ft^2	213.5 ft^2
h_o	2585 BTU/hr-ft^2-°F	2771 BTU/hr-ft^2-°F
F_o	1.55	1.55
F_o'	1.122	1.122
d_{f_c}	0.887	0.887
C_p	0.9985 BTU/lb-°F	0.9985 BTU/lb-°F
W_o	8.905 x 10^5 lb$_m$/hr 1800 gpm	8.905 x 10^5 lb$_m$/hr 1800 gpm

TABLE 7.3-2

METHODS FOR EVALUATING POSITION DEPENDENT CORE FACTORS

Core Factor	Method for Core I	Method for Core II
d_{f_p}	Incore flowmeter data (Chapter 4)	Incore flowmeter data (Chapter 4)
F_r	1. Plate scanning data 2. CITATION results	1. Plate scanning data-CITATION combination 2. CITATION results
F_a	1. Plate scanning data 2. CITATION results	1. Plate scanning data 2. CITATION results
z	1. Plate scanning data 2. CITATION results	1. Plate scanning data 2. CITATION results

For Core II fuel plate scans were only made in fuel element positions where hot spots were located. The following sections show the evaluation of the OLE for Core I and Core II(for both two pump and one pump conditions).

7.3.2.1 Core I

Table 7.3-3 gives the value of the OLE for Core I using plate scanning alone. Note that the one pump value is always lower than the two pump value, also the "expected value" which is determined by setting F_o, F_o', and d_{f_c} equal to 1 is considerably less than the limit of 3.72. The peak value of the OLE occurs on plate 1 of element C-9 at a point approximately 5 1/2 inches from the bottom of the fuel. The peak occurs at this point because C-9 has the lowest element flow and because a power peak occurs at that point as a result of the water filled slot created by the raised control blade. One removable plate element irradiation in C-8 was performed in Core I with a fuel element removed so that the shim bank was in a higher position. Comparing the peaks that occur in C-8 for the two bank heights, the following can be observed:

1) As the shim bank height increases, the height above the fuel bottom where the peak occurs increases and,

2) The value of the OLE increases very slightly as the shim bank height increases.

TABLE 7.3-3

VALUES OF THE OPERATING LIMIT EQUATION FOR CORE I OBTAINED USING PLATE SCANNING DATA

Cases	Axial Position from Fuel Bottom*	Blade Height (inches)	F_r	F_a	z	d_{f_p}	OLE 2 pumps	OLE 1 pump	OLE without Uncertainties (expected values) 2 pumps
C-9, plate 1 next to core housing	4.688	7.6	1.266	2.361	0.4288	0.9377	3.506	3.111	1.509
	5.438	7.6	1.266	2.29	0.5113	0.9377	3.532	3.152	1.55
	6.188	7.6	1.266	2.21	0.5852	0.9377	3.527	3.164	1.576
A-2, plate 1 next to solid dummy in A-1	0.0	7.6	1.333	2.79	0.0	0.9857	3.519	3.032	1.362
	9.688	7.6	1.333	1.259	0.6781	0.9857	2.097	1.923	0.812
C-8, plate 1 next to core housing	0.0	7.6	1.5274	2.2	0.0	1.0112	2.953	2.535	1.044
	5.438	7.6	1.5274	1.88	0.4217	1.0112	3.178	2.835	1.334
	6.188	7.6	1.5274	1.851	0.4834	1.0112	3.246	2.909	1.397
	6.938	7.6	1.5274	1.79	0.5435	1.0112	3.249	2.925	1.422
	7.688	7.6	1.5274	1.67	0.576	1.0112	3.082	2.786	1.343
	8.688	7.6	1.5274	1.536	0.639	1.0112	2.950	2.685	1.296
	9.688	7.6	1.5274	1.29	0.727	1.0112	2.655	2.444	1.170

* Distance in inches

TABLE 7.3-3 (Continued)

Case	Axial Position from Fuel Bottom*	Blade Height (inches)	F_r	F_a	z	d_{f_p}	OLE 2 pumps	1 pump	OLE without Uncertainties (expected values) 2 pumps
B-9, plate 1 next to hexagonal spider	0.0	7.6	1.23	2.79	0.0	1.0919	2.764	2.372	0.931
C-8, plate 8 8th from core housing	0.0	7.6	1.0047	3.31	0.0	1.0112	2.909	2.496	1.019
C-8,	5.438	8.9	1.603	1.723	0.3855	1.0112	3.004	2.677	1.232
plate 1	6.188	8.9	1.603	1.75	0.4432	1.0112	3.181	2.848	1.354
next to	6.938	8.9	1.603	1.70	0.5010	1.0112	3.202	2.88	1.389
core	7.688	8.9	1.603	1.688	0.5622	1.0112	3.306	2.988	1.473
housing	8.688	8.9	1.603	1.624	0.6305	1.0112	3.32	3.017	1.509
	9.688	8.9	1.603	1.481	0.6521	1.0112	3.076	2.807	1.383

* Distance in inches

The increase in OLE may not be real because the value of F_r for the blade raised case was conservatively estimated, also, it could not be directly determined from plate scanning data because the core was not fully loaded and because a series of irradiations was not performed at that blade height. The value of F_r was obtained by using a linear extrapolation of the CITATION predicted increase in F_r for outside channels which neglected xenon poisoning effects.

Note in Table 7.3-3 that the power spikes that occur at the bottom of the fuel plates do not yield the maximum values of the OLE. Plate 8 of position C-8 had a very large spike at the bottom edge, but it was not the limiting position. Table 7.3-4 shows bottom peaks at several element positions:

TABLE 7.3-4

BOTTOM EDGE PEAKS

Bottom Edge Location		F_r	F_a	$F_r F_a$
C-8	plate 1	1.5274	2.2	3.36
C-8	plate 8	1.0047	3.31	3.33
B-9	plate 1	1.23	2.79	3.43
A-2	plate 1	1.333	2.79	3.72

The product $F_r F_a$ represents the peak power at a point relative to the core average. For positions at the core bottom, the peak power occurs in the A-ring elements and decreases toward the outer rings. This trend is expected because the flux peaks under the core in the same manner. Because the flow disparity is less severe for A and B ring elements (with a dummy in the A-ring), the high bottom peaks can be tolerated more easily.

Table 7.3-5 shows the values of the OLE for Core I where the equation is evaluated using CITATION results alone. For the blades at 8 inches, the peak value occurs in plate 1 of C-9 at a position 6 inches above the fuel bottom. For outside edge plates, "CITATION only" results predicts higher values of the OLE than did experimental measurements. For internal elements such as A-2, "CITATION only" predicts values of the OLE almost identical except for positions on the bottom edge spike where "CITATION only" results underpredict the peak. Note that as the shim bank height increases, the CITATION results predict that the height of the position above the fuel bottom where the peak occurs will increase but that the peak value of the OLE will decrease slightly. Thus it appears that the value of the OLE will remain constant or slightly decrease for Core I as the shim bank is raised.

Table 7.3-6 compares the values of Z, F_r, F_a, and $F_r F_a$ obtained using experimental measurements and CITATION results. For points on the outside edge plates, CITATION

TABLE 7.3-5

VALUES OF THE OPERATING LIMIT EQUATION FOR CORE I OBTAINED USING CITATION RESULTS ONLY

Case	Axial Position from Fuel Bottom*	Blade Height (inches)	F_r	F_a	z	d_{f_p}	OLE 2 pumps	OLE 1 pump	OLE without Uncertainties (expected values) 2 pumps
C-8,	0.0	8.0	1.354	2.58	0.0	1.0112	3.124	2.685	1.139
plate 1	2.12	8.0	1.354	2.28	0.215	1.0112	2.988	2.611	1.138
next to	6.06	8.0	1.354	2.2	0.576	1.0112	3.494	3.134	1.545
core	8.06	8.0	1.354	1.67	0.716	1.0112	2.834	2.582	1.230
housing	10.06	8.0	1.354	0.989	0.798	1.0112	1.834	1.713	0.717
C-9, plate 1									
next to	0.0	8.0	1.26	2.66	0.0	0.9377	3.228	2.774	1.206
core	6.06	8.0	1.26	2.37	0.616	0.9377	3.833	3.44	1.756
housing	8.06	8.0	1.26	1.76	0.762	0.9377	3.055	2.785	1.376
A-2, plate 1									
next to	0.0	8.0	1.164	1.98	0.0	0.9857	1.676	1.409	0.340
solid	6.06	8.0	1.164	1.71	0.442	0.9857	1.968	1.748	0.640
dummy	8.06	8.0	1.164	1.59	0.575	0.9857	1.999	1.800	0.700
in A-1	10.06	8.0	1.164	1.39	0.691	0.9857	1.886	1.721	0.676

* Distance in inches

TABLE 7.3-5 (Continued)

Case	Axial Position from Fuel Bottom*	Blade Height (inches)	F_r	F_a	z	d_{f_p}	OLE 2 pumps	OLE 1 pump	OLE without Uncertainties (expected values) 2 pumps
C-8, plate 1 next to core housing	0.0	14.0	1.642	1.91	0.0	1.0112	2.67	2.28	0.885
	2.12	14.0	1.642	1.70	0.16	1.0112	2.57	2.24	0.90
	6.06	14.0	1.642	1.72	0.44	1.0112	3.22	2.88	1.38
	8.06	14.0	1.642	1.66	0.58	1.0112	3.40	3.08	1.54
	10.06	14.0	1.642	1.53	0.71	1.0112	3.41	3.12	1.60
	14.0	14.0	1.642	1.18	0.90	1.0112	3.10	2.89	1.51
	16.0	14.0	1.642	0.44	0.94	1.0112	1.71	1.66	0.79
C-9, plate 1 next to core housing	0.0	14.0	1.60	1.86	0.0	0.9377	2.72	2.32	0.92
	6.06	14.0	1.60	1.77	0.45	0.9377	3.54	3.17	1.58
	8.06	14.0	1.60	1.71	0.59	0.9377	3.73	3.38	1.75
	10.06	14.0	1.60	1.58	0.72	0.9377	3.75	3.43	1.81
	14.06	14.0	1.60	1.21	0.92	0.9377	3.41	3.18	1.71
	16.06	14.0	1.60	0.36	0.95	0.9377	1.71	1.68	0.82
A-2, plate 1 next to solid dummy in A-1	0.0	14.0	1.05	1.85	0.0	0.9857	1.21	1.0	0.08
	8.06	14.0	1.05	1.58	0.55	0.9857	1.63	1.46	0.47
	10.06	14.0	1.05	1.43	0.67	0.9857	1.60	1.45	0.49

* Distance in inches

TABLE 7.3-6

COMPARISON BETWEEN PLATE SCANNING AND CITATION
PREDICTIONS FOR CORE FACTORS IN CORE I

Location in Core	Distance from Bottom Edge of Fuel Meat (inches)	F_r		F_a		$F_r F_a$		z	
		P.S.D.*	CIT**	P.S.D.*	CIT**	P.S.D.*	CIT**	P.S.D.*	CIT**
C-8, plate 1	0.0	1.5274	1.354	2.2	2.58	3.36	3.49	0.0	0.0
C-8, plate 1	6.0	1.5274	1.354	1.851	2.2	2.83	2.98	0.4834	0.576
C-9, plate 1	6.0	1.266	1.26	2.21	2.37	2.80	2.99	0.585	0.616
A-2, plate 1	0.0	1.333	1.164	2.79	1.98	3.72	2.30	0.0	0.0
A-2, plate 1	10.0	1.333	1.164	1.26	1.39	1.68	1.62	0.678	0.691

* - Values are based on plate scanning data (P.S.D.) with blades at 7.6 inches.

** - Values are based on CITATION calculations with blades at 8.0 inches.

yields slightly larger values of $F_r F_a$ than does COREFAC

data. Comparing the Z's shows that CITATION predicts a

larger value of Z than COREFAC. This is the result of

two effects: 1) the large mesh spacing in CITATION

overestimates Z because the actual peak occurs some-

where within the mesh spacing and not at the top of the

large CITATION mesh spacing as is assumed in the OLE cal-

culation (COREFAC has a better resolution because of

greater number of mesh points), 2) cross sections used

in the upper part of the core for the CITATION calcu-

lation result in a greater power depression in the upper

core than is the actual case. Thus, it appears that

while CITATION underestimated the safety limit conditions,

it overestimates the incipient boiling conditions for

Core I type loadings when the peak occurs at an axial

position well above the bottom position.

In Section 7.2.2.1 it was shown that the original

design of the Incore Sample Assembly (ICSA) caused

values of the SI.F to become very close to the limiting

value of 2.9. The largest two pump value of the OLE for

a plate in A-2 in Core I next to the ICSA was 5.07

based on COREFAC results. CITATION results in Chapter 5

had predicted that the OLE would be unacceptable. Be-

cause the initial design of the ICSA caused unacceptable

values of the OLE, the original ICSA was removed from

the reactor before operation above 1.0 kw was allowed.

7.3.2.2 Core II

Core II of the MITR-II was evaluated in a somewhat different manner from Core I. Core II was evaluated by a combination of CITATION results and plate scanning data in addition to being evaluated by "CITATION only" results. As was the case with Core I, the two pump value of the OLE for Core II was always closer to the upper limit than the one pump value.

Table 7.3-7 shows the values of the OLE for core factors that are evaluated for Core II using a combination of CITATION results and plate scanning data. F_a and Z are taken directly from COREFAC results for Core II scans and F_r is obtained by combining plate scanning data and CITATION results in the same manner used to determine F_r in Section 7.2. The peak value of the OLE in Core II occurs on plate 1 of C-13 at a height approximately 10 inches above the bottom of the fuel.

Table 7.3-8 shows the values of the OLE for Core II where the equation is evaluated using CITATION results alone. For the core without fixed absorbers, the peak value of the OLE, as well as, its position up the channel, increases as the height of the shim bank increases. The peak value of the OLE from "CITATION only" results occurs on plate 1 of C-13 at a height of approximately 6 inches above the bottom edge of the fuel.

TABLE 7.3-7

VALUES OF THE OPERATING LIMIT EQUATION FOR CORE II OBTAINED USING A
COMBINATION OF PLATE SCANNING DATA AND CITATION RESULTS

Case	Axial Position from Fuel Bottom*	Blade Height (inches)	F_r	F_a	z	d_{f_p}	OLE 2 pumps	OLE 1 pump	OLE without Uncertainties (expected values) 2 pumps
A-1, plate 1 next to hexagonal spider	0.0	8.6	1.586	1.60	0.0	1.009	2.033	1.727	0.529
	13.688	8.6	1.586	1.33	0.6672	1.009	2.91	2.67	1.267
	22.438	8.6	1.586	0.86	1.0	1.009	2.66	2.53	1.267
B-4, Plate 1 next to radial spider	0.0	8.6	1.495	1.60	0.0	1.032	1.713	1.447	0.348
	13.688	8.6	1.495	1.21	0.6777	1.032	2.296	2.115	0.906
	22.438	8.6	1.495	0.77	1.0	1.032	2.113	2.022	0.9275
C-15, plate 1 next to core housing	0.0	8.6	1.372	2.0	0.0	0.989	2.369	2.023	0.717
	6.688	8.6	1.372	1.82	0.4772	0.989	2.946	2.640	1.195
	7.688	8.6	1.372	1.71	0.5727	0.989	2.926	2.643	1.216

* Distance in inches

TABLE 7.3-7 (Continued)

Case	Axial Position from Fuel Bottom*	Blade Height (inches)	F_r	F_a	z	d_{f_p}	OLE 2 pumps	OLE 1 pump	OLE without Uncertainties (expected values) 2 pumps
C-13,	0.0	8.6	1.54	2.0	0.0	0.944	2.994	2.57	1.068
plate 1	6.688	8.6	1.54	1.65	0.448	0.944	3.240	2.908	1.379
next to	7.688	8.6	1.54	1.59	0.538	0.944	3.313	2.996	1.454
core	9.688	8.6	1.54	1.49	0.655	0.944	3.36	3.07	1.53
housing	11.688	8.6	1.54	1.11	0.760	0.944	2.785	2.588	1.253

* Distance in inches

TABLE 7.3-8

VALUES OF THE OPERATING LIMIT EQUATION FOR CORE II
OBTAINED USING CITATION RESULTS ONLY

Case	Axial Position from Fuel Bottom*	Blade Height (inches)	F_r	F_a	z	d_{f_p}	OLE 2 pumps	OLE 1 pump	OLE without Uncertainties (expected values) 2 pumps
A-1, plate 1 next to hexagonal spider	0.0	8.0	1.245	1.42	0.0	1.009	1.024	0.836	-0.024
	14.0	8.0	1.245	1.157	0.66	1.009	1.720	1.58	0.562
	18.98	8.0	1.245	0.9	0.86	1.009	1.652	1.557	0.591
C-13, plate 1 next to core housing	0.0	8.0	1.20	2.10	0.0	0.944	2.207	1.878	0.631
	6.06	8.0	1.20	1.784	0.468	0.944	2.495	2.229	0.935
	8.06	8.0	1.20	1.47	0.591	0.944	2.189	1.984	0.805
	10.06	8.0	1.2	1.045	0.678	0.944	1.646	1.519	0.539
	14.0	8.0	1.2	0.8	0.809	0.944	1.481	1.398	0.496
	18.98	8.0	1.2	0.51	0.923	0.944	1.227	1.193	0.405
A-1, plate 1 next to hexagonal spider	0.0	14.0	1.137	1.36	0.0	1.009	0.737	0.582	-0.179
	14.0	14.0	1.137	1.222	0.672	1.009	1.576	1.444	0.469
	18.98	14.0	1.137	0.88	0.87	1.009	1.390	1.312	0.431

* Distance in inches

TABLE 7.3-8 (Continued)

Case	Axial Position from Fuel Bottom*	Blade Height (inches)	F_r	F_a	z	d_{f_p}	OLE 2 pumps	OLE 1 pump	OLE without Uncertainties (expected values) 2 pumps
C-13,	6.06	14.0	1.42	1.473	0.379	0.944	2.393	2.135	0.872
plate 1	8.06	14.0	1.42	1.515	0.505	0.944	2.736	2.468	1.107
next to	10.06	14.0	1.42	1.478	0.629	0.944	2.920	2.66	1.254
core	14.0	14.0	1.42	1.28	0.84	0.944	2.967	2.753	1.358
housing	18.98	14.0	1.42	0.424	0.943	0.944	1.551	1.518	0.644

* Distance in inches

Core factors used in the two methods of evaluating the incipient boiling·limit for Core II are compared in Table 7.3-9. Factors F_r and F_a derived entirely from CITATION results appear to be significantly lower than the combination factors and thus, yield lower values of the OLE. For Core II, CITATION results show that the peak value of the OLE increases as the shim bank is raised. Thus, the nearness to the incipient boiling limit is increased as the shim bank height increases. Table 7.3-10 shows the effect of blade height on the value of the OLE for both Core I and Core II. Core I has no limiting shim bank height while Core II is limited to specific heights depending upon whether one or two pumps are in operation.

7.4 Expected Problems for Future Core Loadings

Power peaking problems for future core loadings depend upon the future refueling philosophy and upon the incore loading of solid dummies and experimental facilities. The limiting effects for all considerations are:

A) Local conditions which may cause unacceptable power peaking,

B) The hot spot which occurs in an outer channel of the core at a position above the bottom edge of the fuel as the shim bank height increases.

The problem of unacceptable power peaking caused by local excess light water was demonstrated with the data from the original design of the Incore Sample Assembly

TABLE 7.3-9

COMPARISON BETWEEN PLATE SCANNING-CITATION AND CITATION
ONLY PREDICTIONS FOR CORE FACTORS IN CORE II

Location in Core	Distance from Bottom Edge of Fuel Meat (inches)	F_r		F_a		$F_r F_a$		z	
		Comb.*	CIT**	Comb.*	CIT**	Comb.*	CIT**	Comb.*	CIT**
A-1, plate 1	14.0	1.586	1.245	1.33	1.16	2.11	1.44	0.667	0.66
C-13, plate 1	8.0	1.54	1.2	1.59	1.47	2.45	1.76	0.538	0.591
C-13, plate 1	10.0	1.54	1.2	1.49	1.045	2.29	1.254	0.655	0.678

* - Values based on combination of plate scanning data and CITATION calculations with blades at 8.0 inches.

** - Values based on CITATION calculations only with blades at 8.0 inches.

TABLE 7.3-10

EFFECT OF SHIM BANK HEIGHT ON VALUE OF OPERATING LIMIT EQUATION

Case	Blade Height		Value of OLE from CITATION Calculation	Change in OLE per inch Change in Shim Bank Height	OLE Using Plate Scanning Data	Blade Height Limit[+]
Core I Loading						
C-8, plate 1 next to core housing	8 inches	2 pumps	3.494	2 pumps -0.014	3.249*	no limit
		1 pump	3.134			
	14 inches	2 pumps	3.41	1 pump -0.002	2.925*	no limit
		1 pump	3.12			
Core II Loading						
C-13, plate 1 next to core housing	8 inches	2 pumps	2.495	2 pumps +0.0787	3.36**	13.1 inches
		1 pump	2.229			
	14 inches	2 pumps	2.967	1 pump +0.0873	3.07**	16.0 inches
		1 pump	2.753			

[+] Limit where linear extrapolation of OLE exceeds 3.72.
* Values from Core I plate scanning data with blades at 7.6 inches.
** Values from combination of Core II plate scanning data and CITATION calculations with blades at 8.6 inches.

(ICSA). The problem can be minimized by careful design and consideration of the proper fuel and dummy element placement. For Core II, power peaking caused by water gaps created by removal of the fixed absorbers was minimized by arrangement of the solid dummies.

The problem of the power peak increasing as the shim bank height rises is more critical for core loadings without fixed absorbers. It is more desirable both for experimenters and for operating characteristics to have the upper portion of the core poisoned.

7.4.1 Proposed Refueling Plan

Table 7.4-1 shows the fuel cycle for the MITR-II that was proposed by Kadak (Ref. 7.4-1). The proposed fuel cycle is still valid because it prevents fresh fuel elements from being put into the outer C-ring where the hottest channels are located in the clean core and where the coolant flow disparity is the greatest. The proposed fuel cycle program assumed that 26 fuel elements would be used incore at all times with one A-ring position occupied by a sample assembly. It is unlikely that the reactor will be operated with 26 elements incore because of a desire for incore irradiation space and because of the necessity to load solid dummies for reactivity control. However, the fuel cycle proposed by Kadak can still be used provided that no less than 23 fuel elements are loaded incore or a minimum of 8 elements loaded in the A and B rings.

TABLE 7.4-1

PROPOSED MITR-II FUEL CYCLE

(Ref. 7.4-1)

Time (hrs)	Core Condition	Control Blade Position	Elements in Storage
0	Clean and critical	10"	0
840	Depleting	12"	0
2520	Depleting	14"	0
3000	All elements flipped	12"	0
3690	Depleting	14"	0
4800	Discharge inner and middle store for future refueling refuel with fresh fuel	10"	11
5400	Depleting	12"	11
6500	Depleting	14"	11
7200	Flip entire core	14"	11
7200- 9400	Depleting	14" - 20"	11
9400	Discharge outer 15 elements at greater than 25% burnup; insert depleted 11 inner and middle plus 4 stored elements into outer; refuel with fresh inner and middle.	10"	7

TABLE 7.4-1 (Continued)

Time (hrs)	Core Condition	Control Blade Position	Elements in Storage
10000	Depleting	12"	7
11100	Depleting	14"	7
11800	Flip entire core	14"	7
11800-14000	Depleting	14" - 20"	7
14000	Discharge outer 15 elements at greater than 25% burnup: insert depleted 11 inner and middle plus 4 stored elements into outer; refuel with fresh inner and middle	10"	3
14600	Depleting	12"	3
15700	Depleting	14"	3
16400	Flip entire core	14"	3
16400-18600	Depleting	14" - 20"	3

TABLE 7.4-1 (Continued)

Time (hrs)	Core Condition	Control Blade Position	Elements in Storage
18600	Discharge outer 15 elements at greater than 25% burnup reload entire clean core: place 11 inner and middle into storage for future refuel	10"	14
19440	Depleting	12"	14
21120	Depleting	14"	14
21600	All elements flipped	12"	14
22290	Depleting	14"	14
23300	Discharge inner and middle; store for future refueling; refuel with fresh fuel	10"	25

Elements operated in the A and B rings shall have varied burnups before being loaded into the C ring in future refuelings. The elements that have been depleted the most should be loaded into the higher power corner positions and then into the positions with the greatest flow disparity relative to their power. For a Core I arrangement, the order of loading in terms of most depleted to least depleted should be:

1. C-8
2. C-13
3. C-3
4. C-9
5. C-7
6. C-12
7. C-2
8. C-4
9. C-14
10. C-6
11. C-10
12. C-5
13. C-11
14. C-1
15. C-15 .

Operating with flipped fuel elements will be advantageous because the depleted upper core will depress power

generation in the upper core and prevent the power peak
from rising as the shim bank height increases. Note,
that in the proposed fuel cycle, the shim bank height is
only raised above 14 inches for the cases where the
upper portions of the outside fuel element have been
depleted near their planned limit. The development of
a depletion code that gives the power distribution for
each fuel loading the prime necessity for future core
evaluations.

7.4.2 Sample Assembly and Dummy Element Effects

Loading solid dummies and sample assemblies may cause
unacceptable power peaking for the following reasons:

1. As additional fueled elements are replaced
   by non-fueled assemblies, the remaining fuel
   elements each must produce a greater power
   to keep the total power constant. It may
   not always be true that increasing the
   number of fueled elements will decrease the
   power peaking because adding an additional
   element may decrease the coolant flow to the
   hot plate more than it decreases the power
   generated on that hot plate,

2. The non-fueled assembly may create a local
   condition that results in power peaking,
   e.g., excess light water may create un-
   acceptable peaking,

3. The non-fuel assemblies may adversely affect
   the flow disparity by changing the flow dis-
   tribution or resulting in excessive bypass
   flow.

All of the above effects must be considered in the
design and analysis of a core loadings using various

configurations of irradiation facilities and solid
dummies. Prime concern should be given to minimizing
the bypass flow created by a non-fueled assembly and
to minimizing the amount of water present in the fa-
cility which may cause flux peaking in surrounding
fueled elements.

The reactor should contain the proper amount of fuel
in the loading so that it will go critical at the be-
ginning of life for each core configuration with the
shim bank at approximately 8 to 10 inches with no
xenon build up. This requirement would prevent un-
acceptable peaks from occurring at the bottom edge
power spikes from bank heights below 8 inches, and
would prevent unacceptable peaks from occurring in
the outside edge plates because of high shim bank
positions. Higher shim bank positions would be allow-
able if the upper portions of the outside plates were
heavily depleted.

7.5 Future Safety Limit and Limiting Condition Evaluation

The experience gained in evaluating the initial cores
of the MITR-II should greatly shorten the time required
for evaluation of future core loadings. The MITR-II is
no longer an unknown quantity and some of its features
such as the power peaking near the water filled control
blade slot positions are better understood. Future core

loadings can be more accurately evaluated if the calculational methods are improved as suggested in the following section. Potential changes to some factors in the SLF and the OLE which could increase the flexibility of the reactor by reducing over conservatisms are covered in Section 7.5.2. Section 7.5.3 discusses experimental procedures which could be used as a check on the calculated evaluation.

7.5.1 Calculational Improvements

The major shortcomings of the present 3-D CITATION calculations are as follows:

1) Insufficient detail in the radial direction to accurately predict the higher power plates near the outer edge of the core,

2) Insufficient detail in the axial direction to accurately predict the axial location and Z where the hot spot occurs,

3) CITATION predicts a lower fraction of total power in the upper portion of the core than was shown to exist by experimental measurements,

4) Present CITATION calculations did not include the effects of xenon and burnup in higher blade height cases.

The number of mesh points utilized in a 3-D CITATION calculation is limited by the allowable space in the MIT Information Processing Center Computer. A better mesh spacing representation could be developed to improve the accuracy of CITATION results both for power peaking analysis and for absolute K_{eff} predictions.

The major use of 3-D CITATION calculations should be to
accurately determine the power for each element in a
core loading. This 3-D model must include the effects
of depletion and xenon build up on the individual element
power generation. Basically, the 3-D calculations would
be used to determine the F_r' (ratio of power produced in
a fuel element in the core) for each element for each
loading and blade height case.

Single element calculational models should be
developed to provide the detailed effects that are
not possible with the whole core 3-D calculations
alone. Boundary conditions and the proper burnup ratio
for the single element model would be obtained from the
whole core 3-D calculations. Hence, the single element
calculation is a method of interpretation of the 3-D
results.

The large number of mesh points that could be util-
ized in a single element model would provide good detail
of F_r'', F_a, and Z (definitions   in section 7.2.2.2 and 7.3)
and thus, provide accurate values of the SLF and OLE.
Depletion and xenon effects would also have to be in-
cluded in the single element calculations. Single element
models could be used to calculate the power distribution
in an element next to a control blade slot, a core housing
corner hole, a section of the absorber spider, or an in-
core irradiation facility. The whole core and individual

element calculations would provide good detail for evaluation of the SLF and OLE for future cores.

7.5.2 Suggested Changes in F_p and F_o

The Safety Limit Factor (SLF) contains the factor, F_p, and an uncertainty factor F_H.   The Operating Limit Equation (OLE) contains F_p and uncertainty factors F_o and F_o'. The current evaluation of these factors according to their Technical Specification definitions is overly conservative and reduces flexibility in future core loadings. The following suggestions are made for changing the definitions of F_p and uncertainty factors but neither could be changed without prior approval by the Nuclear Regulatory Commission.

The core factor, F_p, is defined by the MITR-II Technical Specifications as "the fraction of the total power generated by the fuel". In Sections 7.2 and 7.3, the basis for the SLF and OLE were reviewed and it was shown the F_p actually stood for the fraction of total power deposited in the primary coolant that is generated by the fuel. In all cases for the evaluation of Core I and Core II, F_p was assumed to be equal to 1.0 which is the most conservative assumption. By setting F_p equal to 1.0, it is assumed that all of the total power of the reactor is generated by the heat flux on the fuel plates

which results in the coolant temperature rise in the coolant channels.

The total reactor power is based on a heat balance of several reactor systems: the primary coolant system, the D_2O reflector system, and the shield coolant system. The total power obtained from these systems is used as the base power for setting power level trips and determining the operating power level. The fuel surface heat flux is not responsible for all of the power deposited in these systems. For the shield and reflector system, fast neutron and gamma heating are responsible for the power in those systems. For the primary coolant system, neutron and gamma heating, fuel plate surface heating, and heating from experimental facilities are responsible for the power removed by the primary water. The problem of determining the exact fraction for each system is complicated by the heat exchange that can occur between the system at such locations as the outer core tank wall.

The total reactor power which is the sum of all system powers and used for determining the absolute power level may be divided into the following fractions:

F_{P_1} is the fraction of the total power which is deposited in the primary coolant by the fuel plate surfaces,

F_{P_2} is the fraction of the total power which is deposited in the primary coolant by neutron and gamma heating,

F_{P_3} is the fraction of the total power which is deposited in the primary coolant by experimental facilities,

F_{P_4} is the fraction of the total power which is deposited in the reflector system,

F_{P_5} is the fraction of the total power which is deposited in the shield system,

where,

$$F_{P_1} + F_{P_2} + F_{P_3} + F_{P_4} + F_{P_5} = 1.0$$

$$(7.5-1)$$

For the initial reactor cores there were no experimental facilities which deposited heat into the primary coolant, thus, F_{P_3} = 0.0 (although it might be argued that gamma heat in the solid dummies would fall into this classification). Table 7.5-1 shows the values of the remaining fractions based on the predictions by Choi (Ref. 7.5-1) assuming F_{P_3} = 0.0.

TABLE 7.5-1

DISTRIBUTION OF ENERGY RELEASED IN THE
REACTOR FROM FISSION OF URANIUM

Fuel Element Surfaces	F_{P_1}	0.9036
Primary Coolant Neutron and Gamma Heating	F_{P_2}	0.0342
D_2O Reflector	F_{P_4}	0.0531
Shield System	F_{P_5}	0.0091

It was shown in Section 7.2 that the reactor safety limit was related to the amount of power that is generated in the hottest channel. Equations 7.2-7' and 7.2-11 which were combined to give the safety limit are:

$$\frac{P_T}{W_T C_p} = T_{out} - T_{in} \quad , \qquad (7.2\text{-}7')$$

and

$$\frac{P_T F_{H.C.}}{d_f R W_T C_p} = T_{sat} - T_{in} \ . \qquad (7.2\text{-}11)$$

Given that P_T is the total reactor power from all systems, the above equations with the various F_{p_i}'s and F_f included become:

$$(F_{p_1} + F_{p_2} + F_{p_3}) \frac{P_T}{W_T C_p} = T_{out} - T_{in} \quad , \qquad (7.5\text{-}2)$$

and

$$\frac{P_T F_{H.C.} (F_{p_1} + F_{p_2})}{d_f F_f R W_T C_p} = T_{sat} - T_{in} \quad , \qquad (7.5\text{-}3)$$

The quantity $(F_{p_1} + F_{p_2} + F_{p_3})$ in Eq. 7.5-2 represents the fraction of the total reactor power that is deposited in the primary coolant. The quantity $(F_{p_1} + F_{p_2})$ in Eq. 7.5-3 represents the fraction of the total power that is deposited in the coolant that cools the fuel plates. The coolant-moderator in the coolant channels receives

heat from both the fuel plate surfaces and from neutron and gamma heating in the coolant itself. It is conservative to assume that the channel power distribution due to gamma heating is the same as the plate power distribution, i.e., that the channel with the hottest plate surface power also has the hottest channel coolant power from neutron and gamma heating. Equations 7.5-2 and 7.5-3 can be combined and rearranged to yield the following:

$$\frac{P_T}{W_T C_p} \left[(F_{P_1} + F_{P_2} + F_{P_3})(\frac{F_{H.C.}}{d_f F_f R} - 1) - \frac{F_{P_3} F_{H.C.}}{d_f F_f R} \right] =$$

$$T_{sat} - T_{out} \quad . \quad (7.5-4)$$

If there is no power generated by experimental facilities (F_{P_3} = 0), Eq. 7.5-4 reduces to:

$$\frac{P_T}{W_T C_p} \left[(F_{P_1} + F_{P_2})(\frac{F_{H.C.}}{d_f F_f R} - 1) \right] = T_{sat} - T_{out} \quad .$$

$$(7.5-5)$$

The result of having less than 100% of the total reactor power deposited into the primary coolant ($F_{P_1} + F_{P_2} + F_{P_3}$) < 1.0 is that the lines in Fig. 7.2-1 would be shifted upward and to the right, thus, increasing the safety limit margin. If the total reactor power is deposited into the primary coolant system then

$(F_{p_1} + F_{p_2} + F_{p_3}) = 1.0$ and Eq. 7.5-4 becomes:

$$\frac{P_T}{W_T C_p} [\frac{F_{H.C.}(1 - F_{p_3})}{d_f F_f R} -]` = T_{sat} - T_{out} \cdot$$

(7.5-6)

The quantity $(1 - F_{p_3})$ is equivalent to the F_p in the Technical Specifications where F_p is the fraction of the power generated by the fuel. Thus, Eq. 7.5-6 is equivalent to Eq. 7.2-16 which is the present basis of the Technical Specification safety limit. Equation 7.5-4 is actually more precise and less overly conservative than Eq. 7.2-16, but it is somewhat more complicated to evaluate.

The Operating Limit Equation (OLE) which was derived in Section 7.3.1 is formed from the combination of Eqs. 7.3-2, 7.3-3, 7.3-4, 7.3-5, 7.3-6, 7.3-11, and 7.3-12. The following analysis inserts the precise definitions of F_{p_i} into the equations used to develop the OLE. Equations 7.3-2, 7.3-4, and 7.3-11 have no reactor power value, P_T, as a direct component and thus, no F_p factor would be directly included. Eqs. 7.3-3 and 7.3-12 are dependent on the fraction of the reactor power that is generated on the fuel plate surface, F_{p_1}, and thus become :

$$(Q/A)_{MAX} = F_{p_1} F_r F_a P_T/A, \qquad (7.3-3')$$

$$q_{LB}'' = \frac{3.413 P_T F_{P_1}}{\eta A} F_r F_a (10)^6 . \qquad (7.3-12')$$

Equation 7.3-5 is dependent on the fraction of the reactor power that is deposited in the coolant channels, $(F_{P_1} + F_{P_2})$, and thus becomes:

$$T_c(Z) = T_{in} + \frac{(F_{P_1} + F_{P_2}) P_T Z}{d_f F_f W_T C_p} . \qquad (7.3-5')$$

Equation 7.3-6 is dependent on the fraction of the reactor power that is deposited into the primary coolant, $(F_{P_1} + F_{P_2} + F_{P_3})$, and thus becomes:

$$(F_{P_1} + F_{P_2} + F_{P_3}) P_T = W_T C_p (T_{out} - T_{in}) . \qquad (7.3-6')$$

Combining Eqs. 7.3-2, 7.3-3', 7.3-4, 7.3-5', 7.3-6', 7.3-11, and 7.3-12', yields the following form of the OLE:

$$[(\frac{W_T}{W_{T_o}})^{0.2} G + \frac{(F_{P_1} + F_{P_2}) F_r Z}{d_f F_f} - (F_{P_1} + F_{P_2} + F_{P_3})] -$$

$$2.77 [\frac{F_{P_1} F_r F_a}{\eta A}]^{0.466} \leq 3.72, \qquad (7.5-7)$$

where,

$$G = \frac{F_{P_1} F_r F_a W_{T_o} C_p}{(d_f F_f)^{0.8} \eta A h_o} . \qquad (7.5-8)$$

Assuming that all of the reactor power is deposited into the primary coolant $(F_{P_1} + F_{P_2} + F_{P_3} = 1.0)$, and assuming that the neutron and gamma heating of the coolant itself is small $(F_{P_2} \approx 0)$, Eq. 7.5-7 reduces to the fol-

lowing:

$$[(\frac{W_T}{W_{T_o}})^{0.2}G + \frac{F_{p_1}F_r Z}{d_f F_f} - 1] - 2.77[\frac{F_{p_1}F_r F_a}{..A}]^{0.466} \leq 3.72.$$

$$(7.5-9)$$

Equation 7.5-9 is equivalent to the Technical Specification Eq. 7.3-1 assuming that $(F_{p_1} + F_{p_2} + F_{p_3} = 1.0)$, $F_{p_2} \approx 0$, and $F_{p_1} \approx F_p$, with the exception that Eq. 7.5-9 has an additional F_{p_1} in the last term of the expression. Since the factor F_p was assumed equal to 1.0 for Core I and Core II evaluation, the evaluations in Sections 7.2-7.3 were conservative and valid. For future evaluations, the factor F_p should be included into the last term of the OLE as shown in Eq. 7.5-9. While Eq. 7.5-7 is actually more precise than the Technical Specification OLE, it is also somewhat more complicated to evaluate.

The uncertainty factor, F_o, is evaluated in the Technical Specifications in a cumulative manner by a direct product of individual factors. The other uncertainty factors, F_o' and F_H, are also evaluated in similar manner. This cumulative compilation of uncertainties leads to values of the SLF and OLE that are much greater than the "expected values". The tables in Section 7.3 show the expected values of the OLE and the values by the Technical Specification eval-

uation. The inflated value created by the cumulative

combination of uncertainties is somewhat misleading.

When the evaluation of the OLE or SLF approaches the

limiting value, there is much concern but in reality

it is very highly improbable that the limiting condition

is really being approached. This excessive conservatism

can lead to decreased flexibility and competiveness of

the reactor. Incore temperature measurements which

are described in Chapter 8 show good agreement between

the measured temperatures and the "expected values".

While this data is somewhat limited, it shows that the

measured temperatures always fell well below the temp-

erature values which would be obtained using the current

cumulative uncertainties. In the future, attempts

should be made to receive permission from the NRC to

combine the individual uncertainty factors in a semi-

statistical manner. This would yield more flexibility

in the evaluation of the SLF and the OLE and yet maintain

a sufficient margin of safety.

7.5.3 Experimental Procedures

Future core evaluations will rely mostly on analytical

results with some experimental checks. The easiest and

most useful experimental measurements can be made with

flux wire irradiations or by self-powered neutron

detector scans. Flux wire irradiations are useful

because wires can be positioned inside fuel assemblies
and irradiated at powers of less than 1.0 kw. Since
the core factors must be known prior to reactor operation
above 1.0 kw, this technique allows verification of the
analytically determined values prior to exceeding the
1.0 kw level. A description of the flux wire scans
performed on Core I are described in Section 5.4. The
wire experimental flux shapes for Core I were in good
agreement with the shapes obtained by plate scanning and
analytical calculations.

Self-powered neutron detector scans are only possible
at higher powers. At present, scans can be made inside
the absorber spider or in a core housing corner hole.
While the corner hole scan is potentially more useful,
the configuration of the corner hole makes results much
more difficult to interpret. Self-powered detector scans
performed in Core I and II are discussed in Chapter 9.
Future experimental facilities that are inserted into
the core should contain small slots or holes which could
be used for wire irradiation positions at low powers
and for self-powered detector scans at higher powers.
At higher powers, the self-powered scans could be used
to verify the effects of various experimental facility
configurations; e.g., sample in or sample out, or reactor
variations such as, depletion or blade height changes.

CHAPTER 8

TEMPERATURE DISTRIBUTIONS

Steady-state temperature distributions of the MITR-II are discussed in this chaper. Section 8.1 is a review of temperature distribution predictions used in evaluating the initial design of the MITR-II. Temperature predictions for Core I and II, which were determined using power distribution measurements, are discussed in Section 8.2. Steady-state temperature measurements for Core I and Core II are described in Section 8.3. The predicted and measured temperatures are compared in Section 8.4. Secion 8.5 is a summary of temperature distribution results.

8.1 Design Temperature Predictions

As discussed in Chapter 7, the limiting condition for operation is that incipient boiling be prevented in the core. This yields a limit on the peak allowable fuel plate wall temperature. The peak wall temperature does not necessarily occur at the point with the highest heat flux (greatest $F_r F_a$) because the wall temperature is a function of the local heat flux, the coolant channel fluid temperature, and the heat transfer coefficient at that point.

In the design of the MITR-II, the MACABRE computer code (Ref. 8.1-1) was used to perform parametric studies by calculating the heat flux, clad temperature, and channel bulk coolant temperature, due to variations in the average heat flux, radial and axial power peaking factors, coolant flow rate, and the hot channel factors. The design analysis had shown that the hottest fuel plate had a heat flux distribution as shown in Fig. 5.1-1. Figure 8.1-1 shows the calculated variation of the clad surface temperature (T_{WALL}) and the local channel bulk coolant temperature with axial position along this hottest fuel plate for a reactor power of 6 megawatts, primary coolant flow rate of 1800 gpm, an inlet temperature of 118.1° F, and hot channel factors included. Curves are shown for blade heights of 8.0, 10.0, and 14.0 inches. Table 8.1-1 gives a summary of the design results for the peak wall temperature. The temperature required to cause incipient boiling, T_{WIB}, is calculated using Eq. 7.3-10. Thus, the predicted peak wall temperature was shown to be less than the wall temperature required to have incipient boiling. A similar analysis for the one pump case indicated that the two pump case was the more limiting condition.

One problem with the design temperature distributions was that they always showed that the peak wall temperature

FIG. 8.1-1

AXIAL VARIATION OF CLAD SURFACE AND LOCAL (CHANNEL)
BULK COOLANT TEMPERATURES ALONG THE HOTTEST FUEL PLATE

(reactor power: 6 MW + primary coolant flow rate: 1800 GPM)

Temperature at edge of core near D_2O
Curve 1 - blades at 8 inches
Curve 2 - blades at 10 inches
Curve 3 - blades at 14 inches

Wall temp.

1

2

3

4

H_2O bulk channel temp.

1
2
3
4

Temperature on a central fuel plate
Curve 4 - blades at 8 inches

temperature (°F)

245
235
225
215
205
195
185
175
165
155
145
135
125
115

0   2   4   6   8   10   12   14   16   18   20

distance from bottom of fuel   (inches)
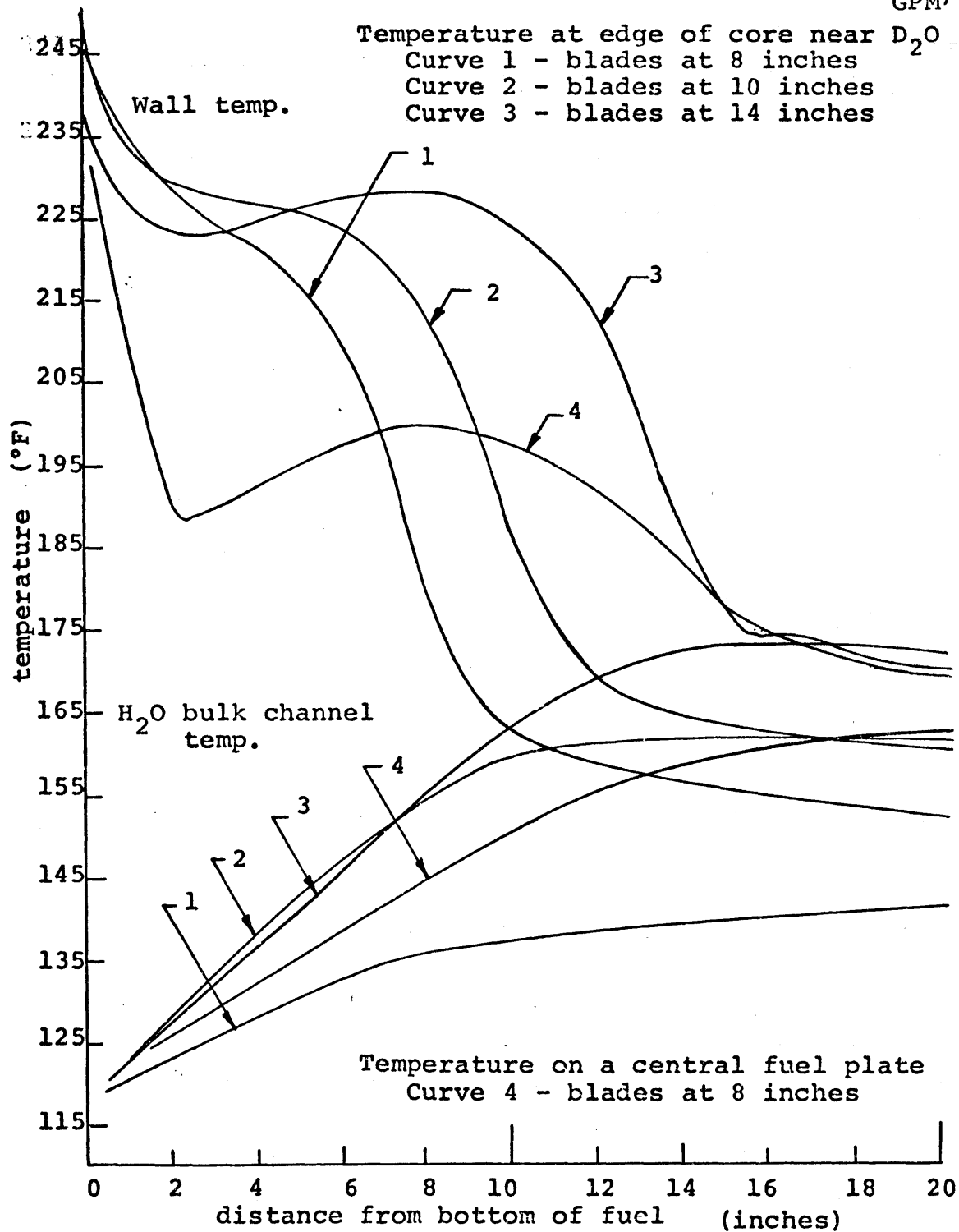
TABLE 8.1-1

SUMMARY OF MAXIMUM CLAD WALL TEMPERATURES, MAXIMUM HEAT FLUXES, AND INCIPIENT
BOILING TEMPERATURES FOR DESIGN PREDICTIONS OF MITR-II

Blade Height (Inches from Bottom)	$(T_{WALL})MAX$ (°F)	$(Q/A)_{max}$ $(BTU/hr\text{-}ft^2)$ (Reactor Power = 6.0 MW and uncertainties included)	T_{WIB} (°F) $(T_{sat} = 230°F)$
8.0	245.7	3.13×10^5	250.6
10.0	244.5	3.10×10^5	250.5
14.0	235.4	2.88×10^5	249.8

occurred at the bottom edge of the fuel. Allowance was made for the possibility that the peak wall temperature could occur further up the channel as the blade height was increased. However, thinking was geared toward the expectation that the peak would always occur at the bottom. For both Core I and Core II, however, the peak wall temperature occurred some distance above the bottom edge even for the lower blade configurations.

8.2 Temperature Predictions from Power Distribution Measurements

Core I and Core II temperatures have been predicted by using the experimentally determined power distributions and nominal heat transfer conditions. Predicted temperatures at various fuel element outlets, fuel channel outlets, and fuel plate surfaces are discussed in Sections 8.2-1, 8.2-2, and 8.2-3, respectively.

8.2.1 Fuel Element Outlet Temperature

The coolant temperature rise across an element can be determined by the following equation:

$$P_E = \dot{m}_E \, C_p \, (\Delta T)_E \tag{8.2-1}$$

where,

P_E is the power generated in the element,

$\dot{m}_E$ is the mass flow rate in the element,

C_p is the coolant heat capacity,

$(\Delta T)_E$ is the coolant temperature rise.

The values of P_E and $\dot{m}_E$ are determined by the following equations:

$$P_E = \frac{P_T F_p F_r'}{N} \ , \tag{8.2-2}$$

$$\dot{m}_E = \frac{W_T d_{f_p} F_f}{N} \ , \tag{8.2-3}$$

where,

P_T is the total reactor thermal power,

F_p is the fraction of the total power generated by the fuel,

F_r' is the ratio of the power produced in a fuel element to the power produced in the average fuel element in the core,

N is the number of fuel elements in the core,

W_T is the reactor coolant flow rate,

d_{f_p} is the ratio of the flow in an element to the flow in the average element,

F_f is the fraction of the primary flow cooling the fuel.

On combining Eqs. 8.2-1, 8.2-2, and 8.2-3 the coolant temperature rise becomes:

$$(\Delta T)_E = \frac{F_r' F_p}{d_{f_p} F_f} \ \frac{P_T}{C_p W_T} \tag{8.2-4}$$

Nominal values of P_T, W_T, and C_p are used in Eq. 8.2-4 in order to compare the predicted ΔT's with the measured ΔT's. Nominal 2 pump values used are:

$$W_T = 2000 \text{ gallons/minute}$$

$$C_p = 0.9985 \text{ BTU/hr-lb}_m$$

$$P_T = 5.0 \text{ MW}$$

Applying the appropriate correction factors to yield correct units, Eq. 8.2-4 becomes:

$$(\Delta T)_E = 17.18 \frac{F_r' F_p}{d_f F_f} \,°F \qquad \text{(2 pumps)} \qquad (8.2\text{-}5)$$

Predicted element temperature rises for Core I using GAMSCAN and CITATION data are shown in Table 8.2-1. The predicted temperatures are compared with several measured temperatures in Section 8.4.

8.2.2 Fuel Channel Outlet Temperatures

By using the method in Section 8.2.1, it can be similarly shown that the temperature rise for an individual channel, $(\Delta T)_C$, of nominal width would be:

$$(\Delta T)_C = 17.18 \frac{F_r F_p}{d_f F_f} \,°F, \qquad \text{(2 pumps)} \qquad (8.2\text{-}6)$$

where,

F_r is the ratio of the power deposited in the channel of interest over the average channel power.

Predicted channel temperature rises for Core I at 5.0 MW using GAMSCAN and CITATION data are shown in Table 8.2-2. The predicted temperatures are compared with measured temperatures in Section 8.4.

TABLE 8.2-1

PREDICTED COOLANT TEMPERATURE RISE FOR ELEMENTS IN CORE I

Element Position in Core	d_{f_p}	F'_r P.S.D.*	F'_r CIT**	ΔT P.S.D.* (°F)	ΔT CIT** (°F)
A-2	1.0167	1.14	1.108	20.3	19.7
A-3	.9857	1.14	1.108	20.9	20.4
B-1	1.0487	1.029	0.936	17.8	16.2
B-3	.9967	1.061	1.022	19.3	18.6
B-4	1.0068	1.141	1.139	20.5	20.5
B-5	1.0574	1.222	1.206	20.9	20.7
B-6	1.0732	1.141	1.139	19.3	19.2
B-7	1.0823	1.061	1.022	17.8	17.1
B-9	1.0919	1.029	0.936	16.1	15.5
C-1	0.942	0.8891	0.855	17.1	16.4
C-2	0.9598	0.9494	0.895	17.9	16.9
C-3	0.9805	0.900	0.927	16.6	17.1
C-4	0.9769	0.9494	0.907	17.6	16.8
C-5	0.9760	0.889	0.935	16.5	17.3
C-6	0.9760	0.85	1.027	15.8	19.1
C-7	0.9454	1.042	1.087	20.0	20.8
C-8	1.0112	1.116	1.117	20.0	20.0

TABLE 8.2-1 (Continued)

Element Position in Core	d_{f_p}	F'_r P.S.D.*	F'_r CIT**	ΔT P.S.D.* ($^\circ$F)	ΔT CIT** ($^\circ$F)
C-9	0.9377	1.042	1.087	20.1	21.0
C-10	0.9811	0.85	1.027	15.7	19.0
C-11	0.9848	0.889	0.935	16.3	17.2
C-12	0.9464	0.9494	0.907	18.2	17.4
C-13	0.9967	0.900	0.927	16.4	16.8
C-14	1.0246	0.9494	0.895	16.8	15.8
C-15	1.0013	0.8891	0.855	16.1	15.5

* Based on plate scanning data

** Based on CITATION results

$F_f = 0.9487$

$P_T = 5.0$ MW

$W_T = 2000$ gpm

TABLE 8.2-2

PREDICTED CHANNEL TEMPERATURE RISE FOR SELECTED CHANNELS IN CORE I

Element Position in Core	Channel Position in Element	F_r P.S.D.*	F_r CIT**	d_{f_p}	ΔT P.S.D.* (°F)	ΔT CIT** (°F)
C-8	1	1.5274	1.529	1.0112	27.4	27.4
C-9	1	1.266	1.321	0.9377	24.4	25.5
C-5	2	1.356	1.425	0.9760	25.2	26.4
	5	0.8833	0.929	0.9760	16.4	17.2
	8	0.822	0.865	0.9760	15.3	16.0
	12	0.7614	0.800	0.9760	14.1	14.8
	15	0.8209	0.863	0.9760	15.2	16.0
B-5	8	1.222	1.206	1.0574	20.9	20.7
A-2	1	1.333	1.295	1.0167	23.7	23.1

* Based on plate scanning data

** Based on combination of plate scanning data and CITATION results (same method as used to determine individual plate relative power in Chapter 6)

$F_f = 0.9487$

$P_T = 5.0$ MW

$W_t = 2000$ gpm

8.2.3 Fuel Plate Surface Temperatures

The fuel plate surface temperature can be calculated by using an equation such as Eq. 5.2-7 or by using the experimentally determined power distribution data as input to a thermal-hydraulic computer code such as MACABRE (Ref. 8.1-1). The latter method was used to predict the fuel plate surface temperatures because of the ability of the the computer code to vary the coolant properties with temperature.

MACABRE is capable of solving the isothermal-hydraulics and nonisothermal-hydraulics and heat transfer of most plate type reactor fuel assemblies cooled by a subcooled fluid in forced convection. It can accommodate two-dimensional time dependent heat generation rates and hydraulic communication between parallel coolant channels. In addition, MACABRE will compute the corrosion of aluminum clad heat transfer surfaces. The code utilizes the Dittus-Boelter forced convection heat transfer correlation with the requirement that the total pressure drop in each coolant channel be equal. The input to MACABRE requires the following:

A. Coolant properties

B. Element geometry

C. Total flow rate

D. Fuel plate properties

E. Power distribution in element.

A listing of MACABRE output can be found in Appendix E.

Temperature distributions in three fuel element positions were calculated by using the MACABRE code. Table 8.2-3 shows input data values for these three positions, C-9, and A-2 in the Core I loading and the position A-1 in the Core II loading. Specific flow and power distribution characteristics of each element were used as input, as well as, fuel element geometry. Nominal values of each were used in order to compare a nominal prediction of the temperature distribution with the measured temperatures.

Figure 8.2-1 shows the predicted fuel surface and bulk coolant temperature distribution on several plates and channels in C-9. The calculated peak wall temperature at 5 MW, which occurs at an axial height of 5.4 inches on plate 1, is 172°F. The outside coolant channel has a smaller temperature rise than interior channels because the MACABRE calculation includes the fact that the outer channels have more than one half the flow of the inner channels for the nominal channel dimensions. MACABRE results (see Table 8.2-4) also show that for given a plate with a slightly different coolant temperatures on each side of the plate at a given axial height, the wall temperature difference between the two sides is small because of the high thermal conductivity of aluminum.

TABLE 8.2-3

FUEL ELEMENT INPUT VALUES TO MACABRE

	Core I Cases		Core II Cases
Element Position in Core	A-2	C-9	A-1
Total Coolant Flow (gpm)	2000	2000	1150
Element Flow Disparity, d_{f_p}	1.0167	0.9377	1.009
F_f	0.9487	0.9487	0.9205
Element Flow lb_m/sec	11.04	10.18	6.672
Total Reactor Power (MW)	5.0	5.0	2.5
Average Heat Flux in Reactor (BTU/hr-ft^2)	7.32×10^4	7.32×10^4	4.0×10^4
T_{inlet} (°F)	116	116	116

FIG. 8.2-1

TEMPERARATURE DISTRIBUTION FROM MACABRE FOR ELEMENT IN POSITION C-9
WITH A CORE I LOADING

reactor power: 5 MW
coolant flow: 2000 GPM
nominal channel dimensions
blades at 7.6 inches

wall temp.

plate 1, next to core
housing and control blade
slot

plate 10

channel bulk temp.

channel 10

channel between
core housing and plate 1

temperature (°F)

distance from bottom of fuel (inches)

TABLE 8.2-4

EXAMPLE OF FUEL PLATE TEMPERATURE GRADIENT

Channel A Bulk Coolant Temperature (°F)	Plate Surface Temperature on Channel A* (°F)	Plate Surface Temperature on Channel B* (°F)	Channel B Bulk Coolant Temperature (°F)
117.8	159.9	160.0	119.3
123.6	171.2	171.7	129.1
128.8	140.3	141.2	136.0
130.1	139.1	139.9	136.9

* Channels A and B are adjacent channels with one plate
between them. Plate surfaces A and B are the two
sides of this plate at the same axial height as the
given value of the bulk coolant temperature.

The predicted temperature distribution in A-2 and
A-1 are shown in Figs. 8.4-6 through 8.4-11 where they
are compared with the measured temperatures.

8.3 Temperature Measurements

Temperature measurements were made incore for both
steady-state and transient conditions. Transient
temperatures were measured as verification of natural
circulation cooling and are not included in this work.
The steady-state temperature measurements were made
for comparison with the predicted temperatures from the
power distribution measurements.

8.3.1 General Descriptions

Temperature measurements were made by inserting
stainless steel clad chromel-alumel type thermocouples
into various core positions. Measurements were made
at selected examples of each of the following:

1. Inlet plenum

2. Individual channel outlets

3. Element outlets

4. Fuel plate surfaces.

Figure 8.3-1 shows where thermocouples were inserted into
the Core I loading.

Leads from the incore thermocouples passed through an
open plug in the top shield lid to a data collection station

FIG. 8.3-1

CORE I THERMOCOUPLE PLACEMENT
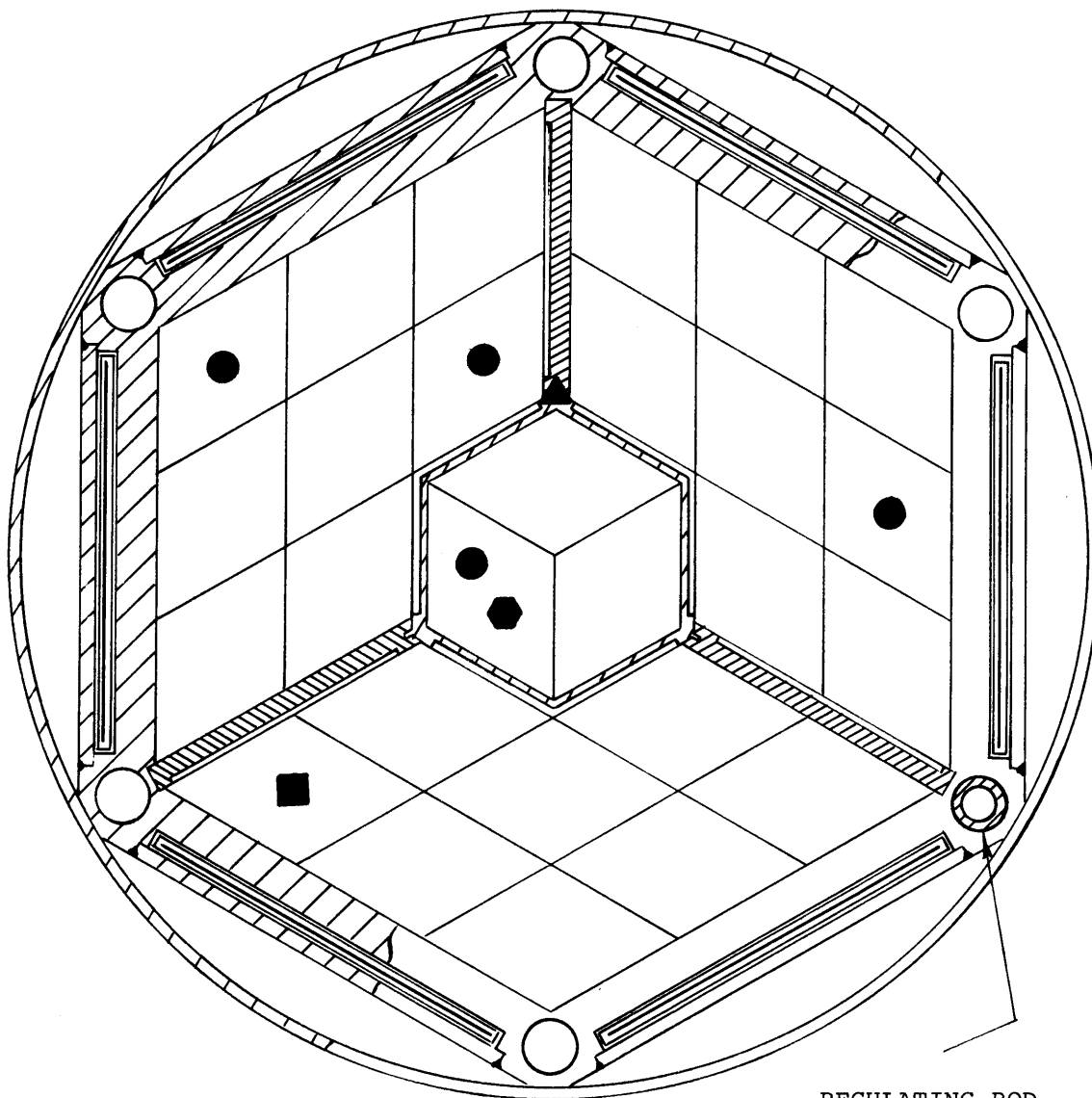
REGULATING ROD

● - fuel element outlet thermocouple

⬢ - fuel surface thermocouple element (4M42)

■ - fuel channel thermocouple element
    (thermocouples at 5 channel outlets)

▲ - inlet plenum thermocouple located at bottom of
    spider hole #3

Not shown:-thermocouple above natural circulation valve
          number 1
          -thermocouple at level of coolant outlet pipe

on the reactor top. The data collection station consisted of a switching arrangement, ice bath reference junction and digital voltmeter for measuring the thermocouple voltage. Standard tables (Ref. 8.3-1) were used to convert the measured voltage to a measured temperature reading. A strip chart recorder was used for transient measurements during natural circulation tests. Figure 8.3-2 shows a block diagram of the thermocouple wiring setup.

One problem that existed in all temperature measurements was an uncertainty in the total reactor power because of disagreement between the core ΔT measurements. The reactor was always operated in a conservative manner so that the licensed limit on power would not be exceeded. The power level for all of the temperature comparisons was based on the reactor power calculated using the primary flow - ΔT recorder in the control room, since this was later found to give the more accurate value (based on calibration against a standard). For purpose of computing the temperature rises, the inlet temperature was obtained by using the inlet plenum thermocouple. Because the thermocouples mounted on the fuel plate surfaces were grounded, their temperature readings fluctuated somewhat when compared with the other ungrounded thermocouples.

FIG. 8.3-2

THERMOCOUPLE WIRING BLOCK DIAGRAM

ice-water
reference
junction

digital
voltmeter

terminal strip

switch

terminal strip

individual
thermocouples

hot junctions

————both wires

— — —one wire
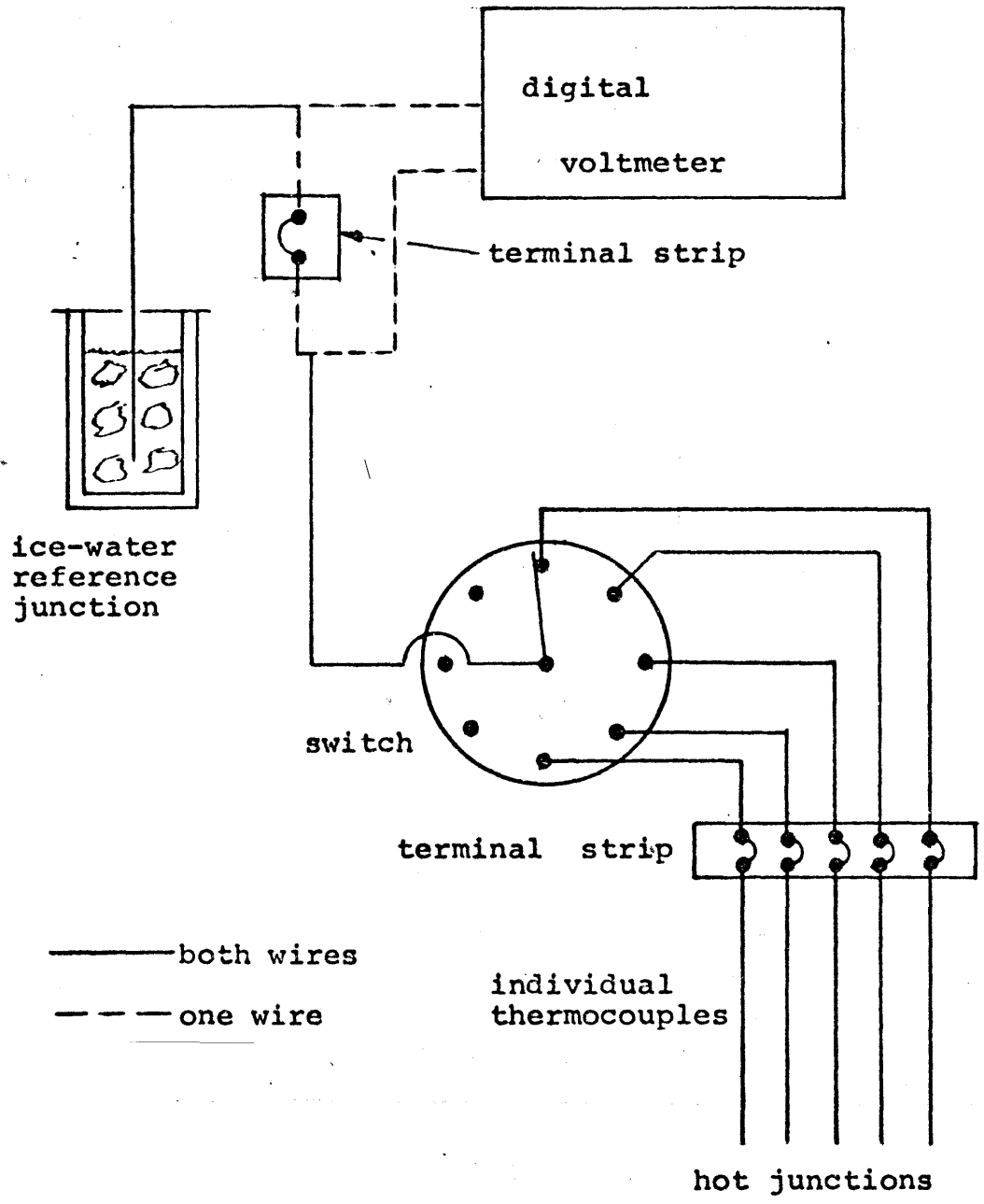
8.3.2 Fuel Element Outlet Temperatures

Figure 8.3-3 shows a fuel element outlet thermocouple holder. Holders of this type were positioned over the outlets of the elements in A-2, B-6, C-8, and C-14 in Core I and above A-1 in Core II. The main problem in the holder design was to affix the holder so that it could not possibly break free during operating conditions and yet would have minimum effect on the element flow. The thermocouple tip is positioned in the element exit plenum but its proximity to the channel exits may mean that the measured temperature may not be the mixed mean element outlet temperature. Table 8.3-1 shows the measured element temperature rise for several reactor powers.

8.3.3 Channel Outlet Temperatures

Thermocouples were positioned at the center of the discharge ends of 5 coolant channels in one fuel element in an attempt to measure the mixed channel outlet temperatures of several coolant channels. A special channel outlet thermocouple holder was constructed to position the thermocouples.

8.3.3.1 Channel Outlet Thermocouple Holder

A channel outlet thermocouple holder was designed to optimize the following requirements:

FIG. 8.3-3

FUEL ELEMENT OUTLET
THERMOCOUPLE HOLDER

12 feet long

fuel element end
nozzle bale
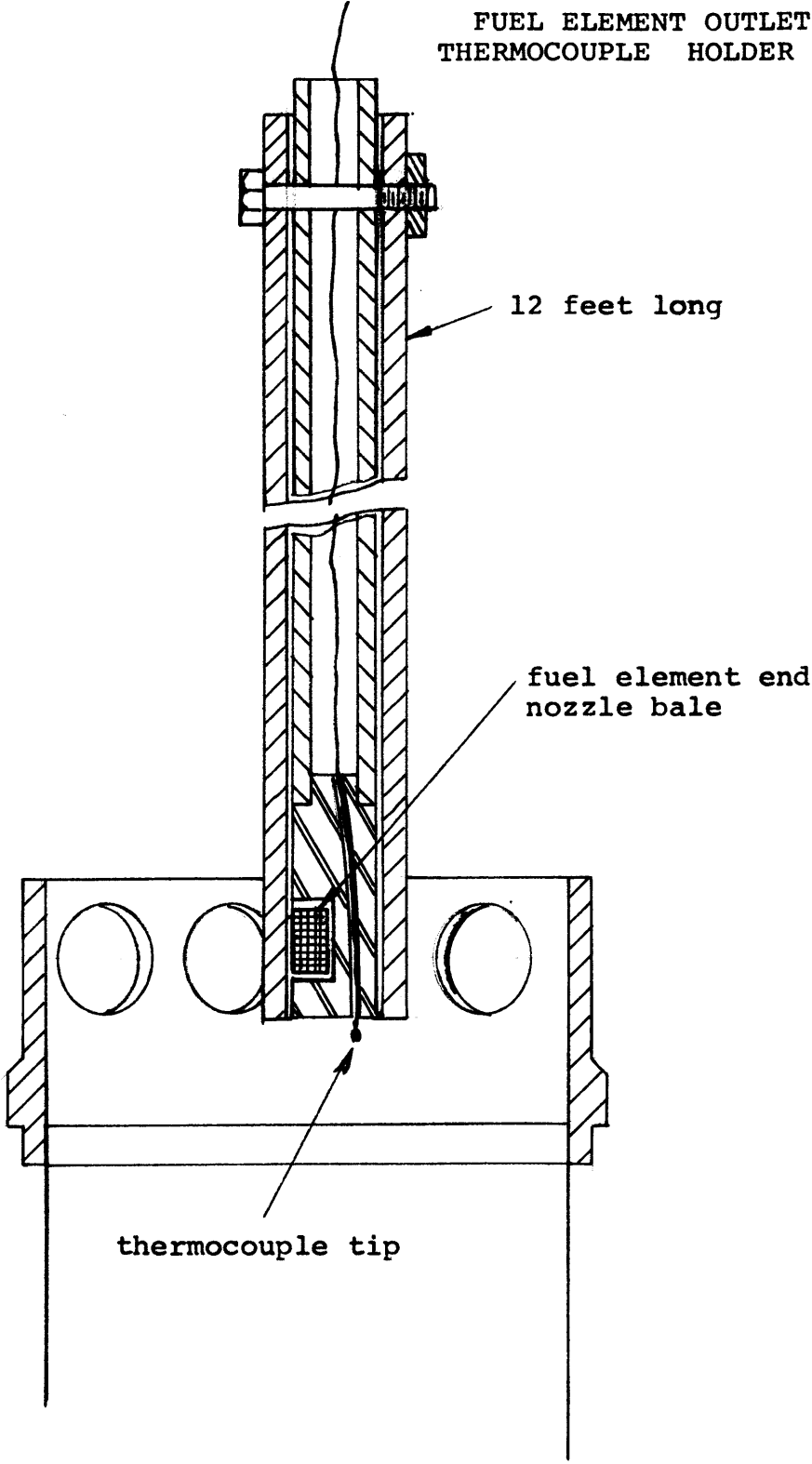
thermocouple tip

TABLE 8.3-1

MEASURED FUEL ELEMENT OUTLET TEMPERATURE RISE

Core I

Case	1	2	3	4
Nominal Power Listed in Reactor Log (MW)	2.5	3.0	3.5	4.0
Power Based on Incore Thermocouples 11 and 19 (MW)*	2.3	2.9	3.3	3.6
Power Based on Flow - ΔT Recorder (MW)	2.1	2.6	2.9	3.1
Coolant Inlet Temperature for Case (°F)	92.6	92.9	91.0	89.3
Temperature Rise in Position A-2 (°F)	7.2	8.6	10.0	11.2
Temperature Rise in Position B-6 (°F)	12.5	14.9	17.4	19.2
Temperature Rise in Position C-8 (°F)	8.5	10.2	12.0	12.9
Temperature Rise in Position C-14 (°F)	9.1	11.5	13.0	14.3

* T/C #11 at bottom of spider hole #1, T/C #19 in upper pool at level of outlet pipes.

TABLE 8.3-1 (Continued)

Core II*

Case	1	2	3	4
Nominal Power Listed in Reactor Log (MW)	1.0	1.75	2.5	2.5
Power Based on Incore Thermocouples 11 and 19 (MW)	1.0	1.66	2.27	2.31
Power Based on Flow - ΔT Recorder (MW)	0.88	1.45	1.9	1.9
Coolant Inlet Temperature for Case (°F)	92.8	92.0	103.8	104.0
Temperature Rise in Position A-1 (°F)	7.7	12.5	15.0	15.1

* 1 Pump Operation

A. Device attachments must have minimal effect on element or channel flow,

B. Device must be firmly attached to the fuel element end nozzle to prevent motion during operation,

C. Device must in no way cause damage to fuel plates or fuel element,

D. Device must be completely removable from irradiated element to allow normal use of element upon completion of the measurements.

Figure 8.3-4 shows the thermocouple holder positioned on a fuel element. Thermocouples were positioned at the discharge of channels 2, 5, 8, 12, and 15. Because the thermocouple holder had to be attached to the fuel element prior to being loaded into the core, the positions where the element could be loaded were restricted by the motion required to return the hold down grid plate to the locked condition. The possible fuel positions were limited to C-5, C-6, B-3, B-4, A-1, A-2, or A-3. The element was loaded into position C-5 for Core I with channel 2 set to be the second channel from the outside wall of the core housing. The channel outlet thermocouple holder was removed from the core prior to the Core II loading.

8.3.3.2 Temperature Data

Channel outlet temperatures were measured in 5 channel discharges of element C-5. Table 8.3-2 shows the measured channel temperature rise for several reactor powers. The measured temperature values are compared to the predicted values in Section 8.4.

extension to reactor top

ball joint

bale clamp
release
mechanism

thermocouple position
clamp

thermocouples (1/16 in. -
stainless
steel clad)

fuel element
end nozzle
bale

tip of thermo-
couple is positioned
above fuel meat
between plates
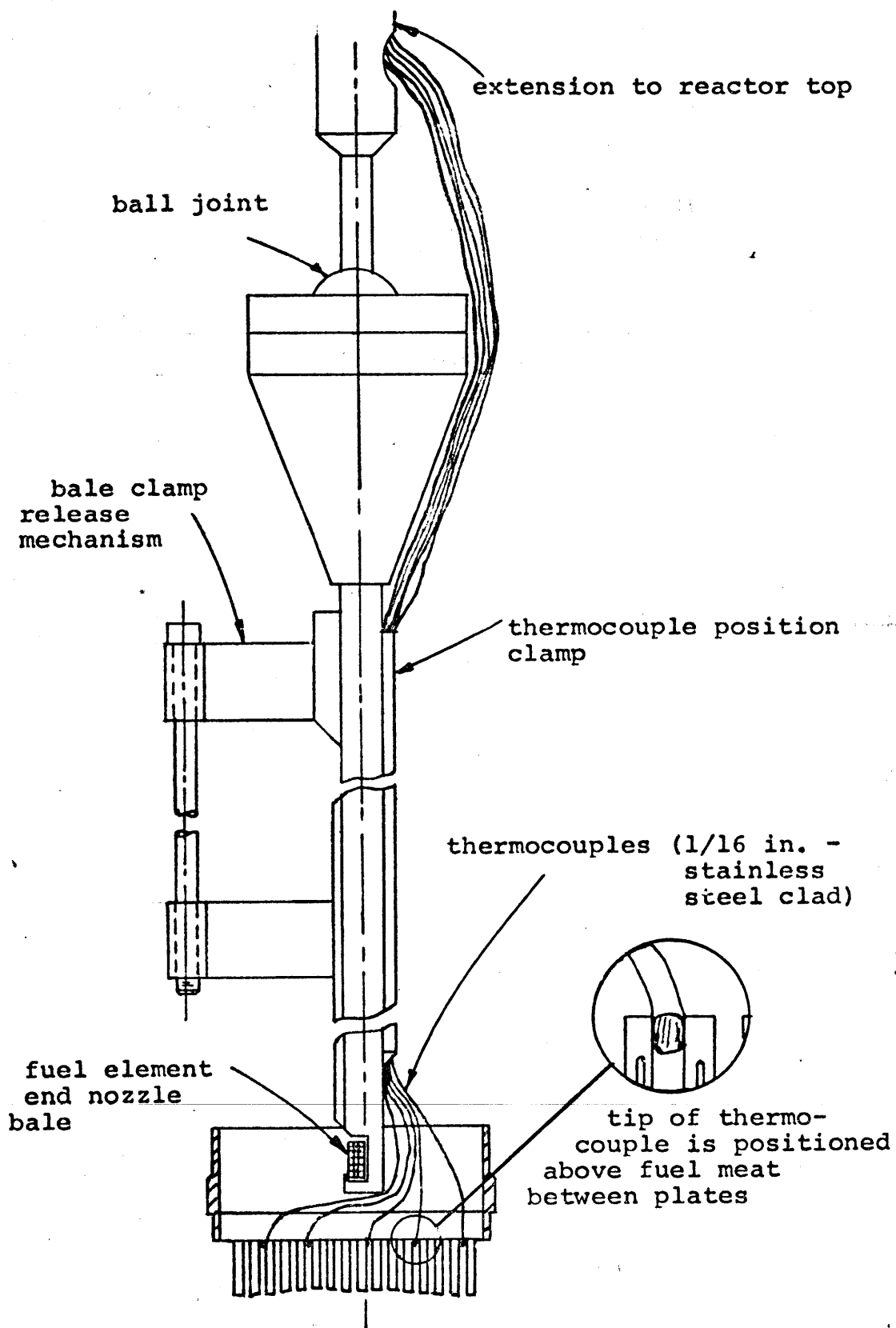
FIG. 8.3-4

COOLANT CHANNEL OUTLET
THERMOCOUPLE HOLDER

TABLE 8.3-2

MEASURED COOLANT CHANNEL TEMPERATURE RISES IN
ELEMENT POSITION C-5 FOR CORE I

Case	1	2	3	4
Nominal Power Listed in Reactor Log (MW)	2.5	3.0	3.5	4.0
Power Based on Incore Thermocouples 11 and 19 (MW)	2.3	2.9	3.3	3.6
Power Based on Flow - ΔT Recorder (MW)	2.1	2.6	2.9	3.1
Coolant Inlet Temperature for Case (°F)	92.6	92.9	91.0	89.3
Temperature Rise in Channel 2 (°F)	14.0	17.1	19.9	21.9
Temperature Rise in Channel 5 (°F)	10.4	12.6	14.9	16.1
Temperature Rise in Channel 8 (°F)	8.8	10.4	12.7	13.3
Temperature Rise in Channel 12 (°F)	7.6	8.9	10.9	11.6
Temperature Rise in Channel 15 (°F)	7.9	9.2	11.3	12.2

8.3.4 Fuel Element Surface Temperature Measurements

Steady-state fuel plate surface temperature measurements were made by using a "Thermocouple fuel element". The "Thermocouple fuel element" was inserted into position A-2 for the initial Core I loading. A comparison between the measured and predicted temperatures is found in Section 8.4.

8.3.4.1 Thermocouple Fuel Element

A special thermocouple instrumented fuel element (4M42), shown in Fig. 8.3-5 and hereafter called the thermocouple fuel element, was constructed by Gulf United Nuclear Fuels (GUNF) as part of the first order for the MITR-II. The thermocouple fuel element is identical with other first core elements with the following exceptions:

A. Thermocouples are crimped between the fins at several plate locations,

B. The top end nozzle is screwed on rather than being welded,

C. A holding pad for the thermocouple leads is located in the top end nozzle.

Stainless steel clad, chromel-alumel thermocouples which were 0.010 inches in diameter and 18 feet long were supplied to GUNF prior to fabrication of the thermocouple element. The thermocouple tips were crimped between the fins at specified locations on fuel plate surfaces on the element. Radiographs had

FIG. 8.3-5

THERMOCOUPLE ELEMENT DETAIL

element number on
top end of this side

T/C-#3

(top end)

xyz

T/C-#4
T/C-#3
T/C-#2

wires fastened
to pad on this
side of inside
of top nozzle

1

plate
#

15

element viewed
from bottom

T/C-#1

0.100

0.230

mounting detail of
thermocouple #3
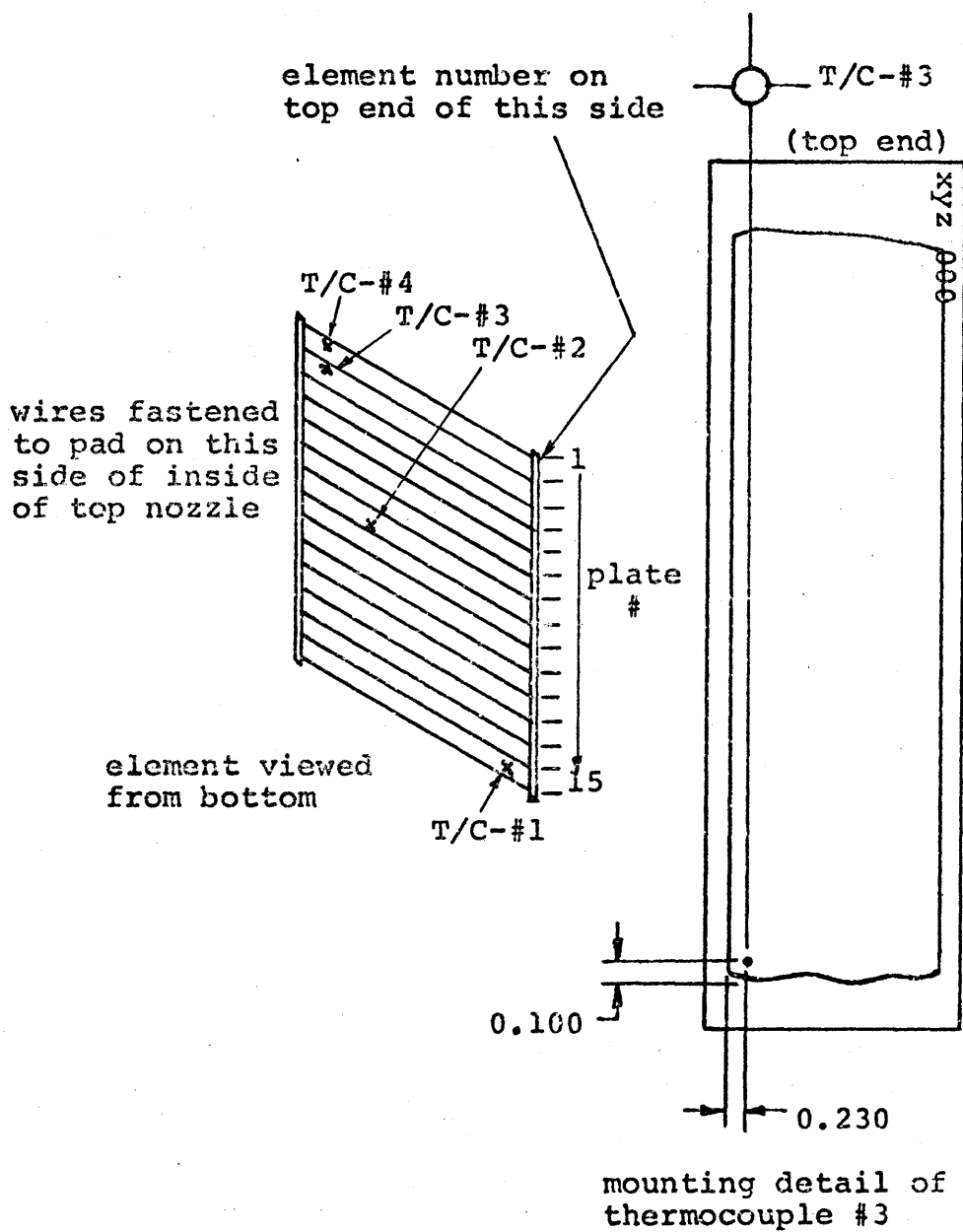
been taken of each plate to which thermocouples were
attached so that the tip position relative to the fuel
meat would be accurately known. Thermocouple leads
were staked between the fins at several locations as
they passed up to the top end of the fuel plate. With
the thermocouple attached, the fuel plates were swaged
into the fuel element. The thermocouple leads were
fed through the upper end nozzle which was then screwed
in position. In the upper end nozzle, the thermocouple
leads were firmly held in position by a holding pad.
Because of the fragility of the 0.010 inch thermocouples,
only four thermocouples remained operable when the
element was loaded into the reactor. Table 8.3-3
shows the positions of the four operable thermocouples
for each core loading. With the thermocouple element
loaded in an incore position, the leads extended from
the holding pad and out of the core region and top
shielding to a data collection station. Because of
the rotating upper grid, the only possible positions
where the thermocouple element could be inserted were
A-1, A-2, A-3, B-3, B-4, C-5, and C-6.

8.3.4.2 Thermocouple Attachment Calibration

The temperature measured by a thermocouple in the
thermocouple element, relative to the actual fuel sur-
face temperature, depends upon the thermocouple attachment

TABLE 8.3-3

OPERABLE THERMOCOUPLE POSITIONS ON THERMOCOUPLE ELEMENT

Core I

T/C#	Element Position	Position of Thermocouple Tip in Element
1	A-2	On inside surface of plate 15 (15th plate from solid dummy in A-1) toward element in A-3 located 4 inches from bottom edge of fuel meat.
2	A-2	On center plate in element (plate 8) toward hexagonal spider located 0.1 inch from bottom edge of fuel meat.
3	A-2	On plate 2 in channel 3 (2nd plate from solid dummy in A-1) toward hexagonal spider located 0.1 inch from bottom edge of fuel meat.
4	A-2	On plate 1, channel 2 side (1st plate, 2nd channel from solid dummy in A-1) toward hexagonal spider 0.1 inch from bottom edge of fuel meat.

Core II

1	A-1	On inside surface of plate 15 (plate 15 is next to solid dummy in A-3) toward hexagonal spider located 4 inches from bottom edge of fuel meat.
2	A-1	On center plate in element (plate 8) towards dummy in A-2 located 0.1 inch from bottom edge of fuel meat.
3	A-1	On plate 2 in channel 3 (2nd plate from hexagonal spider separating from B-1) toward A-2 located 0.1 inch from bottom edge of fuel meat.
4	A-1	On plate 1 in channel 2 (1st plate next to hexagonal spider by B-1) toward A-2 located 0.1 inch from bottom edge of fuel meat.

effectiveness. Figure 8.3-6 shows an example of a "proper" attachment and a "poor" attachment. A properly attached thermocouple will read a temperature that is close to the actual surface temperature while a poorly attached thermocouple will read a temperature that is closer to the bulk coolant temperature. The response of fuel surface thermocouples was studied by Szymczak (Ref. 8.3-2) in experimental heat transfer studies of MITR-II coolant channels.

In order to estimate the difference between the surface temperature and the observed thermocouple temperature, the attachment effectiveness must be determined. Szymczak developed the curves shown in Fig. 8.3-7 which characterized well and poorly installed thermocouples. In Fig. 8.3-7 a thermocouple installation factor, I, is plotted against the experimental ηh where the factors are defined as follows:

$$I = \frac{T_o - T_f}{Q/A} \quad , \quad (8.3-1)$$

where,

Q/A is surface heat flux at thermocouple location (BTU/hr - ft^2),

T_o is the temperature observed by the thermocouple (°F)

T_f is the bulk fluid temperature at the thermocouple location (°F),

η is the fin effectiveness,

h is the heat transfer coefficient obtained using the Boelter correlation (BTU/hr - ft^2 -°F).

FIG. 8.3-6

FUEL SURFACE THERMOCOUPLE DETAILS
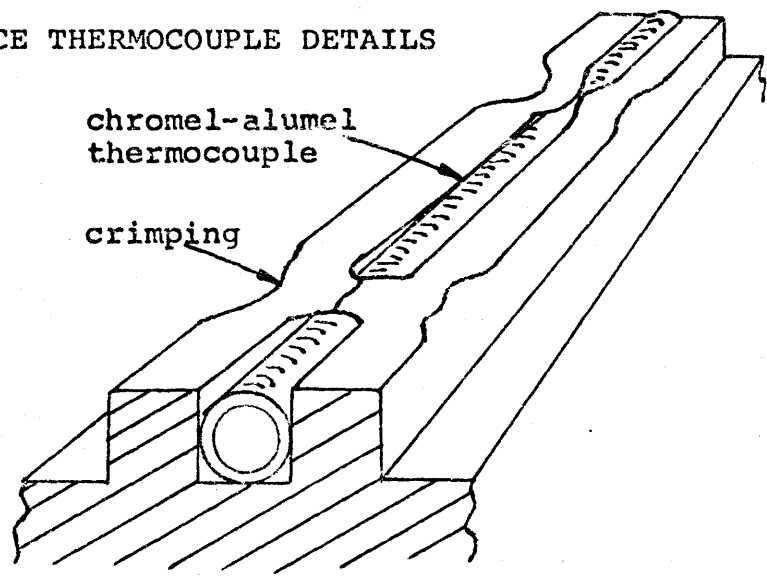
(A) staked fuel surface thermocouple
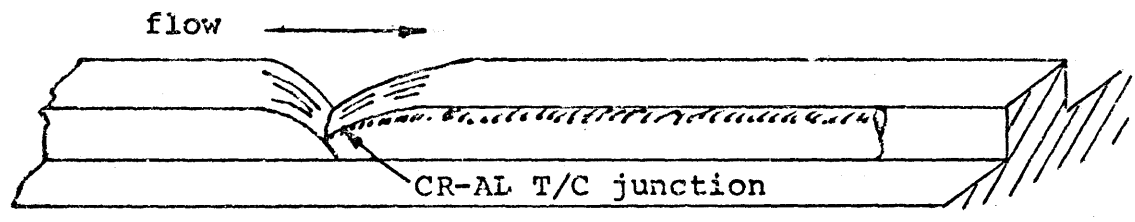
(B) properly crimped fuel surface
thermocouple junction
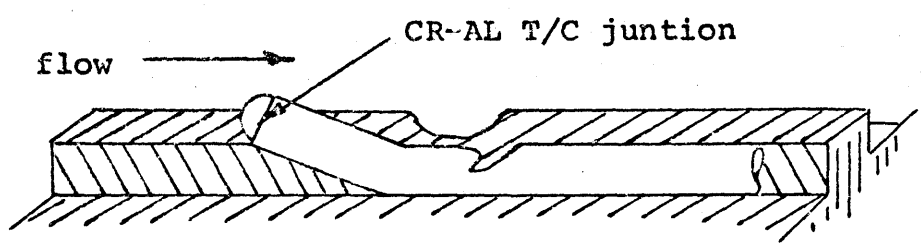
(C) improperly crimped fuel surface
thermocouple junction

FIG. 8.3-7

THERMOCOUPLE INSTALLATION FACTOR

Installation factor, $I = \dfrac{T_o - T_f}{Q/A} \times 10^5$

nh x 10^{-3} (BTU/HR-FT^2-°F)

good thermocouple
installation

poor thermocouple
installation

increasing — — — ➤
values of nh

⬡ – T/C-#1
● – T/C-#2
▪ – T/C-#3
▲ – T/C-#4
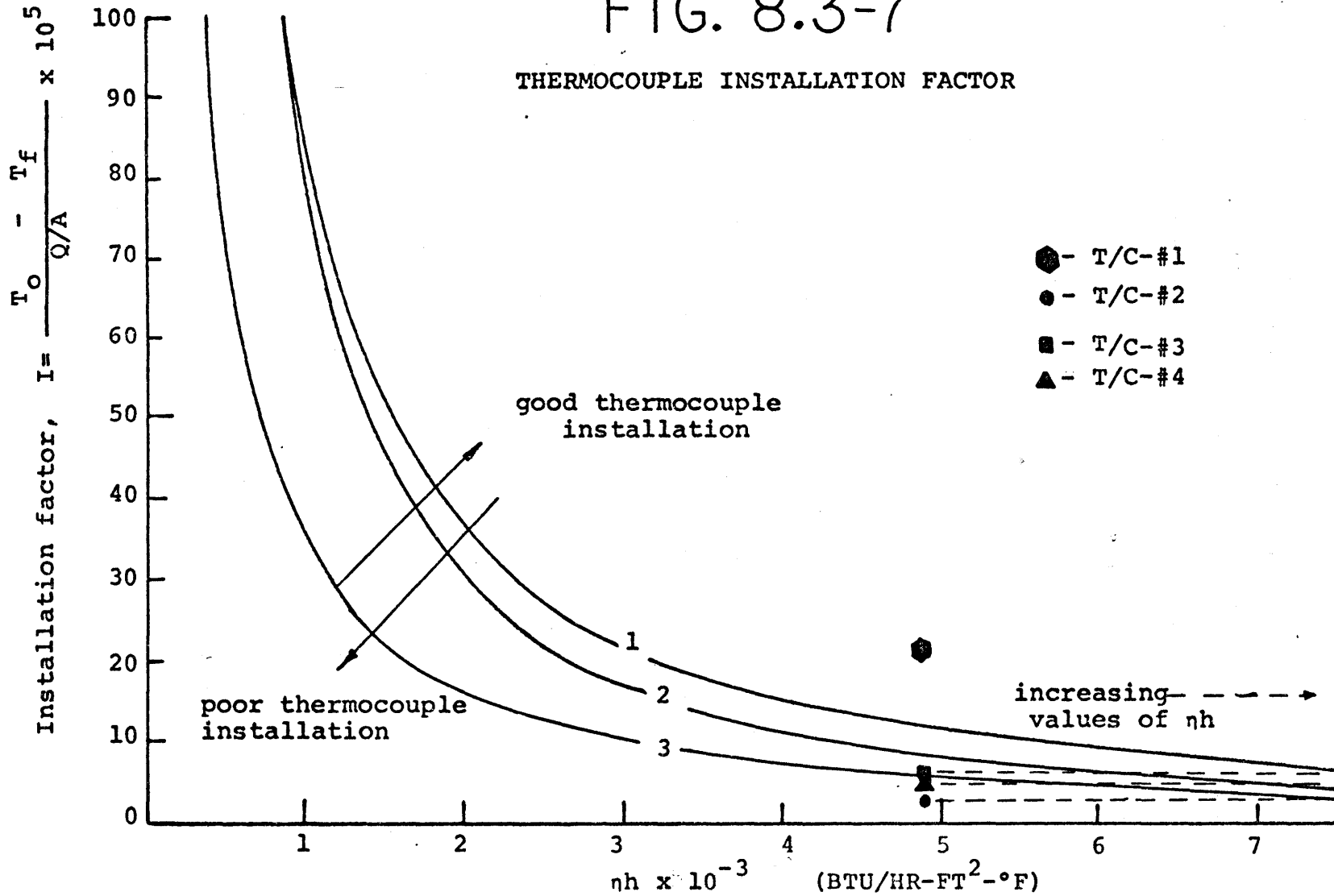
A well installed thermocouple will yield values that lie to the right of curve 1, whereas, a poorly installed thermocouple will yield values that will be in the region of curve 3. The following table lists the values of I obtained for the 4 thermocouples in the thermocouple element based on measured temperatures in Core I at a flow of 2000 gpm.

TABLE 8.3-4

INSTALLATION FACTORS FOR THERMOCOUPLES IN
THERMOCOUPLE ELEMENT

Thermocouple Number	1	2	3	4
Installation Factor, I	21.13	3.42	6.12	5.6

$$\eta h = 4.91 \times 10^3 \text{ BTU/hr-ft}^2\text{-}°F$$

The points are all plotted on Fig. 8.3-7 at the appropriate value of ηh (value for fully developed flow in Core I channel). Thermocouple 1 is clearly shown to be very well installed. Thermocouples 3 and 4 appear to be fairly installed and thermocouple 2 appears to be very poorly installed. These results are somewhat surprising in view of the great care that GUNF used in assembling the thermocouple element and it was expected that all thermocouples would be well installed. The results may not be due to the properness of the thermocouple installation.

Thermocouples 2, 3, and 4 are different from thermocouple 1 in that the former are all on the bottom edge of the fuel meat while the latter is located 4 inches up the plate. The experimentally determined value of I, may be low if the actual heat flux, Q/A, is lower than that used to determine I (Q/A is obtained by the product, $F_r \times F_a \times$ average heat flux, for values of F_r, F_a at that point) or if the actual value of ηh is greater than the one used to determine I. The following effects may be causing a lower than expected Q/A or higher than expected ηh for the thermocouples at the plate tips:

1. Entrance effect increases ηh,

2. Thermocouple is located below fuel meat,

3. Density of fuel at thermocouple location is lower than expected,

4. Axial conduction in fuel plate is high.

   Entrance region effects may cause a higher value of ηh for the thermocouples at the bottom edges than was used in plotting the installation factors in Fig. 8.3-7. The values of ηh used in Fig. 8.3-7 were based on a fully developed flow model. The heat transfer coefficient, h, is directly proportional to the Nusselt number and the ratio of the mean Nusselt number in the entrance region to the Nusselt number for fully developed flow, may be approximated by the following expression (Ref. 8.3-3):

$$\frac{Nu_m}{Nu_\infty} = 1 + \frac{C}{L/D} \quad , \qquad\qquad (8.3-2)$$

where,

L   is the distance from the channel entrance
to the point of interest,

D   is the effective diameter of the channel,

C   is a channel-coolant parameter which is a
function of Reynolds number, Prandtl number,
and entrance geometry,

Nu_m is the mean Nusselt number at a distance
L from the entrance,

Nu_∞ is the fully developed Nusselt number.

For the channel and coolant conditions of the MITR-II, the

value of parameter C will be in the range of 1.5 to 5.

Since several fuel surface thermocouple tips are located a

distance approximately 5 length to diameter ratios from

the channel entrance, the Nusselt number at those tip

locations may be a factor of 1.3 to 2.0 higher than the

Nusselt number for fully developed flow. A higher

Nusselt number (and thus a higher value of h) would have

the effect of shifting the plotted installation points for

thermocouples 2, 3, and 4 to the right along the dotted

lines shown in Fig. 8.3-7. This shift to the right would

bring those thermocouples into the classification of being

well installed.

Radiographs of the fuel plates were used by GUNF to

position the thermocouple tips and thus, it is unlikely

but not impossible that the thermocouple junction is

located below the fuel meat. However, it is highly probable that the fuel density at the thermocouple location is lower than expected. Figure 8.3-8(A) shows the expected density distribution that was assumed in calculating values of F_a from scanning data. Fuel plate radiograph densitometer readings shown in Figs. 5.3-2 through 5.3-6 show that actual fuel plate density at the end of the plate may look like (B) in Fig. 8.3-8. One potential fuel density distribution that caused much concern in the safety analysis of the MITR-II is called the "dogbone" and is (C) in Fig. 8.3-8. Fuel density distributions as shown in (B) and (C) may yield a lower fuel density than expected at the thermo-couple location (for the "dogbone", remember that the thermocouple tip is 0.1 inch from beginning of fuel meat) and thus, the actual heat flux may be lower than expected. During evaluation of the plate scanning data it was observed that the power density at the tip of the fuel meat dropped off faster than could be explained by collimator area averaging, and thus, it appeared that the fuel density decrease shown in the radiographs was real and caused lower power densities than originally expected. However, in the plate scanning evaluation of F_a, an extrapolation was used to determine F_a which neglected this power decrease.

FIG. 8.3-8

FUEL EDGE URANIUM DENSITY DISTRIBUTION
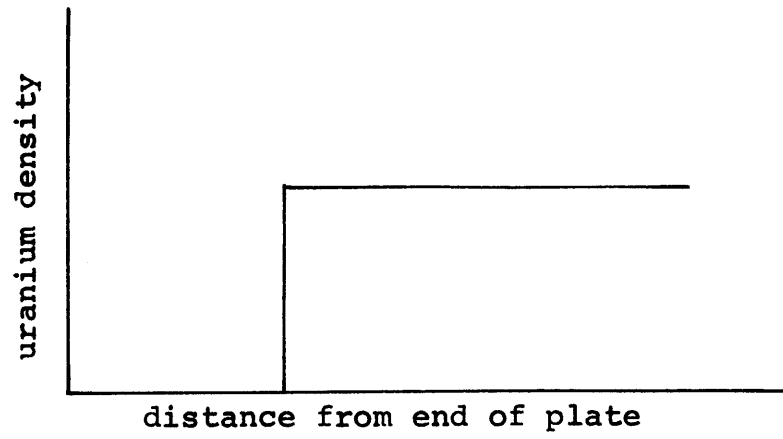
(A) assumed distribution
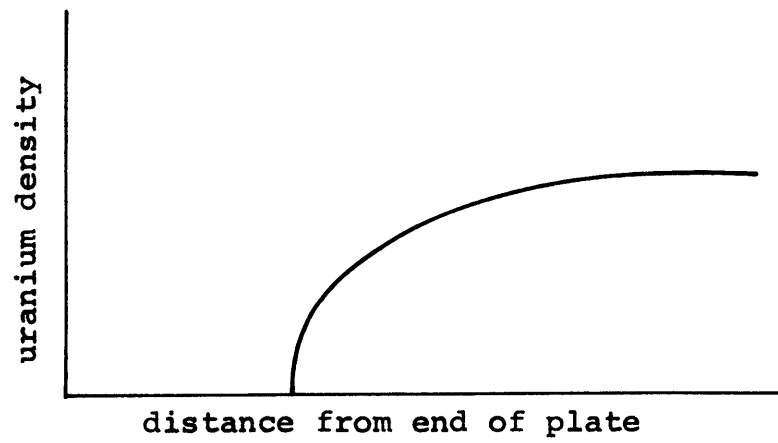
(B) apparent distribution
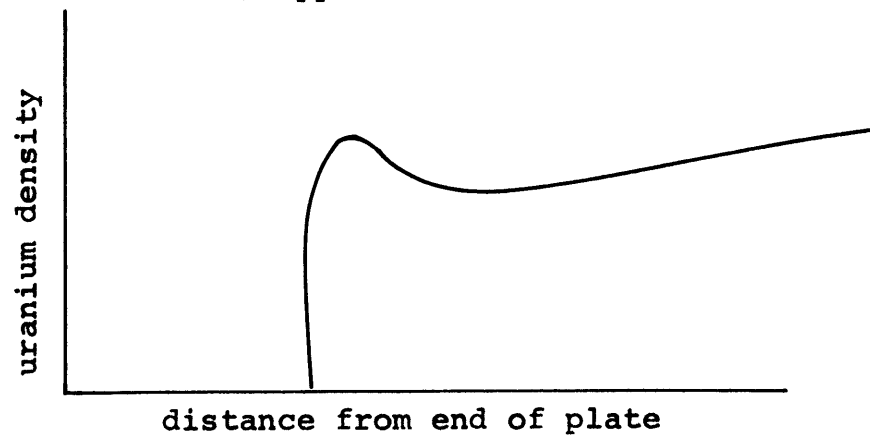
(C) dogbone distribution

The high thermal conductivity of aluminum may also cause lower heat fluxes at the plate end than expected because of heat transfer out the plate end. Axial thermal conductivity was conservatively neglected in calculating fuel plate edge temperatures.

Thus, the thermocouples at the fuel plate lower edges are probably well installed, but conservative assumptions used in determining the heat fluxes and temperatures at the channel entrances result in the thermocouples appearing to be only fairly or poorly installed. The thermocouples at the lower edge give lower than expected plate temperatures because the temperatures are lower than the conservative expected values. Thermocouples 3 and 4 give comparable values of I while the value for 2 is even lower. Thermocouple 2 may indeed be a poor thermocouple because of some data irregularities and spurious results for that particular thermocouple.

The actual wall surface temperature is obtained from the measured wall temperature by knowing a calibration factor. The calibration factor, Z_c, used by Szymczak (Ref. 8.3-2) is defined as follows:

$$Z_c = \frac{T_w - T_o}{T_w - T_f} \quad , \qquad (8.3-3)$$

where,

T_w is the actual surface temperature,

T_o is the temperature measured by the thermocouple,

T_f is the bulk fluid temperature at the thermo-couple tip elevation.

The calibration factor is plotted against ηh in Fig. 8.3-9 for different curves which depend on how well the thermocouple is attached. These curves were generated by summarizing several curves made by Szymczak. Note that for lower values of ηh which would exist in natural circulation cooling, the thermocouples will read close to the actual wall temperature even if they are poorly installed. For Core I and Core II fully developed values of ηh, values of Z_c are summarized in Table 8.3-5. By knowing Z_c and the installation characteristics, the actual wall temperature can be determined.

TABLE 8.3-5

CORE I AND CORE II THERMOCOUPLE CALIBRATION FACTORS

	Core I Z_c ($\eta h = 4.91 \times 10^3$)	Core II Z_c ($\eta h = 3.0 \times 10^3$)
Well Installed	0.4	0.32
Fairly Installed	0.62	0.52
Poorly Installed	0.83	0.77

8.3.4.3 Temperature Data

Tables 8.3-6 and 8.3-7 give representative temperature data for the thermocouples on the thermocouple element for Core I and II, respectively. The data has been normalized

FIG. 8.3-9

THERMOCOUPLE CALIBRATION FACTOR

$z_c = \dfrac{T_W - T_O}{T_W - T_f}$

calibration factor, z_c

$\eta h \times 10^{-3}$ (BTU/HR-FT^2-°F)

poorly installed

fairly installed

well installed
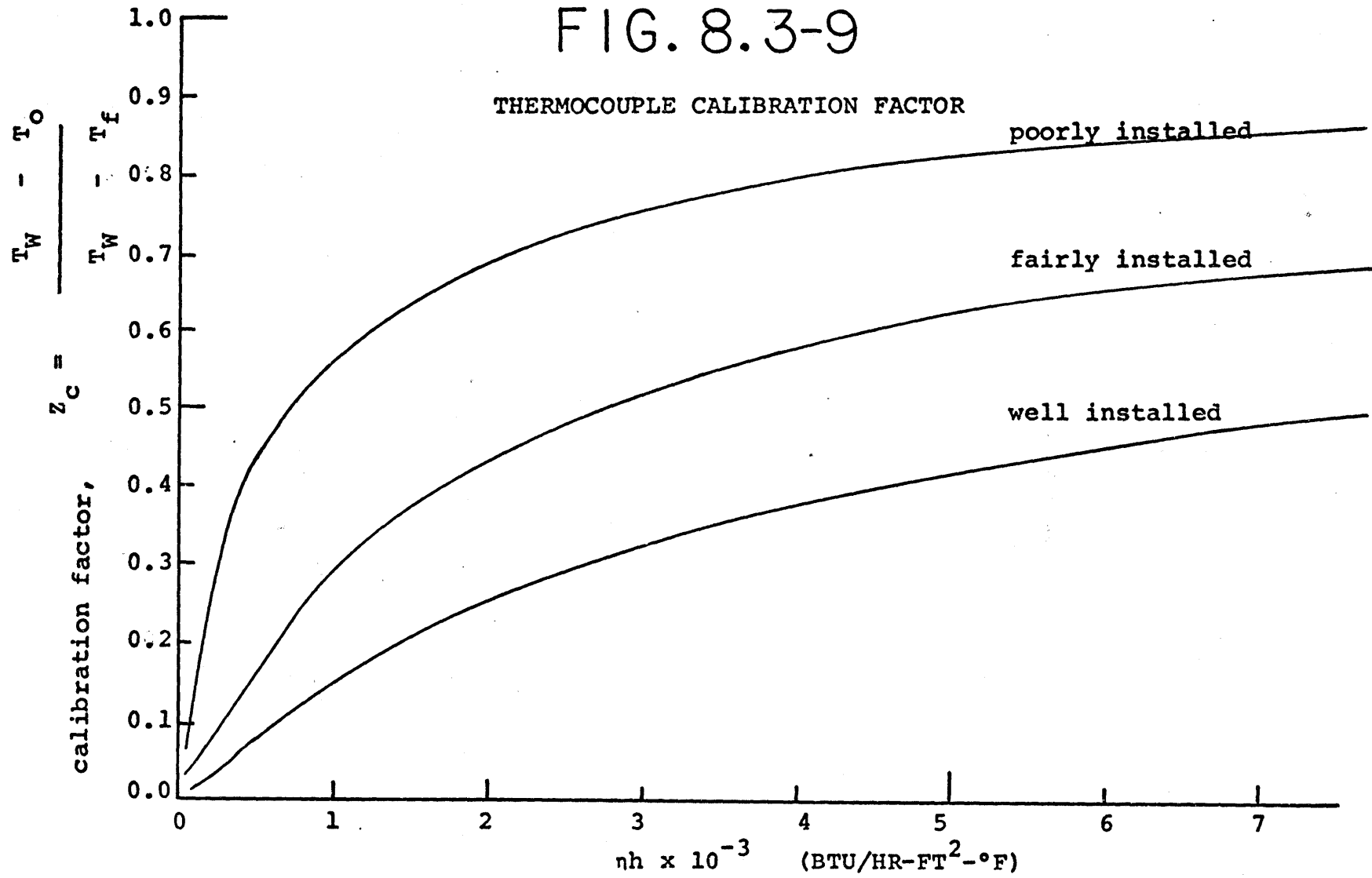
TABLE 8.3-6

CORE I THERMOCOUPLE ELEMENT RESULTS

Fuel Plate Surface Temperature Rise above
Coolant Inlet Temperature

Case	1	2	3	4
Nominal Power Recorded in Reactor Log (MW)	2.5	3.0	3.5	4.0
Reactor Power Calculated from Incore Thermocouples 11 and 19 (MW)	2.3	2.9	3.3	3.6
Reactor Power Calculated from Primary Flow - ΔT Recorder (MW)	2.1	2.6	2.9	3.1
Coolant Inlet Temperature (°F)	92.6	92.9	91.0	89.3
Thermocouple #1 $(T_o - T_{inlet})$ °F	9.1	11.2	15.2	16.9
Thermocouple #2 $(T_o - T_{inlet})$ °F	1.1	1.7	3.6	4.8
Thermocouple #3 $(T_o - T_{inlet})$ °F	4.5	5.0	8.0	9.8
Thermocouple #4 $(T_o - T_{inlet})$ °F	4.3	5.0	7.8	9.3

TABLE 8.3-7

CORE II THERMOCOUPLE ELEMENT RESULTS

Fuel Plate Surface Temperature Rise above
Coolant Inlet Temperature*

Case	1	2	3	4
Nominal Power Recorded in Reactor Log (MW)	1.0	1.75	2.5	2.5
Reactor Power Calculated from Incore Thermo- couples 11 and 19 (MW)	1.0	1.66	2.27	2.5
Reactor Power Calculated from Primary Flow - ΔT Recorder (MW)	0.88	1.45	1.9	1.9
Coolant Inlet Temperature (°F)	92.8	92.0	103.8	104.0
Thermocouple #1 $(T_o - T_{inlet})$, °F	3.3	7.9	9.2	9.7
Thermocouple #2 $(T_o - T_{inlet})$, °F	0.0	0.9	0.0	0.0
Thermocouple #3 $(T_o - T_{inlet})$, °F	0.0	1.7	0.6	0.9
Thermocouple #4 $(T_o - T_{inlet})$, °F	0.0	2.1	1.3	1.62

*   (Core II values for 1 pump operation)

to be the temperature rise at the thermocouple location above the bulk inlet temperature. The quantity, $T_o - T_{inlet}$, is the difference between the observed thermocouple temperature reading, T_o, and the bulk inlet temperature reading, T_{inlet}, for that case.

The temperature data is plotted versus reactor power (measured using Primary flow - ΔT recorder, in Figs. 8.3-10 and 8.3-11 for core I and Core II, respectively. The data is extrapolated to a reactor power of 5 megawatts for Core I and 2.5 megawatts for Core II.

The extrapolated temperature values of the fuel surface thermocouples are listed in Tables 8.3-8 and 8.3-9 for Core I and II, respectively. These values are used to obtain the values of $(T_w - T_f)$ for several calibration factors where T_f is the bulk fluid temperature at the thermocouple tip location and T_w is the fuel plate wall temperature. The value of $(T_o - T_{inlet})$ is changed to $(T_o - T_f)$, by subtracting $T_f - T_{inlet}$. The value of $T_f - T_{inlet}$ is obtained by performing a heat balance in the coolant channel between the channel entrance and the tip elevation. $(T_w - T_f)$ is obtained by knowing Z_c and $(T_o - T_f)$. Taking Eq. 8.3-3 for Z_c:

$$Z_c = \frac{(T_w - T_o)}{(T_w - T_f)} \qquad , \qquad (8.3-3)$$

FIG. 8.3-10

CORE I MEASURED FUEL SURFACE TEMPERATURES IN POSITION A-2

FIG. 8.3-11
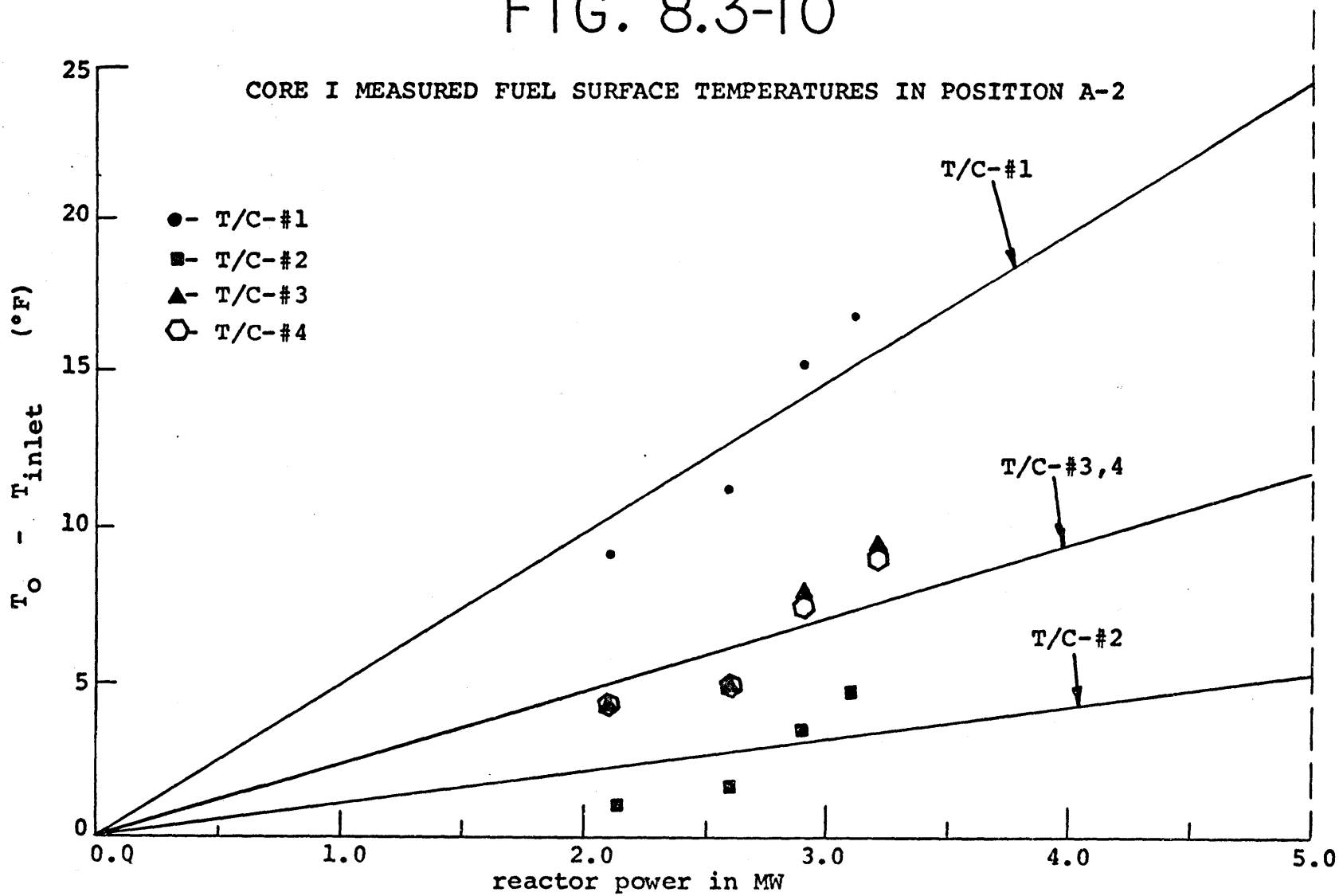
CORE II MEASURED FUEL SURFACE TEMPERATURES IN POSITION A-1
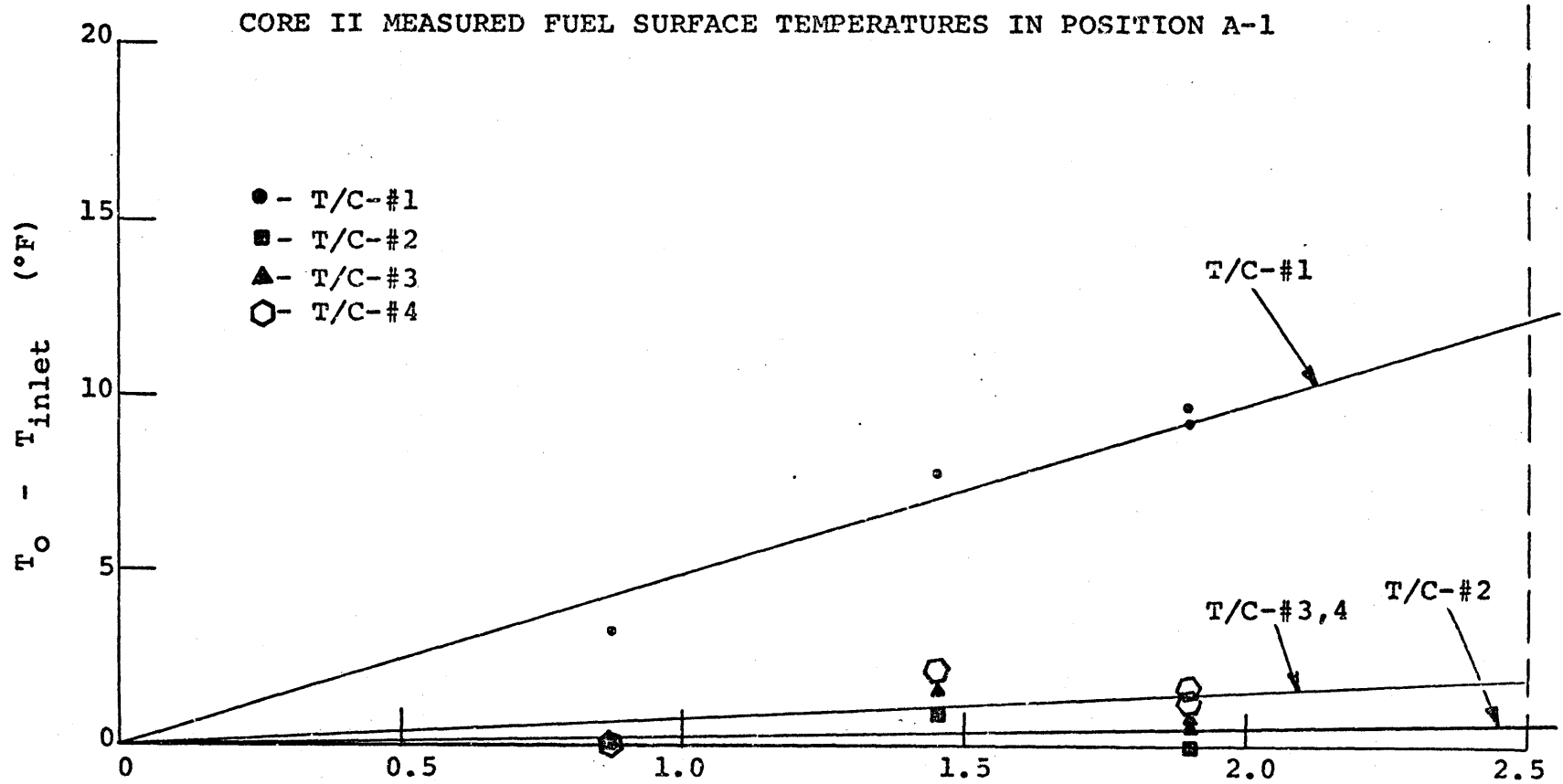
TABLE 8.3-8

CORE I FUEL SURFACE THERMOCOUPLE VALUES OF $T_w - T_f$ FOR SEVERAL CALIBRATION FACTORS, Z_c

Thermocouple Number	$T_o - T_{inlet}$ @5 MW (°F)	$T_f - T_{inlet}$ @5 MW (°F)	$T_o - T_f$ @5 MW (°F)	$(T_w - T_f)$* $Z_c = 0.4$ (°F)	$(T_w - T_f)$** $Z_c = 0.62$ (°F)	$(T_w - T_f)$*** $Z_c = 0.83$ (°F)
1	24.5	5.7	18.8	31.3	49.5	110.6
2	5.3	0.2	5.1	8.5	13.4	30.0
3	11.8	0.25	11.55	19.25	30.4	67.9
4	11.8	0.25	11.55	19.25	30.4	67.9

* Well installed

** Fairly installed

*** Poorly installed

TABLE 8.3-9

CORE II FUEL SURFACE THERMOCOUPLE VALUES OF
$T_w - T_o$ FOR SEVERAL CALIBRATION FACTORS, Z_c^+

Thermocouple Number	$T_o - T_{inlet}$ @2.5 MW (°F)	$T_f - T_{inlet}$ @2.5 MW (°F)	$T_o - T_f$ @2.5 MW (°F)	$(T_w - T_f)$* $Z_c = 0.32$ (°F)	$(T_w - T_f)$** $Z_c = 0.52$ (°F)	$(T_w - T_f)$*** $Z_c = 0.77$ (°F)
1	12.3	3.5	8.8	12.9	18.3	38.3
2	0.7	0.3	0.4	0.6	0.8	1.7
3	2.0	0.3	1.7	2.5	3.5	7.4
4	2.0	0.3	1.7	2.5	3.5	7.4

*   Well installed

**   Fairly installed

*** Poorly installed

+   Core II values for 1 pump operation

and recombining terms and adding and subtracting T_f yields:

$$Z_c(T_w - T_f) = (T_w - T_f) - (T_o - T_f), \qquad (8.3-4)$$

which can be rearranged to yield:

$$(T_w - T_f) = \frac{(T_o - T_f)}{(1 - Z_c)} \qquad (8.3-5)$$

The values found in Tables 8.3-8 and 8.3-9 are compared with the predicted values for the given locations in Section 8.4.

8.4   Comparison of Measured Temperatures with Predicted Temperatures

The following series of figures are a comparison of predicted temperatures with experimental measurements. The comparison is clouded by several effects which include:

1.   Uncertainty in knowing the absolute reactor power,

2.   Uncertainty in thermocouple temperature readings.

The temperature data was plotted against a power based on core average temperature rise measured by the primary flow - ΔT recorder. During Core II operation, this method was found to give the best estimate of core power since the uncertainty in ΔT measurement was ±0.2°C. However, between the operation of Core I and Core II, the ΔT recorder was adjusted and recalibrated, thus, leaving some question as to the accuracy of the Core I power measurements. Recorder calibration is a periodic

and routine procedure and should result in only small differences in accuracy.

The incore thermocouples consistently showed a larger ΔT than was measured on the flow - ΔT recorder in the control room. A thermocouple located at the inlet plenum (#11) and a thermocouple located near the core outlet pipe (#19) were used to obtain the incore thermocouple ΔT measurement which was used to calculate the total power. Figure 8.4-1 shows a comparison between the incore thermocouple measured ΔT and the ΔT measured on the flow - ΔT recorder for Core II. The incore thermocouples give a ΔT that is consistently about 18% higher than the flow - ΔT recorder. For the following comparisons, the measured ΔT's were the difference between the respective thermocouple and the inlet thermocouple and the reactor power was the power based on the flow - ΔT recorder.

Figure 8.4-2 shows a comparison between the measured element average temperature rise and the predicted temperature rise for several element positions in Core I. Considering the previously mentioned uncertainty, the measurements and predictions are in good agreement with the exception of the B-6 position. The B-6 discrepancy is very probably caused by the tip of the B-6 thermocouple not being located in a position to measure the mixed mean

FIG. 8.4-1

COMPARISON OF TWO METHODS OF MEASURING CORE TEMPERATURE RISE

• − ΔT obtained from primary flow-ΔT recorder
■ − ΔT obtained from incore thermocouples #11&19
    (11 is at bottom of spider hole #3 and 19
    is near the core tank outlet pipe)

incore
thermocouples

primary flow-ΔT recorder

core temperature rise, ΔT (°F)

reactor power   (MW)

FIG. 8.4-2

COMPARISON OF MEASURED ELEMENT TEMPERATURE RISE WITH PREDICTED TEMPERATURE
RISE FOR ELEMENT POSITIONS IN CORE I

● - A-2 data

⊕ - A-2 prediction

▣ - C-8 data

⊞ - C-8 prediction

▲ - B-6 data

△ - B-6 prediction

◆ - C-14 data

◈ - C-14 prediction

element outlet temperature. There is a nonuniform power distribution across an element in B-6 caused by the proximity of the element to the fixed absorber spider. The tip of the thermocouple may be measuring the temperature out of the hotter portion of the element. Comparison of natural circulation (no forced convection) temperature measurements indicate that the element in B-6 does not generate more power than expected. An example of natural circulation temperature measurements following three hours of reactor operation with flow at a power of 3.5 nominal megawatts is shown in Table 8.4-1.

Figure 8.4-3 shows comparison between the measured element average temperature rise for position A-1 in Core II and the predicted temperature rise (based on reactor power of 2.5 MW and 1150 gpm primary flow). The measurement and prediction are in good agreement.

Figure 8.4-4 shows a comparison of predicted and measured coolant channel temperature rise in individual channels of an element in C-5. The relative order of temperature rise agrees for the measured and predicted values, but the measured temperature rise shows a larger value than the predicted value. The extrapolated value of the hottest channel (channel 2) is, however, still less than the predicted value which includes hot channel uncertainties. Figure 8.4-5 is also a comparison between the measured and predicted temperatures in C-5 with the

TABLE 8.4-1

NATURAL CIRCULATION TRANSIENT TEMPERATURES IN A-2 AND B-6 FOLLOWING FULL POWER OPERATION

Nominal Power Prior to Shutdown = 3.5 MW

Element Position	A-2	B-6
Plate Scanning Data Predicted Ratio of Element Power to Average Element Power	1.14	1.141

Time after Shutdown and Pump Stoppage	Plenum Inlet Temperature (°C)	A-2 Outlet Temperature (°C)	B-6 Outlet Temperature (°C)
∿ 2 minutes	28.75	53.5	53.5
10 minutes	29.5	46.6	46.9
20 minutes	33.6	47.0	47.2

FIG. 8.4-3

COMPARISON OF MEASURED TEMPERATURE RISE WITH PREDICTED TEMPERATURE
RISE FOR ELEMENT IN POSITION A-1 IN CORE II

● - A-1 data

○ - A-1 prediction
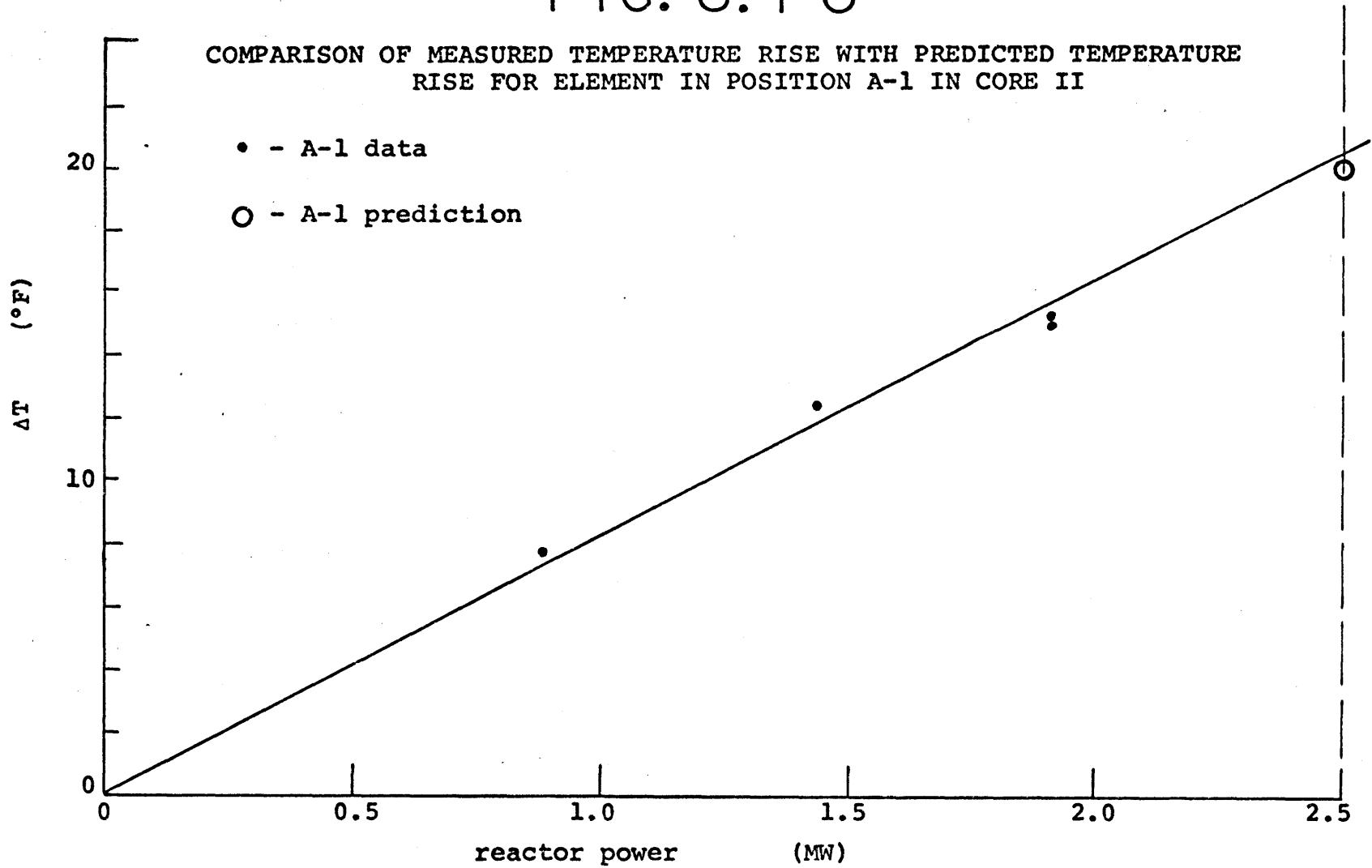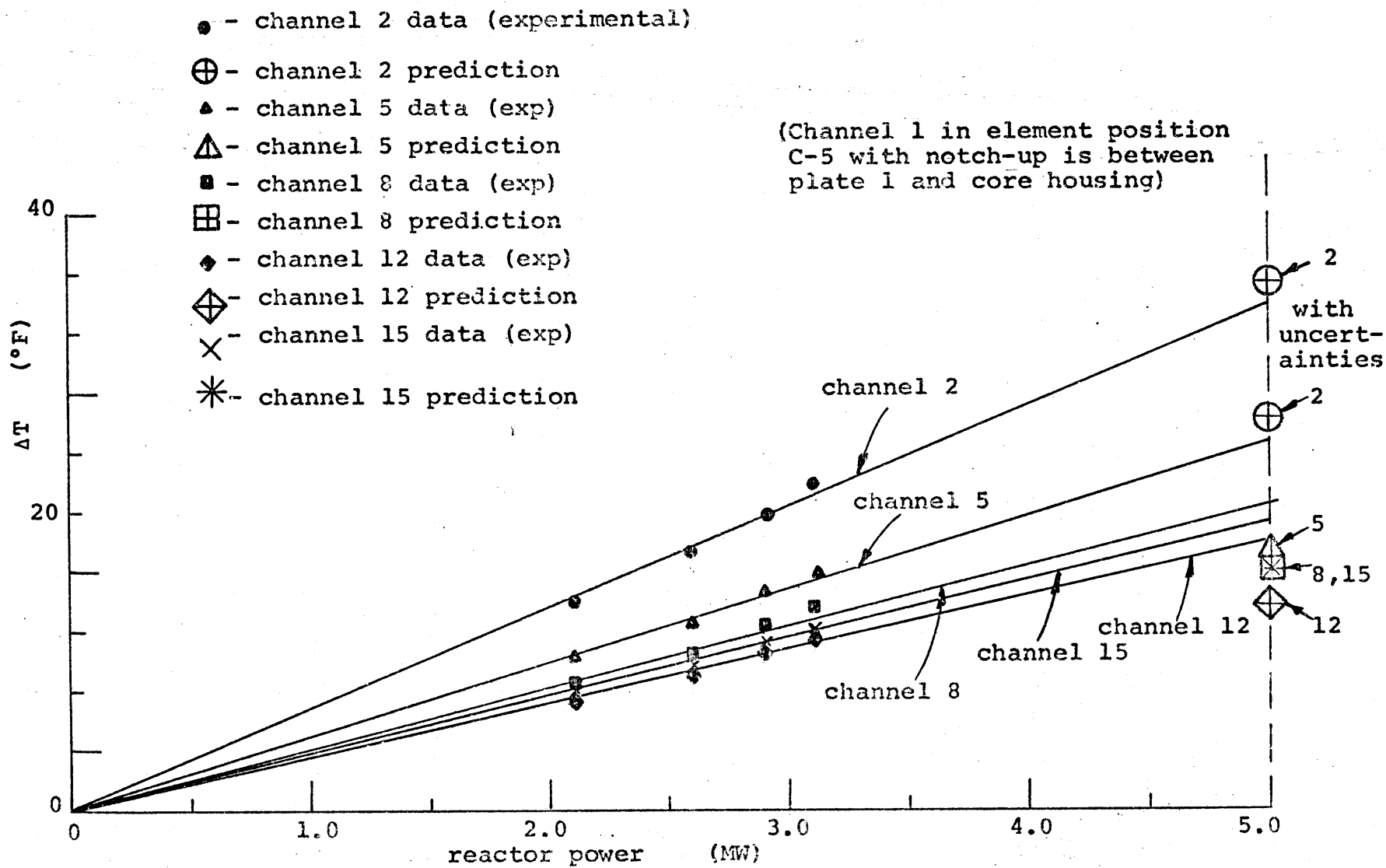
FIG. 8.4-4   COMPARISON OF PREDICTED AND MEASURED COOLANT CHANNEL TEMPERATURE RISE IN SEVERAL CHANNELS OF ELEMENT IN C-5 FOR CORE I

Legend:
- ● – channel 2 data (experimental)
- ⊕ – channel 2 prediction
- ▲ – channel 5 data (exp)
- △ – channel 5 prediction
- ■ – channel 8 data (exp)
- ⊞ – channel 8 prediction
- ◆ – channel 12 data (exp)
- ◇ – channel 12 prediction
- ✕ – channel 15 data (exp)
- ✱ – channel 15 prediction

(Channel 1 in element position C-5 with notch-up is between plate 1 and core housing)

following differences:

1. A "best estimate" of the measured temperature difference is obtained by reducing the measured value by 18% (ΔT difference in Fig. 8.4-1),

2. The predicted values including hot channel uncertainties are plotted.

In all cases the extrapolation of the "best estimate" is well below the predicted value with uncertainties. The predicted value of the hot channel #2 with no uncertainties is very close to the "best estimate" prediction.

Figures 8.4-6 through 8.4-11 show the fuel surface and channel bulk coolant temperature distributions predicted using the experimental power distribution as input to MACABRE for the fuel plates that have surface thermocouples attached. The MACABRE calculations were made using nominal element dimensions, expected element flow with 2000 gpm total primary flow (1150 gpm for Core II), and a reactor total power of 5 MW (2.5 MW for Core II). Thus, the temperature distributions are the expected nominal distributions with an inlet temperature of 116.0°F. The thermocouple element was located in position A-2 in Core I and in position A-1 in Core II (surface thermocouple locations are listed in Table 8.3-3). The observed temperatures are plotted on each of the predicted distributions along with the expected wall temperature if the thermocouple is well, fairly or poorly installed.

FIG. 8.4-5

COMPARISON OF PREDICTED AND MEASURED
COOLANT CHANNEL "BEST ESTIMATE"
TEMPERATURE RISE IN CHANNELS OF ELEMENT
IN C-5 IN CORE I

Legend:

● -channel 2 data
⊕ -channel 2 pred. with uncert.
▲ -channel 5 data
△ -channel 5 pred. with uncert.
▣ -channel 8 data
⊞ -channel 8 pred. with uncert.
◆ -channel 12 data
⬦ -channel 12 pred. with uncert.
✕ -channel 15 data
✳ -channel 15 pred. with uncertainties
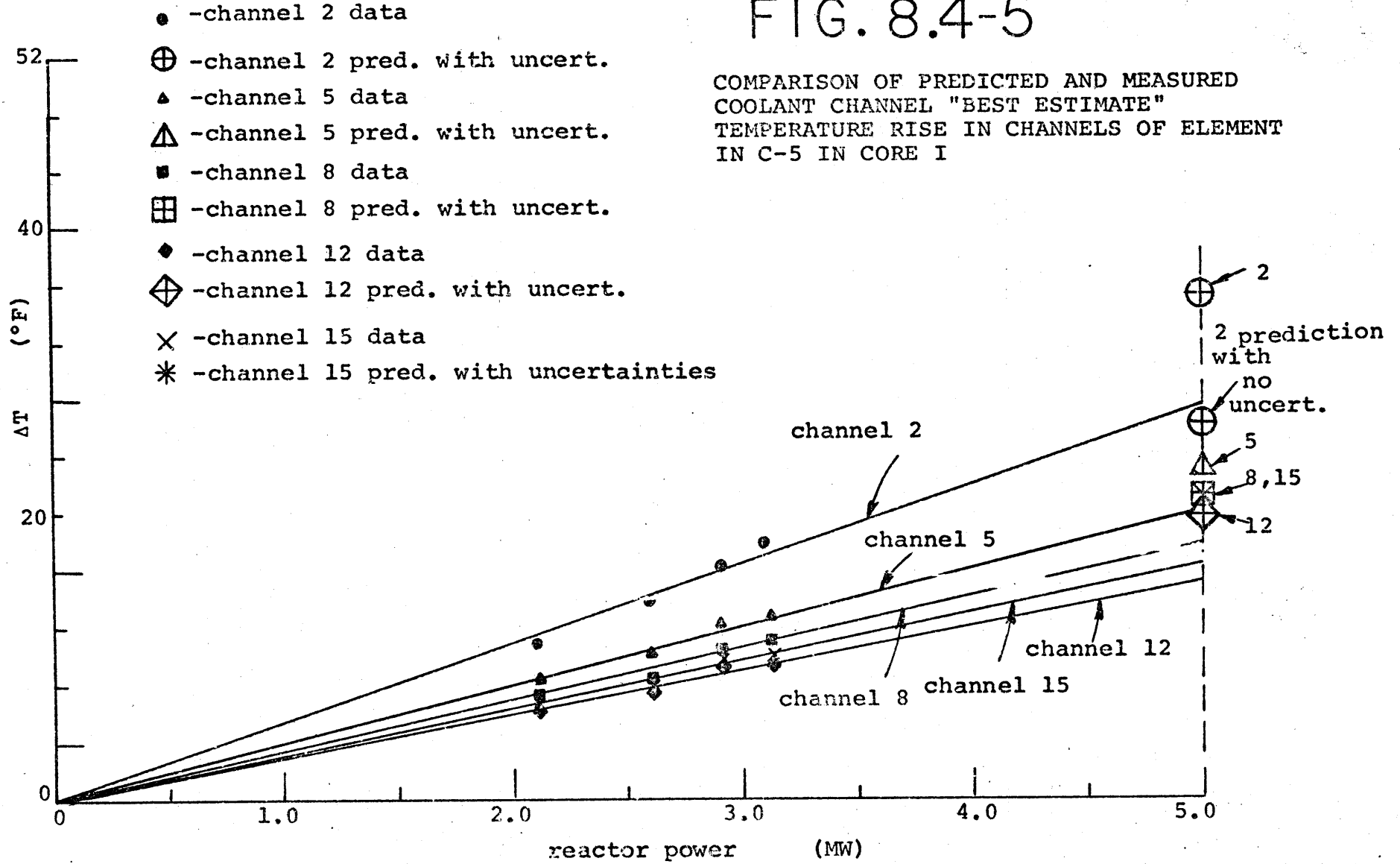
FIG. 8.4-6

COMPARISON OF FUEL SURFACE TEMPERATURE PREDICTION AND MEASURED VALUE ON T/C-#1
FOR CORE I

inlet temp. of coolant: 116 °F
element position: A-2
reactor power: 5MW

T/C-#1 $\begin{cases} \bullet - T_o - \text{observed temp.} \\ \blacksquare - T_W - \text{well installed value} \\ \blacktriangle - T_W - \text{fairly installed value} \end{cases}$

plate 15, channel 15 side
surface temp.

channel 15 bulk coolant temp.

temperature (°F)

distance from bottom of fuel   (inches)
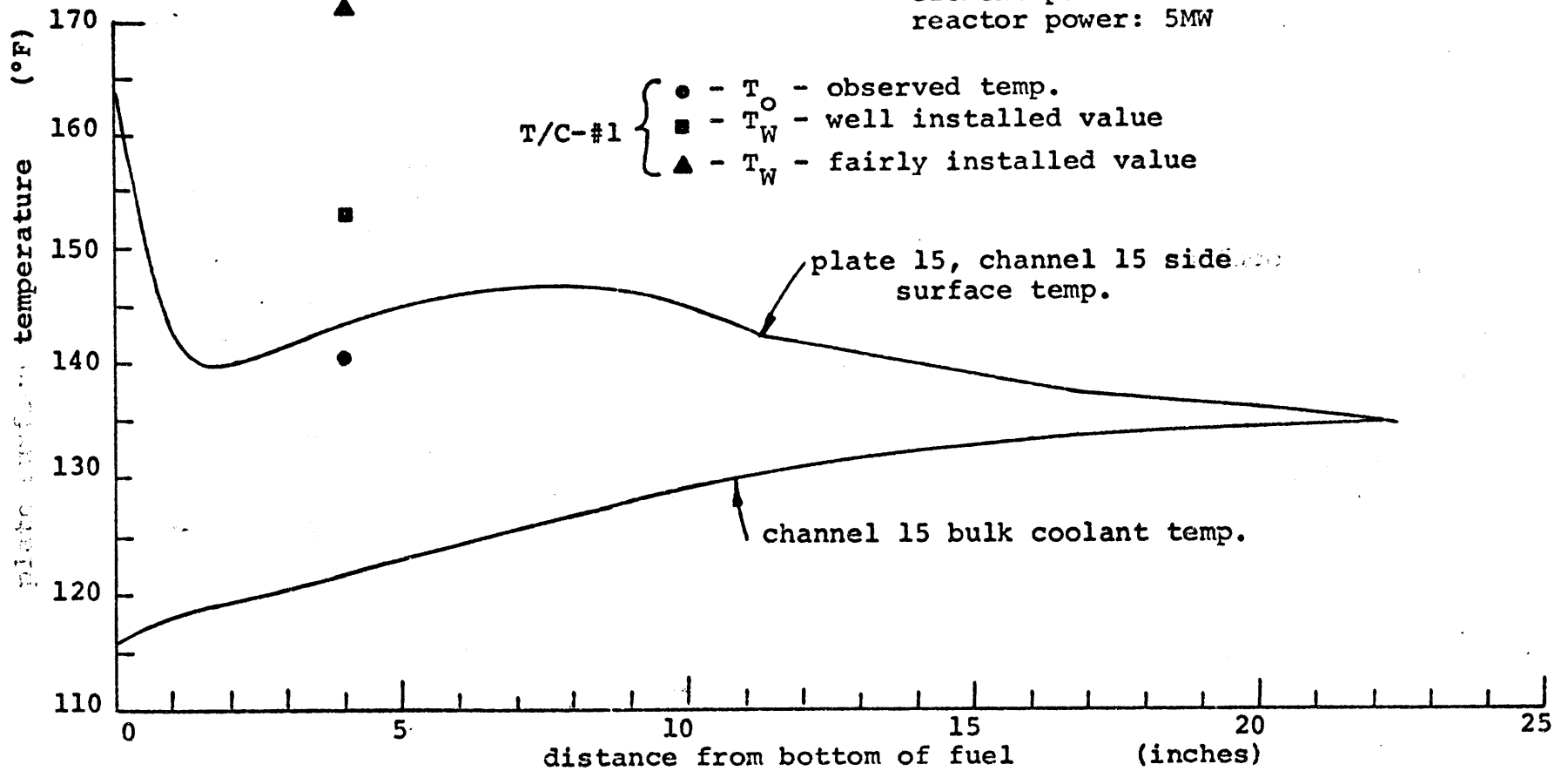
FIG. 8.4-7

COMPARISON OF FUEL SURFACE TEMPERATURE PREDICTION AND MEASURED VALUE ON T/C-#2
FOR CORE I

T/C-#2
- ● -T_o - observed temp.
- ■ -T_W - well installed value
- ▲ -T_W - fairly installed value
- ⬡ -T_W - poorly installed value

coolant flow: 2000 GPM
inlet coolant temp.: 116 °F
element position: A-2
reactor power: 5MW

plate 8 surface temp.

channel 8 bulk coolant temp.

temperature (°F)

distance from bottom of fuel (inches)
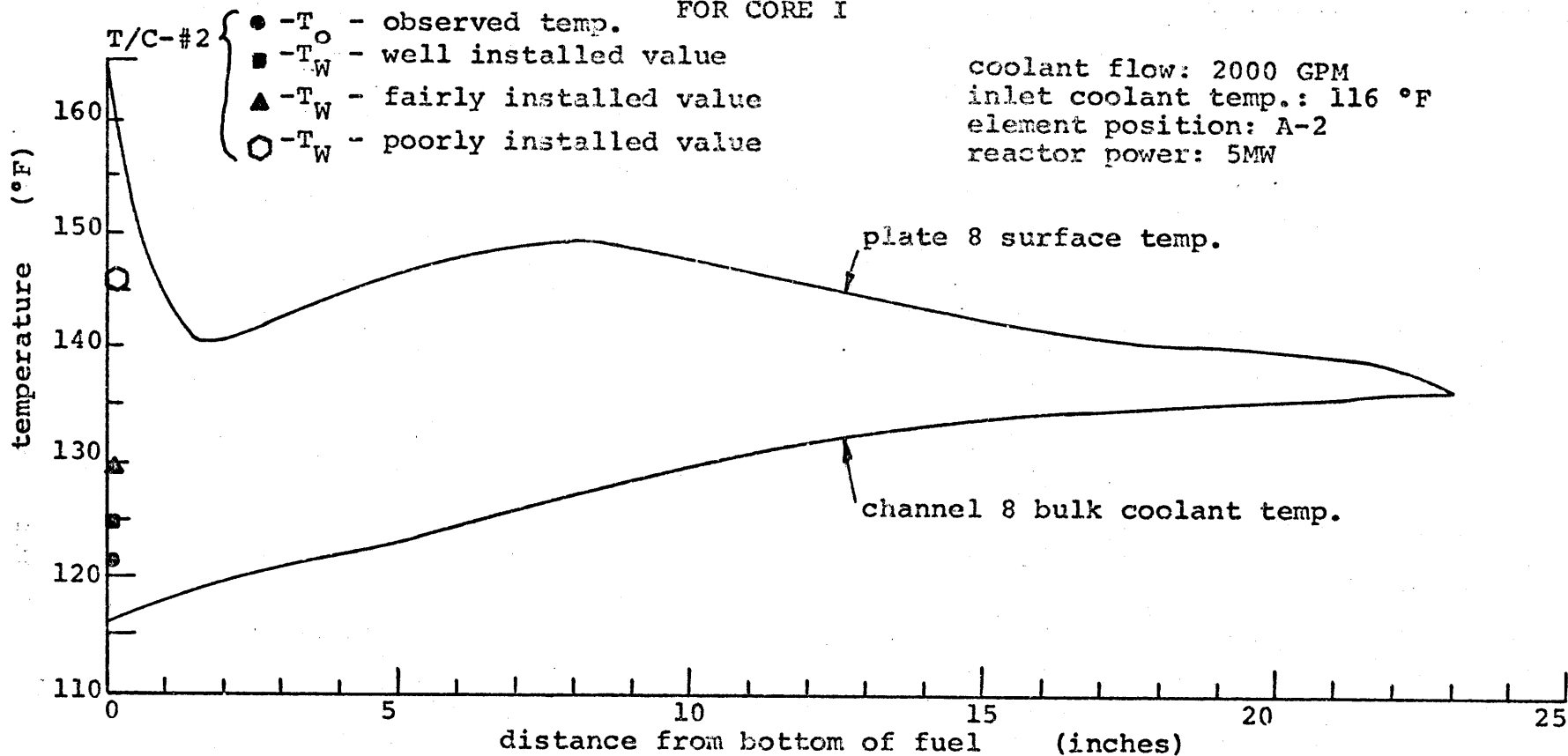
FIG. 8.4-8

COMPARISON OF FUEL SURFACE TEMPERATURE PREDICTIONS AND MEASURED VALUES ON
T/C's #3 AND #4 FOR CORE I

coolant inlet temp.: 116 °F
element position: A-2
reactor power: 5MW
coolant flow: 2000 GPM

T/C-#3
T/C-#4

- T_O - observed temp.
- T_W - well inst. value
- T_W - fair inst. value
- T_W - poor inst. value

plate 1,channel 2 side surface temp.

plate 2,
channel 3 side surface temp.

channels 2&3 bulk coolant temp.

temperature (°F)

distance from bottom of fuel   (inches)

FIG. 8.4-9

COMPARISONSON OF FUEL SURFACE TEMPERATURE PREDICTION AND MEASURED VALUE ON

T/C-#1 FOR CORE II

T/C-#1 {
• - T_o - observed temp.
▪ - T_W - well installed value
▲ - T_W - fairly installed value
}

inlet coolant temp.: 116 °F
element position: A-1
reactor power: 2.5MW
coolant flow: 1150 GPM

plate 15, channel 15 side
surface temp.

channel 15 bulk coolant
temp.

temperature (°F)

145

135

125

115

0   5   10   15   20   25

distance from bottom of fuel   (inches)

FIG. 8.4-10

COMPARISON OF FUEL SURFACE TEMPERATURE PREDICTION AND MEASURED VALUE ON T/C-#2
FOR CORE II

inlet coolant temp.: 116 °F
element position: A-1
reactor power: 2.5 MW
coolant flow: 1150 GPM
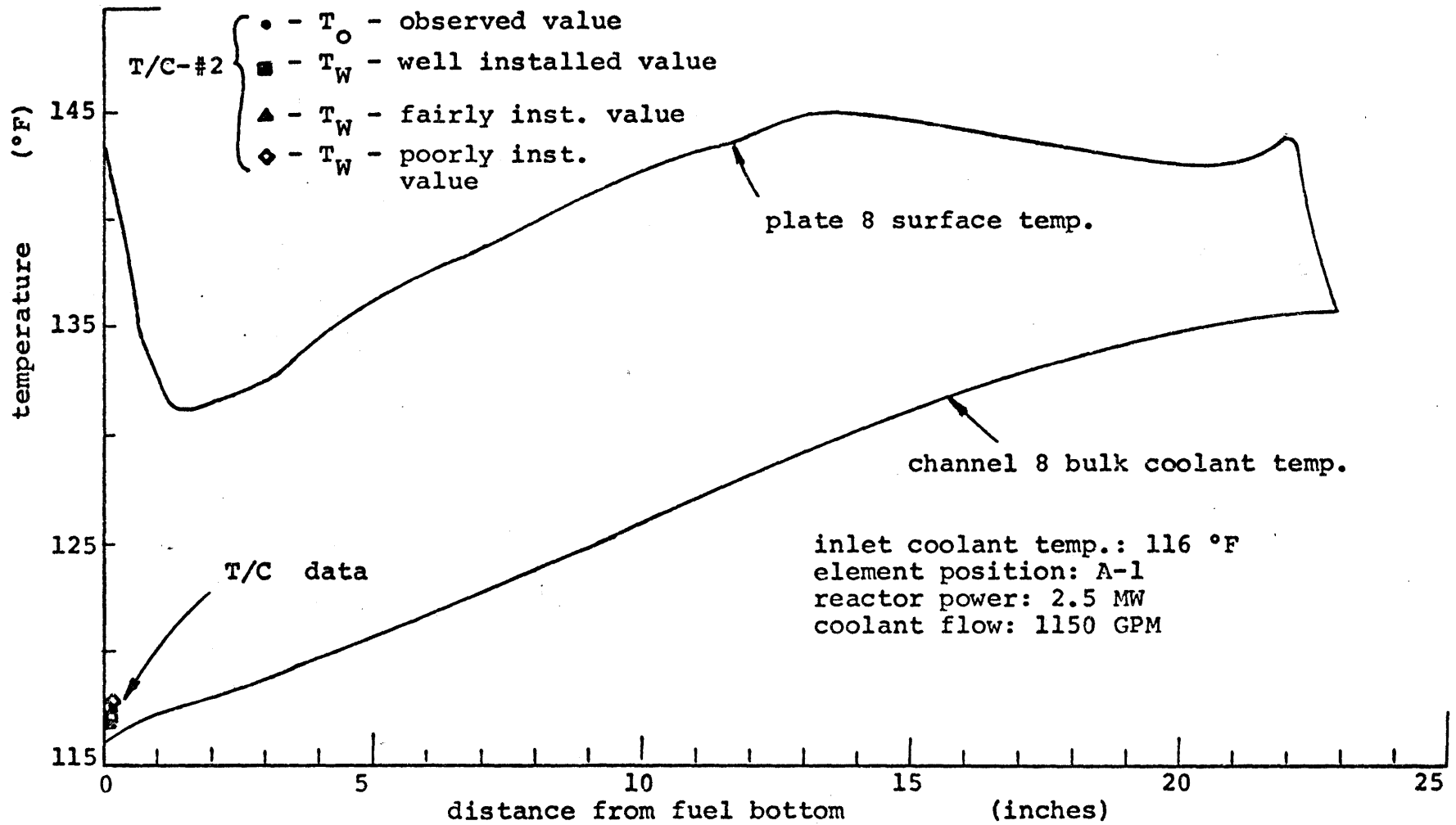
FIG. 8.4-11

COMPARISON OF FUEL SURFACE TEMPERATURE PREDICTIONS AND MEASURED VALUES ON T/C's #3 AND #4 FOR CORE II

$\left.\begin{array}{l} \text{T/C-\#3} \\ \text{T/C-\#4} \end{array}\right\{$
- • – T_0 – observed temp.
- ■ – T_W – welled installed value
- ▲ – T_W – fairly installed value
- ◇ – T_W – poorly installed value

plate 2, channel 3 side surface temp.

plate 1, channel 2 side surface temp.

T/C data

channels 2&3 bulk coolant temp.

inlet coolant temp.: 116 °F
element position: A-1
reactor power: 2.5 MW
coolant flow: 1150 GPM

temperature (°F)

distance from bottom of fuel   (inches)
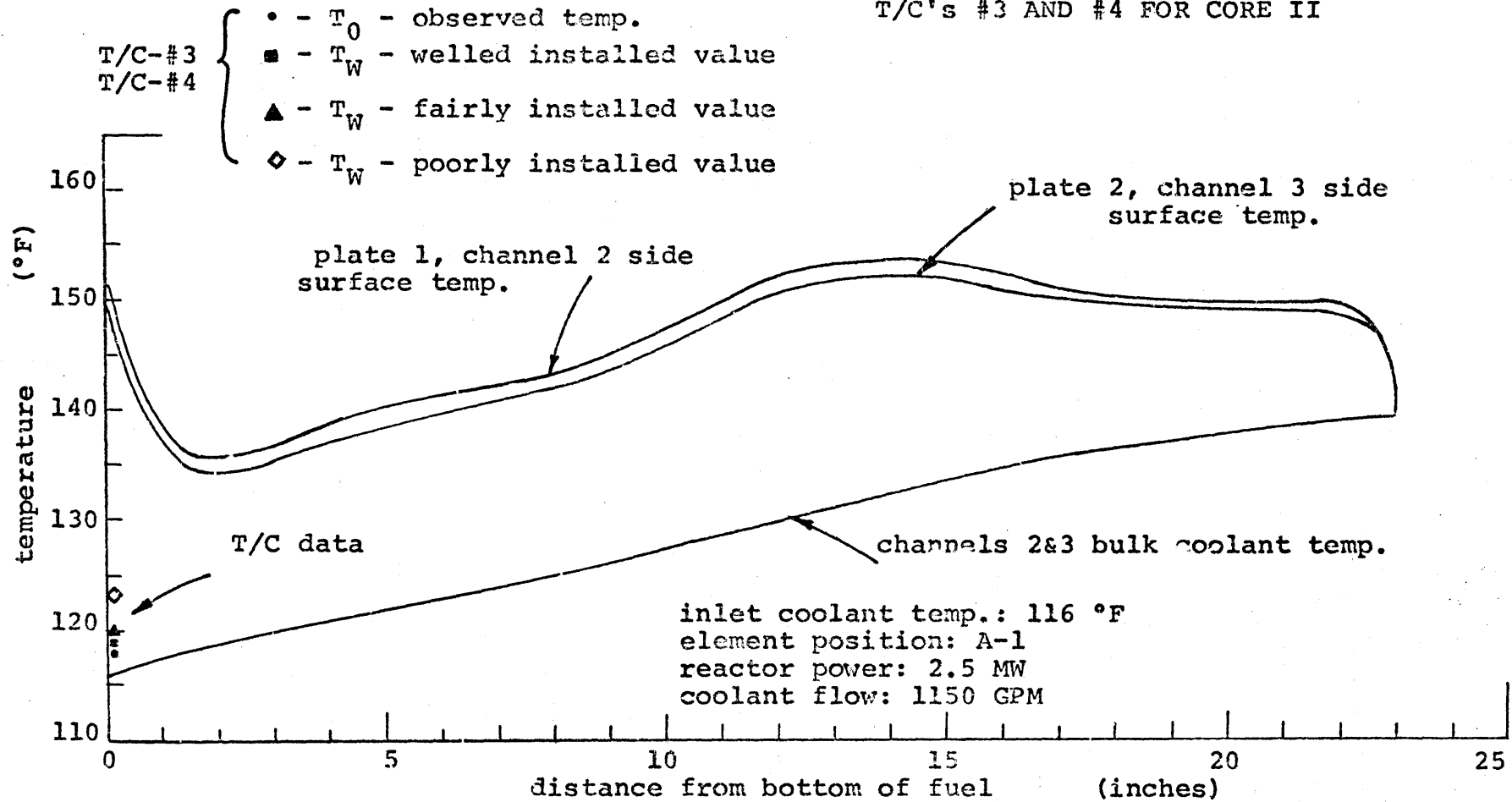
As shown in Fig. 8.3-7, thermocouple #1 was classified as very well installed. Because the thermocouple attachment may have decreased the local heat transfer efficiency and because thermocouple leads are crimped between the fins up the channel reducing the potential heat transfer from the thermocouple to the coolant, the observed temperature may read closer to the actual surface temperature than would be theoretically possible with a well installed thermocouple. Figures 8.4-6 and 8.4-9 show good agreement between the observed surface temperature and predicted temperature for Core I and Core II, respectively. The observed temperature is less than the predicted in both cases.

The results for thermocouples 2, 3, and 4 are somewhat different. The observed temperatures are much less than the predicted temperature based on conservative assumptions at the entrance region and because of the great care used by Gulf United Nuclear Fuel (GUNF) it is very unlikely that all three thermocouples were poorly installed. It appears that for the possible reasons discussed in Section 8.3.4.2, the actual bottom temperature spike does not exist at least for the cases measured.

8.5   Summary of Temperature Distributions

In general, the agreement between predicted and measured temperatures is good. While this chapter only serves to evaluate the steady-state temperature data, it is also useful in the eventual evaluation of the startup temperature data for a detailed natural circulation analysis because it outlines some of the problems in the startup temperature data. The following conditions were observed in analyzing the temperature data:

1.   Some steady-state temperature data is questionable possibly because of lack of sufficient ice in the reference junction temperature bath, reactor building temperature fluctuations at the data collection station, or because readings were taken on the night shift,

2.   The difference in temperature rise measured by the incore thermocouples and temperature rise measured by other means increased with reactor power (see Fig. 8.4-1).

Neither of these effects should exist for the natural circulation results because additional care was taken during natural circulation test measurements and because the reactor was at low powers when the temperature measurements of interest were taken. For the steady-state temperature measurements the following conclusions are valid:

1)   The measured fuel element temperature rise is close to the predicted value,

2) The fuel channel temperature rise is close to the predicted value,

3) The observed fuel surface temperature at the lower fuel meat edge is much lower than the prediction obtained neglecting axial conduction, entrance effects, and edge density decreases.

4) The observed fuel surface temperature at a point up the fuel channel is very close to the predicted value provided that it is assumed that thermocouple #1 is very well installed (calibration factor, $Z_c \approx 0.15$ to 0.3 for flow conditions, for natural circulation, $T_o \approx T_{actual}$).

Uncertainty in the temperature difference measurements based on reading accuracy and data collection station temperature fluctuations is on the order of $\pm 1.0°F$. The error introduced by power level effects and power level uncertainty were covered in Section 8.4 for the data analyzed. While the uncertainty and limited scope of the temperature movements makes it very difficult to use the results to determine new hot channel factors, it is very interesting to note that since the measured temperatures are in good agreement with the predicted temperatures obtained using nominal conditions, that the measured temperatures are well below the temperatures that are predicted when hot channel factors are included.

CHAPTER 9

SELF-POWERED NEUTRON DETECTOR FLUX MAPS

Self-powered neutron detector flux maps in the MITR-I and the MITR-II are discussed in this chapter. Section 9.1 is a general description of self-powered detector neutron scans. Detector characteristics, experimental procedure, and scan results are described in Sections 9.2, 9.3, and 9.4, respectively.

9.1 General Descriptions

Self-powered neutron flux detectors were used to map the neutron flux distribution in several locations in both the MITR-I and the MITR-II. Thus, the neutron flux difference between the two reactors at several locations out of core has been determined, as well as, a comparison of the flux magnitudes and distributions incore. The flux maps of the MITR-I were made prior to its shutdown in 1974, and the flux maps for the MITR-II were made shortly after startup of both Core I and Core II. Table 9.1-1 shows the positions scanned in the MITR-I and MITR-II.

Self-powered neutron detectors were also used to measure the flux distribution change with shim bank height. It indicated in Chapter 7 that changes in the power distri-

TABLE 9.1-1

LOCATION OF RHODIUM SELF-POWERED NEUTRON DETECTOR SCANS

MITR-I

1PH3

3GV2

Incore Position #23

Incore Position #13

MITR-II

Core I	Core II
Incore Spider Hole #1	1PH3
	3GV5
	Incore Spider Hole #1
	Incore Corner Hole #6
	Fuel Storage Rack

bution with shim bank height may provide more limiting conditions on the safety limit and limiting conditions for operation. The scanning techniques described in this chapter can be used to check power distribution changes in future core loadings.

A Reuter-Stokes self-powered flux detector with a rhodium^{103} emitter one centimeter long was used for the neutron flux scans. All results were normalized to the value that would be measured if the reactor was operating at a steady-state power of 4.9 thermal megawatts, which corresponds to the normal full power operating level.

9.2 Self-Powered Neutron Detector Characteristics

Self-powered neutron detectors operate by converting the incident radiation on the detector emitter material to energetic electrons which penetrate the solid insulation surrounding the emitter and come to rest on a collector or its surroundings. Given a circuit shown in Fig. 9.2-1(A), the deficiency of electrons in the emitter results in a positive charge on the center conductor attached to the emitter. With the center conductor connected to the outer collector sheath by a resister, the rate of positive charge produced can be measured as a current. Thus, the current measured is directly proportional to the rate at which radiation is being absorbed by the emitter.

FIG. 9.2-1

SELF-POWERED NEUTRON DETECTOR OPERATION
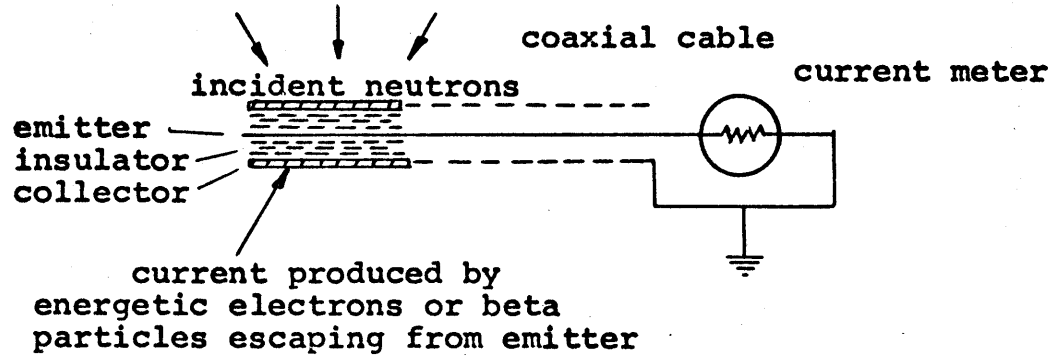
(A)
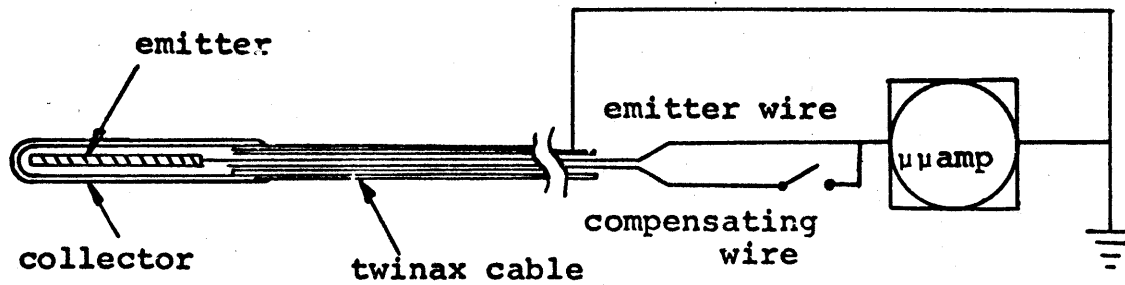
(B)

The self-powered detector used for the MITR scans had a one centimeter long rhodium emitter. The rhodium absorbs neutrons to become beta-active and the beta particles themselves penetrate the surrounding insulator, thus charging the emitter. Other emitter materials are also commercially available which work by beta decay or else by using n-γ-e⁻ or γ-e⁻ reactions, however, rhodium was selected becuase it had the highest neutron sensitivity of possible emitters. The response of rhodium self-powered detectors is delayed by the rhodium beta-decay half-life of 42 seconds. For accurate measurements, the detector must be held in a constant neutron flux for approximately 4 minutes to allow the beta decay to reach its saturation value.

Gamma radiation on the wire connected to the emitter induces a current of the opposite sign of the current caused by neutron absorption in the emitter section. Because the gamma dose rate on the connecting wires is not directly proportional to the emitter neutron fluence, but is more dependent on the amount of wire physically located in the core, the self-powered detectors were gamma compensated. A second connecting wire, which is identical to the wire connected to the emitter but is not attached to the emitter or the outer sheath, is contained in the sheath. Figure 9.2-1(B) shows the electrical

diagram of the self-powered detector measuring circuit.
With only the emitter connected to the current measuring
μμammeter, the meter reads a current that is equal to
the neutron induced current, I_n minus the gamma induced
current, I_g. With both the emitter and the compensating
wire connected to the μμammeter, the meter reads a current
that is equal to neutron induced current minus twice the
gamma induced current. Thus, the neutron induced current
alone can be calculated using the following equation:

$$
\text{Neutron only Signal} = 2 \times \underbrace{(I_n + I_g)}_{\substack{\text{Emitter} \\ \text{Only Reading}}} - \underbrace{(I_n - 2I_g)}_{\substack{\text{Emitter and} \\ \text{Compensating} \\ \text{Wire Reading}}} = I_n \ , \quad (9.2\text{-}1)
$$

The gamma compensation is performed in this manner
because reading the small current of the compensating
wire alone introduces too much uncertainty in the
measurement.

The neutron sensitivity of a 1 centimeter rhodium
self-powered detector is 1.2×10^{-21} amp/nv (Ref. 9.2-1).
Since the neutron fluxes of interest are on the order
of 10^{13}, the electrical currents which must be measured
are on the order of 10^{-8} amps. The currents can be
measured with reasonable accuracy on a good μμammeter.
Since rhodium has a large resonance absorption, the

current measured on the μμammeter is not directly proportional to the thermal neutron flux. The measured current is dependent on both the thermal and epithermal neutron flux at the detector emitter. In order to accurately determine the thermal neutron flux alone, the ratio of epithermal to thermal neutron flux at each point being measured and the effective resonance integral of the emitter must be known. Because of uncertainties in these latter quantities, the epithermal contribution was not accounted for in these results and flux scan distributions are shown as NV for a rhodium detector. All measured currents in amps are divided by the detector sensitivity (1.2 x 10^{-21} amp/nv) and then normalized to 4.9 MW based on the power level at the time of the measurement that was measured on the primary flow – ΔT recorder in the control room.

The self-powered detector has a 1/16" O.D. collector and an 18 feet long connecting cable with a two feet extension cable. The insulating material was M_gO and the outside sheath of the emitter and connecting cable was made of inconel 600. Reuter-Stokes recommended installation methods suggests that there should be at least 1/8 inch of water or equivalent mass between any aluminum and the detector or cable because the 2.87 Mev betas from aluminum can penetrate the detector or cable sheath and

give spurious signals. Because both MITR's were aluminum systems, this suggestion was not always possible to fulfill, but no unusual effects were detected.

9.3 Experimental Procedure

The self-powered neutron flux detector scans were made in the following manner.

A) Detector was inserted in thimble or tube until the detector tip was at the full-in position desired,

B) The detector was connected to the μμammeter in a manner shown in Fig. 9.2-1(B),

C) The reactor power was level at desired condition,

D) Readings were taken with the emitter only and with the emitter and compensating wire combined,

E) The detector would then be withdrawn to the next position of interest (the full-in position was marked on the connecting cable with a piece of tape at the location where the cable first exited the sample tube or shielding). A minimum of 4 minutes elapsed before a reading would be taken after a withdrawal was completed,

F) Readings and withdrawals would be repeated until the scan was complete,

G) The detector was then withdrawn out of the high neutron flux region and allowed to cool for several days prior to removal.

Knowing the full in location of the detector tip was a simple task. In most cases. the detector was irradiated in a sample thimble and it was easily felt

when the detector tip struck the bottom of the thimble.

For the locations in the MITR-II core where an open

ended guide tube was used (see Fig. 9.3-1), the self-

powered detector tip would be positioned at the end of

the guide tube prior to insertion into the core region.

After the guide tube was in position, the detector was

slid down the guide tube to the desired bottom location.

While sliding the detector into position it was quite

easy to feel when the detector tip struck the bottom

of a corner hole, or the interface between the upper

and lower spider or the bottom of the core tank. Either

the original tip location with respect to the guide tube

or tip location with respect to felt incore position could

be marked on the lead cable as a reference. While the

small holes at the bottom of the corner holes were theoreti-

cally large enough to allow passage of the detector tip,

it was never found to be possible to insert the tip more

than 4 inches below the bottom of the large diameter corner

hole. Because of the desire to avoid having a tip stuck

or broken incore, no excessive force was used to aid the

detector tip past this impasse.

The $\mu\mu$ammeter was always allowed to warm up for several

hours prior to use in order to increase its stability.

The detector zero was checked with each reading and care

was taken to insure that both the detector and $\mu\mu$ammeter

were properly grounded. The self-powered detector proved

FIG. 9.3-1

SELF-POWERED DETECTOR GUIDE TUBES

spider hole guide tube

corner hole guide tube

0.730"

14 ft.

15 ft.

3"

spacer
(fluted to
allow water
passage)

12"

1/4 - 20 thread

1/8" minimum
opening

1/4" ID
x 3/8 OD tube
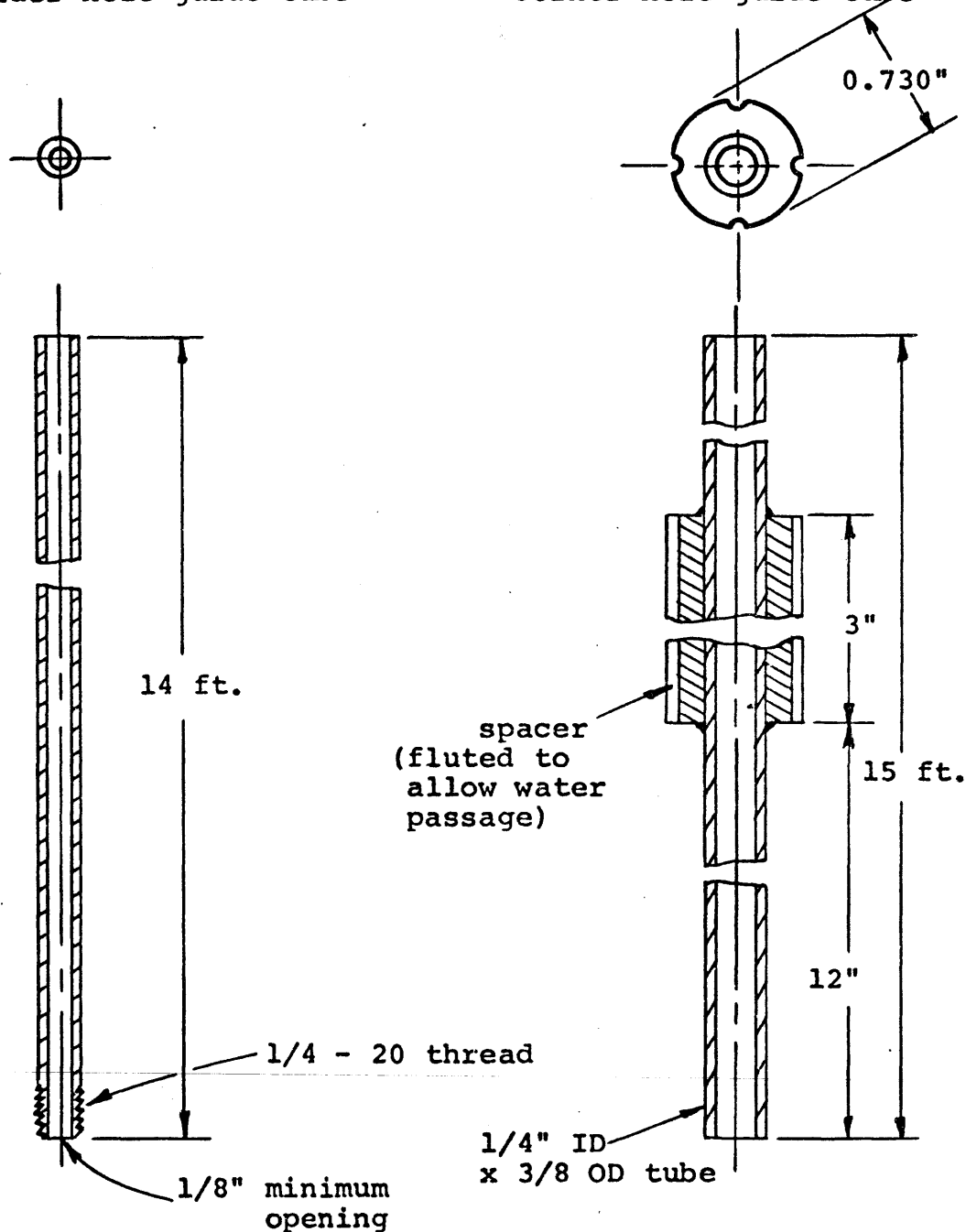
to be both simple and rugged. Between irradiations and
after the detector radiation level had decayed to accept-
able levels, the detector wire cables would require
straightening to allow easy sliding and positioning in
the guide tubes.

9.4 Rhodium Self-Powered Detector Results

The results in this section are all normalized to
a reactor power of 4.9 MW. The neutron flux results
are for a rhodium averaged spectrum and thus, the neutron
flux is plotted as the NV for rhodium. Figure 9.4-1
shows self-powered flux detector scans at two incore
locations in the MITR-I. The peak neutron flux in
the MITR-II occurred at the center of the reactor. The
detectors show a smooth cosine shaped distribution in
the axial direction with a peak in the thimble in position
13 of 5.75 x 10^{13}.

Figure 9.4-2 shows scans in vertical sample thimbles
in the graphite reflector (3GV facilities) for both the
MITR-I and the MITR-II. The MITR-I had a flatter flux
shape over the lower portion of the thimble than does
the MITR-II. The peak flux in the 3GV thimbles for the
MITR-II is about 20% less than the peak MITR-I value.
Table 9.4-1 compares the self-powered detector results
in the pneumatic facility, 1PH3, for the MITR-I and
MITR-II. The peak flux in 1PH3 for the MITR-II is approx-
imately 35% less than the MITR-I value.

FIG. 9.4-1

RHODIUM SELF-POWERED DETECTOR SCANS OF INCORE
POSITIONS IN MITR-I

thimble in
fuel position #13

thimble in fuel position #23

(values normalized to reactor power of
4.9 MW)

(shim bank height = 20 inches, equilibrium
xenon in core)

Rhodium NV x 10^{-13}

distance from bottom of thimble (inches)
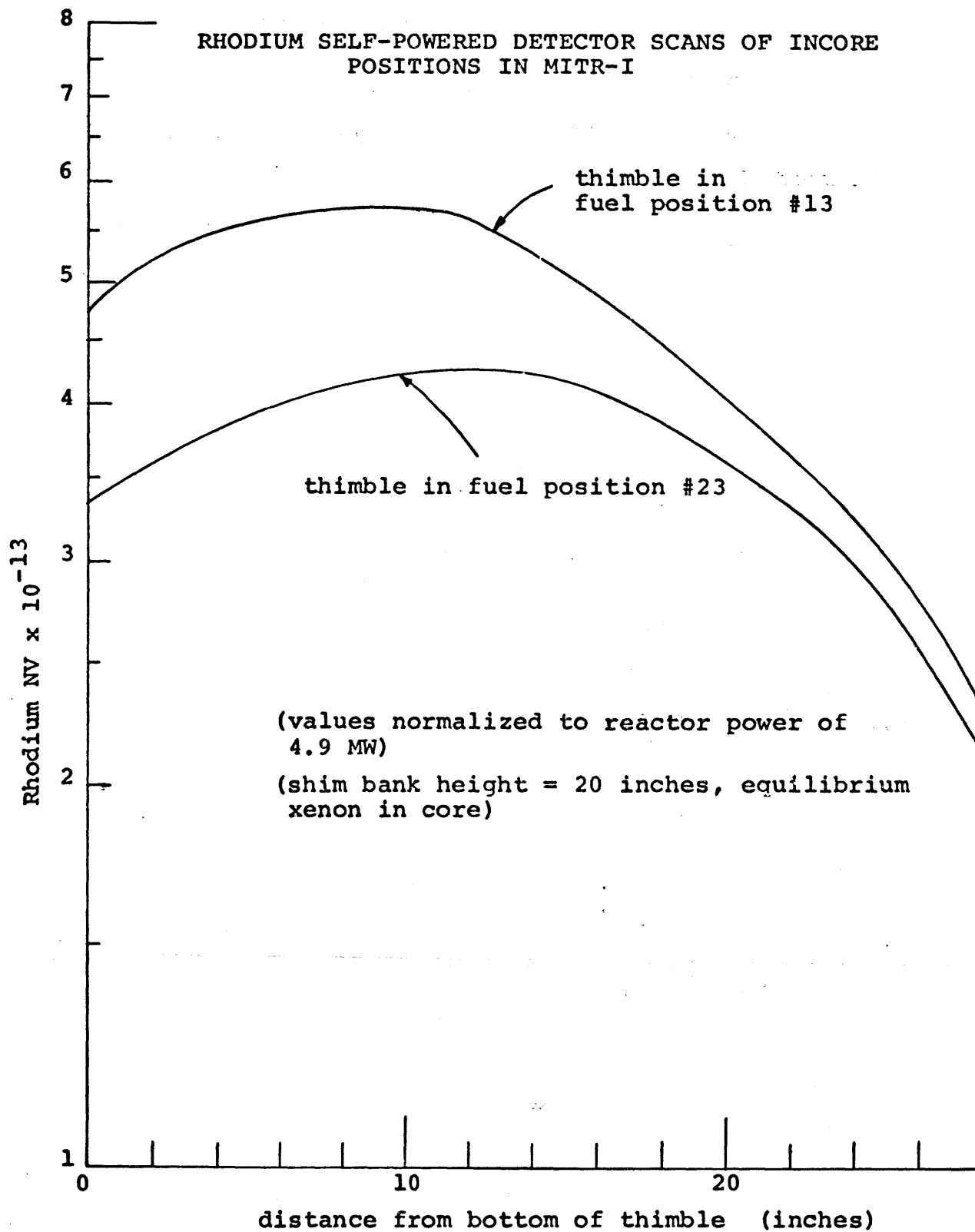
FIG. 9.4-2

COMPARISON OF RHODIUM SELF-POWERED DETECTOR SCANS IN 3GV FACILITIES FOR THE
MITR-I AND CORE II OF THE MITR-II

MITR-I (3GV2)

MITR-II (3GV5)

(values normalized to a reactor power of 4.9 MW)

Rhodium NV x 10^{-13}

distance from bottom of 3GV thimble   (inches)
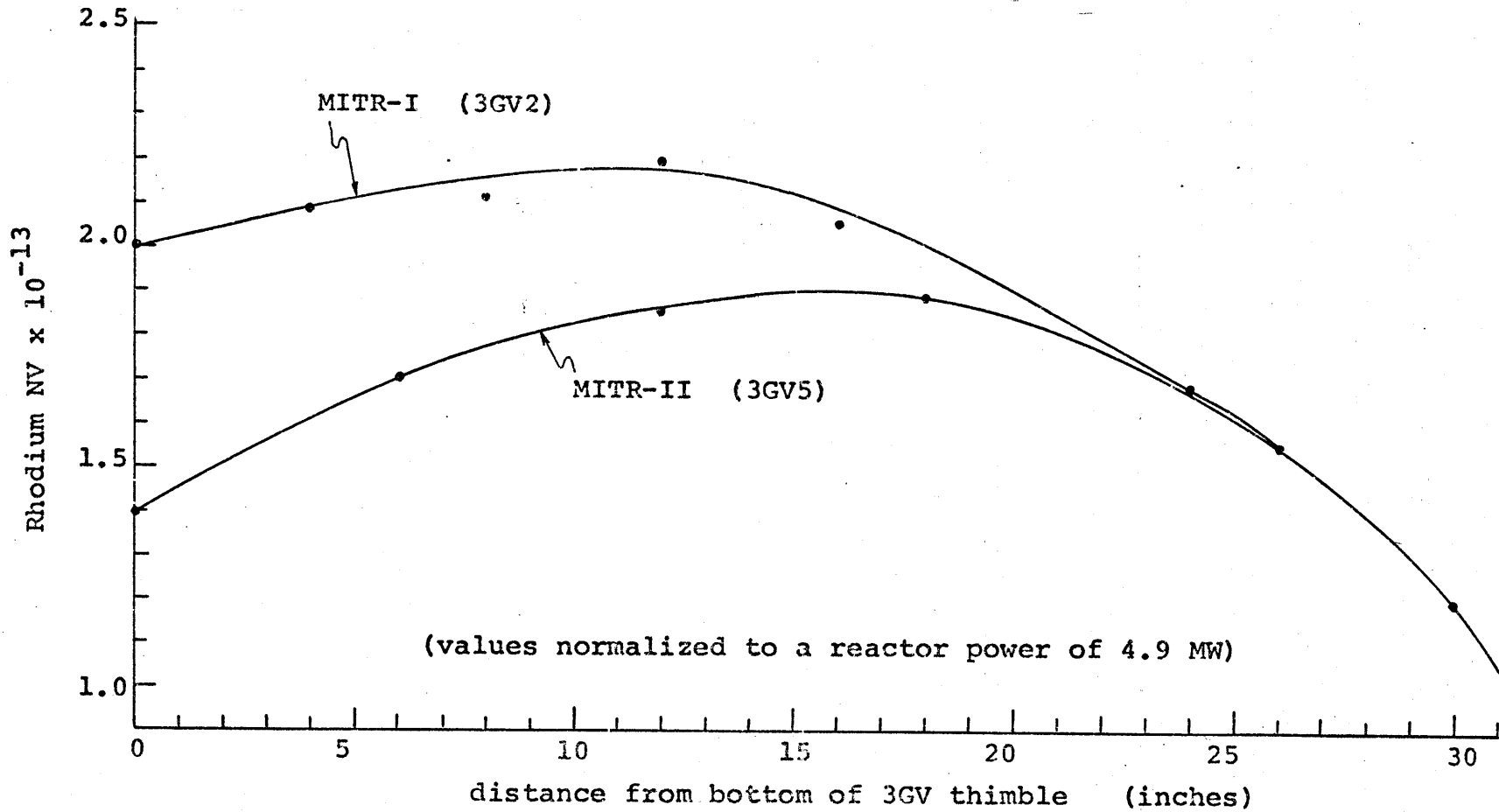
TABLE 9.4-1

RHODIUM SELF-POWERED DETECTOR NEUTRON
FLUX MEASUREMENT IN 1PH3

MITR-I*	MITR-II CORE II*
1.625×10^{13}	1.05×10^{13}

* Readings normalized to a reactor power level of
4.9 MW. Detector tip was located inside the end
of the 1PH3 pneumatic tube in the graphite reflector
region.

Figure 9.4-3 shows a scan of spider hole #1 in Core
I. Note that the peak flux occurs at the bottom edge of
the core and that the flux shape is identical to the
shape determined using copper wires (Section 5.4). The
flux peak that occurs directly above core is greater
than the flux in the graphite pneumatic facilities.
Figure 9.4-4 shows a scan of spider hole #1 in Core II.
The neutron flux is not depressed in the upper portion
of the core as was the case for Core I. The overall
flux level was also higher for the Core II scan of
spider hole #1 because in Core II a fueled element was
in A-1 next to the spider hole, whereas, in Core I a
solid dummy was in A-1.

Figure 9.4-5 shows scans in the core housing corner
hole next to the element containing the hottest channel
in Core II. Scans were performed at different shim bank
heights in order to evaluate the flux shape changes with
shim bank height as equilibrium xenon builds in the core.
These changes were discussed in Section 7.5. The corner
hole scans are very unsatisfying for showing this effect
because of the large effect the corner hole geometry has
on the flux shape at the detector location. Raising
the shim bank does greatly increase the flux level in
the upper portion of the corner hole (which would mean a
corresponding increase in the power level on the nearby

FIG. 9.4-3

RHDOIUM SELF-POWERED DETECTOR SCAN OF SPIDER
HOLE #1 FOR CORE I

├─ bottom edge of fuel meat

├─ top of lower spider

(blades at 10 inches)

(values normalized to reactor power of 4.9 MW)

Rhodium NV   × 10⁻¹³

inches from bottom of lower grid in spider hole #1
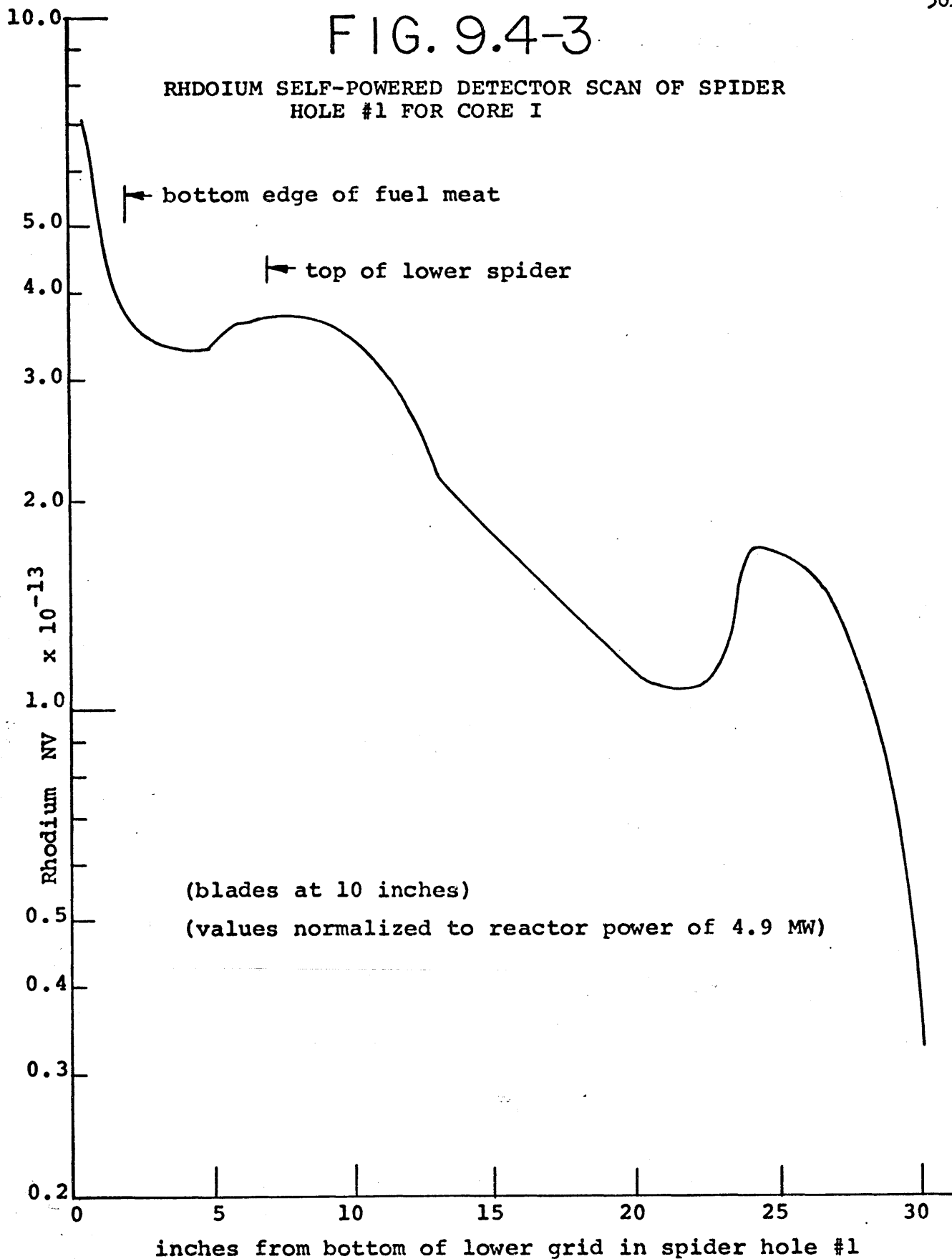
FIG. 9.4-4

RHODIUM SELF-POWERED DETECTOR SCAN OF SPIDER
HOLE #1 FOR CORE II

bottom edge of fuel meat

(blades at 10 inches)

(values normalized to reactor power of 4.9 MW)

inches from bottom of lower grid in spider hole #1
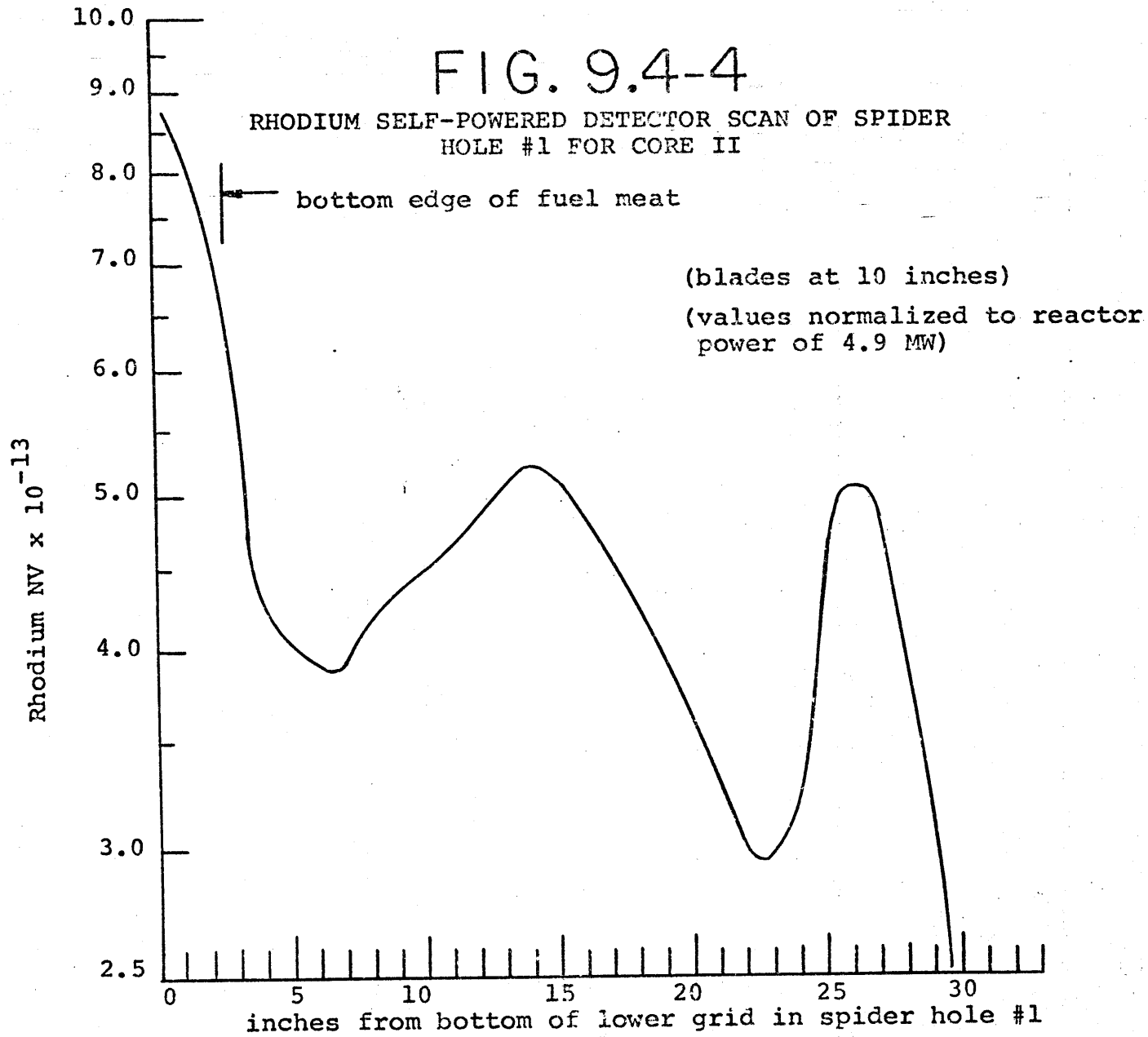
FIG. 9.4-5

EFFECT OF BLADE HEIGHT ON SELF-POWERED
DETECTOR SCANS OF CORNER HOLE #6
IN CORE II

blades at 10.9 inches

blades at 8.74 inches

extrapolated shape estimated using copper wire irradiation data

bottom of corner hole (3/4" section)

Corner hole #6 is next to fuel position C-13.
(values normalized to reactor power of 4.9 MW)

Rhodium NV x 10^{-13}

axial distance from bottom edge of fuel meat incore   (inches)
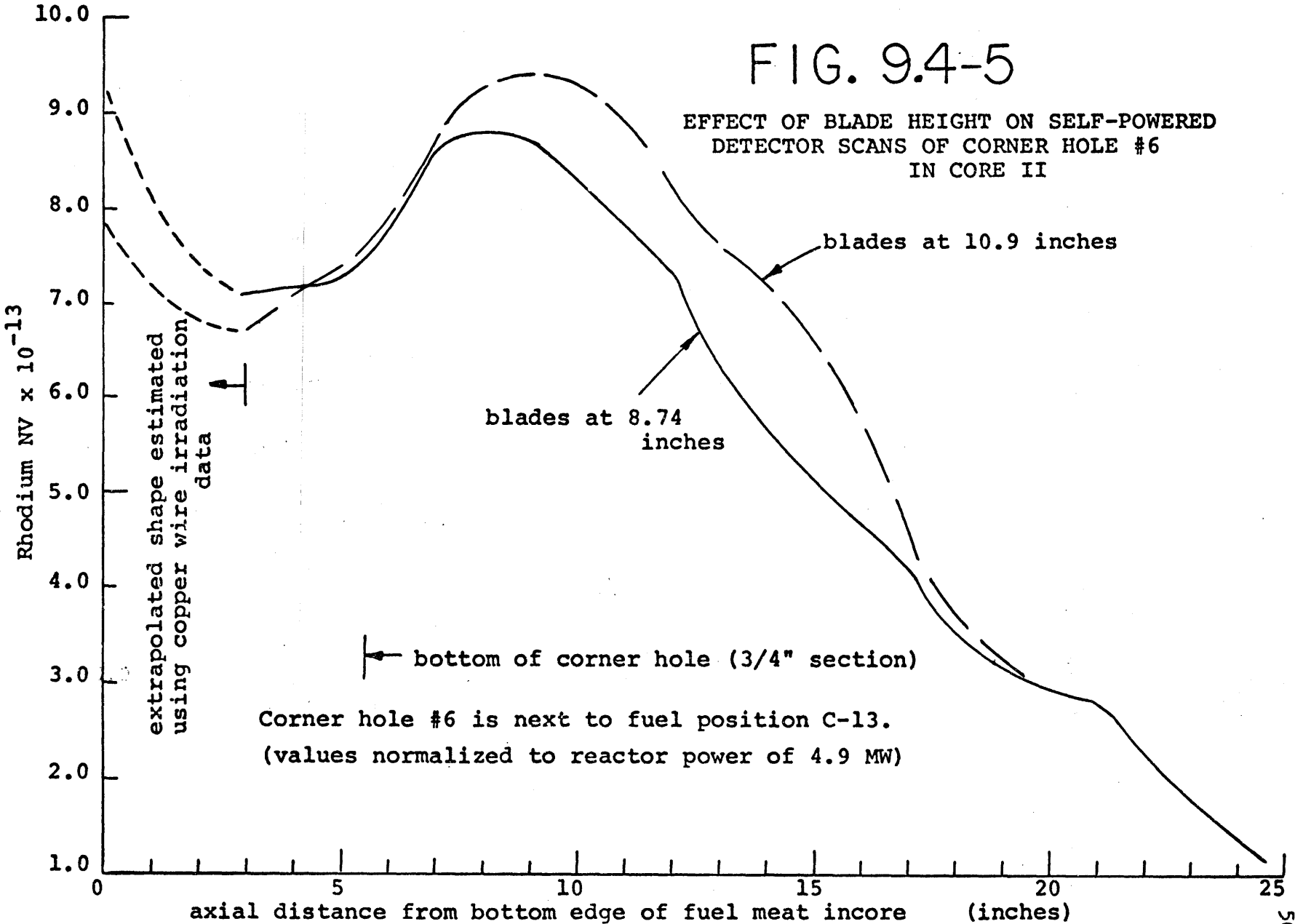
plate). Because it was not possible to insert a self-powered detector to the bottom of the core in a corner hole position, it is not clear as to how much of the increase in power in the upper portion is offset by a decrease in power to the lower portion. The peak flux at an axial height approximately 10 inches from the bottom of the fuel meat increased about 8% as the shim bank was raised from 8.74 inches to 10.90 inches.

Knowing the change in neutron flux level at the beam ports as the shim bank height changes is important to beam port experimenters. Because much of the operating week is spent achieving xenon equilibrium in the reactor, there is a slow and continuous withdrawal of the shim bank during the beginning of the week. Figure 9.4-6 shows the flux level beneath the reactor for Core I at several shim bank heights. For this fuel loading, the flux level decreased about 3.5% for each inch that the shim bank was raised. The flux level beneath the reactor for Core II at several shim bank heights is shown in Fig. 9.4-7. For Core II the flux level decreased about 4.3% for each inch that the shim bank was raised.

Note in Figs. 9.4-6 and 9.4-7 that the absolute flux level appears to be higher at the bottom of Core II than the flux level at the bottom of Core I. This conclusion is not correct. The discrepancy may be caused by one of

FIG. 9.4-6

**CHANGE IN RHODIUM SELF-POWERED DETECTOR READINGS BENEATH CORE I
WITH CHANGES IN SHIM BANK HEIGHT**

Detector tip located at bottom of spider hole #1 at
0.25 inches from core tank bottom.

(values normalized to reactor power of 4.9 MW)

shim bank height   (inches)
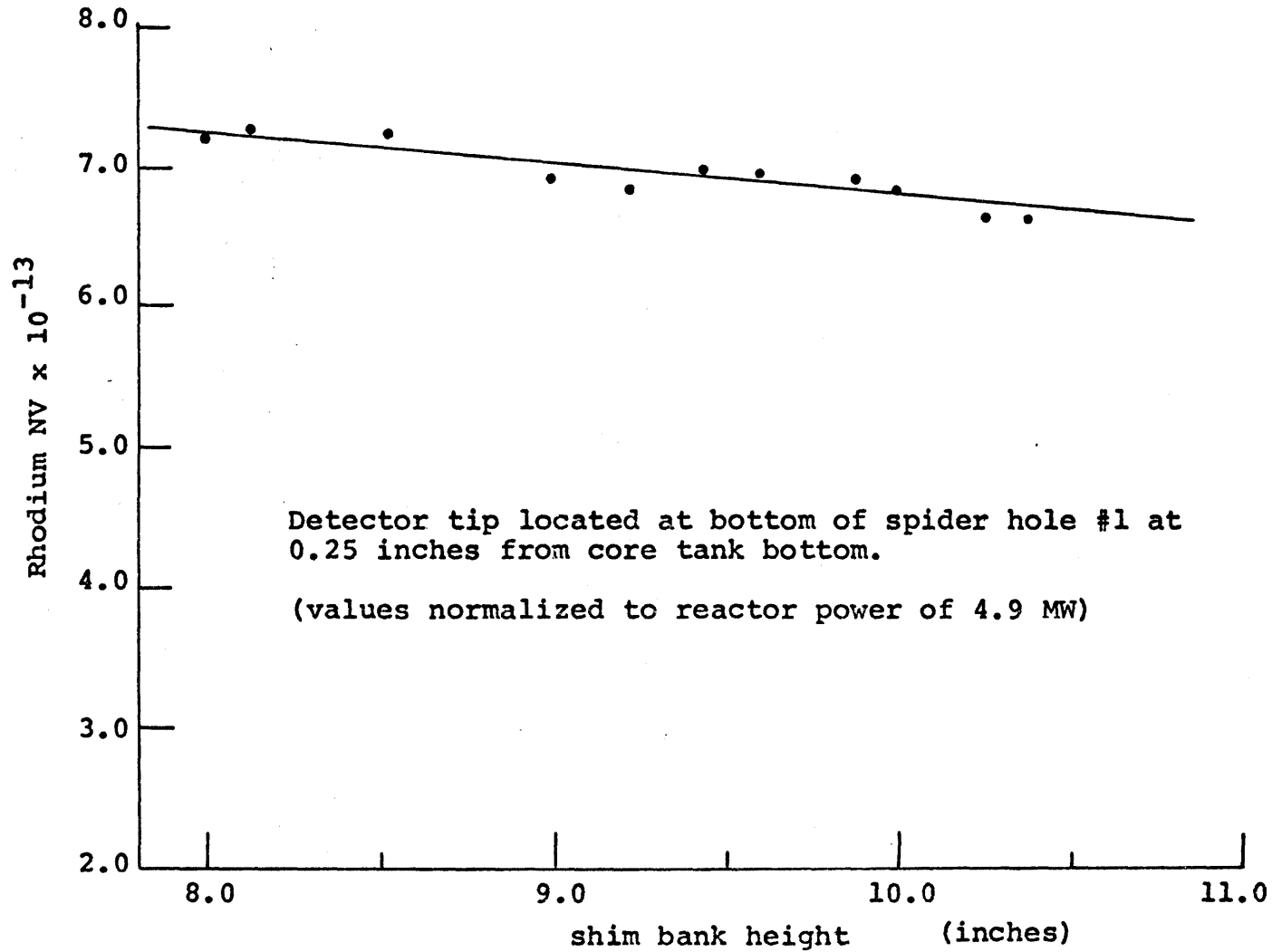
FIG. 9.4-7

CHANGE IN RHODIUM SELF-POWERED DETECTOR READINGS BENEATH CORE II
WITH CHANGES IN SHIM BANK HEIGHT

Detector tip located at bottom of spider hole #1 at
0.25 inches from core tank bottom.

(values normalized to reactor power of 4.9 MW)
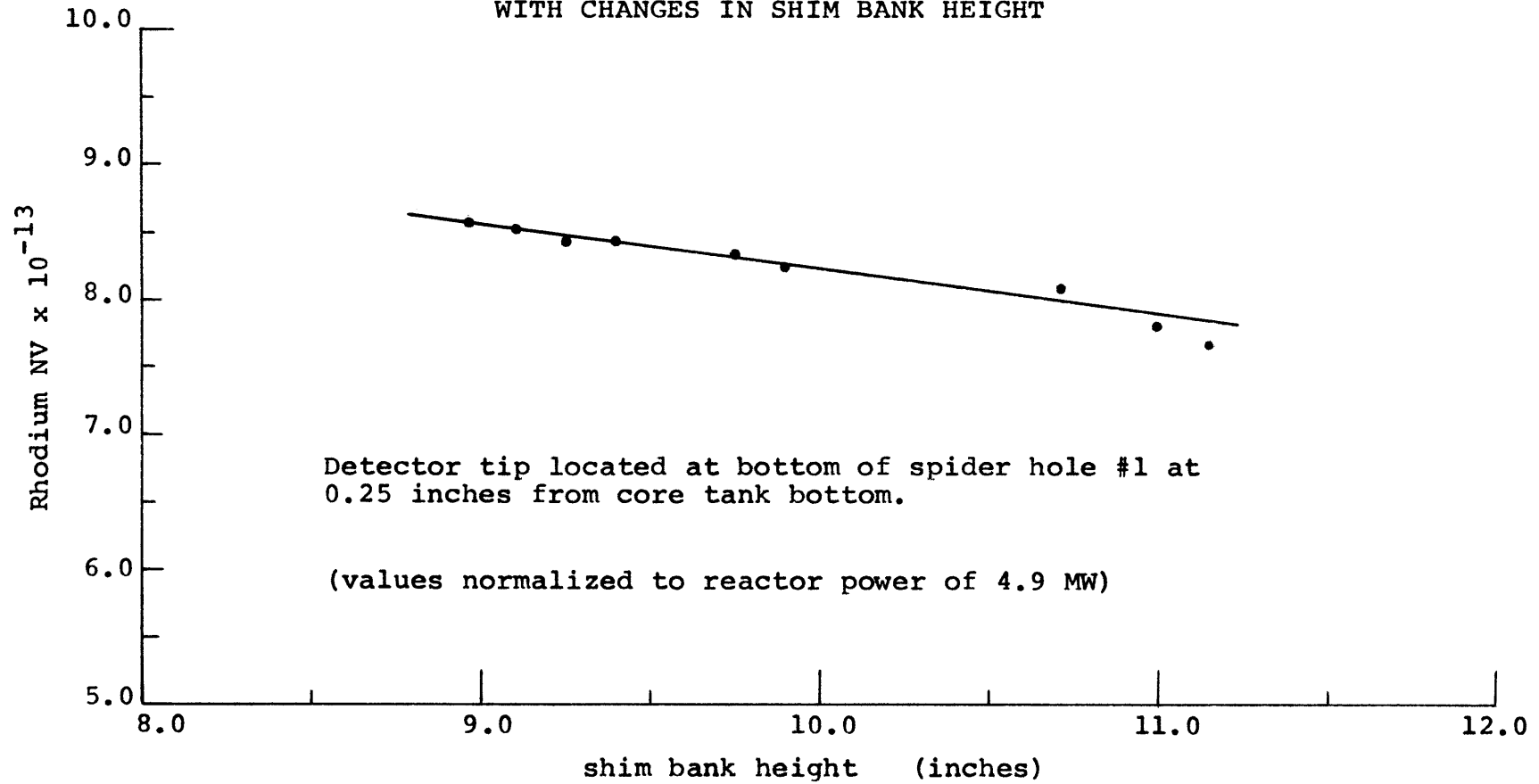
the following reasons:

1) Uncertainty in reactor power level measurements for normalizing data,

2) Uncertainty in the self-powered detector tip location, or

3) Non-uniformity between supposedly identical rhodium self-powered detectors.

Since all total reactor power level measurements were based on the value obtained using the primary flow - ΔT recorder, the power level uncertainty should be small (within a few percent of measured value). The detector tip location is only accurately known to within one half of an inch and thus may yield some error. The same self-powered detector was used in the scans of the MITR-I and Core I of the MITR-II. Shortly after being inserted into Core II and before readings were taken, this detector failed. A second detector with a supposedly identical emitter section as the first was used for all Core II Scans. This second detector appears to give noticeably higher values of absolute flux than the first detector but the first detector had failed before a calibration between the two detectors could be obtained.

Figure 9.4-8 shows a self-powered detector scan of a storage position in the fuel storage rack. This scan of an element in storage is a factor of about 700 below the bottom edge of the fuel meat of an element

FIG. 9.4-8

RHODIUM SELF-POWERED DETECTOR SCAN OF FUEL
STORAGE RACK

location
of bottom
of fuel meat
without inserts in
rack

location of bottom
of fuel meat with
inserts in rack

(values normalized to reactor power
of 4.9MW)

Rhodium NV

1×10^{12}

1×10^{11}

1×10^{10}

1×10^{9}

distance from bottom of fuel storage rack (inches)
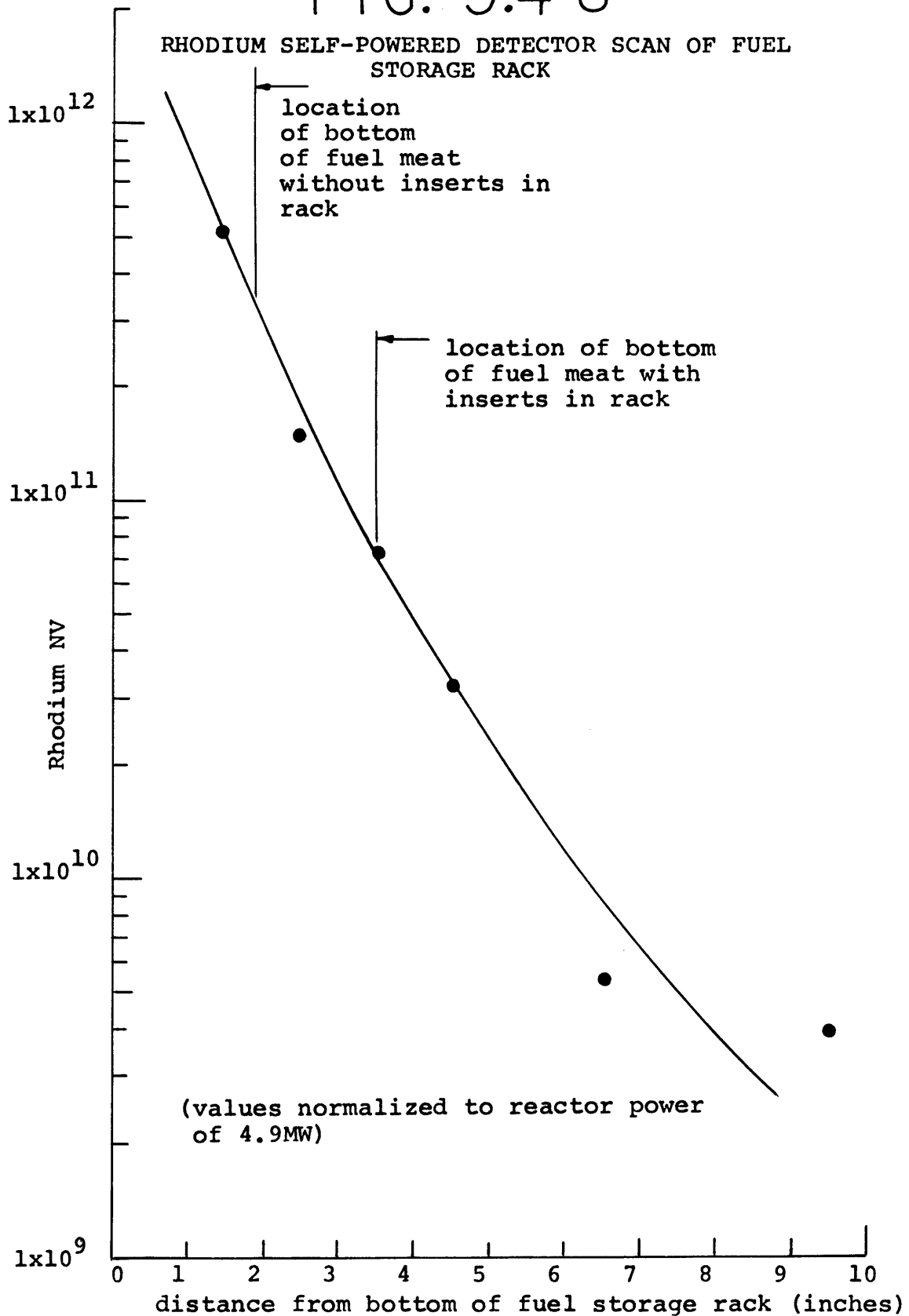
incore provided that poisoned inserts are kept in the fuel storage rack to keep the element raised. The flux drops off very rapidly up the fuel storage rack position thus, the elements may be safely stored in the rack.

CHAPTER 10

CONCLUSIONS

The objectives outlined in Chapter 2 have been completed. Core-wide distributions of the initial cores of the MITR-II have been determined and the Safety Limit Factor (SLF) and Operating Limit Equation (OLE) have also been evaluated. The initial stages of startup are completed and research activity has again commenced at the MITR facility. The following sections summarize the conclusions found in this work.

10.1 Distribution Summaries

Power, coolant flow, and temperature distributions were analytically and experimentally determined for Core I and II of the MITR-II.

10.1.1 Core Power and Neutron Flux

The distributions of core power and neutron flux for Core I and Core II are discussed in Chapters 5 and 6, respectively. Core I was operated with fixed absorbers in the upper portion of the core and Core II was operated without fixed absorbers. Solid aluminum

dummy elements were loaded in both cores for reactivity control. The undermoderated MITR-II core has a non-classical power and neutron flux distribution. The power density peaks at locations where additional moderator is present such as: 1) outer edges of the core (especially at the core housing corner holes and water filled control blade slots with the blades withdrawn), 2) gaps and coolant passages in incore experimental facilities. The peak neutron flux occurs in the reflector beneath the center of the core.

The results of power and neutron flux distribution calculations and measurements for Core I are summarized in Tables 5.5-1, 5.5-2, and 5.5-3. Table 6.4-1 summarizes the power distribution calculations and measurements for Core II. The power and neutron flux distributions of Core I were in good agreement with design expectations. The neutron flux and power densities in the active section of Core I increased with increases in the length of the fixed absorber necessitated by reactivity control requirements. The active height of Core I was approximately 12 inches and the average power density in the active core was about 130 watts/cm^3. Removal of the fixed absorbers to form Core II flattened the power density over the 22 inch fueled core length. The average power density in Core II dropped to about 100 watts/cm^3.

The thermal neutron flux level at the beam ports beneath the core was greater for Core I than for Core II.

10.1.2 Flow

The flow distributions in the MITR-II are discussed in Chapter 4. The B-ring fuel elements receive the highest average element flows. If the A -ing is fully loaded with fueled elements, the A-ring contains the element with the lowest flow. If at least one A-ring position is occupied by a solid dummy or sample assembly, the average flow to the remaining A-ring fueled elements is greatly increased to a value that is slightly below the B-ring average. The C-ring has the lowest average element flow if the A-ring is not fully fueled. The peak flow disparity is approximately 7%, or the element with the lowest flow receives approximately 7% less flow than the average element in the core. The amount of coolant flow that bypasses the core is very dependent on the number of solid dummies and experimental facilities located in the core. For Core I the bypass flow was about 6% and for Core II, the bypass was about 8%.

10.1.3 Temperature

The temperature distributions in Core I and II of the MITR-II are discussed in Chapter 8. The peak wall temperatures for Core I and Core II occurred at locations several inches from the bottom of the fuel in outer C-ring

element positions. The measured temperatures were in good agreement with the temperatures predicted by using nominal conditions with the exception of the lower fuel meat edges. The bottom edge temperature spike appears to be much smaller than was predicted using conservative assumptions. The combination of increased heat transfer at the channel entrance, decreases in bottom edge uranium density, and axial heat conduction, which were neglected in the calculated prediction, result in a low and very acceptable bottom temperature spike. All measured and predicted nominal temperatures fell well below the temperature required to cause boiling in the core.

10.2 Agreement Between Predictions and Measurements

The agreement between measured and predicted values in the MITR-II initial cores is very good with the following exceptions:

1) Measured lower edge wall temperature is much less than predicted,

2) Predicted values of F_r (radial peaking factor) for individual plates are lower than measured plate values while predicted values of F_r for entire elements are in very good agreement with measured values,

3) Predicted values of Z at the hot spot tend to be larger than the measured values because of the lack of axial mesh points in the computer calculation to accurately show the axial position at which the hot spot occurs,

4) Some specific experimental data values in Core I (central plate scans in C-10) are questionable at local points but the discrepancies are averaged out in obtaining core-wide results.

The agreement between experimental and predicted core factor values was best in the hot channel positions. The uncertainty in power density predictions and measurements was less than the 10% uncertainty factor utilized in determining the SLF and OLE.

10.3 Summary of Safety Limit Evaluation

The safety limit of the MITR-II is set to prevent boiling induced flow instabilities which could lead to boiling burnout. The safety limit will not be exceeded provided that the measured system values of reactor power, coolant flow, outlet temperature, and water level are within the limiting safety system settings and that the Safety Limit Factor (SLF) is less than 2.9. The SLF was evaluated for Core I and Core II of the MITR-II and is discussed in Chapter 7. Full power operation of both cores was authorized because the SLF values were less than 2.9. The hottest channels occurred in C-ring elements next to the outside boundary of the core. Using conservative calculations, the value of the SLF increased with shim bank height for both cores, thus imposing an upper limit on allowable shim bank height for initial operation at which the SLF equaled 2.9. Because Core II was operated without fixed absorbers which normally depress the power in the upper core, the raised shim condition was more limiting for Core II than for Core I and the shim bank was limited to being withdrawn less than 14.6 inches. The

higher shim bank calculations are very conservative

because the effects of xenon and burnup are neglected.

10.4 Summary of Limiting Conditions for Operation

The limiting condition for operation above 1.0 kw

is that the core factors have been determined and it has

been shown that incipient boiling is prevented from

occurring anywhere in the reactor core at values of reactor

power, coolant flow, outlet temperature, and water level

that correspond to the limiting safety system settings.

Incipient boiling will not occur in the reactor core if the

value of the Operating Limit Equation (OLE) is less than

or equal to 3.72. The OLE was evaluated for Core I and

Core II of the MITR-II and was shown to be less than

3.72. The derivation of the OLE and its evaluation for

the initial cores was discussed in Chapter 7.

The OLE has its maximum value at the point where the

wall temperature is its maximum value in the core. The

peak wall temperatures for the initial cores occurred on

fuel plates in the C-ring next to the reflector outside

the core. The peaks occurred at axial heights several

inches from the bottom of the fuel meat. While the axial

height of the maximum value of the OLE increased with

increased shim bank height, the value of the OLE remained

approximately constant for Core I. For Core II, the

value of the OLE increased with shim bank height and the

limit of 3.72 was conservatively calculated to be reached

at a bank height of 15.0 inches (1 pump flow).

The initial design of the Incore Sample Assembly (ICSA) could not be utilized in the MITR-II because of large power peaking in the fuel plates of fuel elements nearby the facility. The ICSA contained an excess of water and the resultant thermal neutron peaking would have resulted in the OLE being exceeded if the reactor were operated at powers above 1.0 kw with the ICSA incore. A minor revision of the design can be made to remove the excess water from the core.

10.5 Recommendations

The following recommendations are made for evaluation and loading of future cores:

1) Operation with fixed absorbers is much preferable than operation without fixed absorbers. Fixed absorbers increase the thermal neutron flux beneath the reactor by depressing the power in the upper core. Power peaking and neutron flux changes with shim bank height are more acceptable in the core with fixed absorbers.

2) A full core 3-D calculational method should be developed that would include effects of burnup and fission product poisoning and would yield accurate element average powers.

3) Improved methods should be developed for deriving single element fuel plate powers from the results of the 3-dimensional calculation.

4) The calculational models with burnup and fission product poisoning should be used to evaluate blade height effects.

5) A solid dummy or sample facility should be included in the A-ring in all core loadings in order to insure an acceptable coolant flow distribution.

6) The use of variable plate loadings in fresh fuel elements to decrease the beginning of life power peaking may be worth future study (lower loading in two outside fuel plates).

7) Experimental facilities loaded incore may be used to tailor the power distribution in such a manner than the power peaks occur at a specific location and are insensitive to other system effects such as blade height. Positions for making flux wire and self-power neutron detector scans should be provided in the design of the facility.

8) A fuel management scheme similar to the one suggested by Kadak (Ref.10.5-1) should be used. Fresh fuel should be loaded in the A and B rings and then moved to the C-ring after depletion time step.

9) If the factor, F_{p_2} is to be evaluated and not set equal to 1.0, the definition of F_p in the Technical Specifications should be modified slightly.

10) The hot channel factors should be combined in a semi-statistical manner.

The last two recommendations would require approval by the Nuclear Regulatory Commission prior to use.

REFERENCES

3.3-1   Glasstone, S. and Sesonske, A., Nuclear Reactor
        Engineering, New York, New York: Van Nostrand
        Reinhold Company, 1967.

4.2-1   Daily, J. W. and Harleman, D., Fluid Dynamics,
        Reading, Massachusetts: Addison-Wesley, 1966.

4.2-2   Le Tourneau, B. W. and Gremble, R. E., "Engineering
        Hot Channel Factors for Nuclear Reactor Design,"
        Nuclear Science and Engineering, 1, 1956 339-369.

4.3-1   Dieterich Standard Corporation, "Annubar, Primary
        Flow Elements," Boulder, Colorado, 1970.

4.4-1   MITR Reactor Staff, "Natural Convection Value
        Design Change," MITR-SR#M-75-38, June 24, 1975.

5.1-1   MITR Reactor Staff, "Safety Analysis Report for
        the MIT Research Reactor (MITR-II)," MITNE-115,
        MIT, October, 1970.

5.1-2   Addae, A. K., "The Reactor Physics of the
        Massachusetts Institute of Technology Research
        Reactor Redesign," Ph.D. Thesis, Nuclear
        Engineering Department, MIT, July, 1970, MITNE-118.

5.1-3   Fowler, T. B., et al, "Exterminator-2: A Fortran
        IV Code for Solving Multigroup Diffusion
        Equation in Two Dimensions," ORNL-4078, 1967.

5.1-4   Kadak, Andrew C., "Fuel Managment of the Redesigned
        MIT Research Reactor," Department of Nuclear
        Engineering, MIT, Ph.D. Thesis, April, 1972.

5.2-1   Fowler, T. B., et al, "Nuclear Reactor Core Analysis
        Code: CITATION," ORNL-TM-2496, Rev. 2, 1971.

5.2-2   Emrich, W. J., "Reactivity Studies of the MITR-II,"
        SM Thesis, Nuclear Engineering Department, MIT,
        1974.

5.2-3   Hansen, G. E. and Roach, N. H., Six and Sixteen
        Group Cross Sections for Fast and Intermediate
        Critical Assemblies," LAMS-2543.

5.2-4   Toppel, B. and Baksys, J., "The Argonne Revised
         THERMOS Code," ANL-7023, March 1965.

5.2-5   Lukic, Y. "2-Dimensional MITR-II Beamport Mockup,"
         unpublished report, 1971.

5.2-6   Kennedy, D. J., "Beam Port Optimization for the
         Proposed High-Flux MITR," Sc.D. Thesis,
         Department of Nuclear Engineering, MIT, August,
         1969.

5.2-7   Yeung, M. K., "Reactivity Studies of the MITR-II
         for Initial Loading," 22.90 Report, Department
         of Nuclear Engineering, MIT, June, 1975.

5.3-1   Labbe, D. E., "Gamma Scanner for MITR-II Fuel
         Plates," S.M. Thesis, Department of Nuclear
         Engineering, MIT, August, 1974.

5.3-2   Grill, S. F., "Construction of the Gamma Scanner
         for MITR-II Fuel Plates, " 22.90 Report,
         Department of Nuclear Engineering, MIT, May, 1975.

5.3-3   Labbe, D. E., "Supplementary Report--Gamma Scanner
         for MITR-II Fuel Plates," Supplement to S.M.
         Thesis, Department of Nuclear Engineering, MIT,
         August, 1974.

5.4-1   Mathews, R. L., "Flux Distributions in the MIT
         Reactor", Ph.D. Thesis, Department of Nuclear
         Engineering, MIT, August, 1964.

5.4-2   Kaplan, I. and Travelli, A., "Notes for Nuclear
         Reactor Physics I," Department of Nuclear
         Engineering, MIT, 1964.

5.4-3   Hove, C. M., "Extra Power Peaking in MITR-II
         Due to Manufacturing Tolerances in the Length
         of the Fuel Plates," 22.90 Report, Department
         of Nuclear Engineering, MIT, May, 1973.

7.1-1   MITR Reactor Staff, "Safety Analysis Report for
         the MIT Research Reactor (MITR-II)", MITNE-115,
         MIT, October, 1970.

7.1-2   MITR Reactor Staff, "Technical Specifications for
         the MIT Research Reactor (MITR-II)," MITNE-122,
         MIT, April, 1973.

7.2-1   Griffith, P., "Pressure Drop--Flow Rate Instabilities
        in Two Phase Systems," MIT Course 22.365 Notes
        HH-A, MIT, Spring, 1976.

7.2-2   LeDinegg, M., "Instability of Flow During Natural
        and Forced Circulation," Die Warme, 61, No. 8
        1938; AEC-tr-1861, 1954.

7.2-3   Markels, M., "Effects of Coolant Flow Orificing
        and Monitoring on Safe Pile Power," Chemical
        Engineering Progress, Symp. Ser., 19, 73, 1956.

7.2-4   Maulbetsch, J. and Griffith P., "A Study of
        System-Induced Instabilities in Forced-Convection
        Flows with Subcooled Boiling," Report No. 5382-35,
        Department of Mechanical Engineering, MIT, April
        15, 1965.

7.2-5   Forgan, R. and White, R. H., "Pressure-Drop
        Characteristics for the Flow of Subcooled Water
        at Atmospheric Pressure in Narrow Heated Channels--
        Part 2," AERE-M1739 (Part 2), 1966.

7.2-6   Spurgeon, D., "Preliminary Design Studies for a
        High Flux MIT Reactor," MIT Nuclear Engineering
        Department, S.M. and Nuclear Engineer Thesis,
        May, 1969.

7.2-7   Dormer, T., Jr. and Bergles, A. E., "Pressure
        Drop with Surface Boiling in Small-Diameter
        Tubes," Report No. 8767-31, Department of
        Mechanical Engineering, MIT, September 1, 1964.

7.2-8   Gambill, W. R., "Generalized Prediction of Burnout
        Heat Flux for Flowing, Subcooled, Wetting Liquids,"
        Chemical Engineering Progress, Symp. Ser., 41,
        71, 1963.

7.2-9   Bernath, L., Chemical Engineering Progress, Symp.
        Ser., 30, 56, 1960, 95-116.

7.3-1   Rohsenow and Bergles, "The Determination of
        Forced-Convection Surface-Boiling Heat Transfer,"
        Journal of Heat Transfer, August, 1964.

7.3-2   Taborda, Jesus Alberto, "Design of MITR-II Fuel
        Plates. Heat Transfer in Longitudinal Finned
        Narrow Channels," Nuclear Engineering Department,
        MIT, SM Thesis, September, 1971.

7.3-3   Szymczak, William J., "Experimental Investigation
        of Heat Transfer Characteristics of MITR-II Fuel
        Plates, In-Channel Thermocouple Response and
        Calibration," Nuclear Engineering Department,
        MIT, SM Thesis, September, 1975.

7.4-1   Kadak, Andrew C., "Fuel Management of the Re-
        designed MIT Research Reactor, " Department
        of Nuclear Engineering, MIT, Ph.D. Thesis,
        April, 1972.

7.5-1   Choi, D. K., "Temperature Distribution and
        Natural Convective Shutdown Cooling of the
        MITR-II," MIT Nuclear Engineering Department,
        SM Thesis, May, 1970.

8.1-1   Griebenow, M. L. and Richert, K. D., "MACABRE II,"
        Idaho Nuclear Corporation, IN-1107, September,
        1967.

8.3-1   Weast, R. C., Handbook of Chemistry and Physics,
        9th Edition, Chemical Rubber Company, Cleveland,
        Ohio, 1968.

8.3-2   Szymczak, W. J., "Experimental Investigation of
        Heat Transfer Characteristics of MITR-II Fuel
        Plates, In-Channel Thermocouple Response and
        Calibration," SM Thesis, Department of Nuclear
        Engineering, MIT, September, 1975.

8.3-3   Rohsenow, W. M. and Hartnett, J. P., Handbook
        of Heat Transfer, McGraw-Hill Inc., New York,
        New York, 1973.

9.2-1   Hilborn, J. W., "Self Powered Flux Detectors,"
        Reuter-Stokes pamphlet, Reuter-Stokes Canada
        Limited, Ontario, Canada, 1971.

10.5-1 Kadak, Andrew C., "Fuel Management of the
        Redesigned MIT Research Reactor," Department
        of Nuclear Engineering, MIT, Ph. D Thesis,
        April, 1972.

APPENDIX A

MITR-II Detail Startup Procedures

1) Procedure 5.0.4 - Removable Plate Handling Procedure

2) Procedure 5.9.1 - Neutron Flux and Core Power Mapping

3) Procedure 5.9.2 - Flow Mapping Procedure

Note: Procedures in this section have been condensed from approved form in MITR-II Startup Procedure Manual.

5.0.4 <u>Removable Plate Handling Procedure</u> (page 1 of 2)

Prerequisites

1. Special cask ready if required.

2. Removable plate element handling tools ready.

3. Removable plate element removed from core as per refueling checksheet and stored in storage ring.

4. RPO present on reactor top.

Procedure

1. Slowly raise element to top of reactor pool while RPO surveys radiation level.

2a. If radiation levels are low, transfer element directly to hot shop by hand and proceed to step 11.

2b. If radiation levels are high, attach upper end of fuel element hook to small crane hook and tape hook.

3. Position special cask on transporter on reactor floor below reactor top catwalk.

4. Guide element with rod while element is raised clear of pool using crane.

5. Using crane, position element above special cask.

6. Man standing on catwalk guides removable plate element into special cask.

7. When element is securely in cask, man on catwalk unlatches lifting tool from element and lifting tool is lifted away.

8. Cask and element transferred from reactor floor to hot shop.

9. Squirt alcohol into channels to plates to be removed.

10. Using hook, remove from cask and place in lead cave in hot shop.

*11. Remove 8 screws and end box from element.

12. Use polyethylene dowel to push plate to be removed 3/4" out from other plates and attach clamp to end of plate.

13. Squirt alcohol along edges of plate to be removed. Do not force plates.

14. Slowly slide plate out of element and place in shielded location if hot shop and record plate number and location in element from which it came. (Slot number and if plate number was at "notch" end or "other" end.)

15. Repeat steps 12 - 14 for other plates as necessary.

16. Upon completion of usage of plates, clean plates.

5.04 Removable Plate Handling Procedure

17. Clamp end of plate to be replaced and record number and location.

18. Slide plate in and lubricate with alcohol.

19. Repeat steps 17 and 18 for other plates as necessary.

20. Attach end box with eight screws.

21. Remove element from cave in hot shop to cask if necessary.

22. Return element to reactor building and store in fuel storage rack following standard procedure.

* Note: During handling and use of the fuel element or fuel plates, the fuel must be under surveillance or left in a secure condition. All handling must be within the Tech Spec 3.10.

Procedure 5.9.1   Neutron Flux and Core Power Mapping

Acceptance Criteria

Values of F_r, F_a, F_{HC}, F_p shall be determined together with an estimate of experimental uncertainty.

Prerequisites

1.   Startup checklist 3.1.3 completed.

2.   Reflector and core at normal operating level, as preliminarily determined during preoperational test program. Waters at operating purity.

3.   Main reflector flow, main coolant flow, secondary coolant flow are stopped. Circuit breakers for pump motors in these systems open and tagged open. Flow has been stopped long enough for systems to reach ambient temperature. (Clean up system pumps operating in shutdown cooling mode for reflector system and primary system.)

4.   Scram circuit bypassed for: (if jumper required, jumper must be tagged and recored in Log Book)

   Reflector low flow scram

   Secondary flow scrams and primary flow scram

   Shield coolant low flow scrams

5.   Neutron source(s), in 3GV port attached to be removable.

6.   Nuclear instruments all in place and configured as follows:

   Power range

   Channel 4 - normal port

   Level trip set minimum, corresponding to 20 amps from chamber, and < 100 KW.

   Channel 5 - normal port

   Level trip set at _____ amps corresponding to _____ watts (<200 watts)

Channel 6 - normal port

Level trip set at _____ amps corresponding to _____ watts. (<200 watts)

Channel 7

Normal location, normal adjustments.

Channel 8 - Located for maximum sensitivity in normal well (3GV-3). Meter relay trip set _____.

Channel 9

Normal location, normal adjustments.

Startup Range

Channel 1 - Located in 3IH3. Normal trip setting of > + 10 sec. period. Chamber voltage setting and discriminator setting established and recorded.

Channel 2 - Located in a 4TH1 port. Trip setting of > + 10 sec. period. Chamber voltage setting and discriminator setting established and recorded.

Channel 3 - Located in 4IH4. Normal trip setting (> + 10 sec).

With the startup source(s) in the ICSA or in 3GV, Channels 1 and 2 must be on scale, at least, 10 cpm.

Demonstrate that the startup source(s) or 3GV are causing on scale indication by lifting the source from the ICSA. Observe a decrease in instrument output on the meters to be observed during fuel loading.

Channel 1 _____ Channel 2 _____

7. Procedure 5.1.3 demonstrated that required shutdown margin as required by Technical Specifications exists.

8. Reactivity change due to source removal from ICSA will be _____ % K/K as estimated in procedure 5.1.1. Maximum allowed is (0.2%) K/K per Tech Spec 3.9. Reactivity effect for 3GV will be less.

9. Coolant circulated to remove bubbles, per procedure 5.0.3.

Special Precautions

1. Two low power level scram and two period trip channels shall be operating at all times. Other channels should be operable and operation without a given channel must be recorded in the log and approved by a licensed senior operator and a licensed operator.

2. Estimated power level should be less than 500 watts if a Plutonium-Beryllium source is used.

   Always set the rod positions from the same direction to avoid backlash effects on the reading of the critical position.

Procedure

1. Fuel plate gamma scanner set up in hot shop.

2. Wire counting apparatus set up in hot shop.

3. Foil counting apparatus set up.

4. Using fuel radiographs obtain (0,0) location for each removable fuel plate.

5. Scan the unirradiated fuel plates three times to check (0,0) and obtain background counts (attach data sheets).

6. Dry run of gamma scanning performed and method approved by RPO.

7. Gamma scanning can begin when sustained operation at 100 watts is possible.

8. The following method shall be used for gamma scanning:

   a. Removable plate fuel element uranium and foil loaded in core following standard fuel loading procedure. Foil must be irradiated in repeatable location.

   b. Reactor operated at 100 watts for 30 minutes.

   c. Removable plate element and foil removed from core and placed in transfer shield.

   d. Plates removed from elements and scanned (standard data sheets will be attached).

   e. A cobalt foil shall be irradiated in 1PH2 for every irradiation and saved.

9. Dry run of wire scanning method done and method approved by RPO.

10. At the two fuel element locations that indicate highest power, copper wires shall be attached to the fuel elements and placed in corner holes and spider holes (using self-powered detector guide tube). The wires shall be scanned and the data sheets attached.

11. Dry run of foil counting method done and RPO approves of method.

12. Bare and cadmium covered cobalt, gold, and copper foils shall be irradiated in the following positions and data attached.

    A. 1PH2 - bare only

    B. Sample assembly

13. The rhodium self-powered detector shall be used to scan the corner holes and spider holes and data attached (may be done at higher powers).

14. Based on assembled data the following are found to be:

$F_r =$

$F_a =$

$F_{HC} =$

$F_p =$

Calculations attached.

5.9.2 Flow Mapping Procedure

Acceptance Criteria

Values of F_f and d_f shall be determined with an estimate of experimental uncertainty.

Prerequisites

1. Above core flowmeter constructed.

2. Pitot tube test device constructed and calibrated.

3. 100 inch manometer constructed.

4. Core filled with 24 elements, two solid aluminum dummies and proper ICSA or finned fuel dummy in one central position.

5. Reactor shutdown condition.

6. Startup check sheet 3.1.3 completed and main pump tags cleaned.

Procedure

1. Install above core flowmeter above fuel position C-13 and clamp in place.

2. Connect 100 inch manometer and bleed air out of lines.

3. Connect manometer to primary flow nozzle as per procedure.

4. Start MM1 and throttle to 1150 gpm.

5. Record Δh on both manometers on attached data sheet.

6. Move flowmeter to above each fuel position and record Δh on flowmeter manometer on attached data sheet.

7. Position flowmeter above C-13 and clamp in place.

8. Start MM1A and throttle to 2000 gpm.

9. Record Δh on both manometers on attached data sheet.

10. Move flowmeter to above each fuel position and record Δh on flowmeter manometer on attached data sheet. Keep water temperature constant and repeat measurements as desired.

11. For positions with Solid Dummies and ICSA, the flow is to be measured by fuel shuffling Caution must be taken to assure that the shut down margin is not exceeded. Unload fuel before unloading the Solid Dummy element and moving it to a symmetric position. Use fuel loading procedures. Check for change in flow for elements adjacent to dummy positions.

12. Determine bypass flow for each of the following items. Attach additional sheets to show whether bypass flow is calculated, measured or a combination of both.

BYPASS FLOW

(6)   Control Blades   _____gpm

(6)   Corner Holes   _____gpm

(4)   Check Valves   _____gpm

(2)   Antisyphon Valves   _____gpm

      Annular Partition Gasket   _____gpm

      Annular Partition Gasket
      Housing Joint   _____gpm

(2)   Dummy Elements   _____gpm

            Subtotal A   _____gpm

      Sample Assembly   _____gpm

            Subtotal B   _____gpm

13. Minimum d_f = _____

14. Where W is the total flow for which the bypass flows were determined:

$$F'_f = \frac{W - A}{W}$$

15. When a sample assembly is in use:

$$F'_f = \frac{W - B}{W}$$

Case _____   _____gpm Flow

Position	Main Flow Δh Nozzle (if applicable)	Incore Flowmeter			Incore Flowmeter			Incore Flowmeter			Incore Results	
		h_1	h_2	Δh	h_1	h_2	Δh	h_1	h_2	Δh	AVE Δh	$\Delta h^{0.477}$
A-1												
A-2												
A-3												
B-1												
B-2												
B-3												
B-4												
B-5												
B-6												
B-7												
B-8												
B-9												
C-1												
C-2												
C-3												
C-4												
C-5												

Case _____   _____ gpm Flow

Position	Main Flow Δh Nozzle (if applicable)	Incore Flowmeter			Incore Flowmeter			Incore Flowmeter			Incore Results	
		h_1	h_2	Δh	h_1	h_2	Δh	h_1	h_2	Δh	AVE Δh	$\Delta h^{0.477}$
C-6												
C-7												
C-8												
C-9												
C-10												
C-11												
C-12												
C-13												
C-14												
C-15												

APPENDIX B

Three-Dimensional CITATION Computer Code Output
Listing for Core I Loading

24 Fueled Elements
3 Solid Dummy Elements (A-1, B-2, B-8)

Shim Blades at 8 inches

Fixed Cadmium Absorber at 10 inches from
Fuel Bottom

Reactor Power at 5.0 MW

3 DOMAINS: A1,B2,B3, FIXED AT 10", SHIMS AT 8"

GENERAL CONTROL INPUT - SECTION 001

```
   0   0   1   0   0   0   0   0   0   0   0   0   0   0   0   0   0   0   0   0   0   0   0   6   0   0   0   0
   1   0   0   1   0   0   0   1   1   0   0   0   1   0   0   0   0   0   0   0   0   0   0   0   0   0
 200 100  10   2   3   0   0   0   0   0   0   0   0   0   0   0   0   0   0  20  60  20  60  60 240
 -1.200000E+00  9.000000E-01  9.999999E+09  9.999999E+23  0.0          1.000000E+00
```

NEUTRON FLUX PROBLEM DESCRIPTION - SECTION 003

```
   0   0   0   0  12   0   0   0   0   0   1   1   1   0   0   0   0   0   0   0   0   0   0   0   0
 9.999999E-04  1.000000E-02  9.999999E-05  9.999999E-05  9.999999E-05 , 0.0
 0.0          -1.000000E+00  5.000000E+00  1.000000E+00  5.000000E-01  0.0
```

LEFT,TOP,RIGHT,BOTTOM,FRONT,BACK BOUNDARY CONDITIONS ARE
```
   0.0          0.0          0.0          4.692000E-01  4.692000E-01  4.692000E-01
```

THREE DIMENSIONAL CYLINDRICAL GEOMETRY (R,THETA,Z) WIDTH 3.141590E+00 HEIGHT 1.244000E+02 DEPTH 1.640000E+02

REGION SPECIFICATIONS

PTS	REGION WIDTH	PTS		PTS		PTS		PTS		PTS	
1	4.632500E-02	1	6.069999E-03	1	6.457370E-01	1	2.966700E-01	1	1.047900E-01	1	2.966700E-01
1	6.457370E-01	1	1.047900E-01	1	6.457370E-01	1	2.966700E-01	1	5.239500E-02		

PTS	REGION HEIGHT										
1	3.552000E+00	1	8.960000E-01	1	1.893000E+00	1	5.340000E-01	1	1.750000E+00	1	5.450000E+00
1	4.282000E+00	1	1.000000E+00	1	9.525000E-01	1	4.465000E-01	1	6.335000E-01	1	6.335000E-01
1	9.525000E-01	1	6.870000E-01	1	1.726000E+00	1	1.543500E+01	1	1.543500E+01	1	3.000000E+00
1	6.503999E+01										

PTS	REGION DEPTH										
1	3.048000E+01	1	1.016000E+01	1	1.265000E+01	1	7.570000E+00	1	5.080000E+00	1	1.016000E+01
1	5.002500E+00	1	5.002500E+00	1	1.000500E+01	1	2.695000E+03	1	2.695000E+00	1	1.300000E+00
1	6.000000E-01	1	1.900000E+00	1	3.200000E+00	1	6.000000E-01	1	4.127500E+00	1	4.127500E+00
1	4.127500E+00	1	4.251750E+01									

X-DIR. POINTS 11   Y-DIR. POINTS 19   Z-DIR. POINTS 20

DISTANCES TO MESH INTERVAL INTERFACES

J	DIST.															
2	0.046	3	0.052	4	0.698	5	0.995	6	1.100	7	1.396	8	2.042	9	2.147	10	2.793
11	3.089	12	3.142													

DIST.

2	3.552	3	4.448	4	6.341	5	6.975	6	8.725	7	14.175	8	18.457	9	19.457	10	20.409
11	20.856	12	21.489	13	22.124	14	23.077	15	23.764	16	25.490	17	40.925	18	56.360	19	59.360
20	124.400																

KB	DIST																
2	30.480	3	40.640	4	53.290	5	60.860	6	65.940	7	76.100	8	81.102	9	86.105	10	96.110
11	98.805	12	101.500	13	102.800	14	103.400	15	105.300	16	108.500	17	109.100	18	113.227	19	117.355
20	121.482	21	164.000														

DISTANCES TO FLUX POINTS

J	DIST.																
1	0.023	2	0.049	3	0.375	4	0.846	5	1.047	6	1.248	7	1.719	8	2.094	9	2.470
10	2.941	11	3.115														

I	DIST.																
1	2.512	2	4.025	3	5.477	4	6.666	5	7.899	6	11.770	7	16.456	8	18.964	9	19.939
10	20.633	11	21.175	12	21.809	13	22.606	14	23.423	15	24.642	16	34.092	17	49.251	18	57.879
19	97.465																

KB	DIST																
1	15.240	2	35.560	3	45.965	4	57.075	5	63.400	6	71.020	7	78.601	8	83.604	9	91.107
10	97.457	11	100.152	12	102.150	13	103.100	14	104.350	15	106.900	16	108.800	17	111.164	18	115.291
19	119.419	20	142.741														

ZONE INPUT BY REGION

PLANE NUMBER 1

```
18  18  18  18  18  18  18  18  18  18  18
18  18  18  18  18  18  18  18  18  18
18  18  18  18  18  18  18  18  18  18
18  18  18  18  18  18  18  18  18  18
18  18  18  18  18  18  18  18  18  18
18  18  18  18  18  18  18  18  18  18
18  18  18  18  18  18  18  18  18  18
18  18  18  18  18  18  18  18  18  18
18  18  18  18  18  18  18  18  18  18
 9   9  18  18  18  18  18  18  18  18
18   9  18  18  18  18  18  18  18  18
 9   9   9  18   9  18   9  18  18
18  18  18  18  18  18  18  18  18  18
18  18  18  18  18  18  18  18  18  18
18  18  18  18  18  18  18  18  18  18
18  18  18  18  18  18  18  18  18  18
18  18  18  18  18  18  18  18  18  18
15  15  15  15  15  15  15  15  15  15
16  16  16  16  16  16  16  16  16  16
```

PLANE NUMBER 2

```
2   2   2   2   2   2   2   2   2   2   2
2   2   2   2   2   2   2   2   2   2
2   2   2   2   2   2   2   2   2   2
2   2   2   2   2   2   2   2   2   2
2   2   2   2   2   2   2   2   2   2
2   2   2   2   2   2   2   2   2   2
2   2   2   2   2   2   2   2   2   2
2   2   2   2   2   2   2   2   2   2
2   2   2   2   2   2   2   2   2   2
9   9   2   2   2   2   2   2   2   2
2   9   2   2   2   2   2   2   2   2
9   9   9   9   2   9   9   2   9   9   2
2   2   2   2   2   2   2   2   2   2
2   2   2   2   2   2   2   2   2   2
2   2   2   2   2   2   2   2   2   2
```

```
   2    2    2    2    2    2    2    2    2    2    2
  19   19   19   19   19   19   19   19   19   19   19
  15   15   15   15   15   15   15   15   15   15   15
  16   16   16   16   16   16   16   16   16   16   15
```

PLANE NUMBER 3

```
  11   11   11   11   11   13   13   13   13   13   13
  11   11   11   11   11   13   13   12   13   13   13
  11   11   11   11   13   13   13   13   13   13   13
   9    9    9    9    9    9    9    9    9    9    9
   9    9   14   14   14   14   14    9   14   14   14
   9    9   14   11   11   11   14    9   14   14   14
   9    9   14   14   14   14   14    9   14   14   14
   9    9   14   14   14   14   14    9   14   14   14
   9    9   11   11   11   11   11    9   11   11   11
   9    9   11   11   20   11   11   20   11   11   20
  20    9   11   11   20   11   11   20   11   11   20
   9    9    9    9   20    9    9   20    9    9   20
  11   11   21   21   11   21   21   11   21   21   11
  11   11   11   11   11   11   11   11   11   11   11
   7    7    7    7    7    7    7    7    7    7    7
   7    7    7    7    7    7    7    7    7    7    7
   7    7    7    7    7    7    7    7    7    7    7
  15   15   15   15   15   15   15   15   15   15   15
  16   16   16   16   16   16   16   16   16   16   16
```

PLANE NUMBER 4

```
  11   11   11   11   11   13   13   13   13   13   13
  11   11   11   11   11   13   13   13   13   13   13
  11   11   11   11   13   13   13   13   13   13   13
   9    9    9    9    9    9    9    9    9    9    9
   9    9   14   14   14   14   14    9   14   14   14
   9    9   14   11   11   11   14    9   14   14   14
   9    9   14   14   14   14   14    9   14   14   14
   9    9   14   14   14   14   14    9   14   14   14
   9    9   11   11   11   11   11    9   11   11   11
   9    9   11   11   20   11   11   20   11   11   20
  20    9   11   11   20   11   11   20   11   11   20
   9    9    9    9   20    9    9   20    9    9   20
  11   11   21   21   11   21   21   11   21   21   11
  11   11   11   11   11   11   11   11   11   11   11
   7    7    7    7    7    7    7    7    7    7    7
   7    7    7    7    7    7    7    7    7    7    7
   7    7    7    7    7    7    7    7    7    7    7
  15   15   15   15   15   15   15   15   15   15   15
  16   16   16   16   16   16   16   16   16   16   16
```

PLANE NUMBER 5

```
  11   11   11   11   11   13   13   13   13   13   13
  11   11   11   11   11   13   13   13   13   13   13
  11   11   11   11   13   13   13   13   13   13   13
   9    9    9    9    9    9    9    9    9    9    9
   9    9   14   14   14   14   14    9   14   14   14
   9    9   14   11   11   11   14    9   14   14   14
   9    9   14   14   14   14   14    9   14   14   14
   9    9   14   14   14   14   14    9   14   14   14
   9    9   11   11   11   11   11    9   11   11   11
   9    9   11   11   20   11   11   20   11   11   20
  20    9   11   11   20   11   11   20   11   11   20
   9    9    9    9   20    9    9   20    9    9   20
  11   11   21   21   11   21   21   11   21   21   11
  11   11   11   11   11   11   11   11   11   11   11
   7    7    7    7    7    7    7    7    7    7    7
   7    7    7    7    7    7    7    7    7    7    7
   7    7    7    7    7    7    7    7    7    7    7
  15   15   15   15   15   15   15   15   15   15   15
```

16 16 16 16 16 16 16 16 16 16 16

PLANE NUMBER 6

```
11  11  11  11  11   4   4   4   4   4   4
11  11  11  11  11   4   4   4   4   4   4
11  11  11  11   4   4   4   4   4   4   4
 9   9   9   9   9   9   9   9   9   9   9
 9   9   5   5   5   5   5   9   5   5   5
 9   9   5  11  11  11   5   9   5   5   5
 9   9   5   5   5   5   5   9   5   5   5
 9   9   6   6   6   6   6   9   6   6   6
 9   9  11  11  11  11   9  11  11  11
 9   9  11  11  20  11  11  20  11  11  20
20   9  11  11  20  11  11  20  11  11  20
 9   9   9   9  20   9   9  20   9   9  20
11  11  21  21  11  21  21  11  21  21  11
11  11  11  11  11  11  11  11  11  11  11
 7   7   7   7   7   7   7   7   7   7   7
 7   7   7   7   7   7   7   7   7   7   7
 7   7   7   7   7   7   7   7   7   7   7
15  15  15  15  15  15  15  15  15  15  15
16  16  16  16  16  16  16  16  16  16  16
```

PLANE NUMBER 7

```
11  11  11  11  11   4   4   4   4   4   4
11  11  11  11  11   4   4   4   4   4   4
11  11  11  11   4   4   4   4   4   4
10  10  10  10  10  10  10  10  10  10  10
10  10   5   5   5   5   5  10   5   5   5
10  10   5  11  11  11   5  10   5   5   5
10  10   5   5   5   5   5  10   5   5   5
11  11   6   6   6   6  11   6   6   6
11  11  11  11  11  11  11  11  11  11  11
 9   9  11  11  20  11  11  20  11  11  20
20   9  11  11  20  11  11  20  11  11  20
 9   9   9   9  20   9   9  20   9   9  20
11  11  21  21  11  21  21  11  21  21  11
11  11  11  11  11  11  11  11  11  11  11
 7   7   7   7   7   7   7   7   7   7   7
 7   7   7   7   7   7   7   7   7   7   7
 7   7   7   7   7   7   7   7   7   7   7
15  15  15  15  15  15  15  15  15  15  15
16  16  16  16  16  16  16  16  16  16  16
```

PLANE NUMBER 8

```
11  11  11  11  11   4   4   4   4   4   4
11  11  11  11  11   4   4   4   4   4   4
11  11  11  11   4   4   4   4   4   4
10  10  10  10  10  10  10  10  10  10  10
10  10   5   5   5   5   5  10   5   5   5
10  10   5  11  11  11   5  10   5   5   5
10  10   5   5   5   5   5  10   5   5   5
11  11   6   6   6   6  11   6   6   6
11  11  11  11  11  11  11  11  11  11  11
20  20  11  11  20  11  11  20  11  11  20
20  20  11  11  20  11  11  20  11  11  20
20  20  21  21  20  21  21  20  21  21  20
11  11  21  21  11  21  21  11  21  21  11
11  11  11  11  11  11  11  11  11  11  11
 7   7   7   7   7   7   7   7   7   7   7
 7   7   7   7   7   7   7   7   7   7   7
 7   7   7   7   7   7   7   7   7   7   7
15  15  15  15  15  15  15  15  15  15  15
16  16  16  16  16  16  16  16  16  16  16
```

PLANE NUMBER 9

```
11  11  11  11  11   8   8   8   8   8   8
11  11  11  11  11   8   8   8   8   8   8
11  11  11  11   8   8   8   8   8   8   8
10  10  10  10  10  10  10  10  10  10  10
10  10   5   5   5   5   5  10   5   5   5
10  10   5  11  11  11   5  10   5   5   5
10  10   5   5   5   5   5  10   5   5   5
11  11   6   6   6   6   6  11   6   6   6
11  11  11  11  11  11  11  11  11  11  11
20  20  11  11  20  11  11  20  11  11  20
20  20  11  11  20  11  11  20  11  11  20
20  20  21  21  20  21  21  20  21  21  20
11  11  21  21  11  21  21  11  21  21  11
11  11  11  11  11  11  11  11  11  11  11
 7   7   7   7   7   7   7   7   7   7   7
 7   7   7   7   7   7   7   7   7   7   7
 7   7   7   7   7   7   7   7   7   7   7
15  15  15  15  15  15  15  15  15  15  15
16  16  16  16  16  16  16  16  16  16  16
```

PLANE NUMBER 10

```
11  11  11  11  11   3   3   3   3   3   3
11  11  11  11  11   3   3   3   3   3   3
11  11  11  11   3   3   3   3   3   3   3
10  10  10  10  10  10  10  10  10  10  10
10  10   5   5   5   5   5  10   5   5   5
10  10   5  11  11  11   5  10   5   5   5
10  10   5   5   5   5   5  10   5   5   5
11  11   1   1   1   1   1  11   1   1   1
11  11  11  11  11  11  11  11  11  11  11
20  20  11  11  20  11  11  20  11  11  20
20  20  11  11  20  11  11  20  11  11  20
20  20  21  21  20  21  21  20  21  21  20
11  11  21  21  11  21  21  11  21  21  11
11  11  11  11  11  11  11  11  11  11  11
 7   7   7   7   7   7   7   7   7   7   7
 7   7   7   7   7   7   7   7   7   7   7
 7   7   7   7   7   7   7   7   7   7   7
15  15  15  15  15  15  15  15  15  15  15
16  16  16  16  16  16  16  16  16  16  16
```

PLANE NUMBER 11

```
11  11  11  11  11   3   3   3   3   3   3
11  11  11  11  11   3   3   3   3   3   3
11  11  11  11   3   3   3   3   3   3   3
10  10  10  10  10  10  10  10  10  10  10
10  10   5   5   5   5   5  10   5   5   5
10  10   5  11  11  11   5  10   5   5   5
10  10   5   5   5   5   5  10   5   5   5
11  11   1   1   1   1   1  11   1   1   1
11  11  11  11  11  11  11  11  11  11  11
11  11  11  11  11  11  11  11  11  11  11
11  11   2   2  11   2   2  11   2   2  11
11  11  21  21  11  21  21  11  21  21  11
11  11  21  21  11  21  21  11  21  21  11
11  11  11  11  11  11  11  11  11  11  11
 7   7   7   7   7   7   7   7   7   7   7
 7   7   7   7   7   7   7   7   7   7   7
 7   7   7   7   7   7   7   7   7   7   7
15  15  15  15  15  15  15  15  15  15  15
16  16  16  16  16  16  16  16  16  16  16
```

PLANE NUMBER 12

```
 2   2   2   2   2   2   2   2   2   2   2
 2   2   2   2   2   2   2   2   2   2   2
 2   2   2   2   2   2   2   2   2   2   2
```

```
10  10  10  10  10  10  10  10  10  10  10
 2   2   2   2   2   2   2   2   2   2
 2   2   2   2   2   2   2   2   2   2   2
 2   2   2   2   2   2   2   2   2   2
 2   2   2   2   2   2   2   2   2   2   2
11  11  11  11  11  11  11  11  11  11  11
11  11  11  11  11  11  11  11  11  11  11
11  11   2   2  11   2   2  11   2   2  11
11  11  21  21  11  21  21  11  21  21  11
11  11  21  21  11  21  21  11  21  21  11
11  11  11  11  11  11  11  11  11  11  11
 7   7   7   7   7   7   7   7   7   7   7
 7   7   7   7   7   7   7   7   7   7   7
 7   7   7   7   7   7   7   7   7   7   7
15  15  15  15  15  15  15  15  15  15  15
16  16  16  16  16  16  16  16  16  16  16
```

PLANE NUMBER 13

```
24  24  24  24  24  24  24  24  24  24  24
24  24  24  24  24  24  24  24  24  24  24
24  24  24  24  24  24  24  24  24  24  24
10  10  10  10  10  10  10  10  10  10  10
24  24  24  24  24  24  24  24  24  24  24
24  24  24  24  24  24  24  24  24  24  24
24  24  24  24  24  24  24  24  24  24  24
24  24  24  24  24  24  24  24  24  24  24
11  11  11  11  11  11  11  11  11  11  11
11  11  11  11  11  11  11  11  11  11  11
11  11   2   2  11   2   2  11   2   2  11
11  11  21  21  11  21  21  11  21  21  11
11  11  21  21  11  21  21  11  21  21  11
11  11  11  11  11  11  11  11  11  11  11
 7   7   7   7   7   7   7   7   7   7   7
 7   7   7   7   7   7   7   7   7   7   7
 7   7   7   7   7   7   7   7   7   7   7
15  15  15  15  15  15  15  15  15  15  15
16  16  16  16  16  16  16  16  16  16  16
```

PLANE NUMBER 14

```
 2   2   2   2   2   2   2   2   2   2   2
 2   2   2   2   2   2   2   2   2   2   2
10  10  10  10  10  10  10  10  10  10  10
 2   2   2   2   2   2   2   2   2   2   2
 2   2   2   2   2   2   2   2   2   2   2
 2   2   2   2   2   2   2   2   2   2   2
 2   2   2   2   2   2   2   2   2   2   2
20  20  20  20  20  20  20  20  20  20  20
 2   2   2   2   2   2   2   2   2   2   2
 2   2   2   2   2   2   2   2   2   2   2
21  21  21  21  21  21  21  21  21  21  21
11  11  11  11  11  11  11  11  11  11  11
11  11  11  11  11  11  11  11  11  11  11
 7   7   7   7   7   7   7   7   7   7   7
 7   7   7   7   7   7   7   7   7   7   7
15  15  15  15  15  15  15  15  15  15  15
16  16  16  16  16  16  16  16  16  16  16
```

PLANE NUMBER 15

```
17  17  17  17  17  17  17  17  17  17  17
17  17  17  17  17  17  17  17  17  17  17
17  17  17  17  17  17  17  17  17  17  17
10  10  10  10  10  10  10  10  10  10  10
17  17  17  17  17  17  17  17  17  17  17
17  17  17  17  17  17  17  17  17  17  17
```

```
        2   2   2   2   2   2   2   2   2   2   2
        2   2   2   2   2   2   2   2   2   2   2
        2   2   2   2   2   2   2   2   2   2   2
        2   2   2   2   2   2   2   2   2   2   2
        7   7   7   7   7   7   7   7   7   7   7
        7   7   7   7   7   7   7   7   7   7   7
        7   7   7   7   7   7   7   7   7   7   7
        7   7   7   7   7   7   7   7   7   7   7
        7   7   7   7   7   7   7   7   7   7   7
        7   7   7   7   7   7   7   7   7   7   7
        7   7   7   7   7   7   7   7   7   7   7
        15  15  15  15  15  15  15  15  15  15  15
        16  16  16  16  16  16  16  16  16  16  16

PLANE NUMBER 16
        7   7   20  20  20  20  20  7   20  20  20
        7   7   20  20  20  20  20  7   20  20  20
        20  20  20  20  20  20  20  20  20  20  20
        20  20  20  20  20  20  20  20  20  20  20
        20  20  20  20  20  20  20  20  20  20  20
        20  20  20  20  20  20  20  20  20  20  20
        20  20  20  20  20  20  20  20  20  20  20
        20  20  20  20  20  20  20  20  20  20  20
        17  17  17  17  17  17  17  17  17  17  17
        7   7   7   7   7   7   7   7   7   7   7
        7   7   7   7   7   7   7   7   7   7   7
        7   7   7   7   7   7   7   7   7   7   7
        7   7   7   7   7   7   7   7   7   7   7
        7   7   7   7   7   7   7   7   7   7   7
        7   7   7   7   7   7   7   7   7   7   7
        7   7   7   7   7   7   7   7   7   7   7
        7   7   7   7   7   7   7   7   7   7   7
        15  15  15  15  15  15  15  15  15  15  15
        16  16  16  16  16  16  16  16  16  16  16

PLANE NUMBER 17
        7   7   7   7   7   7   7   7   7   7   7
        7   7   7   7   7   7   7   7   7   7   7
        7   7   7   7   7   7   7   7   7   7   7
        7   7   7   7   7   7   7   7   7   7   7
        7   7   7   7   25  25  25  25  26  26  25
        7   7   7   7   25  25  25  25  26  26  25
        7   7   7   7   27  27  27  27  26  26  25
        7   7   7   7   27  27  27  27  26  26  25
        7   7   7   7   27  29  29  27  28  28  25
        7   7   7   7   27  29  29  27  29  28  25
        7   7   7   7   27  29  29  27  28  28  25
        7   7   7   7   27  29  29  27  28  28  25
        7   7   7   7   27  29  29  27  28  28  25
        7   7   7   7   27  29  29  27  28  28  25
        7   7   7   7   29  30  30  29  30  30  25
        7   7   7   7   27  31  31  7   26  26  29
        15  15  15  15  27  31  31  7   26  26  29
        16  16  16  16  16  32  32  16  32  32  32

PLANE NUMBER 18
        7   7   7   7   7   7   7   7   7   7   7
        7   7   7   7   7   7   7   7   7   7   7
        7   7   7   7   7   7   7   7   7   7   7
        7   7   7   7   7   7   7   7   7   7   7
        7   7   7   7   25  25  25  25  26  26  25
        7   7   7   7   25  25  25  25  26  26  25
        7   7   7   7   27  27  27  27  26  26  25
        7   7   7   7   27  27  27  27  26  26  25
        7   7   7   7   27  29  29  27  28  28  25
```

```
7    7    7    7   27   29   29   27   28   28   25
7    7    7    7   27   29   29   27   28   28   25
7    7    7    7   27   29   29   27   28   28   25
7    7    7    7   27   29   29   27   28   28   25
7    7    7    7   27   29   29   27   28   28   25
7    7    7    7   27   29   29   27   28   28   25
7    7    7    7   29   30   30   29   30   30   25
7    7    7    7   27   31   31    7   26   26   29
15   15   15   15   27   31   31   15   26   26   29
16   16   16   16   16   32   32   16   32   32   32
```

PLANE NUMBER 19

```
7    7    7    7    7    7    7    7    7    7    7
7    7    7    7    7    7    7    7    7    7    7
7    7    7    7    7    7    7    7    7    7    7
7    7    7    7    7    7    7    7    7    7    7
7    7    7    7    7    7    7    7    7    7    7
7    7    7    7    7    7    7    7    7    7    7
7    7    7    7    7    7    7    7    7    7    7
7    7    7    7    7    7    7    7    7    7    7
7    7    7    7    7    7    7    7    7    7    7
7    7    7    7    7    7    7    7    7    7    7
7    7    7    7    7    7    7    7    7    7    7
7    7    7    7    7    7    7    7    7    7    7
7    7    7    7    7    7    7    7    7    7    7
7    7    7    7    7    7    7    7    7    7    7
7    7    7    7    7    7    7    7    7    7    7
15   15   15   15   15   15   15   15   15   15   15
16   16   16   16   16   16   16   16   16   16   16
```

PLANE NUMBER 20

```
7    7    7    7    7    7    7    7    7    7    7
7    7    7    7    7    7    7    7    7    7    7
7    7    7    7    7    7    7    7    7    7    7
7    7    7    7    7    7    7    7    7    7    7
7    7    7    7    7    7    7    7    7    7    7
7    7    7    7    7    7    7    7    7    7    7
7    7    7    7    7    7    7    7    7    7    7
7    7    7    7    7    7    7    7    7    7    7
7    7    7    7    7    7    7    7    7    7    7
7    7    7    7    7    7    7    7    7    7    7
7    7    7    7    7    7    7    7    7    7    7
7    7    7    7    7    7    7    7    7    7    7
7    7    7    7    7    7    7    7    7    7    7
7    7    7    7    7    7    7    7    7    7    7
7    7    7    7    7    7    7    7    7    7    7
15   15   15   15   15   15   15   15   15   15   15
16   16   16   16   16   16   16   16   16   16   16
```

ZONE NUMBER AT EACH MESH INTERVAL

SPECIFICATION FOR LAYER NUMBER   1

```
           1   2   3   4   5   6   7   8   9  10  11

1    18  18  18  18  18  18  18  18  18  18  18
2    18  18  19  18  18  18  18  19  18  18  18
3    18  18  18  18  18  19  18  18  18  18  18
4    18  18  18  18  18  18  18  18  18  18  18
5    18  18  18  18  18  18  18  18  18  18  18
```

```
 5    18 18 18 18  18 18 18 18 18 18 18
 7    18 18 18 18  18 18 18 18 18 18 18
 8    18 18 18 18  18 18 18 18 18 18 18
 9    18 18 18 18  18 18 18 18 18 18 18
10     9  9 18 18  18 18 18 18 18 18 18
11    18  9 18 18  18 18 18 18 18 18 18
12     9  9  9  9  18  9  9 18  9  9 18
13    18 18 18 18  18 18 18 18 18 18 18
14    18 18 18 18  18 18 18 18 18 18 18
15    18 18 18 18  18 18 18 18 18 18 18
16    18 18 18 18  18 18 18 18 18 18 18
17    18 18 18 18  18 18 18 18 18 18 18
18    15 15 15 15  15 15 15 15 15 15 15
19    16 16 16 16  16 16 16 16 16 16 16


     SPECIFICATION FOR LAYER NUMBER  2

           1  2  3  4  5  6  7  8  9 10 11

 1     2  2  2  2  2  2  2  2  2  2  2
 2     2  2  2  2  2  2  2  2  2  2  2
 3     2  2  2  2  2  2  2  2  2  2  2
 4     2  2  2  2  2  2  2  2  2  2
 5     2  2  2  2  2  2  2  2  2  2  2
 6     2  2  2  2  2  2  2  2  2  2
 7     2  2  2  2  2  2  2  2  2  2  2
 8     2  2  2  2  2  2  2  2  2  2
 9     2  2  2  2  2  2  2  2  2  2  2
10     9  9  2  2  2  2  2  2  2  2  2
11     2  9  2  2  2  2  2  2  2  2  2
12     9  9  9  9  2  9  9  2  9  9  2
13     2  2  2  2  2  2  2  2  2  2
14     2  2  2  2  2  2  2  2  2  2
15     2  2  2  2  2  2  2  2  2  2  2
16     2  2  2  2  2  2  2  2  2  2  2
17    19 19 19 19 19 19 19 19 19 19 19
18    15 15 15 15 15 15 15 15 15 15 15
19    16 16 16 16 16 16 16 16 16 16 16


     SPECIFICATION FOR LAYER NUMBER  3

           1  2  3  4  5  6  7  8  9 10 11

 1    11 11 11 11  11 13 13 13 13 13 13
 2    11 11 11 11  11 13 13 13 13 13 13
 3    11 11 11 11  13 13 13 13 13 13 13
 4     9  9  9  9   9  9  9  9  9  9  9
 5     9  9 14 14  14 14 14  9 14 14 14
 6     9  9 14 11  11 11 14  9 14 14 14
 7     9  9 14 14  14 14 14  9 14 14 14
 8     9  9 14 14  14 14 14  9 14 14 14
 9     9  9 11 11  11 11 11  9 11 11 11
10     9  9 11 11  20 11 11 20 11 11 20
11    20  9 11 11  20 11 11 20 11 11 20
12     9  9  9  9  20  9  9 20  9  9 20
13    11 11 21 21  11 21 21 11 21 21 11
14    11 11 11 11  11 11 11 11 11 11 11
15     7  7  7  7   7  7  7  7  7  7  7
16     7  7  7  7   7  7  7  7  7  7  7
17     7  7  7  7   7  7  7  7  7  7  7
18    15 15 15 15  15 15 15 15 15 15 15
19    16 16 16 16  16 16 16 16 16 16 16
```

SPECIFICATION FOR LAYER NUMBER 4

	1	2	3	4	5	6	7	8	9	10	11
1	11	11	11	11	11	13	13	13	13	13	13
2	11	11	11	11	11	13	13	13	13	13	13
3	11	11	11	11	13	13	13	13	13	13	13
4	9	9	9	9	9	9	9	9	9	9	9
5	9	9	14	14	14	14	14	9	14	14	14
6	9	9	14	11	11	14	14	9	14	14	14
7	9	9	14	14	14	14	14	9	14	14	14
8	9	9	14	14	14	14	14	9	14	14	14
9	9	9	11	11	11	11	11	9	11	11	11
10	9	9	11	11	20	11	11	20	11	11	20
11	20	9	11	11	20	11	11	20	11	11	20
12	9	9	9	9	20	9	9	20	9	9	20
13	11	11	21	21	11	21	21	11	21	21	11
14	11	11	11	11	11	11	11	11	11	11	11
15	7	7	7	7	7	7	7	7	7	7	7
16	7	7	7	7	7	7	7	7	7	7	7
17	7	7	7	7	7	7	7	7	7	7	7
18	15	15	15	15	15	15	15	15	15	15	15
19	16	16	16	16	16	16	16	16	16	16	16

SPECIFICATION FOR LAYER NUMBER 5

	1	2	3	4	5	6	7	8	9	10	11
1	11	11	11	11	11	13	13	13	13	13	13
2	11	11	11	11	11	13	13	13	13	13	13
3	11	11	11	11	13	13	13	13	13	13	13
4	9	9	9	9	9	9	9	9	9	9	9
5	9	9	14	14	14	14	14	9	14	14	14
6	9	9	14	11	11	14	14	9	14	14	14
7	9	9	14	14	14	14	14	9	14	14	14
8	9	9	14	14	14	14	14	9	14	14	14
9	9	9	11	11	11	11	11	9	11	11	11
10	9	9	11	11	20	11	11	20	11	11	20
11	20	9	11	11	20	11	11	20	11	11	20
12	9	9	9	9	20	9	9	20	9	9	20
13	11	11	21	21	11	21	21	11	21	21	11
14	11	11	11	11	11	11	11	11	11	11	11
15	7	7	7	7	7	7	7	7	7	7	7
16	7	7	7	7	7	7	7	7	7	7	7
17	7	7	7	7	7	7	7	7	7	7	7
18	15	15	15	15	15	15	15	15	15	15	15
19	16	16	16	16	16	16	16	16	16	16	16

SPECIFICATION FOR LAYER NUMBER 6

	1	2	3	4	5	6	7	8	9	10	11
1	11	11	11	11	11	4	4	4	4	4	4
2	11	11	11	11	11	4	4	4	4	4	4
3	11	11	11	11	4	4	4	4	4	4	4
4	9	9	9	9	9	9	9	9	9	9	9
5	9	9	5	5	5	5	5	9	5	5	5
6	9	9	5	11	11	11	5	9	5	5	5
7	9	9	5	5	5	5	5	9	5	5	5

```
 8    9  9  6  6  6  6  6  9  6  6  6
 9    9  9 11 11 11 11 11  9 11 11 11
10    9  9 11 11 20 11 11 20 11 11 20
11   20  9 11 11 20 11 11 20 11 11 20
12    9  9  9  9 20  9  9 20  9  9 20
13   11 11 21 21 11 21 21 11 21 21 11
14   11 11 11 11 11 11 11 11 11 11 11
15    7  7  7  7  7  7  7  7  7  7  7
16    7  7  7  7  7  7  7  7  7  7  7
17    7  7  7  7  7  7  7  7  7  7  7
18   15 15 15 15 15 15 15 15 15 15 15
19   16 16 16 16 16 16 16 16 16 16 16
```

SPECIFICATION FOR LAYER NUMBER   7

```
       1  2  3  4  5  6  7  8  9 10 11

 1    11 11 11 11 11  4  4  4  4  4  4
 2    11 11 11 11 11  4  4  4  4  4  4
 3    11 11 11 11  4  4  4  4  4  4  4
 4    10 10 10 10 10 10 10 10 10 10 10
 5    10 10  5  5  5  5  5 10  5  5  5
 6    10 10  5 11 11 11  5 10  5  5  5
 7    10 10  5  5  5  5  5 10  5  5  5
 8    11 11  6  6  6  6  6 11  6  6  6
 9    11 11 11 11 11 11 11 11 11 11 11
10     9  9 11 11 20 11 11 20 11 11 20
11    20  9 11 11 20 11 11 20 11 11 20
12     9  9  9  9 20  9  9 20  9  9 20
13    11 11 21 21 11 21 21 11 21 21 11
14    11 11 11 11 11 11 11 11 11 11 11
15     7  7  7  7  7  7  7  7  7  7  7
16     7  7  7  7  7  7  7  7  7  7  7
17     7  7  7  7  7  7  7  7  7  7  7
18    15 15 15 15 15 15 15 15 15 15 15
19    16 16 16 16 16 16 16 16 16 16 16
```

SPECIFICATION FOR LAYER NUMBER   8

```
       1  2  3  4  5  6  7  8  9 10 11

 1    11 11 11 11 11  4  4  4  4  4  4
 2    11 11 11 11 11  4  4  4  4  4  4
 3    11 11 11 11  4  4  4  4  4  4  4
 4    10 10 10 10 10 10 10 10 10 10 10
 5    10 10  5  5  5  5  5 10  5  5  5
 6    10 10  5 11 11 11  5 10  5  5  5
 7    10 10  5  5  5  5  5 10  5  5  5
 8    11 11  6  6  6  6  6 11  6  6  6
 9    11 11 11 11 11 11 11 11 11 11 11
10    20 20 11 11 20 11 11 20 11 11 20
11    20 20 11 11 20 11 11 20 11 11 20
12    20 20 21 21 20 21 21 20 21 21 20
13    11 11 21 21 11 21 21 11 21 21 11
14    11 11 11 11 11 11 11 11 11 11 11
15     7  7  7  7  7  7  7  7  7  7  7
16     7  7  7  7  7  7  7  7  7  7  7
17     7  7  7  7  7  7  7  7  7  7  7
18    15 15 15 15 15 15 15 15 15 15 15
19    16 16 16 16 16 16 16 16 16 16 16
```

SPECIFICATION FOR LAYER NUMBER 9

```
        1  2  3  4  5  6  7  8  9 10 11

 1    11 11 11 11 11 11  8  8  8  8  8  8
 2    11 11 11 11 11 11  8  8  8  8  8  8
 3    11 11 11 11  8  8  8  8  8  8  8
 4    10 10 10 10 10 10 10 10 10 10 10
 5    10 10  5  5  5  5  5 10  5  5  5
 6    10 10  5 11 11 11  5 10  5  5  5
 7    10 10  5  5  5  5  5 10  5  5  5
 8    11 11  6  6  6  6  6 11  6  6  6
 9    11 11 11 11 11 11 11 11 11 11 11
10    20 20 11 11 20 11 11 20 11 11 20
11    20 20 11 11 20 11 11 20 11 11 20
12    20 20 21 21 20 21 21 20 21 21 20
13    11 11 21 21 11 21 21 11 21 21 11
14    11 11 11 11 11 11 11 11 11 11 11
15     7  7  7  7  7  7  7  7  7  7  7
16     7  7  7  7  7  7  7  7  7  7  7
17     7  7  7  7  7  7  7  7  7  7  7
18    15 15 15 15 15 15 15 15 15 15 15
19    16 16 16 16 16 15 16 16 16 16 16
```

SPECIFICATION FOR LAYER NUMBER 10

```
        1  2  3  4  5  6  7  8  9 10 11

 1    11 11 11 11 11  3  3  3  3  3  3
 2    11 11 11 11 11  3  3  3  3  3  3
 3    11 11 11 11  3  3  3  3  3  3
 4    10 10 10 10 10 10 10 10 10 10 10
 5    10 10  5  5  5  5  5 10  5  5  5
 6    10 10  5 11 11 11  5 10  5  5  5
 7    10 10  5  5  5  5  5 10  5  5  5
 8    11 11  1  1  1  1  1 11  1  1  1
 9    11 11 11 11 11 11 11 11 11 11 11
10    20 20 11 11 20 11 11 20 11 11 20
11    20 20 11 11 20 11 11 20 11 11 20
12    20 20 21 21 20 21 21 20 21 21 20
13    11 11 21 21 11 21 21 11 21 21 11
14    11 11 11 11 11 11 11 11 11 11 11
15     7  7  7  7  7  7  7  7  7  7  7
16     7  7  7  7  7  7  7  7  7  7  7
17     7  7  7  7  7  7  7  7  7  7  7
18    15 15 15 15 15 15 15 15 15 15 15
19    16 16 16 16 16 16 16 16 16 16 16
```

SPECIFICATION FOR LAYER NUMBER 11

```
        1  2  3  4  5  6  7  8  9 10 11

 1    11 11 11 11 11  3  3  3  3  3  3
 2    11 11 11 11 11  3  3  3  3  3  3
 3    11 11 11 11  3  3  3  3  3  3
 4    10 10 10 10 10 10 10 10 10 10 10
 5    10 10  5  5  5  5  5 10  5  5  5
 6    10 10  5 11 11 11  5 10  5  5  5
 7    10 10  5  5  5  5  5 10  5  5  5
 8    11 11  1  1  1  1  1 11  1  1  1
 9    11 11 11 11 11 11 11 11 11 11 11
```

Information Processing Center

```
10    11 11 11 11  11 11 11 11  11 11 11
11    11 11  2  2 11  2  2 11  2  2 11
12    11 11 21 21 11 21 21 11 21 21 11
13    11 11 21 21 11 21 21 11 21 21 11
14    11 11 11 11 11 11 11 11 11 11 11
15     7  7  7  7  7  7  7  7  7  7  7
16     7  7  7  7  7  7  7  7  7  7  7
17     7  7  7  7  7  7  7  7  7  7  7
18    15 15 15 15 15 15 15 15 15 15 15
19    16 16 16 16 16 16 16 16 16 16 16
```

SPECIFICATION FOR LAYER NUMBER 12

```
       1  2  3  4  5  6  7  8  9 10 11

 1     2  2  2  2  2  2  2  2  2  2  2
 2     2  2  2  2  2  2  2  2  2  2  2
 3     2  2  2  2  2  2  2  2  2  2  2
 4    10 10 10 10 10 10 10 10 10 10 10
 5     2  2  2  2  2  2  2  2  2  2  2
 6     2  2  2  2  2  2  2  2  2  2  2
 7     2  2  2  2  2  2  2  2  2  2  2
 8     2  2  2  2  2  2  2  2  2  2  2
 9    11 11 11 11 11 11 11 11 11 11 11
10    11 11 11 11 11 11 11 11 11 11 11
11    11 11  2  2 11  2  2 11  2  2 11
12    11 11 21 21 11 21 21 11 21 21 11
13    11 11 21 21 11 21 21 11 21 21 11
14    11 11 11 11 11 11 11 11 11 11 11
15     7  7  7  7  7  7  7  7  7  7  7
16     7  7  7  7  7  7  7  7  7  7  7
17     7  7  7  7  7  7  7  7  7  7  7
18    15 15 15 15 15 15 15 15 15 15 15
19    16 16 16 16 16 16 16 16 16 16 16
```

SPECIFICATION FOR LAYER NUMBER 13

```
       1  2  3  4  5  6  7  8  9 10 11

 1    24 24 24 24 24 24 24 24 24 24 24
 2    24 24 24 24 24 24 24 24 24 24 24
 3    24 24 24 24 24 24 24 24 24 24 24
 4    10 10 10 10 10 10 10 10 10 10 10
 5    24 24 24 24 24 24 24 24 24 24 24
 6    24 24 24 24 24 24 24 24 24 24 24
 7    24 24 24 24 24 24 24 24 24 24 24
 8    24 24 24 24 24 24 24 24 24 24 24
 9    11 11 11 11 11 11 11 11 11 11 11
10    11 11 11 11 11 11 11 11 11 11 11
11    11 11  2  2 11  2  2 11  2  2 11
12    11 11 21 21 11 21 21 11 21 21 11
13    11 11 21 21 11 21 21 11 21 21 11
14    11 11 11 11 11 11 11 11 11 11 11
15     7  7  7  7  7  7  7  7  7  7  7
16     7  7  7  7  7  7  7  7  7  7  7
17     7  7  7  7  7  7  7  7  7  7  7
18    15 15 15 15 15 15 15 15 15 15 15
19    16 16 16 16 16 16 16 16 16 16 16
```

SPECIFICATION FOR LAYER NUMBER 14

	1	2	3	4	5	6	7	8	9	10	11
1	2	2	2	2	2	2	2	2	2	2	2
2	2	2	2	2	2	2	2	2	2	2	2
3	2	2	2	2	2	2	2	2	2	2	2
4	10	10	10	10	10	10	10	10	10	10	10
5	2	2	2	2	2	2	2	2	2	2	2
6	2	2	2	2	2	2	2	2	2	2	2
7	2	2	2	2	2	2	2	2	2	2	2
8	2	2	2	2	2	2	2	2	2	2	2
9	20	20	20	20	20	20	20	20	20	20	20
10	2	2	2	2	2	2	2	2	2	2	2
11	2	2	2	2	2	2	2	2	2	2	2
12	21	21	21	21	21	21	21	21	21	21	21
13	11	11	11	11	11	11	11	11	11	11	11
14	11	11	11	11	11	11	11	11	11	11	11
15	7	7	7	7	7	7	7	7	7	7	7
16	7	7	7	7	7	7	7	7	7	7	7
17	7	7	7	7	7	7	7	7	7	7	7
18	15	15	15	15	15	15	15	15	15	15	15
19	16	16	16	16	16	16	16	16	16	16	16

SPECIFICATION FOR LAYER NUMBER 15

	1	2	3	4	5	6	7	8	9	10	11
1	17	17	17	17	17	17	17	17	17	17	17
2	17	17	17	17	17	17	17	17	17	17	17
3	17	17	17	17	17	17	17	17	17	17	17
4	10	10	10	10	10	10	10	10	10	10	10
5	17	17	17	17	17	17	17	17	17	17	17
6	17	17	17	17	17	17	17	17	17	17	17
7	2	2	2	2	2	2	2	2	2	2	2
8	2	2	2	2	2	2	2	2	2	2	2
9	2	2	2	2	2	2	2	2	2	2	2
10	2	2	2	2	2	2	2	2	2	2	2
11	7	7	7	7	7	7	7	7	7	7	7
12	7	7	7	7	7	7	7	7	7	7	7
13	7	7	7	7	7	7	7	7	7	7	7
14	7	7	7	7	7	7	7	7	7	7	7
15	7	7	7	7	7	7	7	7	7	7	7
16	7	7	7	7	7	7	7	7	7	7	7
17	7	7	7	7	7	7	7	7	7	7	7
18	15	15	15	15	15	15	15	15	15	15	15
19	16	16	16	16	16	16	16	16	16	16	16

SPECIFICATION FOR LAYER NUMBER 16

	1	2	3	4	5	6	7	8	9	10	11
1	7	7	20	20	20	20	20	7	20	20	20
2	7	7	20	20	20	20	20	7	20	20	20
3	20	20	20	20	20	20	20	20	20	20	20
4	20	20	20	20	20	20	20	20	20	20	20
5	20	20	20	20	20	20	20	20	20	20	20
6	20	20	20	20	20	20	20	20	20	20	20
7	20	20	20	20	20	20	20	20	20	20	20
8	20	20	20	20	20	20	20	20	20	20	20
9	17	17	17	17	17	17	17	17	17	17	17
10	7	7	7	7	7	7	7	7	7	7	7
11	7	7	7	7	7	7	7	7	7	7	7

```
12    7  7  7  7  7  7  7  7  7  7  7
13    7  7  7  7  7  7  7  7  7  7  7
14    7  7  7  7  7  7  7  7  7  7  7
15    7  7  7  7  7  7  7  7  7  7  7
16    7  7  7  7  7  7  7  7  7  7  7
17    7  7  7  7  7  7  7  7  7  7  7
18   15 15 15 15 15 15 15 15 15 15 15
19   16 16 16 16 16 16 16 16 16 16 16
```

SPECIFICATION FOR LAYER NUMBER 17

```
      1  2  3  4  5  6  7  8  9 10 11

 1    7  7  7  7  7  7  7  7  7  7  7
 2    7  7  7  7  7  7  7  7  7  7  7
 3    7  7  7  7  7  7  7  7  7  7  7
 4    7  7  7  7  7  7  7  7  7  7  7
 5    7  7  7  7 25 25 25 25 26 26 25
 6    7  7  7  7 25 25 25 25 26 26 25
 7    7  7  7  7 27 27 27 27 26 26 25
 8    7  7  7  7 27 27 27 27 26 26 25
 9    7  7  7  7 27 29 29 27 28 28 25
10    7  7  7  7 27 29 29 27 28 28 25
11    7  7  7  7 27 29 29 27 28 28 25
12    7  7  7  7 27 29 29 27 28 28 25
13    7  7  7  7 27 29 29 27 28 28 25
14    7  7  7  7 27 29 29 27 28 28 25
15    7  7  7  7 27 29 29 27 28 28 25
16    7  7  7  7 29 30 30 29 30 30 25
17    7  7  7  7 27 31 31  7 26 26 29
18   15 15 15 15 27 31 31  7 26 26 29
19   16 16 16 16 16 32 32 16 32 32 32
```

SPECIFICATION FOR LAYER NUMBER 18

```
      1  2  3  4  5  6  7  8  9 10 11

 1    7  7  7  7  7  7  7  7  7  7  7
 2    7  7  7  7  7  7  7  7  7  7  7
 3    7  7  7  7  7  7  7  7  7  7  7
 4    7  7  7  7  7  7  7  7  7  7  7
 5    7  7  7  7 25 25 25 25 26 26 25
 6    7  7  7  7 25 25 25 25 26 26 25
 7    7  7  7  7 27 27 27 27 26 26 25
 8    7  7  7  7 27 27 27 27 26 26 25
 9    7  7  7  7 27 29 29 27 28 28 25
10    7  7  7  7 27 29 29 27 28 28 25
11    7  7  7  7 27 29 29 27 28 28 25
12    7  7  7  7 27 29 29 27 28 28 25
13    7  7  7  7 27 29 29 27 28 28 25
14    7  7  7  7 27 29 29 27 28 28 25
15    7  7  7  7 27 29 29 27 28 28 25
16    7  7  7  7 29 30 30 29 30 30 25
17    7  7  7  7 27 31 31  7 26 26 29
18   15 15 15 15 27 31 31 15 26 26 29
19   16 16 16 16 16 32 32 16 32 32 32
```

SPECIFICATION FOR LAYER NUMBER 19

```
      1  2  3  4  5  6  7  8  9 10 11
```

```
 1    7  7  7  7  7  7  7  7  7  7  7
 2    7  7  7  7  7  7  7  7  7  7  7
 3    7  7  7  7  7  7  7  7  7  7  7
 4    7  7  7  7  7  7  7  7  7  7  7
 5    7  7  7  7  7  7  7  7  7  7  7
 6    7  7  7  7  7  7  7  7  7  7  7
 7    7  7  7  7  7  7  7  7  7  7  7
 8    7  7  7  7  7  7  7  7  7  7  7
 9    7  7  7  7  7  7  7  7  7  7  7
10    7  7  7  7  7  7  7  7  7  7  7
11    7  7  7  7  7  7  7  7  7  7  7
12    7  7  7  7  7  7  7  7  7  7  7
13    7  7  7  7  7  7  7  7  7  7  7
14    7  7  7  7  7  7  7  7  7  7  7
15    7  7  7  7  7  7  7  7  7  7  7
16    7  7  7  7  7  7  7  7  7  7  7
17    7  7  7  7  7  7  7  7  7  7  7
18   15 15 15 15 15 15 15 15 15 15 15
19   16 16 16 16 16 16 16 16 16 16 16
```

SPECIFICATION FOR LAYER NUMBER 20

```
       1  2  3  4  5  6  7  8  9 10 11

 1    7  7  7  7  7  7  7  7  7  7  7
 2    7  7  7  7  7  7  7  7  7  7  7
 3    7  7  7  7  7  7  7  7  7  7  7
 4    7  7  7  7  7  7  7  7  7  7  7
 5    7  7  7  7  7  7  7  7  7  7  7
 6    7  7  7  7  7  7  7  7  7  7  7
 7    7  7  7  7  7  7  7  7  7  7  7
 8    7  7  7  7  7  7  7  7  7  7  7
 9    7  7  7  7  7  7  7  7  7  7  7
10    7  7  7  7  7  7  7  7  7  7  7
11    7  7  7  7  7  7  7  7  7  7  7
12    7  7  7  7  7  7  7  7  7  7  7
13    7  7  7  7  7  7  7  7  7  7  7
14    7  7  7  7  7  7  7  7  7  7  7
15    7  7  7  7  7  7  7  7  7  7  7
16    7  7  7  7  7  7  7  7  7  7  7
17    7  7  7  7  7  7  7  7  7  7  7
18   15 15 15 15 15 15 15 15 15 15 15
19   16 16 16 16 16 16 16 16 16 16 16
```

DESCRIPTION OF REACTOR ZONES

ZN	TO ZN	SUB-ZNS	SIGMA-SET	ID	CLASS	DPL	NEX	NAME
1	1	0	1	0	0	-1	0	CORE
2	2	0	1	0	0	-1	0	H2O+AL
3	6	0	1	0	0	-1	0	CORE
7	7	0	1	0	0	-1	0	D2O+H2O+AL
8	8	0	1	0	0	-1	0	PS
9	9	0	1	0	0	-1	0	CO+AL
10	11	0	1	0	0	-1	0	AL
12	12	0	1	0	0	-1	0	D2O
13	14	0	1	0	0	-1	0	CORE
15	15	0	1	0	0	-1	0	AL+H2O
16	16	0	1	0	0	-1	0	C
17	17	0	1	0	0	-1	0	AL+D2O
18	18	0	1	0	0	-1	0	H2O
19	19	0	1	0	0	-1	0	AL+H2O

```
   20    21     0        1      0    0    -1    0   H2O
   22    23     0        1      0    0    -1    0   CORE+AL-H20
   24    24     0        1      0    0    -1    0   AL+H2O
   25    26     0        1      0    0    -1    0   AL+D2O+VOID
   27    27    .0        1      0    0    -1    0   AL+VOID
   28    32     0        1      0    0    -1    0   AL+D2O+VOID
   33    39     0        1      0    0    -1    0   CORE-H2O
   40    40     0        1      0    0    -1    0   AL+H2O
   41    41     0        1      0    0    -1    0   VOID
   42    42     0        1      0    0    -1    0   H20
```

DESCRIPTION OF MICROSCOPIC CROSS SECTIONS

```
     SET   NUCS   GRPS   UPSC   DNSC   ,          TITLE
      1     57     3      0      2     MICROSCOPIC CROSS-SECTIONS FOR THE HIFR-II
  GROUP   UPPER ENERGY   MEAN ENERGY   1/V X-SECTION   DIST.FUNCT
      1    1.000000E+06   5.477200E+04   1.990000E-09   1.000000
      2    3.000000E+03   1.464000E+01   2.779000E-07   0.0
      3    4.000000E-01   1.000000E-02   4.247000E-06   0.0
    SUM                                                 1.000000
```

INPUT NUCLIDE DENSITIES (NUCLIDE NUMBER - DENSITY)

```
   ZONES  1-  1  SUB-ZONE INDICATOR  0  AND CONTROL OPTION  0
      1  4.39000E-04     2  3.35900E-05     4  3.18300E-02     3  1.54500E-02

   ZONES  2-  2  SUB-ZONE INDICATOR  0  AND CONTROL OPTION  0
     33  1.01200E-02    32  1.65500E-02

   ZONES  3-  3  SUB-ZONE INDICATOR  0  AND CONTROL OPTION  0
      5  4.39000E-04     6  3.35900E-05     8  3.18300E-02     7  1.54500E-02

   ZONES  4-  4  SUB-ZONE INDICATOR  0  AND CONTROL OPTION  0
      9  4.39000E-04    10  3.35900E-05    11  3.18300E-02    12  1.54500E-02

   ZONES  5-  5  SUB-ZONE INDICATOR  0  AND CONTROL OPTION  0
     15  4.39000E-04    16  3.35900E-05    13  3.18300E-02    14  1.54500E-02

   ZONES  6-  6  SUB-ZONE INDICATOR  0  AND CONTROL OPTION  0
     17  4.39000E-04    18  3.35900E-05    20  3.18300E-02    19  1.54500E-02

   ZONES  7-  7  SUB-ZONE INDICATOR  0  AND CONTROL OPTION  0
     21  3.27500E-02    22  1.62100E-04    47  1.64570E-04

   ZONES  8-  8  SUB-ZONE INDICATOR  0  AND CONTROL OPTION  0
     34  3.29500E-02

   ZONES  9-  9  SUB-ZONE INDICATOR  0  AND CONTROL OPTION  0
     36  6.96000E-03    35  5.11950E-02

   ZONES 10- 10  SUB-ZONE INDICATOR  0  AND CONTROL OPTION  0
     38  6.02300E-02

   ZONES 11- 11  SUB-ZONE INDICATOR  0  AND CONTROL OPTION  0
     53  6.02300E-02

   ZONES 12- 12  SUB-ZONE INDICATOR  0  AND CONTROL OPTION  0
     54  6.02300E-02

   ZONES 13- 13  SUB-ZONE INDICATOR  0  AND CONTROL OPTION  0
     24  4.39000E-04    25  3.35900E-05    26  3.18300E-02    27  1.54500E-02

   ZONES 14- 14  SUB-ZONE INDICATOR  0  AND CONTROL OPTION  0
     28  4.39000E-04    29  3.35900E-05    30  3.18300E-02    31  1.54500E-02
```

ZONES 15- 15 SUB-ZONE INDICATOR 0 AND CONTROL OPTION 0
       40 3.01200E-02   39 1.65500E-02   .

ZONES 16- 16 SUB-ZONE INDICATOR 0 AND CONTROL OPTION 0
       41 8.33400E-02

ZONES 17- 17 SUB-ZONE INDICATOR 0 AND CONTROL OPTION 0
       42 1.65400E-02   43 3.12000E-02

ZONES 18- 18 SUB-ZONE INDICATOR 0 AND CONTROL OPTION 0
       44 3.34000E-02

ZONES 19- 19 SUB-ZONE INDICATOR 0 AND CONTROL OPTION 0
       45 3.14300E-02   46 3.01200E-03

ZONES 20- 20 SUB-ZONE INDICATOR 0 AND CONTROL OPTION 0
       47 3.34000E-02

ZONES 21- 21 SUB-ZONE INDICATOR 0 AND CONTROL OPTION 0
       48 3.34000E-02

ZONES 22- 22 SUB-ZONE INDICATOR 0 AND CONTROL OPTION 0
       28 4.39000E-04   29 3.35900E-05   30 5.40400E-02   31 3.09000E-03

ZONES 23- 23 SUB-ZONE INDICATOR 0 AND CONTROL OPTION 0
       15 4.39000E-04   16 3.35900E-05   13 5.40400E-02   14 3.09000E-03

ZONES 24- 24 SUB-ZONE INDICATOR 0 AND CONTROL OPTION 0
       52 6.02300E-03   51 3.00600E-02

ZONES 25- 25 SUB-ZONE INDICATOR 0 AND CONTROL OPTION 0
       21 1.32920E-02   22 5.42160E-03   56 5.10000E-01

ZONES 26- 26 SUB-ZONE INDICATOR 0 AND CONTROL OPTION 0
       21 2.09350E-02   22 3.01200E-03   56 3.20000E-01

ZONES 27- 27 SUB-ZONE INDICATOR 0 AND CONTROL OPTION 0
       22 9.03600E-03   56 8.20000E-01

ZONES 28- 28 SUB-ZONE INDICATOR 0 AND CONTROL OPTION 0
       21 1.52960E-02   22 4.81920E-03   56 4.60000E-01

ZONES 29- 29 SUB-ZONE INDICATOR 0 AND CONTROL OPTION 0
       21 9.96900E-03   22 3.61440E-03   56 3.40000E-01

ZONES 30- 30 SUB-ZONE INDICATOR 0 AND CONTROL OPTION 0
       21 1.72800E-02   22 4.21680E-03   56 4.10000E-01

ZONES 31- 31 SUB-ZONE INDICATOR 0 AND CONTROL OPTION 0
       21 1.99380E-02   22 3.61440E-03   56 3.40000E-01

ZONES 32- 32 SUB-ZONE INDICATOR 0 AND CONTROL OPTION 0
       21 2.59190E-02   22 1.80720E-03   56 1.90000E-01

ZONES 33- 33 SUB-ZONE INDICATOR 0 AND CONTROL OPTION 0
        5 4.39000E-04   6 3.35900E-05   8 3.18300E-02

ZONES 34- 34 SUB-ZONE INDICATOR 0 AND CONTROL OPTION 0
        9 4.39000E-04   10 3.35900E-05   11 3.18300E-02

ZONES 35- 35 SUB-ZONE INDICATOR 0 AND CONTROL OPTION 0
       15 4.39000E-04   16 3.35900E-05   13 3.18300E-02

ZONES 36- 36 SUB-ZONE INDICATOR 0 AND CONTROL OPTION 0
       24 4.39000E-04   25 3.35900E-05   26 3.18300E-02

ZONES 37- 37 SUB-ZONE INDICATOR 0 AND CONTROL OPTION 0
     28 4.39000E-04   29 3.35900E-05   30 3.18300E-02

ZONES 38- 38 SUB-ZONE INDICATOR 0 AND CONTROL OPTION 0
     17 4.39000E-04   18 3.35900E-05   20 3.18300E-02

ZONES 39- 39 SUB-ZONE INDICATOR 0 AND CONTROL OPTION 0
      1 4.39000E-04   2 3.35900E-05   4 3.18300E-02

ZONES 40- 40 SUB-ZONE INDICATOR 0 AND CONTROL OPTION 0
     47 1.49700E-02   54 3.49160E-02

ZONES 41- 41 SUB-ZONE INDICATOR 0 AND CONTROL OPTION 0
     57 1.00000E+00

ZONES 42- 42 SUB-ZONE INDICATOR 0 AND CONTROL OPTION 0
     32 3.34000E-02

FISSILE NUCLIDES---   8 10 14 16
FERTILE NUCLIDES---   6   9 12 15
INTERMEDIATE NUCLIDES---   7 13
OTHER NUCLIDES--- 11 17 18 19 20 21
STRUCTURAL NUCLIDES--- 26 27 31 32 33 34 35 37 38 39 45 46 47
SPECIAL NUCLIDES---   1   2   3   5 23
FISSION PRODUCT NUCLIDES--- 48 49 50 51 52 53 54 55 56 57

CORE STORAGE DIFFERENCE (WORDS) EQUATION CONSTANTS I/O INSTEAD OF STORED   35058

EQUATION CONSTANTS WILL BE STORED IN CORE

NUMBER OF---COLUMNS, ROWS, PLANES, GROUPS, UPSCAT, DOWNSCAT, REGIONS, AND ZONES   11 19 20   3   0 24180 32

MEMORY LOCATIONS RESERVED FOR DATA STORAGE--- 118000
MEMORY LOCATIONS USED FOR THIS PROBLEM------- 113319
MEMORY LOCATIONS NOT USED--------------------   4681

ZONE MACROSCOPIC CROSS SECTIONS

ZONE	NAME	GRP	D	SIGR	SIGA	NUSIGF	BSQ	POWER/FLUX
1	CORE	1	1.62518E+00	3.28883E-02	1.09096E-03	2.00322E-03	0.0	2.60717E-14
		2	8.34367E-01	6.27993E-02	1.96769E-02	3.05681E-02	0.0	4.02591E-13
		3	2.62836E-01	0.0		2.05109E-01	3.95271E-01	0.0	5.22140E-12
2	H2O+AL	1	1.75611E+00	4.09290E-02	1.72222E-04	0.0	0.0	0.0
		2	8.22862E-01	7.34039E-02	1.16531E-03	0.0	0.0	0.0
		3	2.49859E-01	0.0		1.81103E-02	0.0	0.0	0.0
3	CORE	1	1.61766E+00	3.36421E-02	1.08494E-03	2.01097E-03	0.0	2.62119E-14
		2	8.34613E-01	6.21418E-02	1.96273E-02	3.04778E-02	0.0	4.01401E-13
		3	2.62836E-01	0.0		2.05109E-01	3.95271E-01	0.0	5.22140E-12
4	CORE	1	1.78490E+00	3.38145E-02	1.09028E-03	2.01348E-03	0.0	2.62407E-14
		2	8.35597E-01	5.91986E-02	1.93564E-02	3.00046E-02	0.0	3.95170E-13
		3	3.05314E-01	0.0		1.70584E-01	3.26725E-01	0.0	4.31593E-12
5	CORE	1	1.79755E+00	3.32924E-02	1.09130E-03	2.00887E-03	0.0	2.61380E-14

Material	#						
	2	8.35722E-01	5.94504E-02	1.93690E-02	3.00358E-02	0.0	3.95581E-13
	3	3.03235E-01	0.0	1.72317E-01	3.30777E-01	0.0	4.36946E-12
6 CORE	1	1.63257E+00	3.25618E-02	1.08839E-03	1.99930E-03	0.0	2.60108E-14
	2	8.34845E-01	6.16431E-02	1.95829E-02	3.03960E-02	0.0	4.00325E-13
	3	2.62836E-01	0.0	2.05109E-01	3.95271E-01	0.0	5.22140E-12
7 D20+H20+AL	1	1.43073E+00	2.27943E-02	8.27860E-05	0.0	0.0	0.0
	2	1.20494E+00	2.13851E-02	1.05995E-05	0.0	0.0	0.0
	3	7.70232E-01	0.0	1.76033E-04	0.0	0.0	
8 PB	1	1.72041E+00	4.29752E-04	1.02293E-04	0.0	0.0	0.0
	2	9.08600E-01	3.83539E-04	2.83798E-04	0.0	0.0	0.0
	3	9.08926E-01	0.0	1.58160E-03	0.0	0.0	0.0
9 CD+AL	1	2.23690E+00	3.69546E-04	4.44285E-02	0.0	0.0	0.0
	2	2.25806E+00	4.26557E-04	1.07653E-01	0.0	0.0	0.0
	3	3.13902E-01	0.0	2.64731E-04	0.0	0.0	0.0
10 AL	1	2.65500E+00	3.71354E-04	1.71999E-04	0.0	0.0	0.0
	2	4.01942E+00	5.72155E-04	7.42576E-04	0.0	0.0	0.0
	3	3.60168E+00	0.0	9.52056E-03	0.0	0.0	0.0
11 AL	1	2.66638E+00	3.99500E-04	1.97850E-04	0.0	0.0	0.0
	2	4.01738E+00	6.03565E-04	8.94777E-04	0.0	0.0	0.0
	3	3.46091E+00	0.0	1.46606E-02	0.0	0.0	0.0
12 D20	1	2.71624E+00	4.94452E-04	2.20117E-04	0.0	0.0	0.0
	2	4.01476E+00	6.78912E-04	1.02369E-03	0.0	0.0	0.0
	3	3.46093E+00	0.0	1.59357E-02	0.0	0.0	0.0
13 CORE	1	1.78164E+00	3.49311E-02	1.09921E-03	2.02727E-03	0.0	2.64114E-14
	2	8.36273E-01	5.74405E-02	1.92940E-02	2.98306E-02	0.0	3.92862E-13
	3	3.05314E-01	0.0	1.70584E-01	3.26725E-01	0.0	4.31593E-12
14 CORE	1	1.79914E+00	3.36473E-02	1.07665E-03	2.01382E-03	0.0	2.61899E-14
	2	9.07887E-01	5.94802E-02	1.94206E-02	3.00907E-02	0.0	3.96303E-13
	3	3.05314E-01	0.0	1.70584E-01	3.26725E-01	0.0	4.31593E-12
15 AL+H20	1	1.42966E+00	1.01260E-01	1.55308E-04	0.0	0.0	0.0
	2	8.09527E-01	1.08839E-01	1.56547E-03	0.0	0.0	0.0
	3	2.49859E-01	0.0	1.81103E-02	0.0	0.0	0.0
16 C	1	1.29301E+00	9.16490E-03	0.0	0.0	0.0	0.0
	2	9.08544E-01	1.02291E-02	8.47568E-06	0.0	0.0	0.0
	3	8.47624E-01	0.0	2.49286E-04	0.0	0.0	0.0
17 AL+D20	1	1.91839E+00	7.53674E-03	1.72139E-04	0.0	0.0	0.0
	2	1.84655E+00	9.70257E-03	5.52131E-04	0.0	0.0	0.0
	3	1.27290E+00	0.0	8.27121E-03	0.0	0.0	0.0
18 H20	1	1.39896E+00	7.46055E-02	1.55454E-04	0.0	0.0	0.0
	2	4.52630E-01	1.62952E-01	1.41556E-03	0.0	0.0	0.0
	3	1.28445E-01	0.0	2.04662E-02	0.0	0.0	0.0
19 AL+H20	1	1.37749E+00	7.91092E-02	1.43090E-04	0.0	0.0	0.0
	2	4.79095E-01	1.46323E-01	1.34474E-03	0.0	0.0	0.0
	3	1.36227E-01	0.0	2.00560E-02	0.0	0.0	0.0
20 H20	1	1.24040E+00	9.34598E-02	1.20477E-04	0.0	0.0	0.0
	2	4.53494E-01	1.54211E-01	1.35534E-03	0.0	0.0	0.0
	3	1.28445E-01	0.0	2.04662E-02	0.0	0.0	0.0
21 H20	1	1.24195E+00	9.06743E-02	1.16696E-04	0.0	0.0	0.0
	2	4.54609E-01	1.44983E-01	1.29913E-03	0.0	0.0	0.0
	3	1.28445E-01	0.0	2.04662E-02	0.0	0.0	0.0

22	CORE+AL-H2O	1	2.40212E+00	7.02450E-03	1.09647E-03	2.01382E-03	0.0	2.61899E-14
		2	3.09836E+00	1.23471E-02	1.93325E-02	3.00907E-02	0.0	3.96303E-13
		3	7.93444E-01	0.0	1.69736E-01	3.26725E-01	0.0	4.31593E-12
23	CORE+AL-H2O	1	2.39906E+00	6.94948E-03	1.12305E-03	2.00887E-03	0.0	2.61380E-14
		2	2.06529E+00	1.23451E-02	1.92850E-02	3.00358E-02	0.0	3.95581E-13
		3	7.94068E-01	0.0	1.71244E-01	3.30777E-01	0.0	4.36946E-12
24	AL+H2O	1	1.36900E+00	7.13763E-02	1.32019E-04	0.0	0.0	0.0
		2	4.98802E-01	1.30121E-01	1.24397E-03	0.0	0.0	0.0
		3	1.42130E-01	0.0	1.96944E-02	0.0	0.0	0.0
25	AL+D2O+VOID	1	2.64722E+00	9.13870E-03	5.39080E-05	0.0	0.0	0.0
		2	2.37527E+00	8.44473E-03	1.02350E-04	0.0	0.0	0.0
		3	1.64809E+00	0.0	1.44756E-03	0.0	0.0	0.0
26	AL+D2O+VOID	1	1.99327E+00	1.43169E-02	6.36992E-05	0.0	0.0	0.0
		2	1.73227E+00	1.32244E-02	5.72214E-05	0.0	0.0	0.0
		3	1.15862E+00	0.0	8.17563E-04	0.0	0.0	0.0
27	AL+VOID	1	6.39779E+00	1.25266E-04	3.46693E-05	0.0	0.0	0.0
		2	6.93563E+00	1.24372E-04	1.69994E-04	0.0	0.0	0.0
		3	6.43429E+00	0.0	2.39075E-03	0.0	0.0	0.0
28	AL+D2O+VOID	1	2.43792E+00	1.04900E-02	5.65631E-05	0.0	0.0	0.0
		2	2.16531E+00	9.69207E-03	9.10700E-05	0.0	0.0	0.0
		3	1.48433E+00	0.0	1.29014E-03	0.0	0.0	0.0
29	AL+D2O+VOID	1	3.63227E+00	6.84777E-03	3.86975E-05	0.0	0.0	0.0
		2	3.24308E+00	6.32732E-03	6.82628E-05	0.0	0.0	0.0
		3	2.23666E+00	0.0	9.66131E-04	0.0	0.0	0.0
30	AL+D2O+VOID	1	2.25930E+00	1.18413E-02	5.92183E-05	0.0	0.0	0.0
		2	1.98945E+00	1.09394E-02	7.97902E-05	0.0	0.0	0.0
		3	1.35017E+00	0.0	1.13272E-03	0.0	0.0	0.0
31	AL+D2O+VOID	1	2.05519E+00	1.36454E-02	6.35273E-05	0.0	0.0	0.0
		2	1.79384E+00	1.26049E-02	6.85279E-05	0.0	0.0	0.0
		3	1.20426E+00	0.0	9.75963E-04	0.0	0.0	0.0
32	AL+D2O+VOID	1	1.71279E+00	1.76987E-02	7.14903E-05	0.0	0.0	0.0
		2	1.47079E+00	1.63463E-02	3.46081E-05	0.0	0.0	0.0
		3	9.69772E-01	0.0	5.03713E-04	0.0	0.0	0.0

LINE RELAXATION WILL BE DONE ON ROWS - 3 INNER ITERATION(S)

ITERATION	FLUX CHANGE	BETA	MU-1	MU-2	MU-3	K
1	3.05534E+00	1.00000	6.11068	-2.00000	0.0	0.331336
2	4.84941E+00	1.87832	6.43660	0.0	1.01450	0.788224
3	2.84667E+01	1.78304	34.33679	0.00327	0.05753	0.730443
4	3.65237E+01	1.71492	37.80672	0.01874	6.15784	0.843134
5	4.43665E+00	1.66933	4.55812	0.01031	0.25231	0.853388
6	3.61814E+00	1.64014	4.43389	0.01046	0.76330	0.884547
7	1.91502E+00	1.62199	2.44427	0.11058	0.23347	0.891008
8	6.60938E-01	1.61090	1.00607	0.12050	1.04032	0.903593
9	2.67517E-01	1.60420	0.67227	0.41105	0.29671	0.910700
10	2.69360E-01	1.60018	1.27625	0.41565	0.38680	0.917020
11	-1.65894E-01	1.59777	-0.78178	-0.29810	-0.48092	0.921799
12	-7.96422E-02	1.59634	0.40044	0.91126	2.59321	0.925850
13	-6.93774E-02	1.59548	0.80174	0.91863	1.46474	0.929189
14	-5.98297E-02	1.59498	0.80255	0.92361	1.20286	0.931997
15	-5.10637E-02	1.59467	0.80242	0.92691	1.11407	
	-3.43808E-01	EXTRAPOLATION WITH		6.3892		0.949921
16	2.93427E-02	1.00000	-0.54529	-1.00941	6.90737	0.949712
17	3.30458E-02	1.59449	1.15925	1.14178	0.19030	0.949021
18	2.72493E-02	1.59433	0.85184	0.72659	0.90569	0.948870
19	2.29263E-02	1.59429	0.84428	1.03710	0.98407	0.948617
20	1.87790E-02	1.59426	0.83787	0.73166	0.93226	0.948403
21	1.51834E-02	1.59425	0.82373	0.82566	0.91769	0.948204
22	1.23492E-02	1.59424	0.82702	0.89956	0.91102	0.948043
23	-1.13478E-02	1.59424	-0.92877	-0.81700	0.91206	0.947910
24	-1.05920E-02	1.59424	0.92281	0.83137	0.91250	0.947803
25	-9.87619E-03	1.59423	0.92254	0.83299	0.91443	0.947713
26	-9.20129E-03	1.59423	0.92246	0.88406	0.91610	0.947638
27	-8.56197E-03	1.59423	0.92196	0.95407	0.91737	0.947575
28	-7.95221E-03	1.59423	0.92083	0.95245	0.91857	0.947520
29	-7.37333E-03	1.59423	0.91983	0.94971	0.92015	
	-1.05433E-01	EXTRAPOLATION WITH		14.3302		0.946767
30	2.51007E-03	1.00000	-0.33792	-0.38020	14.23802	0.946795
31	-4.07839E-03	1.59423	-1.62889	-1.50571	-0.01266	0.946842
32	-3.44131E-03	1.59423	0.84036	0.72878	0.85690	0.946840
33	-2.97517E-03	1.59423	0.86156	1.15382	0.99416	0.946848
34	-2.49046E-03	1.59423	0.83459	0.84727	0.91308	0.946852
35	-2.04962E-03	1.59423	0.82094	0.74614	0.89831	0.946856
36	-1.69253E-03	1.59423	0.82408	0.93098	0.88330	0.946857
37	-1.40107E-03	1.59423	0.82639	0.93085	0.89126	0.946857
38	1.23405E-03	1.59423	-0.87956	-0.87106	0.88373	0.946854
39	1.14250E-03	1.59423	0.92695	0.83052	0.88897	0.946851
40	1.05476E-03	1.59423	0.92426	0.83170	0.88593	0.946847
41	9.70840E-04	1.59423	0.92140	0.83161	0.88955	
	6.88442E-03	EXTRAPOLATION WITH		7.0977		0.946813
42	1.04904E-03	1.00000	1.08160	0.94558	7.11988	0.946810
43	4.66347E-04	1.59423	0.44501	0.37197	0.01314	0.946809
44	3.28064E-04	1.59423	0.70380	1.09599	0.16551	0.946804

END OF EIGENVALUE CALCULATION - ITERATION TIME 1.683 MINUTES

CONVERGENCE INDICATION BY MINIMIZING THE SUM OF THE SQUARES OF THE RESIDUES - RELATIVE ABSORPTION 0.9999976 K 0.9467986

LEAKAGE 9.10488E+15 TOTAL LOSSES 2.00103E+17 TOTAL PRODUCTIONS 1.89458E+17 REACTOR POWER(WATTS) 5.00000E+06

AVERAGE FLUXES BY ZONE AND GROUP

ZONE 1--CORE

```
                  1.04827E+14  4.27342E+13  4.30269E+13

        ZONE   2--H2O+AL
         9.33460E+12  5.54909E+12  1.69734E+13

        ZONE   3--CORE
          1.73084E+14  6.62549E+13  3.02675E+13

        ZONE   4--CORE
          1.87525E+14  6.79224E+13  2.10479E+13

        ZONE   5--CORE
          1.51612E+14  5.62903E+13  2.07228E+13

        ZONE   6--CORE
          1.07254E+14  4.20585E+13  2.08869E+13

        ZONE   7--D2O+H2O+AL
          2.97409E+12  3.60018E+12  3.99525E+13

        ZONE   8--PB
          0.0          0.0          0.0

        ZONE   9--CD+AL
          3.26098E+13  1.29347E+13  1.69556E+03

        ZONE  10--AL
          1.65312E+14  6.21583E+13  3.52588E+13

        ZONE  11--AL
          7.07611E+13  3.07892E+13  2.61012E+13

        ZONE  12--D2O
          0.0          0.0          0.0

        ZONE  13--CORE
          5.59786E+13  2.09728E+13  4.63760E+12

        ZONE  14--CORE
          4.59007E+13  1.74543E+13  5.19668E+12

        ZONE  15--AL+H2O
          1.66182E+11  3.66578E+11  1.19555E+13

        ZONE  16--C
          5.27521E+09  1.21970E+10  2.00352E+12

        ZONE  17--AL+D2O
          5.54342E+13  3.48326E+13  9.47192E+13

        ZONE  18--H2O
          4.27552E+10  2.41790E+10  2.15897E+11

        ZONE  19--AL+H2O
          8.31029E+10  8.25655E+10  2.69660E+12

        ZONE  20--H2O
          4.90031E+13  2.79871E+13  6.39491E+13

        ZONE  21--H2O
          5.43468E+13  2.94680E+13  5.17933E+13

        ZONE  22--CORE+AL-H2O
          0.0          0.0          0.0

        ZONE  23--CORE+AL-H2O
```

```
          0.0          0.0          0.0

   ZONE  24--AL+H20
       8.24822E+13   4.28092E+13   8.76548E+13

   ZONE  25--AL+D20+VOID
       2.16391E+13   1.89629E+13   8.73934E+13

   ZONE  26--AL+D20+VOID
       4.64331E+12   5.07564E+12   5.04532E+13

   ZONE  27--AL+VOID
       1.25908E+13   1.12388E+13   6.59551E+13

   ZONE  28--AL+D20+VOID
       1.69252E+13   1.65211E+13   8.51538E+13

   ZONE  29--AL+D20+VOID
       1.02731E+13   1.05591E+13   7.04352E+13

   ZONE  30--AL+D20+VOID
       5.25077E+12   7.67233E+12   7.01017E+13

   ZONE  31--AL+D20+VOID
       9.68058E+11   1.97008E+12   4.03061E+13

   ZONE  32--AL+D20+VOID
       1.18902E+10   3.22200E+10   3.49828E+12
```

GROUP 1 FLUX

PLANE NUMBER 1

	1	2	3	4	5	6	7	8	9	10	11
1	2.279E+11	2.279E+11	2.279E+11	2.285E+11	2.286E+11	2.292E+11	2.301E+11	2.310E+11	2.319E+11	2.324E+11	2.324E+11
2	2.239E+11	2.239E+11	2.239E+11	2.246E+11	2.253E+11	2.258E+11	2.273E+11	2.289E+11	2.305E+11	2.315E+11	2.315E+11
3	2.193E+11	2.193E+11	2.194E+11	2.207E+11	2.214E+11	2.220E+11	2.239E+11	2.262E+11	2.285E+11	2.300E+11	2.301E+11
4	2.144E+11	2.144E+11	2.145E+11	2.164E+11	2.172E+11	2.180E+11	2.200E+11	2.229E+11	2.257E+11	2.278E+11	2.279E+11
5	2.090E+11	2.090E+11	2.091E+11	2.115E+11	2.125E+11	2.134E+11	2.156E+11	2.190E+11	2.223E+11	2.250E+11	2.252E+11
6	1.892E+11	1.892E+11	1.894E+11	1.930E+11	1.952E+11	1.965E+11	1.983E+11	2.029E+11	2.079E+11	2.125E+11	2.128E+11
7	1.555E+11	1.556E+11	1.557E+11	1.598E+11	1.610E+11	1.624E+11	1.643E+11	1.685E+11	1.744E+11	1.801E+11	1.804E+11
8	1.381E+11	1.381E+11	1.373E+11	1.407E+11	1.414E+11	1.431E+11	1.450E+11	1.478E+11	1.546E+11	1.600E+11	1.597E+11
9	1.319E+11	1.317E+11	1.304E+11	1.335E+11	1.337E+11	1.358E+11	1.377E+11	1.397E+11	1.470E+11	1.522E+11	1.516E+11
10	1.284E+11	1.281E+11	1.256E+11	1.290E+11	1.283E+11	1.300E+11	1.327E+11	1.340E+11	1.418E+11	1.469E+11	1.458E+11
11	1.248E+11	1.249E+11	1.221E+11	1.249E+11	1.242E+11	1.270E+11	1.289E+11	1.296E+11	1.379E+11	1.428E+11	1.412E+11
12	1.211E+11	1.211E+11	1.188E+11	1.215E+11	1.193E+11	1.236E+11	1.255E+11	1.244E+11	1.343E+11	1.391E+11	1.359E+11
13	1.140E+11	1.139E+11	1.124E+11	1.149E+11	1.130E+11	1.169E+11	1.187E+11	1.178E+11	1.271E+11	1.317E+11	1.289E+11
14	1.064E+11	1.063E+11	1.052E+11	1.075E+11	1.064E+11	1.095E+11	1.112E+11	1.110E+11	1.191E+11	1.234E+11	1.215E+11
15	9.586E+10	9.580E+10	9.503E+10	9.721E+10	9.692E+10	9.894E+10	1.005E+11	1.011E+11	1.077E+11	1.117E+11	1.107E+11
16	2.709E+10	2.708E+10	2.702E+10	2.703E+10	2.806E+10	2.836E+10	2.882E+10	2.970E+10	3.108E+10	3.242E+10	3.245E+10
17	3.371E+09	3.371E+09	3.374E+09	3.472E+09	3.507E+09	3.543E+09	3.605E+09	3.731E+09	3.899E+09	4.074E+09	4.083E+09
18	1.467E+09	1.467E+09	1.469E+09	1.512E+09	1.528E+09	1.543E+09	1.571E+09	1.629E+09	...E+09	1.778E+09	1.782E+09
19	3.244E+08	3.245E+08	3.249E+08	3.345E+08	3.387E+08	3.429E+08	3.522E+08	3.664E+08	3.824E+08	3.982E+08	3.992E+08

PLANE NUMBER 2

	1	2	3	4	5	6	7	8	9	10	11
1	8.277E+12	8.277E+12	8.277E+12	8.271E+12	8.266E+12	8.260E+12	8.269E+12	8.301E+12	8.333E+12	8.354E+12	8.355E+12
2	8.133E+12	8.133E+12	8.134E+12	8.139E+12	8.120E+12	8.132E+12	8.152E+12	8.224E+12	8.296E+12	8.347E+12	8.350E+12
3	7.958E+12	7.958E+12	7.959E+12	7.983E+12	7.970E+12	7.971E+12	8.027E+12	8.136E+12	8.245E+12	8.328E+12	8.333E+12
4	7.750E+12	7.750E+12	7.750E+12	7.811E+12	7.824E+12	7.841E+12	7.907E+12	8.044E+12	8.177E+12	8.294E+12	8.301E+12
5	7.530E+12	7.530E+12	7.524E+12	7.628E+12	7.659E+12	7.689E+12	7.754E+12	7.924E+12	8.075E+12	8.226E+12	8.235E+12
6	6.911E+12	6.912E+12	6.824E+12	7.119E+12	7.180E+12	7.223E+12	7.182E+12	7.394E+12	7.628E+12	7.897E+12	7.912E+12
7	5.415E+12	5.418E+12	5.465E+12	5.680E+12	5.735E+12	5.779E+12	5.802E+12	5.951E+12	6.230E+12	6.535E+12	6.552E+12
8	4.594E+12	4.599E+12	4.660E+12	4.839E+12	4.877E+12	4.927E+12	4.955E+12	5.053E+12	5.335E+12	5.607E+12	5.611E+12
9	4.277E+12	4.252E+12	4.358E+12	4.523E+12	4.549E+12	4.607E+12	4.637E+12	4.703E+12	4.997E+12	5.255E+12	5.247E+12
10	4.069E+12	4.069E+12	4.137E+12	4.292E+12	4.304E+12	4.371E+12	4.402E+12	4.452E+12	4.747E+12	4.992E+12	4.970E+12
11	3.913E+12	3.918E+12	3.963E+12	4.109E+12	4.121E+12	4.186E+12	4.217E+12	4.266E+12	4.549E+12	4.785E+12	4.764E+12
12	3.749E+12	3.752E+12	3.779E+12	3.917E+12	3.922E+12	3.990E+12	4.021E+12	4.053E+12	4.340E+12	4.564E+12	4.538E+12
13	3.539E+12	3.540E+12	3.545E+12	3.673E+12	3.690E+12	3.742E+12	3.771E+12	3.827E+12	4.072E+12	4.283E+12	4.274E+12
14	3.309E+12	3.309E+12	3.313E+12	3.432E+12	3.453E+12	3.497E+12	3.526E+12	3.585E+12	3.808E+12	4.005E+12	4.003E+12
15	2.967E+12	2.967E+12	2.970E+12	3.076E+12	3.099E+12	3.134E+12	3.162E+12	3.223E+12	3.415E+12	3.592E+12	3.595E+12
16	7.672E+11	7.673E+11	7.680E+11	7.930E+11	8.012E+11	8.089E+11	8.202E+11	8.468E+11	8.892E+11	9.320E+11	9.344E+11
17	7.645E+10	7.645E+10	7.652E+10	7.889E+10	7.982E+10	8.062E+10	8.200E+10	8.495E+10	8.903E+10	9.338E+10	9.364E+10
18	2.953E+10	2.953E+10	2.956E+10	3.047E+10	3.093E+10	3.114E+10	3.171E+10	3.289E+10	3.446E+10	3.613E+10	3.623E+10
19	2.076E+09	2.076E+09	2.079E+09	2.142E+09	2.170E+09	2.198E+09	2.257E+09	2.348E+09	2.455E+09	2.561E+09	2.567E+09

PLANE NUMBER 3

	1	2	3	4	5	6	7	8	9	10	11
1	3.490E+13	3.490E+13	3.492E+13	3.523E+13	3.543E+13	3.572E+13	3.662E+13	3.726E+13	3.787E+13	3.818E+13	3.820E+13
2	3.417E+13	3.417E+13	3.419E+13	3.447E+13	3.468E+13	3.496E+13	3.599E+13	3.680E+13	3.761E+13	3.814E+13	3.817E+13
3	3.144E+13	3.145E+13	3.351E+13	3.370E+13	3.384E+13	3.413E+13	3.520E+13	3.609E+13	3.714E+13	3.793E+13	3.799E+13
4	3.263E+13	3.266E+13	3.297E+13	3.309E+13	3.320E+13	3.345E+13	3.459E+13	3.527E+13	3.678E+13	3.790E+13	3.797E+13
5	3.191E+13	3.196E+13	3.286E+13	3.284E+13	3.301E+13	3.328E+13	3.461E+13	3.475E+13	3.710E+13	3.863E+13	3.872E+13
6	2.954E+13	2.967E+13	3.204E+13	3.100E+13	3.117E+13	3.150E+13	3.409E+13	3.278E+13	3.746E+13	4.016E+13	4.032E+13
7	2.213E+13	2.230E+13	2.532E+13	2.671E+13	2.708E+13	2.721E+13	2.710E+13	2.459E+13	2.964E+13	3.222E+13	3.243E+13

	1	2	3	4	5	6	7	8	9	10	11
8	1.797E+13	1.807E+13	1.970E+13	2.082E+13	2.130E+13	2.123E+13	2.110E+13	1.993E+13	2.306E+13	2.497E+13	2.532E+13
9	1.655E+13	1.665E+13	1.791E+13	1.887E+13	1.925E+13	1.924E+13	1.917E+13	1.832E+13	2.095E+13	2.260E+13	2.288E+13
10	1.565E+13	1.571E+13	1.692E+13	1.779E+13	1.774E+13	1.815E+13	1.811E+13	1.700E+13	1.978E+13	2.129E+13	2.110E+13
11	1.469E+13	1.489E+13	1.616E+13	1.696E+13	1.622E+13	1.730E+13	1.729E+13	1.576E+13	1.889E+13	2.029E+13	1.932E+13
12	1.389E+13	1.401E+13	1.520E+13	1.593E+13	1.487E+13	1.626E+13	1.626E+13	1.464E+13	1.776E+13	1.905E+13	1.770E+13
13	1.328E+13	1.330E+13	1.354E+13	1.417E+13	1.400E+13	1.446E+13	1.448E+13	1.393E+13	1.581E+13	1.694E+13	1.665E+13
14	1.269E+13	1.269E+13	1.259E+13	1.316E+13	1.337E+13	1.343E+13	1.345E+13	1.339E+13	1.469E+13	1.572E+13	1.588E+13
15	1.128E+13	1.127E+13	1.121E+13	1.170E+13	1.188E+13	1.194E+13	1.197E+13	1.200E+13	1.307E+13	1.398E+13	1.410E+13
16	2.400E+12	2.400E+12	2.398E+12	2.485E+12	2.514E+12	2.537E+12	2.569E+12	2.646E+12	2.801E+12	2.961E+12	2.973E+12
17	3.504E+11	3.505E+11	3.506E+11	3.619E+11	3.662E+11	3.700E+11	3.770E+11	3.908E+11	4.108E+11	4.318E+11	4.331E+11
18	1.146E+11	1.146E+11	1.146E+11	1.182E+11	1.196E+11	1.209E+11	1.233E+11	1.280E+11	1.344E+11	1.412E+11	1.416E+11
19	4.131E+09	4.131E+09	4.135E+09	4.262E+09	4.322E+09	4.378E+09	4.502E+09	4.685E+09	4.901E+09	5.115E+09	5.128E+09

PLANE NUMBER 4

	1	2	3	4	5	6	7	8	9	10	11
1	6.231E+13	6.232E+13	6.235E+13	6.293E+13	6.330E+13	6.384E+13	6.555E+13	6.680E+13	6.798E+13	6.859E+13	6.862E+13
2	6.093E+13	6.093E+13	6.097E+13	6.148E+13	6.188E+13	6.242E+13	6.445E+13	6.606E+13	6.766E+13	6.868E+13	6.874E+13
3	5.956E+13	5.957E+13	5.968E+13	6.002E+13	6.029E+13	6.086E+13	6.306E+13	6.487E+13	6.696E+13	6.848E+13	6.856E+13
4	5.806E+13	5.810E+13	5.866E+13	5.883E+13	5.905E+13	5.956E+13	6.196E+13	6.344E+13	6.639E+13	6.850E+13	6.862E+13
5	5.670E+13	5.679E+13	5.834E+13	5.820E+13	5.856E+13	5.912E+13	6.194E+13	6.252E+13	6.701E+13	6.986E+13	7.002E+13
6	5.234E+13	5.257E+13	5.666E+13	5.490E+13	5.526E+13	5.592E+13	6.087E+13	5.899E+13	6.770E+13	7.268E+13	7.297E+13
7	3.924E+13	3.954E+13	4.479E+13	4.698E+13	4.766E+13	4.799E+13	4.838E+13	4.426E+13	5.349E+13	5.815E+13	5.853E+13
8	3.192E+13	3.209E+13	3.491E+13	3.669E+13	3.754E+13	3.752E+13	3.772E+13	3.589E+13	4.163E+13	4.507E+13	4.566E+13
9	2.942E+13	2.960E+13	3.177E+13	3.331E+13	3.399E+13	3.407E+13	3.431E+13	3.301E+13	3.785E+13	4.080E+13	4.131E+13
10	2.783E+13	2.794E+13	3.003E+13	3.142E+13	3.136E+13	3.215E+13	3.242E+13	3.065E+13	3.575E+13	3.845E+13	3.811E+13
11	2.615E+13	2.649E+13	2.870E+13	2.999E+13	2.873E+13	3.068E+13	3.098E+13	2.844E+13	3.415E+13	3.666E+13	3.493E+13
12	2.473E+13	2.494E+13	2.702E+13	2.820E+13	2.635E+13	2.885E+13	2.916E+13	2.642E+13	3.214E+13	3.445E+13	3.202E+13
13	2.365E+13	2.368E+13	2.411E+13	2.512E+13	2.483E+13	2.570E+13	2.600E+13	2.515E+13	2.___E+13	3.066E+13	3.012E+13
14	2.261E+13	2.260E+13	2.243E+13	2.335E+13	2.373E+13	2.389E+13	2.418E+13	2.419E+13	2.663E+13	2.848E+13	2.875E+13
15	2.013E+13	2.013E+13	2.000E+13	2.081E+13	2.112E+13	2.1_3E+13	2.156E+13	2.17_E+13	2.373E+13	2.536E+13	2.556E+13
16	4.301E+12	4.300E+12	4.296E+12	4.438E+12	4.495E+12	4.638E+12	4.792E+12	5.085E+12	5.368E+12	5.388E+12	
17	6.253E+11	6.253E+11	6.253E+11	6.439E+11	6.520E+11	6.597E+11	6.768E+11	7.035E+11	7.405E+11	7.768E+11	7.790E+11
18	2.039E+11	2.038E+11	2.038E+11	2.098E+11	2.124E+11	2.149E+11	2.207E+11	2.296E+11	2.414E+11	2.529E+11	2.537E+11
19	6.508E+09	6.508E+09	6.513E+09	6.716E+09	6.821E+09	6.921E+09	7.144E+09	7.439E+09	7.783E+09	8.111E+09	8.131E+09

PLANE NUMBER 5

	1	2	3	4	5	6	7	8	9	10	11
1	8.551E+13	8.551E+13	8.555E+13	8.640E+13	8.692E+13	8.771E+13	9.014E+13	9.191E+13	9.358E+13	9.444E+13	9.449E+13
2	8.349E+13	8.350E+13	8.356E+13	8.431E+13	8.489E+13	8.567E+13	8.858E+13	9.088E+13	9.316E+13	9.458E+13	9.467E+13
3	8.151E+13	8.152E+13	8.168E+13	8.219E+13	8.259E+13	8.343E+13	8.686E+13	8.923E+13	9.219E+13	9.430E+13	9.442E+13
4	7.937E+13	7.943E+13	8.018E+13	8.043E+13	8.077E+13	8.153E+13	8.505E+13	8.722E+13	9.138E+13	9.427E+13	9.444E+13
5	7.740E+13	7.752E+13	7.962E+13	7.941E+13	7.994E+13	8.078E+13	8.495E+13	8.591E+13	9.218E+13	9.607E+13	9.629E+13
6	7.118E+13	7.150E+13	7.700E+13	7.462E+13	7.517E+13	7.613E+13	8.323E+13	8.089E+13	9.291E+13	9.961E+13	1.000E+14
7	5.331E+13	5.371E+13	6.076E+13	6.354E+13	6.450E+13	6.503E+13	6.603E+13	6.062E+13	7.325E+13	7.941E+13	7.991E+13
8	4.333E+13	4.355E+13	4.729E+13	4.954E+13	5.070E+13	5.075E+13	5.141E+13	4.911E+13	5.691E+13	6.141E+13	6.221E+13
9	3.991E+13	4.015E+13	4.302E+13	4.496E+13	4.591E+13	4.607E+13	4.675E+13	4.514E+13	5.172E+13	5.558E+13	5.626E+13
10	3.774E+13	3.789E+13	4.066E+13	4.241E+13	4.235E+13	4.347E+13	4.417E+13	4.190E+13	4.885E+13	5.237E+13	5.189E+13
11	3.545E+13	3.590E+13	3.886E+13	4.047E+13	3.879E+13	4.148E+13	4.219E+13	3.886E+13	4.665E+13	4.992E+13	4.754E+13
12	3.352E+13	3.379E+13	3.658E+13	3.805E+13	3.557E+13	3.901E+13	3.971E+13	3.607E+13	4.390E+13	4.689E+13	4.356E+13
13	3.205E+13	3.208E+13	3.262E+13	3.388E+13	3.350E+13	3.473E+13	3.539E+13	3.300E+13	3.910E+13	4.171E+13	4.095E+13
14	3.063E+13	3.061E+13	3.034E+13	3.148E+13	3.201E+13	3.227E+13	3.290E+13	3.300E+13	3.633E+13	3.872E+13	3.908E+13
15	2.725E+13	2.724E+13	2.704E+13	2.804E+13	2.848E+13	2.874E+13	2.931E+13	2.960E+13	3.236E+13	3.445E+13	3.472E+13
16	5.731E+12	5.730E+12	5.720E+12	5.894E+12	5.972E+12	6.043E+12	6.207E+12	6.425E+12	6.816E+12	7.174E+12	7.200E+12
17	8.186E+11	8.186E+11	8.183E+11	8.409E+11	8.519E+11	8.627E+11	8.895E+11	9.257E+11	9.741E+11	1.019E+12	1.022E+12
18	2.657E+11	2.657E+11	2.656E+11	2.729E+11	2.765E+11	2.800E+11	2.899E+11	3.009E+11	3.162E+11	3.306E+11	3.315E+11
19	8.042E+09	8.042E+09	8.047E+09	8.305E+09	8.452E+09	8.585E+09	8.883E+09	9.252E+09	9.674E+09	1.007E+10	1.009E+10

PLANE NUMBER 6

	1	2	3	4	5	6	7	8	9	10	11
1	1.206E+14	1.206E+14	1.207E+14	1.221E+14	1.230E+14	1.243E+14	1.281E+14	1.308E+14	1.333E+14	1.346E+14	1.347E+14
2	1.175E+14	1.175E+14	1.176E+14	1.189E+14	1.199E+14	1.213E+14	1.259E+14	1.294E+14	1.328E+14	1.348E+14	1.350E+14
3	1.145E+14	1.145E+14	1.148E+14	1.157E+14	1.165E+14	1.179E+14	1.231E+14	1.270E+14	1.314E+14	1.344E+14	1.345E+14
4	1.114E+14	1.115E+14	1.126E+14	1.130E+14	1.136E+14	1.149E+14	1.207E+14	1.240E+14	1.301E+14	1.340E+14	1.343E+14

	1	2	3	4	5	6	7	8	9	10	11
5	1.085E+14	1.087E+14	1.116E+14	1.112E+14	1.120E+14	1.134E+14	1.203E+14	1.219E+14	1.310E+14	1.362E+14	1.365E+14
6	9.941E+13	9.984E+13	1.073E+14	1.034E+14	1.043E+14	1.058E+14	1.170E+14	1.142E+14	1.310E+14	1.398E+14	1.403E+14
7	7.457E+13	7.512E+13	8.472E+13	8.799E+13	8.937E+13	9.026E+13	9.278E+13	8.562E+13	1.032E+14	1.110E+14	1.117E+14
8	6.038E+13	6.066E+13	6.590E+13	6.859E+13	7.033E+13	7.043E+13	7.216E+13	6.911E+13	8.003E+13	8.578E+13	8.694E+13
9	5.551E+13	5.581E+13	5.949E+13	6.177E+13	6.318E+13	6.344E+13	6.511E+13	6.340E+13	7.214E+13	7.699E+13	7.798E+13
10	5.242E+13	5.250E+13	5.617E+13	5.821E+13	5.821E+13	5.900E+13	6.144E+13	5.874E+13	6.806E+13	7.245E+13	7.184E+13
11	4.915E+13	4.975E+13	5.363E+13	5.549E+13	5.323E+13	5.702E+13	5.864E+13	5.436E+13	6.494E+13	6.900E+13	6.571E+13
12	4.637E+13	4.675E+13	5.045E+13	5.213E+13	4.872E+13	5.357E+13	5.514E+13	5.034E+13	6.104E+13	6.476E+13	6.009E+13
13	4.428E+13	4.432E+13	4.491E+13	4.635E+13	4.581E+13	4.762E+13	4.905E+13	4.781E+13	5.427E+13	5.749E+13	5.637E+13
14	4.227E+13	4.224E+13	4.170E+13	4.300E+13	4.373E+13	4.418E+13	4.552E+13	4.591E+13	5.033E+13	5.328E+13	5.375E+13
15	3.753E+13	3.751E+13	3.710E+13	3.823E+13	3.895E+13	3.928E+13	4.048E+13	4.109E+13	4.474E+13	4.732E+13	4.766E+13
16	7.639E+12	7.637E+12	7.613E+12	7.811E+12	7.920E+12	8.023E+12	8.303E+12	8.616E+12	9.125E+12	9.558E+12	9.591E+12
17	1.061E+12	1.061E+12	1.060E+12	1.086E+12	1.101E+12	1.116E+12	1.157E+12	1.206E+12	1.268E+12	1.322E+12	1.325E+12
18	3.423E+11	3.423E+11	3.420E+11	3.506E+11	3.554E+11	3.603E+11	3.737E+11	3.897E+11	4.091E+11	4.263E+11	4.274E+11
19	9.802E+09	9.803E+09	9.807E+09	1.014E+10	1.035E+10	1.053E+10	1.092E+10	1.138E+10	1.188E+10	1.235E+10	1.238E+10

PLANE NUMBER 7

	1	2	3	4	5	6	7	8	9	10	11
1	1.716E+14	1.716E+14	1.718E+14	1.749E+14	1.767E+14	1.795E+14	1.868E+14	1.915E+14	1.958E+14	1.979E+14	1.980E+14
2	1.672E+14	1.672E+14	1.674E+14	1.705E+14	1.710E+14	1.768E+14	1.861E+14	1.921E+14	1.978E+14	2.007E+14	2.009E+14
3	1.636E+14	1.616E+14	1.639E+14	1.663E+14	1.692E+14	1.732E+14	1.843E+14	1.912E+14	1.983E+14	2.022E+14	2.024E+14
4	1.613E+14	1.613E+14	1.623E+14	1.631E+14	1.653E+14	1.685E+14	1.813E+14	1.878E+14	1.966E+14	2.013E+14	2.016E+14
5	1.584E+14	1.595E+14	1.606E+14	1.586E+14	1.639E+14	1.639E+14	1.792E+14	1.847E+14	1.960E+14	2.017E+14	2.020E+14
6	1.450E+14	1.452E+14	1.501E+14	1.411E+14	1.424E+14	1.451E+14	1.664E+14	1.698E+14	1.865E+14	1.945E+14	1.950E+14
7	1.115E+14	1.119E+14	1.184E+14	1.198E+14	1.216E+14	1.233E+14	1.311E+14	1.299E+14	1.455E+14	1.525E+14	1.532E+14
8	9.023E+13	9.030E+13	9.191E+13	9.350E+13	9.590E+13	9.630E+13	1.017E+14	1.051E+14	1.124E+14	1.177E+14	1.192E+14
9	8.237E+13	8.235E+13	8.228E+13	8.365E+13	8.568E+13	8.617E+13	9.086E+13	9.608E+13	E+14	1.049E+14	1.063E+14
10	7.679E+13	7.657E+13	7.732E+13	7.854E+13	7.866E+13	8.091E+13	8.531E+13	8.785E+13	9.426E+13	9.827E+13	9.750E+13
11	7.056E+13	7.104E+13	7.354E+13	7.465E+13	7.160E+13	7.591E+13	8.110E+13	7.955E+13	8.958E+13	9.329E+13	8.873E+13
12	6.525E+13	6.567E+13	6.885E+13	6.985E+13	6.513E+13	7.196E+13	7.588E+13	7.204E+13	8.379E+13	8.719E+13	8.061E+13
13	6.147E+13	6.147E+13	6.082E+13	6.170E+13	6.090E+13	6.355E+13	6.696E+13	6.735E+13	7.390E+13	7.688E+13	7.518E+13
14	5.821E+13	5.809E+13	5.611E+13	5.695E+13	5.797E+13	5.865E+13	6.171E+13	6.416E+13	6.808E+13	7.085E+13	7.145E+13
15	5.109E+13	5.099E+13	4.960E+13	5.037E+13	5.125E+13	5.186E+13	5.452E+13	5.677E+13	6.011E+13	6.257E+13	6.304E+13
16	9.593E+12	9.589E+12	9.525E+12	9.710E+12	9.855E+12	9.990E+12	1.044E+13	1.091E+13	1.146E+13	1.190E+13	1.195E+13
17	1.271E+12	1.270E+12	1.268E+12	1.296E+12	1.316E+12	1.335E+12	1.393E+12	1.455E+12	1.523E+12	1.590E+12	1.584E+12
18	4.061E+11	4.061E+11	4.055E+11	4.149E+11	4.212E+11	4.276E+11	4.459E+11	4.658E+11	4.872E+11	5.054E+11	5.067E+11
19	1.098E+10	1.098E+10	1.099E+10	1.144E+10	1.178E+10	1.201E+10	1.247E+10	1.295E+10	1.351E+10	1.402E+10	1.406E+10

PLANE NUMBER 8

	1	2	3	4	5	6	7	8	9	10	11
1	1.948E+14	1.949E+14	1.950E+14	1.987E+14	2.009E+14	2.042E+14	2.127E+14	2.180E+14	2.230E+14	2.253E+14	2.255E+14
2	1.898E+14	1.898E+14	1.900E+14	1.937E+14	1.967E+14	2.010E+14	2.120E+14	2.188E+14	2.253E+14	2.286E+14	2.288E+14
3	1.857E+14	1.857E+14	1.861E+14	1.890E+14	1.925E+14	1.972E+14	2.100E+14	2.179E+14	2.259E+14	2.302E+14	2.305E+14
4	1.832E+14	1.832E+14	1.844E+14	1.853E+14	1.879E+14	1.918E+14	2.065E+14	2.139E+14	2.240E+14	2.291E+14	2.294E+14
5	1.801E+14	1.802E+14	1.828E+14	1.804E+14	1.828E+14	1.865E+14	2.043E+14	2.104E+14	2.234E+14	2.296E+14	2.299E+14
6	1.654E+14	1.657E+14	1.715E+14	1.602E+14	1.617E+14	1.649E+14	1.902E+14	1.937E+14	2.130E+14	2.214E+14	2.219E+14
7	1.292E+14	1.297E+14	1.389E+14	1.395E+14	1.413E+14	1.436E+14	1.536E+14	1.501E+14	1.701E+14	1.775E+14	1.780E+14
8	1.051E+14	1.053E+14	1.103E+14	1.114E+14	1.148E+14	1.192E+14	1.217E+14	1.218E+14	1.344E+14	1.399E+14	1.408E+14
9	9.614E+13	9.626E+13	9.759E+13	9.865E+13	1.005E+14	1.016E+14	1.076E+14	1.112E+14	1.187E+14	1.234E+14	1.245E+14
10	8.782E+13	8.827E+13	9.128E+13	9.226E+13	9.171E+13	9.505E+13	1.007E+14	1.015E+14	1.110E+14	1.152E+14	1.135E+14
11	7.934E+13	8.016E+13	8.656E+13	8.746E+13	8.280E+13	9.011E+13	9.542E+13	9.151E+13	1.052E+14	1.091E+14	1.025E+14
12	7.152E+13	7.195E+13	7.828E+13	7.912E+13	7.439E+13	8.151E+13	8.627E+13	8.227E+13	9.509E+13	9.859E+13	9.182E+13
13	6.668E+13	6.672E+13	6.756E+13	6.830E+13	6.898E+13	7.042E+13	7.441E+13	7.651E+13	8.196E+13	8.503E+13	8.493E+13
14	6.341E+13	6.335E+13	6.237E+13	6.319E+13	6.543E+13	6.507E+13	6.866E+13	7.271E+13	7.560E+13	7.847E+13	8.042E+13
15	5.595E+13	5.590E+13	5.515E+13	5.593E+13	5.757E+13	5.758E+13	6.069E+13	6.412E+13	6.679E+13	6.936E+13	7.062E+13
16	1.044E+13	1.043E+13	1.039E+13	1.058E+13	1.076E+13	1.089E+13	1.141E+13	1.197E+13	1.250E+13	1.296E+13	1.302E+13
17	1.359E+12	1.359E+12	1.356E+12	1.387E+12	1.410E+12	1.432E+12	1.497E+12	1.565E+12	1.633E+12	1.691E+12	1.696E+12
18	4.324E+11	4.324E+11	4.318E+11	4.423E+11	4.499E+11	4.570E+11	4.775E+11	4.931E+11	5.206E+11	5.391E+11	5.405E+11
19	1.141E+10	1.141E+10	1.142E+10	1.198E+10	1.245E+10	1.270E+10	1.318E+10	1.369E+10	1.423E+10	1.476E+10	1.483E+10

PLANE NUMBER 9

	1	2	3	4	5	6	7	8	9	10	11
1	2.081E+14	2.081E+14	2.084E+14	2.124E+14	2.149E+14	2.186E+14	2.278E+14	2.334E+14	2.385E+14	2.410E+14	2.411E+14

	1	2	3	4	5	6	7	8	9	10	11
2	2.028E+14	2.028E+14	2.031E+14	2.073E+14	2.107E+14	2.155E+14	2.272E+14	2.343E+14	2.410E+14	2.444E+14	2.446E+14
3	1.987E+14	1.987E+14	1.991E+14	2.024E+14	2.065E+14	2.117E+14	2.253E+14	2.334E+14	2.417E+14	2.460E+14	2.463E+14
4	1.963E+14	1.964E+14	1.977E+14	1.988E+14	2.017E+14	2.060E+14	2.216E+14	2.290E+14	2.396E+14	2.448E+14	2.451E+14
5	1.935E+14	1.936E+14	1.968E+14	1.968E+14	1.965E+14	2.005E+14	2.194E+14	2.254E+14	2.391E+14	2.453E+14	2.457E+14
6	1.787E+14	1.791E+14	1.858E+14	1.722E+14	1.737E+14	1.770E+14	2.051E+14	2.090E+14	2.288E+14	2.373E+14	2.377E+14
7	1.419E+14	1.424E+14	1.544E+14	1.542E+14	1.559E+14	1.585E+14	1.695E+14	1.634E+14	1.871E+14	1.946E+14	1.951E+14
8	1.157E+14	1.160E+14	1.242E+14	1.250E+14	1.268E+14	1.285E+14	1.362E+14	1.330E+14	1.497E+14	1.554E+14	1.563E+14
9	1.058E+14	1.060E+14	1.093E+14	1.100E+14	1.119E+14	1.132E+14	1.197E+14	1.215E+14	1.316E+14	1.364E+14	1.375E+14
10	9.650E+13	9.718E+13	1.019E+14	1.026E+14	1.019E+14	1.055E+14	1.117E+14	1.107E+14	1.227E+14	1.270E+14	1.251E+14
11	8.692E+13	8.802E+13	9.638E+13	9.707E+13	9.159E+13	9.984E+13	1.056E+14	9.972E+13	1.160E+14	1.201E+14	1.125E+14
12	7.747E+13	7.855E+13	8.683E+13	8.749E+13	8.185E+13	8.998E+13	9.515E+13	8.939E+13	1.045E+14	1.081E+14	1.003E+14
13	7.233E+13	7.242E+13	7.437E+13	7.506E+13	7.553E+13	7.719E+13	8.149E+13	8.239E+13	8.944E+13	9.259E+13	9.232E+13
14	6.864E+13	6.863E+13	6.828E+13	6.902E+13	7.146E+13	7.097E+13	7.481E+13	7.866E+13	8.208E+13	8.504E+13	8.720E+13
15	6.036E+13	6.034E+13	6.006E+13	6.079E+13	6.262E+13	6.251E+13	6.581E+13	6.919E+13	7.218E+13	7.492E+13	7.626E+13
16	1.086E+13	1.096E+13	1.084E+13	1.104E+13	1.124E+13	1.137E+13	1.192E+13	1.250E+13	1.301E+13	1.346E+13	1.354E+13
17	1.384E+12	1.384E+12	1.382E+12	1.421E+12	1.452E+12	1.476E+12	1.545E+12	1.614E+12	1.677E+12	1.734E+12	1.740E+12
18	4.389E+11	4.398E+11	4.384E+11	4.517E+11	4.627E+11	4.707E+11	4.923E+11	5.137E+11	5.338E+11	5.518E+11	5.537E+11
19	1.141E+10	1.141E+10	1.142E+10	1.221E+10	1.301E+10	1.326E+10	1.372E+10	1.417E+10	1.469E+10	1.526E+10	1.537E+10

PLANE NUMBER 10

	1	2	3	4	5	6	7	8	9	10	11
1	1.696E+14	1.697E+14	1.699E+14	1.744E+14	1.771E+14	1.815E+14	1.908E+14	1.956E+14	2.000E+14	2.020E+14	2.021E+14
2	1.648E+14	1.649E+14	1.651E+14	1.700E+14	1.739E+14	1.799E+14	1.907E+14	1.963E+14	2.016E+14	2.042E+14	2.044E+14
3	1.614E+14	1.614E+14	1.619E+14	1.660E+14	1.713E+14	1.771E+14	1.888E+14	1.949E+14	2.013E+14	2.047E+14	2.048E+14
4	1.600E+14	1.601E+14	1.615E+14	1.633E+14	1.664E+14	1.706E+14	1.836E+14	1.886E+14	1.973E+14	2.012E+14	2.015E+14
5	1.582E+14	1.594E+14	1.625E+14	1.602E+14	1.625E+14	1.660E+14	1.814E+14	1.843E+14	1.962E+14	2.008E+14	2.010E+14
6	1.456E+14	1.460E+14	1.533E+14	1.388E+14	1.397E+14	1.424E+14	1.676E+14	1.672E+14	1.857E+14	1.913E+14	1.916E+14
7	1.153E+14	1.159E+14	1.285E+14	1.284E+14	1.297E+14	1.314E+14	1.395E+14	1.311E+14	1.530E+14	1.586E+14	1.590E+14
8	9.375E+13	9.417E+13	1.039E+14	1.047E+14	1.062E+14	1.072E+14	1.127E+14	1.064E+14	1.232E+14	1.277E+14	1.284E+14
9	8.565E+13	8.599E+13	9.028E+13	9.111E+13	9.256E+13	9.333E+13	9.793E+13	9.717E+13	1.071E+14	1.110E+14	1.118E+14
10	7.820E+13	7.830E+13	8.381E+13	8.460E+13	8.394E+13	8.669E+13	9.149E+13	8.872E+13	9.943E+13	1.030E+14	1.014E+14
11	7.067E+13	7.164E+13	7.906E+13	7.982E+13	7.535E+13	8.180E+13	8.515E+13	8.019E+13	9.381E+13	9.713E+13	9.105E+13
12	6.373E+13	6.419E+13	7.085E+13	7.161E+13	6.736E+13	7.334E+13	7.636E+13	7.233E+13	8.409E+13	8.709E+13	8.127E+13
13	5.939E+13	5.943E+13	6.022E+13	6.104E+13	6.221E+13	6.348E+13	6.546E+13	6.749E+13	7.420E+13	7.492E+13	7.069E+13
14	5.639E+13	5.630E+13	5.504E+13	5.591E+13	5.877E+13	5.731E+13	5.946E+13	6.405E+13	6.536E+13	6.794E+13	7.069E+13
15	4.953E+13	4.944E+13	4.826E+13	4.912E+13	5.134E+13	5.036E+13	5.253E+13	5.633E+13	5.733E+13	5.966E+13	6.166E+13
16	8.969E+12	8.963E+12	8.881E+12	9.130E+12	9.354E+12	9.459E+12	9.892E+12	1.043E+13	1.071E+13	1.109E+13	1.118E+13
17	1.171E+12	1.171E+12	1.168E+12	1.225E+12	1.279E+12	1.306E+12	1.364E+12	1.419E+12	1.463E+12	1.512E+12	1.521E+12
18	3.736E+11	3.736E+11	3.729E+11	3.938E+11	4.188E+11	4.257E+11	4.437E+11	4.591E+11	4.747E+11	4.911E+11	4.952E+11
19	1.021E+10	1.021E+10	1.023E+10	1.135E+10	1.292E+10	1.299E+10	1.331E+10	1.358E+10	1.405E+10	1.465E+10	1.490E+10

PLANE NUMBER 11

	1	2	3	4	5	6	7	8	9	10	11
1	1.443E+14	1.443E+14	1.445E+14	1.483E+14	1.507E+14	1.545E+14	1.622E+14	1.660E+14	1.694E+14	1.709E+14	1.710E+14
2	1.402E+14	1.402E+14	1.404E+14	1.446E+14	1.479E+14	1.534E+14	1.621E+14	1.665E+14	1.706E+14	1.726E+14	1.727E+14
3	1.372E+14	1.372E+14	1.376E+14	1.412E+14	1.461E+14	1.511E+14	1.603E+14	1.650E+14	1.701E+14	1.727E+14	1.729E+14
4	1.358E+14	1.359E+14	1.372E+14	1.387E+14	1.414E+14	1.449E+14	1.551E+14	1.587E+14	1.653E+14	1.689E+14	1.691E+14
5	1.345E+14	1.347E+14	1.388E+14	1.369E+14	1.388E+14	1.416E+14	1.539E+14	1.553E+14	1.656E+14	1.692E+14	1.694E+14
6	1.234E+14	1.238E+14	1.307E+14	1.178E+14	1.185E+14	1.206E+14	1.415E+14	1.406E+14	1.560E+14	1.609E+14	1.610E+14
7	9.760E+13	9.814E+13	1.095E+14	1.094E+14	1.103E+14	1.117E+14	1.182E+14	1.103E+14	1.291E+14	1.337E+14	1.340E+14
8	7.895E+13	7.927E+13	8.884E+13	8.959E+13	9.020E+13	9.149E+13	9.579E+13	9.004E+13	1.044E+14	1.083E+14	1.081E+14
9	7.149E+13	7.183E+13	7.658E+13	7.736E+13	7.717E+13	7.905E+13	8.269E+13	8.073E+13	9.019E+13	9.349E+13	9.251E+13
10	6.636E+13	6.665E+13	7.109E+13	7.188E+13	7.049E+13	7.347E+13	7.681E+13	7.496E+13	8.376E+13	8.685E+13	8.494E+13
11	6.257E+13	6.273E+13	6.594E+13	6.676E+13	6.633E+13	6.024E+13	7.129E+13	7.070E+13	7.773E+13	8.065E+13	7.942E+13
12	5.959E+13	5.860E+13	5.857E+13	5.944E+13	6.160E+13	6.077E+13	6.337E+13	6.623E+13	6.907E+13	7.180E+13	7.369E+13
13	5.432E+13	5.419E+13	5.035E+13	5.132E+13	5.658E+13	5.454E+13	6.144E+13	5.943E+13	6.197E+13	6.760E+13	6.760E+13
14	5.084E+13	5.057E+13	4.639E+13	4.739E+13	5.263E+13	4.848E+13	5.030E+13	5.755E+13	5.478E+13	5.723E+13	6.281E+13
15	4.398E+13	4.378E+13	4.098E+13	4.193E+13	4.529E+13	4.292E+13	4.449E+13	4.986E+13	4.843E+13	5.063E+13	5.396E+13
16	7.986E+12	7.978E+12	7.865E+12	8.138E+12	8.400E+12	8.484E+12	8.870E+12	9.389E+12	9.547E+12	9.878E+12	9.988E+12
17	1.064E+12	1.064E+12	1.061E+12	1.129E+12	1.202E+12	1.228E+12	1.280E+12	1.327E+12	1.363E+12	1.409E+12	1.420E+12
18	3.411E+11	3.410E+11	3.404E+11	3.660E+11	4.056E+11	4.088E+11	4.246E+11	4.353E+11	4.502E+11	4.661E+11	4.733E+11
19	9.610E+09	9.612E+09	9.638E+09	1.091E+10	1.293E+10	1.285E+10	1.310E+10	1.328E+10	1.373E+10	1.435E+10	1.469E+10

PLANE NUMBER 12

	1	2	3	4	5	6	7	8	9	10	11
1	1.158E+14	1.158E+14	1.159E+14	1.173E+14	1.178E+14	1.183E+14	1.206E+14	1.226E+14	1.240E+14	1.253E+14	1.254E+14
2	1.129E+14	1.130E+14	1.131E+14	1.149E+14	1.156E+14	1.151E+14	1.200E+14	1.227E+14	1.254E+14	1.267E+14	1.268E+14
3	1.104E+14	1.104E+14	1.105E+14	1.121E+14	1.125E+14	1.139E+14	1.190E+14	1.225E+14	1.258E+14	1.275E+14	1.276E+14
4	1.093E+14	1.083E+14	1.083E+14	1.092E+14	1.092E+14	1.120E+14	1.181E+14	1.221E+14	1.257E+14	1.278E+14	1.279E+14
5	1.062E+14	1.062E+14	1.057E+14	1.054E+14	1.065E+14	1.092E+14	1.154E+14	1.205E+14	1.237E+14	1.260E+14	1.262E+14
6	9.701E+13	9.702E+13	9.701E+13	9.410E+13	9.473E+13	9.621E+13	1.048E+14	1.098E+14	1.148E+14	1.180E+14	1.182E+14
7	7.725E+13	7.742E+13	7.975E+13	7.969E+13	8.028E+13	8.120E+13	8.571E+13	8.689E+13	9.375E+13	9.693E+13	9.710E+13
8	6.321E+13	6.334E+13	6.505E+13	6.558E+13	6.605E+13	6.684E+13	7.000E+13	7.112E+13	7.639E+13	7.913E+13	7.918E+13
9	5.837E+13	5.846E+13	6.004E+13	6.071E+13	6.110E+13	6.190E+13	6.468E+13	6.571E+13	7.054E+13	7.313E+13	7.308E+13
10	5.524E+13	5.532E+13	5.658E+13	5.730E+13	5.757E+13	5.843E+13	6.099E+13	6.222E+13	6.648E+13	6.898E+13	6.890E+13
11	5.278E+13	5.278E+13	5.295E+13	5.371E+13	5.492E+13	5.478E+13	5.710E+13	5.946E+13	6.222E+13	6.463E+13	6.556E+13
12	4.996E+13	4.988E+13	4.763E+13	4.845E+13	4.176E+13	4.943E+13	5.141E+13	5.632E+13	5.598E+13	5.828E+13	6.170E+13
13	4.657E+13	4.642E+13	4.173E+13	4.269E+13	4.797E+13	4.352E+13	4.512E+13	5.255E+13	4.906E+13	5.125E+13	5.710E+13
14	4.371E+13	4.342E+13	3.906E+13	4.001E+13	4.484E+13	4.036E+13	4.229E+13	4.935E+13	4.597E+13	4.807E+13	5.329E+13
15	3.795E+13	3.775E+13	3.492E+13	3.582E+13	3.943E+13	3.661E+13	3.789E+13	4.293E+13	4.114E+13	4.303E+13	4.608E+13
16	7.154E+12	7.146E+12	7.037E+12	7.334E+12	7.609E+12	7.716E+12	8.079E+12	8.554E+12	8.637E+12	8.921E+12	9.017E+12
17	9.772E+11	9.770E+11	9.739E+11	1.053E+12	1.151E+12	1.174E+12	1.222E+12	1.260E+12	1.290E+12	1.334E+12	1.349E+12
18	3.146E+11	3.146E+11	3.142E+11	3.447E+11	4.086E+11	4.029E+11	4.166E+11	4.208E+11	4.374E+11	4.539E+11	4.665E+11
19	9.119E+09	9.121E+09	9.152E+09	1.055E+10	1.301E+10	1.274E+10	1.294E+10	1.304E+10	1.347E+10	1.411E+10	1.455E+10

PLANE NUMBER 13

	1	2	3	4	5	6	7	8	9	10	11
1	1.004E+14	1.004E+14	1.004E+14	1.015E+14	1.020E+14	1.025E+14	1.043E+14	1.058E+14	1.072E+14	1.079E+14	1.080E+14
2	9.811E+13	9.811E+13	9.818E+13	9.943E+13	1.001E+14	1.008E+14	1.037E+14	1.059E+14	1.080E+14	1.091E+14	1.092E+14
3	9.610E+13	9.610E+13	9.617E+13	9.731E+13	9.798E+13	9.901E+13	1.030E+14	1.059E+14	1.085E+14	1.100E+14	1.101E+14
4	9.536E+13	9.536E+13	9.536E+13	9.606E+13	9.697E+13	9.821E+13	1.030E+14	1.063E+14	1.099E+14	1.111E+14	1.112E+14
5	9.203E+13	9.202E+13	9.179E+13	9.178E+13	9.269E+13	9.398E+13	9.940E+13	1.033E+14	1.064E+14	1.083E+14	1.084E+14
6	8.314E+13	8.314E+13	8.314E+13	8.120E+13	8.170E+13	8.283E+13	8.940E+13	9.36..E+13	9.786E+13	1.005E+14	1.006E+14
7	6.616E+13	6.626E+13	6.771E+13	6.770E+13	6.899E+13	6.878E+13	7.249E+13	7.410E+13	7.940E+13	8.202E+13	8.216E+13
8	5.520E+13	5.527E+13	5.625E+13	5.672E+13	5.718E+13	5.759E+13	6.038E+13	6.191E+13	6.595E+13	6.828E+13	6.847E+13
9	5.285E+13	5.291E+13	5.368E+13	5.430E+13	5.488E+13	5.529E+13	5.773E+13	5.937E+13	6.297E+13	6.523E+13	6.557E+13
10	5.019E+13	5.021E+13	5.048E+13	5.115E+13	5.201E+13	5.203E+13	5.633E+13	5.642E+13	5.921E+13	6.145E+13	6.206E+13
11	4.817E+13	4.812E+13	4.702E+13	4.775E+13	4.979E+13	4.863E+13	5.066E+13	5.417E+13	5.516E+13	5.732E+13	5.934E+13
12	4.599E+13	4.572E+13	4.249E+13	4.328E+13	4.727E+13	4.410E+13	4.582E+13	5.164E+13	4.988E+13	5.191E+13	5.626E+13
13	4.247E+13	4.231E+13	3.752E+13	3.838E+13	4.354E+13	3.912E+13	4.053E+13	4.785E+13	4.404E+13	4.597E+13	5.173E+13
14	3.997E+13	3.971E+13	3.587E+13	3.677E+13	4.085E+13	3.751E+13	3.881E+13	4.506E+13	4.214E+13	4.405E+13	4.846E+13
15	3.483E+13	3.465E+13	3.218E+13	3.304E+13	3.556E+13	3.374E+13	3.491E+13	3.936E+13	3.786E+13	3.958E+13	4.212E+13
16	6.746E+12	6.739E+12	6.639E+12	6.949E+12	7.230E+12	7.356E+12	7.712E+12	8.160E+12	8.210E+12	8.469E+12	8.554E+12
17	9.348E+11	9.346E+11	9.319E+11	1.017E+12	1.131E+12	1.150E+12	1.196E+12	1.230E+12	1.257E+12	1.301E+12	1.318E+12
18	3.018E+11	3.018E+11	3.014E+11	3.348E+11	4.154E+11	4.032E+11	4.157E+11	4.155E+11	4.342E+11	4.511E+11	4.680E+11
19	8.878E+09	8.881E+09	8.913E+09	1.037E+10	1.307E+10	1.270E+10	1.286E+10	1.292E+10	1.335E+10	1.400E+10	1.448E+10

PLANE NUMBER 14

	1	2	3	4	5	6	7	8	9	10	11
1	8.398E+13	8.386E+13	8.390E+13	8.463E+13	8.505E+13	8.551E+13	8.681E+13	8.785E+13	8.884E+13	8.935E+13	8.938E+13
2	8.215E+13	8.216E+13	8.220E+13	8.303E+13	8.358E+13	8.420E+13	8.623E+13	8.789E+13	8.946E+13	9.027E+13	9.031E+13
3	8.063E+13	8.064E+13	8.067E+13	8.146E+13	8.209E+13	8.286E+13	8.562E+13	8.782E+13	8.991E+13	9.100E+13	9.107E+13
4	7.999E+13	7.989E+13	7.990E+13	8.045E+13	8.110E+13	8.195E+13	8.522E+13	8.780E+13	9.021E+13	9.150E+13	9.157E+13
5	7.679E+13	7.678E+13	7.675E+13	7.693E+13	7.754E+13	7.840E+13	8.295E+13	8.492E+13	8.755E+13	8.900E+13	8.908E+13
6	6.826E+13	6.827E+13	6.827E+13	6.720E+13	6.758E+13	6.831E+13	7.278E+13	7.612E+13	7.955E+13	8.150E+13	8.160E+13
7	5.407E+13	5.411E+13	5.474E+13	5.477E+13	5.490E+12	5.533E+13	5.815E+13	6.008E+13	6.389E+13	6.591E+13	6.601E+13
8	4.594E+13	4.595E+13	4.619E+13	4.659E+13	4.693E+13	4.715E+13	4.931E+13	5.116E+13	5.395E+13	5.581E+13	5.611E+13
9	4.256E+13	4.255E+13	4.241E+13	4.293E+13	4.355E+13	4.351E+13	4.539E+13	4.749E+13	4.955E+13	5.134E+13	5.194E+13
10	4.002E+13	4.087E+13	4.017E+13	4.079E+13	4.186E+13	4.138E+13	4.310E+13	4.574E+13	4.696E+13	4.874E+13	4.982E+13
11	3.976E+13	3.968E+13	3.849E+13	3.916E+13	4.064E+13	3.976E+13	4.135E+13	4.449E+13	4.501E+13	4.677E+13	4.831E+13
12	3.782E+13	3.769E+13	3.579E+13	3.653E+13	3.859E+13	3.713E+13	3.854E+13	4.240E+13	4.189E+13	4.360E+13	4.579E+13
13	3.646E+13	3.629E+13	3.181E+13	3.462E+13	3.711E+13	3.522E+13	3.650E+13	4.095E+13	3.959E+13	4.129E+13	4.397E+13
14	3.490E+13	3.474E+13	3.241E+13	3.323E+13	3.553E+13	3.384E+13	3.504E+13	3.925E+13	3.798E+13	3.963E+13	4.204E+13
15	3.064E+13	3.051E+13	2.870E+13	2.950E+13	3.120E+13	3.010E+13	3.116E+13	3.454E+13	3.370E+13	3.517E+13	3.687E+13
16	6.207E+12	6.201E+12	6.115E+12	6.445E+12	6.737E+12	6.892E+12	7.240E+12	7.651E+12	7.657E+12	7.883E+12	7.950E+12
17	8.787E+11	8.785E+11	8.765E+11	9.694E+11	1.108E+12	1.122E+12	1.165E+12	1.191E+12	1.216E+12	1.258E+12	1.279E+12
18	2.848E+11	2.848E+11	2.846E+11	3.219E+11	4.319E+11	4.063E+11	4.170E+11	4.100E+11	4.322E+11	4.499E+11	4.740E+11

| 19 | 8.558E+09 | 8.560E+09 | 8.595E+09 | 1.014E+10 | 1.315E+10 | 1.263E+10 | 1.275E+10 | 1.276E+10 | 1.319E+10 | 1.385E+10 | 1.441E+10 |

PLANE NUMBER 15

	1	2	3	4	5	6	7	8	9	10	11
1	6.358E+13	6.359E+13	6.361E+13	6.404E+13	6.430E+13	6.458E+13	6.535E+13	6.598E+13	6.659E+13	6.690E+13	6.692E+13
2	6.223E+13	6.223E+13	6.226E+13	6.272E+13	6.304E+13	6.340E+13	6.456E+13	6.561E+13	6.663E+13	6.714E+13	6.716E+13
3	6.085E+13	6.085E+13	6.087E+13	6.130E+13	6.162E+13	6.202E+13	6.353E+13	6.498E+13	6.639E+13	6.709E+13	6.712E+13
4	5.961E+13	5.961E+13	5.962E+13	5.991E+13	6.014E+13	6.049E+13	6.221E+13	6.393E+13	6.564E+13	6.646E+13	6.649E+13
5	5.757E+13	5.757E+13	5.758E+13	5.769E+13	5.774E+13	5.802E+13	5.991E+13	6.186E+13	6.389E+13	6.481E+13	6.482E+13
6	5.042E+13	5.042E+13	5.042E+13	5.007E+13	4.978E+13	4.994E+13	5.229E+13	5.467E+13	5.739E+13	5.862E+13	5.857E+13
7	3.761E+13	3.762E+13	3.774E+13	3.782E+13	3.710E+13	3.713E+13	3.882E+13	4.042E+13	4.347E+13	4.470E+13	4.465E+13
8	3.223E+13	3.223E+13	3.217E+13	3.252E+13	3.204E+13	3.222E+13	3.365E+13	3.487E+13	3.712E+13	3.827E+13	3.835E+13
9	3.031E+13	3.030E+13	3.012E+13	3.057E+13	3.021E+13	3.042E+13	3.175E+13	3.289E+13	3.477E+13	3.588E+13	3.605E+13
10	2.923E+13	2.920E+13	2.891E+13	2.943E+13	2.919E+13	2.938E+13	3.065E+13	3.181E+13	3.341E+13	3.450E+13	3.476E+13
11	2.833E+13	2.830E+13	2.790E+13	2.847E+13	2.835E+13	2.850E+13	2.972E+13	3.093E+13	3.229E+13	3.336E+13	3.370E+13
12	2.718E+13	2.714E+13	2.662E+13	2.724E+13	2.727E+13	2.736E+13	2.852E+13	2.980E+13	3.085E+13	3.190E+13	3.233E+13
13	2.594E+13	2.579E+13	2.515E+13	2.582E+13	2.602E+13	2.604E+13	2.711E+13	2.853E+13	2.921E+13	3.023E+13	3.075E+13
14	2.434E+13	2.429E+13	2.361E+13	2.431E+13	2.460E+13	2.462E+13	2.565E+13	2.699E+13	2.750E+13	2.848E+13	2.900E+13
15	2.192E+13	2.187E+13	2.124E+13	2.194E+13	2.228E+13	2.235E+13	2.328E+13	2.451E+13	2.483E+13	2.572E+13	2.617E+13
16	5.123E+12	5.119E+12	5.073E+12	5.457E+12	5.799E+12	6.035E+12	6.381E+12	6.730E+12	6.620E+12	6.771E+12	6.796E+12
17	7.647E+11	7.647E+11	7.643E+11	8.765E+11	1.089E+12	1.079E+12	1.116E+12	1.125E+12	1.147E+12	1.188E+12	1.222E+12
18	2.501E+11	2.502E+11	2.504E+11	2.978E+11	5.139E+11	4.159E+11	4.421E+11	4.111E+11	4.496E+11	4.707E+11	5.235E+11
19	7.889E+09	7.892E+09	7.931E+09	9.628E+09	1.341E+10	1.249E+10	1.253E+10	1.244E+10	1.284E+10	1.353E+10	1.427E+10

PLANE NUMBER 16

	1	2	3	4	5	6	7	8	9	10	11
1	5.100E+13	5.099E+13	5.081E+13	5.110E+13	5.129E+13	5.151E+13	5.215E+13	5.286E+13	5.309E+13	5.327E+13	5.329E+13
2	5.013E+13	5.010E+13	4.969E+13	5.003E+13	5.027E+13	5.054E+13	5.146E+13	5.275E+13	5.305E+13	5.340E+13	5.342E+13
3	4.861E+13	4.861E+13	4.860E+13	4.896E+13	4.917E+13	4.945E+13	5.059E+13	5.175E+13	5.283E+13	5.336E+13	5.338E+13
4	4.813E+13	4.813E+13	4.814E+13	4.838E+13	4.819E+13	4.834E+13	4.963E+13	5.100E+13	5.259E+13	5.320E+13	5.311E+13
5	4.583E+13	4.583E+13	4.584E+13	4.592E+13	4.428E+13	4.419E+13	4.553E+13	4.703E+13	4.958E+13	5.022E+13	4.951E+13
6	4.001E+13	4.001E+13	4.003E+13	3.999E+13	3.815E+13	3.818E+13	3.986E+13	4.154E+13	4.464E+13	4.552E+13	4.466E+13
7	2.998E+13	2.998E+13	3.006E+13	3.041E+13	2.744E+13	2.762E+13	2.891E+13	2.968E+13	3.430E+13	3.519E+13	3.453E+13
8	2.591E+13	2.590E+13	2.586E+13	2.648E+13	2.432E+13	2.502E+13	2.624E+13	2.634E+13	2.957E+13	3.037E+13	3.001E+13
9	2.485E+13	2.484E+13	2.474E+13	2.544E+13	2.337E+13	2.459E+13	2.579E+13	2.533E+13	2.807E+13	2.884E+13	2.875E+13
10	2.388E+13	2.387E+13	2.371E+13	2.447E+13	2.262E+13	2.385E+13	2.502E+13	2.456E+13	2.695E+13	2.769E+13	2.767E+13
11	2.292E+13	2.290E+13	2.269E+13	2.350E+13	2.185E+13	2.306E+13	2.419E+13	2.376E+13	2.586E+13	2.657E+13	2.659E+13
12	2.190E+13	2.188E+13	2.162E+13	2.247E+13	2.106E+13	2.221E+13	2.331E+13	2.295E+13	2.474E+13	2.542E+13	2.547E+13
13	2.070E+13	2.068E+13	2.036E+13	2.125E+13	2.014E+13	2.121E+13	2.225E+13	2.201E+13	2.344E+13	2.409E+13	2.416E+13
14	1.949E+13	1.946E+13	1.912E+13	2.002E+13	1.921E+13	2.019E+13	2.119E+13	2.105E+13	2.215E+13	2.275E+13	2.283E+13
15	1.766E+13	1.763E+13	1.729E+13	1.820E+13	1.780E+13	1.866E+13	1.959E+13	1.958E+13	2.023E+13	2.077E+13	2.082E+13
16	4.430E+12	4.423E+12	4.402E+12	4.855E+12	5.314E+12	5.628E+12	5.987E+12	6.370E+12	6.078E+12	6.177E+12	6.171E+12
17	6.862E+11	6.862E+11	6.871E+11	8.160E+11	1.134E+12	1.077E+12	1.109E+12	1.100E+12	1.125E+12	1.166E+12	1.223E+12
18	2.259E+11	2.260E+11	2.266E+11	2.835E+11	7.143E+11	5.164E+11	5.178E+11	4.416E+11	5.177E+11	5.451E+11	6.611E+11
19	7.392E+09	7.395E+09	7.438E+09	9.231E+09	1.361E+10	1.232E+10	1.229E+10	1.216E+10	1.252E+10	1.323E+10	1.411E+10

PLANE NUMBER 17

	1	2	3	4	5	6	7	8	9	10	11
1	3.559E+13	3.559E+13	3.560E+13	3.593E+13	3.596E+13	3.611E+13	3.650E+13	3.681E+13	3.710E+13	3.724E+13	3.725E+13
2	3.474E+13	3.474E+13	3.475E+13	3.506E+13	3.523E+13	3.543E+13	3.601E+13	3.654E+13	3.702E+13	3.726E+13	3.727E+13
3	3.382E+13	3.392E+13	3.384E+13	3.421E+13	3.440E+13	3.463E+13	3.538E+13	3.609E+13	3.680E+13	3.713E+13	3.715E+13
4	3.288E+13	3.289E+13	3.291E+13	3.334E+13	3.345E+13	3.367E+13	3.455E+13	3.538E+13	3.634E+13	3.675E+13	3.675E+13
5	3.179E+13	3.180E+13	3.182E+13	3.234E+13	3.266E+13	3.291E+13	3.389E+13	3.476E+13	3.586E+13	3.633E+13	3.635E+13
6	2.784E+13	2.784E+13	2.788E+13	2.858E+13	2.902E+13	2.936E+13	3.057E+13	3.154E+13	3.309E+13	3.370E+13	3.374E+13
7	2.164E+13	2.164E+13	2.169E+13	2.272E+13	2.330E+13	2.376E+13	2.489E+13	2.514E+13	2.671E+13	2.730E+13	2.738E+13
8	1.882E+13	1.882E+13	1.884E+13	2.004E+13	2.116E+13	2.211E+13	2.325E+13	2.290E+13	2.343E+13	2.393E+13	2.414E+13
9	1.778E+13	1.778E+13	1.778E+13	1.903E+13	2.029E+13	2.131E+13	2.244E+13	2.202E+13	2.229E+13	2.275E+13	2.295E+13
10	1.703E+13	1.703E+13	1.701E+13	1.828E+13	1.965E+13	2.059E+13	2.170E+13	2.137E+13	2.150E+13	2.194E+13	2.208E+13
11	1.644E+13	1.644E+13	1.641E+13	1.770E+13	1.915E+13	2.004E+13	2.113E+13	2.087E+13	2.088E+13	2.129E+13	2.141E+13
12	1.576E+13	1.575E+13	1.571E+13	1.702E+13	1.857E+13	1.941E+13	2.047E+13	2.028E+13	2.014E+13	2.053E+13	2.062E+13
13	1.491E+13	1.491E+13	1.485E+13	1.616E+13	1.786E+13	1.863E+13	1.966E+13	1.956E+13	1.922E+13	1.957E+13	1.964E+13
14	1.406E+13	1.405E+13	1.399E+13	1.529E+13	1.716E+13	1.788E+13	1.887E+13	1.884E+13	1.827E+13	1.860E+13	1.863E+13
15	1.281E+13	1.290E+13	1.273E+13	1.399E+13	1.616E+13	1.679E+13	1.772E+13	1.782E+13	1.687E+13	1.716E+13	1.714E+13

	1	2	3	4	5	6	7	8	9	10	11
16	3.599E+12	3.599E+12	3.596E+12	4.141E+12	5.061E+12	5.329E+12	5.702E+12	6.210E+12	5.665E+12	5.722E+12	5.745E+12
17	5.905E+11	5.907E+11	5.931E+11	7.426E+11	1.158E+12	1.081E+12	1.109E+12	1.074E+12	1.109E+12	1.152E+12	1.229E+12
18	1.964E+11	1.964E+11	1.974E+11	2.659E+11	8.172E+11	6.092E+11	6.063E+11	4.920E+11	6.006E+11	6.350E+11	7.647E+11
19	6.777E+09	6.780E+09	6.827E+09	8.731E+09	1.392E+10	1.212E+10	1.203E+10	1.180E+10	1.217E+10	1.289E+10	1.391E+10

PLANE NUMBER 18

	1	2	3	4	5	6	7	8	9	10	11
1	2.197E+13	2.187E+13	2.188E+13	2.213E+13	2.225E+13	2.238E+13	2.270E+13	2.287E+13	2.304E+13	2.311E+13	2.312E+13
2	2.129E+13	2.128E+13	2.130E+13	2.178E+13	2.203E+13	2.227E+13	2.279E+13	2.301E+13	2.320E+13	2.330E+13	2.331E+13
3	2.065E+13	2.066E+13	2.070E+13	2.143E+13	2.183E+13	2.221E+13	2.293E+13	2.316E+13	2.334E+13	2.347E+13	2.343E+13
4	2.004E+13	2.005E+13	2.010E+13	2.112E+13	2.172E+13	2.232E+13	2.319E+13	2.337E+13	2.345E+13	2.362E+13	2.367E+13
5	1.933E+13	1.938E+13	1.944E+13	2.076E+13	2.186E+13	2.246E+13	2.343E+13	2.359E+13	2.356E+13	2.377E+13	2.386E+13
6	1.700E+13	1.701E+13	1.709E+13	1.894E+13	2.071E+13	2.156E+13	2.273E+13	2.281E+13	2.259E+13	2.285E+13	2.303E+13
7	1.353E+13	1.353E+13	1.363E+13	1.592E+13	1.906E+13	1.989E+13	2.103E+13	2.075E+13	1.918E+13	1.935E+13	1.961E+13
8	1.179E+13	1.180E+13	1.188E+13	1.411E+13	1.756E+13	1.863E+13	1.974E+13	1.923E+13	1.720E+13	1.731E+13	1.761E+13
9	1.113E+13	1.113E+13	1.121E+13	1.340E+13	1.690E+13	1.791E+13	1.839E+13	1.858E+13	1.650E+13	1.659E+13	1.683E+13
10	1.066E+13	1.067E+13	1.074E+13	1.289E+13	1.642E+13	1.730E+13	1.835E+13	1.810E+13	1.602E+13	1.609E+13	1.623E+13
11	1.031E+13	1.031E+13	1.037E+13	1.250E+13	1.604E+13	1.683E+13	1.787E+13	1.773E+13	1.563E+13	1.569E+13	1.584E+13
12	9.892E+12	9.896E+12	9.955E+12	1.203E+13	1.560E+13	1.631E+13	1.732E+13	1.729E+13	1.515E+13	1.521E+13	1.533E+13
13	9.379E+12	9.392E+12	9.436E+12	1.145E+13	1.506E+13	1.569E+13	1.666E+13	1.674E+13	1.455E+13	1.459E+13	1.469E+13
14	8.864E+12	8.868E+12	8.916E+12	1.086E+13	1.452E+13	1.507E+13	1.619E+13	1.619E+13	1.391E+13	1.394E+13	1.400E+13
15	8.111E+12	8.114E+12	8.156E+12	9.976E+12	1.374E+13	1.420E+13	1.508E+13	1.539E+13	1.294E+13	1.296E+13	1.290E+13
16	2.577E+12	2.579E+12	2.593E+12	3.227E+12	4.456E+12	4.655E+12	5.010E+12	5.608E+12	4.833E+12	4.945E+12	4.902E+12
17	4.576E+11	4.579E+11	4.617E+11	6.244E+11	1.111E+12	1.016E+12	9.578E+11	1.000E+12	1.042E+12	1.145E+12	
18	1.543E+11	1.544E+11	1.558E+11	2.286E+11	8.051E+11	5.916E+11	5.749E+11	3.362E+11	5.628E+11	5.977E+11	7.388E+11
19	5.783E+09	5.786E+09	5.836E+09	7.776E+09	1.311E+10	1.144E+10	1.130E+10	1.064E+10	1.135E+10	1.206E+10	1.314E+10

PLANE NUMBER 19

	1	2	3	4	5	6	7	8	9	10	11
1	1.494E+13	1.494E+13	1.495E+13	1.515E+13	1.525E+13	1.536E+13	1.560E+13	1.572E+13	1.583E+13	1.588E+13	1.588E+13
2	1.451E+13	1.451E+13	1.453E+13	1.493E+13	1.513E+13	1.531E+13	1.586E+13	1.597E+13	1.602E+13	1.602E+13	1.602E+13
3	1.406E+13	1.406E+13	1.410E+13	1.471E+13	1.502E+13	1.532E+13	1.590E+13	1.601E+13	1.608E+13	1.613E+13	1.613E+13
4	1.364E+13	1.364E+13	1.368E+13	1.450E+13	1.496E+13	1.539E+13	1.600E+13	1.614E+13	1.613E+13	1.619E+13	1.620E+13
5	1.318E+13	1.318E+13	1.323E+13	1.426E+13	1.492E+13	1.548E+13	1.629E+13	1.629E+13	1.617E+13	1.623E+13	1.627E+13
6	1.158E+13	1.159E+13	1.166E+13	1.322E+13	1.436E+13	1.527E+13	1.631E+13	1.612E+13	1.568E+13	1.575E+13	1.582E+13
7	9.316E+12	9.322E+12	9.408E+12	1.134E+13	1.353E+13	1.455E+13	1.561E+13	1.509E+13	1.367E+13	1.365E+13	1.376E+13
8	8.143E+12	8.148E+12	8.228E+12	1.012E+13	1.227E+13	1.345E+13	1.441E+13	1.399E+13	1.241E+13	1.238E+13	1.247E+13
9	7.694E+12	7.699E+12	7.776E+12	9.630E+12	1.183E+13	1.291E+13	1.387E+13	1.352E+13	1.192E+13	1.189E+13	1.196E+13
10	7.380E+12	7.395E+12	7.459E+12	9.278E+12	1.149E+13	1.255E+13	1.346E+13	1.317E+13	1.157E+13	1.152E+13	1.159E+13
11	7.127E+12	7.143E+12	7.214E+12	9.003E+12	1.122E+13	1.224E+13	1.313E+13	1.289E+13	1.128E+13	1.123E+13	1.130E+13
12	6.857E+12	6.862E+12	6.931E+12	8.680E+12	1.090E+13	1.187E+13	1.274E+13	1.255E+13	1.094E+13	1.089E+13	1.095E+13
13	6.511E+12	6.516E+12	6.581E+12	8.273E+12	1.049E+13	1.141E+13	1.223E+13	1.211E+13	1.053E+13	1.045E+13	1.050E+13
14	6.165E+12	6.169E+12	6.231E+12	7.856E+12	1.005E+13	1.091E+13	1.170E+13	1.164E+13	1.004E+13	9.989E+12	1.003E+13
15	5.657E+12	5.661E+12	5.718E+12	7.236E+12	9.371E+12	1.015E+13	1.088E+13	1.090E+13	9.339E+12	9.290E+12	9.329E+12
16	1.938E+12	1.940E+12	1.958E+12	2.519E+12	3.357E+12	3.609E+12	3.903E+12	4.261E+12	3.724E+12	3.720E+12	3.763E+12
17	3.629E+11	3.632E+11	3.672E+11	5.110E+11	8.552E+11	7.982E+11	8.164E+11	7.737E+11	7.985E+11	8.311E+11	9.045E+11
18	1.234E+11	1.235E+11	1.250E+11	1.842E+11	4.681E+11	3.629E+11	3.609E+11	2.807E+11	3.524E+11	3.733E+11	4.465E+11
19	4.914E+09	4.917E+09	4.965E+09	6.762E+09	1.132E+10	1.025E+10	1.012E+10	9.281E+09	1.013E+10	1.078E+10	1.170E+10

PLANE NUMBER 20

	1	2	3	4	5	6	7	8	9	10	11
1	7.351E+11	7.351E+11	7.355E+11	7.428E+11	7.466E+11	7.595E+11	7.597E+11	7.646E+11	7.691E+11	7.711E+11	7.712E+11
2	7.164E+11	7.164E+11	7.172E+11	7.310E+11	7.379E+11	7.448E+11	7.599E+11	7.657E+11	7.706E+11	7.725E+11	7.726E+11
3	6.968E+11	6.969E+11	6.980E+11	7.186E+11	7.286E+11	7.386E+11	7.595E+11	7.654E+11	7.702E+11	7.718E+11	7.719E+11
4	6.782E+11	6.791E+11	6.797E+11	7.063E+11	7.321E+11	7.574E+11	7.626E+11	7.663E+11	7.675E+11	7.675E+11	
5	6.580E+11	6.592E+11	6.599E+11	6.929E+11	7.090E+11	7.248E+11	7.546E+11	7.587E+11	7.609E+11	7.616E+11	7.616E+11
6	5.984E+11	5.996E+11	5.914E+11	6.440E+11	6.704E+11	6.959E+11	7.300E+11	7.368E+11	7.321E+11	7.307E+11	7.307E+11
7	4.897E+11	4.890E+11	4.925E+11	5.607E+11	5.988E+11	6.338E+11	6.818E+11	6.713E+11	6.534E+11	6.495E+11	6.495E+11
8	4.347E+11	4.309E+11	4.384E+11	5.081E+11	5.492E+11	5.857E+11	6.328E+11	6.210E+11	5.996E+11	5.951E+11	5.951E+11
9	4.138E+11	4.140E+11	4.175E+11	4.872E+11	5.290E+11	5.657E+11	6.121E+11	6.004E+11	5.778E+11	5.733E+11	5.733E+11
10	3.990E+11	3.993E+11	4.028E+11	4.720E+11	5.142E+11	5.503E+11	5.965E+11	5.849E+11	5.619E+11	5.573E+11	5.573E+11
11	3.876E+11	3.879E+11	3.913E+11	4.602E+11	5.025E+11	5.389E+11	5.841E+11	5.727E+11	5.493E+11	5.447E+11	5.447E+11
12	3.744E+11	3.746E+11	3.780E+11	4.461E+11	4.885E+11	5.246E+11	5.690E+11	5.579E+11	5.343E+11	5.298E+11	5.298E+11

	1	2	3	4	5	6	7	8	9	10	11
13	3.579E+11	3.582E+11	3.615E+11	4.284E+11	4.706E+11	5.062E+11	5.495E+11	5.389E+11	5.153E+11	5.108E+11	5.108E+11
14	3.413E+11	3.416E+11	3.448E+11	4.101E+11	4.518E+11	4.867E+11	5.287E+11	5.188E+11	4.954E+11	4.910E+11	4.910E+11
15	3.170E+11	3.172E+11	3.203E+11	3.829E+11	4.235E+11	4.570E+11	4.969E+11	4.882E+11	4.654E+11	4.613E+11	4.613E+11
16	1.360E+11	1.361E+11	1.378E+11	1.731E+11	1.983E+11	2.176E+11	2.394E+11	2.416E+11	2.302E+11	2.287E+11	2.290E+11
17	3.187E+10	3.190E+10	3.237E+10	4.343E+10	5.392E+10	5.810E+10	6.200E+10	6.098E+10	6.047E+10	6.162E+10	6.263E+10
18	1.126E+10	1.127E+10	1.144E+10	1.559E+10	2.073E+10	2.165E+10	2.287E+10	2.197E+10	2.234E+10	2.291E+10	2.363E+10
19	7.848E+08	7.856E+08	7.977E+08	1.117E+09	1.495E+09	1.564E+09	1.588E+09	1.521E+09	1.580E+09	1.663E+09	1.711E+09

GROUP 2 FLUX

PLANE NUMBER 1

	1	2	3	4	5	6	7	8	9	10	11
1	1.266E+11	1.266E+11	1.266E+11	1.268E+11	1.270E+11	1.271E+11	1.275E+11	1.279E+11	1.281E+11	1.286E+11	1.286E+11
2	1.244E+11	1.244E+11	1.244E+11	1.249E+11	1.251E+11	1.253E+11	1.259E+11	1.267E+11	1.275E+11	1.280E+11	1.280E+11
3	1.219E+11	1.219E+11	1.219E+11	1.226E+11	1.229E+11	1.232E+11	1.240E+11	1.252E+11	1.263E+11	1.272E+11	1.272E+11
4	1.191E+11	1.191E+11	1.191E+11	1.202E+11	1.206E+11	1.210E+11	1.218E+11	1.233E+11	1.247E+11	1.259E+11	1.260E+11
5	1.160E+11	1.160E+11	1.161E+11	1.176E+11	1.191E+11	1.195E+11	1.191E+11	1.211E+11	1.229E+11	1.243E+11	1.244E+11
6	1.047E+11	1.047E+11	1.049E+11	1.081E+11	1.089E+11	1.095E+11	1.097E+11	1.121E+11	1.148E+11	1.174E+11	1.175E+11
7	8.581E+10	8.583E+10	8.612E+10	8.875E+10	8.951E+10	9.018E+10	9.091E+10	9.325E+10	9.645E+10	9.968E+10	9.985E+10
8	7.533E+10	7.516E+10	7.577E+10	7.805E+10	7.866E+10	7.939E+10	8.016E+10	8.205E+10	8.543E+10	8.854E+10	8.861E+10
9	7.121E+10	7.123E+10	7.181E+10	7.395E+10	7.449E+10	7.526E+10	7.602E+10	7.771E+10	8.115E+10	8.419E+10	8.422E+10
10	6.901E+10	6.882E+10	6.904E+10	7.109E+10	7.156E+10	7.234E+10	7.311E+10	7.467E+10	7.816E+10	8.112E+10	8.110E+10
11	6.751E+10	6.754E+10	6.691E+10	6.889E+10	6.931E+10	7.017E+10	7.090E+10	7.233E+10	7.584E+10	7.875E+10	7.870E+10
12	6.597E+10	6.608E+10	6.545E+10	6.740E+10	6.675E+10	6.867E+10	6.937E+10	6.965E+10	7.426E+10	7.713E+10	7.594E+10
13	6.303E+10	6.301E+10	6.259E+10	6.440E+10	6.335E+10	6.560E+10	6.634E+10	6.607E+10	7. 10	7.372E+10	7.219E+10
14	5.903E+10	5.901E+10	5.870E+10	6.035E+10	5.992E+10	6.147E+10	6.221E+10	6.241E+10	6.665E+10	6.923E+10	6.824E+10
15	5.344E+10	5.342E+10	5.322E+10	5.470E+10	5.445E+10	5.571E+10	5.702E+10	6.048E+10	6.236E+10	6.238E+10	
16	1.611E+10	1.611E+10	1.612E+10	1.660E+10	1.676E+10	1.693E+10	1.720E+10	1.774E+10	1.855E+10	1.936E+10	1.939E+10
17	1.987E+09	1.987E+09	1.989E+09	2.048E+09	2.069E+09	2.090E+09	2.127E+09	2.202E+09	2.302E+09	2.405E+09	2.411E+09
18	1.766E+09	1.766E+09	1.768E+09	1.822E+09	1.841E+09	1.860E+09	1.895E+09	1.965E+09	2.053E+09	2.146E+09	2.151E+09
19	6.983E+08	6.983E+08	6.994E+08	7.205E+08	7.300E+08	7.394E+08	7.600E+08	7.910E+08	8.250E+08	8.583E+08	8.602E+08

PLANE NUMBER 2

	1	2	3	4	5	6	7	8	9	10	11
1	5.239E+12	5.238E+12	5.236E+12	5.211E+12	5.194E+12	5.174E+12	5.147E+12	5.151E+12	5.156E+12	5.163E+12	5.163E+12
2	5.153E+12	5.153E+12	5.153E+12	5.138E+12	5.115E+12	5.086E+12	5.063E+12	5.088E+12	5.116E+12	5.141E+12	5.142E+12
3	5.038E+12	5.038E+12	5.039E+12	5.045E+12	5.014E+12	4.993E+12	4.976E+12	5.021E+12	5.070E+12	5.115E+12	5.118E+12
4	4.895E+12	4.895E+12	4.806E+12	4.938E+12	4.933E+12	4.924E+12	4.898E+12	4.960E+12	5.023E+12	5.089E+12	5.093E+12
5	4.720E+12	4.720E+12	4.716E+12	4.794E+12	4.824E+12	4.835E+12	4.794E+12	4.876E+12	4.946E+12	5.033E+12	5.038E+12
6	4.205E+12	4.207E+12	4.229E+12	4.584E+12	4.627E+12	4.639E+12	4.426E+12	4.519E+12	4.647E+12	4.808E+12	4.818E+12
7	3.330E+12	3.334E+12	3.393E+12	3.589E+12	3.613E+12	3.650E+12	3.605E+12	3.687E+12	3.849E+12	4.039E+12	4.053E+12
8	2.783E+12	2.792E+12	2.915E+12	3.082E+12	3.140E+12	3.140E+12	3.115E+12	3.215E+12	3.341E+12	3.523E+12	3.554E+12
9	2.543E+12	2.555E+12	2.731E+12	2.890E+12	2.960E+12	2.946E+12	2.925E+12	3.031E+12	3.143E+12	3.320E+12	3.365E+12
10	2.397E+12	2.395E+12	2.580E+12	2.730E+12	2.816E+12	2.785E+12	2.766E+12	2.898E+12	2.976E+12	3.147E+12	3.207E+12
11	2.320E+12	2.321E+12	2.454E+12	2.597E+12	2.711E+12	2.650E+12	2.634E+12	2.801E+12	2.835E+12	3.000E+12	3.093E+12
12	2.249E+12	2.258E+12	2.344E+12	2.480E+12	2.605E+12	2.531E+12	2.517E+12	2.702E+12	2.710E+12	2.869E+12	2.976E+12
13	2.216E+12	2.221E+12	2.274E+12	2.403E+12	2.502E+12	2.452E+12	2.442E+12	2.600E+12	2.631E+12	2.785E+12	2.866E+12
14	2.119E+12	2.142E+12	2.187E+12	2.308E+12	2.384E+12	2.355E+12	2.349E+12	2.480E+12	2.531E+12	2.678E+12	2.736E+12
15	1.992E+12	1.995E+12	2.029E+12	2.137E+12	2.190E+12	2.180E+12	2.178E+12	2.283E+12	2.349E+12	2.485E+12	2.520E+12
16	7.272E+11	7.275E+11	7.308E+11	7.583E+11	7.694E+11	7.750E+11	7.848E+11	8.142E+11	8.500E+11	8.924E+11	8.957E+11
17	7.564E+10	7.565E+10	7.582E+10	7.838E+10	7.930E+10	8.011E+10	8.156E+10	8.464E+10	8.856E+10	9.281E+10	9.308E+10
18	4.267E+10	4.267E+10	4.275E+10	4.413E+10	4.465E+10	4.511E+10	4.598E+10	4.774E+10	4.997E+10	5.235E+10	5.249E+10
19	4.513E+09	4.514E+09	4.521E+09	4.664E+09	4.728E+09	4.790E+09	4.923E+09	5.124E+09	5.350E+09	5.574E+09	5.587E+09

PLANE NUMBER 3

	1	2	3	4	5	6	7	8	9	10	11
1	1.342E+13	1.342E+13	1.342E+13	1.351E+13	1.355E+13	1.374E+13	1.421E+13	1.448E+13	1.472E+13	1.485E+13	1.486E+13
2	1.313E+13	1.313E+13	1.314E+13	1.325E+13	1.333E+13	1.349E+13	1.383E+13	1.409E+13	1.440E+13	1.463E+13	1.464E+13
3	1.278E+13	1.278E+13	1.285E+13	1.296E+13	1.301E+13	1.308E+13	1.323E+13	1.342E+13	1.387E+13	1.424E+13	1.426E+13
4	1.213E+13	1.216E+13	1.253E+13	1.267E+13	1.254E+13	1.250E+13	1.250E+13	1.227E+13	1.317E+13	1.370E+13	1.373E+13
5	1.128E+13	1.131E+13	1.252E+13	1.285E+13	1.205E+13	1.284E+13	1.274E+13	1.169E+13	1.353E+13	1.427E+13	1.431E+13

	1	2	3	4	5	6	7	8	9	10	11
6	9.368E+12	9.443E+12	1.205E+13	1.286E+13	1.291E+13	1.294E+13	1.270E+13	1.020E+13	1.390E+13	1.507E+13	1.514E+13
7	6.996E+12	7.074E+12	9.814E+12	1.085E+13	1.102E+13	1.103E+13	1.051E+13	7.817E+12	1.145E+13	1.260E+13	1.270E+13
8	6.646E+12	6.697E+12	8.294E+12	9.077E+12	9.470E+12	9.277E+12	8.960E+12	7.580E+12	9.764E+12	1.066E+13	1.098E+13
9	6.685E+12	6.821E+12	7.945E+12	9.676E+12	9.175E+12	9.881E+12	8.606E+12	7.704E+12	9.390E+12	1.022E+13	1.064E+13
10	6.721E+12	6.864E+12	7.845E+12	8.552E+12	9.059E+12	8.758E+12	8.502E+12	8.009E+12	9.267E+12	1.008E+13	1.051E+13
11	6.843E+12	6.984E+12	7.763E+12	8.451E+12	8.770E+12	8.657E+12	8.415E+12	8.228E+12	9.173E+12	9.964E+12	1.021E+13
12	6.738E+12	6.808E+12	7.620E+12	8.280E+12	8.353E+12	8.482E+12	8.261E+12	8.201E+12	9.004E+12	9.767E+12	9.769E+12
13	6.778E+12	6.789E+12	7.473E+12	8.048E+12	8.086E+12	8.238E+12	8.093E+12	8.105E+12	8.817E+12	9.315E+12	9.452E+12
14	6.776E+12	6.802E+12	7.203E+12	7.733E+12	7.999E+12	7.914E+12	7.809E+12	8.056E+12	8.502E+12	9.147E+12	9.349E+12
15	6.628E+12	6.650E+12	6.958E+12	7.449E+12	7.660E+12	7.623E+12	7.540E+12	7.780E+12	8.208E+12	8.815E+12	8.960E+12
16	3.163E+12	3.165E+12	3.190E+12	3.328E+12	3.374E+12	3.405E+12	3.447E+12	3.578E+12	3.747E+12	3.947E+12	3.963E+12
17	7.273E+11	7.279E+11	7.304E+11	7.562E+11	7.693E+11	7.742E+11	7.900E+11	8.216E+11	8.591E+11	8.996E+11	9.021E+11
18	2.627E+11	2.628E+11	2.634E+11	2.724E+11	2.750E+11	2.788E+11	2.846E+11	2.959E+11	3.097E+11	3.244E+11	3.253E+11
19	9.393E+09	9.390E+09	9.406E+09	9.710E+09	9.850E+09	9.983E+09	1.027E+10	1.069E+10	1.117E+10	1.164E+10	1.166E+10

PLANE NUMBER 4

	1	2	3	4	5	6	7	8	9	10	11
1	2.259E+13	2.259E+13	2.261E+13	2.282E+13	2.295E+13	2.346E+13	2.472E+13	2.538E+13	2.599E+13	2.628E+13	2.630E+13
2	2.206E+13	2.206E+13	2.209E+13	2.235E+13	2.256E+13	2.309E+13	2.416E+13	2.483E+13	2.554E+13	2.602E+13	2.605E+13
3	2.148E+13	2.149E+13	2.160E+13	2.184E+13	2.205E+13	2.243E+13	2.319E+13	2.370E+13	2.468E+13	2.541E+13	2.545E+13
4	2.047E+13	2.051E+13	2.114E+13	2.137E+13	2.125E+13	2.134E+13	2.186E+13	2.162E+13	2.343E+13	2.444E+13	2.450E+13
5	1.915E+13	1.921E+13	2.138E+13	2.167E+13	2.172E+13	2.182E+13	2.235E+13	2.060E+13	2.415E+13	2.555E+13	2.562E+13
6	1.609E+13	1.622E+13	2.089E+13	2.130E+13	2.139E+13	2.149E+13	2.231E+13	1.793E+13	2.475E+13	2.710E+13	2.723E+13
7	1.197E+13	1.211E+13	1.705E+13	1.856E+13	1.893E+13	1.893E+13	1.844E+13	1.361E+13	2.036E+13	2.243E+13	2.263E+13
8	1.131E+13	1.140E+13	1.418E+13	1.539E+13	1.611E+13	1.578E+13	1.545E+13	1.312E+13	1.701E+13	1.860E+13	1.919E+13
9	1.137E+13	1.159E+13	1.349E+13	1.464E+13	1.555E+13	1.503E+13	1.474E+13	1.333E+13	1.621E+13	1.767E+13	1.847E+13
10	1.143E+13	1.167E+13	1.331E+13	1.443E+13	1.540E+13	1.482E+13	1.455E+13	1.389E+13	1.601E+13	1.742E+13	1.829E+13
11	1.165E+13	1.187E+13	1.317E+13	1.426E+13	1.494E+13	1.465E+13	1.440E+13	1.428E+13	1.___E+13	1.722E+13	1.777E+13
12	1.143E+13	1.155E+13	1.295E+13	1.399E+13	1.422E+13	1.437E+13	1.416E+13	1.419E+13	1.557E+13	1.690E+13	1.694E+13
13	1.149E+13	1.151E+13	1.277E+13	1.368E+13	1.368E+13	1.405E+13	1.395E+13	1.39_E+13	1.533E+13	1.653E+13	1.629E+13
14	1.199E+13	1.153E+13	1.228E+13	1.312E+13	1.353E+13	1.345E+13	1.342E+13	1.384E+13	1.473E+13	1.582E+13	1.611E+13
15	1.128E+13	1.133E+13	1.189E+13	1.267E+13	1.301E+13	1.300E+13	1.294E+13	1.342E+13	1.425E+13	1.529E+13	1.550E+13
16	5.474E+12	5.477E+12	5.520E+12	5.741E+12	5.825E+12	5.887E+12	6.005E+12	6.247E+12	6.557E+12	6.893E+12	6.919E+12
17	1.226E+12	1.227E+12	1.231E+12	1.271E+12	1.288E+12	1.304E+12	1.339E+12	1.395E+12	1.460E+12	1.525E+12	1.529E+12
18	4.511E+11	4.512E+11	4.522E+11	4.665E+11	4.726E+11	4.784E+11	4.910E+11	5.118E+11	5.362E+11	5.605E+11	5.620E+11
19	1.467E+10	1.467E+10	1.469E+10	1.518E+10	1.543E+10	1.566E+10	1.617E+10	1.684E+10	1.759E+10	1.830E+10	1.835E+10

PLANE NUMBER 5

	1	2	3	4	5	6	7	8	9	10	11
1	3.057E+13	3.057E+13	3.059E+13	3.090E+13	3.108E+13	3.182E+13	3.365E+13	3.461E+13	3.549E+13	3.592E+13	3.595E+13
2	2.984E+13	2.984E+13	2.988E+13	3.025E+13	3.054E+13	3.132E+13	3.293E+13	3.390E+13	3.493E+13	3.560E+13	3.564E+13
3	2.904E+13	2.905E+13	2.920E+13	2.952E+13	2.994E+13	3.042E+13	3.160E+13	3.238E+13	3.377E+13	3.479E+13	3.485E+13
4	2.767E+13	2.773E+13	2.857E+13	2.886E+13	2.871E+13	2.887E+13	2.978E+13	2.953E+13	3.206E+13	3.345E+13	3.352E+13
5	2.589E+13	2.597E+13	2.890E+13	2.917E+13	2.925E+13	2.942E+13	3.040E+13	2.814E+13	3.304E+13	3.494E+13	3.505E+13
6	2.174E+13	2.192E+13	2.821E+13	2.848E+13	2.861E+13	2.876E+13	3.031E+13	2.448E+13	3.392E+13	3.697E+13	3.715E+13
7	1.616E+13	1.635E+13	2.295E+13	2.486E+13	2.529E+13	2.539E+13	2.499E+13	1.8_5E13	2.769E+13	3.042E+13	3.068E+13
8	1.521E+13	1.533E+13	1.900E+13	2.052E+13	2.150E+13	2.107E+13	2.082E+13	1._2E.13	2.299E+13	2.5_	2.585E+13
9	1.526E+13	1.556E+13	1.804E+13	1.948E+13	2.073E+13	2.00_E+_	.982E+13	1.807E+13	2.187E+13	2.375E+13	2.485E+13
10	1.534E+13	1.565E+13	1.780E+13	1.919E+13	2.0_4E+13	1.975E+13	1.956E+13	1.882E+13	2.159E+13	2.340E+13	2.461E+13
11	1.562E+13	1.590E+13	1.762E+13	1.897E+13	1.993E+13	1.953E+13	1.936E+13	1.932E+13	2.136E+13	2.313E+13	2.390E+13
12	1.531E+13	1.547E+13	1.731E+13	1.862E+13	1.893E+13	1.916E+13	1.903E+13	1.914E+13	2.099E+13	2.269E+13	2.274E+13
13	1.537E+13	1.540E+13	1.709E+13	1.822E+13	1.819E+13	1.873E+13	1.876E+13	1.875E+13	2.066E+13	2.220E+13	2.192E+13
14	1.536E+13	1.543E+13	1.640E+13	1.743E+13	1.799E+13	1.792E+13	1.801E+13	1.863E+13	1.981E+13	2.120E+13	2.157E+13
15	1.509E+13	1.514E+13	1.587E+13	1.683E+13	1.728E+13	1.730E+13	1.749E+13	1.804E+13	1.916E+13	2.047E+13	2.074E+13
16	7.178E+12	7.182E+12	7.234E+12	7.501E+12	7.611E+12	7.702E+12	7.900E+12	8.230E+12	8.639E+12	9.055E+12	9.087E+12
17	1.576E+12	1.577E+12	1.581E+12	1.630E+12	1.652E+12	1.674E+12	1.726E+12	1.800E+12	1.884E+12	1.964E+12	1.969E+12
18	5.809E+11	5.810E+11	5.820E+11	5.993E+11	6.074E+11	6.154E+11	6.349E+11	6.619E+11	6.933E+11	7.229E+11	7.248E+11
19	1.803E+10	1.803E+10	1.805E+10	1.867E+10	1.901E+10	1.933E+10	2.000E+10	2.083E+10	2.175E+10	2.260E+10	2.266E+10

PLANE NUMBER 6

	1	2	3	4	5	6	7	8	9	10	11
1	4.237E+13	4.237E+13	4.240E+13	4.280E+13	4.304E+13	4.403E+13	4.650E+13	4.783E+13	4.905E+13	4.965E+13	4.969E+13
2	4.141E+13	4.141E+13	4.146E+13	4.192E+13	4.231E+13	4.333E+13	4.561E+13	4.701E+13	4.849E+13	4.942E+13	4.947E+13

	1	2	3	4	5	6	7	8	9	10	11
3	4.035E+13	4.036E+13	4.056E+13	4.093E+13	4.133E+13	4.210E+13	4.397E+13	4.516E+13	4.716E+13	4.853E+13	4.861E+13
4	3.849E+13	3.857E+13	3.973E+13	3.999E+13	3.977E+13	4.001E+13	4.169E+13	4.150E+13	4.507E+13	4.692E+13	4.702E+13
5	3.602E+13	3.613E+13	4.023E+13	4.023E+13	4.035E+13	4.065E+13	4.273E+13	3.964E+13	4.663E+13	4.917E+13	4.931E+13
6	3.035E+13	3.058E+13	3.919E+13	3.882E+13	3.900E+13	3.923E+13	4.249E+13	3.466E+13	4.768E+13	5.180E+13	5.203E+13
7	2.279E+13	2.302E+13	3.176E+13	3.395E+13	3.454E+13	3.474E+13	3.481E+13	2.654E+13	3.868E+13	4.210E+13	4.244E+13
8	2.126E+13	2.139E+13	2.586E+13	2.761E+13	2.896E+13	2.841E+13	2.851E+13	2.527E+13	3.154E+13	3.403E+13	3.514E+13
9	2.121E+13	2.156E+13	2.451E+13	2.616E+13	2.789E+13	2.696E+13	2.707E+13	2.547E+13	2.991E+13	3.217E+13	3.370E+13
10	2.125E+13	2.160E+13	2.418E+13	2.578E+13	2.766E+13	2.658E+13	2.672E+13	2.635E+13	2.952E+13	3.170E+13	3.339E+13
11	2.152E+13	2.183E+13	2.393E+13	2.549E+13	2.686E+13	2.629E+13	2.644E+13	2.684E+13	2.921E+13	3.133E+13	3.243E+13
12	2.099E+13	2.119E+13	2.352E+13	2.501E+13	2.548E+13	2.580E+13	2.599E+13	2.639E+13	2.870E+13	3.074E+13	3.081E+13
13	2.104E+13	2.107E+13	2.321E+13	2.450E+13	2.440E+13	2.524E+13	2.560E+13	2.574E+13	2.824E+13	3.008E+13	2.947E+13
14	2.101E+13	2.109E+13	2.221E+13	2.339E+13	2.412E+13	2.408E+13	2.450E+13	2.554E+13	2.699E+13	2.865E+13	2.913E+13
15	2.057E+13	2.063E+13	2.147E+13	2.256E+13	2.316E+13	2.323E+13	2.367E+13	2.468E+13	2.606E+13	2.762E+13	2.797E+13
16	9.397E+12	9.401E+12	9.453E+12	9.759E+12	9.907E+12	1.003E+13	1.036E+13	1.082E+13	1.134E+13	1.183E+13	1.187E+13
17	2.007E+12	2.007E+12	2.011E+12	2.069E+12	2.098E+12	2.128E+12	2.205E+12	2.301E+12	2.406E+12	2.501E+12	2.507E+12
18	7.397E+11	7.397E+11	7.406E+11	7.610E+11	7.717E+11	7.826E+11	8.113E+11	8.467E+11	8.860E+11	9.211E+11	9.233E+11
19	2.185E+10	2.185E+10	2.188E+10	2.267E+10	2.317E+10	2.360E+10	2.448E+10	2.548E+10	2.658E+10	2.759E+10	2.766E+10

PLANE NUMBER 7

	1	2	3	4	5	6	7	8	9	10	11
1	5.994E+13	5.994E+13	5.998E+13	6.069E+13	6.111E+13	6.287E+13	6.736E+13	6.972E+13	7.189E+13	7.288E+13	7.294E+13
2	5.906E+13	5.906E+13	5.912E+13	5.988E+13	6.050E+13	6.272E+13	6.760E+13	7.021E+13	7.272E+13	7.402E+13	7.410E+13
3	5.833E+13	5.834E+13	5.850E+13	5.909E+13	6.013E+13	6.223E+13	6.705E+13	6.967E+13	7.272E+13	7.441E+13	7.450E+13
4	5.767E+13	5.772E+13	5.841E+13	5.868E+13	5.939E+13	6.063E+13	6.570E+13	6.752E+13	7.172E+13	7.375E+13	7.386E+13
5	5.639E+13	5.642E+13	5.834E+13	5.663E+13	5.720E+13	5.826E+13	6.521E+13	6.605E+13	7.170E+13	7.416E+13	7.430E+13
6	5.127E+13	5.133E+13	5.518E+13	5.151E+13	5.178E+13	5.227E+13	6.102E+13	6.025E+13	6.871E+13	7.217E+13	7.237E+13
7	4.202E+13	4.205E+13	4.555E+13	4.555E+13	4.630E+13	4.677E+13	4.934E+13	5.008E+13	5.743E+13	5.779E+13	
8	3.766E+13	3.763E+13	3.598E+13	3.701E+13	3.874E+13	3.815E+13	3.986E+13	4.618E+13	4.333E+13	4.599E+13	4.743E+13
9	3.610E+13	3.595E+13	3.397E+13	3.501E+13	3.724E+13	3.614E+13	3.763E+13	4.495E+13	4.147E+13	4.332E+13	4.533E+13
10	3.496E+13	3.456E+13	3.345E+13	3.446E+13	3.690E+13	3.559E+13	3.704E+13	4.369E+13	4.082E+13	4.262E+13	4.484E+13
11	3.297E+13	3.268E+13	3.303E+13	3.403E+13	3.568E+13	3.515E+13	3.659E+13	4.117E+13	4.031E+13	4.207E+13	4.334E+13
12	3.033E+13	3.060E+13	3.234E+13	3.330E+13	3.355E+13	3.440E+13	3.580E+13	3.796E+13	3.944E+13	4.115E+13	4.078E+13
13	2.995E+13	2.997E+13	3.149E+13	3.236E+13	3.198E+13	3.328E+13	3.481E+13	3.576E+13	3.831E+13	3.991E+13	3.867E+13
14	2.965E+13	2.966E+13	2.979E+13	3.062E+13	3.149E+13	3.157E+13	3.293E+13	3.527E+13	3.616E+13	3.765E+13	3.816E+13
15	2.853E+13	2.853E+13	2.861E+13	2.941E+13	3.012E+13	3.032E+13	3.159E+13	3.368E+13	3.471E+13	3.613E+13	3.649E+13
16	1.159E+13	1.159E+13	1.159E+13	1.188E+13	1.206E+13	1.223E+13	1.274E+13	1.335E+13	1.392E+13	1.443E+13	1.447E+13
17	2.361E+12	2.362E+12	2.363E+12	2.426E+12	2.463E+12	2.501E+12	2.606E+12	2.722E+12	2.838E+12	2.937E+12	2.944E+12
18	8.682E+11	8.683E+11	8.684E+11	8.910E+11	9.049E+11	9.193E+11	9.574E+11	9.999E+11	1.043E+12	1.080E+12	1.083E+12
19	2.438E+10	2.438E+10	2.441E+10	2.548E+10	2.629E+10	2.687E+10	2.791E+10	2.896E+10	3.019E+10	3.129E+10	3.139E+10

PLANE NUMBER 8

	1	2	3	4	5	6	7	8	9	10	11
1	6.766E+13	6.766E+13	6.770E+13	6.852E+13	6.902E+13	7.107E+13	7.631E+13	7.906E+13	8.157E+13	8.272E+13	8.278E+13
2	6.664E+13	6.664E+13	6.671E+13	6.757E+13	6.831E+13	7.090E+13	7.661E+13	7.963E+13	8.253E+13	8.401E+13	8.409E+13
3	6.579E+13	6.580E+13	6.599E+13	6.662E+13	6.793E+13	7.028E+13	7.595E+13	7.898E+13	8.247E+13	8.436E+13	8.447E+13
4	6.499E+13	6.504E+13	6.582E+13	6.606E+13	6.684E+13	6.827E+13	7.425E+13	7.634E+13	8.115E+13	8.341E+13	8.353E+13
5	6.358E+13	6.362E+13	6.596E+13	6.377E+13	6.441E+13	6.565E+13	7.395E+13	7.468E+13	8.139E+13	8.409E+13	8.424E+13
6	5.824E+13	5.840E+13	6.282E+13	5.778E+13	5.808E+13	5.866E+13	6.953E+13	6.834E+13	7.835E+13	8.200E+13	8.221E+13
7	4.904E+13	4.908E+13	5.197E+13	5.245E+13	5.317E+13	5.366E+13	5.743E+13	5.751E+13	6.361E+13	6.640E+13	6.668E+13
8	4.551E+13	4.547E+13	4.341E+13	4.404E+13	4.536E+13	4.539E+13	4.788E+13	5.346E+13	5.277E+13	5.475E+13	5.570E+13
9	4.447E+13	4.428E+13	4.152E+13	4.217E+13	4.378E+13	4.351E+13	4.577E+13	5.223E+13	5.038E+13	5.218E+13	5.347E+13
10	4.341E+13	4.290E+13	4.117E+13	4.182E+13	4.331E+13	4.316E+13	4.537E+13	5.089E+13	4.995E+13	5.170E+13	5.290E+13
11	4.101E+13	4.094E+13	4.094E+13	4.159E+13	4.169E+13	4.293E+13	4.512E+13	4.792E+13	4.967E+13	5.140E+13	5.090E+13
12	3.750E+13	3.761E+13	4.006E+13	4.068E+13	3.863E+13	4.197E+13	4.415E+13	4.376E+13	4.857E+13	5.025E+13	4.705E+13
13	3.512E+13	3.513E+13	3.699E+13	3.759E+13	3.633E+13	3.875E+13	4.075E+13	4.092E+13	4.477E+13	4.631E+13	4.409E+13
14	3.462E+13	3.461E+13	3.441E+13	3.504E+13	3.581E+13	3.611E+13	3.790E+13	4.031E+13	4.159E+13	4.303E+13	4.344E+13
15	3.299E+13	3.298E+13	3.282E+13	3.344E+13	3.412E+13	3.445E+13	3.615E+13	3.835E+13	3.965E+13	4.103E+13	4.134E+13
16	1.261E+13	1.261E+13	1.260E+13	1.289E+13	1.309E+13	1.327E+13	1.387E+13	1.454E+13	1.513E+13	1.563E+13	1.567E+13
17	2.512E+12	2.512E+12	2.512E+12	2.580E+12	2.625E+12	2.668E+12	2.795E+12	2.909E+12	3.028E+12	3.127E+12	3.134E+12
18	9.217E+11	9.216E+11	9.216E+11	9.465E+11	9.631E+11	9.790E+11	1.022E+12	1.067E+12	1.112E+12	1.149E+12	1.151E+12
19	2.531E+10	2.532E+10	2.535E+10	2.667E+10	2.780E+10	2.849E+10	2.959E+10	3.060E+10	3.188E+10	3.305E+10	3.318E+10

PLANE NUMBER 9

	1	2	3	4	5	6	7	8	9	10	11
11	8.385E+11	8.388E+11	8.435E+11	9.337E+11	9.827E+11	1.027E+12	1.002E+12	1.090E+12	1.079E+12	1.072E+12	1.077E+12
12	8.130E+11	8.143E+11	8.189E+11	9.092E+11	9.587E+11	1.003E+12	1.067E+12	1.066E+12	1.054E+12	1.052E+12	1.052E+12
13	7.832E+11	7.835E+11	7.881E+11	8.783E+11	9.281E+11	9.726E+11	1.036E+12	1.035E+12	1.022E+12	1.020E+12	1.020E+12
14	7.519E+11	7.522E+11	7.568E+11	8.462E+11	8.962E+11	9.404E+11	1.003E+12	1.002E+12	9.884E+11	9.868E+11	9.868E+11
15	7.055E+11	7.058E+11	7.103E+11	7.982E+11	8.480E+11	8.916E+11	9.526E+11	9.520E+11	9.382E+11	9.365E+11	9.366E+11
16	3.548E+11	3.550E+11	3.583E+11	4.252E+11	4.669E+11	5.016E+11	5.459E+11	5.522E+11	5.418E+11	5.410E+11	5.413E+11
17	9.808E+10	9.817E+10	9.938E+10	1.269E+11	1.497E+11	1.606E+11	1.711E+11	1.697E+11	1.706E+11	1.738E+11	1.756E+11
18	3.413E+10	3.416E+10	3.460E+10	4.511E+10	5.646E+10	5.943E+10	6.292E+10	6.120E+10	6.244E+10	6.389E+10	6.526E+10
19	1.994E+09	1.996E+09	2.025E+09	2.781E+09	3.699E+09	4.037E+09	4.139E+09	3.871E+09	4.159E+09	4.373E+09	4.477E+09

GROUP 3 FLUX

PLANE NUMBER 1

	1	2	3	4	5	6	7	8	9	10	11
1	1.135E+12	1.135E+12	1.135E+12	1.139E+12	1.140E+12	1.142E+12	1.148E+12	1.152E+12	1.156E+12	1.158E+12	1.158E+12
2	1.114E+12	1.114E+12	1.114E+12	1.120E+12	1.123E+12	1.125E+12	1.133E+12	1.140E+12	1.147E+12	1.151E+12	1.151E+12
3	1.090E+12	1.090E+12	1.091E+12	1.099E+12	1.102E+12	1.106E+12	1.115E+12	1.124E+12	1.134E+12	1.141E+12	1.141E+12
4	1.064E+12	1.064E+12	1.065E+12	1.075E+12	1.080E+12	1.084E+12	1.095E+12	1.105E+12	1.117E+12	1.126E+12	1.126E+12
5	1.035E+12	1.035E+12	1.036E+12	1.049E+12	1.054E+12	1.058E+12	1.068E+12	1.082E+12	1.096E+12	1.108E+12	1.109E+12
6	9.199E+11	9.201E+11	9.231E+11	9.459E+11	9.532E+11	9.594E+11	9.659E+11	9.873E+11	1.006E+12	1.026E+12	1.028E+12
7	6.574E+11	6.590E+11	6.815E+11	7.092E+11	7.267E+11	7.209E+11	7.248E+11	7.694E+11	7.646E+11	7.906E+11	8.017E+11
8	3.306E+11	3.376E+11	4.362E+11	4.633E+11	5.396E+11	4.712E+11	4.693E+11	6.048E+11	4.971E+11	5.205E+11	5.911E+11
9	1.477E+11	1.575E+11	3.130E+11	3.364E+11	4.644E+11	2.422E+11	3.389E+11	5.404E+11	3.594E+11	3.793E+11	5.041E+11
10	3.065E+06	4.167E+06	1.997E+11	2.164E+11	4.129E+11	2.202E+11	2.170E+11	2.110E+11	2.303E+11	2.445E+11	4.429E+11
11	9.003E+09	1.206E+06	9.950E+10	1.088E+11	3.757E+11	1.107E+11	7.084E+11	4.645E+11	1.???E+11	1.232E+11	3.983E+11
12	1.415E+06	1.262E+06	2.945E+06	3.321E+06	3.415E+11	3.378E+06	3.241E+06	4.323E+11	3.451E+06	3.808E+06	3.559E+11
13	9.930E+10	9.930E+10	9.930E+10	1.083E+11	3.399E+11	1.103E+11	1.078E+11	4.247E+11	1.153E+11	1.245E+11	3.619E+11
14	1.761E+11	1.761E+11	1.764E+11	1.903E+11	3.447E+11	1.??9E+11	1.909E+11	4.20?E+11	2.044E+11	2.189E+11	3.731E+11
15	2.452E+11	2.453E+11	2.459E+11	2.629E+11	3.485E+11	1.680E+11	2.657E+11	4.105E+11	2.845E+11	3.026E+11	3.842E+11
16	1.949E+11	1.949E+11	1.957E+11	2.030E+11	2.073E+11	2.077E+11	2.114E+11	2.225E+11	2.273E+11	2.365E+11	2.387E+11
17	4.781E+10	4.782E+10	4.796E+10	4.960E+10	5.029E+10	5.069E+10	5.223E+10	5.411E+10	5.602E+10	5.787E+10	5.801E+10
18	1.247E+11	1.248E+11	1.250E+11	1.294E+11	1.315E+11		1.383E+11	1.427E+11	1.469E+11	1.501E+11	1.503E+11
19	4.236E+11	4.217E+11	4.246E+11	4.397E+11	4.472E+11	4.540E+11	4.721E+11	4.862E+11	4.999E+11	5.088E+11	5.093E+11

PLANE NUMBER 2

	1	2	3	4	5	6	7	8	9	10	11
1	1.648E+13	1.648E+13	1.648E+13	1.661E+13	1.669E+13	1.672E+13	1.696E+13	1.706E+13	1.715E+13	1.720E+13	1.721E+13
2	1.615E+13	1.615E+13	1.616E+13	1.633E+13	1.641E+13	1.655E+13	1.675E+13	1.689E+13	1.702E+13	1.710E+13	1.711E+13
3	1.583E+13	1.583E+13	1.584E+13	1.604E+13	1.619E+13	1.630E+13	1.649E+13	1.665E+13	1.682E+13	1.695E+13	1.695E+13
4	1.555E+13	1.556E+13	1.558E+13	1.580E+13	1.590E+13	1.600E+13	1.616E+13	1.634E+13	1.655E+13	1.673E+13	1.674E+13
5	1.519E+13	1.519E+13	1.523E+13	1.548E+13	1.557E+13	1.565E+13	1.599E+13	1.625E+13	1.648E+13	1.649E+13	
6	1.343E+13	1.344E+13	1.356E+13	1.387E+13	1.399E+13	1.406E+13	1.424E+13	1.450E+13	1.489E+13	1.529E+13	1.533E+13
7	9.068E+12	9.099E+12	9.540E+12	1.013E+13	1.044E+13	1.023E+13	1.090E+13	1.134E+13	1.155E+13		
8	4.372E+12	4.868E+12	5.915E+12	6.360E+12	7.616E+12	6.477E+12	6.238E+12	8.602E+12	6.732E+12	7.180E+12	8.369E+12
9	2.007E+12	2.132E+12	4.094E+12	4.559E+12	6.610E+12	4.644E+12	4.503E+12	7.926E+12	4.789E+12	5.167E+12	7.192E+12
10	6.941E+07	9.854E+07	2.657E+12	2.996E+12	6.040E+12	3.052E+12	2.939E+12	7.417E+12	3.128E+12	3.404E+12	6.511E+12
11	8.676E+10	2.720E+07	1.444E+12	1.649E+12	5.670E+12	1.689E+12	1.605E+12	7.162E+12	1.709E+12	1.878E+12	6.075E+12
12	3.339E+07	3.129E+07	7.023E+07	8.230E+07	5.429E+12	8.401E+07	7.929E+07	6.999E+12	8.469E+07	9.497E+07	5.795E+12
13	1.511E+12	1.517E+12	1.603E+12	1.830E+12	5.566E+12	1.874E+12	7.031E+12	1.940E+12	2.131E+12	6.009E+12	
14	2.656E+12	2.670E+12	2.865E+12	3.222E+12	5.830E+12	3.304E+12	3.224E+12	7.242E+12	3.459E+12	3.753E+12	6.375E+12
15	3.886E+12	3.905E+12	4.169E+12	4.625E+12	6.193E+12	4.745E+12	4.676E+12	7.431E+12	5.017E+12	5.387E+12	6.876E+12
16	6.456E+12	6.461E+12	6.535E+12	6.843E+12	6.988E+12	7.037E+12	7.202E+12	7.555E+12	7.720E+12	7.987E+12	8.041E+12
17	2.451E+12	2.451E+12	2.462E+12	2.553E+12	2.591E+12	2.625E+12	2.703E+12	2.799E+12	2.893E+12	2.975E+12	2.981E+12
18	1.433E+12	1.434E+12	1.439E+12	1.491E+12	1.513E+12	1.555E+12	1.637E+12	1.692E+12	1.737E+12	1.740E+12	
19	1.230E+12	1.230E+12	1.233E+12	1.279E+12	1.302E+12	1.324E+12	1.375E+12	1.416E+12	1.457E+12	1.485E+12	1.486E+12

PLANE NUMBER 3

	1	2	3	4	5	6	7	8	9	10	11
1	1.423E+12	1.424E+12	1.431E+12	1.568E+12	1.647E+12	2.366E+12	3.705E+12	4.097E+12	4.420E+12	4.536E+12	4.543E+12
2	1.126E+12	1.126E+12	1.135E+12	1.316E+12	1.475E+12	2.474E+12	3.484E+12	3.713E+12	3.901E+12	3.986E+12	3.990E+12
3	8.404E+11	8.409E+11	8.486E+11	1.004E+12	1.442E+12	2.164E+12	2.601E+12	2.701E+12	2.800E+12	2.864E+12	2.868E+12

	1	2	3	4	5	6	7	8	9	10	11
1	7.236E+13	7.236E+13	7.241E+13	7.272E+13	7.379E+13	7.595E+13	8.147E+13	8.433E+13	8.695E+13	8.815E+13	8.821E+13
2	7.130E+13	7.131E+13	7.138E+13	7.227E+13	7.305E+13	7.578E+13	8.178E+13	8.491E+13	8.791E+13	8.944E+13	8.953E+13
3	7.044E+13	7.045E+13	7.063E+13	7.128E+13	7.255E+13	7.515E+13	8.107E+13	8.420E+13	8.781E+13	8.975E+13	8.985E+13
4	6.964E+13	6.959E+13	7.049E+13	7.070E+13	7.152E+13	7.301E+13	7.926E+13	8.139E+13	8.639E+13	8.869E+13	8.882E+13
5	6.824E+11	6.828E+13	7.079E+13	6.839E+13	6.904E+11	7.033E+13	7.906E+13	7.967E+13	8.675E+13	8.952E+13	8.967E+13
6	6.292E+13	6.299E+13	6.787E+13	6.212E+13	6.242E+13	6.303E+13	7.477E+13	7.323E+13	8.396E+13	8.766E+13	8.787E+13
7	5.379E+13	5.384E+13	5.724E+13	5.738E+13	5.609E+13	5.884E+13	6.286E+13	6.226E+13	6.939E+13	7.219E+13	7.246E+13
8	5.027E+13	5.023E+13	4.828E+13	4.865E+13	4.991E+13	5.005E+13	5.292E+13	5.812E+13	5.814E+13	6.007E+13	6.096E+13
9	4.922E+13	4.902E+13	4.627E+13	4.667E+13	4.821E+13	4.807E+13	5.069E+13	5.687E+13	5.563E+13	5.734E+13	5.858E+13
10	4.805E+13	4.748E+13	4.589E+13	4.628E+13	4.771E+13	4.769E+13	5.026E+13	5.545E+13	5.516E+13	5.683E+13	5.794E+13
11	4.532E+13	4.538E+13	4.563E+13	4.603E+13	4.579E+13	4.743E+13	4.999E+13	5.222E+13	5.495E+13	5.650E+13	5.563E+13
12	4.130E+13	4.146E+13	4.453E+13	4.492E+13	4.219E+13	4.627E+13	4.870E+13	4.753E+13	5.350E+13	5.511E+13	5.112E+13
13	3.855E+13	3.857E+13	4.073E+13	4.116E+13	3.948E+13	4.236E+13	4.463E+13	4.433E+13	4.888E+13	5.036E+13	4.767E+13
14	3.797E+13	3.795E+13	3.765E+13	3.813E+13	3.899E+13	3.924E+13	4.126E+13	4.366E+13	4.514E+13	4.653E+13	4.692E+13
15	3.606E+13	3.604E+13	3.579E+13	3.629E+13	3.696E+13	3.733E+13	3.923E+13	4.145E+13	4.290E+13	4.423E+13	4.455E+13
16	1.314E+13	1.314E+13	1.312E+13	1.340E+13	1.362E+13	1.392E+13	1.447E+13	1.515E+13	1.573E+13	1.621E+13	1.625E+13
17	2.560E+12	2.560E+12	2.560E+12	2.644E+12	2.702E+12	2.754E+12	2.880E+12	3.003E+12	3.115E+12	3.211E+12	3.218E+12
18	9.365E+11	9.365E+11	9.363E+11	9.677E+11	9.911E+11	1.010E+12	1.056E+12	1.100E+12	1.142E+12	1.174E+12	1.181E+12
19	2.537E+10	2.537E+10	2.542E+10	2.724E+10	2.917E+10	3.004E+10	3.112E+10	3.188E+10	3.326E+10	3.452E+10	3.476E+10

PLANE NUMBER 10

	1	2	3	4	5	6	7	8	9	10	11
1	6.387E+13	6.387E+13	6.389E+13	6.435E+13	6.464E+13	6.581E+13	6.891E+13	7.062E+13	7.218E+13	7.291E+13	7.296E+13
2	6.302E+13	6.302E+13	6.307E+13	6.352E+13	6.396E+13	6.535E+13	6.873E+13	7.069E+13	7.258E+13	7.356E+13	7.361E+13
3	6.221E+13	6.222E+13	6.236E+13	6.263E+13	6.322E+13	6.449E+13	6.793E+13	6.997E+13	7.232E+13	7.357E+13	7.364E+13
4	6.132E+13	6.137E+13	6.204E+13	6.204E+13	6.226E+13	6.296E+13	6.660E+13	6.807E+13	7.1??E+13	7.279E+13	7.287E+13
5	5.999E+13	5.991E+13	6.141E+13	5.998E+13	6.032E+13	6.105E+13	6.634E+13	6.696E+13	7.1??E+13	7.333E+13	7.343E+13
6	5.485E+13	5.499E+13	5.753E+13	5.559E+13	5.594E+13	5.623E+13	6.243E+13	6.235E+13	6.882E+13	7.123E+13	7.136E+13
7	4.670E+13	4.672E+13	4.834E+13	4.901E+13	4.945E+13	5.007E+13	5.251E+13	5.323E+13	5.745E+13	5.932E+13	5.941E+13
8	4.309E+13	4.306E+13	4.136E+13	4.169E+13	4.213E+13	4.274E+13	4.495E+13	4.914E+13	4.909E+13	5.031E+13	5.041E+13
9	4.202E+13	4.188E+13	3.986E+13	4.012E+13	4.062E+13	4.119E+13	4.333E+13	4.791E+13	4.729E+13	4.837E+13	4.854E+13
10	4.089E+13	4.056E+13	3.958E+13	3.984E+13	4.013E+13	4.091E+13	4.303E+13	4.658E+13	4.697E+13	4.804E+13	4.800E+13
11	3.859E+13	3.892E+13	3.940E+13	3.967E+13	3.857E+13	4.073E+13	4.284E+13	4.394E+13	4.677E+13	4.784E+13	4.621E+13
12	3.557E+13	3.572E+13	3.809E+13	3.839E+13	3.548E+13	3.941E+13	4.142E+13	4.051E+13	4.519E+13	4.631E+13	4.281E+13
13	3.365E+13	3.365E+13	3.440E+13	3.482E+13	3.397E+13	3.573E+13	3.745E+13	3.835E+13	4.091E+13	4.199E+13	4.036E+13
14	3.314E+13	3.306E+13	3.172E+13	3.227E+13	3.335E+13	3.311E+13	3.462E+13	3.776E+13	3.768E+13	3.886E+13	3.972E+13
15	3.135E+13	3.127E+13	3.017E+13	3.069E+13	3.164E+13	3.149E+13	3.290E+13	3.575E+13	3.579E+13	3.694E+13	3.764E+13
16	1.130E+13	1.129E+13	1.122E+13	1.155E+13	1.179E+13	1.193E+13	1.255E+13	1.317E+13	1.353E+13	1.392E+13	1.397E+13
17	2.237E+12	2.237E+12	2.235E+12	2.356E+12	2.458E+12	2.519E+12	2.729E+12	2.815E+12	2.900E+12	2.911E+12	
18	8.149E+11	8.147E+11	8.143E+11	8.619E+11	9.127E+11	9.310E+11	9.710E+11	1.004E+12	1.038E+12	1.071E+12	1.073E+12
19	2.296E+10	2.296E+10	2.303E+10	2.559E+10	2.931E+10	3.022E+10	3.106E+10	3.111E+10	3.277E+10	3.417E+10	3.470E+10

PLANE NUMBER 11

	1	2	3	4	5	6	7	8	9	10	11
1	6.029E+13	6.029E+13	6.030E+13	6.048E+13	6.059E+13	6.100E+13	6.236E+13	6.333E+13	6.425E+13	6.471E+13	6.473E+13
2	5.941E+13	5.942E+13	5.944E+13	5.962E+13	5.983E+13	6.010E+13	6.173E+13	6.305E+13	6.433E+13	6.501E+13	6.505E+13
3	5.843E+13	5.843E+13	5.852E+13	5.855E+13	5.855E+13	5.880E+13	6.077E+13	6.236E+13	6.399E+13	6.488E+13	6.493E+13
4	5.720E+13	5.723E+13	5.768E+13	5.756E+13	5.729E+13	5.746E+13	5.969E+13	6.128E+13	6.321E+13	6.424E+13	6.430E+13
5	5.593E+13	5.593E+13	5.613E+13	5.545E+13	5.560E+13	5.601E+13	5.925E+13	6.103E+13	6.323E+13	6.445E+13	6.452E+13
6	5.127E+13	5.127E+13	5.155E+13	5.261E+13	5.286E+13	5.315E+13	5.542E+13	5.767E+13	6.044E+13	6.212E+13	6.221E+13
7	4.339E+13	4.339E+13	4.307E+13	4.392E+13	4.415E+13	4.476E+13	4.647E+13	4.914E+13	5.066E+13	5.204E+13	5.198E+13
8	3.861E+13	3.850E+13	3.735E+13	3.759E+13	3.686E+13	3.842E+13	4.049E+13	4.375E+13	4.399E+13	4.484E+13	4.369E+13
9	3.659E+13	3.656E+13	3.618E+13	3.630E+13	3.500E+13	3.714E+13	3.915E+13	4.145E+13	4.262E+13	4.334E+13	4.151E+13
10	3.518E+13	3.521E+13	3.591E+13	3.604E+13	3.410E+13	3.687E+13	3.986E+13	4.231E+13	4.303E+13		4.042E+13
11	3.418E+13	3.420E+13	3.528E+13	3.545E+13	3.315E+13	3.627E+13	3.820E+13	3.873E+13	4.158E+13	4.237E+13	3.951E+13
12	3.318E+13	3.318E+13	3.365E+13	3.385E+13	3.254E+13	3.463E+13	3.636E+13	3.760E+13	3.955E+13	4.050E+13	3.853E+13
13	3.213E+13	3.211E+13	3.044E+13	3.090E+13	3.169E+13	3.162E+13	3.302E+13	3.643E+13	3.587E+13	3.698E+13	3.750E+13
14	3.132E+13	3.115E+13	2.942E+13	2.897E+13	3.097E+13	2.966E+13	3.097E+13	3.551E+13	3.350E+13	3.464E+13	3.661E+13
15	2.918E+13	2.904E+13	2.704E+13	2.760E+13	2.827E+13	2.827E+13	2.941E+13	3.314E+13	3.190E+13	3.300E+13	3.433E+13
16	1.035E+13	1.034E+13	1.024E+13	1.061E+13	1.087E+13	1.105E+13	1.159E+13	1.218E+13	1.243E+13	1.277E+13	1.283E+13
17	2.073E+12	2.073E+12	2.072E+12	2.214E+12	2.349E+12	2.409E+12	2.515E+12	2.598E+12	2.673E+12	2.754E+12	2.768E+12
18	7.536E+11	7.536E+11	7.533E+11	8.107E+11	8.896E+11	9.016E+11	9.378E+11	9.615E+11	9.945E+11	1.027E+12	1.039E+12
19	2.175E+10	2.175E+10	2.182E+10	2.474E+10	2.948E+10	3.035E+10	3.107E+10	3.070E+10	3.256E+10	3.404E+10	3.477E+10

	1	2	3	4	5	6	7	8	9	10	11
14	1.498E+13	1.397E+13	1.488E+13	1.561E+13	1.579E+13	1.616E+13	1.677E+13	1.604E+13	1.717E+13	1.747E+12	1.784E+13
15	1.402E+13	1.401E+13	1.392E+13	1.469E+13	1.523E+13	1.551E+13	1.612E+13	1.631E+13	1.629E+13	1.656E+13	1.650E+13
16	5.919E+12	5.918E+12	5.918E+12	6.564E+12	7.143E+12	7.564E+12	8.039E+12	8.529E+12	8.263E+12	8.341E+12	8.302E+12
17	1.316E+12	1.317E+12	1.323E+12	1.609E+12	2.208E+12	2.153E+12	2.214E+12	2.181E+12	2.263E+12	2.343E+12	2.431E+12
18	4.732E+11	4.734E+11	4.760E+11	6.205E+11	1.769E+12	1.353E+12	1.352E+12	1.147E+12	1.366E+12	1.438E+12	1.671E+12
19	1.594E+10	1.585E+10	1.596E+10	2.024E+10	3.201E+10	3.210E+10	3.216E+10	2.862E+10	3.279E+10	3.474E+10	3.696E+10

PLANE NUMBER 18

	1	2	3	4	5	6	7	8	9	10	11
1	2.333E+13	2.333E+13	2.333E+13	2.341E+13	2.346E+13	2.352E+13	2.367E+13	2.380E+13	2.393E+13	2.400E+13	2.401E+13
2	2.286E+13	2.286E+13	2.287E+13	2.297E+13	2.302E+13	2.308E+13	2.330E+13	2.354E+13	2.378E+13	2.391E+13	2.392E+13
3	2.235E+13	2.235E+13	2.236E+13	2.248E+13	2.252E+13	2.255E+13	2.285E+13	2.320E+13	2.356E+13	2.374E+13	2.375E+13
4	2.183E+13	2.183E+13	2.184E+13	2.199E+13	2.197E+13	2.202E+13	2.232E+13	2.274E+13	2.325E+13	2.348E+13	2.348E+13
5	2.125E+13	2.125E+13	2.126E+13	2.148E+13	2.155E+13	2.162E+13	2.195E+13	2.239E+13	2.296E+13	2.324E+13	2.326E+13
6	1.915E+13	1.915E+13	1.918E+13	1.963E+13	1.979E+13	1.990E+13	2.034E+13	2.084E+13	2.165E+13	2.200E+13	2.205E+13
7	1.592E+13	1.592E+13	1.597E+13	1.692E+13	1.754E+13	1.779E+13	1.830E+13	1.839E+13	1.887E+13	1.917E+13	1.924E+13
8	1.410E+13	1.411E+13	1.435E+13	1.550E+13	1.655E+13	1.707E+13	1.761E+13	1.745E+13	1.731E+13	1.754E+13	1.768E+13
9	1.368E+13	1.368E+13	1.392E+13	1.494E+13	1.611E+13	1.663E+13	1.721E+13	1.700E+13	1.675E+13	1.696E+13	1.708E+13
10	1.324E+13	1.325E+13	1.328E+13	1.453E+13	1.580E+13	1.624E+13	1.642E+13	1.677E+13	1.638E+13	1.657E+13	1.665E+13
11	1.290E+13	1.290E+13	1.294E+13	1.421E+13	1.555E+13	1.594E+13	1.652E+13	1.655E+13	1.608E+13	1.626E+13	1.632E+13
12	1.250E+13	1.250E+13	1.254E+13	1.383E+13	1.526E+13	1.559E+13	1.610E+13	1.629E+13	1.572E+13	1.588E+13	1.593E+13
13	1.200E+13	1.200E+13	1.203E+13	1.334E+13	1.490E+13	1.517E+13	1.576E+13	1.595E+13	1.526E+13	1.540E+13	1.543E+13
14	1.149E+13	1.148E+13	1.151E+13	1.282E+13	1.454E+13	1.475E+13	1.533E+13	1.562E+13	1.476E+13	1.489E+13	1.490E+13
15	1.070E+13	1.070E+13	1.073E+13	1.203E+13	1.413E+13	1.470E+13	1.512E+13	1.401E+13	1.412E+13	1.409E+13	
16	4.659E+12	4.661E+12	4.681E+12	5.454E+12	6.481E+12	6.808E+12	7.297E+12	7.881E+12	7.345E+12	7.381E+12	7.397E+12
17	1.077E+12	1.077E+12	1.086E+12	1.398E+12	2.143E+12	2.009E+12	2.056E+12	1.973E+12	2.079E+12	2.158E+12	2.298E+12
18	3.852E+11	3.855E+11	3.888E+11	5.430E+11	1.754E+12	1.313E+12	1.301E+12	8.555E+11	1.303E+12	1.377E+12	1.632E+12
19	1.367E+10	1.368E+10	1.380E+10	1.815E+10	3.051E+10	3.093E+10	3.089E+10	2.609E+10	3.1xx+xx	3.330E+10	3.564E+10

PLANE NUMBER 19

	1	2	3	4	5	6	7	8	9	10	11
1	1.845E+13	1.845E+13	1.845E+13	1.857E+13	1.863E+13	1.870E+13	1.886E+13	1.897E+13	1.906E+13	1.911E+13	1.912E+13
2	1.806E+13	1.806E+13	1.807E+13	1.828E+13	1.838E+13	1.843E+13	1.875E+13	1.890E+13	1.904E+13	1.912E+13	1.912E+13
3	1.764E+13	1.764E+13	1.765E+13	1.796E+13	1.811E+13	1.827E+13	1.862E+13	1.881E+13	1.898E+13	1.908E+13	1.909E+13
4	1.722E+13	1.722E+13	1.724E+13	1.764E+13	1.787E+13	1.809E+13	1.849E+13	1.869E+13	1.887E+13	1.899E+13	1.900E+13
5	1.676E+13	1.676E+13	1.679E+13	1.729E+13	1.761E+13	1.793E+13	1.836E+13	1.857E+13	1.874E+13	1.888E+13	1.899E+13
6	1.513E+13	1.513E+13	1.517E+13	1.598E+13	1.652E+13	1.696E+13	1.757E+13	1.776E+13	1.789E+13	1.808E+13	1.812E+13
7	1.268E+13	1.268E+13	1.274E+13	1.394E+13	1.495E+13	1.569E+13	1.626E+13	1.619E+13	1.586E+13	1.600E+13	1.606E+13
8	1.136E+13	1.137E+13	1.142E+13	1.272E+13	1.393E+13	1.452E+13	1.528E+13	1.520E+13	1.465E+13	1.474E+13	1.480E+13
9	1.085E+13	1.086E+13	1.091E+13	1.224E+13	1.351E+13	1.419E+13	1.444E+13	1.479E+13	1.417E+13	1.426E+13	1.431E+13
10	1.049E+13	1.050E+13	1.055E+13	1.188E+13	1.320E+13	1.386E+13	1.450E+13	1.449E+13	1.382E+13	1.390E+13	1.394E+13
11	1.021E+13	1.022E+13	1.027E+13	1.161E+13	1.296E+13	1.359E+13	1.424E+13	1.425E+13	1.355E+13	1.362E+13	1.366E+13
12	9.885E+12	9.888E+12	9.947E+12	1.128E+13	1.266E+13	1.328E+13	1.391E+13	1.396E+13	1.322E+13	1.328E+13	1.332E+13
13	9.475E+12	9.478E+12	9.531E+12	1.086E+13	1.228E+13	1.287E+13	1.345E+13	1.358E+13	1.280E+13	1.285E+13	1.288E+13
14	9.057E+12	9.061E+12	9.112E+12	1.042E+13	1.187E+13	1.233E+13	1.304E+13	1.317E+13	1.235E+13	1.240E+13	1.243E+13
15	8.439E+12	8.442E+12	8.490E+12	9.755E+12	1.122E+13	1.174E+13	1.233E+13	1.252E+13	1.167E+13	1.171E+13	1.173E+13
16	3.741E+12	3.743E+12	3.769E+12	4.500E+12	5.391E+12	5.721E+12	6.142E+12	6.568E+12	6.131E+12	6.148E+12	6.186E+12
17	8.865E+11	8.871E+11	8.958E+11	1.179E+12	1.754E+12	1.689E+12	1.729E+12	1.653E+12	1.738E+12	1.806E+12	1.920E+12
18	3.161E+11	3.163E+11	3.196E+11	4.462E+11	1.013E+12	8.329E+11	8.317E+11	6.530E+11	8.290E+11	8.737E+11	1.009E+12
19	1.171E+10	1.172E+10	1.183E+10	1.587E+10	2.643E+10	2.727E+10	2.723E+10	2.280E+10	2.759E+10	2.933E+10	3.129E+10

PLANE NUMBER 20

	1	2	3	4	5	6	7	8	9	10	11
1	1.429E+12	1.429E+12	1.430E+12	1.439E+12	1.444E+12	1.449E+12	1.461E+12	1.468E+12	1.475E+12	1.478E+12	1.478E+12
2	1.401E+12	1.401E+12	1.402E+12	1.418E+12	1.427E+12	1.435E+12	1.455E+12	1.464E+12	1.473E+12	1.477E+12	1.477E+12
3	1.370E+12	1.371E+12	1.372E+12	1.396E+12	1.408E+12	1.420E+12	1.446E+12	1.458E+12	1.468E+12	1.472E+12	1.472E+12
4	1.341E+12	1.341E+12	1.342E+12	1.373E+12	1.388E+12	1.403E+12	1.435E+12	1.447E+12	1.457E+12	1.461E+12	1.462E+12
5	1.306E+12	1.308E+12	1.310E+12	1.348E+12	1.366E+12	1.385E+12	1.422E+12	1.435E+12	1.445E+12	1.449E+12	1.449E+12
6	1.194E+12	1.194E+12	1.197E+12	1.257E+12	1.297E+12	1.315E+12	1.369E+12	1.379E+12	1.385E+12	1.389E+12	1.390E+12
7	1.022E+12	1.022E+12	1.026E+12	1.109E+12	1.151E+12	1.190E+12	1.254E+12	1.256E+12	1.252E+12	1.253E+12	1.253E+12
8	9.245E+11	9.248E+11	9.294E+11	1.017E+12	1.063E+12	1.106E+12	1.171E+12	1.171E+12	1.162E+12	1.162E+12	1.162E+12
9	8.866E+11	8.869E+11	8.915E+11	9.808E+11	1.028E+12	1.072E+12	1.137E+12	1.136E+12	1.126E+12	1.125E+12	1.125E+12
10	8.595E+11	8.599E+11	8.645E+11	9.544E+11	1.003E+12	1.047E+12	1.112E+12	1.111E+12	1.100E+12	1.098E+12	1.098E+12

11	8.385E+11	8.388E+11	8.435E+11	9.337E+11	9.827E+11	1.027E+12	1.092E+12	1.090E+12	1.079E+12	1.077E+12	1.077E+12
12	8.139E+11	8.143E+11	8.189E+11	9.092E+11	9.587E+11	1.003E+12	1.067E+12	1.066E+12	1.054E+12	1.052E+12	1.052E+12
13	7.832E+11	7.835E+11	7.881E+11	8.783E+11	9.281E+11	9.726E+11	1.035E+12	1.035E+12	1.022E+12	1.020E+12	1.020E+12
14	7.519E+11	7.522E+11	7.568E+11	8.462E+11	8.962E+11	9.404E+11	1.003E+12	1.002E+12	9.884E+11	9.868E+11	9.868E+11
15	7.055E+11	7.058E+11	7.103E+11	7.982E+11	8.480E+11	8.916E+11	9.525E+11	9.520E+11	9.392E+11	9.365E+11	9.366E+11
16	3.548E+11	3.550E+11	3.583E+11	4.252E+11	4.659E+11	5.016E+11	5.459E+11	5.522E+11	5.419E+11	5.410E+11	5.413E+11
17	9.808E+10	9.817E+10	9.938E+10	1.269E+11	1.497E+11	1.605E+11	1.711E+11	1.697E+11	1.706E+11	1.738E+11	1.756E+11
18	3.413E+10	3.416E+10	3.460E+10	4.511E+10	5.646E+10	5.943E+10	6.292E+10	6.129E+10	6.244E+10	6.389E+10	6.526E+10
19	1.994E+09	1.996E+09	2.025E+09	2.781E+09	3.699E+09	4.037E+09	4.139E+09	3.871E+09	4.159E+09	4.373E+09	4.477E+09

GROUP 3 FLUX

PLANE NUMBER 1

	1	2	3	4	5	6	7	8	9	10	11
1	1.135E+12	1.135E+12	1.135E+12	1.139E+12	1.140E+12	1.142E+12	1.148E+12	1.152E+12	1.156E+12	1.158E+12	1.158E+12
2	1.114E+12	1.114E+12	1.114E+12	1.120E+12	1.123E+12	1.125E+12	1.133E+12	1.140E+12	1.147E+12	1.151E+12	1.151E+12
3	1.090E+12	1.090E+12	1.090E+12	1.091E+12	1.099E+12	1.102E+12	1.115E+12	1.124E+12	1.134E+12	1.141E+12	1.141E+12
4	1.064E+12	1.064E+12	1.065E+12	1.075E+12	1.090E+12	1.084E+12	1.093E+12	1.105E+12	1.117E+12	1.126E+12	1.126E+12
5	1.035E+12	1.035E+12	1.036E+12	1.049E+12	1.054E+12	1.058E+12	1.068E+12	1.092E+12	1.095E+12	1.109E+12	1.109E+12
6	9.199E+11	9.201E+11	9.231E+11	9.459E+11	9.532E+11	9.584E+11	9.659E+11	9.873E+11	1.006E+12	1.026E+12	1.028E+12
7	6.574E+11	6.590E+11	6.815E+11	7.092E+11	7.267E+11	7.209E+11	7.244E+11	7.694E+11	7.646E+11	7.906E+11	8.017E+11
8	3.306E+11	3.376E+11	4.362E+11	4.633E+11	5.396E+11	4.712E+11	4.693E+11	6.048E+11	4.971E+11	5.205E+11	5.911E+11
9	1.477E+11	1.575E+11	3.130E+11	3.364E+11	4.644E+11	3.422E+11	3.389E+11	5.404E+11	3.594E+11	3.793E+11	5.041E+11
10	3.065E+06	4.167E+06	1.997E+11	2.164E+11	4.128E+11	2.202E+11	2.170E+11	4.966E+11	2.303E+11	2.445E+11	4.429E+11
11	9.003E+09	1.206E+06	9.950E+10	1.088E+11	3.757E+11	1.094E+11	1.094E+11	4.645E+11	1.152E+11	1.232E+11	3.983E+11
12	1.415E+06	1.262E+06	2.945E+06	3.321E+06	3.411E+11	3.378E+06	3.241E+06	4.323E+11	3.451E+06	3.808E+06	3.559E+11
13	9.930E+10	9.930E+10	9.930E+10	1.083E+11	3.399E+11	1.073E+11	9.678E+10	1.155E+11	1.245E+11	3.618E+11	
14	1.761E+11	1.761E+11	1.764E+11	1.903E+11	3.447E+11	1.939E+11	1.909E+11	4.200E+11	2.044E+11	2.189E+11	3.731E+11
15	2.452E+11	2.453E+11	2.459E+11	2.629E+11	3.495E+11	2.680E+11	2.657E+11	4.105E+11	2.845E+11	3.026E+11	3.842E+11
16	1.949E+11	1.949E+11	1.957E+11	2.030E+11	2.073E+11	2.077E+11	2.114E+11	2.225E+11	2.273E+11	2.365E+11	2.387E+11
17	4.781E+10	4.782E+10	4.796E+10	4.960E+10	5.029E+10	5.089E+10	5.223E+10	5.411E+10	5.602E+10	5.787E+10	5.801E+10
18	1.247E+11	1.248E+11	1.250E+11	1.294E+11	1.315E+11	1.336E+11	1.383E+11	1.427E+11	1.469E+11	1.501E+11	1.503E+11
19	4.236E+11	4.237E+11	4.246E+11	4.397E+11	4.472E+11	4.540E+11	4.721E+11	4.862E+11	4.939E+11	5.088E+11	5.093E+11

PLANE NUMBER 2

	1	2	3	4	5	6	7	8	9	10	11
1	1.648E+13	1.648E+13	1.648E+13	1.661E+13	1.669E+13	1.678E+13	1.696E+13	1.706E+13	1.715E+13	1.720E+13	1.721E+13
2	1.615E+13	1.615E+13	1.616E+13	1.633E+13	1.643E+13	1.656E+13	1.675E+13	1.689E+13	1.702E+13	1.710E+13	1.711E+13
3	1.583E+13	1.583E+13	1.584E+13	1.604E+13	1.619E+13	1.630E+13	1.649E+13	1.665E+13	1.682E+13	1.695E+13	1.695E+13
4	1.555E+13	1.556E+13	1.558E+13	1.580E+13	1.590E+13	1.600E+13	1.615E+13	1.634E+13	1.655E+13	1.673E+13	1.674E+13
5	1.519E+13	1.519E+13	1.523E+13	1.548E+13	1.557E+13	1.565E+13	1.579E+13	1.599E+13	1.625E+13	1.648E+13	1.649E+13
6	1.343E+13	1.344E+13	1.356E+13	1.387E+13	1.399E+13	1.409E+13	1.424E+13	1.450E+13	1.489E+13	1.529E+13	1.533E+13
7	9.068E+12	9.099E+12	9.540E+12	1.013E+13	1.044E+13	1.030E+13	1.023E+13	1.090E+13	1.093E+13	1.134E+13	1.155E+13
8	4.372E+12	4.468E+12	5.815E+12	6.360E+12	7.636E+12	6.477E+12	6.339E+12	8.602E+12	6.732E+12	7.180E+12	8.369E+12
9	2.007E+12	2.132E+12	4.094E+12	4.559E+12	6.619E+12	4.644E+12	4.503E+12	7.826E+12	4.789E+12	5.167E+12	7.192E+12
10	6.841E+07	9.854E+07	2.657E+12	2.996E+12	6.040E+12	3.052E+12	2.939E+12	7.417E+12	3.128E+12	3.404E+12	6.511E+12
11	8.678E+10	2.720E+07	1.444E+12	1.649E+12	5.670E+12	1.680E+12	1.680E+12	7.162E+12	1.709E+12	1.878E+12	6.075E+12
12	3.339E+07	3.129E+07	7.023E+07	8.230E+07	5.429E+12	8.401E+07	7.929E+07	6.999E+12	8.469E+07	9.497E+07	5.795E+12
13	1.511E+12	1.517E+12	1.603E+12	1.830E+12	5.566E+12	1.874E+12	1.808E+12	7.091E+12	1.940E+12	2.131E+12	6.009E+12
14	2.656E+12	2.670E+12	2.865E+12	3.222E+12	5.830E+12	3.304E+12	3.224E+12	7.242E+12	3.459E+12	3.753E+12	6.375E+12
15	3.896E+12	3.905E+12	4.169E+12	4.625E+12	6.193E+12	4.745E+12	4.676E+12	7.431E+12	5.017E+12	5.387E+12	6.876E+12
16	6.456E+12	6.461E+12	6.535E+12	6.843E+12	6.988E+12	7.037E+12	7.202E+12	7.555E+12	7.720E+12	7.987E+12	8.041E+12
17	2.451E+12	2.451E+12	2.462E+12	2.553E+12	2.591E+12	2.625E+12	2.703E+12	2.799E+12	2.893E+12	2.975E+12	2.981E+12
18	1.433E+12	1.434E+12	1.439E+12	1.491E+12	1.513E+12	1.535E+12	1.583E+12	1.637E+12	1.692E+12	1.737E+12	1.740E+12
19	1.230E+12	1.230E+12	1.233E+12	1.279E+12	1.302E+12	1.324E+12	1.375E+12	1.416E+12	1.457E+12	1.485E+12	1.486E+12

PLANE NUMBER 3

	1	2	3	4	5	6	7	8	9	10	11
1	1.423E+12	1.424E+12	1.431E+12	1.568E+12	1.647E+12	2.366E+12	3.705E+12	4.097E+12	4.420E+12	4.536E+12	4.543E+12
2	1.126E+12	1.126E+12	1.135E+12	1.316E+12	1.475E+12	2.474E+12	3.484E+12	3.713E+12	3.901E+12	3.986E+12	3.990E+12
3	8.404E+11	8.409E+11	8.486E+11	1.004E+12	1.442E+12	2.164E+12	2.601E+12	2.701E+12	2.800E+12	2.864E+12	2.868E+12

17	1.786E+12	1.786E+12	1.786E+12	1.975E+12	2.206E+12	2.256E+12	2.346E+12	2.397E+12	2.460E+12	2.537E+12	2.562E+12
18	6.467E+11	6.467E+11	6.472E+11	7.286E+11	9.475E+11	9.052E+11	9.312E+11	9.208E+11	9.698E+11	1.006E+12	1.049E+12
19	1.958E+10	1.959E+10	1.968E+10	2.317E+10	3.020E+10	3.084E+10	3.131E+10	3.003E+10	3.245E+10	3.409E+10	3.529E+10

PLANE NUMBER 15

	1	2	3	4	5	6	7	8	9	10	11
1	3.943E+13	3.944E+13	3.945E+13	3.958E+13	3.966E+13	3.974E+13	4.000E+13	4.024E+13	4.050E+13	4.063E+13	4.064E+13
2	3.884E+13	3.885E+13	3.887E+13	3.896E+13	3.904E+13	3.914E+13	3.951E+13	3.995E+13	4.043E+13	4.068E+13	4.069E+13
3	3.826E+13	3.826E+13	3.826E+13	3.831E+13	3.837E+13	3.846E+13	3.893E+13	3.960E+13	4.028E+13	4.062E+13	4.064E+13
4	3.777E+13	3.777E+13	3.776E+13	3.777E+13	3.779E+13	3.785E+13	3.837E+13	3.919E+13	4.002E+13	4.043E+13	4.045E+13
5	3.657E+13	3.657E+13	3.656E+13	3.651E+13	3.644E+13	3.645E+13	3.700E+13	3.797E+13	3.897E+13	3.944E+13	3.945E+13
6	3.265E+13	3.256E+13	3.253E+13	3.246E+13	3.220E+13	3.210E+13	3.274E+13	3.409E+13	3.555E+13	3.620E+13	3.619E+13
7	2.546E+13	2.546E+13	2.539E+13	2.542E+13	2.495E+13	2.491E+13	2.573E+13	2.689E+13	2.857E+13	2.926E+13	2.923E+13
8	2.279E+13	2.278E+13	2.260E+13	2.279E+13	2.241E+13	2.251E+13	2.333E+13	2.426E+13	2.555E+13	2.620E+13	2.623E+13
9	2.197E+13	2.195E+13	2.168E+13	2.194E+13	2.159E+13	2.172E+13	2.253E+13	2.341E+13	2.452E+13	2.516E+13	2.524E+13
10	2.167E+13	2.165E+13	2.127E+13	2.156E+13	2.131E+13	2.141E+13	2.221E+13	2.316E+13	2.408E+13	2.472E+13	2.487E+13
11	2.155E+13	2.152E+13	2.106E+13	2.141E+13	2.119E+13	2.127E+13	2.206E+13	2.307E+13	2.386E+13	2.451E+13	2.470E+13
12	2.132E+13	2.129E+13	2.074E+13	2.113E+13	2.097E+13	2.102E+13	2.180E+13	2.289E+13	2.352E+13	2.418E+13	2.443E+13
13	2.103E+13	2.098E+13	2.032E+13	2.075E+13	2.071E+13	2.070E+13	2.147E+13	2.269E+13	2.310E+13	2.376E+13	2.410E+13
14	2.042E+13	2.037E+13	1.969E+13	2.015E+13	2.016E+13	2.015E+13	2.090E+13	2.212E+13	2.244E+13	2.309E+13	2.344E+13
15	1.917E+13	1.913E+13	1.851E+13	1.900E+13	1.903E+13	1.907E+13	1.979E+13	2.091E+13	2.118E+13	2.179E+13	2.208E+13
16	7.563E+12	7.560E+12	7.515E+12	8.003E+12	8.239E+12	8.577E+12	9.073E+12	9.448E+12	9.497E+12	9.669E+12	9.662E+12
17	1.605E+12	1.606E+12	1.608E+12	1.831E+12	2.152E+12	2.187E+12	2.266E+12	2.293E+12	2.352E+12	2.428E+12	2.468E+12
18	5.799E+11	5.800E+11	5.812E+11	6.828E+11	1.126E+12	9.781E+11	9.943E+11	9.358E+11	1.020E+12	1.064E+12	1.162E+12
19	1.819E+10	1.820E+10	1.830E+10	2.213E+10	3.090E+10	3.132E+10	3.162E+10	2.957E+10	3.254E+10	3.430E+10	3.590E+10

PLANE NUMBER 16

	1	2	3	4	5	6	7	8	9	10	11
1	3.563E+13	3.562E+13	3.541E+13	3.547E+13	3.553E+13	3.560E+13	3.587E+13	3.633E+13	3.631E+13	3.639E+13	3.640E+13
2	3.527E+13	3.526E+13	3.482E+13	3.483E+13	3.487E+13	3.493E+13	3.526E+13	3.613E+13	3.613E+13	3.633E+13	3.634E+13
3	3.425E+13	3.425E+13	3.422E+13	3.418E+13	3.416E+13	3.418E+13	3.456E+13	3.523E+13	3.586E+13	3.610E+13	3.619E+13
4	3.412E+13	3.412E+13	3.411E+13	3.400E+13	3.375E+13	3.369E+13	3.411E+13	3.492E+13	3.586E+13	3.624E+13	3.620E+13
5	3.260E+13	3.260E+13	3.259E+13	3.236E+13	3.131E+13	3.110E+13	3.150E+13	3.243E+13	3.394E+13	3.436E+13	3.402E+13
6	2.899E+13	2.899E+13	2.897E+13	2.875E+13	2.747E+13	2.724E+13	2.775E+13	2.991E+13	3.092E+13	3.147E+13	3.110E+13
7	2.214E+13	2.213E+13	2.211E+13	2.213E+13	2.039E+13	2.037E+13	2.095E+13	2.151E+13	2.432E+13	2.489E+13	2.460E+13
8	1.989E+13	1.913E+13	1.978E+13	2.004E+13	1.899E+13	1.914E+13	1.977E+13	1.989E+13	2.184E+13	2.235E+13	2.222E+13
9	1.948E+13	1.947E+13	1.932E+13	1.964E+13	1.825E+13	1.889E+13	1.953E+13	1.931E+13	2.115E+13	2.164E+13	2.161E+13
10	1.932E+13	1.931E+13	1.911E+13	1.948E+13	1.809E+13	1.875E+13	1.941E+13	1.919E+13	2.095E+13	2.143E+13	2.142E+13
11	1.919E+13	1.917E+13	1.892E+13	1.933E+13	1.797E+13	1.864E+13	1.931E+13	1.913E+13	2.079E+13	2.128E+13	2.128E+13
12	1.892E+13	1.889E+13	1.860E+13	1.905E+13	1.773E+13	1.840E+13	1.908E+13	1.893E+13	2.048E+13	2.096E+13	2.097E+13
13	1.849E+13	1.845E+13	1.810E+13	1.810E+13	1.738E+13	1.803E+13	1.870E+13	1.861E+13	2.000E+13	2.047E+13	2.050E+13
14	1.786E+13	1.784E+13	1.747E+13	1.801E+13	1.694E+13	1.755E+13	1.822E+13	1.819E+13	1.940E+13	1.985E+13	1.987E+13
15	1.679E+13	1.676E+13	1.641E+13	1.699E+13	1.634E+13	1.674E+13	1.739E+13	1.746E+13	1.837E+13	1.878E+13	1.878E+13
16	6.821E+12	6.819E+12	6.795E+12	7.350E+12	7.536E+12	8.007E+12	8.507E+12	8.846E+12	8.804E+12	8.924E+12	8.859E+12
17	1.476E+12	1.476E+12	1.480E+12	1.731E+12	2.193E+12	2.166E+12	2.236E+12	2.240E+12	2.303E+12	2.381E+12	2.442E+12
18	5.320E+11	5.321E+11	5.340E+11	6.550E+11	1.594E+12	1.184E+12	1.386E+12	1.032E+12	1.203E+12	1.263E+12	1.487E+12
19	1.714E+10	1.715E+10	1.726E+10	2.130E+10	3.145E+10	3.177E+10	3.193E+10	2.917E+10	3.269E+10	3.456E+10	3.650E+10

PLANE NUMBER 17

	1	2	3	4	5	6	7	8	9	10	11
1	3.018E+13	3.018E+13	3.017E+13	3.020E+13	3.023E+13	3.027E+13	3.041E+13	3.061E+13	3.078E+13	3.007E+13	3.087E+13
2	2.964E+13	2.964E+13	2.961E+13	2.952E+13	2.949E+13	2.948E+13	2.964E+13	3.006E+13	3.042E+13	3.061E+13	3.062E+13
3	2.899E+13	2.899E+13	2.899E+13	2.876E+13	2.860E+13	2.850E+13	2.867E+13	2.927E+13	2.991E+13	3.019E+13	3.020E+13
4	2.833E+13	2.833E+13	2.831E+13	2.795E+13	2.743E+13	2.720E+13	2.738E+13	2.814E+13	2.917E+13	2.951E+13	2.946E+13
5	2.755E+13	2.755E+13	2.753E+13	2.708E+13	2.642E+13	2.619E+13	2.637E+13	2.719E+13	2.844E+13	2.883E+13	2.878E+13
6	2.469E+13	2.468E+13	2.466E+13	2.426E+13	2.331E+13	2.304E+13	2.336E+13	2.431E+13	2.616E+13	2.666E+13	2.657E+13
7	1.999E+13	1.999E+13	1.998E+13	2.002E+13	1.894E+13	1.899E+13	1.946E+13	1.976E+13	2.194E+13	2.244E+13	2.236E+13
8	1.809E+13	1.809E+13	1.806E+13	1.841E+13	1.784E+13	1.825E+13	1.704E+13	1.870E+13	2.002E+13	2.044E+13	2.049E+13
9	1.743E+13	1.742E+13	1.738E+13	1.784E+13	1.740E+13	1.790E+13	1.847E+13	1.831E+13	1.938E+13	1.977E+13	1.983E+13
10	1.696E+13	1.696E+13	1.690E+13	1.743E+13	1.709E+13	1.756E+13	1.815E+13	1.802E+13	1.997E+13	1.934E+13	1.938E+13
11	1.660E+13	1.659E+13	1.653E+13	1.711E+13	1.684E+13	1.729E+13	1.789E+13	1.780E+13	1.864E+13	1.900E+13	1.903E+13
12	1.616E+13	1.616E+13	1.609E+13	1.671E+13	1.654E+13	1.698E+13	1.759E+13	1.753E+13	1.825E+13	1.859E+13	1.860E+13
13	1.560E+13	1.559E+13	1.551E+13	1.619E+13	1.617E+13	1.658E+13	1.720E+13	1.719E+13	1.773E+13	1.806E+13	1.805E+13

PLANE NUMBER 12

	1	2	3	4	5	6	7	8	9	10	11
1	5.679E+13	5.679E+13	5.680E+13	5.681E+13	5.678E+13	5.663E+13	5.696E+13	5.752E+13	5.808E+13	5.838E+13	5.840E+13
2	5.575E+13	5.575E+13	5.576E+13	5.579E+13	5.563E+13	5.534E+13	5.610E+13	5.705E+13	5.800E+13	5.851E+13	5.853E+13
3	5.430E+13	5.430E+13	5.431E+13	5.427E+13	5.379E+13	5.374E+13	5.499E+13	5.630E+13	5.753E+13	5.822E+13	5.825E+13
4	5.196E+13	5.196E+13	5.193E+13	5.193E+13	5.194E+13	5.211E+13	5.358E+13	5.511E+13	5.638E+13	5.714E+13	5.718E+13
5	5.179E+13	5.174E+13	5.099E+13	5.107E+13	5.126E+13	5.158E+13	5.343E+13	5.610E+13	5.669E+13	5.758E+13	5.763E+13
6	4.762E+13	4.754E+13	4.644E+13	4.862E+13	4.891E+13	4.920E+13	4.948E+13	5.316E+13	5.372E+13	5.499E+13	5.505E+13
7	4.007E+13	3.998E+13	3.869E+13	3.918E+13	3.933E+13	3.981E+13	4.143E+13	4.508E+13	4.519E+13	4.634E+13	4.628E+13
8	3.495E+13	3.491E+13	3.429E+13	3.448E+13	3.390E+13	3.515E+13	3.691E+13	3.941E+13	4.017E+13	4.096E+13	4.006E+13
9	3.311E+13	3.312E+13	3.338E+13	3.351E+13	3.253E+13	3.420E+13	3.600E+13	3.736E+13	3.914E+13	3.983E+13	3.845E+13
10	3.234E+13	3.238E+13	3.302E+13	3.316E+13	3.185E+13	3.385E+13	3.562E+13	3.650E+13	3.873E+13	3.942E+13	3.763E+13
11	3.167E+13	3.169E+13	3.204E+13	3.224E+13	3.120E+13	3.290E+13	3.457E+13	3.575E+13	3.757E+13	3.832E+13	3.684E+13
12	3.083E+13	3.082E+13	3.002E+13	3.035E+13	3.040E+13	3.094E+13	3.241E+13	3.441E+13	3.519E+13	3.609E+13	3.586E+13
13	2.976E+13	2.972E+13	2.712E+13	2.761E+13	2.937E+13	2.817E+13	2.931E+13	3.360E+13	3.178E+13	3.281E+13	3.460E+13
14	2.892E+13	2.873E+13	2.574E+13	2.630E+13	2.856E+13	2.684E+13	2.795E+13	3.265E+13	3.015E+13	3.122E+13	3.360E+13
15	2.680E+13	2.665E+13	2.455E+13	2.511E+13	2.662E+13	2.565E+13	2.661E+13	3.030E+13	2.879E+13	2.982E+13	3.129E+13
16	9.555E+12	9.548E+12	9.451E+12	9.843E+12	1.011E+13	1.031E+13	1.083E+13	1.137E+13	1.155E+13	1.185E+13	1.191E+13
17	1.939E+12	1.939E+12	1.938E+12	2.101E+12	2.273E+12	2.332E+12	2.431E+12	2.500E+12	2.569E+12	2.647E+12	2.666E+12
18	7.036E+11	7.036E+11	7.036E+11	7.712E+11	8.974E+11	8.932E+11	9.252E+11	9.365E+11	9.736E+11	1.007E+12	1.029E+12
19	2.074E+10	2.075E+10	2.083E+10	2.401E+10	2.977E+10	3.055E+10	3.115E+10	3.038E+10	3.248E+10	3.403E+10	3.496E+10

PLANE NUMBER 13

	1	2	3	4	5	6	7	8	9	10	11
1	5.210E+13	5.210E+13	5.210E+13	5.220E+13	5.224E+13	5.230E+13	5.266E+13	5.314E+13	5.360E+13	5.386E+13	5.387E+13
2	5.116E+13	5.116E+13	5.117E+13	5.126E+13	5.125E+13	5.125E+13	5.196E+13	5.279E+13	5.359E+13	5.403E+13	5.405E+13
3	4.999E+13	4.999E+13	5.000E+13	5.004E+13	4.996E+13	5.003E+13	5.110E+13	5.225E+13	5.331E+13	5.392E+13	5.396E+13
4	4.865E+13	4.864E+13	4.862E+13	4.867E+13	4.875E+13	4.892E+13	5.011E+13	5.145E+13	5.291E+13	5.326E+13	5.330E+13
5	4.773E+13	4.770E+13	4.737E+13	4.749E+13	4.767E+13	4.795E+13	4.945E+13	5.138E+13	5.235E+13	5.312E+13	5.317E+13
6	4.336E+13	4.332E+13	4.273E+13	4.395E+13	4.415E+13	4.443E+13	4.517E+13	4.793E+13	4.901E+13	5.011E+13	5.016E+13
7	3.636E+13	3.631E+13	3.562E+13	3.596E+13	3.604E+13	3.641E+13	3.790E+13	4.057E+13	4.139E+13	4.244E+13	4.242E+13
8	3.236E+13	3.235E+13	3.212E+13	3.231E+13	3.190E+13	3.284E+13	3.442E+13	3.628E+13	3.749E+13	3.828E+13	3.766E+13
9	3.207E+13	3.209E+13	3.234E+13	3.249E+13	3.167E+13	3.312E+13	3.403E+13	3.612E+13	3.786E+13	3.855E+13	3.740E+13
10	3.136E+13	3.139E+13	3.180E+13	3.196E+13	3.098E+13	3.259E+13	3.424E+13	3.532E+13	3.722E+13	3.792E+13	3.656E+13
11	3.072E+13	3.072E+13	3.015E+13	3.039E+13	3.033E+13	3.095E+13	3.245E+13	3.461E+13	3.525E+13	3.602E+13	3.577E+13
12	2.986E+13	2.985E+13	2.787E+13	2.823E+13	2.948E+13	2.874E+13	3.000E+13	3.365E+13	3.255E+13	3.343E+13	3.472E+13
13	2.834E+13	2.829E+13	2.497E+13	2.548E+13	2.799E+13	2.591E+13	2.689E+13	3.191E+13	2.910E+13	3.009E+13	3.292E+13
14	2.752E+13	2.734E+13	2.455E+13	2.511E+13	2.866E+13	2.557E+13	2.650E+13	3.097E+13	2.866E+13	2.968E+13	3.191E+13
15	2.547E+13	2.533E+13	2.340E+13	2.396E+13	2.530E+13	2.442E+13	2.532E+13	2.871E+13	2.736E+13	2.833E+13	2.967E+13
16	9.163E+12	9.156E+12	9.066E+12	9.473E+12	9.736E+12	9.957E+12	1.047E+13	1.099E+13	1.113E+13	1.141E+13	1.146E+13
17	1.873E+12	1.873E+12	1.873E+12	2.047E+12	2.242E+12	2.298E+12	2.393E+12	2.455E+12	2.521E+12	2.598E+12	2.620E+12
18	6.791E+11	6.791E+11	6.793E+11	7.527E+11	9.141E+11	8.959E+11	9.255E+11	9.283E+11	9.697E+11	1.004E+12	1.034E+12
19	2.025E+10	2.025E+10	2.033E+10	2.365E+10	2.994E+10	3.067E+10	3.121E+10	3.022E+10	3.245E+10	3.405E+10	3.509E+10

PLANE NUMBER 14

	1	2	3	4	5	6	7	8	9	10	11
1	4.598E+13	4.598E+13	4.599E+13	4.615E+13	4.625E+13	4.637E+13	4.673E+13	4.709E+13	4.744E+13	4.763E+13	4.764E+13
2	4.526E+13	4.526E+13	4.526E+13	4.541E+13	4.551E+13	4.565E+13	4.623E+13	4.687E+13	4.750E+13	4.784E+13	4.786E+13
3	4.454E+13	4.454E+13	4.455E+13	4.466E+13	4.476E+13	4.491E+13	4.572E+13	4.663E+13	4.751E+13	4.798E+13	4.801E+13
4	4.426E+13	4.426E+13	4.425E+13	4.434E+13	4.445E+13	4.462E+13	4.553E+13	4.661E+13	4.762E+13	4.817E+13	4.820E+13
5	4.257E+13	4.256E+13	4.250E+13	4.261E+13	4.273E+13	4.292E+13	4.394E+13	4.525E+13	4.635E+13	4.698E+13	4.701E+13
6	3.797E+13	3.796E+13	3.778E+13	3.920E+13	3.826E+13	3.849E+13	3.934E+13	4.122E+13	4.261E+13	4.349E+13	4.353E+13
7	3.188E+13	3.186E+13	3.161E+13	3.180E+13	3.178E+13	3.199E+13	3.325E+13	3.509E+13	3.640E+13	3.730E+13	3.731E+13
8	2.891E+13	2.889E+13	2.866E+13	2.887E+13	2.878E+13	2.914E+13	3.041E+13	3.200E+13	3.316E+13	3.396E+13	3.387E+13
9	2.788E+13	2.795E+13	2.751E+13	2.776E+13	2.776E+13	2.809E+13	2.932E+13	3.097E+13	3.191E+13	3.270E+13	3.268E+13
10	2.727E+13	2.722E+13	2.653E+13	2.684E+13	2.709E+13	2.719E+13	2.815E+11	3.036E+13	3.078E+13	3.159E+13	3.184E+13
11	2.686E+13	2.679E+13	2.575E+13	2.610E+13	2.666E+13	2.641E+13	2.754E+13	2.994E+13	2.987E+13	3.070E+13	3.130E+13
12	2.618E+13	2.606E+13	2.437E+13	2.482E+13	2.594E+13	2.515E+13	2.612E+13	2.924E+13	2.827E+13	2.916E+13	3.041E+13
13	2.586E+13	2.571E+13	2.346E+13	2.399E+13	2.558E+13	2.433E+13	2.520E+13	2.896E+13	2.722E+13	2.817E+13	2.991E+13
14	2.549E+13	2.514E+13	2.327E+13	2.380E+13	2.523E+13	2.416E+13	2.502E+13	2.855E+13	2.701E+13	2.796E+13	2.949E+13
15	2.361E+13	2.350E+13	2.193E+13	2.247E+13	2.347E+13	2.281E+13	2.365E+13	2.646E+13	2.550E+13	2.638E+13	2.742E+13
16	8.640E+12	8.635E+12	8.556E+12	8.986E+12	9.244E+12	9.493E+12	9.994E+12	1.046E+13	1.058E+13	1.083E+13	1.086E+13

	1	2	3	4	5	6	7	8	9	10	11
4	3.849E+07	3.853E+07	7.989E+07	9.357E+07	7.066E+07	8.115E+07	8.201E+07	4.107E+07	8.784E+07	9.407E+07	9.438E+07
5	1.341E+06	2.490E+08	2.637E+12	3.073E+12	3.092E+12	3.084E+12	2.727E+12	2.813E+07	2.911E+12	3.249E+12	3.265E+12
6	1.154E+06	1.715E+08	3.940E+12	3.837E+12	3.844E+12	3.852E+12	4.172E+12	2.033E+07	4.570E+12	5.166E+12	5.199E+12
7	7.641E+05	6.950E+07	3.165E+12	3.597E+12	3.760E+12	3.655E+12	3.403E+12	8.734E+06	3.712E+12	4.207E+12	4.334E+12
8	4.302E+05	2.344E+07	1.419E+12	1.973E+12	3.127E+12	1.911E+12	1.584E+12	3.469E+06	1.727E+12	2.215E+12	3.307E+12
9	2.585E+05	9.511E+07	6.239E+11	1.102E+12	3.095E+12	1.124E+12	7.532E+11	7.371E+07	8.215E+11	1.325E+12	3.095E+12
10	2.322E+07	7.614E+07	5.356E+11	9.651E+11	5.900E+12	9.857E+11	6.590E+11	5.399E+12	7.183E+11	1.173E+12	5.781E+12
11	8.627E+11	1.262E+08	4.680E+11	8.559E+11	1.057E+13	8.743E+11	5.833E+11	1.094E+13	6.354E+11	1.049E+12	1.041E+13
12	3.069E+08	2.949E+08	1.513E+08	1.923E+08	1.520E+13	1.993E+08	1.804E+08	1.671E+13	1.939E+08	2.289E+08	1.647E+13
13	5.534E+12	5.594E+12	9.958E+12	1.120E+13	1.711E+13	1.160E+13	1.165E+13	1.892E+13	1.250E+13	1.313E+13	1.924E+13
14	6.573E+12	7.042E+12	1.447E+13	1.633E+13	1.733E+13	1.656E+13	1.721E+13	1.915E+13	1.840E+13	1.911E+13	1.955E+13
15	9.834E+12	1.025E+13	1.611E+13	1.801E+13	1.895E+13	1.869E+13	1.900E+13	2.074E+13	2.032E+13	2.107E+13	2.138E+13
16	2.792E+13	2.796E+13	2.853E+13	2.995E+13	3.037E+13	3.091E+13	3.184E+13	3.301E+13	3.399E+13	3.489E+13	3.496E+13
17	2.021E+13	2.021E+13	2.031E+13	2.106E+13	2.138E+13	2.167E+13	2.240E+13	2.316E+13	2.390E+13	2.446E+13	2.449E+13
18	1.005E+13	1.095E+13	1.010E+13	1.047E+13	1.062E+13	1.079E+13	1.113E+13	1.150E+13	1.188E+13	1.217E+13	1.219E+13
19	1.814E+12	1.814E+12	1.818E+12	1.088E+12	1.922E+12	1.957E+12	2.031E+12	2.093E+12	2.153E+12	2.195E+12	2.198E+12

PLANE NUMBER 4

	1	2	3	4	5	6	7	8	9	10	11
1	2.050E+12	2.050E+12	2.063E+12	2.308E+12	2.444E+12	3.725E+12	6.154E+12	6.891E+12	7.503E+12	7.728E+12	7.741E+12
2	1.586E+12	1.597E+12	1.602E+12	1.914E+12	2.181E+12	3.964E+12	5.832E+12	6.283E+12	6.656E+12	6.823E+12	6.833E+12
3	1.159E+12	1.158E+12	1.172E+12	1.442E+12	2.220E+12	3.525E+12	4.373E+12	4.585E+12	4.791E+12	4.919E+12	4.926E+12
4	5.150E+07	5.156E+07	1.197E+08	1.377E+08	1.070E+08	1.264E+08	1.360E+08	6.768E+07	1.489E+08	1.603E+08	1.609E+08
5	3.730E+05	4.083E+08	4.343E+12	4.733E+12	4.760E+12	4.772E+12	4.599E+12	4.600E+07	5.025E+12	5.634E+12	5.664E+12
6	2.798E+05	2.845E+08	6.574E+12	5.444E+12	5.451E+12	5.474E+12	7.053E+12	3.306E+07	7.947E+12	9.024E+12	9.083E+12
7	1.970E+05	1.162E+08	5.341E+12	5.094E+12	6.157E+12	6.005E+12	5.799E+12	1.362E+07	6.422E+12	7.294E+12	7.506E+12
8	1.833E+05	3.837E+07	2.355E+12	3.042E+12	3.111E+12	2.647E+12	4.775E+06	2.923E+12	3.729E+12	5.506E+12	
9	1.876E+05	1.529E+08	1.004E+12	1.741E+12	4.903E+12	1.781E+12	1.219E+12	1.171E+08	1. 12	2.157E+12	5.032E+12
10	3.955E+07	1.222E+08	8.599E+11	1.522E+12	9.384E+12	1.558E+12	1.063E+12	8.635E+12	1.174E+12	1.906E+12	9.398E+12
11	1.469E+12	2.087E+08	7.504E+11	1.349E+12	1.658E+13	1.380E+12	9.397E+11	1.719E	1.037E+12	1.701E+12	1.659E+13
12	4.567E+08	4.359E+08	2.147E+08	2.964E+08	2.312E+13	3.059E+08	2.798E+08	2.545E+13	3.028E+08	3.581E+08	2.528E+13
13	8.178E+12	8.254E+12	1.534E+13	1.716E+13	2.533E+13	1.777E+13	1.793E+13	2.810E+13	1.934E+13	2.031E+13	2.874E+13
14	9.721E+12	1.043E+13	2.161E+13	2.430E+13	2.569E+13	2.524E+13	2.570E+13	2.843E+13	2.757E+13	2.862E+13	2.917E+13
15	1.458E+13	1.521E+13	2.404E+13	2.678E+13	2.796E+13	2.739E+13	2.835E+13	3.081E+13	3.041E+13	3.152E+13	3.192E+13
16	4.091E+11	4.097E+11	4.183E+13	4.382E+13	4.457E+13	4.521E+13	4.666E+13	4.840E+13	4.989E+13	5.119E+13	5.128E+13
17	2.774E+13	2.775E+13	2.789E+13	2.887E+13	2.930E+13	2.972E+13	3.073E+13	3.179E+13	3.280E+13	3.356E+13	3.361E+13
18	1.420E+13	1.420E+13	1.427E+13	1.476E+13	1.498E+13	1.520E+13	1.571E+13	1.625E+13	1.679E+13	1.720E+13	1.722E+13
19	2.307E+12	2.307E+12	2.313E+12	2.404E+12	2.452E+12	2.499E+12	2.593E+12	2.672E+12	2.749E+12	2.803E+12	2.806E+12

PLANE NUMBER 5

	1	2	3	4	5	6	7	8	9	10	11
1	3.008E+12	3.010E+12	3.026E+12	3.346E+12	3.531E+12	5.227E+12	8.456E+12	9.447E+12	1.027E+13	1.058E+13	1.060E+13
2	2.353E+12	2.354E+12	2.375E+12	2.789E+12	3.152E+12	5.497E+12	7.985E+12	8.601E+12	9.114E+12	9.344E+12	9.357E+12
3	1.736E+12	1.737E+12	1.755E+12	2.110E+12	3.125E+12	4.835E+12	5.975E+12	6.292E+12	6.562E+12	6.739E+12	6.749E+12
4	7.719E+07	7.727E+07	1.693E+08	1.922E+08	1.453E+08	1.708E+08	1.854E+08	9.259E+07	2.039E+08	2.194E+08	2.201E+08
5	5.042E+05	5.511E+08	5.865E+12	6.324E+12	6.361E+12	6.386E+12	6.245E+12	6.274E+07	6.874E+12	7.702E+12	7.742E+12
6	3.781E+05	3.816E+08	8.863E+12	7.192E+12	7.231E+12	7.237E+12	9.569E+12	4.501E+07	1.062E+13	1.230E+13	1.238E+13
7	2.660E+05	1.564E+08	7.191E+12	7.876E+12	8.225E+12	8.039E+12	7.855E+12	1.849E+07	8.735E+12	9.686E+12	1.016E+13
8	2.465E+05	5.174E+07	3.175E+12	4.058E+12	4.156E+12	3.589E+12	6.485E+06	3.977E+12	5.029E+12	7.372E+12	
9	2.520E+05	2.083E+08	1.369E+12	2.323E+12	6.456E+12	2.380E+12	1.668E+12	1.540E+08	1.848E+12	2.905E+12	6.698E+12
10	5.303E+07	1.668E+08	1.174E+12	2.031E+12	1.226E+13	2.083E+12	1.455E+12	1.131E+13	1.612E+12	2.566E+12	1.239E+13
11	1.970E+12	2.823E+08	1.025E+12	1.800E+12	2.143E+13	1.845E+12	1.287E+12	2.232E+13	1.424E+12	2.289E+12	2.159E+13
12	5.753E+08	5.471E+08	3.031E+08	3.814E+08	2.944E+13	3.937E+08	3.617E+08	3.254E+13	3.924E+08	4.635E+08	3.231E+13
13	1.026E+13	1.036E+13	1.958E+13	2.181E+13	3.193E+13	2.259E+13	2.288E+13	3.551E+13	2.472E+13	2.594E+13	3.626E+13
14	1.219E+13	1.308E+13	2.718E+13	3.049E+13	3.229E+13	3.168E+13	3.230E+13	3.588E+13	3.471E+13	3.601E+13	3.676E+13
15	1.822E+13	1.901E+13	3.014E+13	3.349E+13	3.501E+13	3.475E+13	3.552E+13	3.874E+13	3.815E+13	3.952E+13	4.007E+13
16	2.600E+13	5.011E+13	5.116E+13	5.347E+13	5.437E+13	5.515E+13	5.698E+13	5.914E+13	6.095E+13	5.250E+13	6.261E+13
17	3.283E+13	3.294E+13	3.300E+13	3.411E+13	3.461E+13	3.510E+13	3.632E+13	3.757E+13	3.877E+13	3.964E+13	3.969E+13
18	1.698E+13	1.698E+13	1.695E+13	1.752E+13	1.777E+13	1.803E+13	1.865E+13	1.930E+13	1.994E+13	2.041E+13	2.044E+13
19	2.586E+12	2.587E+12	2.593E+12	2.699E+12	2.755E+12	2.810E+12	2.917E+12	3.005E+12	3.092E+12	3.152E+12	3.156E+12

PLANE NUMBER 6

	1	2	3	4	5	6	7	8	9	10	11

	1	2	3	4	5	6	7	8	9	10	11
1	5.403E+12	5.404E+12	5.426E+12	5.838E+12	6.076E+12	8.250E+12	1.240E+13	1.370E+13	1.479E+13	1.519E+13	1.522E+13
2	4.406E+12	4.408E+12	4.434E+12	4.976E+12	5.472E+12	8.429E+12	1.163E+13	1.246E+13	1.316E+13	1.347E+13	1.349E+13
3	3.404E+12	3.405E+12	3.427E+12	3.873E+12	5.113E+12	7.210E+12	8.696E+12	9.121E+12	9.539E+12	9.787E+12	9.801E+12
4	1.546E+08	1.547E+08	2.824E+08	3.112E+08	2.151E+08	2.479E+08	2.695E+08	1.396E+08	2.970E+08	3.181E+08	3.191E+08
5	4.376E+06	7.690E+08	8.186E+12	8.762E+12	8.817E+12	8.868E+12	8.810E+12	9.330E+07	9.750E+12	1.087E+13	1.092E+13
6	4.241E+06	5.297E+08	1.223E+13	9.978E+12	9.996E+12	1.005E+13	1.333E+13	6.762E+07	1.519E+13	1.709E+13	1.719E+13
7	3.468E+06	2.175E+08	9.927E+12	1.073E+13	1.117E+13	1.098E+13	1.091E+13	3.092E+07	1.218E+13	1.362E+13	1.397E+13
8	2.541E+06	6.639E+07	4.567E+12	5.631E+12	8.872E+12	5.782E+12	5.194E+12	1.365E+07	5.759E+12	7.033E+12	9.967E+12
9	2.090E+06	3.176E+08	2.075E+12	3.320E+12	8.830E+12	3.414E+12	2.548E+12	2.162E+08	2.817E+12	4.170E+12	9.260E+12
10	7.307E+07	2.569E+08	1.808E+12	2.929E+12	1.647E+13	3.014E+12	2.254E+12	1.533E+13	2.489E+12	3.711E+12	1.680E+13
11	2.715E+12	4.133E+08	1.592E+12	2.606E+12	2.837E+13	2.682E+12	2.005E+12	2.992E+13	2.213E+12	3.321E+12	2.877E+13
12	7.563E+08	7.171E+08	4.102E+08	5.096E+08	3.839E+13	5.265E+08	4.895E+08	4.286E+13	5.317E+08	6.221E+08	8.228E+13
13	1.345E+13	1.354E+13	2.564E+13	2.833E+13	4.123E+13	2.934E+13	2.988E+13	4.620E+13	3.233E+13	3.381E+13	4.691E+13
14	1.594E+13	1.708E+13	3.517E+13	3.917E+13	4.164E+13	4.064E+13	4.161E+13	4.662E+13	4.476E+13	4.634E+13	4.749E+13
15	2.353E+13	2.455E+13	3.878E+13	4.282E+13	4.486E+13	4.440E+13	4.553E+13	4.997E+13	4.894E+13	5.059E+13	5.142E+13
16	6.162E+13	6.171E+13	6.298E+13	6.557E+13	6.664E+13	6.757E+13	6.992E+13	7.259E+13	7.481E+13	7.660E+13	7.673E+13
17	3.894E+13	3.895E+13	3.913E+13	4.035E+13	4.092E+13	4.151E+13	4.298E+13	4.445E+13	4.586E+13	4.684E+13	4.690E+13
18	2.004E+13	2.004E+13	2.016E+13	2.078E+13	2.108E+13	2.138E+13	2.215E+13	2.292E+13	2.367E+13	2.421E+13	2.424E+13
19	2.888E+12	2.898E+12	2.896E+12	3.019E+12	3.087E+12	3.152E+12	3.273E+12	3.370E+12	3.467E+12	3.534E+12	3.538E+12

PLANE NUMBER 7

	1	2	3	4	5	6	7	8	9	10	11
1	1.581E+13	1.581E+13	1.583E+13	1.612E+13	1.629E+13	1.788E+13	2.130E+13	2.262E+13	2.377E+13	2.424E+13	2.427E+13
2	1.569E+13	1.569E+13	1.571E+13	1.609E+13	1.632E+13	1.863E+13	2.193E+13	2.313E+13	2.418E+13	2.467E+13	2.470E+13
3	1.575E+13	1.575E+13	1.575E+13	1.619E+13	1.723E+13	1.930E+13	2.199E+13	2.315E+13	2.420E+13	2.473E+13	2.476E+13
4	1.620E+13	1.619E+13	1.607E+13	1.656E+13	1.764E+13	1.876E+13	2.151E+13	2.283E+13	2.385E+13	2.440E+13	2.444E+13
5	1.668E+13	1.669E+13	1.797E+13	1.702E+13	1.740E+13	1.798E+13	2.158E+13	2.293E+13	2.395E+13	2.469E+13	2.473E+13
6	1.686E+13	1.697E+13	1.833E+13	1.476E+13	1.492E+13	1.493E+13	2.051E+13	2.326E+13	2.	13	2.432E+13	2.439E+13
7	1.404E+13	1.404E+13	1.477E+13	1.504E+13	1.560E+13	1.544E+13	1.661E+13	2.407E+13	1.839E+13	1.924E+13	1.965E+13
8	9.987E+12	9.985E+12	9.640E+12	1.077E+13	1.510E+13	1.112E+13	1.150E+13	2.441E+13	1.227E+13	1.337E+13	1.732E+13
9	7.910E+12	7.902E+12	7.779E+12	9.351E+12	1.680E+13	9.680E+12	9.346E+12	2.449E+13	1.017E+13	1.151E+13	1.846E+13
10	9.054E+08	1.800E+09	7.137E+12	8.583E+12	2.646E+13	8.892E+12	8.590E+12	3.473E+13	9.344E+12	1.060E+13	2.796E+13
11	4.354E+12	1.203E+09	6.476E+12	7.797E+12	4.118E+13	8.080E+12	7.804E+12	5.021E+13	8.488E+12	9.646E+12	4.267E+13
12	1.310E+09	1.244E+09	8.135E+08	9.331E+08	5.306E+13	9.647E+08	9.559E+08	6.236E+13	1.036E+09	1.135E+09	5.879E+13
13	2.310E+13	2.324E+13	3.602E+13	3.863E+13	5.633E+13	3.990E+13	4.117E+13	6.191E+13	4.452E+13	4.603E+13	6.431E+13
14	2.665E+13	2.801E+13	4.950E+13	5.345E+13	5.673E+13	5.524E+13	5.706E+13	6.420E+13	6.130E+13	6.305E+13	6.490E+13
15	3.608E+13	3.724E+13	5.357E+13	5.753E+13	6.095E+13	5.943E+13	6.143E+13	6.742E+13	6.603E+13	6.777E+13	6.895E+13
16	7.363E+13	7.372E+13	7.496E+13	7.739E+13	7.850E+13	7.955E+13	8.245E+13	8.550E+13	8.812E+13	8.998E+13	9.011E+13
17	4.404E+13	4.405E+13	4.422E+13	4.543E+13	4.604E+13	4.668E+13	4.835E+13	4.997E+13	5.152E+13	5.251E+13	5.259E+13
18	2.270E+13	2.271E+13	2.278E+13	2.341E+13	2.373E+13	2.407E+13	2.495E+13	2.580E+13	2.662E+13	2.718E+13	2.721E+13
19	3.085E+12	3.086E+12	3.094E+12	3.236E+12	3.321E+12	3.397E+12	3.526E+12	3.627E+12	3.731E+12	3.803E+12	3.807E+12

PLANE NUMBER 8

	1	2	3	4	5	6	7	8	9	10	11
1	2.015E+13	2.016E+13	2.017E+13	2.040E+13	2.054E+13	2.185E+13	2.483E+13	2.609E+13	2.721E+13	2.769E+13	2.771E+13
2	2.002E+13	2.002E+13	2.003E+13	2.031E+13	2.051E+13	2.233E+13	2.528E+13	2.651E+13	2.761E+13	2.812E+13	2.815E+13
3	2.000E+13	2.000E+13	1.999E+13	2.028E+13	2.104E+13	2.265E+13	2.518E+13	2.643E+13	2.754E+13	2.811E+13	2.814E+13
4	2.021E+13	2.021E+13	2.010E+13	2.037E+13	2.105E+13	2.188E+13	2.444E+13	2.587E+13	2.688E+13	2.744E+13	2.747E+13
5	2.056E+13	2.056E+13	2.131E+13	2.015E+13	2.044E+13	2.096E+13	2.469E+13	2.606E+13	2.730E+13	2.807E+13	2.811E+13
6	2.139E+13	2.139E+13	2.121E+13	1.783E+13	1.799E+13	1.801E+13	2.361E+13	2.703E+13	2.671E+13	2.777E+13	2.784E+13
7	2.317E+13	2.314E+13	1.900E+13	1.896E+13	1.929E+13	1.947E+13	2.111E+13	3.045E+13	2.332E+13	2.415E+13	2.429E+13
8	2.590E+13	2.590E+13	2.412E+13	2.516E+13	2.597E+13	2.597E+13	2.674E+13	3.417E+13	2.919E+13	3.065E+13	3.137E+13
9	2.732E+13	2.744E+13	2.986E+13	3.149E+13	3.368E+13	3.254E+13	3.311E+13	3.587E+13	3.602E+13	3.802E+13	3.911E+13
10	3.785E+13	3.377E+13	3.079E+13	3.244E+13	4.506E+13	3.353E+13	3.411E+13	4.940E+13	3.711E+13	3.918E+13	5.113E+13
11	5.219E+13	4.097E+13	3.164E+13	3.330E+13	6.157E+13	3.443E+13	3.504E+13	6.866E+13	3.812E+13	4.024E+13	6.837E+13
12	6.109E+13	5.937E+13	4.862E+13	5.066E+13	7.263E+13	5.229E+13	5.389E+13	8.065E+13	5.858E+13	6.104E+13	8.327E+13
13	5.951E+13	5.958E+13	7.063E+13	7.315E+13	7.538E+13	7.538E+13	7.848E+13	7.911E+13	8.496E+13	8.718E+13	8.304E+13
14	6.016E+13	6.076E+13	7.014E+13	7.282E+13	7.233E+13	7.500E+13	7.816E+13	7.940E+13	8.415E+13	8.570E+13	8.350E+13
15	6.385E+13	6.440E+13	7.213E+13	7.481E+13	7.491E+13	7.703E+13	8.025E+13	8.209E+13	8.631E+13	8.788E+13	8.652E+13
16	8.116E+13	8.122E+13	8.207E+13	8.417E+13	8.518E+13	8.633E+13	8.953E+13	9.254E+13	9.557E+13	9.739E+13	9.745E+13
17	4.664E+13	4.665E+13	4.680E+13	4.797E+13	4.859E+13	4.925E+13	5.102E+13	5.268E+13	5.428E+13	5.529E+13	5.533E+13
18	2.401E+13	2.401E+13	2.407E+13	2.469E+13	2.503E+13	2.538E+13	2.631E+13	2.719E+13	2.804E+13	2.859E+13	2.862E+13
19	3.172E+12	3.173E+12	3.181E+12	3.336E+12	3.435E+12	3.519E+12	3.652E+12	3.752E+12	3.859E+12	3.934E+12	3.939E+12

PLANE NUMBER 9

	1	2	3	4	5	6	7	8	9	10	11
1	2.530E+13	2.530E+13	2.530E+13	2.539E+13	2.545E+13	2.601E+13	2.763E+13	2.854E+13	2.933E+13	2.976E+13	2.979E+13
2	2.522E+13	2.522E+13	2.521E+13	2.528E+13	2.536E+13	2.601E+13	2.780E+13	2.885E+13	2.978E+13	3.023E+13	3.025E+13
3	2.522E+13	2.522E+13	2.516E+13	2.516E+13	2.524E+13	2.593E+13	2.775E+13	2.898E+13	2.990E+13	3.037E+13	3.040E+13
4	2.549E+13	2.547E+13	2.514E+13	2.509E+13	2.529E+13	2.567E+13	2.753E+13	2.934E+13	2.968E+13	3.005E+13	3.007E+13
5	2.605E+13	2.604E+13	2.466E+13	2.379E+13	2.395E+13	2.471E+13	2.729E+13	3.002E+13	2.972E+13	3.033E+13	3.036E+13
6	2.812E+13	2.809E+13	2.354E+13	2.249E+13	2.255E+13	2.265E+13	2.589E+13	3.262E+13	2.898E+13	2.988E+13	2.993E+13
7	3.388E+13	3.381E+13	2.234E+13	2.220E+13	2.245E+13	2.273E+13	2.450E+13	3.936E+13	2.692E+13	2.761E+13	2.766E+13
8	3.913E+13	3.912E+13	3.480E+13	3.556E+13	3.611E+13	3.655E+13	3.776E+13	4.539E+13	4.106E+13	4.258E+13	4.238E+13
9	4.134E+13	4.158E+13	4.579E+13	4.703E+13	4.772E+13	4.838E+13	4.955E+13	4.795E+13	5.376E+13	5.591E+13	5.540E+13
10	5.361E+13	4.970E+13	4.706E+13	4.832E+13	5.983E+13	4.972E+13	5.091E+13	6.279E+13	5.523E+13	5.747E+13	6.829E+13
11	7.057E+13	5.824E+13	4.810E+13	4.937E+13	7.697E+13	5.081E+13	5.203E+13	8.341E+13	5.644E+13	5.874E+13	8.617E+13
12	8.183E+13	7.944E+13	6.605E+13	6.743E+13	8.747E+13	6.931E+13	7.166E+13	9.503E+13	7.769E+13	8.021E+13	1.002E+14
13	8.075E+13	8.078E+13	8.817E+13	8.942E+13	8.602E+13	9.174E+13	9.575E+13	9.273E+13	1.034E+14	1.054E+14	9.890E+13
14	8.113E+13	8.146E+13	8.679E+13	8.788E+13	8.634E+13	9.002E+13	9.407E+13	9.304E+13	1.011E+14	1.023E+14	9.930E+13
15	8.353E+13	8.394E+13	8.814E+13	8.927E+13	9.141E+13	9.549E+13	9.535E+13	1.025E+14	1.038E+14	1.017E+14	
16	8.859E+13	8.862E+13	8.913E+13	9.056E+13	9.135E+13	9.246E+13	9.584E+13	9.866E+13	1.020E+14	1.037E+14	1.036E+14
17	4.895E+13	4.896E+13	4.907E+13	5.015E+13	5.074E+13	5.141E+13	5.323E+13	5.490E+13	5.648E+13	5.740E+13	5.744E+13
18	2.508E+13	2.509E+13	2.513E+13	2.574E+13	2.609E+13	2.646E+13	2.741E+13	2.829E+13	2.912E+13	2.964E+13	2.967E+13
19	3.230E+12	3.231E+12	3.240E+12	3.415E+12	3.541E+12	3.636E+12	3.770E+12	3.865E+12	3.977E+12	4.054E+12	4.061E+12

PLANE NUMBER 10

	1	2	3	4	5	6	7	8	9	10	11
1	3.383E+13	3.383E+13	3.381E+13	3.334E+13	3.306E+13	3.001E+13	2.552E+13	2.485E+13	2.443E+13	2.439E+13	2.439E+13
2	3.422E+13	3.421E+13	3.418E+13	3.359E+13	3.312E+13	2.823E+13	2.527E+13	2.542E+13	2.542E+13	2.558E+13	2.558E+13
3	3.444E+13	3.444E+13	3.436E+13	3.373E+13	3.124E+13	2.766E+13	2.686E+13	2.762E+13	2.7??E+13	2.810E+13	2.811E+13
4	3.441E+13	3.419E+13	3.405E+13	3.353E+13	3.302E+13	3.256E+13	3.276E+13	3.487E+13	3.400E+13	3.402E+13	3.402E+13
5	3.437E+13	3.433E+13	2.788E+13	2.835E+13	2.833E+13	2.832E+13	2.853E+13	3.61?E+13	3.009E+13	3.007E+13	3.008E+13
6	3.561E+13	3.554E+13	2.303E+13	3.007E+13	3.017E+13	3.019E+13	2.473E+13	3.926E+13	2.668E+13	2.683E+13	2.685E+13
7	4.248E+13	4.236E+13	2.189E+13	2.242E+13	2.266E+13	2.282E+13	2.357E+13	4.722E+13	2.559E+13	2.584E+13	2.591E+13
8	4.817E+13	4.811E+13	3.780E+13	3.860E+13	3.946E+13	3.938E+13	4.020E+13	5.352E+13	4.346E+13	4.489E+13	4.514E+13
9	5.018E+13	5.020E+13	5.120E+13	5.238E+13	5.362E+13	5.343E+13	5.439E+13	5.580E+13	5.861E+13	6.078E+13	6.102E+13
10	5.920E+13	5.534E+13	5.238E+13	5.356E+13	6.280E+13	5.465E+13	5.564E+13	6.654E+13	5.997E+13	6.219E+13	7.075E+13
11	7.113E+13	6.133E+13	5.324E+13	5.441E+13	7.524E+13	5.553E+13	5.656E+13	8.065E+13	6.097E+13	6.321E+13	8.369E+13
12	7.861E+13	7.716E+13	6.845E+13	6.938E+13	8.241E+13	7.073E+13	7.288E+13	8.764E+13	7.852E+13	8.063E+13	9.327E+13
13	7.721E+13	7.727E+13	8.733E+13	8.744E+13	8.094E+13	8.895E+13	9.279E+13	8.496E+13	9.959E+13	1.007E+14	9.181E+13
14	7.777E+13	7.832E+13	8.697E+13	8.649E+13	8.153E+13	8.775E+13	9.188E+13	8.552E+13	9.814E+13	9.835E+13	9.251E+13
15	8.059E+13	8.109E+13	8.810E+13	8.767E+13	8.409E+13	8.891E+13	8.839E+13	9.927E+13	9.953E+13	9.533E+13	
16	8.628E+13	8.632E+13	8.686E+13	8.744E+13	8.758E+13	8.940E+13	9.140E+13	9.356E+13	9.674E+13	9.796E+13	9.785E+13
17	4.753E+13	4.753E+13	4.763E+13	4.864E+13	4.913E+13	4.981E+13	5.148E+13	5.309E+13	5.441E+13	5.519E+13	5.518E+13
18	2.416E+13	2.416E+13	2.420E+13	2.483E+13	2.510E+13	2.565E+13	2.652E+13	2.733E+13	2.804E+13	2.849E+13	2.852E+13
19	3.146E+12	3.147E+12	3.156E+12	3.349E+12	3.519E+12	3.618E+12	3.744E+12	3.82?E+12	3.942E+12	4.021E+12	4.032E+12

PLANE NUMBER 11

	1	2	3	4	5	6	7	8	9	10	11
1	3.969E+13	3.969E+13	3.967E+13	3.927E+13	3.902E+13	3.613E+13	3.211E+13	3.156E+13	3.123E+13	3.122E+13	3.122E+13
2	4.040E+13	4.040E+13	4.038E+13	3.986E+13	3.932E+13	3.491E+13	3.191E+13	3.200E+13	3.222E+13	3.240E+13	3.241E+13
3	4.117E+13	4.117E+13	4.120E+13	4.076E+13	3.824E+13	3.492E+13	3.429E+13	3.478E+13	3.537E+13	3.566E+13	3.568E+13
4	4.204E+13	4.206E+13	4.233E+13	4.222E+13	4.308E+13	4.342E+13	4.401E+13	4.450E+13	4.547E+13	4.578E+13	4.580E+13
5	4.065E+13	4.062E+13	3.488E+13	3.495E+13	3.521E+13	3.543E+13	3.636E+13	3.805E+13	3.819E+13	3.821E+13	
6	4.067E+13	4.061E+13	3.012E+13	3.497E+13	3.505E+13	3.510E+13	3.173E+13	4.435E+13	3.407E+13	3.436E+13	3.440E+13
7	4.749E+13	4.737E+13	2.835E+13	2.872E+13	2.907E+13	2.905E+13	2.998E+13	5.213E+13	3.244E+13	3.287E+13	3.309E+13
8	5.549E+13	5.541E+13	4.234E+13	4.328E+13	4.631E+13	4.390E+13	4.463E+13	6.052E+13	4.801E+13	4.975E+13	5.240E+13
9	5.951E+13	5.929E+13	5.604E+13	5.750E+13	6.304E+13	5.832E+13	5.896E+13	6.464E+13	6.333E+13	6.594E+13	7.101E+13
10	6.272E+13	6.242E+13	5.710E+13	5.856E+13	6.580E+13	5.940E+13	6.008E+13	6.791E+13	6.453E+13	6.717E+13	7.408E+13
11	6.516E+13	6.512E+13	6.340E+13	6.462E+13	6.818E+13	6.555E+13	6.660E+13	7.043E+13	7.176E+13	7.420E+13	7.675E+13
12	6.779E+13	6.781E+13	7.806E+13	7.858E+13	7.080E+13	7.314E+13	7.678E+13	8.034E+13	9.018E+13	7.970E+13	
13	7.079E+13	7.090E+13	8.939E+13	8.883E+13	7.385E+13	8.984E+13	9.378E+13	7.629E+13	1.003E+14	1.010E+14	8.317E+13
14	7.285E+13	7.370E+13	8.713E+13	8.587E+13	7.606E+13	8.657E+13	9.068E+13	7.849E+13	9.659E+13	9.631E+13	8.569E+13
15	7.761E+13	7.829E+13	8.793E+13	8.052E+13	8.677E+13	9.145E+13	8.344E+13	9.733E+13	9.716E+13	9.060E+13	
16	8.465E+13	8.469E+13	8.525E+13	8.542E+13	8.513E+13	8.581E+13	8.861E+13	9.046E+13	9.352E+13	9.455E+13	9.437E+13
17	4.660E+13	4.661E+13	4.670E+13	4.769E+13	4.810E+13	4.881E+13	5.040E+13	5.201E+13	5.318E+13	5.389E+13	5.384E+13

	1	2	3	4	5	6	7	8	9	10	11
18	2.359E+13	2.360E+13	2.364E+13	2.429E+13	2.498E+13	2.527E+13	2.608E+13	2.685E+13	2.752E+19	2.795E+13	2.800E+13
19	3.096E+12	3.097E+12	3.106E+12	3.306E+12	3.499E+12	3.598E+12	3.721E+12	3.796E+12	3.913E+12	3.993E+12	4.006E+12

PLANE NUMBER 12

	1	2	3	4	5	6	7	8	9	10	11
1	6.666E+13	6.667E+13	6.679E+13	6.952E+13	7.231E+13	7.607E+13	8.052E+13	8.186E+13	8.298E+13	8.343E+13	8.345E+13
2	6.510E+13	6.510E+13	6.517E+13	6.679E+13	6.987E+13	7.497E+13	7.832E+13	7.953E+13	8.063E+13	8.116E+13	8.119E+13
3	6.352E+13	6.353E+13	6.362E+13	6.474E+13	6.956E+13	7.184E+13	7.369E+13	7.483E+13	7.605E+13	7.667E+13	7.670E+13
4	6.225E+13	6.228E+13	6.258E+13	6.282E+13	6.353E+13	6.416E+13	6.539E+13	6.609E+13	6.747E+13	6.805E+13	6.808E+13
5	6.501E+13	6.535E+13	7.021E+13	6.918E+13	6.949E+13	6.999E+13	7.274E+13	6.886E+13	7.610E+13	7.717E+13	7.722E+13
6	6.526E+13	6.573E+13	7.249E+13	5.964E+13	5.940E+13	5.986E+13	7.495E+13	7.012E+13	8.067E+13	8.232E+11	8.242E+13
7	6.531E+13	6.541E+13	6.697E+13	6.652E+13	6.681E+13	6.682E+13	6.946E+13	7.090E+13	7.522E+13	7.692E+13	7.723E+13
8	6.645E+13	6.634E+13	6.477E+13	6.570E+13	6.860E+13	6.630E+13	6.757E+13	7.176E+13	7.268E+13	7.513E+13	7.767E+13
9	6.628E+13	6.604E+13	6.259E+13	6.389E+13	6.821E+13	6.455E+13	6.536E+13	7.119E+13	7.012E+13	7.280E+13	7.665E+13
10	6.756E+13	6.712E+13	6.116E+13	6.443E+13	6.952E+13	6.510E+13	6.594E+13	7.239E+13	7.074E+13	7.340E+13	7.804E+13
11	6.888E+13	6.885E+13	6.872E+13	6.967E+13	7.094E+13	7.033E+13	7.168E+13	7.364E+13	7.696E+13	7.926E+13	7.957E+13
12	7.064E+13	7.067E+13	8.068E+13	8.086E+13	7.277E+13	8.149E+13	8.396E+13	7.530E+13	8.992E+13	9.167E+13	8.153E+13
13	7.294E+13	7.303E+13	8.917E+13	8.822E+13	7.507E+13	8.859E+13	9.209E+13	7.745E+13	9.824E+13	9.889E+13	8.399E+13
14	7.465E+13	7.539E+13	8.707E+13	8.545E+13	7.687E+13	8.919E+13	8.192E+13	7.915E+13	9.477E+13	9.457E+13	8.595E+13
15	7.873E+13	7.933E+13	8.774E+13	8.622E+13	8.058E+13	8.626E+13	8.984E+13	8.118E+13	9.537E+13	9.527E+13	8.988E+13
16	8.313E+13	8.316E+13	8.364E+13	8.350E+13	8.277E+13	8.331E+13	8.593E+13	8.761E+13	9.047E+13	9.136E+13	9.115E+13
17	4.570E+13	4.571E+13	4.580E+13	4.678E+13	4.709E+13	4.786E+13	4.937E+13	5.104E+13	5.204E+13	5.269E+13	5.259E+13
18	2.306E+13	2.307E+13	2.311E+13	2.382E+13	2.498E+13	2.511E+13	2.586E+13	2.656E+13	2.724E+13	2.766E+13	2.779E+13
19	3.049E+12	3.049E+12	3.059E+12	3.264E+12	3.478E+12	3.575E+12	3.694E+12	3.763E+12	3.882E+12	3.962E+12	3.978E+12

PLANE NUMBER 13

	1	2	3	4	5	6	7	8	9	10	11
1	8.934E+13	8.935E+13	8.945E+13	9.149E+13	9.302E+13	9.470E+13	9.775E+13	9.897E+13	1.000E+14	1.005E+14	1.005E+14
2	8.626E+13	8.626E+13	8.632E+13	8.771E+13	8.957E+13	9.184E+13	9.448E+13	9.575E+13	9.692E+13	9.751E+13	9.754E+13
3	8.173E+13	8.173E+13	8.180E+13	8.265E+13	8.475E+13	8.624E+13	8.803E+13	8.933E+13	9. 13	9.137E+13	9.141E+13
4	7.096E+13	7.097E+13	7.114E+13	7.129E+13	7.178E+13	7.228E+13	7.348E+13	7.441E+13	7.571E+13	7.633E+13	7.637E+13
5	8.282E+13	8.297E+13	8.504E+13	8.410E+13	8.432E+13	8.473E+13	8.727E+13	8.677E+13	9.111E+13	9.227E+13	9.233E+13
6	8.567E+13	8.592E+13	8.938E+13	8.122E+13	8.006E+13	8.118E+13	9.104E+13	9.030E+13	9.772E+13	9.961E+13	9.971E+13
7	8.211E+13	8.216E+13	8.287E+13	8.211E+13	8.206E+13	8.203E+13	8.490E+13	8.770E+13	9.198E+13	9.404E+13	9.430E+13
8	7.700E+13	7.699E+13	7.538E+13	7.587E+13	7.785E+13	7.617E+13	7.785E+13	8.226E+13	8.380E+13	8.628E+13	8.815E+13
9	6.798E+13	6.775E+13	6.449E+13	6.569E+13	6.951E+13	6.630E+13	6.717E+13	7.281E+13	7.205E+13	7.471E+13	7.819E+13
10	6.905E+13	6.884E+13	6.519E+13	6.634E+13	7.074E+13	6.692E+13	6.784E+13	7.375E+13	7.275E+13	7.536E+13	7.935E+13
11	7.021E+13	7.020E+13	7.234E+13	7.290E+13	7.201E+13	7.327E+13	7.477E+13	7.480E+13	8.006E+13	8.227E+13	8.068E+13
12	7.196E+13	7.199E+13	8.267E+13	8.236E+13	7.378E+13	8.253E+13	8.497E+13	7.634E+13	9.077E+13	9.228E+13	8.250E+13
13	7.501E+13	7.512E+13	8.825E+13	8.678E+13	7.663E+13	8.651E+13	8.964E+13	7.896E+13	9.529E+13	9.571E+13	8.538E+13
14	7.652E+13	7.715E+13	8.705E+13	8.529E+13	7.814E+13	8.504E+13	8.840E+13	8.037E+13	9.381E+13	9.372E+13	8.696E+13
15	7.997E+13	8.048E+13	8.774E+13	8.607E+13	8.113E+13	8.575E+13	8.904E+13	8.363E+13	9.440E+13	9.441E+13	9.004E+13
16	8.234E+13	8.237E+13	8.281E+13	8.250E+13	8.150E+13	8.200E+13	8.452E+13	8.612E+13	8.888E+13	8.970E+13	8.948E+13
17	4.523E+13	4.523E+13	4.532E+13	4.631E+13	4.655E+13	4.736E+13	4.884E+13	5.054E+13	5.144E+13	5.200E+13	5.194E+13
18	2.279E+13	2.279E+13	2.284E+13	2.358E+13	2.515E+13	2.514E+13	2.585E+13	2.649E+13	2.720E+13	2.762E+13	2.781E+13
19	3.024E+12	3.025E+12	3.034E+12	3.242E+12	3.467E+12	3.562E+12	3.679E+12	3.745E+12	3.865E+12	3.945E+12	3.963E+12

PLANE NUMBER 14

	1	2	3	4	5	6	7	8	9	10	11
1	9.992E+13	9.992E+13	9.996E+13	1.008E+14	1.013E+14	1.018E+14	1.031E+14	1.039E+14	1.046E+14	1.049E+14	1.050E+14
2	9.604E+13	9.604E+13	9.606E+13	9.667E+13	9.723E+13	9.784E+13	9.918E+13	1.002E+14	1.012E+14	1.017E+14	1.017E+14
3	9.030E+13	9.030E+13	9.032E+13	9.059E+13	9.108E+13	9.159E+13	9.279E+13	9.398E+13	9.517E+13	9.582E+13	9.586E+13
4	8.121E+13	8.121E+13	8.126E+13	8.121E+13	8.145E+13	8.175E+13	8.281E+13	8.394E+13	8.518E+13	8.585E+13	8.588E+13
5	9.094E+13	9.096E+13	9.129E+13	9.044E+13	9.045E+13	9.063E+13	9.230E+13	9.368E+13	9.592E+13	9.694E+13	9.700E+13
6	9.664E+13	9.669E+13	9.748E+13	9.342E+13	9.204E+13	9.278E+13	9.721E+13	9.935E+13	1.037E+14	1.054E+14	1.055E+14
7	9.226E+13	9.227E+13	9.243E+13	9.114E+13	9.054E+13	9.034E+13	9.295E+13	9.634E+13	1.007E+14	1.028E+14	1.030E+14
8	8.889E+13	8.897E+13	8.863E+13	8.801E+13	8.789E+13	8.747E+13	8.965E+13	9.302E+13	9.655E+13	9.875E+13	9.922E+13
9	8.890E+13	8.891E+13	8.895E+13	8.851E+13	8.835E+13	8.811E+13	9.030E+13	9.324E+13	9.695E+13	9.909E+13	9.944E+13
10	8.417E+13	8.427E+13	8.564E+13	8.499E+13	8.395E+13	8.450E+13	8.662E+13	8.787E+13	9.263E+13	9.437E+13	9.388E+13
11	8.310E+13	8.329E+13	8.607E+13	8.607E+13	8.299E+13	8.455E+13	8.678E+13	8.650E+13	9.260E+13	9.405E+13	9.252E+13
12	8.261E+13	8.297E+13	8.824E+13	8.679E+13	8.290E+13	8.611E+13	8.875E+13	8.591E+13	9.439E+13	9.520E+13	9.213E+13
13	7.932E+13	7.982E+13	8.710E+13	8.516E+13	8.012E+13	8.443E+13	8.733E+13	8.230E+13	9.255E+13	9.269E+13	8.865E+13
14	7.959E+13	8.009E+13	8.710E+13	8.517E+13	8.034E+13	8.447E+13	8.742E+13	8.251E+13	9.264E+13	9.273E+13	8.884E+13

	1	2	3	4	5	6	7	8	9	10	11
13	8.195E+13	8.235E+13	8.798E+13	8.597E+13	8.209E+13	8.515E+13	8.890E+13	8.445E+13	9.315E+13	9.332E+13	9.044E+13
16	8.126E+13	8.129E+13	8.166E+13	8.115E+13	7.973E+13	8.018E+13	8.258E+13	8.407E+13	8.679E+13	8.743E+13	8.717E+13
17	4.458E+13	4.459E+13	4.467E+13	4.566E+13	4.583E+13	4.668E+13	4.810E+13	4.987E+13	5.068E+13	5.124E+13	5.104E+13
18	2.242E+13	2.242E+13	2.246E+13	2.326E+13	2.554E+13	2.526E+13	2.592E+13	2.646E+13	2.723E+13	2.767E+13	2.797E+13
19	2.990E+12	2.991E+12	3.000E+12	3.211E+12	3.451E+12	3.544E+12	3.658E+12	3.720E+12	3.842E+12	3.922E+12	3.941E+12

PLANE NUMBER 15

	1	2	3	4	5	6	7	8	9	10	11
1	9.606E+13	9.606E+13	9.603E+13	9.613E+13	9.620E+13	9.629E+13	9.660E+13	9.696E+13	9.726E+13	9.744E+13	9.745E+13
2	9.462E+13	9.462E+13	9.455E+13	9.441E+13	9.442E+13	9.447E+13	9.435E+13	9.554E+13	9.613E+13	9.649E+13	9.651E+13
3	9.299E+13	9.299E+13	9.296E+13	9.254E+13	9.247E+13	9.245E+13	9.288E+13	9.384E+13	9.480E+13	9.534E+13	9.537E+13
4	9.194E+13	9.194E+13	9.191E+13	9.123E+13	9.106E+13	9.098E+13	9.149E+13	9.266E+13	9.389E+13	9.455E+13	9.459E+13
5	9.325E+13	9.324E+13	9.320E+13	9.202E+13	9.165E+13	9.142E+13	9.197E+13	9.345E+13	9.504E+13	9.588E+13	9.592E+13
6	9.622E+13	9.622E+13	9.615E+13	9.334E+13	9.231E+13	9.166E+13	9.269E+13	9.510E+13	9.797E+13	9.934E+13	9.939E+13
7	9.743E+13	9.742E+13	9.738E+13	9.462E+13	9.226E+13	9.141E+13	9.285E+13	9.577E+13	1.008E+14	1.027E+14	1.027E+14
8	9.329E+13	9.332E+13	9.361E+13	9.112E+13	8.876E+13	8.838E+13	8.973E+13	9.162E+13	9.628E+13	9.787E+13	9.778E+13
9	9.176E+13	9.180E+13	9.245E+13	8.992E+13	8.741E+13	8.714E+13	8.858E+13	8.981E+13	9.447E+13	9.584E+13	9.563E+13
10	9.067E+13	9.075E+13	9.186E+13	8.926E+13	8.655E+13	8.652E+13	8.799E+13	8.857E+13	9.343E+13	9.455E+13	9.414E+13
11	9.021E+13	9.031E+13	9.171E+13	8.904E+13	8.621E+13	8.630E+13	8.779E+13	8.801E+13	9.301E+13	9.400E+13	9.347E+13
12	8.968E+13	8.950E+13	9.147E+13	8.879E+13	8.584E+13	8.609E+13	8.764E+13	8.756E+13	9.273E+13	9.362E+13	9.294E+13
13	8.862E+13	8.877E+13	9.088E+13	8.826E+13	8.515E+13	8.569E+13	8.735E+13	8.684E+13	9.231E+13	9.306E+13	9.215E+13
14	8.794E+13	8.810E+13	9.031E+13	8.777E+13	8.464E+13	8.526E+13	8.699E+13	8.630E+13	9.182E+13	9.249E+13	9.152E+13
15	8.726E+13	8.741E+13	8.945E+13	8.705E+13	8.402E+13	8.456E+13	8.634E+13	8.585E+13	9.099E+13	9.159E+13	9.070E+13
16	7.882E+13	7.884E+13	7.905E+13	7.814E+13	7.540E+13	7.598E+13	7.813E+13	7.932E+13	8.171E+13	8.226E+13	8.183E+13
17	4.310E+13	4.311E+13	4.318E+13	4.422E+13	4.399E+13	4.513E+13	4.642E+13	4.841E+13	4.881E+13	4.936E+13	4.896E+13
18	2.159E+13	2.159E+13	2.163E+13	2.258E+13	2.801E+13	2.649E+13	2.698E+13	2.708E+13	2.825E+13	2.874E+13	2.961E+13
19	2.913E+12	2.914E+12	2.923E+12	3.139E+12	3.413E+12	3.498E+12	3.607E+12	3.659E+12	3.785E+12	3.865E+12	3.889E+12

PLANE NUMBER 16

	1	2	3	4	5	6	7	8	9	10	11
1	1.026E+14	1.026E+14	1.047E+14	1.048E+14	1.048E+14	1.048E+14	1.046E+14	1.027E+14	1.051E+14	1.056E+14	1.056E+14
2	1.011E+14	1.011E+14	1.038E+14	1.033E+14	1.031E+14	1.029E+14	1.027E+14	1.007E+14	1.041E+14	1.047E+14	1.047E+14
3	1.028E+14	1.028E+14	1.028E+14	1.015E+14	1.010E+14	1.006E+14	1.005E+14	1.028E+14	1.034E+14	1.035E+14	1.035E+14
4	1.013E+14	1.012E+14	1.012E+14	9.942E+13	9.845E+13	9.784E+13	9.777E+13	9.919E+13	1.009E+14	1.017E+14	1.017E+14
5	1.025E+14	1.025E+14	1.024E+14	9.980E+13	9.825E+13	9.736E+13	9.711E+13	9.886E+13	1.013E+14	1.023E+14	1.022E+14
6	1.031E+14	1.031E+14	1.030E+14	9.862E+13	9.552E+13	9.419E+13	9.427E+13	9.674E+13	1.010E+14	1.024E+14	1.021E+14
7	1.027E+14	1.026E+14	1.025E+14	9.709E+13	8.990E+13	8.903E+13	8.915E+13	9.056E+13	9.859E+13	1.003E+14	9.960E+13
8	9.729E+13	9.729E+13	9.736E+13	9.288E+13	8.714E+13	8.694E+13	8.721E+13	8.768E+13	9.356E+13	9.495E+13	9.460E+13
9	9.402E+13	9.404E+13	9.433E+13	9.001E+13	8.502E+13	8.494E+13	8.519E+13	8.511E+13	9.011E+13	9.127E+13	9.111E+13
10	9.341E+13	9.344E+13	9.389E+13	8.977E+13	8.479E+13	8.481E+13	8.517E+13	8.498E+13	8.998E+13	9.108E+13	9.085E+13
11	9.256E+13	9.260E+13	9.326E+13	8.942E+13	8.456E+13	8.467E+13	8.520E+13	8.492E+13	8.934E+13	9.097E+13	9.065E+13
12	9.168E+13	9.174E+13	9.259E+13	8.896E+13	8.418E+13	8.435E+13	8.500E+13	8.464E+13	8.964E+13	9.058E+13	9.018E+13
13	9.060E+13	9.069E+13	9.173E+13	8.833E+13	8.363E+13	8.385E+13	8.462E+13	8.420E+13	8.910E+13	8.996E+13	8.944E+13
14	8.962E+13	8.971E+13	9.084E+13	8.763E+13	8.309E+13	8.328E+13	8.413E+13	8.376E+13	8.845E+13	8.923E+13	8.865E+13
15	8.826E+13	8.834E+13	8.947E+13	8.652E+13	8.225E+13	8.237E+13	8.332E+13	8.312E+13	8.739E+13	8.809E+13	8.745E+13
16	7.664E+13	7.665E+13	7.679E+13	7.567E+13	7.077E+13	7.219E+13	7.415E+13	7.492E+13	7.730E+13	7.771E+13	7.695E+13
17	4.183E+13	4.183E+13	4.191E+13	4.301E+13	4.210E+13	4.372E+13	4.430E+13	4.725E+13	4.720E+13	4.772E+13	4.699E+13
18	2.099E+13	2.089E+13	2.093E+13	2.209E+13	3.056E+13	3.067E+13	3.067E+13	2.977E+13	3.215E+13	3.280E+13	3.518E+13
19	2.945E+12	2.846E+12	2.856E+12	3.074E+12	3.375E+12	3.452E+12	3.557E+12	3.600E+12	3.730E+12	3.810E+12	3.837E+12

PLANE NUMBER 17

	1	2	3	4	5	6	7	8	9	10	11
1	1.078E+14	1.078E+14	1.078E+14	1.073E+14	1.071E+14	1.069E+14	1.065E+14	1.066E+14	1.068E+14	1.069E+14	1.069E+14
2	1.075E+14	1.075E+14	1.075E+14	1.061E+14	1.055E+14	1.049E+14	1.042E+14	1.047E+14	1.055E+14	1.059E+14	1.059E+14
3	1.074E+14	1.074E+14	1.072E+14	1.047E+14	1.035E+14	1.025E+14	1.015E+14	1.026E+14	1.039E+14	1.046E+14	1.046E+14
4	1.071E+14	1.071E+14	1.069E+14	1.033E+14	1.009E+14	9.941E+13	9.827E+13	9.984E+13	1.022E+14	1.031E+14	1.030E+14
5	1.069E+14	1.069E+14	1.066E+14	1.020E+14	9.874E+13	9.728E+13	9.609E+13	9.783E+13	1.008E+14	1.018E+14	1.017E+14
6	1.058E+14	1.057E+14	1.054E+14	9.880E+13	9.368E+13	9.182E+13	9.086E+13	9.302E+13	9.775E+13	9.916E+13	9.897E+13
7	1.019E+14	1.019E+14	1.016E+14	9.448E+13	8.688E+13	8.618E+13	8.579E+13	8.653E+13	9.342E+13	9.495E+13	9.459E+13
8	9.792E+13	9.792E+13	9.780E+13	9.185E+13	8.533E+13	8.526E+13	8.506E+13	8.514E+13	9.016E+13	9.143E+13	9.134E+13
9	9.627E+13	9.627E+13	9.623E+13	9.078E+13	8.470E+13	8.471E+13	8.463E+13	8.461E+13	8.899E+13	9.015E+13	9.014E+13
10	9.516E+13	9.516E+13	9.518E+13	9.006E+13	8.423E+13	8.416E+13	8.420E+13	8.423E+13	8.833E+13	8.942E+13	8.936E+13
11	9.429E+13	9.430E+13	9.437E+13	8.950E+13	8.396E+13	8.374E+13	8.386E+13	8.394E+13	8.783E+13	8.887E+13	8.877E+13

	1	2	3	4	5	6	7	8	9	10	11
12	9.329E+13	9.330E+13	9.343E+13	8.884E+13	8.343E+13	8.326E+13	8.346E+13	8.360E+13	8.725E+13	8.822E+13	8.808E+13
13	9.205E+13	9.206E+13	9.224E+13	8.799E+13	8.290E+13	8.265E+13	8.295E+13	8.319E+13	8.651E+13	8.741E+13	8.721E+13
14	9.078E+13	9.079E+13	9.102E+13	8.706E+13	8.236E+13	8.201E+13	8.240E+13	8.278E+13	8.573E+13	8.656E+13	8.630E+13
15	8.898E+13	8.890E+13	8.916E+13	8.561E+13	8.159E+13	8.106E+13	8.157E+13	8.220E+13	8.454E+13	8.528E+13	8.492E+13
16	7.384E+13	7.385E+13	7.391E+13	7.258E+13	6.809E+13	6.916E+13	7.097E+13	7.248E+13	7.378E+13	7.407E+13	7.338E+13
17	4.021E+13	4.022E+13	4.029E+13	4.150E+13	4.151E+13	4.249E+13	4.354E+13	4.580E+13	4.571E+13	4.622E+13	4.586E+13
18	2.000E+13	2.001E+13	2.005E+13	2.146E+13	3.766E+13	3.269E+13	3.283E+13	3.167E+13	3.426E+13	3.499E+13	3.731E+13
19	2.759E+12	2.760E+12	2.770E+12	2.990E+12	3.323E+12	3.397E+12	3.497E+12	3.523E+12	3.664E+12	3.744E+12	3.776E+12

PLANE NUMBER 18

	1	2	3	4	5	6	7	8	9	10	11
1	1.048E+14	1.048E+14	1.048E+14	1.043E+14	1.041E+14	1.039E+14	1.035E+14	1.035E+14	1.036E+14	1.037E+14	1.037E+14
2	1.047E+14	1.047E+14	1.047E+14	1.033E+14	1.027E+14	1.022E+14	1.015E+14	1.019E+14	1.024E+14	1.027E+14	1.027E+14
3	1.045E+14	1.045E+14	1.044E+14	1.022E+14	1.010E+14	1.001E+14	9.908E+13	9.994E+13	1.010E+14	1.015E+14	1.015E+14
4	1.042E+14	1.042E+14	1.040E+14	1.009E+14	9.875E+13	9.744E+13	9.630E+13	9.753E+13	9.942E+13	1.001E+14	1.001E+14
5	1.039E+14	1.038E+14	1.036E+14	9.956E+13	9.683E+13	9.556E+13	9.438E+13	9.575E+13	9.807E+13	9.894E+13	9.889E+13
6	1.021E+14	1.020E+14	1.018E+14	9.611E+13	9.199E+13	9.042E+13	8.937E+13	9.113E+13	9.477E+13	9.599E+13	9.592E+13
7	9.746E+13	9.744E+13	9.719E+13	9.138E+13	8.600E+13	8.545E+13	8.502E+13	8.559E+13	9.018E+13	9.145E+13	9.132E+13
8	9.398E+13	9.387E+13	9.369E+13	8.885E+13	8.443E+13	8.444E+13	8.417E+13	8.421E+13	8.718E+13	8.823E+13	8.831E+13
9	9.242E+13	9.241E+13	9.226E+13	8.781E+13	8.376E+13	8.375E+13	8.357E+13	8.365E+13	8.607E+13	8.704E+13	8.715E+13
10	9.134E+13	9.133E+13	9.120E+13	8.704E+13	8.326E+13	8.306E+13	8.295E+13	8.324E+13	8.537E+13	8.629E+13	8.634E+13
11	9.049E+13	9.048E+13	9.036E+13	8.642E+13	8.296E+13	8.254E+13	8.248E+13	8.292E+13	8.482E+13	8.569E+13	8.571E+13
12	8.947E+13	8.946E+13	8.936E+13	8.566E+13	8.229E+13	8.193E+13	8.194E+13	8.255E+13	8.417E+13	8.499E+13	8.498E+13
13	8.817E+13	8.816E+13	8.808E+13	8.468E+13	8.180E+13	8.119E+13	8.126E+13	8.203E+13	8.334E+13	8.410E+13	8.404E+13
14	8.680E+13	8.679E+13	8.673E+13	8.360E+13	8.122E+13	8.043E+13	8.057E+13	8.164E+13	8.247E+13	8.317E+13	8.306E+13
15	8.473E+13	8.472E+13	8.468E+13	8.193E+13	8.037E+13	7.931E+13	7.955E+13	8.099E+13	8.115E+13	8.177E+13	8.158E+13
16	6.807E+13	6.807E+13	6.808E+13	6.722E+13	6.505E+13	6.551E+13	6.709E+13	6.947E+13	6.948E+13	6.970E+13	6.934E+13
17	3.702E+13	3.702E+13	3.709E+13	3.859E+13	4.049E+13	4.130E+13	4.279E+13	4.322E+13	4.378E+13	4.416E+13	
18	1.832E+13	1.832E+13	1.836E+13	1.992E+13	3.748E+13	3.206E+13	3.209E+13	2.553E+13	3.342E+13	3.419E+13	3.679E+13
19	2.585E+12	2.586E+12	2.595E+12	2.812E+12	3.155E+12	3.240E+12	3.333E+12	3.31..E+2	3.48?E	3.567E+12	3.600E+12

PLANE NUMBER 19

	1	2	3	4	5	6	7	8	9	10	11
1	9.788E+13	9.799E+13	9.787E+13	9.760E+13	9.748E+13	9.736E+13	9.715E+13	9.716E+13	9.718E+13	9.722E+13	9.722E+13
2	9.770E+13	9.770E+13	9.766E+13	9.698E+13	9.670E+13	9.643E+13	9.624E+13	9.624E+13	9.648E+13	9.666E+13	9.667E+13
3	9.742E+13	9.741E+13	9.735E+13	9.624E+13	9.578E+13	9.535E+13	9.481E+13	9.523E+13	9.571E+13	9.603E+13	9.605E+13
4	9.701E+13	9.701E+13	9.692E+13	9.542E+13	9.480E+13	9.424E+13	9.361E+13	9.423E+13	9.495E+13	9.540E+13	9.542E+13
5	9.653E+13	9.652E+13	9.642E+13	9.451E+13	9.375E+13	9.307E+13	9.235E+13	9.318E+13	9.414E+13	9.471E+13	9.476E+13
6	9.447E+13	9.445E+13	9.429E+13	9.130E+13	9.000E+13	8.904E+13	8.827E+13	8.959E+13	9.125E+13	9.216E+13	9.223E+13
7	8.980E+13	8.979E+13	8.963E+13	8.648E+13	8.512E+13	8.434E+13	8.400E+13	8.499E+13	8.677E+13	8.772E+13	8.781E+13
8	8.644E+13	8.643E+13	8.630E+13	8.361E+13	8.253E+13	8.207E+13	8.195E+13	8.280E+13	8.405E+13	8.488E+13	8.497E+13
9	8.507E+13	8.506E+13	8.495E+13	8.244E+13	8.163E+13	8.110E+13	8.107E+13	8.193E+13	8.299E+13	8.376E+13	8.384E+13
10	8.405E+13	8.404E+13	8.394E+13	8.158E+13	8.099E+13	8.037E+13	8.040E+13	8.131E+13	8.221E+13	8.295E+13	8.302E+13
11	8.324E+13	8.324E+13	8.314E+13	8.089E+13	8.030E+13	7.978E+13	7.987E+13	8.081E+13	8.160E+13	8.231E+13	8.237E+13
12	8.228E+13	8.227E+13	8.218E+13	8.006E+13	7.959E+13	7.907E+13	7.921E+13	8.021E+13	8.087E+13	8.155E+13	8.160E+13
13	8.103E+13	8.103E+13	8.094E+13	7.898E+13	7.867E+13	7.815E+13	7.836E+13	7.944E+13	7.994E+13	8.057E+13	8.061E+13
14	7.972E+13	7.972E+13	7.964E+13	7.783E+13	7.767E+13	7.714E+13	7.743E+13	7.861E+13	7.895E+13	7.955E+13	7.958E+13
15	7.773E+13	7.772E+13	7.766E+13	7.607E+13	7.610E+13	7.557E+13	7.598E+13	7.729E+13	7.745E+13	7.799E+13	7.801E+13
16	6.163E+13	6.163E+13	6.164E+13	6.137E+13	6.150E+13	6.157E+13	6.299E+13	6.511E+13	6.503E+13	6.526E+13	6.526E+13
17	3.356E+13	3.357E+13	3.363E+13	3.517E+13	3.817E+13	3.761E+13	3.829E+13	3.884E+13	3.992E+13	4.048E+13	4.111E+13
18	1.654E+13	1.655E+13	1.659E+13	1.785E+13	2.577E+13	2.342E+13	2.358E+13	2.086E+13	2.450E+13	2.503E+13	2.642E+13
19	2.390E+12	2.391E+12	2.400E+12	2.603E+12	2.906E+12	3.004E+12	3.091E+12	3.065E+12	3.233E+12	3.305E+12	3.333E+12

PLANE NUMBER 20

	1	2	3	4	5	6	7	8	9	10	11
1	3.642E+13	3.642E+13	3.642E+13	3.645E+13	3.646E+13	3.648E+13	3.652E+13	3.656E+13	3.659E+13	3.660E+13	3.660E+13
2	3.622E+13	3.622E+13	3.622E+13	3.626E+13	3.628E+13	3.631E+13	3.638E+13	3.643E+13	3.648E+13	3.651E+13	3.651E+13
3	3.599E+13	3.599E+13	3.599E+13	3.604E+13	3.607E+13	3.611E+13	3.620E+13	3.627E+13	3.634E+13	3.638E+13	3.638E+13
4	3.574E+13	3.574E+13	3.574E+13	3.580E+13	3.584E+13	3.588E+13	3.599E+13	3.608E+13	3.617E+13	3.621E+13	3.622E+13
5	3.546E+13	3.546E+13	3.546E+13	3.554E+13	3.558E+13	3.563E+13	3.576E+13	3.587E+13	3.597E+13	3.602E+13	3.602E+13
6	3.441E+13	3.441E+13	3.442E+13	3.452E+13	3.459E+13	3.466E+13	3.486E+13	3.501E+13	3.516E+13	3.524E+13	3.524E+13
7	3.254E+13	3.254E+13	3.255E+13	3.271E+13	3.281E+13	3.292E+13	3.320E+13	3.339E+13	3.357E+13	3.366E+13	3.366E+13
8	3.132E+13	3.132E+13	3.133E+13	3.153E+13	3.165E+13	3.178E+13	3.210E+13	3.230E+13	3.249E+13	3.258E+13	3.259E+13

1 DUMMIES: A1,B2,3J, FIXED AT 10", SHIES AT 8"

POINT POWER DISTRIBUTION (WATTS/CC)

PLANE NUMBER 1

	1	2	3	4	5	6	7	8	9	10	11
1	0.0	0.0	0.0	0.0	0.0	0.0	0.0	0.0	0.0	0.0	0.0
2	0.0	0.0	0.0	0.0	0.0	0.0	0.0	0.0	0.0	0.0	0.0
3	0.0	0.0	0.0	0.0	0.0	0.0	0.0	0.0	0.0	0.0	0.0
4	0.0	0.0	0.0	0.0	0.0	0.0	0.0	0.0	0.0	0.0	0.0
5	0.0	0.0	0.0	0.0	0.0	0.0	0.0	0.0	0.0	0.0	0.0
6	0.0	0.0	0.0	0.0	0.0	0.0	0.0	0.0	0.0	0.0	0.0
7	0.0	0.0	0.0	0.0	0.0	0.0	0.0	0.0	0.0	0.0	0.0
8	0.0	0.0	0.0	0.0	0.0	0.0	0.0	0.0	0.0	0.0	0.0
9	0.0	0.0	0.0	0.0	0.0	0.0	0.0	0.0	0.0	0.0	0.0
10	0.0	0.0	0.0	0.0	0.0	0.0	0.0	0.0	0.0	0.0	0.0
11	0.0	0.0	0.0	0.0	0.0	0.0	0.0	0.0	0.0	0.0	0.0
12	0.0	0.0	0.0	0.0	0.0	0.0	0.0	0.0	0.0	0.0	0.0
13	0.0	0.0	0.0	0.0	0.0	0.0	0.0	0.0	0.0	0.0	0.0
14	0.0	0.0	0.0	0.0	0.0	0.0	0.0	0.0	0.0	0.0	0.0
15	0.0	0.0	0.0	0.0	0.0	0.0	0.0	0.0	0.0	0.0	0.0
16	0.0	0.0	0.0	0.0	0.0	0.0	0.0	0.0	0.0	0.0	0.0
17	0.0	0.0	0.0	0.0	0.0	0.0	0.0	0.0	0.0	0.0	0.0
18	0.0	0.0	0.0	0.0	0.0	0.0	0.0	0.0	0.0	0.0	0.0
19	0.0	0.0	0.0	0.0	0.0	0.0	0.0	0.0	0.0	0.0	0.0

PLANE NUMBER 2

	1	2	3	4	5	6	7	8	9	10	11
1	0.0	0.0	0.0	0.0	0.0	0.0	0.0	0.0	0.0	0.0	0.0
2	0.0	0.0	0.0	0.0	0.0	0.0	0.0	0.0	0.0	0.0	0.0
3	0.0	0.0	0.0	0.0	0.0	0.0	0.0	0.0	0.0	0.0	0.0
4	0.0	0.0	0.0	0.0	0.0	0.0	0.0	0.0	0.0	0.0	0.0
5	0.0	0.0	0.0	0.0	0.0	0.0	0.0	0.0	0.0	0.0	0.0
6	0.0	0.0	0.0	0.0	0.0	0.0	0.0	0.0	0.0	0.0	0.0
7	0.0	0.0	0.0	0.0	0.0	0.0	0.0	0.0	0.0	0.0	0.0
8	0.0	0.0	0.0	0.0	0.0	0.0	0.0	0.0	0.0	0.0	0.0
9	0.0	0.0	0.0	0.0	0.0	0.0	0.0	0.0	0.0	0.0	0.0
10	0.0	0.0	0.0	0.0	0.0	0.0	0.0	0.0	0.0	0.0	0.0
11	0.0	0.0	0.0	0.0	0.0	0.0	0.0	0.0	0.0	0.0	0.0
12	0.0	0.0	0.0	0.0	0.0	0.0	0.0	0.0	0.0	0.0	0.0
13	0.0	0.0	0.0	0.0	0.0	0.0	0.0	0.0	0.0	0.0	0.0
14	0.0	0.0	0.0	0.0	0.0	0.0	0.0	0.0	0.0	0.0	0.0
15	0.0	0.0	0.0	0.0	0.0	0.0	0.0	0.0	0.0	0.0	0.0
16	0.0	0.0	0.0	0.0	0.0	0.0	0.0	0.0	0.0	0.0	0.0
17	0.0	0.0	0.0	0.0	0.0	0.0	0.0	0.0	0.0	0.0	0.0
18	0.0	0.0	0.0	0.0	0.0	0.0	0.0	0.0	0.0	0.0	0.0
19	0.0	0.0	0.0	0.0	0.0	0.0	0.0	0.0	0.0	0.0	0.0

PLANE NUMBER 3

	1	2	3	4	5	6	7	8	9	10	11
1	0.0	0.0	0.0	0.0	0.0	1.556E+01	2.254E+01	2.436E+01	2.586E+01	2.642E+01	2.645E+01
2	0.0	0.0	0.0	0.0	0.0	1.590E+01	2.142E+01	2.254E+01	2.349E+01	2.396E+01	2.398E+01
3	0.0	0.0	0.0	0.0	1.222E+01	1.538E+01	1.735E+01	1.788E+01	1.851E+01	1.896E+01	1.898E+01
4	0.0	0.0	0.0	0.0	0.0	0.0	0.0	0.0	0.0	0.0	0.0
5	0.0	0.0	1.720E+01	1.922E+01	1.930E+01	1.927E+01	1.772E+01	0.0	1.890E+01	2.069E+01	2.078E+01
6	0.0	0.0	2.262E+01	0.0	0.0	0.0	2.393E+01	0.0	2.617E+01	2.932E+01	2.949E+01
7	0.0	0.0	1.821E+01	2.052E+01	2.131E+01	2.086E+01	1.956E+01	0.0	2.133E+01	2.399E+01	2.459E+01

	1	2	3	4	5	6	7	8	9	10	11
8	0.0	0.0	9.925E+00	1.223E+01	1.781E+01	1.248E+01	1.094E+01	0.0	1.193E+01	1.444E+01	1.928E+01
9	0.0	0.0	0.0	0.0	0.0	0.0	0.0	0.0	0.0	0.0	0.0
10	0.0	0.0	0.0	0.0	0.0	0.0	0.0	0.0	0.0	0.0	0.0
11	0.0	0.0	0.0	0.0	0.0	0.0	0.0	0.0	0.0	0.0	0.0
12	0.0	0.0	0.0	0.0	0.0	0.0	0.0	0.0	0.0	0.0	0.0
13	0.0	0.0	0.0	0.0	0.0	0.0	0.0	0.0	0.0	0.0	0.0
14	0.0	0.0	0.0	0.0	0.0	0.0	0.0	0.0	0.0	0.0	0.0
15	0.0	0.0	0.0	0.0	0.0	0.0	0.0	0.0	0.0	0.0	0.0
16	0.0	0.0	0.0	0.0	0.0	0.0	0.0	0.0	0.0	0.0	0.0
17	0.0	0.0	0.0	0.0	0.0	0.0	0.0	0.0	0.0	0.0	0.0
18	0.0	0.0	0.0	0.0	0.0	0.0	0.0	0.0	0.0	0.0	0.0
19	0.0	0.0	0.0	0.0	0.0	0.0	0.0	0.0	0.0	0.0	0.0

PLANE NUMBER 4

	1	2	3	4	5	6	7	8	9	10	11
1	0.0	0.0	0.0	0.0	0.0	2.698E+01	3.800E+01	4.148E+01	4.439E+01	4.549E+01	4.555E+01
2	0.0	0.0	0.0	0.0	0.0	2.783E+01	3.637E+01	3.862E+01	4.055E+01	4.149E+01	4.154E+01
3	0.0	0.0	0.0	0.0	1.984E+01	2.564E+01	2.965E+01	3.081E+01	3.214E+01	3.302E+01	3.307E+01
4	0.0	0.0	0.0	0.0	0.0	0.0	0.0	0.0	0.0	0.0	0.0
5	0.0	0.0	2.874E+01	3.054E+01	3.068E+01	3.079E+01	3.030E+01	0.0	3.301E+01	3.627E+01	3.643E+01
6	0.0	0.0	3.814E+01	0.0	0.0	0.0	4.089E+01	0.0	4.588E+01	5.159E+01	5.190E+01
7	0.0	0.0	3.098E+01	3.402E+01	3.530E+01	3.468E+01	3.361E+01	0.0	3.718E+01	4.190E+01	4.289E+01
8	0.0	0.0	1.669E+01	2.019E+01	2.910E+01	2.066E+01	1.853E+01	0.0	2.045E+01	2.464E+01	3.256E+01
9	0.0	0.0	0.0	0.0	0.0	0.0	0.0	0.0	0.0	0.0	0.0
10	0.0	0.0	0.0	0.0	0.0	0.0	0.0	0.0	0.0	0.0	0.0
11	0.0	0.0	0.0	0.0	0.0	0.0	0.0	0.0	0.0	0.0	0.0
12	0.0	0.0	0.0	0.0	0.0	0.0	0.0	0.0	0.0	0.0	0.0
13	0.0	0.0	0.0	0.0	0.0	0.0	0.0	0.0	0.0	0.0	0.0
14	0.0	0.0	0.0	0.0	0.0	0.0	0.0	0.0	0.0	0.0	0.0
15	0.0	0.0	0.0	0.0	0.0	0.0	0.0	0.0	0.0	0.0	0.0
16	0.0	0.0	0.0	0.0	0.0	0.0	0.0	0.0	0.0	0.0	0.0
17	0.0	0.0	0.0	0.0	0.0	C.0	0.0	0.0	0.0	0.0	0.0
18	0.0	0.0	0.0	0.0	0.0	0.0	0.0	0.0	0.0	0.0	0.0
19	0.0	0.0	0.0	0.0	0.0	0.0	0.0	0.0	0.0	0.0	0.0

PLANE NUMBER 5

	1	2	3	4	5	6	7	8	9	10	11
1	0.0	0.0	0.0	0.0	0.0	3.738E+01	5.210E+01	5.680E+01	6.075E+01	6.226E+01	6.235E+01
2	0.0	0.0	0.0	0.0	0.0	3.829E+01	4.974E+01	5.284E+01	5.552E+01	5.681E+01	5.689E+01
3	0.0	0.0	0.0	0.0	2.739E+01	3.502E+01	4.049E+01	4.215E+01	4.403E+01	4.524E+01	4.531E+01
4	0.0	0.0	0.0	0.0	0.0	0.0	0.0	0.0	0.0	0.0	0.0
5	0.0	0.0	3.885E+01	4.094E+01	4.114E+01	4.134E+01	4.120E+01	0.0	4.518E+01	4.961E+01	4.983E+01
6	0.0	0.0	5.145E+01	0.0	0.0	0.0	5.549E+01	0.0	6.269E+01	7.037E+01	7.079E+01
7	0.0	0.0	4.173E+01	4.551E+01	4.721E+01	4.646E+01	4.553E+01	0.0	5.059E+01	5.680E+01	5.812E+01
8	0.0	0.0	2.247E+01	2.694E+01	3.860E+01	2.761E+01	2.509E+01	0.0	2.777E+01	3.324E+01	4.369E+01
9	0.0	0.0	0.0	0.0	0.0	0.0	0.0	0.0	0.0	0.0	0.0
10	0.0	0.0	0.0	0.0	0.0	0.0	0.0	0.0	0.0	0.0	0.0
11	0.0	0.0	0.0	0.0	0.0	0.0	0.0	0.0	0.0	0.0	0.0
12	0.0	0.0	0.0	0.0	0.0	0.0	0.0	0.0	0.0	0.0	0.0
13	0.0	0.0	0.0	0.0	0.0	0.0	0.0	0.0	0.0	0.0	0.0
14	0.0	0.0	0.0	0.0	0.0	0.0	0.0	0.0	0.0	0.0	0.0
15	0.0	0.0	0.0	0.0	0.0	0.0	0.0	0.0	0.0	0.0	0.0
16	0.0	0.0	0.0	0.0	0.0	0.0	0.0	0.0	0.0	0.0	0.0
17	0.0	0.0	0.0	0.0	0.0	0.0	0.0	0.0	0.0	0.0	0.0
18	0.0	0.0	0.0	0.0	0.0	0.0	0.0	0.0	0.0	0.0	0.0
19	0.0	0.0	0.0	0.0	0.0	0.0	0.0	0.0	0.0	0.0	0.0

PLANE NUMBER 6

	1	2	3	4	5	6	7	8	9	10	11
1	0.0	0.0	0.0	0.0	0.0	5.627E+01	7.527E+01	8.147E+01	8.670E+01	8.873E+01	8.884E+01
2	0.0	0.0	0.0	0.0	0.0	5.669E+01	7.150E+01	7.574E+01	7.943E+01	8.122E+01	8.132E+01
3	0.0	0.0	0.0	0.0	4.146E+01	5.085E+01	5.813E+01	6.054E+01	6.325E+01	6.494E+01	6.504E+01
4	0.0	0.0	0.0	0.0	0.0	0.0	0.0	0.0	0.0	0.0	0.0

	1	2	3	4	5	6	7	8	9	10	11
5	0.0	0.0	5.360E+01	5.711E+01	5.742E+01	5.779E+01	5.854E+01	0.0	6.447E+01	7.049E+01	7.079E+01
6	0.0	0.0	7.176E+01	0.0	0.0	0.0	7.810E+01	0.0	9.867E+01	9.881E+01	9.935E+01
7	0.0	0.0	5.815E+01	6.262E+01	6.481E+01	6.406E+01	6.393E+01	0.0	7.122E+01	7.908E+01	8.073E+01
8	0.0	0.0	3.591E+01	4.224E+01	5.975E+01	4.340E+01	4.041E+01	0.0	4.478E+01	5.258E+01	6.837E+01
9	0.0	0.0	0.0	0.0	0.0	0.0	0.0	0.0	0.0	0.0	0.0
10	0.0	0.0	0.0	0.0	0.0	0.0	0.0	0.0	0.0	0.0	0.0
11	0.0	0.0	0.0	0.0	0.0	0.0	0.0	0.0	0.0	0.0	0.0
12	0.0	0.0	0.0	0.0	0.0	0.0	0.0	0.0	0.0	0.0	0.0
13	0.0	0.0	0.0	0.0	0.0	0.0	0.0	0.0	0.0	0.0	0.0
14	0.0	0.0	0.0	0.0	0.0	0.0	0.0	0.0	0.0	0.0	0.0
15	0.0	0.0	0.0	0.0	0.0	0.0	0.0	0.0	0.0	0.0	0.0
16	0.0	0.0	0.0	0.0	0.0	0.0	0.0	0.0	0.0	0.0	0.0
17	0.0	0.0	0.0	0.0	0.0	0.0	0.0	0.0	0.0	0.0	0.0
18	0.0	0.0	0.0	0.0	0.0	0.0	0.0	0.0	0.0	0.0	0.0
19	0.0	0.0	0.0	0.0	0.0	0.0	0.0	0.0	0.0	0.0	0.0

PLANE NUMBER 7

	1	2	3	4	5	6	7	8	9	10	11
1	0.0	0.0	0.0	0.0	0.0	1.067E+02	1.235E+02	1.302E+02	1.361E+02	1.386E+02	1.388E+02
2	0.0	0.0	0.0	0.0	0.0	1.098E+02	1.262E+02	1.326E+02	1.383E+02	1.410E+02	1.411E+02
3	0.0	0.0	0.0	0.0	1.025E+02	1.124E+02	1.262E+02	1.325E+02	1.384E+02	1.414E+02	1.416E+02
4	0.0	0.0	0.0	0.0	0.0	0.0	0.0	0.0	0.0	0.0	0.0
5	0.0	0.0	1.058E+02	1.009E+02	1.029E+02	1.059E+02	1.248E+02	0.0	1.381E+02	1.425E+02	1.427E+02
6	0.0	0.0	1.058E+02				1.181E+02		1.337E+02	1.394E+02	1.403E+02
7	0.0	0.0	8.527E+01	8.684E+01	8.955E+01	8.917E+01	9.551E+01	0.0	1.058E+02	1.108E+02	1.127E+02
8	0.0	0.0	6.713E+01	7.348E+01	9.686E+01	7.584E+01	7.709E+01	0.0	8.460E+01	9.130E+01	1.125E+02
9	0.0	0.0	0.0	0.0	0.0	0.0	0.0	0.0	0.0	0.0	0.0
10	0.0	0.0	0.0	0.0	0.0	0.0	0.0	0.0	0.0	0.0	0.0
11	0.0	0.0	0.0	0.0	0.0	0.0	0.0	0.0	0.0	0.0	0.0
12	0.0	0.0	0.0	0.0	0.0	0.0	0.0	0.0	0.0	0.0	0.0
13	0.0	0.0	0.0	0.0	0.0	0.0	0.0	0.0	0.0	0.0	0.0
14	0.0	0.0	0.0	0.0	0.0	0.0	0.0	0.0	0.0	0.0	0.0
15	0.0	0.0	0.0	0.0	0.0	0.0	0.0	0.0	0.0	0.0	0.0
16	0.0	0.0	0.0	0.0	0.0	0.0	0.0	0.0	0.0	0.0	0.0
17	0.0	0.0	0.0	0.0	0.0	0.0	0.0	0.0	0.0	0.0	0.0
18	0.0	0.0	0.0	0.0	0.0	0.0	0.0	0.0	0.0	0.0	0.0
19	0.0	0.0	0.0	0.0	0.0	0.0	0.0	0.0	0.0	0.0	0.0

PLANE NUMBER 8

	1	2	3	4	5	6	7	8	9	10	11
1	0.0	0.0	0.0	0.0	0.0	1.278E+02	1.429E+02	1.496E+02	1.555E+02	1.581E+02	1.582E+02
2	0.0	0.0	0.0	0.0	0.0	1.297E+02	1.449E+02	1.516E+02	1.577E+02	1.606E+02	1.607E+02
3	0.0	0.0	0.0	0.0	1.226E+02	1.307E+02	1.442E+02	1.510E+02	1.574E+02	1.607E+02	1.609E+02
4	0.0	0.0	0.0	0.0	0.0	0.0	0.0	0.0	0.0	0.0	0.0
5	0.0	0.0	1.240E+02	1.180E+02	1.196E+02	1.224E+02	1.425E+02	0.0	1.573E+02	1.619E+02	1.622E+02
6	0.0	0.0	1.220E+02	0.0		1.356E+02			1.533E+02	1.5??E+02	1.600E+02
7	0.0	0.0	1.072E+02	1.072E+02	1.090E+02	1.101E+02	1.190E+02	0.0	1.315E+02	1.30?E+02	1.371E+02
8	0.0	0.0	1.462E+02	1.519E+02	1.599E+02	1.568E+02	1.620E+02	0.0	1.770E+02	1.856E+02	1.898E+02
9	0.0	0.0	0.0	0.0	0.0	0.0	0.0	0.0	0.0	0.0	0.0
10	0.0	0.0	0.0	0.0	0.0	0.0	0.0	0.0	0.0	0.0	0.0
11	0.0	0.0	0.0	0.0	0.0	0.0	0.0	0.0	0.0	0.0	0.0
12	0.0	0.0	0.0	0.0	0.0	0.0	0.0	0.0	0.0	0.0	0.0
13	0.0	0.0	0.0	0.0	0.0	0.0	0.0	0.0	0.0	0.0	0.0
14	0.0	0.0	0.0	0.0	0.0	0.0	0.0	0.0	0.0	0.0	0.0
15	0.0	0.0	0.0	0.0	0.0	0.0	0.0	0.0	0.0	0.0	0.0
16	0.0	0.0	0.0	0.0	0.0	0.0	0.0	0.0	0.0	0.0	0.0
17	0.0	0.0	0.0	0.0	0.0	0.0	0.0	0.0	0.0	0.0	0.0
18	0.0	0.0	0.0	0.0	0.0	0.0	0.0	0.0	0.0	0.0	0.0
19	0.0	0.0	0.0	0.0	0.0	0.0	0.0	0.0	0.0	0.0	0.0

PLANE NUMBER 9

	1	2	3	4	5	6	7	8	9	10	11
1	0.0	0.0	0.0	0.0	0.0	1.480E+02	1.574E+02	1.626E+02	1.674E+02	1.696E+02	1.697E+02

	1	2	3	4	5	6	7	8	9	10	11
2	0.0	0.0	0.0	0.0	0.0	1.478E+02	1.583E+02	1.642E+02	1.696E+02	1.722E+02	1.724E+02
3	0.0	0.0	0.0	0.0	1.434E+02	1.472E+02	1.577E+02	1.645E+02	1.701E+02	1.730E+02	1.732E+02
4	0.0	0.0	0.0	0.0	0.0	0.0	0.0	0.0	0.0	0.0	0.0
5	0.0	0.0	1.409E+02	1.361E+02	1.371E+02	1.393E+02	1.560E+02	0.0	1.704E+02	1.743E+02	1.746E+02
6	0.0	0.0	1.346E+02	0.0	0.0	0.0	1.481E+02	0.0	1.658E+02	1.714E+02	1.718E+02
7	0.0	0.0	1.241E+02	1.217E+02	1.252E+02	1.268E+02	1.363E+02	0.0	1.500E+02	1.543E+02	1.546E+02
8	0.0	0.0	2.043E+02	2.084E+02	2.118E+02	2.143E+02	2.219E+02	0.0	2.415E+02	2.504E+02	2.498E+02
9	0.0	0.0	0.0	0.0	0.0	0.0	0.0	0.0	0.0	0.0	0.0
10	0.0	0.0	0.0	0.0	0.0	0.0	0.0	0.0	0.0	0.0	0.0
11	0.0	0.0	0.0	0.0	0.0	0.0	0.0	0.0	0.0	0.0	0.0
12	0.0	0.0	0.0	0.0	0.0	0.0	0.0	0.0	0.0	0.0	0.0
13	0.0	0.0	0.0	0.0	0.0	0.0	0.0	0.0	0.0	0.0	0.0
14	0.0	0.0	0.0	0.0	0.0	0.0	0.0	0.0	0.0	0.0	0.0
15	0.0	0.0	0.0	0.0	0.0	0.0	0.0	0.0	0.0	0.0	0.0
16	0.0	0.0	0.0	0.0	0.0	0.0	0.0	0.0	0.0	0.0	0.0
17	0.0	0.0	0.0	0.0	0.0	0.0	0.0	0.0	0.0	0.0	0.0
18	0.0	0.0	0.0	0.0	0.0	0.0	0.0	0.0	0.0	0.0	0.0
19	0.0	0.0	0.0	0.0	0.0	0.0	0.0	0.0	0.0	0.0	0.0

PLANE NUMBER 10

	1	2	3	4	5	6	7	8	9	10	11
1	0.0	0.0	0.0	0.0	0.0	1.879E+02	1.659E+02	1.632E+02	1.618E+02	1.619E+02	1.619E+02
2	0.0	0.0	0.0	0.0	0.0	1.786E+02	1.641E+02	1.655E+02	1.672E+02	1.684E+02	1.685E+02
3	0.0	0.0	0.0	0.0	1.930E+02	1.750E+02	1.725E+02	1.774E+02	1.800E+02	1.816E+02	1.817E+02
4	0.0	0.0	0.0	0.0	0.0	0.0	0.0	0.0	0.0	0.0	0.0
5	0.0	0.0	1.504E+02	1.518E+02	1.519E+02	1.522E+02	1.556E+02	0.0	1.649E+02	1.657E+02	1.657E+02
6	0.0	0.0	1.274E+02	0.0	0.0	0.0	1.371E+02	0.0	1.486E+02	1.504E+02	1.506E+02
7	0.0	0.0	1.181E+02	1.207E+02	1.220E+02	1.230E+02	1.274E+02	0.0	1.385E+02	1.405E+02	1.408E+02
8	0.0	0.0	2.167E+02	2.211E+02	2.259E+02	2.256E+02	2.313E+02	0.0	E+02	2.580E+02	2.593E+02
9	0.0	0.0	0.0	0.0	0.0	0.0	0.0	0.0	0.0	0.0	0.0
10	0.0	0.0	0.0	0.0	0.0	0.0	0.0	0.0	0.0	0.0	0.0
11	0.0	0.0	0.0	0.0	0.0	0.0	0.0	0.0	0.0	0.0	0.0
12	0.0	0.0	0.0	0.0	0.0	0.0	0.0	0.0	0.0	0.0	0.0
13	0.0	0.0	0.0	0.0	0.0	0.0	0.0	0.0	0.0	0.0	0.0
14	0.0	0.0	0.0	0.0	0.0	0.0	0.0	0.0	0.0	0.0	0.0
15	0.0	0.0	0.0	0.0	0.0	0.0	0.0	0.0	0.0	0.0	0.0
16	0.0	0.0	0.0	0.0	0.0	0.0	0.0	0.0	0.0	0.0	0.0
17	0.0	0.0	0.0	0.0	0.0	0.0	0.0	0.0	0.0	0.0	0.0
18	0.0	0.0	0.0	0.0	0.0	0.0	0.0	0.0	0.0	0.0	0.0
19	0.0	0.0	0.0	0.0	0.0	0.0	0.0	0.0	0.0	0.0	0.0

PLANE NUMBER 11

	1	2	3	4	5	6	7	8	9	10	11
1	0.0	0.0	0.0	0.0	0.0	2.172E+02	1.969E+02	1.946E+02	1.933E+02	1.934E+02	1.935E+02
2	0.0	0.0	0.0	0.0	0.0	2.091E+02	1.956E+02	1.967E+02	1.985E+02	1.998E+02	1.999E+02
3	0.0	0.0	0.0	0.0	2.270E+02	2.099E+02	2.076E+02	2.109E+02	2.148E+02	2.168E+02	2.169E+02
4	0.0	0.0	0.0	0.0	0.0	0.0	0.0	0.0	0.0	0.0	0.0
5	0.0	0.0	1.783E+02	1.782E+02	1.795E+02	1.807E+02	1.863E+02	0.0	1.956E+02	1.968E+02	1.969E+02
6	0.0	0.0	1.554E+02	0.0	0.0	0.0	1.643E+02	0.0	1.768E+02	1.789E+02	1.791E+02
7	0.0	0.0	1.438E+02	1.457E+02	1.473E+02	1.476E+02	1.525E+02	0.0	1.652E+02	1.677E+02	1.687E+02
8	0.0	0.0	2.384E+02	2.434E+02	2.590E+02	2.471E+02	2.518E+02	0.0	2.711E+02	2.806E+02	2.940E+02
9	0.0	0.0	0.0	0.0	0.0	0.0	0.0	0.0	0.0	0.0	0.0
10	0.0	0.0	0.0	0.0	0.0	0.0	0.0	0.0	0.0	0.0	0.0
11	0.0	0.0	0.0	0.0	0.0	0.0	0.0	0.0	0.0	0.0	0.0
12	0.0	0.0	0.0	0.0	0.0	0.0	0.0	0.0	0.0	0.0	0.0
13	0.0	0.0	0.0	0.0	0.0	0.0	0.0	0.0	0.0	0.0	0.0
14	0.0	0.0	0.0	0.0	0.0	0.0	0.0	0.0	0.0	0.0	0.0
15	0.0	0.0	0.0	0.0	0.0	0.0	0.0	0.0	0.0	0.0	0.0
16	0.0	0.0	0.0	0.0	0.0	0.0	0.0	0.0	0.0	0.0	0.0
17	0.0	0.0	0.0	0.0	0.0	0.0	0.0	0.0	0.0	0.0	0.0
18	0.0	0.0	0.0	0.0	0.0	0.0	0.0	0.0	0.0	0.0	0.0
19	0.0	0.0	0.0	0.0	0.0	0.0	0.0	0.0	0.0	0.0	0.0

PLANE NUMBER 12

	1	2	3	4	5	6	7	8	9	10	11
1	0.0	0.0	0.0	0.0	0.0	0.0	0.0	0.0	0.0	0.0	0.0
2	0.0	0.0	0.0	0.0	0.0	0.0	0.0	0.0	0.0	0.0	0.0
3	0.0	0.0	0.0	0.0	0.0	0.0	0.0	0.0	0.0	0.0	0.0
4	0.0	0.0	0.0	0.0	0.0	0.0	0.0	0.0	0.0	0.0	0.0
5	0.0	0.0	0.0	0.0	0.0	0.0	0.0	0.0	0.0	0.0	0.0
6	0.0	0.0	0.0	0.0	0.0	0.0	0.0	0.0	0.0	0.0	0.0
7	0.0	0.0	0.0	0.0	0.0	0.0	0.0	0.0	0.0	0.0	0.0
8	0.0	0.0	0.0	0.0	0.0	0.0	0.0	0.0	0.0	0.0	0.0
9	0.0	0.0	0.0	0.0	0.0	0.0	0.0	0.0	0.0	0.0	0.0
10	0.0	0.0	0.0	0.0	0.0	0.0	0.0	0.0	0.0	0.0	0.0
11	0.0	0.0	0.0	0.0	0.0	0.0	0.0	0.0	0.0	0.0	0.0
12	0.0	0.0	0.0	0.0	0.0	0.0	0.0	0.0	0.0	0.0	0.0
13	0.0	0.0	0.0	0.0	0.0	0.0	0.0	0.0	0.0	0.0	0.0
14	0.0	0.0	0.0	0.0	0.0	0.0	0.0	0.0	0.0	0.0	0.0
15	0.0	0.0	0.0	0.0	0.0	0.0	0.0	0.0	0.0	0.0	0.0
16	0.0	0.0	0.0	0.0	0.0	0.0	0.0	0.0	0.0	0.0	0.0
17	0.0	0.0	0.0	0.0	0.0	0.0	0.0	0.0	0.0	0.0	0.0
18	0.0	0.0	0.0	0.0	0.0	0.0	0.0	0.0	0.0	0.0	0.0
19	0.0	0.0	0.0	0.0	0.0	0.0	0.0	0.0	0.0	0.0	0.0

PLANE NUMBER 13

	1	2	3	4	5	6	7	8	9	10	11
1	0.0	0.0	0.0	0.0	0.0	0.0	0.0	0.0	0.0	0.0	0.0
2	0.0	0.0	0.0	0.0	0.0	0.0	0.0	0.0	0.0	0.0	0.0
3	0.0	0.0	0.0	0.0	0.0	0.0	0.0	0.0	0.0	0.0	0.0
4	0.0	0.0	0.0	0.0	0.0	0.0	0.0	0.0	0.0	0.0	0.0
5	0.0	0.0	0.0	0.0	0.0	0.0	0.0	0.0	0.0	0.0	0.0
6	0.0	0.0	0.0	0.0	0.0	0.0	0.0	0.0	0.0	0.0	0.0
7	0.0	0.0	0.0	0.0	0.0	0.0	0.0	0.0	0.0	0.0	0.0
8	0.0	0.0	0.0	0.0	0.0	0.0	0.0	0.0	0.0	0.0	0.0
9	0.0	0.0	0.0	0.0	0.0	0.0	0.0	0.0	0.0	0.0	0.0
10	0.0	0.0	0.0	0.0	0.0	0.0	0.0	0.0	0.0	0.0	0.0
11	0.0	0.0	0.0	0.0	0.0	0.0	0.0	0.0	0.0	0.0	0.0
12	0.0	0.0	0.0	0.0	0.0	0.0	0.0	0.0	0.0	0.0	0.0
13	0.0	0.0	0.0	0.0	0.0	0.0	0.0	0.0	0.0	0.0	0.0
14	0.0	0.0	0.0	0.0	0.0	0.0	0.0	0.0	0.0	0.0	0.0
15	0.0	0.0	0.0	0.0	0.0	0.0	0.0	0.0	0.0	0.0	0.0
16	0.0	0.0	0.0	0.0	0.0	0.0	0.0	0.0	0.0	0.0	0.0
17	0.0	0.0	0.0	0.0	0.0	0.0	0.0	0.0	0.0	0.0	0.0
18	0.0	0.0	0.0	0.0	0.0	0.0	0.0	0.0	0.0	0.0	0.0
19	0.0	0.0	0.0	0.0	0.0	0.0	0.0	0.0	0.0	0.0	0.0

PLANE NUMBER 14

	1	2	3	4	5	6	7	8	9	10	11
1	0.0	0.0	0.0	0.0	0.0	0.0	0.0	0.0	0.0	0.0	0.0
2	0.0	0.0	0.0	0.0	0.0	0.0	0.0	0.0	0.0	0.0	0.0
3	0.0	0.0	0.0	0.0	0.0	0.0	0.0	0.0	0.0	0.0	0.0
4	0.0	0.0	0.0	0.0	0.0	0.0	0.0	0.0	0.0	0.0	0.0
5	0.0	0.0	0.0	0.0	0.0	0.0	0.0	0.0	0.0	0.0	0.0
6	0.0	0.0	0.0	0.0	0.0	0.0	0.0	0.0	0.0	0.0	0.0
7	0.0	0.0	0.0	0.0	0.0	0.0	0.0	0.0	0.0	0.0	0.0
8	0.0	0.0	0.0	0.0	0.0	0.0	0.0	0.0	0.0	0.0	0.0
9	0.0	0.0	0.0	0.0	0.0	0.0	0.0	0.0	0.0	0.0	0.0
10	0.0	0.0	0.0	0.0	0.0	0.0	0.0	0.0	0.0	0.0	0.0
11	0.0	0.0	0.0	0.0	0.0	0.0	0.0	0.0	0.0	0.0	0.0
12	0.0	0.0	0.0	0.0	0.0	0.0	0.0	0.0	0.0	0.0	0.0
13	0.0	0.0	0.0	0.0	0.0	0.0	0.0	0.0	0.0	0.0	0.0
14	0.0	0.0	0.0	0.0	0.0	0.0	0.0	0.0	0.0	0.0	0.0
15	0.0	0.0	0.0	0.0	0.0	0.0	0.0	0.0	0.0	0.0	0.0
16	0.0	0.0	0.0	0.0	0.0	0.0	0.0	0.0	0.0	0.0	0.0
17	0.0	0.0	0.0	0.0	0.0	0.0	0.0	0.0	0.0	0.0	0.0
18	0.0	0.0	0.0	0.0	0.0	0.0	0.0	0.0	0.0	0.0	0.0

19	0.0	0.0	0.0	0.0	0.0	0.0	0.0	0.0	0.0	0.0	0.0

PLANE NUMBER 15

	1	2	3	4	5	6	7	8	9	10	11
1	0.0	0.0	0.0	0.0	0.0	0.0	0.0	0.0	0.0	0.0	0.0
2	0.0	0.0	0.0	0.0	0.0	0.0	0.0	0.0	0.0	0.0	0.0
3	0.0	0.0	0.0	0.0	0.0	0.0	0.0	0.0	0.0	0.0	0.0
4	0.0	0.0	0.0	0.0	0.0	:.0	0.0	0.0	0.0	0.0	0.0
5	0.0	0.0	0.0	0.0	0.0	0.0	0.0	0.0	0.0	0.0	0.0
6	0.0	0.0	0.0	0.0	0.0	0.0	0.0	0.0	0.0	0.0	0.0
7	0.0	0.0	0.0	0.0	0.0	0.0	0.0	0.0	0.0	0.0	0.0
8	0.0	0.0	0.0	0.0	0.0	0.0	0.0	0.0	0.0	0.0	0.0
9	0.0	0.0	0.0	0.0	0.0	0.0	0.0	0.0	0.0	0.0	0.0
10	0.0	0.0	0.0	0.0	0.0	0.0	0.0	0.0	0.0	0.0	0.0
11	0.0	0.0	0.0	0.0	0.0	0.0	0.0	0.0	0.0	0.0	0.0
12	0.0	0.0	0.0	0.0	0.0	0.0	0.0	0.0	0.0	0.0	0.0
13	0.0	0.0	0.0	0.0	0.0	0.0	0.0	0.0	0.0	0.0	0.0
14	0.0	0.0	0.0	0.0	0.0	0.0	0.0	0.0	0.0	0.0	0.0
15	0.0	0.0	0.0	0.0	0.0	0.0	0.0	0.0	0.0	0.0	0.0
16	0.0	0.0	0.0	0.0	0.0	0.0	0.0	0.0	0.0	0.0	0.0
17	0.0	0.0	0.0	0.0	0.0	0.0	0.0	0.0	0.0	0.0	0.0
18	0.0	0.0	0.0	0.0	0.0	0.0	0.0	0.0	0.0	0.0	0.0
19	0.0	0.0	0.0	0.0	0.0	0.0	0.0	0.0	0.0	0.0	

PLANE NUMBER 16

	1	2	3	4	5	6	7	8	9	10	11
1	0.0	0.0	0.0	0.0	0.0	0.0	0.0	0.0	0.0	0.0	0.0
2	0.0	0.0	0.0	0.0	0.0	0.0	0.0	0.0	0.0	0.0	0.0
3	0.0	0.0	0.0	0.0	0.0	0.0	0.0	0.0	0.0	0.0	0.0
4	0.0	0.0	0.0	0.0	0.0	0.0	0.0	0.0	0.0	0.0	0.0
5	0.0	0.0	0.0	0.0	0.0	0.0	0.0	0.0	0.0	0.0	0.0
6	0.0	0.0	0.0	0.0	0.0	0.0	0.0	0.0	0.0	0.0	0.0
7	0.0	0.0	0.0	0.0	0.0	0.0	0.0	0.0	0.0	0.0	0.0
8	0.0	0.0	0.0	0.0	0.0	0.0	0.0	0.0	0.0	0.0	0.0
9	0.0	0.0	0.0	0.0	0.0	0.0	0.0	0.0	0.0	0.0	0.0
10	0.0	0.0	0.0	0.0	0.0	0.0	0.0	0.0	0.0	0.0	0.0
11	0.0	0.0	0.0	0.0	0.0	0.0	0.0	0.0	0.0	0.0	0.0
12	0.0	0.0	0.0	0.0	0.0	0.0	0.0	0.0	0.0	0.0	0.0
13	0.0	0.0	0.0	0.0	0.0	0.0	0.0	0.0	0.0	0.0	0.0
14	0.0	0.0	0.0	0.0	0.0	0.0	0.0	0.0	0.0	0.0	0.0
15	0.0	0.0	0.0	0.0	0.0	0.0	0.0	0.0	0.0	0.0	0.0
16	0.0	0.0	0.0	0.0	0.0	0.0	0.0	0.0	0.0	0.0	0.0
17	0.0	0.0	0.0	0.0	0.0	0.0	0.0	0.0	0.0	0.0	0.0
18	0.0	0.0	0.0	0.0	0.0	0.0	0.0	0.0	0.0	0.0	0.0
19	0.0	0.0	0.0	0.0	0.0	0.0	0.0	0.0	0.0	0.0	

PLANE NUMBER 17

	1	2	3	4	5	6	7	8	9	10	11
1	0.0	0.0	0.0	0.0	0.0	0.0	0.0	0.0	0.0	0.0	0.0
2	0.0	0.0	0.0	0.0	0.0	0.0	0.0	0.0	0.0	0.0	0.0
3	0.0	0.0	0.0	0.0	0.0	0.0	0.0	0.0	0.0	0.0	0.0
4	0.0	0.0	0.0	0.0	0.0	0.0	0.0	0.0	0.0	0.0	0.0
5	0.0	0.0	0.0	0.0	C.0	0.0	0.0	0.0	0.0	0.0	0.0
6	0.0	0.0	0.0	0.0	0.0	0.0	0.0	0.0	0.0	0.0	0.0
7	0.0	0.0	0.0	0.0	0.0	0.0	0.0	0.0	0.0	0.0	0.0
8	0.0	0.0	0.0	0.0	0.0	0.0	0.0	0.0	0.0	0.0	0.0
9	0.0	0.0	0.0	0.0	0.0	0.0	0.0	0.0	0.0	0.0	0.0
10	0.0	0.0	0.0	0.0	0.0	0.0	0.0	0.0	0.0	0.0	0.0
11	0.0	0.0	0.0	0.0	0.0	0.0	0.0	0.0	0.0	0.0	0.0
12	0.0	0.0	0.0	0.0	0.0	0.0	0.0	0.0	0.0	0.0	0.0
13	0.0	0.0	0.0	0.0	0.0	0.0	0.0	0.0	0.0	0.0	0.0
14	0.0	0.0	0.0	0.0	0.0	0.0	0.0	0.0	0.0	0.0	0.0
15	0.0	0.0	0.0	0.0	0.0	0.0	0.0	0.0	0.0	0.0	0.0

Information Processing Center

```
16   0.0      0.0      0.0      0.0      0.0      0.0      0.0      0.0      0.0      0.0      0.0
17   0.0      0.0      0.0      0.0      0.0      0.0      0.0      0.0      0.0      0.0      0.0
18   0.0      0.0      0.0      0.0      0.0      0.0      0.0      0.0      0.0      0.0      0.0
19   0.0      0.0      0.0      0.0      0.0      0.0      0.0      0.0      0.0      0.0      0.0
```

PLANE NUMBER 18

	1	2	3	4	5	6	7	8	9	10	11
1	0.0	0.0	0.0	0.0	0.0	0.0	0.0	0.0	0.0	0.0	0.0
2	0.0	0.0	0.0	0.0	0.0	0.0	0.0	0.0	0.0	0.0	0.0
3	0.0	0.0	0.0	0.0	0.0	0.0	0.0	0.0	0.0	0.0	0.0
4	0.0	0.0	0.0	0.0	0.0	0.0	0.0	0.0	0.0	0.0	0.0
5	0.0	0.0	0.0	0.0	0.0	0.0	0.0	0.0	0.0	0.0	0.0
6	0.0	0.0	0.0	0.0	0.0	0.0	0.0	0.0	0.0	0.0	0.0
7	0.0	0.0	0.0	0.0	0.0	0.0	0.0	0.0	0.0	0.0	0.0
8	0.0	0.0	0.0	0.0	0.0	0.0	0.0	0.0	0.0	0.0	0.0
9	0.0	0.0	0.0	0.0	0.0	0.0	0.0	0.0	0.0	0.0	0.0
10	0.0	0.0	0.0	0.0	0.0	0.0	0.0	0.0	0.0	0.0	0.0
11	0.0	0.0	0.0	0.0	0.0	0.0	0.0	0.0	0.0	0.0	0.0
12	0.0	0.0	0.0	0.0	0.0	0.0	0.0	0.0	0.0	0.0	0.0
13	0.0	0.0	0.0	0.0	0.0	0.0	0.0	0.0	0.0	0.0	0.0
14	0.0	0.0	0.0	0.0	0.0	0.0	0.0	0.0	0.0	0.0	0.0
15	0.0	0.0	0.0	0.0	0.0	0.0	0.0	0.0	0.0	0.0	0.0
16	0.0	0.0	0.0	0.0	0.0	0.0	0.0	0.0	0.0	0.0	0.0
17	0.0	0.0	0.0	0.0	0.0	0.0	0.0	0.0	0.0	0.0	0.0
18	0.0	0.0	0.0	0.0	0.0	0.0	0.0	0.0	0.0	0.0	0.0
19	0.0	0.0	0.0	0.0	0.0	0.0	0.0	0.0	0.0	0.0	0.0

PLANE NUMBER 19

	1	2	3	4	5	6	7	8	9	10	11
1	0.0	0.0	0.0	0.0	0.0	0.0	0.0	0.0	0.0	0.0	0.0
2	0.0	0.0	0.0	0.0	0.0	0.0	0.0	0.0	0.0	0.0	0.0
3	0.0	0.0	0.0	0.0	0.0	0.0	0.0	0.0	0.0	0.0	0.0
4	0.0	0.0	0.0	0.0	0.0	0.0	0.0	0.0	0.0	0.0	0.0
5	0.0	0.0	0.0	0.0	0.0	0.0	0.0	0.0	0.0	0.0	0.0
6	0.0	0.0	0.0	0.0	0.0	0.0	0.0	0.0	0.0	0.0	0.0
7	0.0	0.0	0.0	0.0	0.0	0.0	0.0	0.0	0.0	0.0	0.0
8	0.0	0.0	0.0	0.0	0.0	0.0	0.0	0.0	0.0	0.0	0.0
9	0.0	0.0	0.0	0.0	0.0	0.0	0.0	0.0	0.0	0.0	0.0
10	0.0	0.0	0.0	0.0	0.0	0.0	0.0	0.0	0.0	0.0	0.0
11	0.0	0.0	0.0	0.0	0.0	0.0	0.0	0.0	0.0	0.0	0.0
12	0.0	0.0	0.0	0.0	0.0	0.0	0.0	0.0	0.0	0.0	0.0
13	0.0	0.0	0.0	0.0	0.0	0.0	0.0	0.0	0.0	0.0	0.0
14	0.0	0.0	0.0	0.0	0.0	0.0	0.0	0.0	0.0	0.0	0.0
15	0.0	0.0	0.0	0.0	0.0	0.0	0.0	0.0	0.0	0.0	0.0
16	0.0	0.0	0.0	0.0	0.0	0.0	0.0	0.0	0.0	0.0	0.0
17	0.0	0.0	0.0	0.0	0.0	0.0	0.0	0.0	0.0	0.0	0.0
18	0.0	0.0	0.0	0.0	0.0	0.0	0.0	0.0	0.0	0.0	0.0
19	0.0	0.0	0.0	0.0	0.0	0.0	0.0	0.0	0.0	0.0	0.0

PLANE NUMBER 20

	1	2	3	4	5	6	7	8	9	10	11
1	0.0	0.0	0.0	0.0	0.0	0.0	0.0	0.0	0.0	0.0	0.0
2	0.0	0.0	0.0	0.0	0.0	0.0	0.0	0.0	0.0	0.0	0.0
3	0.0	0.0	0.0	0.0	0.0	0.0	0.0	0.0	0.0	0.0	0.0
4	0.0	0.0	0.0	0.0	0.0	0.0	0.0	0.0	0.0	0.0	0.0
5	0.0	0.0	0.0	0.0	0.0	0.0	0.0	0.0	0.0	0.0	0.0
6	0.0	0.0	0.0	0.0	0.0	0.0	0.0	0.0	0.0	0.0	0.0
7	0.0	0.0	0.0	0.0	0.0	0.0	0.0	0.0	0.0	0.0	0.0
8	0.0	0.0	0.0	0.0	0.0	0.0	0.0	0.0	0.0	0.0	0.0
9	0.0	0.0	0.0	0.0	0.0	0.0	0.0	0.0	0.0	0.0	0.0
10	0.0	0.0	0.0	0.0	0.0	0.0	0.0	0.0	0.0	0.0	0.0
11	0.0	0.0	0.0	0.0	0.0	0.0	0.0	0.0	0.0	0.0	0.0
12	0.0	0.0	0.0	0.0	0.0	0.0	0.0	0.0	0.0	0.0	0.0

13	0.0	0.0	0.0	0.0	0.0	0.0	0.0	0.0	0.0	0.0	0.0
14	0.0	0.0	0.0	0.0	0.0	0.0	0.0	0.0	0.0	0.0	0.0
15	0.0	0.0	0.0	0.0	0.0	0.0	0.0	0.0	0.0	0.0	0.0
16	0.0	0.0	0.0	0.0	0.0	0.0	0.0	0.0	0.0	0.0	0.0
17	0.0	0.0	0.0	0.0	0.0	0.0	0.0	0.0	0.0	0.0	0.0
18	0.0	0.0	0.0	0.0	0.0	0.0	0.0	0.0	0.0	0.0	0.0
19	0.0	0.0	0.0	0.0	0.0	0.0	0.0	0.0	0.0	0.0	0.0

APPENDIX C

Computer Code GAMSCAN

```
C    GAMSCAN
C    CODE ANALYZING DATA FROM GAMMA SCANS OF MITR2 FUEL PLATES
C    EACH J CORRESPONDS TO A PARTICULAR X AND Y.FOR EACH RUN(K) USE THE SAME
C    POINTS (X,Y) IN THE SAME ORDER (J)
C PART 1.CORRECTION OF DATA FOR BACKGROUND AND ACTIVITY OF PREVIOUS IRRADIATIONS
      REAL MULT,MUL,NEW,NEWX,NEWY
      DIMENSION MP(14),LI(14),B(14),DT(15),P(14,7),X(14,67),Y(14,67),
     CXX(67),YY(67),TI(14,67),C(14,67),DELT(15,15),T(14,14,67,7),
     CMULT(14,67),SUBT(14,67),MUL(14,67),CCRCCU(14,67),RATIO(14,67),
     CWIDTH(14,67),BKN(14,67)
C    NO IS THE NUMBER OF TIMES THE FUEL PLATE IS IRRADIATED
C    A IS AN ARBITRARY REFERENCE POWER LEVEL,EG.,100 WATTS
C    NZG IS THE NUMBER OF PLATES SCANNED IN EACH IRRADIATION
C    MZS IS THE CONSTANT NUMBER OF POINTS SCANNED ON EACH IRRADIATION
      READ (5,3000)NO,NZG,MZS,A
3000  FORMAT(3I5,F7.2)
C    MP(K) IS THE NUMBER OF POINTS SCANNED IN THE KTH IRRADIATION
C    LI(K) IS THE NUMBER OF 10 MINUTE INTERVALS THE FUEL PLATE IS IRRADIATED
C    B(K) IS THE AVERAGE BACKGROUND FOR THE KTH SCAN
C    DT(K) IS THE TIME BETWEEN IRRADIATIONS,EG.,DT(3)IS THE TIME BETWEEN
C    THE STARTS OF IRRADIATIONS 2 AND 3
C    P(K,I) IS THE POWER LEVEL OF THE ITH 10 MINUTE IRRADIATION INTERVAL OF
C    THE KTH IRRADIATION,EG.,P(1,2)=75 WATTS (USE SAME UNITS AS A)
C    INDICATE THE POWER LEVEL FOR  7 INTERVALS
      READ(5,20) (MP(K),LI(K),DT(K),(P(K,I),I=1,7),K=1,NO)
20    FORMAT(2I3,F7.1/7F8.3)
C    XX(I),YY(I) ARE THE X AND Y COORDINATES OF THE ITH POINT
      READ(5,3001) (XX(I),YY(I),I=1,MZS)
3001  FORMAT(10F8.4)
C    X(K,J) IS THE DISTANCE ALONG THE LENGTH FROM THE LEFT LOWER CORNER OF THE
C    FUEL PLATE TO THE JTH POINT OF THE KTH IRRADIATION IN INCHES
C    Y(K,J) IS THE DISTANCE ALONG THE WIDTH FROM THE LEFT LOWER CORNER
C    TI(K,J) IS THE TIME BETWEEN THE START OF THE KTH IRRADIATION AND THE
C     MIDDLE OF THE COUNTING OF THE JTH POINT
C    C(K,J) IS THE COUNTS/MINUTE RECORDED AT POINT J FOR THE KTH IRRADIATION
      DO 3002 JZZ=1,NZG
```

```
       WRITE(6,3004) JZZ
3004   FORMAT (1H1,'THE FOLLCWING DATA IS FOR PLATE NO.',I3)
       DO 32 K=1,NC
       N=MP(K)
       DO 3003 II=1,MZS
       X(K,II)=XX(II)
3003   Y(K,II)=YY(II)
       READ(5,3005) P(K)
3005   FORMAT (F8.2)
       READ(5,30) (TI(K,J),C(K,J),J=1,N)
30     FORMAT (F7.2,9F8.2)
       DO 31 J=1,N
  31   WIDTH(K,J)=C.5
  32   CONTINUE
C  DELT(L,K) IS THE TIME DIFFERENCE BETWEEN THE STARTS OF IRRADIATIONS L AND K
       DO 35 L=1,NC
  35   DELT(L,L)=C.0
       L1=NC-1
       DO 40 L=1,L1
       L2=L+1
       DO 40 K=L2,NO
       M=K-1
  40   DELT(L,K)=DELT(L,M)+DT(K)
       DO 101 L=1,NO
       DO 101 K=L,NC
       N=MP(K)
       DO 101 J=1,N
       R=10.0
       N1=LI(K)
       DO 101 I=1,N1
C  T(L,K,J,I) IS THE DIFFERENCE IN TIME BETWEEN THE SCAN OF THE JTH POINT OF THE
C  KTH IRRADIATICN AND THE ITH 1C MINUTE IRRADIATION INTERVAL OF THE RTH
C  IRRADIATICN
       T(L,K,J,I)=DELT(L,K)+TI(K,J)-R
       R=R+10.0
       S=T(L,K,J,I)
```

```
      IF(S.GT.130.C) GO TO 41
      IF(S.LE.115.C)U=1.1817+0.08*(115.0-S)/5.C
      IF(S.GT.115.0.AND.S.LE.120.0)U=1.1045+0.0772*(120.0-S)/5.0
      IF(S.GT.120.0.AND.S.LE.125.0)U=1.0474+0.0571*(125.0-S)/5.0
      IF(S.GT.125.0.AND.S.LE.130.0)U=1.0+0.0474*(130.0-S)/5.0
41    IF(S.GT.190.0)GC TO 42
      IF (S.LE.130.C)GO TO 100
      IF(S.GT.130.0.AND.S.LE.140.0)U=0.88366+C.11634*(140.0-S)/10.0
      IF(S.GT.140.0.AND.S.LE.150.0)U=0.79472+C.08894*(150.0-S)/10.0
      IF(S.GT.150.C.AND.S.LE.180.0)U=0.61252+C.18220*(180.0-S)/30.0
      IF(S.GT.180.C.AND.S.LE.190.0)U=0.5592+0.05332*(190.0-S)/10.C
42    IF(S.GT.285.C)GO TO 43
      IF(S.LE.190.C)GO TO 100
      IF(S.GT.190.C.AND.S.LE.210.0)U=0.47671+0.0825*(210.0-S)/20.C
      IF(S.GT.210.C.AND.S.LE.241.0)U=0.39403+C.0827*(241.0-S)/31.0
      IF(S.GT.241.C.AND.S.LE.261.0)U=0.34452+0.04951*(261.0-S)/20.0
      IF(S.GT.261.0.AND.S.LE.285.0)U=0.30186+C.04266*(285.0-S)/24.0
43    IF(S.GT.440.C)GO TO 44
      IF(S.LE.285.C)GO TO 100
      IF(S.GT.285.0.AND.S.LE.330.0)U=0.24824+C.05362*(330.0-S)/45.0
      IF(S.GT.330.0.AND.S.LE.360.0)U=0.21712+C.03112*(360.0-S)/30.0
      IF(S.GT.360.0.AND.S.LE.380.0)U=0.20225+0.01487*(380.0-S)/20.0
      IF(S.GT.380.0.AND.S.LE.440.0)U=0.16830+0.03395*(440.0-S)/60.0
44    IF(S.GT.680.C)GO TO 45
      IF(S.LE.440.C)GO TO 100
      IF(S.GT.440.C.AND.S.LF.500.0)U=0.15137+C.01693*(500.0-S)/60.0
      IF(S.GT.500.C.AND.S.LF.560.0)U=0.13356+0.01781*(560.0-S)/60.0
      IF(S.GT.560.C.AND.S.LE.620.0)U=0.12456+C.009*(620.0-S)/60.0
      IF(S.GT.620.0.AND.S.LE.680.0)U=0.11429+C.01027*(680.0-S)/60.0
45    IF(S.GT.1940.C)GC TO 46
      IF(S.LE.680.0)GO TO 100
      IF(S.GT.680.C.AND.S.LE.740.0)U=0.10734+C.00695*(740.0-S)/60.0
      IF(S.GT.740.0.AND.S.LE.1340.C)U=0.0635+C.04384*(1340.0-S)/600.0
      IF(S.GT.1340.C.AND.S.LE.1580.C)U=0.0499+0.0136*(1580.0-S)/240.0
      IF(S.GT.1580.C.AND.S.LE.1940.C)U=0.04119+C.00871*(1940.0-S)/360.0
46    IF(S.LE.1940.0)GO TO 100
```

```
          IF(S.GT.1940.0.AND.S.IE.2805.0)U=0.02299+0.0182*(2805.0-S)/865.0
          IF(S.GT.2805.0.AND.S.IE.3254.0)U=0.01859+C.0044*(3254.0-S)/449.0
          IF(S.GT.3254.0.AND.S.IE.4286.0)U=0.0136+0.00499*(4286.0-S)/1032.0
          IF(S.GT.4286.0.AND.S.IF.5880.0)U=0.00783+0.00577*(5880.0-S)/1594.0
          IF(S.GT.5880.0.AND.S.IE.7260.0)U=0.00616+0.00167*(7260.0-S)/1380.0
          IF(S.GT.7260.0)U=C.00431+0.00185*(10140.0-S)/2880.0
100       CONTINUE
          IF(U.LE.C.0)U=0.00001
101       T(L,K,J,I)=U
C
C    BACK SCATTERING CORRECTICN RCUTINE
C
          DO 4000 K=1,NC
          DZB=0.0
          DO 4000 J=1,MZS
          DZB=DZB+1.0
          IF(DZB.GT.12.0.AND.DZB.LE.15.0)DZR=15.0
          IF(DZB.GT.15.0.AND.DZB.IE.18.0)DZR=18.0
          IF(DZB.GT.18.0.AND.DZB.LE.21.0)DZR=21.0
          IF(DZB.GT.21.0.AND.DZB.IF.24.0)DZR=24.0
          IF(DZB.GT.24.0.AND.DZB.LE.27.0)DZR=27.0
          IF(DZL.LE.12.0)BKN(K,J)=0.8*B(K)
          IF(DZB.GT.12.0.AND.DZB.LE.27.0)BKN(K,J)=B(K)*(0.8+
         10.49*(DZR-12.0)/15.0)
          IF(DZB.GT.27.0.AND.DZB.LE.54.0)BKN(K,J)=1.29*B(K)
          IF(DZB.GT.54.0.AND.DZB.LE.57.0)BKN(K,J)=1.22+B(K)
          IF(DZB.GT.57.0.AND.DZB.IE.60.0)BKN(K,J)=B(K)
          IF(DZB.GT.60.0.AND.DZB.LE.63.0)BKN(K,J)=C.65*B(K)
          IF(DZB.GT.63.0.AND.DZB.IE.67.0)BKN(K,J)=0.56*B(K)
4000      CONTINUE
C    MULT(N,J) IS THE DECAY FACTCR FOR THE NTH IRRADIATION
C    SUBT(K,J) IS THE ACTIVITY DUE TO PREVIOUS IRRADIATIONS AND WILL BE SUBTRACTED
          N=MP(1)
          DO 105 J=1,N
105       SUBT(1,J)=0.0
          DO 140 K=1,NC
```

```
          N3=MP(K)
          DO 140 J=1,N3
          KA=K-1
          IF(KA.EQ.0)GC TO 125
          SUBT(K,J)=C.0
          DO 120 M=1,KA
          N=K-M
          MULT(N,J)=0.0
          N99=LI(N)
          DO 110 I=1,N99
 110      MULT(N,J)=MULT(N,J)+P(N,I)/A*T(N,K,J,I)
 120      SUBT(K,J)=(CORCOU(N,J)*MULT(N,J))/LI(K)+SUBT(K,J)
C    MUL(K,J) IS THE DECAY FACTCR FOR THE KTH IRRADIATION
C    CORCOU(K,J) IS THE CORRECTED COUNTS PER MINUTE FOR THE JTH POINT
 125      MUL(K,J)=0.0
          CXS=SUBT(K,J)
          IF(CXS.GT.0.001)GO TO 3015
          SUBT(K,J)=C.001
 3015     N4=LI(K)
          DO 130 I=1,N4
 130      MUL(K,J)=MUL(K,J)+P(K,I)/A/T(K,K,J,I)
          CORCOU(K,J)=(((C(K,J)-EKN(K,J))-SUBT(K,J))*MUL(K,J))/LI(K)
          CXR=CORCOU(K,J)
          IF(CXR.GT.1.C)GO TO 140
          CORCOU(K,J)=1.0
 140      CONTINUE
C    PRINT CUT MEASURED POWER LEVEL FOR COMPARISON
          WRITE(6,145)
 145      FORMAT(1H1)
          WRITE(6,150)(K,(P(K,I),I=1,7),K=1,NC)
 150      FORMAT(25HCMEASURED POWER LEVELS K=,I2//1H ,7P8.3)
          COR1=1000.C
          DO 155 K=1,NC
          N6=MP(K)
          DO 155 J=1,N6
 155      RATIO(K,J)=CORCOU(K,J)/COR1
```

```
C    PRINT OUT THE CORRECTED DATA POINTS
      DO 156 K=1,NO
      N7=MP(K)
      WRITE(6,160)(JZZ,K,J,X(K,J),Y(K,J),RATIO(K,J),CORCOU(K,J),
     1C(K,J),SUBT(K,J),BKN(K,J),J=1,N7)
  160 FORMAT(1H1, 'CORRECTED DATA POINTS',//,1H ,2X,'P.N.',4X,'K',
     14X,'J',4X,'X(K,J)',4X,'Y(K,J)',4X,'RATIO(K,J)',4X,
     2'CORCOU(K,J)',4X,'C(K,J)',7X,'SUBT(K,J)',6X,'BKN(K,J)',//
     3(1H,2X,I2,3X,I3,3X,I3,3X,F7.3,3X,F7.3,4X,F8.3,6X,F9.1,7X,
     4F8.2,6X,F8.2,5X,F8.2))
      WRITE(7,4001)(CORCOU(K,J),J=1,N7)
 4001 FORMAT(10F8.2)
  156 CONTINUE
 3002 CONTINUE
      STOP
      END
```

APPENDIX D

Computer Code COREFAC

```
C    COREFAC
C
C    CODE  USING GAMSCAN DATA TO DETERMINE CORE PEAKING FACTORS
C
      DIMENSION COB(14),X(67),Y(67),NWT(14,5),CCRRAT(14,67),UNIT(67),
     $CTAR(67),PTRAT(67),PLTAVG(14,5),PLTWT(14,5),PLTRAT(14,5),ARWT(67)
C
C    INPUT SECTION
C
      READ(5,10) NO,NZG,MZS
C NO IS THE NUMBER OF IRRADIATIONS PERFORMED
C NZG IS THE NUMBER OF PLATES SCANNED PER IRRADIATION
C MZS IS THE NUMBER OF POINTS SCANNED PER PLATE
10    FORMAT (3I5)
      READ (5,15) (COB(K),K=1,NC)
C COB(K) IS THE COBALT FOIL COUNT FOR THE KTH IRRADIATION
15    FORMAT (10F8.2)
      SMCOB=9999999.
      DO 17 K=1,NO
17    IF (COB(K).IF.SMCOB)  SMCCB=COB(K)
C SMCOB IS THE SMALLEST COBALT FOIL COUNT
      READ (5,20) (X(I),Y(I),I=1,MZS)
C X(I),Y(I) ARE THE X AND Y CCCRDINATES OF THE  ITH POINT
20    FORMAT (10F8.4)
      READ (5,22) ((NWT(K,JZZ),JZZ=1,NZG),K=1,NO)
C NWT(K,JZZ) IS THE WEIGHTING FACTOR FOR THE JZZ PLATE IN THE
C    KTH IRRADIATION
22    FORMAT (10I8)
      READ (5,23) (ARWT(I),I=1,MZS)
C ARWT(I) IS THE EFFECTIVE AREA OF THE ITH POINT
23    FORMAT (10F8.5)
C
C    FA CALCULATION
C
      DO 200  JZZ=1,NZG
      DO 100 K=1,NO
```

```
      READ (5,30) (CORRAT(K,J),J=1,MZS)
C  CORRAT(K,J) IS THE CORRECTED COUNTS FROM GAMSCAN FOR THE
C     KTH IRRADIATION AND THE JTH POINT
30    FORMAT (10F8.2)
      SUM=0.0
C
C    COBALT FOIL CORRECTION
C
      DO 45  J=1,MZS
      CORRAT(K,J)=CORRAT(K,J)*(SMCOB/COB(K))
      UNIT(J)=(CORRAT(K,J))/(.5*.125)
C  UNIT(J) IS THE COUNT PER UNIT AREA FOR THE JTH POINT
      CTAR(J)=(UNIT(J))*ARWT(J)
C  CTAR(J) IS THE NUMBER CF COUNTS FOR THE JTH POINT
      SUM=SUM+CTAR(J)
45    CONTINUE
      PLTAVG(K,JZZ)=SUM/45.504
C  PLTAVG(K,JZZ) IS THE AVERAGE COUNT PER UNIT AREA FOR THE
C     JZZ PLATE IN THE KTH IRRADIATION
      DO  47  J=1,MZS
      PTRAT(J)=UNIT(J)/PLTAVG(K,JZZ)
C  PTRAT(J) IS THE RATIO OF THE COUNTS AT THE JTH POINT TO THE
C     PLATE AVERAGE COUNTS
47    CONTINUE
      WRITE (6,50) (JZZ,K,X(J),Y(J),CORRAT(K,J),UNIT(J),ARWT(J),
     $CTAR(J),PTRAT(J),J=1,MZS)
50    FORMAT (1H1,5X,'PLATE NO',2X,'K',5X,'X',8X,'Y',9X,'CORRAT',9X,
     $'UNIT',5X,'AREA WT',5X,'CTAR',9X,'PTRAT',//(7X,I2,6X,I2,3X,
     $F7.3,2X,F7.3,2X,F9.1,4X,F9.1,4X,F8.5,4X,F9.1,4X,F7.4))
      WRITE (6,55) JZZ,PLTAVG(K,JZZ)
55    FORMAT (5X,'THE AVERAGE COUNTS FOR PLATE NO ',I2,' IS  ',F9.2)
100   CONTINUE
200   CONTINUE
C
C    FR CALCULATION
C
```

```fortran
      SUMM=0.0
      DO   400 K=1,NO
      DO   300  JZZ=1,NZG
      PLTWT(K,JZZ)=(PLTAVG(K,JZZ))*(NWT(K,JZZ))
C  PLTWT(K,JZZ) IS THE AVERAGE COUNTS FOR THE JZZ PLATE IN THE
C     KTH IRRADIATION MULTIPLIED BY THE   WEIGHTING FACTOR OF
C     THE PLATE
300   SUMM=SUMM+PLTWT(K,JZZ)
400   CONTINUE
      CORAVG=SUMM/360
C  CORAVG IS THE COUNT FOR THE AVERAGE PLATE IN THE CORE
      DO   450  K=1,NO
      DO   420  JZZ=1,NZG
420   PLTRAT(K,JZZ)=(PLTAVG(K,JZZ))/CORAVG
450   CONTINUE
      WRITE   (6,460)
460   FORMAT (1H1,'THE FOLLOWING DATA IS FOR THE WHOLE CORE')
      WRITE (6,470)
470   FORMAT (3X,'IRR NO',3X,'PLATE NO',8X,'PLATE AVG',3X,'WEIGHT ',
     $'FACTOR',6X,'PLATE RATIO')
      WRITE (6,480) ((K,JZZ,PLTAVG(K,JZZ),NWT(K,JZZ),PLTRAT(K,JZZ),
     $JZZ=1,NZG),K=1,NO)
480   FORMAT (4X,I2,9X,I2,9X,F9.1,9X,I3,9X,F8.4)
      WRITE (6,500)  CORAVG
500   FORMAT (2X,'THE AVERAGE COUNTS FOR THE WHOLE CORE IS ',F9.2)
      STOP
      END
```

APPENDIX E

MACABRE Computer Code Output for
Element in Position A-2 in Core I

Reactor Power = 5.0 MW

Primary Coolant Flow = 2000 gpm

Inlet Coolant Temp. = 116.0° F.

Nominal Fuel Channel Dimensions

MITR2 TEMP DISTRIBUTION CORE 1 A-2

INTEGER ARRAY

| 1 | 64 | 16 | 1 | 1 | 24 | 1 | 1 | 1 | 2 | 64 | 0 | 0 | 0 |

FLOATING POINT SINGLE VALUE ARRAY

0.0	2.7886D+00	2.2900D-01	2.2900D-01	2.0000D-02	2.0000D-02	2.0000D-02	3.0000D-02
0.0	0.0	1.1600D+02	0.0	1.1040D+01	1.0000D+00	1.0000D+00	5.0000D-01
5.0000D-01	5.0000D-01	5.0000D-01	2.0000D+00	1.4640D+05	1.2000D+03	1.2000D+03	1.9000D+00
5.0000D-03	1.5600D+01	4.4300D+02	8.2900D+03	7.7800D-01	2.4000D+01	0.0	0.0
0.0	0.0	0.0	0.0	0.0	0.0	0.0	0.0
0.0	0.0	0.0	0.0	0.0	0.0	0.0	0.0
0.0	0.0	0.0	0.0	0.0	0.0	0.0	

MULM ARRAY

1.9000D+00	1.9000D+00	1.9000D+00	1.9000D+00	1.9000D+00	1.9000D+00	1.9000D+00	1.9000D+00
1.9000D+00	1.9000D+00	1.9000D+00	1.9000D+00	1.9000D+00	1.9000D+00	1.9000D+00	1.9000D+00

FLOATING POINT ARRAY DATA

30	1	0	1	1	5.0000D-02	0	2	1	2.1000D-01	0	3	1	3.6600D-01	207
30	1	0	4	1	5.2400D-01	0	5	1	6.8200D-01	0	6	1	8.4000D-01	208
30	1	0	7	1	9.9800D-01	0	8	1	1.1560D+00	0	9	1	1.3140D+00	209
30	1	0	10	1	1.4720D+00	0	11	1	1.6300D+00	0	12	1	1.7880D+00	210
30	1	0	13	1	1.9460D+00	0	14	1	2.1040D+00	0	15	1	2.2620D+00	212
30	1217	0	1	1	1.2000D-01	0	2	1	2.7800D-01	0	3	1	4.3600D-01	213
30	1217	0	4	1	5.9400D-01	0	5	1	7.5200D-01	0	6	1	9.1000D-01	214
30	1217	0	7	1	1.0680D+00	0	8	1	1.2260D+00	0	9	1	1.3840D+00	215
30	1217	0	10	1	1.5420D+00	0	11	1	1.7000D+00	0	12	1	1.8580D+00	216
30	1217	0	13	1	2.0160D+00	0	14	1	2.1740D+00	0	15	1	2.3320D+00	217
20	2433	0	0	1	2.9600D-02	0	0	64	5.2100D-02	0	0	0	0.0	218
20	2497	0	1	0	1.2430D-01	0	15	0	1.2430D-01	0	0	0	0.0	219
30	2516	0	1	0	7.0000D+00	0	2	0	7.6000D+00	0	16	0	7.0000D+00	220
10	2536	0	1	0	5.0000D-01	0	0	0	0.0	0	0	0	0.0	221
10	2556	0	1	0	5.0000D-01	0	0	0	0.0	0	0	0	0.0	222
20	2576	0	1	0	1.0000D+00	0	16	0	1.0000D+00	0	0	0	0.0	223

20	2596	0	1	0	1.0000D+00	0	16	0	1.0000D+00	0	0	0	0.0	224
10	2616	0	0	1	6.0000D-03	0	0	0	0.0	0	0	0	0.0	225
10	2617	1	1	1	1.0C00D-06	0	0	0	0.0	0	0	0	0.0	226
10	2680	0	0	1	2.3760D+00	0	0	0	0.0	0	0	0	0.0	227
10	2744	0	0	1	2.0000D-02	0	0	0	0.0	0	0	0	0.0	228
11	2808	0	0	1	2.0C00D-02	0	0	0	0.0	0	0	0	0.0	229

HORIZCNTAL PEAKING

```
    1.33    1.27    1.21    1.17    1.15    1.13    1.11    1.10    1.09    1.08    1.08    1.08    1.08    1.08
    1.09
```

```
PLATE NC.          1    2    3    4    5    6    7    8    9   10   11   12   13   14   15
VP PROFILE         1    1    2    2    2    2    2    2    2    2    2    2    2    2    2
```

VERTICAL PEAKING FOR PROFILE   1

```
    2.80    1.56    1.45    1.46    1.46    1.45    1.44    1.43    1.38    1.30    1.17    1.05    0.94    0.81
    0.70    C.62    0.56    0.51    0.47    0.44    0.41    0.37    0.32    0.01
```

VERTICAL PEAKING FOR PROFILE   2

```
    2.80    1.35    1.30    1.35    1.43    1.47    1.47    1.47    1.44    1.35    1.22    1.10    0.98    0.87
    0.76    C.69    0.60    0.55    0.50    0.46    0.41    0.37    0.32    0.01
```

FLOFED=   11.04000 LBS./SEC.   AVEPL=   3.27596

MESH POINT - 1

DX = C.0 FT.

CHANNEL	VEL FT/SEC	TOTPL PSI	TBULK DEG. F.	TSURFACE DEG. F.	FILMTH INCHES	TINTFACE DEG. F.	TINTFACE DEG. F.	FILMTH INCHES	TSURFACE DEG. F.	Q / A BTU/HR*FT2	Q / A BTU/HR*FT2	WINDOW
	4.28	0.18										
1	7.67	0.59	116.0									
				174.1	1.0000-06	174.1	174.0	1.0C00-06	174.0	2.71760+05	2.74670+05	
2	7.83	0.61	116.0									
				170.4	1.0000-06	170.4	170.6	1.0000-06	170.6	2.57420+05	2.56570+05	
3	7.72	0.60	116.0									
				168.4	1.0000-06	168.5	168.5	1.0C00-06	168.5	2.46580+05	2.46810+05	
4	7.71	0.59	116.0									
				168.6	1.0000-06	166.6	166.7	1.0000-06	166.7	2.37870+05	2.38100+05	
5	7.71	0.59	116.0									
				165.9	1.0000-06	165.9	166.0	1.0000-06	166.0	2.34450+05	2.34690+05	
6	7.71	0.59	116.0									
				165.0	1.0000-06	165.1	165.1	1.0C00-06	165.1	2.30410+05	2.30640+05	
7	7.71	0.59	116.0									
				164.4	1.0000-06	164.4	164.5	1.0000-06	164.5	2.27380+05	2.27600+05	
8	7.71	0.59	116.0									
				163.8	1.0000-06	163.8	163.8	1.0C00-06	163.8	2.24340+05	2.24560+05	
9	7.70	0.59	116.0									
				163.3	1.0000-06	163.4	163.4	1.0C00-06	163.4	2.22320+05	2.22540+05	
10	7.70	0.59	116.0									
				163.1	1.0C00-06	163.1	163.2	1.0000-06	163.2	2.21310+05	2.21540+05	
11	7.70	0.59	116.0									
				163.1	1.0000-06	163.2	163.2	1.0000-06	163.2	2.21320+05	2.21550+05	
12	7.70	0.59	116.0									
				163.1	1.0000-06	163.2	163.2	1.0000-03	163.2	2.21320+05	2.21550+05	
13	7.70	0.59	116.0									
				163.1	1.0000-06	163.2	163.2	1.0000-06	163.2	2.21320+05	2.21540+05	
14	7.70	0.59	116.0									
				163.1	1.0000-06	163.2	163.2	1.0C00-06	163.2	2.21350+05	2.21520+05	
15	7.70	0.59	116.0									
				163.5	1.0C00-06	163.5	163.6	1.0000-06	163.6	2.22920+05	2.22180+05	
16	7.65	0.59	116.0									
	4.28	0.18										

MITR2 TEMP DISTRIBUTION CORE 1 A-2

MESH POINT - 3

DX = 0.02960 FT.

CHANNEL	VEL FT/SEC	TOTPL PSI	TBULK DEG. F.	TSURFACE DEG. F.	FILMTH INCHES	TINTFACE DEG. F.	TINTFACE DEG. F.	FILMTH INCHES	TSURFACE DEG. F.	Q / A BTU/HR*FT2	Q / A BTU/HR*FT2	WINDOW
	4.28	0.28										
1	7.67	0.68	117.0									
				156.9	1.000D-06	156.9	156.9	1.000D-06	156.9	1.8770D+05	1.8682D+05	
2	7.83	0.71	117.8									
				154.2	1.000D-06	154.2	154.5	1.000D-06	154.5	1.7386D+05	1.7404D+05	
3	7.72	0.69	117.8									
				150.3	1.000D-06	150.3	150.4	1.000D-06	150.4	1.5402D+05	1.5485D+05	
4	7.71	0.69	117.7									
				149.1	1.000D-06	149.1	149.2	1.000D-06	149.2	1.4877D+05	1.4940D+05	
5	7.71	0.69	117.6									
				149.6	1.000D-06	148.6	148.7	1.000D-06	148.7	1.4674D+05	1.4729D+05	
6	7.71	0.69	117.6									
				148.1	1.000D-06	148.1	148.2	1.000D-06	148.2	1.4423D+05	1.4476D+05	
7	7.71	0.69	117.6									
				147.7	1.000D-06	147.7	147.8	1.000D-06	147.8	1.4238D+05	1.4288D+05	
8	7.71	0.69	117.6									
				147.3	1.000D-06	147.3	147.4	1.000D-06	147.3	1.4051D+05	1.4099D+05	
9	7.71	0.69	117.5									
				147.0	1.000D-06	147.0	147.1	1.000D-06	147.1	1.3929D+05	1.3973D+05	
10	7.71	0.69	117.5									
				146.9	1.000D-06	146.9	146.9	1.000D-06	146.9	1.3868D+05	1.3910D+05	
11	7.71	0.69	117.5									
				146.9	1.000D-06	146.9	147.0	1.000D-06	146.9	1.3870D+05	1.3910D+05	
12	7.71	0.69	117.5									
				146.9	1.000D-06	146.9	147.0	1.000D-06	146.9	1.3870D+05	1.3910D+05	
13	7.71	0.69	117.5									
				146.9	1.000D-06	146.9	147.0	1.000D-06	146.9	1.3870D+05	1.3910D+05	
14	7.71	0.69	117.5									
				146.9	1.000D-06	146.9	147.0	1.000D-06	147.0	1.3873D+05	1.3908D+05	
15	7.70	0.69	117.5									
				146.8	1.000D-06	146.8	146.8	1.000D-06	146.8	1.3840D+05	1.4089D+05	
16	7.65	0.68	116.8									
	4.28	0.28										

MITR2 TEMP DISTRIBUTION   CORE 1   A-2

MESH POINT -   5

DX =   0.02960 FT.

CHANNEL	VEL FT/SEC	TOTPL PSI	TBULK DEG. F.	TSURFACE DEG. F.	FILMTH INCHES	TINTFACE DEG. F.	TINTFACE DEG. F.	FILMTH INCHES	TSURFACE DEG. F.	Q / A BTU/HR*FT2	Q / A BTU/HR*FT2	WINDOW
	4.28	0.38										
1	7.67	0.77	117.7									
				149.3	1.000D-06	149.4	149.5	1.000D-06	149.5	1.494?D+05	1.4596D+05	
2	7.84	0.80	119.1									
				147.2	1.000D-06	147.2	147.5	1.000D-06	147.4	1.3502D+05	1.3599D+05	
3	7.72	0.78	118.9									
				142.8	1.000D-06	142.9	143.0	1.000D-06	143.0	1.1406D+05	1.1547D+05	
4	7.72	0.78	118.7									
				141.9	1.000D-06	141.9	142.1	1.000D-06	142.1	1.1052D+05	1.1137D+05	
5	7.71	0.78	118.6									
				141.6	1.000D-06	141.6	141.7	1.000D-06	141.7	1.0909D+05	1.0981D+05	
6	7.71	0.79	118.6									
				141.2	1.000D-06	141.2	141.3	1.000D-06	141.3	1.0726D+05	1.0795D+05	
7	7.71	0.78	118.6									
				140.8	1.000D-06	140.9	141.0	1.000D-06	141.0	1.0591D+05	1.0657D+05	
8	7.71	0.78	118.5									
				140.5	1.000D-06	140.5	140.6	1.000D-06	140.6	1.0455D+05	1.0517D+05	
9.	7.71	0.78	118.5									
				140.3	1.000D-06	140.3	140.4	1.000D-06	140.4	1.0367D+05	1.0424D+05	
10	7.71	0.78	118.5									
				140.2	1.000D-06	140.2	140.3	1.000D-06	140.3	1.0325D+05	1.0377D+05	
11	7.71	0.78	118.5									
				140.2	1.000D-06	140.2	140.3	1.000D-06	140.3	1.0327D+05	1.0377D+05	
12	7.71	0.78	118.5									
				140.2	1.000D-06	140.2	140.3	1.000D-06	140.3	1.0327D+05	1.0377D+05	
13	7.71	0.78	118.5									
				140.2	1.000D-06	140.2	140.3	1.000D-06	140.3	1.0328D+05	1.0377D+05	
14	7.71	0.78	118.5									
				140.2	1.000D-06	140.2	..3	1.000D-06	140.3	1.0330D+05	1.0375D+05	
15	7.70	0.78	118.5									
				139.9	1.000D-06	139.9	139.9	1.000D-06	139.9	1.0181D+05	1.0639D+05	
16	7.66	0.77	117.3									
	4.28	0.38										

PITR2 TEMP DISTRIBUTION CORE 1 A-2

MESH POINT -   7

DX =   0.02960 FT.

CHANNEL	VEL FT/SEC	TOTPL PSI	TBULK DEG. F.	TSURFACE DEG. F.	FILMTH INCHES	TINTFACE DEG. F.	TINTFACE CEG. F.	FILMTH INCHES	TSURFACE DEG. F.	Q / A BTU/HR*FT2	Q / A WINDOW BTU/HR*FT2
	4.28	0.48									
1	7.67	0.87	118.3								
				148.8	1.000D-06	148.8	149.0	1.0C0D-06	149.0	1.4431D+05	1.3891D+05
2	7.84	0.89	120.2								
				146.7	1.C00D-06	146.8	147.1	1.000D-06	147.1	1.2828D+05	1.2976D+05
3	7.72	0.88	119.9								
				143.2	1.000D-06	143.2	143.3	1.000D-06	143.3	1.1130D+05	1.1320D+05
4	7.72	0.88	119.6								
				142.3	1.C00D-06	142.3	142.4	1.000D-06	142.4	1.0810D+05	1.0914D+05
5	7.72	0.88	119.6								
				141.9	1.0C0D-06	141.9	142.1	1.000D-06	142.1	1.0674D+05	1.0762D+05
6	7.71	0.88	119.5								
				141.5	1.000D-06	141.5	141.6	1.000D-06	141.6	1.0497D+05	1.0581D+05
7	7.71	0.88	119.5								
				141.2	1.000D-06	141.2	141.3	1.0C0D-06	141.3	1.0367D+05	1.0446D+05
8	7.71	0.88	119.4								
				140.9	1.C00D-06	140.9	14I.0	1.000D-06	141.0	1.0235D+05	1.0309D+05
9	7.71	0.88	119.4								
				140.7	1.000D-06	140.7	140.8	1.0C0D-06	140.8	1.0151D+05	1.0218D+05
10	7.71	0.87	119.3								
				140.6	1.000D-06	140.6	140.7	1.000D-06	140.7	1.0111D+05	1.0171D+05
11	7.71	0.87	119.3								
				140.6	1.000D-06	140.6	140.7	1.000D-06	140.7	1.0114D+05	1.0172D+05
12	7.71	0.87	119.3								
				140.6	1.000D-06	140.6	140.7	1.000D-06	140.7	1.0114D+05	1.0172D+05
13	7.71	0.87	119.3								
				140.6	1.000D-06	140.6	140.7	1.000D-06	140.7	1.0115D+05	1.0171D+05
14	7.71	0.87	119.3								
				140.6	1.000D-06	140.6	140.7	1.000D-06	140.7	1.0115D+05	1.0171D+05
15	7.70	0.87	119.3								
				140.1	1.000D-06	140.1	140.0	1.0C0D-06	140.0	9.8895D+04	1.0513D+05
16	7.66	0.86	117.7								
	4.28	0.48									

MESH POINT - 9

DX = C.02960 FT.

CHANNEL	VEL FT/SEC	TOTPL PSI	TBULK DEG. F.	TSURFACE DEG. F.	FILMTH INCHES	TINTFACE DEG. F.	TINTFACE DEG. F.	FILMTH INCHES	TSURFACE DEG. F.	Q / A BTU/HR*FT2	Q / A BTU/HR*FT2	WINDOW
	4.28	0.58										
1	7.67	0.96	118.9									
				149.7	1.0000-06	149.7	149.9	1.0000-06	149.9	1.4585D+05	1.3876D+05	
2	7.84	0.99	121.3									
				147.6	1.0000-06	147.6	148.0	1.0000-06	148.0	1.2794D+05	1.2986D+05	
3	7.72	0.97	121.0									
				144.6	1.0000-06	144.6	144.8	1.0000-06	144.7	1.1357D+05	1.1592D+05	
4	7.72	0.97	120.6									
				143.6	1.0000-06	143.6	143.8	1.0000-06	143.8	1.1052D+05	1.1178D+05	
5	7.72	0.97	120.5									
				143.3	1.0000-06	143.3	143.4	1.0000-06	143.4	1.0919D+05	1.1023D+05	
6	7.72	0.97	120.4									
				142.8	1.0000-06	142.8	143.0	1.0000-06	143.0	1.0740D+05	1.0839D+05	
7	7.71	0.97	120.3									
				142.5	1.0000-06	142.5	142.6	1.0000-06	142.6	1.0609D+05	1.0702D+05	
8	7.71	0.97	120.3									
				142.2	1.0000-06	142.2	142.3	1.0000-06	142.3	1.0477D+05	1.0563D+05	
9	7.71	0.97	120.2									
				142.0	1.0000-06	142.0	142.1	1.0000-06	142.1	1.0393D+05	1.0470D+05	
10	7.71	0.97	120.2									
				141.9	1.0000-06	141.9	142.0	1.0000-06	142.0	1.0353D+05	1.0423D+05	
11	7.71	0.97	120.2									
				141.9	1.0000-06	141.9	142.0	1.0000-06	142.0	1.0357D+05	1.0423D+05	
12	7.71	0.97	120.2									
				141.9	1.0000-06	141.9	142.0	1.0000-06	142.0	1.0357D+05	1.0423D+05	
13	7.71	0.97	120.2									
				141.9	1.0000-06	141.9	142.0	1.0000-06	142.0	1.0357D...	..0423D+05	
14	7.71	0.97	120.2									
				141.9	1.0000-06	141.9	142.0	1.0000-06	142.0	1.0356D+05	1.0425D+05	
15	7.71	0.97	120.2									
				141.2	1.0000-06	141.2	141.2	1.0000-06	141.1	1.0060D+05	1.0843D+05	
16	7.66	0.96	118.2									
	4.28	0.58										

MITR2 TEMP DISTRIBUTION CORE 1 A-2

MESH POINT - 11

DX = 0.02960 FT.

CHANNEL	VEL FT/SEC	TOTPL PSI	TBULK DEG. F.	TSURFACE DEG. F.	FILMTH INCHES	TINTFACE DEG. F.	TINTFACE DEG. F.	FILMTH INCHES	TSURFACE DEG. F.	Q / A BTU/HR*FT2	Q / A BTU/HR*FT2	WINDOW
	4.28	0.68										
1	7.67	1.05	119.5									
				150.4	1.000D-06	150.4	150.7	1.000D-06	150.7	1.4685D+05	1.3807D+05	
2	7.84	1.08	122.3									
				148.4	1.000D-06	148.4	148.8	1.000D-06	148.8	1.2712D+05	1.2943D+05	
3	7.73	1.06	122.0									
				146.3	1.000D-06	146.3	146.5	1.000D-06	146.5	1.1731D+05	1.2006D+05	
4	7.72	1.06	121.6									
				145.3	1.000D-06	145.3	145.5	1.000D-06	145.5	1.1427D+05	1.1576D+05	
5	7.72	1.06	121.4									
				144.9	1.000D-06	144.9	145.1	1.000D-06	145.1	1.1293D+05	1.1417D+05	
6	7.72	1.06	121.3									
				144.4	1.000D-06	144.4	144.6	1.000D-06	144.6	1.1108D+05	1.1226D+05	
7	7.72	1.06	121.3									
				144.1	1.000D-06	144.1	144.3	1.000D-06	144.3	1.0975D+05	1.1085D+05	
8	7.71	1.06	121.2									
				143.7	1.000D-06	143.7	143.9	1.000D-06	143.9	1.0839D+05	1.0941D+05	
9	7.71	1.06	121.1									
				143.5	1.000D-06	143.5	143.7	1.000D-06	143.7	1.0753D+05	1.0845D+05	
10	7.71	1.06	121.1									
				143.4	1.000D-06	143.4	143.6	1.000D-06	143.6	1.0713D+05	1.0796D+05	
11	7.71	1.06	121.1									
				143.4	1.000D-06	143.4	143.6	1.000D-06	143.6	1.0718D+05	1.0796D+05	
12	7.71	1.06	121.1									
				143.4	1.000D-06	143.4	143.6	1.000D-06	143.6	1.0718D+05	1.0796D+05	
13	7.71	1.06	121.1									
				143.4	1.000D-06	143.4	143.6	1.000D-06	143.6	1.0718D+05	1.0796D+05	
14	7.71	1.06	121.1									
				143.4	1.000D-06	143.4	143.6	1.000D-06	143.6	1.0715D+05	1.0800D+05	
15	7.71	1.06	121.1									
				142.6	1.000D-06	142.6	142.5	1.000D-06	142.5	1.0350D+05	1.1294D+05	
16	7.66	1.05	118.6									
	4.28	0.68										

DX = 0.02960 FT.

CHANNEL	VEL FT/SEC	TOTPL PSI	TBULK DEG. F.	TSURFACE DEG. F.	FILMTH INCHES	TINTFACE DEG. F.	TINTFACE DEG. F.	FILMTH INCHES	TSURFACE DEG. F.	Q / A BTU/HR*FT2	Q / A BTU/HR*FT2	WINDOW
	4.28	0.78										
1	7.68	1.15	120.1									
				151.1	1.0000-06	151.1	151.4	1.0000-06	151.4	1.4744D+05	1.3696D+05	
2	7.84	1.17	123.4									
				149.1	1.0000-06	149.1	149.5	1.0000-06	149.5	1.2599D+05	1.2861D+05	
3	7.73	1.16	123.0									
				147.9	1.0000-06	147.9	148.1	1.0000-06	148.1	1.2058D+05	1.2367D+05	
4	7.72	1.16	122.6									
				146.8	1.0000-06	146.8	147.1	1.0000-06	147.1	1.1750D+05	1.1923D+05	
5	7.72	1.16	122.4									
				146.4	1.0000-06	146.4	146.6	1.0000-06	146.6	1.1616D+05	1.1759D+05	
6	7.72	1.16	122.3									
				145.9	1.0000-06	146.0	146.2	1.0000-06	146.1	1.1427D+05	1.1564D+05	
7	7.72	1.16	122.2									
				145.6	1.0000-06	145.6	145.8	1.0000-06	145.8	1.1291D+05	1.1419D+05	
8	7.72	1.16	122.1									
				145.2	1.0000-06	145.2	145.4	1.0000-06	145.4	1.1152D+05	1.1271D+05	
9	7.72	1.16	122.1									
				145.0	1.0000-06	145.0	145.2	1.0000-06	145.2	1.1065D+05	1.1172D+05	
10	7.71	1.15	122.0									
				144.9	1.0000-06	144.9	145.1	1.0000-06	145.1	1.1025D+05	1.1121D+05	
11	7.71	1.15	122.0									
				144.9	1.0000-06	144.9	145.1	1.0000-06	145.1	1.1031D+05	1.1121D+05	
12	7.71	1.15	122.0									
				144.9	1.0000-06	144.9	145.1	1.0000-06	145.1	1.1031D+05	1.1121D+05	
13	7.71	1.15	122.0									
				144.9	1.0000-06	144.9	145.1	1.0000-06	145.1	1.1031D+05	1.1121D+05	
14	7.71	1.15	122.0									
				144.9	1.0000-06	144.9	145.1	1.0000-06	145.0	1.1025D+05	1.1128D+05	
15	7.71	1.15	122.0									
				143.9	1.0000-06	143.9	143.8	1.0000-06	143.8	1.0590D+05	1.1699D+05	
16	7.66	1.14	119.1									
	4.28	0.78										

DX = 0.02960 FT.

CHANNEL	VEL FT/SEC	TOTPL PSI	TBULK DEG. F.	TSURFACE DEG. F.	FILMTH INCHES	TINTFACE DEG. F.	TINTFACE DEG. F.	FILMTH INCHES	TSURFACE DEG. F.	Q / A BTU/HR*FT2	Q / A BTU/HR*FT2	WINDOW
	4.28	0.88										
1	7.68	1.24	120.8									
				151.6	1.0000-06	151.6	152.0	1.0000-06	152.0	1.4760D+05	1.3542D+05	
2	7.85	1.27	124.5									
				149.8	1.0000-06	149.8	150.2	1.0000-06	150.2	1.2457D+05	1.2742D+05	
3	7.73	1.25	124.1									
				149.2	1.0000-06	149.2	149.4	1.0000-06	149.4	1.2236D+05	1.2572D+05	
4	7.73	1.25	123.6									
				148.1	1.0000-06	148.1	148.4	1.0000-06	148.3	1.1925D+05	1.2122D+05	
5	7.72	1.25	123.4									
				147.7	1.0000-06	147.7	147.9	1.0000-06	147.9	1.1793D+05	1.1955D+05	
6	7.72	1.25	123.3									
				147.2	1.0000-06	147.2	147.4	1.0000-06	147.4	1.1602D+05	1.1757D+05	
7	7.72	1.25	123.2									
				146.8	1.0000-06	146.8	147.0	1.0000-06	147.0	1.1465D+05	1.1610D+05	
8	7.72	1.25	123.1									
				146.4	1.0000-06	146.5	146.7	1.0000-06	146.7	1.1326D+05	1.1461D+05	
9	7.72	1.25	123.0									
				146.2	1.0000-06	146.2	146.4	1.0000-06	146.4	1.1239D+05	1.1360D+05	
10	7.72	1.25	123.0									
				146.1	1.0000-06	146.1	146.3	1.0000-06	146.3	1.1200D+05	1.1308D+05	
11	7.72	1.25	123.0									
				146.1	1.0000-06	146.1	146.3	1.0000-06	146.3	1.1206D+05	1.1308D+05	
12	7.72	1.25	123.0									
				146.1	1.0000-06	146.1	146.3	1.0000-06	146.3	1.1206D+05	1.1308D+05	
13	7.72	1.25	123.0									
				146.1	1.0000-06	146.1	146.3	1.0000-06	146.3	1.1206D+05	1.1308D+05	
14	7.72	1.25	123.0									
				146.1	1.0000-06	146.1	146.3	1.0000-06	146.3	1.1197D+05	1.1318D+05	
15	7.71	1.25	122.9									
				145.0	1.0000-06	145.0	144.8	1.0000-06	144.8	1.0691D+05	1.1968D+05	
16	7.66	1.24	119.6									
	4.28	0.88										

MITR2 TEMP DISTRIBUTION CORE 1 A-2

MESH POINT - 17

DX = C.02960 FT.

CHANNEL	VEL FT/SEC	TOTPL PSI	TBULK DEG. F.	TSURFACE DEG. F.	FILMTH INCHES	TINTFACE DEG. F.	TINTFACE DEG. F.	FILMTH INCHES	TSURFACE DEG. F.	Q / A BTU/HR*FT2	Q / A BTU/HR*FT2	WINDOW
	4.28	0.98										
1	7.68	1.33	121.4									
				152.2	1.0000-06	152.2	152.6	1.0000-06	152.6	1.4775D+05	1.3389D+05	
2	7.85	1.36	125.5									
				150.4	1.0000-06	150.4	150.9	1.0000-06	150.9	1.2319D+05	1.2623D+05	
3	7.73	1.34	125.1									
				150.0	1.0000-06	150.0	150.3	1.0000-06	150.3	1.2175D+05	1.2534D+05	
4	7.73	1.34	124.6									
				148.9	1.0000-06	148.9	149.2	1.0000-06	149.2	1.1865D+05	1.2087D+05	
5	7.73	1.34	124.4									
				148.5	1.0000-06	148.5	148.7	1.0000-06	148.7	1.1739D+05	1.1921D+05	
6	7.72	1.34	124.3									
				148.0	1.0000-06	148.0	148.2	1.0000-06	148.2	1.1550D+05	1.1725D+05	
7	7.72	1.34	124.2									
				147.6	1.0000-06	147.6	147.8	1.0000-06	147.8	1.1416D+05	1.1579D+05	
8	7.72	1.34	124.1									
				147.2	1.0000-06	147.2	147.5	1.0000-06	147.5	1.1279D+05	1.1430D+05	
9	7.72	1.34	124.0									
				147.0	1.0000-06	147.0	147.2	1.0000-06	147.2	1.1195D+05	1.1330D+05	
10	7.72	1.34	123.9									
				146.8	1.0000-06	146.9	147.1	1.0000-06	147.1	1.1157D+05	1.1278D+05	
11	7.72	1.34	123.9									
				146.8	1.0000-06	146.9	147.1	1.0000-06	147.1	1.1164D+05	1.1277D+05	
12	7.72	1.34	123.9									
				146.8	1.0000-06	146.9	147.1	1.0000-06	147.1	1.1164D+05	1.1277D+05	
13	7.72	1.34	123.9									
				146.8	1.0000-06	146.9	147.1	1.0000-06	147.1	1.1164D+05	1.1277D+05	
14	7.72	1.34	123.9									
				146.8	1.0000-06	146.8	147.1	1.0000-06	147.0	1.1150D+05	1.1292D+05	
15	7.72	1.34	123.8									
				145.6	1.0000-06	145.6	145.4	1.0000-06	145.4	1.0571D+05	1.2021D+05	
16	7.66	1.33	120.1									
	4.28	0.98										

MITR2 TEMP DISTRIBUTION CORE 1 A-2

MESH POINT - 19

DX = 0.02960 FT.

CHANNEL	VEL FT/SEC	TOTPL PSI	TBULK DEG. F.	TSURFACE DEG. F.	FILMTH INCHES	TINTFACE DEG. F.	TINTFACE DEG. F.	FILMTH INCHES	TSURFACE DEG. F.	Q / A BTU/HR*FT2	Q / A BTU/HR*FT2	WINDOW
	4.28	1.08										
1	7.68	1.42	122.0									
				152.8	1.000D-06	152.8	153.2	1.000D-06	153.2	1.4788D+05	1.3237D+05	
2	7.85	1.45	126.6									
				151.1	1.000D-06	151.1	151.6	1.000D-06	151.6	1.2185D+05	1.2506D+05	
3	7.74	1.44	126.2									
				150.8	1.000D-06	150.8	151.1	1.000D-06	151.1	1.2106D+05	1.2488D+05	
4	7.73	1.44	125.7									
				149.7	1.000D-06	149.7	150.0	1.000D-06	150.0	1.1798D+05	1.2043D+05	
5	7.73	1.43	125.4									
				149.2	1.000D-06	149.2	149.5	1.000D-06	149.5	1.1677D+05	1.1879D+05	
6	7.73	1.43	125.3									
				148.7	1.000D-06	148.7	149.0	1.000D-06	149.0	1.1491D+05	1.1684D+05	
7	7.72	1.43	125.1									
				148.3	1.000D-06	148.4	148.6	1.000D-06	148.6	1.1359D+05	1.1539D+05	
8	7.72	1.43	125.0									
				148.0	1.000D-06	148.0	148.2	1.000D-06	148.2	1.1224D+05	1.1392D+05	
9	7.72	1.43	124.9									
				147.7	1.000D-06	147.7	148.0	1.000D-06	148.0	1.1142D+05	1.1291D+05	
10	7.72	1.43	124.9									
				147.6	1.000C-06	147.6	147.9	1.000D-06	147.9	1.1107D+05	1.1239D+05	
11	7.72	1.43	124.9									
				147.6	1.000D-06	147.6	147.9	1.000D-06	147.8	1.1114D+05	1.1239D+05	
12	7.72	1.43	124.9									
				147.6	1.000D-06	147.6	147.9	1.000D-06	147.8	1.1114D+05	1.1239D+05	
13	7.72	1.43	124.9									
				147.6	1.000C-06	147.6	147.9	1.000D-06	147.8	1.1114D+05	1.1239D+05	
14	7.72	1.43	124.9									
				147.6	1.000D-06	147.6	147.8	1.000D-06	147.8	1.1096D+05	1.1258D+05	
15	7.72	1.43	124.8									
				146.1	1.000D-06	146.1	145.9	1.000D-06	145.9	1.0444D+05	1.2067D+05	
16	7.66	1.42	120.6									
	4.28	1.08										

MITR2 TEMP DISTRIBUTION CORE 1 A-2

MESH POINT - 21

DX = 0.02960 FT.

CHANNEL	VEL FT/SEC	TOTPL PSI	TBULK DEG. F.	TSURFACE DEG. F.	FILMTH INCHES	TINTFACE DEG. F.	TINTFACE DEG. F.	FILMTH INCHES	TSURFACE DEG. F.	Q / A BTU/HR*FT2	Q / A WINDOW BTU/HR*FT2
	4.28	1.18									
1	7.68	1.52	122.6								
				153.2	1.0000-06	153.2	153.7	1.0000-06	153.7	1.4760D+05	1.3045D+05
2	7.86	1.54	127.6								
				151.7	1.000D-06	151.7	152.2	1.000D-06	152.2	1.2015D+05	1.2351D+05
3	7.74	1.53	127.2								
				151.5	1.CCOD-06	151.5	151.9	1.000D-06	151.8	1.2012D+05	1.2414D+05
4	7.73	1.53	126.7								
				150.4	1.0000-06	150.4	150.7	1.0000-06	150.7	1.1704D+05	1.1974D+05
5	7.73	1.53	126.4								
				149.9	1.0000-06	150.0	150.3	1.0000-06	150.3	1.1590D+05	1.1811D+05
6	7.73	1.53	126.3								
				149.4	1.0000-06	149.4	149.7	1.0000-06	149.7	1.1407D+05	1.1618D+05
7	7.73	1.53	126.1								
				149.1	1.0000-06	149.1	149.3	1.000D-06	149.3	1.1278D+05	1.1475D+05
8	7.73	1.53	126.0								
				148.7	1.0000-06	148.7	149.0	1.000D-06	149.0	1.1146D+05	1.1329D+05
9	7.72	1.53	125.9								
				148.4	1.0000-06	148.4	148.7	1.000D-06	148.7	1.1066D+05	1.1229D+05
10	7.72	1.53	125.8								
				148.3	1.0000-06	148.3	148.6	1.0C0D-06	148.6	1.1032D+05	1.1177D+05
11	7.72	1.53	125.8								
				149.3	1.0000-06	148.3	148.6	1.0000-06	148.6	1.1040D+05	1.1176D+05
12	7.72	1.53	125.8								
				148.3	1.0000-06	148.3	148.6	1.0000-06	148.6	1.1040D+05	1.1176D+05
13	7.72	1.53	125.8								
				148.3	1.000D-C6	148.3	148.6	1.0000-06	148.6	1.1040D+05	1.1177D+05
14	7.72	1.53	125.8								
				148.2	1.CCOD-06	148.3	148.5	1.000D-06	148.5	1.1017D+05	1.1201D+05
15	7.72	1.52	125.7								
				146.7	1.0000-06	146.7	146.4	1.0000-06	146.4	1.0295D+05	1.2088D+05
16	7.66	1.51	121.2								
	4.28	1.18									

MESH POINT - 23

DX = 0.02960 FT.

CHANNEL	VEL FT/SEC	TOTPL PSI	TBULK DEG. F.	TSURFACE DEG. F.	FILMTH INCHES	TINTFACE DEG. F.	TINTFACE CEG. F.	FILMTH INCHES	TSURFACE DEG. F.	Q / A BTU/HR*FT2	Q / A BTU/HR*FT2	WINDOW
	4.28	1.28										
1	7.68	1.61	123.2									
				153.2	1.000D-06	153.2	153.8	1.000D-06	153.8	1.4497D+05	1.2615D+05	
2	7.86	1.63	128.6									
				151.8	1.000D-06	151.8	152.3	1.000D-06	152.3	1.1623D+05	1.1973D+05	
3	7.74	1.62	128.2									
				151.9	1.000D-06	151.9	152.3	1.000D-06	152.3	1.1760D+05	1.2181D+05	
4	7.74	1.62	127.7									
				150.8	1.000D-06	150.8	151.2	1.000D-06	151.2	1.1458D+05	1.1751D+05	
5	7.73	1.62	127.4									
				150.4	1.000D-06	150.4	150.7	1.000D-06	150.7	1.1351D+05	1.1591D+05	
6	7.73	1.62	127.2									
				149.8	1.000D-06	149.9	150.2	1.000D-06	150.2	1.1173D+05	1.1403D+05	
7	7.73	1.62	127.1									
				149.5	1.000D-06	149.5	149.8	1.000D-06	149.8	1.1050D+05	1.1264D+05	
8	7.73	1.62	126.9									
				149.1	1.000D-06	149.1	149.4	1.000D-06	149.4	1.0922D+05	1.1121D+05	
9	7.73	1.62	126.8									
				148.8	1.000D-06	148.8	149.1	1.000D-06	149.1	1.0846D+05	1.1023D+05	
10	7.73	1.62	126.8									
				148.7	1.000D-06	148.7	149.0	1.000D-06	149.0	1.0815D+05	1.0971D+05	
11	7.73	1.62	126.7									
				148.7	1.000D-06	148.7	149.0	1.000D-06	149.0	1.0823D+05	1.0970D+05	
12	7.73	1.62	126.7									
				148.7	1.000D-06	148.7	149.0	1.0C0D-06	149.0	1.0823D+05	1.0970D+05	
13	7.73	1.62	126.7									
				148.7	1.C00D-06	148.7	149.0	1.000D-06	149.0	1.0823D+05	1.0971D+05	
14	7.73	1.62	126.7									
				148.6	1.000D-06	148.6	148.9	1.000D-06	148.9	1.0794D+05	1.1001D+05	
15	7.72	1.62	126.6									
				146.9	1.000D-06	146.9	146.6	1.0C0D-06	146.6	1.0001D+05	1.1966D+05	
16	7.66	1.60	121.7									
	4.28	1.28										

MITR2 TEMP DISTRIBUTION CORE 1 A-2

MESH POINT - 25

DX = C.02960 FT.

CHANNEL	VEL FT/SEC	TOTPL PSI	TBULK DEG. F.	TSURFACE DEG. F.	FILMTH INCHES	TINTFACE DEG. F.	TINTFACE DEG. F.	FILMTH INCHES	TSURFACE DEG. F.	Q / A BTU/HR*FT2	Q / A BTU/HR*FT2	WINDOW
	4.28	1.38										
1	7.68	1.70	123.9									
				152.9	1.000D-06	152.9	152.9	1.000D-06	153.5	1.4070D+05	1.2033D+05	
2	7.86	1.72	129.6									
				151.6	1.000D-06	151.6	152.2	1.000D-06	152.2	1.1089D+05	1.1452D+05	
3	7.74	1.71	129.2									
				151.7	1.000D-06	151.7	152.1	1.000D-06	152.1	1.1233D+05	1.1671D+05	
4	7.74	1.71	128.7									
				150.7	1.000D-06	150.7	151.0	1.000D-06	151.0	1.0944D+05	1.1261D+05	
5	7.74	1.71	128.4									
				150.2	1.000D-06	150.2	150.6	1.000D-06	150.6	1.0849D+05	1.1109D+05	
6	7.73	1.71	128.2									
				149.7	1.000D-06	149.7	150.1	1.000D-06	150.1	1.0682D+05	1.0930D+05	
7	7.73	1.71	128.0									
				149.3	1.000D-06	149.3	149.7	1.000D-06	149.7	1.0567D+05	1.0797D+05	
8	7.73	1.71	127.9									
				148.9	1.000D-06	149.0	149.3	1.000D-06	149.3	1.0447D+05	1.0661D+05	
9	7.73	1.71	127.7									
				148.7	1.000D-06	148.7	149.0	1.000D-06	149.0	1.0377D+05	1.0567D+05	
10	7.73	1.71	127.7									
				148.6	1.000D-06	148.5	148.9	1.000D-05	148.9	1.0349D+05	1.0517D+05	
11	7.73	1.71	127.6									
				148.6	1.000D-06	148.6	148.9	1.000D-06	148.9	1.0358D+05	1.0516D+05	
12	7.73	1.71	127.6									
				148.6	1.000D-06	148.6	148.9	1.000D-06	148.9	1.0358D+05	1.0516D+05	
13	7.73	1.71	127.6									
				148.6	1.000D-06	148.6	148.9	1.000D-06	148.9	1.0358D+05	1.0517D+05	
14	7.73	1.71	127.6									
				148.5	1.000D-06	148.5	148.8	1.000D-06	148.8	1.0323D+05	1.0554D+05	
15	7.72	1.71	127.4									
				146.6	1.000D-06	146.6	146.3	1.000D-06	146.3	9.4593D+04	1.1594D+05	
16	7.66	1.70	122.2									
	4.28	1.38										

MITR2 TEMP DISTRIBUTION   CORE 1   A-2

MESH POINT - 27

DX = 0.02960 FT.

CHANNEL	VEL FT/SEC	TOTPL PSI	TBULK DEG. F.	TSURFACE DEG. F.	FILMTH INCHES	TINTFACE DEG. F.	TINTFACE DEG. F.	FILMTH INCHES	TSURFACE DEG. F.	Q / A BTU/HR*FT2	Q / A BTU/HR*FT2	WINDOW
	4.28	1.48										
1	7.69	1.79	124.4									
				152.2	1.000D-06	152.2	152.8	1.000D-06	152.8	1.3488D+05	1.1285D+05	
2	7.86	1.82	130.5									
				151.1	1.000D-06	151.1	151.7	1.000D-06	151.7	1.0394D+05	1.0769D+05	
3	7.75	1.80	130.1									
				151.2	1.000D-06	151.2	151.6	1.000D-06	151.6	1.0528D+05	1.0982D+05	
4	7.74	1.80	129.6									
				150.1	1.000D-06	150.1	150.5	1.000D-06	150.5	1.0261D+05	1.0600D+05	
5	7.74	1.80	129.3									
				149.7	1.000D-06	149.7	150.1	1.000D-06	150.1	1.0180D+05	1.0457D+05	
6	7.74	1.80	129.1									
				149.2	1.000D-06	149.2	149.6	1.000D-06	149.6	1.0026D+05	1.0290D+05	
7	7.73	1.80	128.9									
				148.8	1.000D-06	148.8	149.2	1.000D-06	149.2	9.9204D+04	1.0166D+05	
8	7.73	1.80	128.7									
				148.5	1.000D-06	148.5	148.8	1.000D-06	148.8	9.8103D+04	1.0039D+05	
9	7.73	1.80	128.6									
				148.2	1.000D-06	148.2	148.6	1.000D-06	148.6	9.7483D+04	9.9506D+04	
10	7.73	1.80	128.5									
				148.1	1.000D-06	148.1	148.4	1.000D-06	148.4	9.7246D+04	9.9033D+04	
11	7.73	1.80	128.5									
				148.1	1.000D-06	148.1	148.4	1.000D-06	148.4	9.7343D+04	9.9020D+04	
12	7.73	1.80	128.5									
				148.1	1.000D-06	148.1	148.4	1.000D-06	148.4	9.7344D+04	9.9020D+04	
13	7.73	1.80	128.5									
				148.1	1.000D-06	148.1	148.4	1.000D-06	148.4	9.7334D+04	9.9030D+04	
14	7.73	1.80	128.5									
				148.0	1.000D-06	148.0	148.3	1.000D-06	148.3	9.6916D+04	9.9475D+04	
15	7.73	1.80	128.3									
				145.9	1.000D-06	145.9	145.6	1.000D-06	145.6	8.7605D+04	1.1059D+05	
16	7.67	1.79	122.6									
	4.28	1.48										

MESH POINT - 29

DX = 0.02960 FT.

CHANNEL	VEL FT/SEC	TOTPL PSI	TBULK DEG. F.	TSURFACE DEG. F.	FILMTH INCHES	TINTFACE DEG. F.	TINTFACE DEG. F.	FILMTH INCHES	TSURFACE DEG. F.	Q / A BTU/HR*FT2	Q / A BTU/HR*FT2	WINDOW
	4.28	1.58										
1	7.69	1.88	125.0									
				151.0	1.0000-06	151.0	151.7	1.0000-06	151.7	1.2663D+05	1.0308D+05	
2	7.86	1.91	131.3									
				150.0	1.0000-06	150.0	150.7	1.0000-06	150.6	9.4791D+04	9.8682D+04	
3	7.75	1.89	131.0									
				150.2	1.0000-06	150.2	150.7	1.0000-06	150.6	9.6522D+04	1.0123D+05	
4	7.74	1.89	130.4									
				149.2	1.0000-06	149.2	149.7	1.0000-06	149.7	9.4163D+04	9.7755D+04	
5	7.74	1.89	130.1									
				148.8	1.0000-06	148.8	149.2	1.0000-06	149.2	9.3548D+04	9.6482D+04	
6	7.74	1.89	129.9									
				148.3	1.0000-06	148.4	148.7	1.0000-06	148.7	9.2173D+04	9.4968D+04	
7	7.74	1.89	129.7									
				148.0	1.0000-06	148.0	148.4	1.0000-06	148.4	9.1241D+04	9.3843D+04	
8	7.73	1.89	129.5									
				147.6	1.0000-06	147.6	148.0	1.0000-06	148.0	9.0261D+04	9.2675D+04	
9	7.73	1.89	129.4									
				147.4	1.0000-06	147.4	147.8	1.0000-06	147.8	8.9727D+04	9.1861D+04	
10	7.73	1.89	129.3									
				147.3	1.0000-06	147.3	147.6	1.0000-06	147.6	8.9537D+04	9.1419D+04	
11	7.73	1.89	129.3									
				147.3	1.0000-06	147.3	147.6	1.0000-06	147.6	8.9641D+04	9.1404D+04	
12	7.73	1.89	129.3									
				147.3	1.0000-06	147.3	147.6	1.0000-06	147.6	8.9642D+04	9.1404D+04	
13	7.73	1.89	129.3									
				147.3	1.0000-06	147.3	147.6	1.0000-06	147.6	8.9628D+04	9.1419D+04	
14	7.73	1.89	129.3									
				147.2	1.0000-06	147.2	1/7.5	1.0000-06	147.5	8.913	9.1943D+04	
15	7.73	1.89	129.0									
				144.9	1.0000-06	144.9	144.6	1.0000-06	144.6	7.9193D+04	1.0373D+05	
16	7.67	1.88	123.1									
	4.28	1.58										

MESH POINT - 31

DX = 0.02960 FT.

CHANNEL	VEL FT/SEC	TOTPL PSI	TBULK DEG. F.	TSURFACE DEG. F.	FILMTH INCHES	TINTFACE DEG. F.	TINTFACE DEG. F.	FILMTH INCHES	TSURFACE DEG. F.	Q / A BTU/HR*FT2	Q / A BTU/HR*FT2	WINDOW
	4.28	1.68										
1	7.69	1.98	125.5									
				149.8	1.000D-06	149.9	150.6	1.000D-06	150.6	1.1894D+05	9.4029D+04	
2	7.86	2.00	132.1									
				149.1	1.000D-06	149.1	149.7	1.000D-06	149.7	8.6332D+04	9.0332D+04	
3	7.75	1.99	131.8									
				149.3	1.000D-06	149.3	149.8	1.0C0D-06	149.8	8.8416D+04	9.3260D+04	
4	7.74	1.99	131.2									
				148.4	1.000D-06	148.4	148.8	1.000D-06	148.8	8.6293D+04	9.0087D+04	
5	7.74	1.99	130.9									
				148.0	1.000D-06	148.0	148.4	1.000D-06	148.4	8.5828D+04	8.8926D+04	
6	7.74	1.98	130.7									
				147.5	1.000D-06	147.6	148.0	1.0C0D-06	147.9	8.4611D+04	8.7555D+04	
7	7.74	1.98	130.5									
				147.2	1.000D-06	147.2	147.6	1.000D-06	147.6	8.3815D+04	8.6550D+04	
8	7.74	1.98	130.3									
				146.9	1.000D-06	146.9	147.2	1.000D-06	147.2	8.2965D+04	8.5498D+04	
9	7.73	1.98	130.1									
				146.6	1.000D-06	146.7	147.0	1.000D-06	147.0	8.2527D+04	8.4761D+04	
10	7.73	1.98	130.1									
				146.5	1.000D-06	146.5	146.9	1.000D-06	146.9	8.2391D+04	8.4357D+04	
11	7.73	1.98	130.0									
				146.5	1.C00D-06	146.5	146.9	1.000D-06	146.9	8.2502D+04	8.4344D+04	
12	7.73	1.98	130.0									
				146.5	1.C00D-06	146.5	146.9	1.000D-06	146.9	8.2503D+04	8.4344D+04	
13	7.73	1.98	130.0									
				146.5	1.000D-06	146.5	146.9	1.000D-06	146.9	8.2486D+04	8.4362D+04	
14	7.73	1.98	130.0									
				146.4	1.000D-06	146.4	146.7	1.0C0D-06	146.7	8.1916D+04	8.4971D+04	
15	7.73	1.98	129.7									
				144.0	1.C00D-06	144.0	143.7	1.000D-06	143.7	7.1427D+04	9.7349D+04	
16	7.67	1.97	123.5									
	4.28	1.68										

MITR2 TEMP DISTRIBUTION CORE 1 A-2

MESH POINT - 33

DX = 0.02960 FT.

CHANNEL	VEL FT/SEC	TOTPL PSI	TBULK DEG. F.	TSURFACE DEG. F.	FILMTH INCHES	TINTFACE DEG. F.	TINTFACE DEG. F.	FILMTH INCHES	TSURFACE DEG. F.	Q / A BTU/HR*FT2	Q / A BTU/HR*FT2	WINDOW
	4.28	1.78										
1	7.69	2.07	126.0									
				148.8	1.000D-06	148.8	149.5	1.000D-06	149.5	1.1158D+05	8.5466D+04	
2	7.87	2.09	132.8									
				148.1	1.000D-06	148.2	148.8	1.000D-06	148.8	7.8338D+04	8.2419D+04	
3	7.75	2.08	132.5									
				148.4	1.000D-06	148.4	148.9	1.000D-06	148.9	8.0428D+04	8.5386D+04	
4	7.75	2.08	132.0									
				147.5	1.000D-06	147.5	148.0	1.000D-06	148.0	7.8532D+04	8.2509D+04	
5	7.74	2.08	131.6									
				147.1	1.000D-06	147.1	147.6	1.000D-06	147.6	7.8211D+04	8.1458D+04	
6	7.74	2.08	131.4									
				146.7	1.000D-06	146.7	147.1	1.000D-06	147.1	7.7137D+04	8.0222D+04	
7	7.74	2.08	131.2									
				146.4	1.000D-06	146.4	146.8	1.000D-06	146.8	7.6452D+04	7.9318D+04	
8	7.74	2.08	131.0									
				146.1	1.000D-06	146.1	146.5	1.000D-06	146.4	7.5712D+04	7.8365D+04	
9	7.74	2.07	130.8									
				145.8	1.000D-06	145.9	146.2	1.000D-06	146.2	7.5353D+04	7.6692D+04	
10	7.73	2.07	130.7									
				145.7	1.000D-06	145.8	146.1	1.000D-06	146.1	7.5259D+04	7.7317D+04	
11	7.73	2.07	130.7									
				145.7	1.000D-06	145.7	146.1	1.000D-06	146.1	7.5375D+04	7.7302D+04	
12	7.73	2.07	130.7									
				145.7	1.000D-06	145.7	146.1	1.000D-06	146.1	7.5376D+04	7.7302D+04	
13	7.73	2.07	130.7									
				145.7	1.000D-06	145.7	146.1	1.000D-06	146.1	7.5354D+04	7.7325D+04	
14	7.73	2.07	130.7									
				145.6	1.000D-06	145.6	145.9	1.000D-06	145.9	7.4706D+04	7.8020D+04	
15	7.73	2.07	130.3									
				143.1	1.000D-06	143.1	142.7	1.000D-06	142.7	6.3779D+04	9.0951D+04	
16	7.67	2.06	123.9									
	4.28	1.78										

MITR2 TEMP DISTRIBUTION CORE 1 A-2

MESH POINT - 35

DX = 0.02960 FT.

CHANNEL	VEL FT/SEC	TOTPL PSI	TBULK DEG. F.	TSURFACE DEG. F.	FILMTH INCHES	TINTFACE DEG. F.	TINTFACE DEG. F.	FILMTH INCHES	TSURFACE DEG. F.	Q / A BTU/HR*FT2	Q / A BTU/HR*FT2	WINDOW
	4.28	1.88										
1	7.69	2.16	126.4									
				147.7	1.0000-06	147.7	148.5	1.0C0D-06	148.5	1.0434D+05	7.7157D+04	
2	7.87	2.18	133.4									
				147.2	1.0000-06	147.2	147.9	1.0C0D-06	147.9	7.0586D+04	7.4731D+04	
3	7.75	2.17	133.2									
				147.5	1.0000-06	147.5	148.0	1.0000-06	148.0	7.2572D+04	7.7626D+04	
4	7.75	2.17	132.6									
				146.6	1.0000-06	146.7	147.1	1.0000-06	147.1	7.0903D+04	7.5040D+04	
5	7.74	2.17	132.2									
				146.3	1.0C00-06	146.3	146.7	1.0000-06	146.7	7.0720D+04	7.4098D+04	
6	7.74	2.17	132.0									
				145.9	1.0000-06	145.9	146.3	1.0000-06	146.3	6.9785D+04	7.2994D+04	
7	7.74	2.17	131.8									
				145.5	1.0000-06	145.5	145.9	1.0C0D-06	145.9	6.9208D+04	7.2189D+04	
8	7.74	2.17	131.6									
				145.2	1.0000-06	145.2	145.6	1.0000-06	145.6	6.8575D+04	7.1333D+04	
9	7.74	2.17	131.4									
				145.0	1.0000-06	145.0	145.4	1.0000-06	145.4	6.8292D+04	7.0722D+04	
10	7.74	2.17	131.4									
				144.9	1.0000-06	144.9	145.3	1.0C0D-06	145.3	6.8240D+04	7.0377D+04	
11	7.74	2.17	131.3									
				144.9	1.0C00-06	144.9	145.3	1.0000-06	145.3	6.8360D+04	7.0360D+04	
12	7.74	2.17	131.3									
				144.9	1.0C00-06	144.9	145.3	1.0000-06	145.3	6.8361D+04	7.0361D+04	
13	7.74	2.17	131.3									
				144.9	1.0000-06	144.9	145.3	1.0000-06	145.3	6.8334D+04	7.0390D+04	
14	7.74	2.17	131.3									
				144.8	1.0000-06	144.8	145.1	1.0000-06	145.1	6.7601D+04	7.1177D+04	
15	7.73	2.16	130.9									
				142.1	1.0C00-06	142.1	141.7	1.0C0D-06	141.7	5.6280D+04	8.4563D+04	
16	7.67	2.15	124.3									
	4.28	1.88										

DX = C.02960 FT.

CHANNEL	VEL FT/SEC	TOTPL PSI	TBULK DEG. F.	TSURFACE DEG. F.	FILMTH INCHES	TINTFACE DEG. F.	TINTFACE DEG. F.	FILMTH INCHES	TSURFACE DEG. F.	Q / A BTU/HR*FT2	Q / A BTU/HR*FT2	WINDOW
	4.28	1.98										
1	7.69	2.25	126.9									
				146.4	1.000D-06	146.4	147.2	1.0C0D-06	147.2	9.5812D+04	6.7659D+04	
2	7.87	2.27	134.0									
				146.0	1.0C0D-06	146.0	146.7	1.000D-06	146.7	6.1724D+04	6.5911D+04	
3	7.75	2.26	133.8									
				146.6	1.000D-06	146.6	147.1	1.0C0D-06	147.1	6.5344D+04	7.0462D+04	
4	7.75	2.26	133.2									
				145.8	1.000D-06	145.8	146.3	1.000D-06	146.3	6.3870D+04	6.8147D+04	
5	7.74	2.26	132.8									
				145.4	1.000D-06	145.4	145.9	1.000D-06	145.9	6.3811D+04	6.7305D+04	
6	7.74	2.26	132.6									
				145.1	1.0000-06	145.1	145.5	1.0000-06	145.5	6.3005D+04	6.6322D+04	
7	7.74	2.26	132.4									
				144.7	1.0000-06	144.8	145.2	1.0000-06	145.2	6.2528D+04	6.5609D+04	
8	7.74	2.26	132.2									
				144.5	1.0C0D-06	144.5	144.9	1.000D-06	144.9	6.1993D+04	6.4843D+04	
9	7.74	2.26	132.0									
				144.3	1.000D-06	144.3	144.7	1.0C0D-06	144.7	6.1779D+04	6.4289D+04	
10	7.74	2.26	131.9									
				144.2	1.0C0D-06	144.2	144.6	1.000D-06	144.6	6.1765D+04	6.3971D+04	
11	7.74	2.26	131.9									
				144.2	1.000D-06	144.2	144.6	1.000D-06	144.6	6.1889D+04	6.3953D+04	
12	7.74	2.26	131.9									
				144.2	1.000D-06	144.2	144.6	1.0C0D-06	144.6	6.1890D+04	6.3954D+04	
13	7.74	2.26	131.9									
				144.2	1.000D-06	144.2	144.6	1.000D-06	144.6	6.1856D+04	6.3989D+04	
14	7.74	2.26	131.9									
				144.0	1.000D-06	144.0	144.3	1.000D-06	144.3	6.1037D+04	6.4872D+04	
15	7.73	2.26	131.4									
				141.3	1.000D-06	141.3	140.8	1.000D-06	140.8	4.9398D+04	7.8645D+04	
16	7.67	2.25	124.6									
	4.28	1.98										

MITR2 TEMP DISTRIBUTION CORE 1 A-2

MESH POINT - 39

DX = 0.02960 FT.

CHANNEL	VEL FT/SEC	TOTPL PSI	TBULK DEG. F.	TSURFACE DEG. F.	FILMTH INCHES	TINTFACE DEG. F.	TINTFACE DEG. F.	FILMTH INCHES	TSURFACE DEG. F.	Q / A BTU/HR*FT2	Q / A BTU/HR*FT2	WINDOW
	4.28	2.08										
1	7.69	2.34	127.3									
				145.2	1.000D-06	145.2	146.0	1.000D-06	146.0	8.8167D+04	5.9224D+04	
2	7.87	2.36	134.5									
				145.0	1.0000-06	145.0	145.7	1.0000-06	145.7	5.3870D+04	5.8050D+04	
3	7.75	2.35	134.3									
				145.7	1.000D-06	145.7	146.2	1.CC0D-06	146.2	5.8186D+04	6.3326D+04	
4	7.75	2.35	133.8									
				145.0	1.000D-06	145.0	145.5	1.0000-06	145.4	5.6884D+04	6.1285D+04	
5	7.75	2.35	133.4									
				144.6	1.000D-06	144.6	145.1	1.000D-06	145.1	5.6947D+04	6.0543D+04	
6	7.74	2.35	133.1									
				144.2	1.0000-06	144.2	144.7	1.0000-06	144.7	5.6268D+04	5.9680D+04	
7	7.74	2.35	132.9									
				143.9	1.0000-06	143.9	144.4	1.0000-06	144.4	5.5888D+04	5.9057D+04	
8	7.74	2.35	132.7									
				143.6	1.C000-06	143.7	144.1	1.0C00-06	144.1	5.5449D+04	5.8380D+04	
9	7.74	2.35	132.5									
				143.5	1.CC0D-06	143.5	143.9	1.000D-06	143.9	5.5304D+04	5.7884D+04	
10	7.74	2.35	132.4									
				143.4	1.000C-06	143.4	143.8	1.000D-06	143.8	5.5326D+04	5.7592D+04	
11	7.74	2.35	132.4									
				143.4	1.C00D-06	143.4	143.8	1.0000-06	143.8	5.5453D+04	5.7573D+04	
12	7.74	2.35	132.4									
				143.4	1.C00D-06	143.4	143.8	1.0000-06	143.8	5.5454D+04	5.7574D+04	
13	7.74	2.35	132.4									
				143.4	1.0000-06	143.4	143.8	1.0000-06	143.8	5.5414D+04	5.7617D+04	
14	7.74	2.35	132.4									
				143.2	1.C00D-06	143.2	143.5	1.0000-06	143.5	5.4506D+04	5.8597D+04	
15	7.73	2.35	131.9									
				140.3	1.0000-06	140.4	139.9	1.0000-06	139.9	4.2614D+04	7.2695D+04	
16	7.67	2.34	125.0									
	4.28	2.08										

MITR2 TEMP DISTRIBUTION CORE 1 A-2

MESH POINT - 41

OX = 0.02960 FT.

CHANNEL	VEL FT/SEC	TOTPL PSI	TBULK DEG. F.	TSURFACE DEG. F.	FILMTH INCHES	TINTFACE DEG. F.	TINTFACE DEG. F.	FILMTH INCHES	TSURFACE DEG. F.	Q / A BTU/HR*FT2	Q / A BTU/HR*FT2	WINDOW
	4.28	2.18										
1	7.69	2.43	127.6									
				144.1	1.0000-06	144.1	145.0	1.0000-06	145.0	8.1461D+04	5.1398D+04	
2	7.87	2.45	134.9									
				144.1	1.0000-06	144.1	144.8	1.0C0D-06	144.8	4.7059D+04	5.1200D+04	
3	7.75	2.44	134.7									
				144.9	1.C00D-06	144.9	145.4	1.0000-06	145.4	5.1825D+04	5.6960D+04	
4	7.75	2.44	134.2									
				144.2	1.0000-06	144.2	144.7	1.0000-06	144.7	5.0662D+04	5.5166D+04	
5	7.75	2.44	133.8									
				143.8	1.0000-06	143.8	144.3	1.0000-06	144.3	5.0831D+04	5.4513D+04	
6	7.74	2.44	133.6									
				143.5	1.0000-06	143.5	143.9	1.0000-06	143.9	5.0265D+04	5.3758D+04	
7	7.74	2.44	133.3									
				143.2	1.0000-06	143.2	143.6	1.0000-06	143.6	4.9971D+04	5.3215D+04	
8	7.74	2.44	133.1									
				142.9	1.0000-06	142.9	143.4	1.0000-06	143.4	4.9619D+04	5.2616D+04	
9	7.74	2.44	133.0									
				142.8	1.0000-06	142.8	143.2	1.0000-06	143.2	4.9533D+04	5.2171D+04	
10	7.74	2.44	132.9									
				142.7	1.0000-06	142.7	143.1	1.C000-06	143.1	4.9587D+04	5.1904D+04	
11	7.74	2.44	132.8									
				142.7	1.0000-06	142.7	143.1	1.0000-06	143.1	4.9718D+04	5.1884D+04	
12	7.74	2.44	132.8									
				142.7	1.0000-06	142.7	143.1	1.0000-06	143.1	4.9718D+04	5.1885D+04	
13	7.74	2.44	132.8									
				142.7	1.0000-06	142.7	143.1	1.0000-06	143.1	4.9671D+04	5.1936D+04	
14	7.74	2.44	132.8									
				142.4	1.0000-06	142.4	142.8	1.0000-06	142.8	4.8675D+04	5.3015D+04	
15	7.73	2.44	132.3									
				139.5	1.0000-06	139.6	139.1	1.0000-06	139.1	3.6602D+04	6.7371D+04	
16	7.67	2.43	125.3									
	4.28	2.18										

MITR2 TEMP DISTRIBUTION CORE 1 A-2

MESH POINT - 43

DX = 0.02960 FT.

CHANNEL	VEL FT/SEC	TOTPL PSI	TBULK DEG. F.	TSURFACE DEG. F.	FILMTH INCHES	TINTFACE DEG. F.	TINTFACE CEG. F.	FILMTH INCHES	TSURFACE DEG. F.	Q / A BTU/HR*FT2	Q / A BTU/HR*FT2	WINDOW
	4.28	2.28										
1	7.69	2.52	127.9									
				143.4	1.000D-06	143.4	144.2	1.0C0D-06	144.2	7.6144D+04	4.6124D+04	
2	7.87	2.54	135.3									
				143.4	1.0C0D-06	143.4	144.1	1.000D-06	144.1	4.1707D+04	4.5775D+04	
3	7.76	2.53	135.2									
				144.4	1.000D-06	144.4	145.0	1.000D-06	145.0	4.7295D+04	5.2395D+04	
4	7.75	2.53	134.7									
				143.7	1.000D-06	143.7	144.2	1.CC0D-06	144.2	4.6196D+04	5.0787D+04	
5	7.75	2.53	134.3									
				143.4	1.0C0D-06	143.4	143.9	1.000D-06	143.9	4.6442D+04	5.0198D+04	
6	7.75	2.53	134.0									
				143.0	1.000C-06	143.0	143.5	1.000D-06	143.5	4.5958D+04	4.9520D+04	
7	7.74	2.53	133.8									
				142.8	1.000C-06	142.8	143.2	1.0C0D-06	14...	4.5727D+04	4.9035D+04	
8	7.74	2.53	133.6									
				142.5	1.000D-06	142.5	143.0	1.000D-06	143.0	4.5437D+04	4.8492D+04	
9	7.74	2.53	133.4									
				142.3	1.000D-06	142.3	142.8	1.000D-06	142.8	4.5396D+04	4.8084D+04	
10	7.74	2.53	133.3									
				142.3	1.000D-06	142.3	142.7	1.000D-06	142.7	4.5473D+04	4.7834D+04	
11	7.74	2.53	133.3									
				142.3	1.000D-06	142.3	142.7	1.000D-06	142.7	4.5606D+04	4.7813D+04	
12	7.74	2.53	133.3									
				142.3	1.000D-06	142.3	142.7	1.000D-06	142.7	4.5607D+04	4.7814D+04	
13	7.74	2.53	133.2									
				142.2	1.000D-06	142.2	142.7	1.000D-06	142.7	4.5551D+04	4.7873D+04	
14	7.74	2.53	133.2									
				142.0	1.000D-06	142.0	142.4	1.000D-06	142.4	4.4468D+04	4.9051D+04	
15	7.73	2.53	132.7									
				139.0	1.000D-06	139.0	138.6	1.000D-06	138.6	3.2295D+04	6.3602D+04	
16	7.67	2.52	125.5									
	4.28	2.28										

MESH POINT - 45

DX = C.02960 FT.

CHANNEL	VEL FT/SEC	TOTPL PSI	TBULK DEG. F.	TSURFACE DEG. F.	FILMTH INCHES	TINTFACE DEG. F.	TINTFACE CEG. F.	FILMTH INCHES	TSURFACE DEG. F.	Q / A BTU/HR*FT2	Q / A BTU/HR*FT2	WINDOW
	4.28	2.38										
1	7.70	2.61	128.3									
				142.8	1.000D-06	142.8	143.7	1.0C0D-06	143.7	7.1986D+04	4.1645D+04	
2	7.87	2.63	135.6									
				142.9	1.0C0D-06	142.9	143.7	1.000D-06	143.7	3.7565D+04	4.1545D+04	
3	7.76	2.62	135.5									
				143.7	1.000D-06	143.7	144.2	1.000D-06	144.2	4.1687D+04	4.6745D+04	
4	7.75	2.62	135.1									
				143.0	1.000D-06	143.0	143.6	1.000D-06	143.6	4.0695D+04	4.5361D+04	
5	7.75	2.62	134.7									
				142.7	1.000D-06	142.7	143.2	1.000D-05	143.2	4.1031D+04	4.4851D+04	
6	7.75	2.62	134.4									
				142.4	1.0C0D-06	142.4	142.9	1.0C0D-06	142.8	4.0647D+04	4.4267D+04	
7	7.74	2.62	134.1									
				142.1	1.0C0D-06	142.1	142.6	1.0000-06	142.0	4.0492D+04	4.3853D+04	
8	7.74	2.62	133.9									
				141.9	1.0000-06	141.7	142.3	1.0000-06	142.3	4.0277D+04	4.3380D+04	
9	7.74	2.62	133.8									
				141.7	1.0000-06	141.7	142.1	1.0C0D-06	142.1	4.0288D+04	4.3017D+04	
10	7.74	2.62	133.7									
				141.6	1.0C0D-06	141.6	142.1	1.0000-06	142.1	4.0393D+04	4.2788D+04	
11	7.74	2.62	133.6									
				141.6	1.0000-06	141.6	142.1	1.0000-06	142.1	4.0527D+04	4.2767D+04	
12	7.74	2.62	133.6									
				141.6	1.0000-06	141.6	142.1	1.0000-06	142.1	4.0527D+04	4.2769D+04	
13	7.74	2.62	133.6									
				141.6	1.0000-06	141.6	142.0	1.0000-06	142.0	4.0463D+04	4.2837D+0‹	
14	7.74	2.62	133.6									
				141.3	1.0000-06	141.3	141.7	1.00 - 5	141.7	3.9293D+0‹	4.4114D+04	
15	7.74	2.62	133.0									
				138.3	1.0000 06	138.3	137.8	1.0000-06	137.8	2.7042D+04	5.8827D+04	
16	7.67	2.61	125.8									
	4.28	2.38										

MITR2 TEMP DISTRIBUTION CORE 1 A-2

MESH POINT - 47

DX = 0.02960 FT.

CHANNEL	VEL FT/SEC	TOTPL PSI	TBULK DEG. F.	TSURFACE DEG. F.	FILMTH INCHES	TINTFACE DEG. F.	TINTFACE DEG. F.	FILMTH INCHES	TSURFACE DEG. F.	Q / A BTU/HR*FT2	Q / A BTU/HR*FT2	WINDOW
	4.28	2.48										
1	7.70	2.70	128.6									
				142.3	1.0000-06	142.4	143.2	1.0000-06	143.2	6.8273D+04	3.7702D+04	
2	7.87	2.72	135.9									
				142.5	1.0000-06	142.5	143.2	1.0000-06	143.2	3.3908D+04	3.7816D+04	
3	7.76	2.71	135.9									
				143.1	1.0000-06	143.1	143.7	1.0C0D-06	143.7	3.7167D+04	4.2193D+04	
4	7.75	2.71	135.4									
				142.5	1.CC0D-06	142.5	143.0	1.0000-06	143.0	3.6267D+04	4.0988D+04	
5	7.75	2.71	135.0									
				142.2	1.0000-06	142.2	142.7	1.0C00-06	142.7	3.6674D+04	4.0542D+04	
6	7.75	2.71	134.7									
				141.9	1.0000-06	141.9	142.3	1.0000-06	142.3	3.6370D+04	4.0034D+04	
7	7.74	2.71	134.5									
				141.6	1.0000-06	141.6	142.1	1.0000-06	142.1	3.6276D+04	3.9677D+04	
8	7.74	2.71	134.3									
				141.4	1.0000-06	141.4	141.8	1.0000-06	141.8	3.6122D+04	3.9261D+04	
9	7.74	2.71	134.1									
				141.2	1.0000-06	141.2	141.7	1.0000-06	141.7	3.6175D+04	3.8934D+04	
10	7.74	2.71	134.0									
				141.1	1.0000-06	141.1	141.6	1.0C00-06	141.6	3.6302D+04	3.8723D+04	
11	7.74	2.71	134.0									
				141.1	1.0000-06	141.1	141.6	1.0C00-06	141.6	3.6438D+04	3.8701D+04	
12	7.74	2.71	134.0									
				141.1	1.0000-06	141.1	141.6	1.0000-06	141.6	3.6438D+04	3.8703D+04	
13	7.74	2.71	134.0									
				141.1	1.0000-06	141.1	141.6	1.0C00-06	141.6	3.6364D+04	3.8781D+04	
14	7.74	2.71	133.9									
				140.8	1.0000-06	140.8	141.2	1.0000-06	141.2	3.5108D+04	4.0158D+04	
15	7.74	2.71	133.3									
				137.8	1.0000-06	137.8	137.3	1.0000-06	137.3	2.2846D+04	5.4973D+04	
16	7.67	2.70	126.0									
	4.28	2.48										

MITR2 TEMP DISTRIBUTION CORE 1 A-2

MESH POINT - 49

DX = 0.02960 FT.

CHANNEL	VEL FT/SEC	TOTPL PSI	TBULK DEG. F.	TSURFACE DEG. F.	FILMTH INCHES	TINTFACE DEG. F.	TINTFACE DEG. F.	FILMTH INCHES	TSURFACE DEG. F.	Q / A BTU/HR*FT2	Q / A BTU/HR*FT2	WINDOW
	4.28	2.58										
1	7.70	2.79	128.8									
				141.9	1.0000-06	141.9	142.8	1.0000-06	142.8	6.4931D+04	3.4208D+04	
2	7.87	2.81	136.2									
				142.2	1.0000-06	142.2	142.9	1.0000-06	142.9	3.0647D+04	3.4498D+04	
3	7.76	2.80	136.2									
				142.8	1.0000-06	142.8	143.4	1.0000-06	143.4	3.3988D+04	3.8975D+04	
4	7.75	2.80	135.7									
				142.2	1.0000-06	142.2	142.7	1.0000-06	142.7	3.3137D+04	3.7901D+04	
5	7.75	2.80	135.3									
				141.9	1.0000-06	141.9	142.4	1.0000-06	142.4	3.3594D+04	3.7501D+04	
6	7.75	2.80	135.0									
				141.6	1.0000-06	141.6	142.1	1.0000-06	142.1	3.3348D+04	3.7047D+04	
7	7.75	2.80	134.8									
				141.3	1.0000-06	141.3	141.8	1.0000-06	14?.?	3.3298D+04	3.6730D+04	
8	7.74	2.80	134.6									
				141.1	1.0000-06	141.1	141.5	1.0000-06	141.5	3.3188D+04	3.6354D+04	
9	7.74	2.80	134.4									
				140.9	1.0000-06	140.9	141.4	1.0000-06	141.4	3.3271D+04	3.6052D+04	
10	7.74	2.80	134.3									
				140.9	1.0000-06	140.9	141.3	1.0000-06	141.3	3.3413D+04	3.5853D+04	
11	7.74	2.80	134.3									
				140.9	1.0000-06	140.9	141.3	1.0000-06	141.3	3.3550D+04	3.5831D+04	
12	7.74	2.80	134.3									
				140.9	1.0000-06	140.9	141.3	1.0000-06	141.3	3.3550D+04	3.5834D+04	
13	7.74	2.80	134.3									
				140.8	1.0000-06	140.8	141.3	1.0000-06	141.3	3.3467D+04	3.5923D+04	
14	7.74	2.80	134.2									
				140.5	1.0000-06	140.5	140.9	1.0000-06	140.9	3.2128D+04	3.7396D+04	
15	7.74	2.80	133.5									
				137.4	1.0000-06	137.4	1?.?	1.0000-06	136.9	1.9908D+04	5.2271D+04	
16	7.67	2.79	126.3									
	4.28	2.58										

MITR2 TEMP DISTRIBUTION CORE 1 A-2

MESH POINT - 51

DX = 0.02960 FT.

CHANNEL	VEL FT/SEC	TOTPL PSI	TBULK DEG. F.	TSURFACE DEG. F.	FILMTH INCHES	TINTFACE DEG. F.	TINTFACE DEG. F.	FILMTH INCHES	TSURFACE DEG. F.	Q / A BTU/HR*FT2	Q / A BTU/HR*FT2	WINDOW
	4.28	2.68										
1	7.70	2.89	129.1									
				141.6	1.000D-06	141.6	142.5	1.000D-06	142.5	6.2196D+04	3.1399D+04	
2	7.87	2.90	136.5									
				141.9	1.000D-06	141.9	142.6	1.000D-06	142.6	2.8062D+04	3.1810D+04	
3	7.76	2.89	136.5									
				142.5	1.000D-06	142.5	143.0	1.000D-06	143.0	3.0832D+04	3.5775D+04	
4	7.75	2.89	136.0									
				141.9	1.000D-06	141.9	142.4	1.000D-06	142.4	3.0032D+04	3.4831D+04	
5	7.75	2.89	135.6									
				141.6	1.000D-06	141.6	142.1	1.000D-06	142.1	3.0538D+04	3.4476D+04	
6	7.75	2.89	135.3									
				141.3	1.000D-06	141.3	141.8	1.000D-06	141.8	3.0349D+04	3.4075D+04	
7	7.75	2.89	135.1									
				141.0	1.000D-06	141.0	141.5	1.000D-06	14...	3.0342D+04	3.3799D+04	
8	7.74	2.89	134.9									
				140.8	1.000D-06	140.8	141.3	1.000D-06	141.3	3.0274D+04	3.3462D+04	
9	7.74	2.89	134.7									
				140.6	1.000D-06	140.7	141.1	1.000D-06	141.1	3.0387D+04	3.3185D+04	
10	7.74	2.89	134.6									
				140.6	1.000D-06	140.6	141.0	1.000D-06	141.0	3.0544D+04	3.2999D+04	
11	7.74	2.89	134.5									
				140.6	1.000D-06	140.6	141.0	1.000D-06	141.0	3.0682D+04	3.2976D+04	
12	7.74	2.89	134.5									
				140.6	1.000D-06	140.6	141.0	1.000D-06	141.0	3.0682D+04	3.2980D+04	
13	7.74	2.89	134.5									
				140.6	1.000D-06	140.6	141.0	1.000D-06	141.0	3.0588D+04	3.3080D+04	
14	7.74	2.89	134.5									
				140.2	1.000D-06	140.2	140.6	1.000D-06	140.6	2.9168D+04	3.4649D+04	
15	7.74	2.89	133.7									
				137.1	1.000D-06	137.1	136.6	1.000D-06	136.6	1.7017D+04	4.9556D+04	
16	7.67	2.88	126.5									
	4.28	2.68										

MITR2 TEMP DISTRIBUTION CORE 1 A-2

MESH POINT - 53

DX = 0.02960 FT.

CHANNEL	VEL FT/SEC	TOTPL PSI	TBULK DEG. F.	TSURFACE DEG. F.	FILMTH INCHES	TINTFACE DEG. F.	TINTFACE DEG. F.	FILMTH INCHES	TSURFACE DEG. F.	Q / A BTU/HR*FT2	Q / A BTU/HR*FT2	WINDOW
	4.28	2.78										
1	7.70	2.98	129.4									
				141.4	1.0000-06	141.4	142.3	1.0000-06	142.3	5.9807D+04	2.9080D+04	
2	7.87	2.99	136.7									
				141.7	1.0000-06	141.7	142.5	1.0000-06	142.5	2.5909D+04	2.9578D+04	
3	7.76	2.98	136.7									
				142.2	1.0000-06	142.2	142.7	1.0000-06	142.7	2.8111D+04	3.3012D+04	
4	7.75	2.98	136.3									
				141.6	1.0000-06	141.6	142.2	1.0000-06	142.2	2.7357D+04	3.2179D+04	
5	7.75	2.98	135.9									
				141.3	1.0000-06	141.3	141.8	1.0000-06	141.8	2.7903D+04	3.1864D+04	
6	7.75	2.98	135.6									
				141.0	1.0000-06	141.0	141.5	1.0000-06	141.5	2.7763D+04	3.1509D+04	
7	7.75	2.98	135.3									
				140.8	1.0000-06	140.8	141.2	1.0000-06	141.2	2.7793D+04	3.1268D+04	
8	7.74	2.98	135.1									
				140.6	1.0000-06	140.6	141.0	1.0000-06	141.0	2.7762D+04	3.0964D+04	
9	7.74	2.98	134.9									
				140.4	1.0000-06	140.4	140.9	1.0000-06	140.9	2.7900D+04	3.0710D+04	
10	7.74	2.98	134.8									
				140.3	1.0000-06	140.3	140.8	1.0000-06	140.8	2.8070D+04	3.0534D+04	
11	7.74	2.98	134.8									
				140.3	1.0000-06	140.3	140.8	1.0000-06	140.8	2.8209D+04	3.0511D+04	
12	7.74	2.98	134.8									
				140.3	1.0000-06	140.3	140.8	1.0000-06	140.8	2.8208D+04	3.0515D+04	
13	7.74	2.98	134.8									
				140.3	1.0000-06	140.3	140.8	1.0000-06	140.8	2.8103D+04	3.0628D+04	
14	7.74	2.98	134.7									
				140.0	1.0000-06	140.0	140.3	1.0000-06	140.3	2.6606D+04	3.2291D+04	
15	7.74	2.98	134.0									
				136.8	1.0000-06	136.8	136.3	1.0000-06	136.3	1.4552D+04	4.7200D+04	
16	7.67	2.97	126.7									
	4.28	2.78										

MITR2 TEMP DISTRIBUTION   CORE 1   A-2

MESH POINT - 55

DX = 0.02960 FT.

CHANNEL	VEL FT/SEC	TOTPL PSI	TBULK DEG. F.	TSURFACE DEG. F.	FILMTH INCHES	TINTFACE DEG. F.	TINTFACE DEG. F.	FILMTH INCHES	TSURFACE DEG. F.	Q / A. BTU/HR*FT2	Q / A BTU/HR*FT2	WINDOW
	4.28	2.88										
1	7.70	3.07	129.6									
				141.2	1.000D-06	141.2	142.1	1.000D-06	142.1	5.7791D+04	2.7017D+04	
2	7.87	3.08	136.9									
				141.5	1.000C-06	141.6	142.3	1.000D-06	142.3	2.3987D+04	2.7584D+04	
3	7.76	3.07	136.9									
				141.9	1.000D-06	141.9	142.4	1.0C0D-06	142.4	2.5455D+04	3.0320D+04	
4	7.75	3.07	136.5									
				141.4	1.C00D-06	141.4	141.9	1.000D-06	141.9	2.4754D+04	2.9593D+04	
5	7.75	3.07	136.1									
				141.1	1.000D-06	141.1	141.6	1.CC0D-06	141.6	2.5338D+04	2.9317D+04	
6	7.75	3.07	135.8									
				140.8	1.000D-06	140.8	141.3	1.000D-06	141.3	2.5247D+04	2.9007D+04	
7	7.75	3.07	135.6									
				140.5	1.000D-06	140.5	141.0	1.000D-06	141.0	2.5312D+04	2.8799D+04	
8	7.75	3.07	135.4									
				140.3	1.000D-06	140.3	140.8	1.CC0D-06	140.8	2.5318D+04	2.8528D+04	
9	7.74	3.07	135.2									
				140.2	1.C00D-06	140.2	140.6	1.000D-06	140.6	2.5479D+04	2.8295D+04	
10	7.74	3.07	135.1									
				140.1	1.000D-06	140.1	140.6	1.0C0D-06	140.6	2.5662D+04	2.8130D+04	
11	7.74	3.07	135.0									
				140.1	1.000D-06	140.1	140.6	1.000D-06	140.6	2.5801D+04	2.8107D+04	
12	7.74	3.07	135.0									
				140.1	1.CC0D-06	140.1	140.6	1.000D-06	140.6	2.5799D+04	2.8112D+04	
13	7.74	3.07	135.0									
				140.1	1.C00D-06	140.1	140.5	1.0C0D-06	140.5	2.5684D+04	2.8237D+04	
14	7.74	3.07	135.0									
				139.7	1.0C0D-06	139.7	140.1	1.000D-06	140.0	2.4110D+04	2.9992D+04	
15	7.74	3.07	134.1									
				136.5	1.000D-06	136.5	136.0	1.000D-06	136.0	1.2175D+04	4.4881D+04	
16	7.68	3.06	126.9									
	4.28	2.88										

MESH POINT - 57

DX = 0.02960 FT.

CHANNEL	VEL FT/SEC	TOTPL PSI	TBULK DEG. F.	TSURFACE DEG. F.	FILMTH INCHES	TINTFACE DEG. F.	TINTFACE DEG. F.	FILMTH INCHES	TSURFACE DEG. F.	Q / A BTU/HR*FT2	Q / A BTU/HR*FT2 WINDOW
	4.28	2.98									
1	7.70	3.16	129.8								
				141.0	1.0000-06	141.0	141.9	1.0000-06	141.9	5.5679D+04	2.4970D+04
2	7.87	3.17	137.1								
				141.4	1.0000-06	141.4	142.1	1.0C00-06	142.1	2.2068D+04	2.5609D+04
3	7.76	3.16	137.2								
				141.5	1.0000-06	141.5	142.1	1.0000-06	142.1	2.2341D+04	2.7182D+04
4	7.75	3.16	136.8								
				141.0	1.0000-06	141.0	141.5	1.0C00-06	141.5	2.1726D+04	2.6573D+04
5	7.75	3.16	136.3								
				140.7	1.0000-06	140.7	141.2	1.0C0D-06	141.2	2.2354D+04	2.6342D+04
6	7.75	3.16	136.1								
				140.4	1.0000-06	140.4	140.9	1.0000-06	140.9	2.2318D+04	2.6084D+04
7	7.75	3.16	135.8								
				140.2	1.0000-06	140.2	140.6	1.0000-06	140.6	2.2423D+04	2.5915D+04
8	7.75	3.16	135.6								
				140.0	1.0000-06	140.0	140.4	1.0000-06	140.4	2.2470D+04	2.5683D+04
9	7.74	3.16	135.4								
				139.8	1.0000-06	139.8	140.3	1.0000-06	140.3	2.2658D+04	2.5475D+04
10	7.74	3.16	135.3								
				139.8	1.0C00-06	139.8	140.2	1.0000-06	140.2	2.2855D+04	2.5322D+04
11	7.74	3.16	135.3								
				139.8	1.0C00-06	139.8	140.2	1.0000-06	140.2	2.2994D+04	2.5299D+04
12	7.74	3.16	135.3								
				139.8	1.0000-06	139.8	140.2	1.0000-06	140.2	2.2992D+04	2.5305D+04
13	7.74	3.16	135.3								
				139.7	1.0000-06	139.7	140.2	1.0C0D-06	140.2	2.2864D+04	2.5443D+04
14	7.74	3.16	135.2								
				139.3	1.0000-06	139.4	139.7	1.0000-06	139.7	2.1218D+04	2.7268D+04
15	7.74	3.16	134.3								
				136.2	1.0000-06	136.2	135.6	1.0000-06	135.6	9.4116D+03	4.2139D+04
16	7.68	3.16	127.1								
	4.28	2.98									

MITR2 TEMP DISTRIBUTION   CORE 1   A-2

MESH POINT -   59

DX = 0.02960 FT.

CHANNEL	VEL FT/SEC	TOTPL PSI	TBULK DEG. F.	TSURFACE DEG. F.	FILMTH INCHES	TINTFACE DEG. F.	TINTFACE CEG. F.	FILMTH INCHES	TSURFACE DEG. F.	Q / A BTU/HR*FT2	Q / A BTU/HR*FT2	WINDOW
	4.28	3.08										
1	7.70	3.25	130.1									
				140.7	1.0000-06	140.7	141.6	1.0000-06	141.6	5.2974D+04	2.2342D+04	
2	7.88	3.26	137.3									
				141.1	1.0000-06	141.1	141.8	1.0000-06	141.8	1.9604D+04	2.3102D+04	
3	7.76	3.25	137.3									
				141.2	1.0000-06	141.2	141.7	1.0000-06	141.7	1.9783D+04	2.4603D+04	
4	7.76	3.25	137.0									
				140.7	1.0000-06	140.7	141.2	1.0000-06	141.2	1.9247D+04	2.4089D+04	
5	7.75	3.25	136.5									
				140.4	1.0000-06	140.4	140.9	1.0000-06	140.9	1.9908D+04	2.3896D+04	
6	7.75	3.25	136.3									
				140.1	1.0000-06	140.1	140.6	1.0000-06	140.6	1.9917D+04	2.3681D+04	
7	7.75	3.25	136.0									
				139.9	1.0000-06	139.9	140.4	1.0000-06	14.	2.0056D+04	2.3544D+04	
8	7.75	3.25	135.8									
				139.7	1.0000-06	139.7	140.2	1.0000-06	140.2	2.0136D+04	2.3343D+04	
9	7.74	3.25	135.6									
				139.6	1.0000-06	139.6	140.0	1.0000-06	140.0	2.0347D+04	2.3156D+04	
10	7.74	3.25	135.5									
				139.5	1.0000-06	139.5	140.0	1.0000-06	140.0	2.0555D+04	2.3014D+04	
11	7.74	3.25	135.5									
				139.5	1.0000-06	139.5	140.0	1.0000-06	140.0	2.0694D+04	2.2990D+04	
12	7.74	3.25	135.5									
				139.5	1.0000-06	139.5	140.0	1.0000-06	140.0	2.0691D+04	2.2998D+04	
13	7.74	3.25	135.5									
				139.5	1.0000-06	139.5	139.9	1.0000-06	139.9	2.0551D+04	2.3149D+04	
14	7.74	3.25	135.4									
				139.1	1.0000-06	139.1	139.4	1.0000-06	139.4	1.8835D+04	2.5082D+04	
15	7.74	3.25	134.5									
				135.9	1.0000-06	135.9	135.3	1.0000-06	135.3	7.1883D+03	3.9867D+04	
16	7.68	3.25	127.2									
	4.28	3.08										

MESH POINT - 61

DX = C.02960 FT.

CHANNEL	VEL FT/SEC	TOTPL PSI	TBULK DEG. F.	TSURFACE DEG. F.	FILMTH INCHES	TINTFACE DEG. F.	TINTFACE DEG. F.	FILMTH INCHES	TSURFACE DEG. F.	Q / A BTU/HR*FT2	Q / A BTU/HR*FT2	WINDOW
	4.28	3.18										
1	7.70	3.34	130.3									
				140.3	1.0000-06	140.3	141.2	1.0000-06	141.2	4.9845D+04	1.9317D+04	
2	7.88	3.35	137.5									
				140.7	1.0000-06	140.7	141.4	1.0000-06	141.4	1.6779D+04	2.0230D+04	
3	7.76	3.34	137.5									
				140.8	1.0000-06	140.8	141.4	1.0000-06	141.4	1.7079D+04	2.1868D+04	
4	7.76	3.34	137.1									
				140.4	1.0000-06	140.4	140.9	1.0000-06	140.9	1.6627D+04	2.1455D+04	
5	7.75	3.34	136.7									
				140.1	1.0000-06	140.1	140.6	1.0000-06	140.6	1.7322D+04	2.1302D+04	
6	7.75	3.34	136.4									
				139.8	1.0000-06	139.8	140.3	1.0000-06	140.3	1.7380D+04	2.1132D+04	
7	7.75	3.34	136.2									
				139.6	1.0000-06	139.6	140.1	1.0000-06	14C...	1.7554D+04	2.1029D+04	
8	7.75	3.34	136.0									
				139.4	1.0000-06	139.4	139.9	1.0000-06	139.8	1.7669D+04	2.0862D+04	
9	7.74	3.34	135.8									
				139.3	1.0000-06	139.3	139.7	1.0000-06	139.7	1.7903D+04	2.0698D+04	
10	7.74	3.34	135.7									
				139.2	1.0000-06	139.2	139.7	1.0000-06	139.7	1.8122D+04	2.0566D+04	
11	7.74	3.34	135.6									
				139.2	1.0000-06	139.2	139.6	1.0000-06	139.6	1.8261D+04	2.0543D+04	
12	7.74	3.34	135.6									
				139.2	1.0000-06	139.2	139.6	1.0000-06	139.6	1.8256D+04	2.0551D+04	
13	7.74	3.34	135.6									
				139.2	1.0000-06	139.2	139.6	1.0000-06	139.6	1.6105D+04	2.0717D+04	
14	7.74	3.34	135.5									
				138.7	1.0000-06	130.7	139 1	1.0000-06	139.1	1.6321D	.2735D+04	
15	7.74	3.34	134.6									
				135.5	1.0000-06	135.5	135.0	1.0000-06	135.0	4.8469D+03	3.7435D+04	
16	7.68	3.34	127.4									
	4.28	3.18										

MESH POINT - 63

DX = 0.02960 FT.

CHANNEL	VEL FT/SEC	TOTPL PSI	TBULK DEG. F.	TSURFACE DEG. F.	FILMTH INCHES	TINTFACE DEG. F.	TINTFACE DEG. F.	FILMTH INCHES	TSURFACE DEG. F.	Q / A BTU/HR*FT2	Q / A BTU/HR*FT2 WINDOW
	4.28	3.28									
1	7.70	3.43	130.4								
				139.6	1.0000-06	139.6	140.5	1.0000-06	140.5	4.5821D+04	1.5273D+04
2	7.88	3.44	137.5								
				140.0	1.0000-06	140.0	140.8	1.0000-06	140.8	1.2988D+04	1.6428D+04
3	7.76	3.43	137.6								
				140.2	1.0000-06	140.2	140.8	1.0C0D-06	140.8	1.3466D+04	1.8240D+04
4	7.76	3.43	137.2								
				139.8	1.0000-06	139.8	140.3	1.0000-06	140.3	1.3136D+04	1.7959D+04
5	7.75	3.43	136.8								
				139.5	1.0000-06	139.5	140.0	1.0000-06	140.0	1.3881D+04	1.7856D+04
6	7.75	3.43	136.5								
				139.2	1.0000-06	139.2	139.7	1.0000-06	139.7	1.4000D+04	1.7746D+04
7	7.75	3.43	136.3								
				139.0	1.0000-06	139.0	139.5	1.0000-06	13°.5	1.4219D+04	1.7688D+04
8	7.75	3.43	136.0								
				138.8	1.0000-06	138.8	139.3	1.0C0D-06	139.3	1.4380D+04	1.7566D+04
9	7.75	3.43	135.9								
				138.7	1.0000-06	138.7	139.2	1.0000-06	139.2	1.4644D+04	1.7431D+04
10	7.74	3.43	135.7								
				138.7	1.0000-06	138.7	139.1	1.0C0C-06	139.1	1.4878D+04	1.7314D+04
11	7.74	3.43	135.7								
				138.6	1.0000-06	138.6	139.1	1.0C0D-06	139.1	1.5018D+04	1.7291D+04
12	7.74	3.43	135.7								
				138.6	1.0C0D-06	138.6	139.1	1.0000-06	139.1	1.5013D+04	1.73C0D+04
13	7.74	3.43	135.7								
				138.6	1.0000-06	138.6	139.0	1.0C0D-06	139.0	1.4854D+04	1.7473D+04
14	7.74	3.43	135.6								
				138.2	1.0000-06	138.2	138.5	1.0000-06	138.5	1.3035D+04	1.9537D+04
15	7.74	3.43	134.6								
				135.0	1.0000-06	135.0	134.4	1.0000-06	134.4	1.6162D+03	3.4204D+04
16	7.68	3.43	127.5								
	4.28	3.28									

APPENDIX F

Sample Data Sheets

1)   Irradiation Data Sheet (Element Irradiation)

2)   Plate Scanning Data Sheet

3)   GAMSCAN INPUT DATA SHEET

4)   Irradiation Data Sheet (Copper Wire Irradiation)

5)   Copper Wire Data Sheet

6)   Copper Wire Resonance Correction Sheet

IRRADIATION DATA SHEET

IRRADIATION **#2**   DATE **October 16, 1975**

GAMSCAN REFERENCE IRRADIATION **#1***

TIME REACTOR POWER LEVELED   **1422**

TIME REACTOR SHUTDOWN   **1522**

#4M41

C-9

C-8
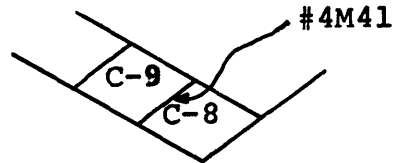
ELEMENT POSITION **C-9**

Ten Minute Interval	Channel 7	Channel 5	Channel 6	Ave. on Channel 7 for Interval
1	$.5 \times 10^{-6}$	19 μa		$.5 \times 10^{-6}$
2	$.5 \times 10^{-6}$	19 μa		$.5 \times 10^{-6}$
3	$.5 \times 10^{-6}$	19 μa		$.5 \times 10^{-6}$
4	$.5 \times 10^{-6}$	19 μa		$.5 \times 10^{-6}$
5	$.5 \times 10^{-6}$	19 μa		$.5 \times 10^{-6}$
6	$.5 \times 10^{-6}$	19 μa		$.5 \times 10^{-6}$

Note*   Irradiation numbers in GAMSCAN and COREFAC are 1
        less than the irradiation number listed in the
        raw data sheet because the actual irradiation #1
        was only a trial irradiation.

PLATE SCANNING DATA SHEET

IRRADIATION   # 2   PLATE   # GP-64   DATE October 16, 1975

GAMSCAN IRRADIATION   # 1   Co FOIL   # 2   SHEET   #1

Time	Lath Table Readings			Fuel Meat Coordinates		U Foil Counts	Point Number	Corrected Counts from GAMSCAN
	Y	X	Original Count	Y^1	X^1			
1739	3	23	739					
1742	3	22 7/8	974					
1744	3	22 3/4	1330	1.0	-0.125	5645	J=1,2,3	1084
1746	2 5/16	22 11/16	1079	1.6875	0.0	5782	4	728
1747	3	22 11/16	1638	1.0	0.0		15	1577
1750	3 11/16	22 11/16	1388	0.3125	0.0		6	1233
1752	2 5/16	22 5/8	1850	1.6875	0.0625	5463	7	1984
1753	3	22 5/8	6152	1.0	0.0625		8	8837
1754	3 11/16	22 5/8	4172	0.3125	0.0625		9	5737
1756	2 5/16	22 9/16	4542	1.6875	0.125		10	6437
1757	3	22 9/16	11807	1.0	0.125		11	18430
1758	3 11/16	22 9/16	8650	0.3125	0.125		12	13356
1800	2 5/16	22 1/2	8706	1.6875	0.1875		13	13561

IRRADIATION   #   2   PLATE   #   GP-64   DATE   October 16, 1975

GAMSCAN IRRADIATION   #   1   Co FOIL   #   2   SHEET   #2

Time	Lath Table Readings Y	X	Original Count	Fuel Meat Coordinates Y^1	X^1	U Foil Counts	Point Number	Corrected Counts from GAMSCAN
1801	3	22 1/2	16769	1.0	0.1875		14	27396
1802	3 11/16	22 1/2	13336	0.3125	0.1875		15	21916
1804	2 5/16	22 3/8	13093	1.6875	0.3125		16	21537
1805	3	22 3/8	15106	1.0	0.3125		17	25243.6
1807	3 11/16	22 3/8	14628	0.3125	0.3125	4926	18	24795
1808	2 5/16	22 1/4	12757	1.6875	0.4375		19	21499
1809	3	22 1/4	14280	1.0	0.4375		20	24436
1811	3 11/16	22 1/4	13740	0.3125	0.4375	4959	21	23845
1812	2 5/16	22	12424	1.6875	0.6875		22	21463
1814	3	22 1/4	13332	1.0	0.6875		23	23493
1815	3 11/16	22 1/4	13186	0.3125	0.6875		24	23390
1818	2 5/16	21 1/2	12319	1.6875	1.1875	4777	25	22098

| Time | Lath Table Readings | | Original Count | Fuel Meat Coordinates | | U Foil Counts | Point Number | Corrected Counts from GAMSCAN |
	Y	X		Y^1	X^1			
1819	3	21 1/2	12483	1.0	1.1875		26	22589
1820	3 11/16	21 1/2	12444	0.3125	1.1875		27	22687
1822	2 5/16	21	12812	1.6875	1.6875		28	23782
1823	3	21	12371	1.0	1.6875		29	23056
1825	3 11/16	21	11809	0.3125	1.6875		30	22229
1827	2 5/16	20	13394	1.6875	2.6875		31	25837
1828	3	20	13200	1.0	2.6875	4603	32	25616
1829	3 11/16	20	12637	0.3125	2.6875		33	24615
1831	2 5/16	19	12949	1.6875	3.6875		34	25643
1832	3	19	13418	1.0	3.6875		35	26843
1834	3 11/16	19	12855	0.3125	3.6875	4504	36	25971
1835	2 5/16	18	12931	1.6875	4.6875		37	26311

IRRADIATION # __2__   PLATE # __GP-64__   DATE __October 16, 1975__

GAMSCAN IRRADIATION # __1__   Co FOIL # __2__   SHEET __#4__

Time	Lath Table Readings Y	X	Original Count	Fuel Meat Coordinates Y^1	X^1	U Foil Counts	Point Number	Corrected Counts from GAMSCAN
1838	3	18	13413	1.0	4.6875		38	27926
1839	3 11/16	18	12822	0.3125	4.6875		39	26783
1843	3	17 1/4	12631	1.6875	5.4375		40	27079
1844	2 5/16	17 1/4	11965	1.0	5.4375	4336	41	25701
1846	3 11/16	17 1/4	11508	0.3125	5.4375		42	24960
1848	2 5/16	16 1/2	11652	1.6875	6.1875		43	25639
1849	3	16 1/2	11778	1.0	6.1875		44	26115
1850	3 11/16	16 1/2	11096	0.3125	6.1875		45	24636
1851	2 5/16	15 3/4	10442	1.6875	6.9375		46	23205
1853	3	15 3/4	10442	1.0	6.9375		47	23516
1854	3 11/16	15 3/4	10143	0.3125	6.9375		48	22912
1856	2 5/16	15	8477	1.6875	7.6875		49	18989
1857	3	15	8244	1.0	7.6875		50	18966

640

Time	Lath Table Readings		Original Count	Fuel Meat Coordinates		U Foil Counts	Point Number	Corrected Counts from GAMSCAN
	Y	X		Y^1	X^1			
1858	3 11/16	15	8148	0.3125	7.6875		51	18383
1900	2 5/16	14	5503	1.6875	8.6875		52	11770
1901	3	14	5223	1.0	8.6875		53	11116
1903	3 11/16	14	5252	0.3125	8.6875		54	10807
1904	2 5/16	13	3763	1.6875	9.6875		55	7590
1906	3	13	3668	1.0	9.6875		56	7427
1907	3 11/16	13	3865	0.3125	9.6875		57	8005
1908	2 5/16	9	2439	1.6875	13.6875		58	4620
1910	3	9	2505	1.0	13.6875		59	4859
1911	3 11/16	9	2360	0.3125	13.6875		60	4488
1913	2 5/16	3	1303	1.6875	19.6875		61	2307
1914	3	3	1352	1.0	19.6875		62	2458

IRRADIATION   #   2   PLATE   #   GP-64   DATE   October 16, 1975

GAMSCAN IRRADIATION   #   1   Co FOIL   #   2   SHEET #6

| Time | Lath Table Readings | | Original Count | Fuel Meat Coordinates | | U Foil Counts | Point Number | Corrected Counts from GAMSCAN |
	Y	X		Y^1	X^1			
1916	3 11/16	3	1302	0.3125	19.6875		63	2365
1917	3	0	776	1.0	22.0000		64,65,66	1040
1919	2	23	463	1.0				

642

GAMSCAN INPUT DATA PREPARATION SHEET

IRRADIATION #2   PLATE   #6P-64   (Plate 1)

REFERENCE GAMSCAN IRRADIATION #1

J	TI (J) Time from Start of Irradiation in Min.	C(J) Original Counts
1	202	1330
2	202	1330
3	202	1330
4	204	1079
5	205	1638
6	208	1388
7	210	1850
8	211	6152
9	212	4172
10	214	4542
11	215	11807
12	216	8650
13	218	8706
14	219	16769
15	221	13336

IRRADIATION #2   PLATE   #6P-64

J	TI(J) Time from Start of Irradiation in Min.	C(J) Original Counts
16	222	13093
17	223	15106
18	225	14628
19	226	12757
20	227	14280
21	229	13740
22	230	12424
23	232	13332
24	233	13186
25	236	12319
26	237	12483
27	238	12444
28	240	12812
29	241	12371
30	243	11809
31	245	13394
32	246	13200
33	247	12637
34	249	12949
35	250	13418

IRRADIATION **#2**   PLATE **#6P-64**

J	TI(J) Time from Start of Irradiation in Min.	C(J) Original Counts
36	252	12855
37	253	12931
38	256	13413
39	257	12822
40	261	12631
41	262	11965
42	264	11508
43	266	11652
44	267	11778
45	268	11096
46	269	10442
47	271	10442
48	272	10143
49	274	8477
50	275	8244
51	276	8148
52	278	5503
53	279	5223
54	281	5052
55	282	3763

IRRADIATION #2   PLATE   #6P-64

J	TI(J) Time from Start of Irradiation in Min.	C(J) Original Counts
56	284	3668
57	285	3865
59	288	2505
60	289	2360
61	291	1303
62	292	1352
63	294	1309
64	295	776
65	295	776
66	295	776

IRRADIATION DATA SHEET

IRRADIATION #17   DATE   November 7, 1975

TIME REACTOR POWER LEVELED   1120

TIME REACTOR SHUTDOWN   1220

SPECIAL DETAILS OF
    IRRADIATION

 Period Channel Levels

Channel #1 - 3.1×10^{-6} Wire N   Spider hole #1

Channel #2 - 9.5×10^{-7} Wire M   Deep Drill Hole #4 7-3/4

Channel #3 - 1.8×10^{-7} Wire F   3GV5   below
                                                                bottom
                                         Wire E   Channel 11 ⎫
                                                             ⎬ A2(4M41)
                                                  Channel 2 ⎭

Ten Minute Interval	Channel 7		Channel 5	Channel 6	Ave. on Channel 7 for Interval
	Recorder	µµammeter			
1	50.2	48.8	18.8	9.0	49.8
2	49.8	48.4	18.8	9.0	49.9
3	49.8	48.4	18.8	9.0	50.0
4	49.9	48.4	18.8	9.0	49.9
5	49.9	48.4	18.8	9.0	49.9
6	49.9	48.4	18.8	9.0	49.9

COPPER WIRE DATA SHEET

IRRADIATION #17   Co FOIL   #17

DATE November 7, 1975   LOCATION OF WIRE TIP: Spider Hole #1

WIRE #   N   Tip of Wire 27" from Tip
                                              of holder

Time of Start of Count	Lath Table Readings		(4 minute counts) Original Counts	Distance from Tip of Wire x^1 (inch)	Decay Time (minutes)	Counts Corrected for Background and Decay
	X	Y				
1324	23	3	216		64	0
1328	22 3/8	3	4357	-1 5/16	68	4402.6
1333	22	3	4311	- 11/16	73	4373.4
1337	21	3	3158	5/16	77	3153.3
1342	20	3	2246	1 5/16	82	2185.6
1346	19	3	1958	2 5/16	86	1882.3

Time at Start of Count	Lath Table Readings		(4 minute counts) Original Counts	Distance from Tip of Wire x^1 (inch)	Decay Time (minutes)	Counts Corrected for Background and Decay
	X	Y				
1351	18	3	1863	3 5/16	91	1787.7
1355	17	3	1857	4 5/16	95	1787.6
1359	16	3	1879	5 5/16	99	1818.1
1403	15	3	1946	6 5/16	103	1898.2
1408	14	3	889	7 5/16	108	1844.0
1413	13	3	1720	8 5/16	113	1665.2
1417	12	3	1640	9 5/16	117	1582.3
1422	11	3	1549	10 5/16	122	1487.9
1427	10	3	1445	11 5/16	127	1378.0

Time at Start of Count	Lath Table Readings		(4 minute counts) Original Counts	Distance from Tip of Wire X^1 (inch)	Decay Time (minutes)	Counts Corrected for Background and Decay
	X	Y				
1431	8	3	1053	13 5/16	131	941.8
1436	5	3	881	16 5/16	136	751.7
1440	1	3	631	20 5/16	140	470.8

COPPER WIRE RESONANCE CORRECTION SHEET

CASE #11

WIRE N

LOCATION OF WIRE TIP: 27 1/4
from top edge of hold down
grid plate - Spider Hole #1

Distance from Wire Tip to Collimator Centerline	Counts Corrected for Background, Decay, and Power	$\dfrac{\emptyset_2}{\emptyset_3}$ From CITATION	Counts Due to Thermal Activation of Copper
5/16	4376.7	.47	2889.5
11/16	4347.7	.57	2676.9
1 11/16	3135.0	.8	1671.1
2 11/16	2172.8	1.35	876.7
3 11/16	1871.2	1.74	644.0
4 11/16	1777.2	2.6	460.6
5 11/16	1777.2	2.6	460.6
6 11/16	1807.4	2.6	460.6
7 11/16	1887.0	3.15	424.1
8 11/16	1833.2	3.15	412.0
9 11/16	1655.4	3.15	372.0

Distance from Wire Tip to Collimator Centerline	Counts Corrected for Background, Decay, and Power	$\dfrac{\phi_2}{\phi_3}$ From CITATION	Counts Due to Thermal Activation of Copper
10 11/16	1573.0	3.15	353.5
11 11/16	1479.2	3.5	309.8
12 11/16	1369.9	3.5	283.4
14 11/16	936.3	9.25	84.1
17 11/16	747.3	13.0	49.0
21 11/16	468.0	21.0	19.5

George Charman Allen, Jr. was born on February 13, 1948 in Upper Darby, Pennsylvania. His elementary and secondary education were obtained in Drexel Hill, Pennsylvania and Toms River, New Jersey.

Upon graduation he enrolled at Massachusetts Institute of Technology, Cambridge, Massachusetts. While an undergraduate he was a member of Sigma Phi Epsilon, a social fraternity, M.I.T. varsity heavyweight crew team, Mangla Dam study group, and he was elected vice president of the local student chapter of the American Society of Civil Engineers. In 1969, he was accepted into a five year program with the Department of Civil Engineering and the Department of Nuclear Engineering. During the fifth year he was a teaching assistant for the courses, "Nuclear Power Reactors" and "Radiation Shielding." Among the honors he received as an undergraduate was election to Chi Epsilon, a national civil engineering honor society, and twice being a silver medalist in the national intercollegiate rowing championships. In June, 1971, he received a S.B. degree in Civil Engineering and a S.M. degree in Nuclear Engineering. The title of his master's thesis was, "Aspects of a Seismic Analysis of the MITR-II."

Mr. Allen was accepted into the M.I.T. Department of Nuclear Engineering Ph.D. program and awarded the first

Theos J. Thompson Fellowship. He was elected secretary
and then president of the local student branch of the
American Nuclear Society. In October, 1972, he accepted
employment at the M.I.T. Research Reactor as a senior
shift supervisor and later as the supervisor for mechanical
engineering on the MITR-II modification. Prior technical
employment had consisted of three summers with Bechtel
Corporation and one summer with the Army Corps. of Engineers.

Mr. Allen is married to the former Carol Iris Gibbs of
Skillman, New Jersey.